FABRICATION AND CHARACTERIZATION OF A POLYDIMETHYLSILOXANE MICROFLUIDIC PUMP FOR DIRECT-SAMPLING NEUROSCIENCE EXPERIMENTS, WITH IN-LINE CAPILLARY ELECTROPHORESIS – LASER-INDUCED FLUORESCENCE CHEMICAL ANALYSIS

A DISSERTATION
SUBMITTED TO THE FACULTY OF THE GRADUATE SCHOOL
OF THE UNIVERSITY OF MINNESOTA
BY

Neil J. Graf

IN PARTIAL FULFILLMENT OF THE REQUIREMENTS
FOR THE DEGREE OF
DOCTOR OF PHILOSOPHY

Michael T. Bowser, Advisor

May, 2011

Acknowledgements

I would like to first acknowledge my graduate research advisor, Michael T. Bowser, for a truly memorable graduate research experience. Throughout my graduate research career, I was allowed to grow, learn, and function, in the most positive ways. The resources and opportunities that Mike has provided along the way, have no question had a tremendous impact on me both personally, as well as professionally. I am grateful I have never felt limited, in any way. Beyond his scientific talents, Mike possesses remarkable balance, and a certain sort of, "coolness," that is very rare, and hard to come across. Mike has also shown what a kind, down-to-earth, decent, and generous individual he is, with integrity and ethics that is second to none. I thank him for everything.

I would like to acknowledge my other Analytical Chemistry Professors, namely Edgar A. Arriaga, Philippe Bühlmann, and Peter W. Carr. Along the way, they have all had a very positive impact on my growth and development as a scientist. They too, possess nothing less than the highest levels of excellence and integrity, in too many ways to list. I have many fond memories of all three, on both personal and professional levels, and would like to thank each of them for their involvement, advice, and generosity, throughout my entire graduate research career.

I am especially grateful to Dave Hultman and co-workers, of the University of Minnesota's Electrical Engineering Machine Shop. Dave is without a question, one of the most passionate and creative machinists this world has to offer. The results presented within the forthcoming Chapters, have been made possible in large-part, with Dave's

very hard work and dedicated efforts. Dave's most notable deliverables include fabrication of the injection mold, microvalves, and micropositioners. Without Dave's speedy and rapid turnaround time in fabricating the second generation micropositioners, several Chapters would not exist. I have many positive memories of Dave and his Shop over the years, and will most certainly miss my regular and frequent visits. I genuinely thank him for everything.

Lastly, I would like to graciously acknowledge Jian Sheng, for his very helpful discussions, regarding pump analysis. My discussions with Jian came very late in my graduate research career, where I wish I had had the opportunity to meet him earlier along the way. His helpful input and expert pump knowledge was extremely positive, and I genuinely thank him for both his time, and generosity.

Dedication

To Mom, for all her unwavering love and support on too many levels to mention, in any, every, and all ways possible, as far back as I can remember. And to the memory of Dad, and all the special memories we shared hunting and fishing together, and further to all that he instilled in me, in making me who I am, and the person I continue to be. And finally, to the rest of my Family and Friends, for their presence and positive influences throughout my entire life. You all know who you are, and all that you have done for me, thank you.

Abstract

A polydimethylsiloxane (PDMS) peristaltic micropump was designed, fabricated, and characterized, for intended use within rodent brain direct-sampling neuroscience experiments, with capillary electrophoresis - laser-induced fluorescence (CE-LIF) chemical analysis.

The micropump was fabricated in-part using replica molding (REM) and injection molding. The micropump channel was formed by bonding an open PDMS Gaussian-shaped micromolded channel, to a featureless slab of PDMS. Two pieces of capillary tube interconnects were sealed within the closed-off microchannel, and used to make connections with the outside world. The micropump was actuated using piezoelectric cantilevers, with a precision machined microvalve attached to the tip of each cantilever actuator. Registration of the cantilevers and microvalves over the PDMS microchannel, was accomplished with the aid of in-house machined micropositioners.

The micropump was thoroughly characterized, for use and application as a bio-analytical add-on attachment device, to an already existing CE-LIF instrument. The micropump was characterized for: various microchannel geometries; different microvalve sizes, tilt, positioning, and shutoff performance; micropositioner design and performance; and, flow rate, backpressure, and peristaltic signal analysis.

A P-Q (or H-Q) plot was formed, to represent the performance of the micropump for maximum attainable backpressure (P), versus flow rate (Q). The linear plot was formed by experimentally collecting fourteen individual data points, each corresponding

to a unique micropump, "state." The P-Q plot as discussed within Chapter VIII, is very potent, in providing a 5-for-1 benefit ratio. The P-Q plot allows an experimentalist to obtain: 1) a means to understand how the micropump output performance for both flow rate and backpressure, can be optimized for any particular microfluidic application, 2) an experimentally characterized micropump performance curve/s, 3) an experimentally characterized system curve, 4) the maximum power output of the micropump, and 5) a means to acquire a quantitative measure of the suction lift requirements associated with rodent brain direct-sampling neuroscience experiments. A control volume analysis is provided, to additionally articulate and facilitate discussion of the direct-sampling methodology. Preliminary pilot study direct-sampling data is also provided, as a means to justify and prove viability of the direct-sampling technique, for future characterization and optimization direct-sampling CE-LIF neuroscience studies.

Table of Contents

List of Tables

List of Figures

List of Abbreviations

2D	Two-Dimensional
3D	Three-Dimensional
A.U.	Arbitrary Unit/s
Bio-MEMS	Biological Microelectromechanical Systems
CAD	Computer Aided Design
CCD	Charged Coupled Device
CD	Compact Disc
CE	Capillary Electrophoresis
CE-LIF	Capillary Electrophoresis with Laser-Induced Fluorescence
CF	CompactFlash
cm	centimeter
CMOS	Complementary Metal-Oxide-Semiconductor
CNC	Computer Numerically Controlled
COP	Cyclo Olefin Polymer
CSF	Cerebral Spinal Fluid
dc	Direct Current
EDM	Electrical Discharge Machine

EOF	Electroosmotic Flow
FET	Field-Effect Transistor
FIA	Flow Injection Analysis
FSCV	Fast Scanning Cyclic Voltammetry
HARMS	High Aspect Ratio Microstructures
HPLC	High-Performance Liquid Chromatography
Hz	hertz
IC	Integrated Circuit
ID	Inner Diameter
InGaAs	Indium Gallium Arsenide
IPA	Isopropyl Alcohol
IR	Infrared
kPa	kilopascal
LIF	Laser-Induced Fluorescence
LIGA	Lithographie, Galvano-formung, Abformung
LOC	Lab-on-a-Chip
µm	Micrometer -or- Micron
µM	Micromolar
µPIV	Micro-Particle Image Velocimetry
µPOS	Micropositioner/s
µTAS	Micro Total Analysis System/s

μTM	Microtransfer Molding
M	Molar
MEMS	Microelectromechanical Systems
MIMIC	Micromolding in Capillaries
min	minute
mm	millimeter
mM	millimolar
MTV	Molecular Tagging Velocimetry
mV	millivolt
nL	nanoliter
nW	nanowatt
N	newton
NMR	Nuclear Magnetic Resonance
OD	Outer Diameter
OED	Optical Emission Detection
psi	Pounds per Square Inch
Pa	pascal
PCB	Printed Circuit Board
PDMS	Polydimethylsiloxane
PEB	Post Exposure Bake
PIV	Particle Image Velocimetry
PMBSF	Posteriomedial Barrel Subfield

PMMA	Polymethylmethacrylate
PMT	Photomultiplier Tube
POC	Point-of-Care
PZT	Lead Zirconate Titanate
REM - or - RM	Replica Molding
RI	Refractive Index
RPM	Revolutions Per Minute
RTV	Room Temperature Vulcanization
s	second
SD	Secure Digital
SI	Primary Somatosensory Cortex
SPR	Surface Plasmon Resonance
V	volt

Preface

Chapter II was produced in-part with permission from:

Neil J. Graf and Michael T. Bowser, "A Soft-Polymer Piezoelectric Bimorph Cantilever-Actuated Peristaltic Micropump," *Lab on a Chip*, 2008, **8**, 1664 – 1670.

Chapter I : *A Compendium, on Microfluidic Device Technology*

Microfluidics, a Brief Overview

1) Microfluidics, Defined

Microfluidics is, "…the science and technology of systems that process or manipulate small (10^{-9} to 10^{-18} liters) amounts of fluids, using channels with dimensions of tens to hundreds of micrometers." [1] The field of microfluidics is highly interdisciplinary, with research and development efforts found within nearly every subdiscipline of chemistry, physics, engineering, biology, and medicine.[2-6] Microfluidics is uniquely sandwiched between millifluidic,[7] and nanofluidic technology,[8, 9] with both channel geometries and fluidic quantities being regarded as, larger vs. smaller, for millifluidic vs. nanofluidic devices, respectively. As a reference in terms of length, a meter stick contains 1000 millimeters (mm), or, 1,000,000 micrometers (micron or μm), or, 1,000,000,000 nanometers (nm).

The field of microfluidics is often associated with, and interchangeably referenced as, lab-on-a-chip (LOC) device technology, and/or, micro total analysis systems (μTAS). The emphasis of LOC technology, is to integrate multiple fluidic, chemical, mechanical, and electrical processes onto a single chip, with the chip ideally having dimensions similar to that of a camera memory card (e.g. CompactFlash (CF) or Secure Digital (SD) card). Therefore, the LOC concept is best summarized as, the goal or process of scaling down macroscopic fluidic, chemical, mechanical, and electrical processes, into analogous microscopic formats. This concept is clearly understood with reference to Figure I-1, where it can be visualized the processes and instrumentation employed within a modern laboratory, are ideally placed onto a single microfluidic substrate chip.[10]

A)

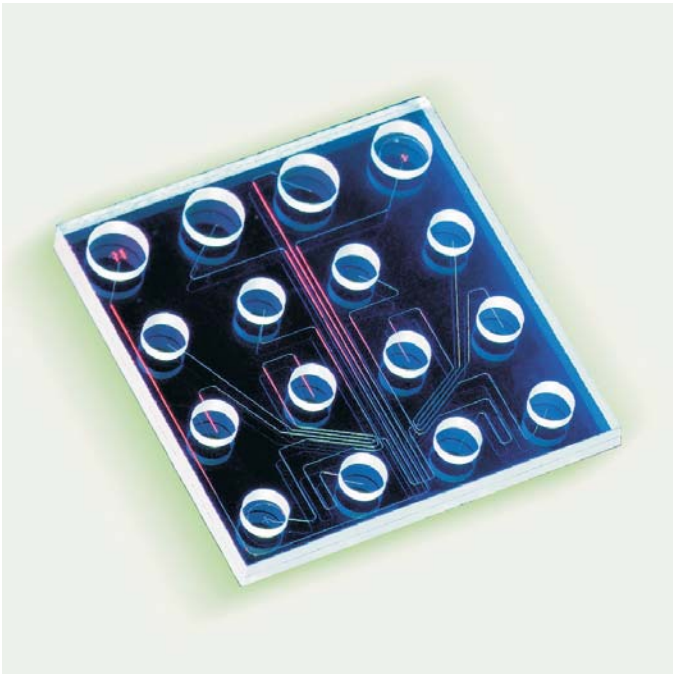

B)

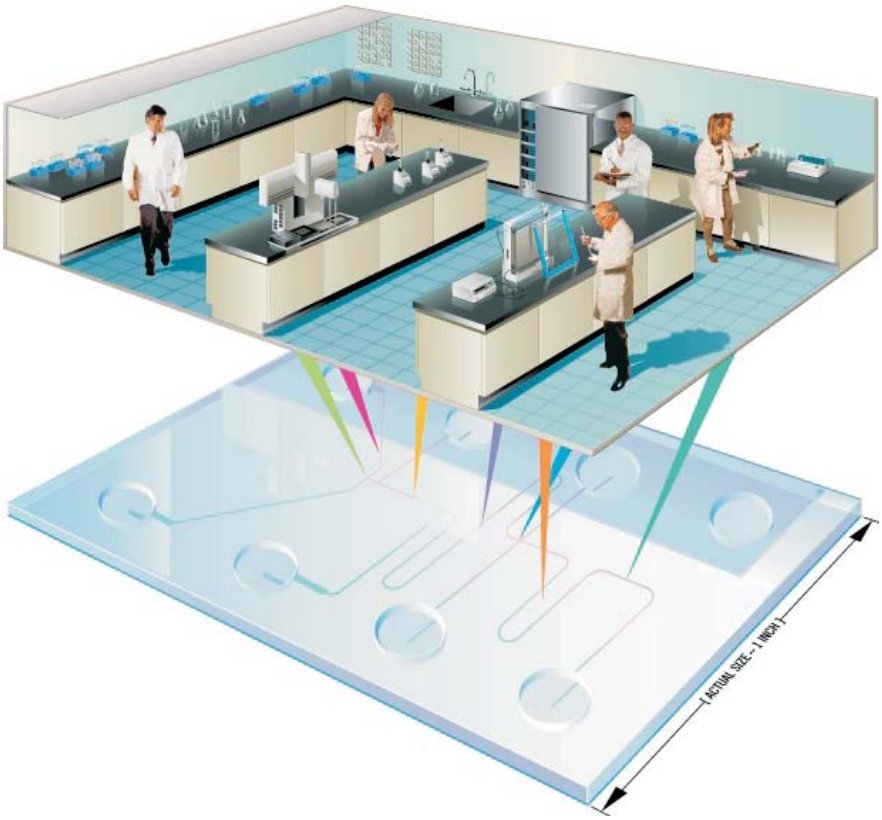

Figure I-1: A) Microfluidic chip fabricated in glass; B) Miniaturizing and integrating laboratory processes onto a microchip device. (Figure I-1 adapted from Chow, 2002)[10]

A realistic perspective of a modern lab-on-a-chip device, can be seen within Figure I-2. It can be observed within this Figure, that the chip dimensions are on the order of 2-3 cm per side, and less than 1 mm in thickness.[11]

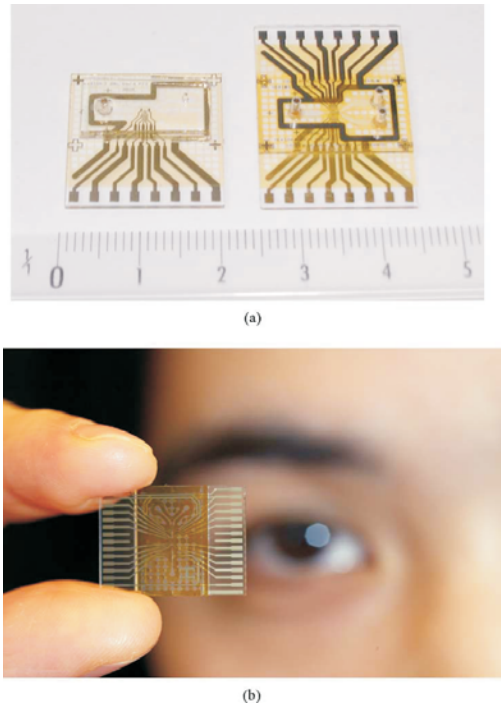

Figure I-2: (a) Microfluidic cytological tool, for cell counting and separation, consisting of an integrated microfabricated chip with a PDMS cover and molded fluidic connections. (b) Latest design iteration of chip. (Figure I-2 adapted from Erickson and Li, 2004)[11]

2) Origins of Microfluidic Device Technology

"On the west end of the 4th floor of Building 1 of Bell Labs at Murray Hill, hangs a small plaque with a picture of the first point contact transistor and the following inscription: "*The transistor, a solid-state electronic amplifier which revolutionized world communications, was invented in this laboratory on December 23rd, 1947.*" " [12] A trio of scientists; 1) Walter Brattain, Ph.D. graduate of the University of Minnesota, under

Professor John Tate, 2) William Shockley, Ph.D. graduate of MIT, under Professor John Slater, and 3) John Bardeen, Ph.D. graduate of Princeton University, under Professor Eugene Wigner, and later a Professor at the University of Minnesota, jointly were awarded the 1956 Nobel Prize in Physics "for their researches on semiconductors and their discovery of the transistor effect." [13] Brattain and Bardeen's point-contact transistor was first invented, with the commercial success of the transistor being solidified with Shockley's invention of the bipolar junction transistor, one month later.[13]

"Miniaturization of electronic circuits was a frequent topic of discussion in the late 1950's, especially in the U.S. armed forces because of their needs for compact, lightweight electrical equipment. But it took the inventive genius of electrical engineer Jack Kilby to come up with a practical way to achieve this goal. On July 24, 1958, he penned a prophetic entry into his Texas Instruments logbook: "*Extreme miniaturization of many electrical circuits could be achieved by making resistors, capacitors and transistors & diodes on a single slice of silicon.*" [13] The integrated circuit (IC), is an electronic chip fabricated with millions/billions of transistors, by which nearly all electronic equipment relies upon, to process and output information. In 2000, Jack Kilby won the Nobel Prize in Physics, "for his part in the invention of the integrated circuit." [13]

Arguably, the most famous integrated circuit is associated with, the Intel Pentium Processor. In 1965, Intel co-founder, Gordon Moore wrote a paper in the April issue of *Electronics*, where he envisioned the explosive growth and demand for integrated circuit device technology, where he also predicted within this same article, that the number of transistors on an integrated circuit would double approximately every year.[13, 14] This

prediction was slightly modified in 1975, where Moore refined his prediction in stating that the number of transistors on an IC chip would double approximately every *two* years. Moore's transistor density growth prediction on an IC chip, has long since been coined, "Moore's Law." Figure I-3 is a plot of Moore's Law, representing the increased transistor density, as a function of time.[14]

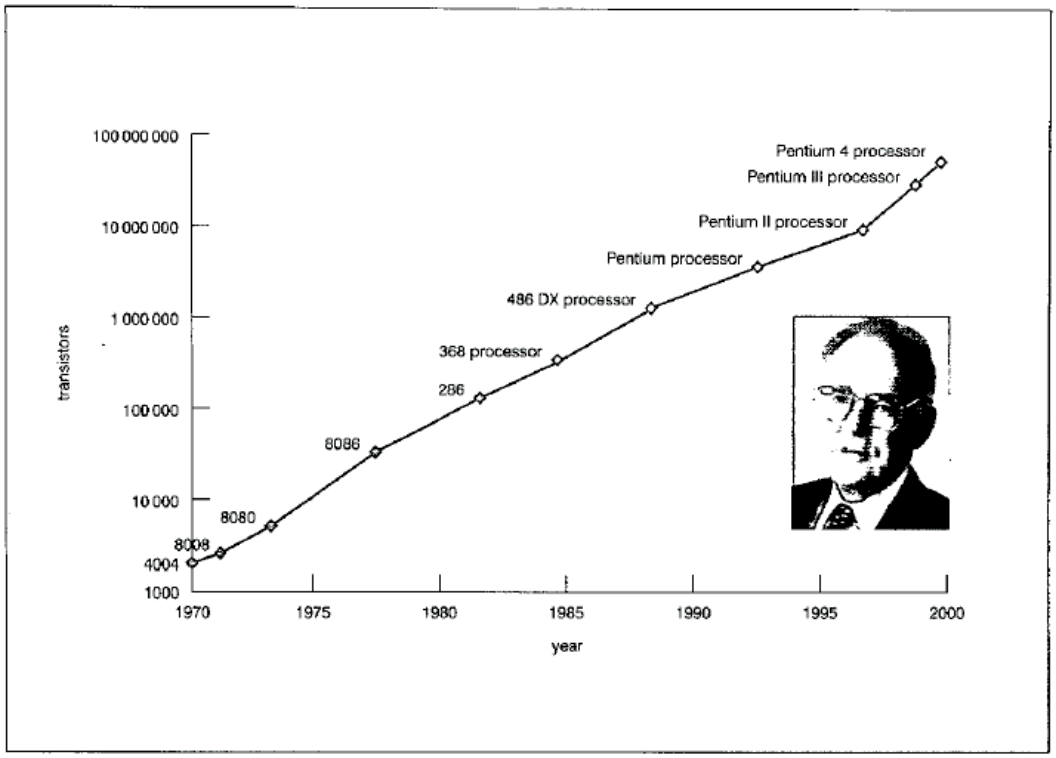

Figure I-3: Moore's Law, with inset, Gordon Moore. (Figure I-3 from Warren, 2002)[14]

Eventually, Moore's Law will hit a physical limit, slowing or stopping the continued growth of increased transistor density on IC chips. This physical limit is expected to occur some time around the year 2020, where alternative computing architectures will need to be invented, if computing power is to continue increasing past the limits as predicted by Moore's Law.[15]

It is not the intent of this dissertation to provide a history lesson in electronics, however the origins and growth of electrical device technology, parallels that of the same for microfluidic device technology. The two seemingly disparate fields are actually, and maybe surprisingly so to the non-specialist, inextricably connected on many levels. Comparisons between IC and LOC technologies, are not uncommon to come across. Figure I-4 is a representation of one such comparison, where it can be seen the stages of growth and development for microfluidic device technology, are compared one-for-one with microelectronic device technology.[16]

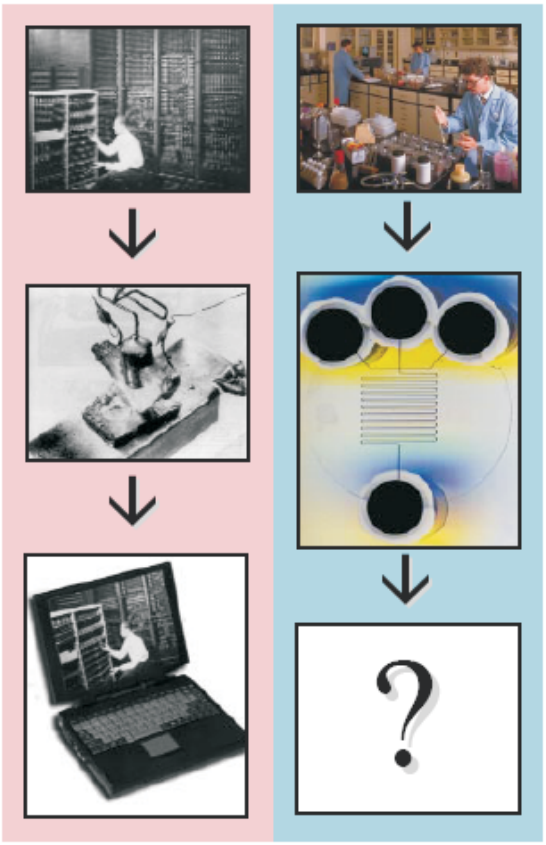

Figure I-4: A pictorial history of the development of microelectronics and microfluidics. On the left: the path leading to today's digital computers, from the ENIAC, to the transistor and thereafter modern day laptop computer. On the right: the biochemist's laboratory. Will microfabricated fluidic devices lead to a similar expansion in experimental power? (Figure I-4 from Ramsey, 1999)[16]

If a transistor is taken as the basic fundamental unit operation device on an integrated circuit, perhaps, it might be stated the analogous equivalent on a microfluidic chip, is a microvalve, or micropump. Microvalves are unit operation devices that direct/route fluid flows on microfluidic chips, with micropumps the unit operation devices that drive fluids throughout the internal conduits of a microfluidic chip. Micropumps are quite often composed of one or more microvalves, where actuation of the microvalve/s in turn creates a micropump. A literature search would reveal that one of the very first documented reports of using a micropump to pumps fluids, is found in 1975,[17, 18] with the first patent for a micropump created from IC technology being discovered in, 1984.[19]

The analogous equivalent of an IC chip format, for microfluidic device technology, is better known as LOC or μTAS chip technology. Other related and sometimes interchangeable terms used to reference LOC technology are; MEMS, Bio-MEMS, and MEMS-Fluidics.[2, 20-22] If Jack Kilby is the pioneer of the integrated circuit, Andreas Manz is regarded by many as, the pioneer of LOC, or μTAS chip technology. The μTAS concept was introduced by Manz in 1990,[23] with an experimental presentation of a capillary electrophoresis microfluidic chip presented by Manz and Team, in 1992.[24] Since the early 1990's, microfluidic device technology has been growing at an exponential pace, both in terms of research activity, as well as integrated unit operation densities. Figure I-5 is a comparison of Moore's Law for the growth rate of transistor density on a semiconductor chip, to that of valve densities on a polymeric fluidic chip.[25]

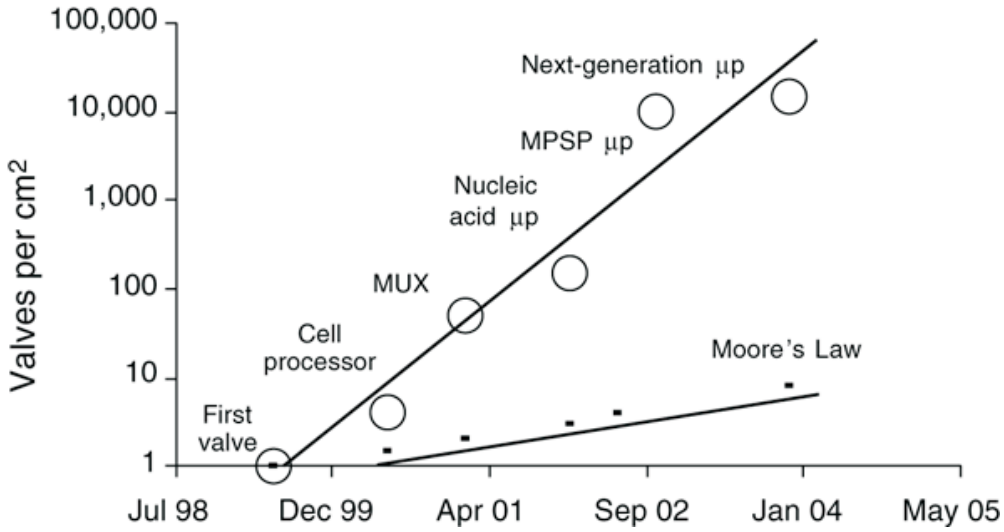

Figure I-5: The analog of Moore's Law for nanofluidic systems. Valve densities in fluidic chips fabricated with soft lithography have increased exponentially with time. The current rate of growth is four times faster than the rate of growth of transistor densities in the semiconductor industry – it remains to be seen how long this can be maintained. MPSP, massively partitioning sniper processor; μp, microprocessor; MUX, multiplexer. (Figure I-5 from Hong and Quake, 2003).[25]

It can be seen the growth rate on microfluidic chips is four times faster than that on semiconductor chips. High density integrated microfluidic device technology has most notably been explored by Steve Quake, a second pioneer in the field of microfluidic device technology. A modern high-density-microvalve integrated microfluidic chip developed within the Quake Lab, is shown in Figure I-6. This Figure shows a polymeric microfluidic chip containing 256 compartments, with 2056 microvalves, for both chip length and width dimensions of approximately 5.5 cm.

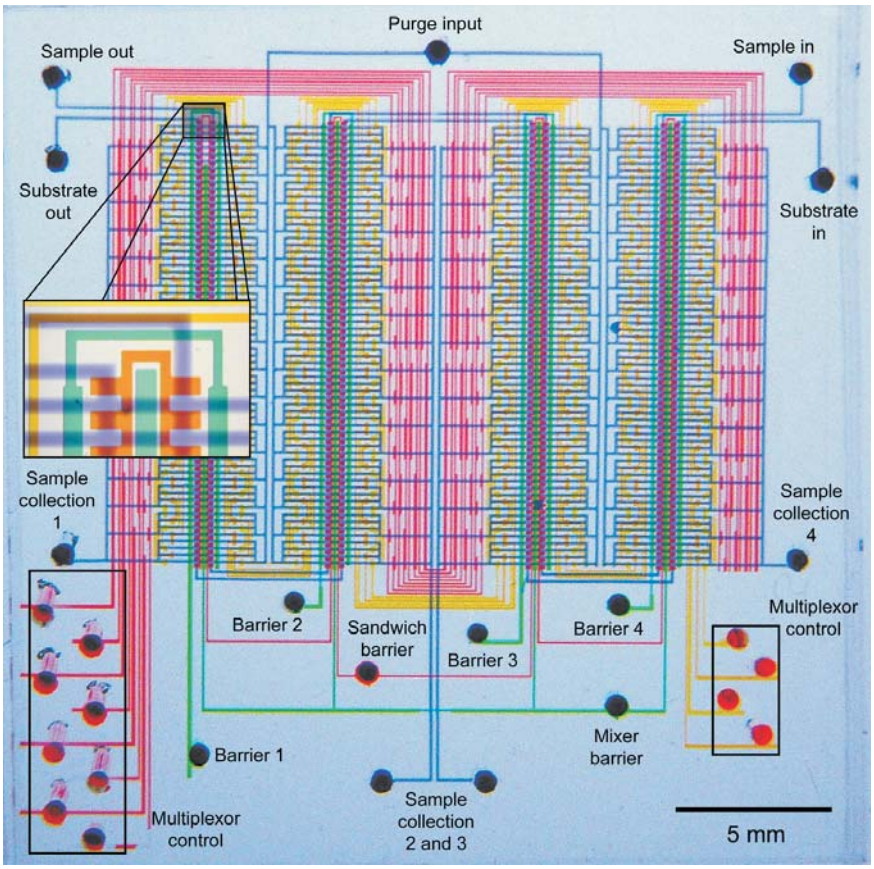

Figure I-6: Optical micrograph of a nanofluidic system that can be used for parallelized high-throughput screening of fluorescence-based single cell assays. The various inputs have been loaded with food dyes to show the channels and subelements of the fluidic logic. This chip has 2056 valves, which are used to manipulate 256 compartments containing bacterial cells expressing an enzyme of interest (or a library of mutants of that enzyme) that are combined on a pairwise basis with 256 other compartments containing a fluorogenic substrate used to assay for a desired activity. Cells that display a particularly interesting activity can be selected and recovered from the chip using valve-based addressing of the compartments. (Figure I-6 from Hong and Quake, 2003)[25]

It is not an exaggeration to state that the invention of the transistor, and subsequent proliferation of the integrated circuit, has been anything less than revolutionary. Modern civilization was radically transformed as a result of these two electronic inventions. While many comparisons have been made between microfluidics and microelectronics, it remains to be seen whether or not microfluidic device technology, will have the same revolutionary effect on modern human civilization, as did

that of the microelectronics revolution. Various assessments have been provided by experts in the microfluidics field, as to why the impact and commercial success has been slower than expected.[1, 26-33] The current state of microfluidic device technology, and foreseen future, will be explored more deeply in the sections that follow.

3) Why Microfluidic Device Technology?

The proposed and realized benefits of microfluidic device technology are numerous, and growing. Unlike bulk solution chemistry, microfluidic devices have a very high surface area to volume ratio, where this high surface area to volume ratio creates many unique and interesting properties, which can be exploited and used to a scientist or engineer's advantage. Many advantages associated with microfluidic systems can be understood and predicted based upon scaling laws. These laws can be used to compare the expected performance of a macroscopic instrument, to the same instrument when scaled down into a microscopic format.[23, 24, 34-40] A list of some of the advantages and performance improvements associated with microfluidic devices would include: decreased reagent and labor cost savings; increased sensitivity and response times; improved analytical performance; increased yield and selectivity of chemical reactions; integration of on-chip functions and parallel operations; improved automation and decreased need/dependence of robotic laboratory apparatus equipment; small sample size requirements; lightweight and portability; increased throughput; low power consumption; increased efficiency with heat dissipation in CE separations, and therefore in turn allowing use of higher electric field strengths, to produce faster separations; short reaction times; low cost and rapid prototyping options; economy of scale; possibility for

plug and play connectivity; shorter fluid transport times and controlled mixing; exploitable physical phenomena at the micro-scale, with the ability to strictly control and manipulate variables such as temperature, pressure, chemical concentrations, chemical gradients, chemical interactions, and liquid interfaces; decreased sample handling and contamination; decreased dead volume; potential to create devices with novel functionalities not currently available; length scales comparable to prokaryotic and eukaryotic cell studies; ability to spatially and temporally control cell growth by mimicking extracellular environments in terms of geometry and biochemistry; and disposibility.[1, 16, 23, 24, 34, 41-61] With such and array of benefits, it is not surprising it has been stated that as a technology, microfluidics seems too good to be true, since there are so many advantages associated with the miniaturization of microfluidic devices, yet at the same time, so few disadvantages.[1]

4) Microfluidics, Present and Beyond

Since the beginning of modern microfluidic device technology in the early 1990's, the field of microfluidics as a whole has been exponentially growing in a number of areas, and shows no signs of slowing down any time soon. Key indicators of this rapid growth activity can be found by examining: 1) the steady increase in the number of scholarly publications reported each year since the early 1990's,[62-69] with nearly 10,000 papers being published between 2000 - 2010;[70] 2) the growing number of scholarly conferences[71, 72] and journals[73-75] devoted exclusively to the field of microfluidics, and; 3) the steady increase in microfluidics commercialization activities.[31, 68]

While it is true there has been a steady increase in commercialized microfluidic

device technology, the growth experienced to-date has not been as rapid as initially hoped, and expected. Many expert assessments have been provided, to account for this slower-than-expected growth activity of microfluidics within industry, with these expert opinions most clearly articulated, by grouping these assessments into one of three categories, for: 1) academic-related reasons, 2) industry-related reasons, or 3) a hybrid of both academic and industry-related reasons.

Microfluidics originated within academia, and therefore it should come as no surprise that the evolution of microfluidic technology has more closely mirrored academic initiatives, as opposed to industrial-related goals and activities. It has been suggested by many, that academic research is too highly focused on fanciful prototypes and proof-of-concept device platforms, as a result of a tenure system that does not overly reward those that conceive and develop practical technology, in actually solving a real-world problem or satisfying a user's end-need.[27, 32] Criticisms of this mind-set/approach, have been that not enough academic researchers are *aware* of end-user needs, with technology being developed that is too specialized or too finicky for most non-specialist users of the technology.[27, 32] As one expert notes, "*When you go to the commercial landscape, technology doesn't make money, applications make money*." [32] Other experts have noted that academic laboratories are working on fundamental development, and therefore tend to be random and poorly focused on technology innovation.[30] One last reason attributed to academia, for its role in contributing to the slower-than-expected microfluidic commercialization activities, relates to the academic structure in which researchers perform their research activities. Microfluidics is a highly

interdisciplinary field, requiring the knowledge and skills of many to fully develop a complicated microfluidic device/platform, where many academic disciplines are structured in such a way so as to operate in isolation, and therefore remain disconnected from many other science and engineering communities.[27, 30, 32] In a response to such structures and impediments, collaborative centers focused on microfluidic device technology development have been formed, to bring together many diverse academic groups to share ideas, expertise, and tools.[30]

The barriers to entry are high, for microfluidic device acceptance within an industrial setting, as is the case with any new form of technology. Modern microfluidic devices are relatively new, and therefore greeted with much caution and skepticism, in making big investment decisions to research and develop microfluidic chip technology, to solve real-world problems. A so-called "first-user premium" has been associated with microfluidics device technology, and therefore in-turn cited as a barrier to entry, for wide-spread acceptance and adoption of microfluidic device technology, into the marketplace.[1] It is said, the "first-user premium" burdens the first commercial user of the/a newly-developed technology, where this forerunner pays a disproportionate share of the costs tied to the development of the new technology, and also accepts a disproportionate share of the risk associated with introduction of the new technology.[1] Many have stated, until a killer application (a.k.a. "killer app") is found or discovered, it will be difficult to see high investment activity, in developing mature microfluidic technologies.[1, 26, 30, 32] A "killer app" would justify, or mitigate investor concerns, on seeing a return on their investment. Some however, have changed their focus from

finding the elusive microfluidics "killer app," to making use of microfluidics technology as an enabling technology platform, for integration into other mature technologies already in existence within the marketplace.[30, 32]

A final force cited as working against widespread uptake and acceptance of commercial microfluidic technologies within industry, has been associated with the response of the established industry, to such an external threat.[33] A plot known as, "The Dueck Hubris Curve" explains this fascinating link between technology development, and that of individual, social, and institutional psychology. It is noted, hubris is defined as, "…extreme haughtiness, pride or arrogance. Hubris often indicates being out of touch with reality and overestimating one's own competence or capabilities, especially for people in positions of power" [76] Figure I-7 is a plot of The Dueck Hubris Curve. As Gunter Dueck, an IBM Distinguished Engineer and innovation researcher notes in-part, "*The technology trigger is often overlooked or ignored during the "plateau of ignorance." At one point however, the hype of the new technology draws a response, first in the "dip of alarmed unamusedness" a more irritated behavior in the sense of "what the hell is this?," often in combination with an air of supremacy ("we have been working in this field for so long, we know all the tricks") and disgust about the hype about the new technology. The reaction to the disillusionment is labeled as "the peak of false pride" usually accompanied by a feeling of relief that one can stay in the establishment comfort zone. While the new technology is making its comeback and eventually becomes a significant force in the market, the conventional industry faces a bifurcation point which is strongly related to the onset of one or more killer apps. If the*

new technology can come up with these killer apps and the established players do not react, they can in the worst case disappear from the scene rather quickly (remember Polaroid instant cameras?). The normal course of events however is a frantic struggle to adopt the innovation or more frequently, depending on the size of the war-chest, the simple take-over of the innovating company which correlates in many cases with the desired exit-route for the start-up founders and investors." [33]

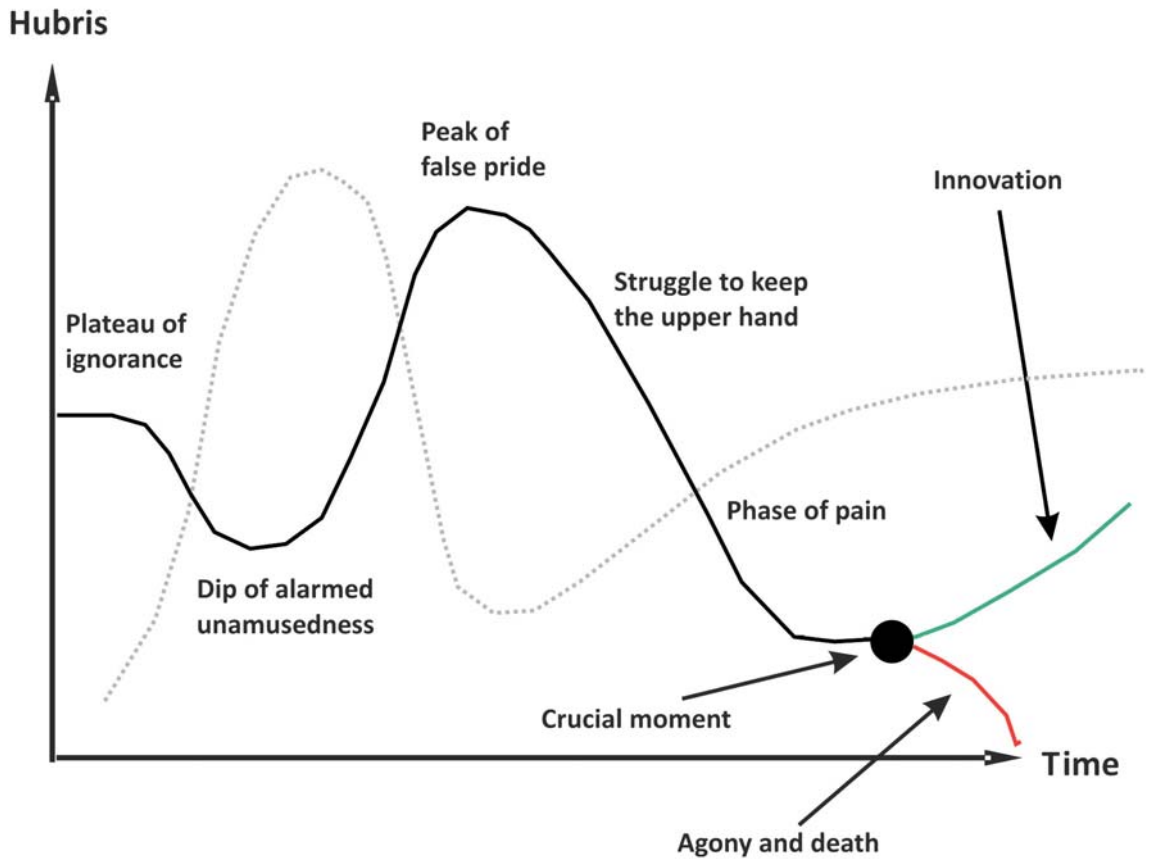

Figure I-7: The Dueck Hubris Curve. Solid line representative of the Dueck Hubris Curve, with dotted line representative of the Gardner Hype Cycle Model. (Figure I-7 from Becker, 2009)[33]

A final force working against the widespread commercialization of microfluidic device technology can be attributed to both, academia, as well as industry. It has been stated that many newly created, as well as some long-time established technologies, have not been clearly distinguished or recognized as, microfluidics technology.[32] Some long-time well known successful microfluidics technologies not typically associated with microfluidics are the ink-jet printer, and home pregnancy tests.[32] It has been estimated the annual market for inkjet printer heads is around $2.5 billion (USD), just for the microfabricated component in the inkjet cartridge alone.[33] Other newer microfluidics corporate success stories such as Fluidigm, Raindance, and Caliper, are choosing not to recognize their true roots or market their products as "microfluidics," and rather opting to market their products more directly to their target audiences needs and applications.[32] Therefore, microfluidics adoption into the marketplace faces challenges associated with mind-set, as well as recognition, where one prominent analytical chemist notes, "*none of these technologies (successfully commercialized microfluidic devices) comes to mind when analytical chemists think of the word "microfluidics*." " [32]

In spite of all the concern and skepticism as to whether or not microfluidics will remain relevant and continue to grow, some experts see the slow growth of microfluidic commercial activities as nothing less than, normal. The Gartner Hype Cycle, developed in 1995, has been applied and used to explain the growth activities witnessed within the microfluidics device industry.[32, 33] Figure I-8 is a plot of the Gartner Hype Cycle, displaying the various phases associated with the birth of a new technology, with the dotted line of Figure I-7 also displaying the Gartner Hype Cycle curve, overlaid upon the

Dueck Hubris Curve. As noted by Gartner, an information technology research and advisory company, "*The Gartner Hype Cycle Model explains five key phases of a technology's life cycle. The first step is the technology trigger that occurs when a breakthrough takes place. Stories in the media set off publicity, but the commercial viability of the technology is unproven. During the peak of inflated expectations, the early publicity produces some success stories but lots of failures. Some companies may jump on the bandwagon, but many don't. The trough of disillusionment creeps in as the technology fails to be implemented. During the slope of enlightenment, people better understand how the technology can benefit the scientific enterprise and society. At the plateau of productivity, the technology becomes mainstream and the criteria for assessing its viability become clearly defined.*" [32]

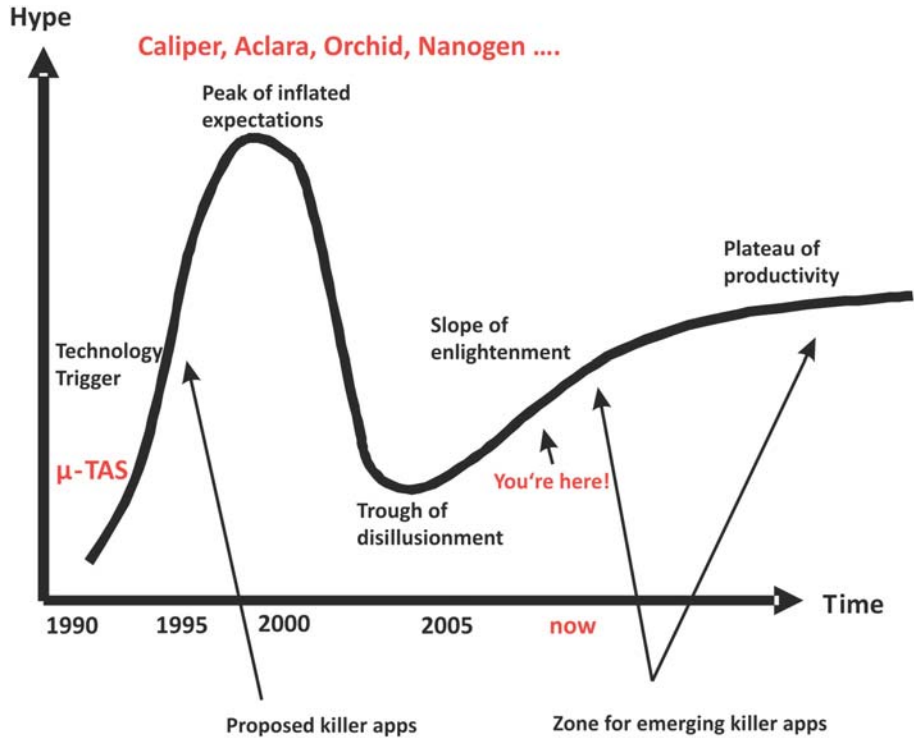

Figure I-8: The Gartner Hype Cycle Model for microfluidics. (Figure I-8 from Becker, 2009)[33]

Figure I-9 is a final assessment concerning the growth and progression of microfluidics technology within the marketplace.[33] This Figure is a classical technology adoption life cycle curve, as applied specifically to the field of microfluidics.

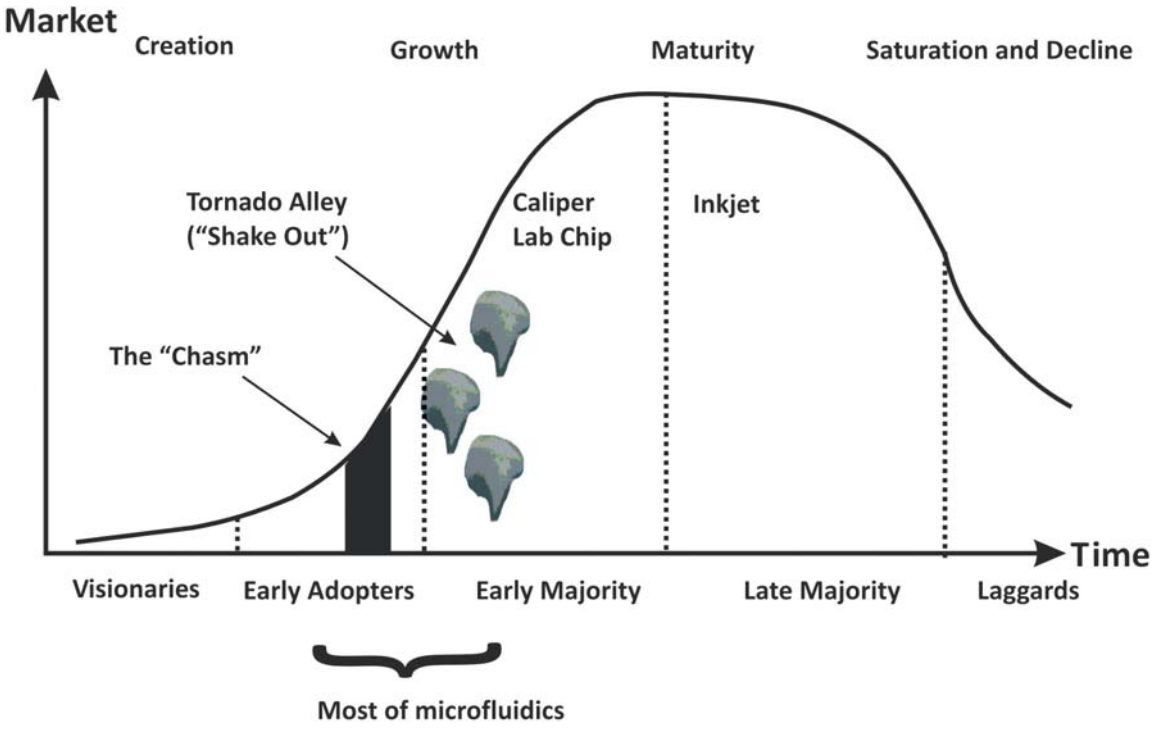

Figure I-9: The technology adoption life cycle. (Figure I-9 from Becker, 2009)[33]

It can be seen within this Figure, that microfluidics is believed to be within the very earliest growth stages of development. It has been stated, this curve can be used as a gauge to assess the likelihood and timing for the discovery of, "microfluidic killer app/s." [33] In spite of the sought after microfluidic "killer app" not turning up as of yet, the search still continues.[26, 29] Recent forecasts have cited the microfluidics market to grow to $1.9 billion (USD) by 2012,[31] and in other cases to $6.2 billion (USD) by 2011,[77, 78] with many of worlds most revered corporations such as 3M, GE, IBM, Abbott, Agilent,

Beckman Coulter, St. Jude Medical, and Medtronic, taking notice of microfluidics technology, as evidenced by their technology portfolios. Regardless of the current state of commercial activity, microfluidics must turn out commercial products, if the field is to be sustained over time.[28] Some of the future opportunities that may exist, for microfluidics to play a key role in, are: nanofluidics, digital microfluidics, cell biology, stackable systems, development of new fluids/fluidics/materials, interface technology and standards, biomedical analysis for disease biomarkers, organic synthesis, medicine, 5-dimensional analytical devices, and other new and early-stage technologies for emerging or unknown markets.[27, 28, 79] The highly interdisciplinary, beautiful, and nascent field of microfluidics is well poised to play a significant role in shaping the future of chemistry, education, and society.[80, 81] The evolution of the field as a whole in the years to come, will most certainly be exciting to observe and follow, for those scientists and engineers actively engaged with the research and development of new and exciting microfluidic device technologies.

Fabrication and Analysis of Microfluidic Devices

5) Fabrication Materials

At the very core of any prototype microfluidic device, is an idea, and materials. Once an idea is conceived, a technologist must determine proper choice of materials and associated fabrication methodologies. With microfluidic device technology originating within the microelectronics field, it is not surprising that most of the pre-1990 microfluidic devices were fabricated primarily from microelectronic materials such as

silicon and glass, along with other supporting inorganic materials such as silicon dioxide, silicon nitride, aluminum, and stainless steel. These microelectronic materials have many favorable characteristics when fabricating mechanical and electronic devices, but are not necessarily the best choice of materials for use within microfluidic device platforms. Since the early 1990's, microfluidic devices have increasingly become fabricated from polymeric materials, as opposed to other hard microelectronic materials such as silicon and glass. The transition in materials usage has been driven in part by cost, where it has been reported that soft polymer materials such as polydimethylsiloxane (PDMS), are around 50 times cheaper than silicon on a per volume basis.[82-85] Polymeric materials also possess a wide array of unique and different physical properties, in comparison to other common inorganic microelectronic materials. It has been said, polymeric materials exhibit a "Jekyll and Hide" character, where polymers possess a very broad range of chemical, mechanical, electrical, and optical properties, that allow a technologist to select the optimal material for nearly any intended application.[86] In spite of polymeric fabrication materials having inherent versatility and numerous advantages over traditional microelectronic materials, many microfluidic devices are fabricated from both microelectronic and common polymeric microfluidic materials. Use of both materials has many advantages, in allowing a technologist to leverage the strength of both materials within the same device. Integration of both materials within a single microfluidic device however, does create certain challenges, where many of the common solvents and processing technologies of either class of materials, are incompatible with one another. Table I-1 is a general comparison between glass and polymers, and can be used as a

baseline reference for comparing the properties of these two disparate fabrication materials. Comparisons between other discrete microfluidic polymer compounds, can be found elsewhere.[69, 86-92]

	Polymers	Glass
Manufacturing costs	Low in cost relative to glass, especially for mass-production	Higher in cost, especially for relatively large-area substrates. Higher costs are also associated with clean-room facilities
Fabrication complexity	Fabrication steps are simpler than glass, and no wet chemistry is needed	Time consuming and expensive, and wet chemistry is used
Clean-room facilities	Clean-room facilities are necessary for applications where avoiding contamination with dust is critical. In certain cases, particles may become pressed into the polymer during processing without having an effect on device functionality	Clean-room facilities are needed to avoid contamination
Properties	Wide selection of polymers, hence mechanical, optical, chemical and biological properties can be tailored	Less variability in available properties relative to polymers
Operation temperature	Limited for polymers because of relatively low T_g compared to glass	Wider range of operation temperature relative to polymers
Optical properties and fluorescenc detection	Optical transparency is lower than glass. Except for special grades, polymers also have higher autofluorescenc relative to glass	Excellent optical properties; autofluorescenc levels do not affect detection capabilities
Bonding	Different bonding options are available, for example: adhesives, thermal fusion, ultrasonic welding and mechanical clamping	Time consuming relative to polymers. Bonding options include thermal, adhesive and anodic bonding
Surface treatment	Surface treatment methods are available for polymers, but routine, well-established derivatization techniques are not available	Established chemical modificatio procedures for glass are available using organosilanes
Compatibility with organic solvents or strong acids	Except for some special grades, polymers are generally not compatible with most organic solvents and in some cases, strong bases or acids	Good resistance to organic solvents and acids
Joule heating	Subject to significan Joule heating because of low thermal conductivity	More resistant to Joule heating relative to polymers
Electro-osmotic flo (EOF)	Smaller EOF produced relative to glass, because of lack of ionisable functional groups	Higher EOF relative to polymers
Geometrical flexibilit	Polymer processing techniques offer more flexibilit for geometrical designs, including for example different cross-section (curved, vertical or V-groove), high aspect ratio square channels, channels with a define but arbitrary wall angle, or channels with different heights	Limited to 2 -D designs. Due to the isotropic nature of the etching process, only shallow, low aspect ratio, mainly semicircular channel cross-sections are possible in glass substrates
Permeability to gasses	Higher gas permeability relative to glass	Glass does not have the gas permeability required for some biological applications, such as living mammalian cells

Table I-1: A comparison between polymers and glass properties with respect to their use for microfluidic applications. (Table I-1 from Attia et al., 2009)[88]

Polymers are a class of chemical compounds with high molecular mass, and composed of multiple repeating subunits called monomers. One classification scheme for polymers is based upon thermophysical behavior, with a polymer being classified as either a thermoplastic, elastomer, or thermoset chemical compound.[87] Thermoplastics are those polymers that soften and flow upon heating, with this class of polymers consisting of unlinked or weakly linked chain molecules.[87] Elastomeric polymers also have very weakly cross-linked polymer chains, however this class of polymers can be mechanically deformed and stretched with application of external forces, where after a force is removed, the elastomer can return to its original state.[87] And finally, thermosets are heavily cross-linked polymers that are normally rigid, brittle, and intractable, where this class of polymers is thermally stable and will not melt or reflow upon heating.[87] Of the many polymeric materials available for device fabrication, PDMS and SU-8 are two of the most popular polymers utilized for microfluidic device fabrication purposes.

Polydimethylsiloxane (PDMS) is an elastomeric polymer, and belongs to a group of polyorganosiloxane compounds. Polyorganosiloxanes are also commonly referenced as either silicones, or silicone rubbers.[93] PDMS contains repeating monomer units of $-OSi(CH_3)_2-$, where the PDMS backbone molecule can be seen within Figure I-10.

Polydimethylsiloxane (PDMS)

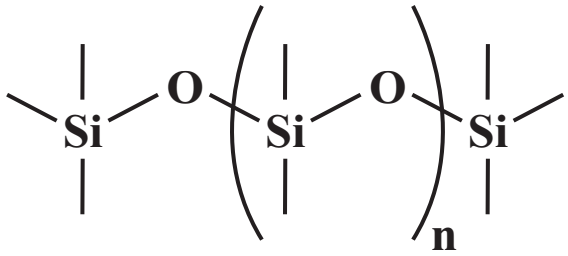

Figure I-10: Polydimethylsiloxane (PDMS) polymer.

PDMS is commercially supplied as a two-part kit containing: 1) a liquid silicon rubber base (i.e. a vinyl-terminated PDMS), and 2) a catalyst or curing agent (i.e. a mixture of a platinum complex and copolymers of methylhydrosiloxane and dimethylsiloxane).[94] When these two components are mixed, a solid elastomer is formed via a hydrosilylation reaction between vinyl ($SiCH=CH_2$) groups and hydrosilane (SiH) groups.[94]

PDMS like that of any material, has advantages and disadvantages, for use within microfluidic systems. The particular application is the most important variable in determining whether the physical properties of PDMS are positive, or negative. Many studies have characterized the physical[95-100] and processing[101-103] characteristics of PDMS, with this information useful when evaluating PDMS for its strengths and weaknesses as a microfluidic device working material. Some of the positive properties associated with PDMS are: 1) a significant body of literature exists for use of PDMS within microfluidic systems; 2) PDMS can be cured and molded to planar, as well as nonplanar surfaces; 3) PDMS is relatively inexpensive, and therefore can be readily employed as a cheap rapid-prototyping material; 4) PDMS is relatively simple and easy

to use, requiring minimal capital investment for equipment and fabrication facilities; 5) PDMS is chemically inert and thermally stable up to about 186 °C in air, and is not hygroscopic (and therefore will not swell with humidity);[94] 6) nonpolar gasses such as O_2, N_2, and CO_2 readily pass through bulk-cured PDMS slabs;[104] 7) PDMS is extremely durable, where a PDMS diaphragm valving system was tested continuously for 10^5 opening and closings, where the valves did not show any marked deterioration;[105] 8) PDMS is very flexible, allowing for elongation up to ~160%;[106] 9) by controlling the amount of cross linking between monomer backbones, the Young's modulus of PDMS can be tuned over two orders of magnitude;[82] 10) PDMS can be irreversibly sealed to itself, and additionally to a wide range of other materials including silicon, glass, SiO_2, quartz, silicon nitride, polyethylene, polystyrene, and glassy carbon, with the bond strength being reported as 30-50 psi;[107] 11) PDMS can seal to other surfaces by simple van der Waals interactions, and form a water-tight seal with seal pressures up to ~5 psi;[108] 12) PDMS has a low surface energy that facilitates release from templates and other structures; 13) PDMS is optically transparent from 240 – 1100 nm;[109] 14) cross linking of PDMS can be performed either thermally or optically, and; 15) PDMS surfaces can be modified for specific chemical reactivities, or altered to convert the hydrophobic surface into a hydrophilic surface.[49, 82, 86, 94, 104, 106-109] Likewise, a list of some of the reported drawbacks associated with PDMS, when used as a microfluidic device fabrication material includes: 1) upon curing, PDMS can shrink by as much as 1-3%;[94] 2) PDMS is hydrophobic, and therefore results in poor wettability with aqueous solvents, rendering the channels susceptible to air bubble trapping, and also rendering the surfaces

susceptible to nonspecific adsorption of proteins and cells;[49] 3) evaporation of water can occur through PDMS membranes, in turn causing osmolarity changes within a microfluidic device, and therefore possibly having a negative effect on cell culture conditions within a microfluidic device;[109] 4) PDMS shows autofluorescence characteristics, with intensity levels in excess of the intrinsic values reported for glass;[109, 110] 5) PDMS has been classified as a clean-room contaminant;[111] 6) PDMS swells and readily absorbs many nonpolar solvents;[112-114] 7) PDMS has been shown to exhibit leaching of uncured oligomers from bulk PDMS microchannel networks, and in turn affecting cell functions on a microfluidic chip,[115] and; 8) due to the elasticity and thermal expansion of PDMS, distortion and registration of PDMS molds can be a problem, especially for larger molds and multilayer device designs.[49, 94, 109-116]

As a result of the popularity and widespread use of PDMS for fabrication of microfluidic devices, many chemical derivatization studies have been reported, to either augment PDMS as a working material, or to work around its disadvantages for a particular application. Some of the chemical modifications reported for PDMS include altering or embedding PDMS with other materials to change the antimicrobial,[117, 118] optical,[119, 120] electrical,[121-125] magnetic,[126] and mechanical[127-130] properties of PDMS. PDMS has also been chemically modified, for the purpose of transforming the polymer into a photodefinable material.[123, 127, 131-133] And finally, due to the high surface area to volume ratio that exists for microfluidic devices, PDMS surface chemistry is an important variable to consider for any microfluidic application. PDMS surface modifications[134-140] have been reported for both patterned and surface coated

microchannel inorganic materials,[141-155] organic materials,[156-176] biological materials,[177-182] and plasma treatements.[183-188] To a slightly lesser extent, PDMS surface structural modifications have been reported within the literature.[189, 190]

While PDMS remains the microfluidics workhorse fabrication and prototyping material, other alternative materials are also being explored for their use in fabrication and processing protocols. Outside of other common polymeric fabrication materials such as polymethylmethacrylate (PMMA),[191-193] polymers such as polymethylhydrosiloxane,[194] thermoset polyester,[195-197] thiolene resins,[198, 199] epoxies,[200] polyurethanes,[201, 202] perfluoropolymers,[203-206] photocurable liquid Teflon,[207] liquid crystal polymers,[208] various copolymer materials,[93, 209-215] and other elastomeric adhesives,[216] have been reported as promising alternatives to PDMS, for their use within microfluidic systems. Additional materials under investigation have included paper-based materials,[217-221] ceramics,[222-224] and composite ceramic materials.[225, 226] In the years to come, newly developed materials will surely play a significant role in advancing microfluidic device platforms, for use as relevant and practical technology.

If PDMS is the most widely reported polymer in-use as a microfluidic fabrication material, many would say SU-8 is the second most widely employed polymeric fabrication material. SU-8 was developed by IBM in the 1980's, for use as a photolithography photoresist.[227, 228] The SU-8 monomer can be seen within Figure I-11.

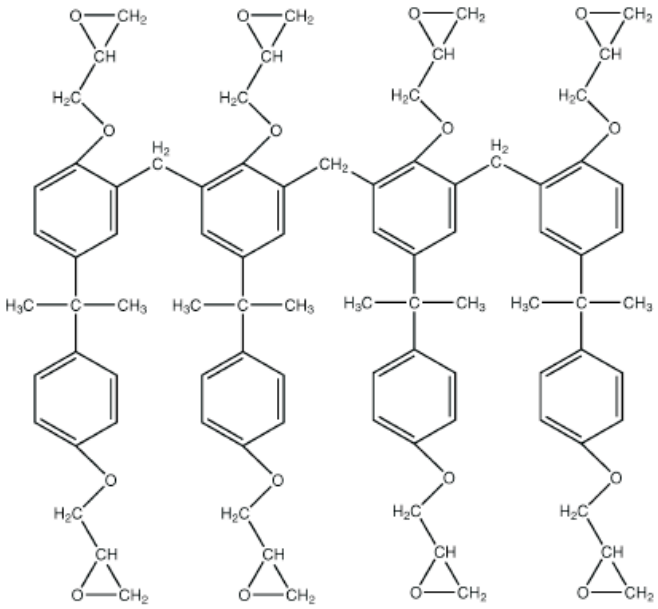

Figure I-11: Chemical structure of the monomer SU-8 with eight epoxy-groups. (Figure I-11 from Liu et al., 2010)[229]

SU-8 is a negative tone photoresist, based upon the EPON SU-8 epoxy resin.[228] The resin is made photosensitive by mixing the SU-8 monomer with an onium salt photo-acid generator. Upon exposure to UV radiation or an electron beam, the onium salt decomposes and in turn generates a strong acid which initiates cationic polymerization by ring opening and subsequent cross-linking of the epoxy groups.[228] An SU-8 monomer contains eight reactive epoxy functional groups, and therefore is known for its high reactivity, good sensitivity, and low molecular weight, where these properties in turn provide for a negative tone photoresist with both high contrast and high solubility.[228] SU-8 is also known for its good UV transparency, high refractive index, excellent chemical resistance, and low Young's modulus.[228, 230]

One of the first reported applications of SU-8 was to use the photoresist as a fabrication material for production of high aspect ratio microstructures (HARMS). It has

been suggested, that SU-8 can be used as a "Poor man's LIGA," to replace the expensive high aspect ratio synchrotron x-ray LIGA (Lithographie, Galvano-formung, Abformung) fabrication process.[227, 231] Thin films of SU-8 readily produce HARMS with aspect ratios (a structures [height / width] ratio) in excess of 20,[232-234] and in some cases producing HARMS with aspect ratios in excess of 190.[235] SU-8 is often processed as a thick film, with film thicknesses commonly reported within the range of 1-2 mm.[232, 236-238]

As a result of the widespread use of SU-8, many reports exist for characterization of SU-8's adhesion and removal,[231, 233, 239] exposure dose,[232, 240, 241] soft and post-exposure bake steps,[228, 242, 243] sidewall morphologies,[235, 244] chemical swelling/resistance properties,[245] and zeta-potential surface properties.[246] These and other processing protocols have been used to create SU-8 structures such as microlens',[247, 248] waveguides,[249, 250] microimpellers,[251] pins,[238, 252] membranes,[253] nanochannels,[254] microchannels,[255, 256] and microfluidic device structures.[230, 236, 257-260]

6) Fundamental Microfluidic Process and Fabrication Technologies

The origins of microfluidic microfabrication technologies, are deeply rooted within the microelectronics and MEMS industries. The field of microfabrication as a whole, is ever evolving and constantly reinventing itself, frequently churning out new and creative fabrication strategies, that allow for fabrication of increasingly complex microstructures with typical dimensions < 500 μm. Microfabrication is a beautiful, rich, diverse, eclectic, and highly interdisciplinary field, encompassing many disciplines within both science and engineering. This sentiment is reflected in the preface of the most highly regarded microelectronics fabrication text in existence, "The Science and

Engineering of Microelectronic Fabrication" by Stephen A. Campbell, which states in part; "*Magic. That is the word that I often hear used to describe the process of fabricating integrated circuits. Society regards the electronics industry, and microelectronics in particular, as a pinnacle of "high-tech." Even engineers, sometimes the very ones who design the circuits being built, consider the fabrication process to be something mysterious. There are a variety of reasons for this phenomenon. The rate of technology evolution is so rapid that narrow specialization is required in order to stay current. The fabrication line further requires a number of subspecialties, each of which is rooted in some combination of physics, chemistry, statistics, chemical engineering, electrical engineering, and mechanical engineering. Jargon develops among specialists that reduces information flow outside the discipline."* [261]

As one might expect with reference to Campbell's preface quote, the field of microfabrication is immense, and dense with regards to published scientific information. A comprehensive microfabrication discussion, is well beyond the scope of this dissertation. Therefore, should there be a need to take in a deeper and more comprehensive microfabrication perspective, readers are directed to Campbell's second edition text.[262] Campbell's second edition continues to serve as *the* definitive microfabrication reference text, where a United States Patent and Trademark Office EAST database search reveals, nearly all inventors cite this text as the definitive microelectronics fabrication resource, since its debut in 1996. Other great texts are also in existence, to serve as microfabrication reference resources.[21, 263-267]

Microfluidic device fabrication prior to 1990, was predominantly performed using

glass and silicon, with associated microelectronic processing protocols and clean-room instrumentation. Since the early 1990's however, microfluidic device fabrication strategies have evolved rapidly. As opposed to once relying upon glass and silicon, microfluidic devices are now predominantly fabricated from polymeric compounds. Fabrication of these polymeric devices still relies upon traditional microelectronic processing technologies, however microfluidic device fabrication protocols have also integrated newer fabrication approaches, which are more suitable for polymeric materials processing. The two techniques most widely employed for fabrication of modern microfluidic devices includes photolithography and soft lithography, with Figure I-12 highlighting other available microstructure fabrication options.[268]

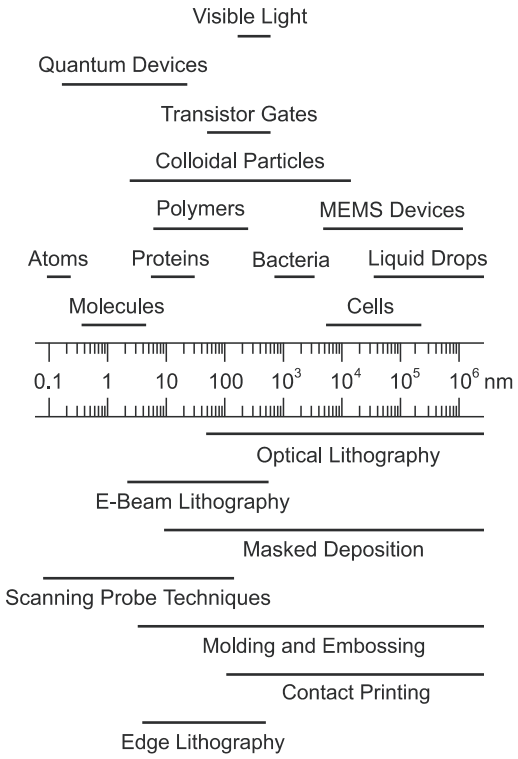

Figure I-12: Patterning on various length scales. The scale bar indicates the range of dimensions for a specific object (above the ruler), and the range of feature sizes that have been demonstrated for each type of patterning technique (below the ruler). (Figure I-12 from Geissler and Xia, 2004)[268]

Photolithography is a microfabrication process used to transfer geometric patterns from a photomask, onto a thin film applied across a substrate surface. In photolithography, a substrate such as silicon or glass is spin-coated with a photo-sensitive polymer called a photoresist, or just resist for short. A photomask plate is typically composed of quartz, with an opaque thin film such as chromium coated across the quartz surface. A photomask pattern is created by patterning two-dimensional structures across the chromium thin film. Radiation transmission occurs through the substrate where patterned areas exist, with blockage of radiation transfer for all other opaque areas. The process of transferring the geometric pattern/s of a photomask onto a separate substrate begins by spin-coating a photoresist onto a separate substrate, such as a silicon wafer. When the photomask is placed in contact with the photoresist-coated silicon wafer, the transparent regions of the photomask allow radiation to expose the underlying regions of the photoresist-coated silicon surface. If the photoresist is a positive tone substance, the *exposed* regions will be eroded away in a developing solution. If the photoresist is a negative tone compound, the underlying *unexposed* portions of the photoresist-coated silicon substrate will be removed by the developing solution. These patterned photoresist surfaces can then be used to build functional devices through deposition of thin films, and/or removal of bulk substrate regions. The removal of materials in microfabrication is called etching. Etching can be achieved with many techniques, but is usually accomplished with either wet or dry etching. Plasmas are used for dry etching, where wet etching in contrast relies upon liquid solutions. This photolithography discussion can be referenced with respect to Figure I-13.[21]

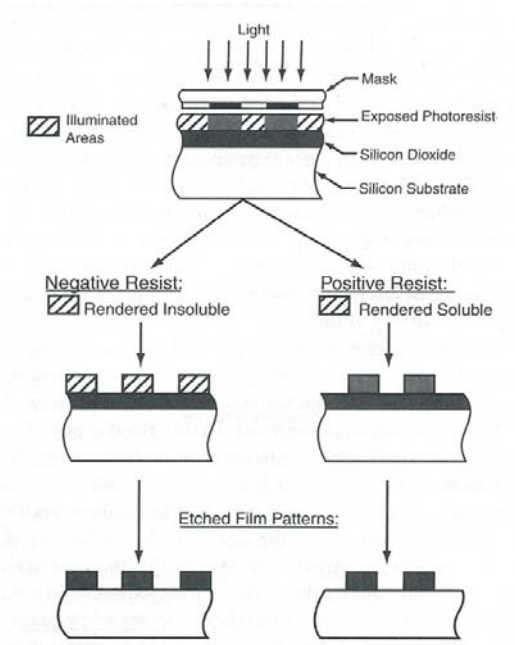

Figure I-13: Positive and negative photoresist: exposure, development, and pattern transfer. Positive resists develop and remove in the exposed region. Negative resists remain in the exposed region. (Figure I-13 from Madou, 2002)[21]

Figure I-14 is a realistic perspective, of the types of microstructures that can be created using photolithography.[269] This Figure shows a three-level SU-8 micropatterned surface, to be used as a tissue engineering scaffold.

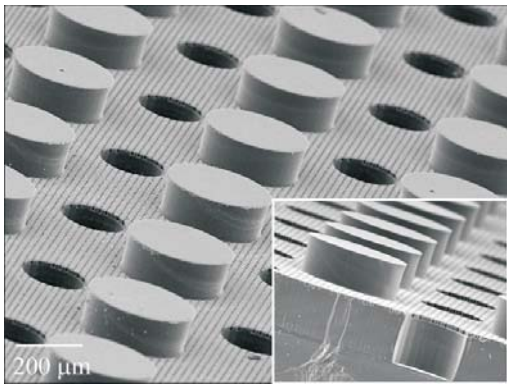

Figure I-14: Scanning electron microscope image showing a three-level SU-8 microstructure similar to that used to create tissue engineering scaffolds with an overall height of ~260 µm. The cross section (inset) shows the 300 µm diameter, 100 µm high columns and 200 µm diameter, 150 µm deep holes as well as 10 µm diameter and 10 µm deep holes. (Figure I-14 from Mata el al., 2006)[269]

Soft lithography is a general term used to reference a suite of non-photolithographic microstructure fabrication techniques. More specifically, soft lithography has been characterized as "*a collection of novel patterning techniques based on printing, molding, and embossing with a transparent elastomeric stamp – representing a new conceptual approach to the fabrication and manufacturing of new types of structures and devices on planar, curved, or flexible substrates at low cost*." [270] Figure I-15 is a schematic reference of some of the most commonly employed soft lithography fabrication techniques.[106]

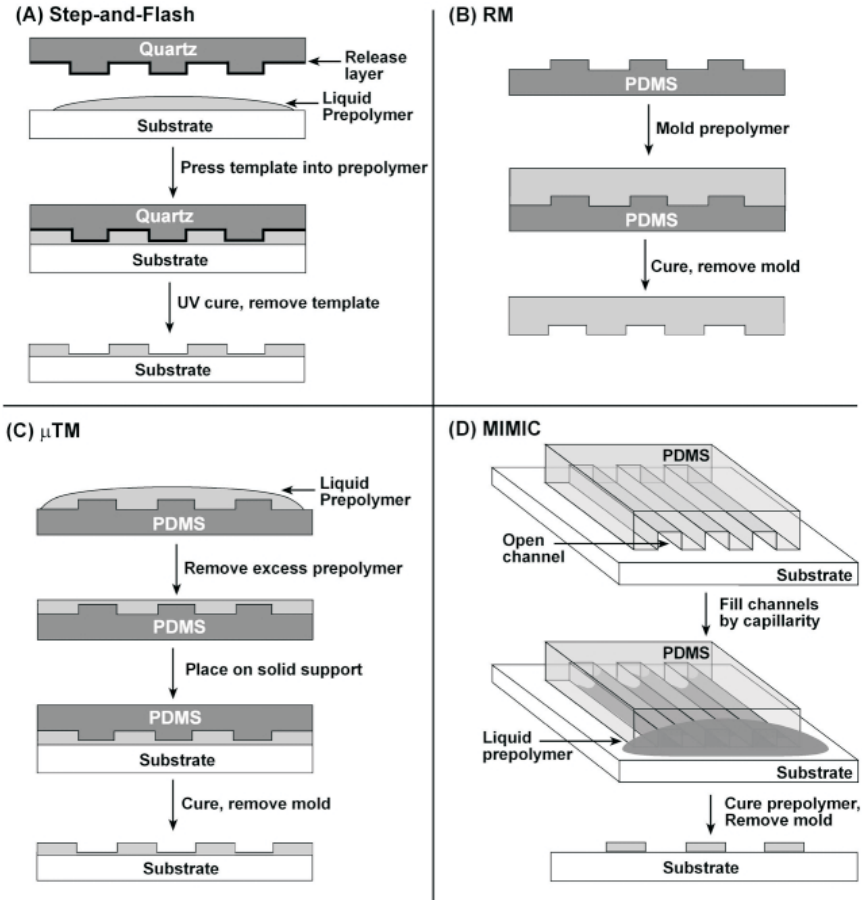

Figure I-15: Schematic diagrams of four soft lithography approaches: (A) step-and-flash lithography, (B) replica molding (RM), (C) microtransfer molding (μTM), and (D) micromolding in capillaries (MIMIC). (Figure I-15 from Gates et al., 2004)[106]

Soft lithography was developed by George Whitesides, one of the greatest pioneers in the field of microfluidics.[94, 107, 271-276] The term soft lithography was coined in 1998, with this fabrication approach being developed as a non-photolithographic fabrication alternative, that could compliment traditional and more well established photolithography fabrication practices.[270, 271] Soft lithography typically begins with creation of a photolithographic-generated template, which is used in turn as a soft lithography molding template. Soft lithography techniques share a common feature of using a patterned elastomer as a stamp, mold, or mask (rather than a rigid photomask) to generate micropatterns and microstructures.[94] While photolithography is the dominant lithographic technique used for microtechnology, it may not always be the best option for some applications.[94, 277] Soft lithography has become very popular among both scientists and engineers for a variety of reasons, with this fabrication approach having inherent advantages over photolithography such as, soft lithography: 1) is a cheap and affordable fabrication process;[94, 104, 271] 2) does not have a diffraction limit;[271] 3) is capable of conforming to nonplanar surfaces;[107, 278-280] 4) makes use of many optically transparent materials;[271, 281, 282] 5) can generate three-dimensional topologies;[105, 283] 6) has good control over surface chemistry;[163, 164, 180] and 7) uses technology that is very accessible to biologists and the medical community.[11, 41, 271, 284-287] Soft lithography does however have disadvantages as well. They include: 1) distortion of the mold or stamp due to the elastomeric nature of the materials used;[271, 288] 2) difficulty in achieving accurate registration;[105, 271, 289-296] and 3) limited compatibility with current photolithography fabrication processing protocols.[114, 271]

Soft lithography has been used extensively to create a wide range of soft polymeric microstructures.[297-307] Figure I-16 illustrates the incredible versatility of this lithographic fabrication process, in producing a wide array of unique microstructures with replica molding, microtransfer molding (μTM), and micromolding in capillaries (MIMIC).[273] It has recently been reported that soft lithography has been established as an atomic-level replication process, where a replica mold with elementary steps of 3 – 5 angstroms (0.3 – 0.5 nm - a distance that defines the minimum separation between molecular layers in a crystal lattice) in height has been produced.[130]

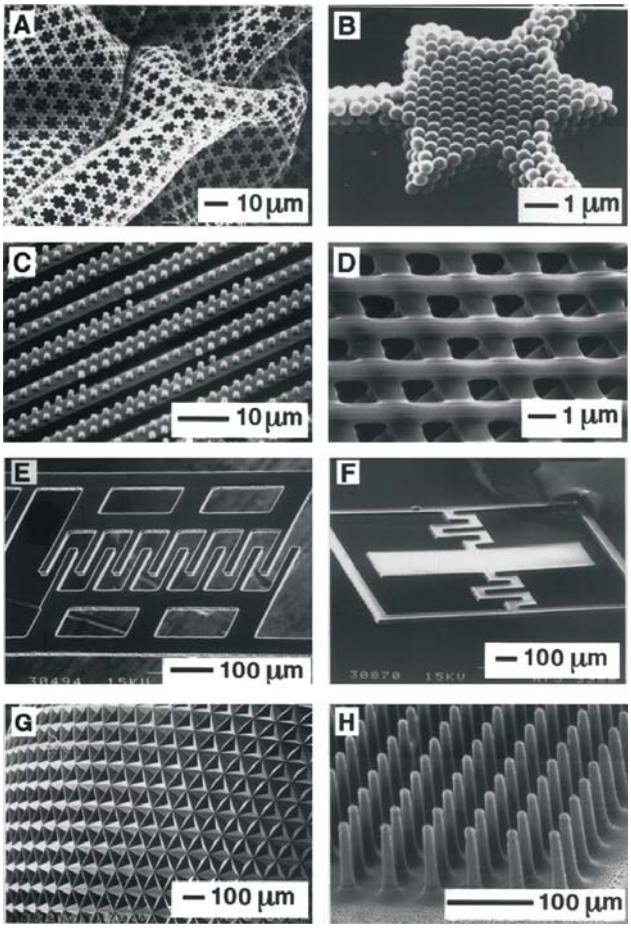

Figure I-16: Scanning electron microscope images of microstructures fabricated using: A, B – MIMIC; C, D, E, F - μTM; and G, H replica molding. (Figure I-16 from Qin et al., 1998)[273]

The polymeric structures illustrated within Figure I-16, demonstrates the fidelity with which polymeric structures can be produced, using soft lithography. Upon implementation into microfluidic and other device platforms, these soft structures can deform in deleterious ways, and in turn affect the performance of the device. Figure I-17 illustrates the sagging and collapse characteristics sometimes associated with soft lithography molded microstructures.[275] Optimal aspect ratios are shown within this Figure, and can be used as a general guideline, for optimal design and implementation of soft lithography fabricated microstructures.[275] Formulation of hardened PDMS has been one route taken in an attempt to improve upon, or eliminate these sagging and collapse limitations of soft lithography.[127, 129, 130] Improving upon these limitations also improves upon the registration challenges associated with multilayered soft lithography microstructures.[105, 271, 289-296]

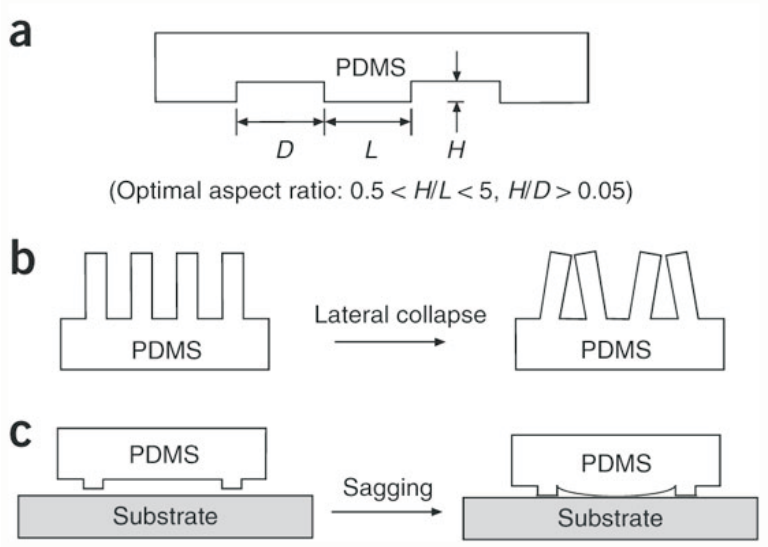

Figure I-17: Schematic illustrations of a PDMS stamp (a) and two possible problems that may arise from the softness of an elastomer: (b) lateral collapse of relief structures (or commonly known as "pairing") with aspect ratios H/L > 5; and (c) sagging of recessed structures with aspect ratios H/L < 0.5. (Figure I-17 from Qin et al., 2010)[275]

A wide array of structures and device designs has been reported within the academic literature, with three-dimensional (3D) micro devices regarded as some of the most challenging devices to fabricate.[308-324] Many 3D designs have been reported using soft lithography, with Figure I-18 illustrating one possible 3D soft lithography fabrication scheme.[325] Bonding of the replica molded PDMS layers is accomplished with an oxygen plasma,[104, 107, 108, 274] where bonding is also possible, if two PDMS layers containing different ratios of base to curing agent are brought into contact with one another.[283, 326, 327]

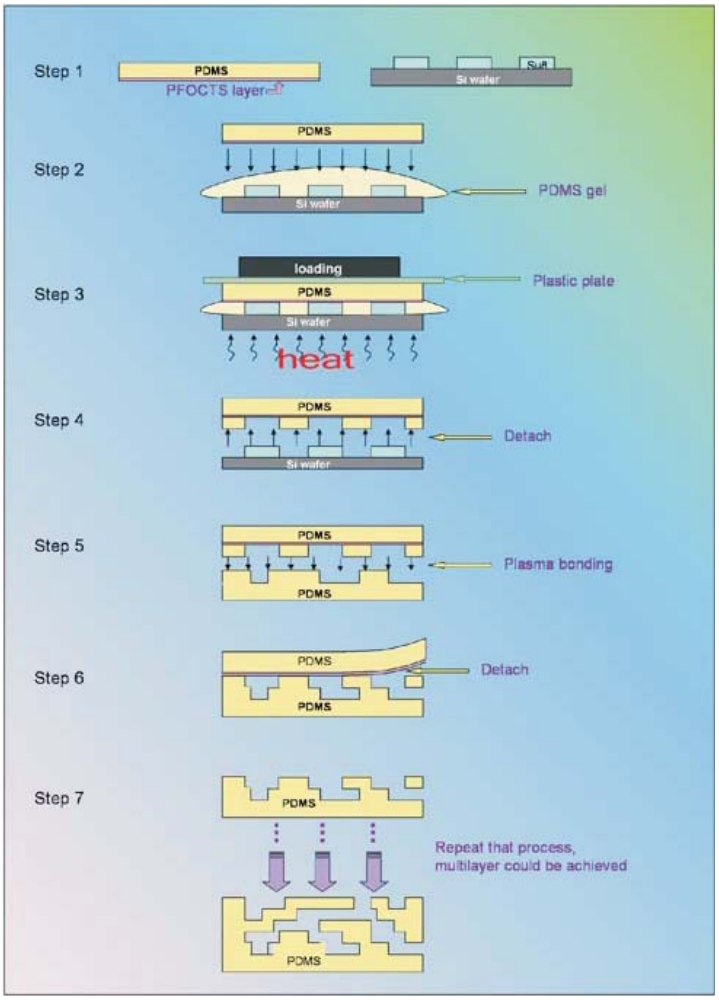

Figure I-18: Schematic view of a three-dimensional soft lithography fabrication process, using replica molded PDMS layers and oxygen plasma bonding. (Figure I-18 from Zhang et al., 2010)[325]

While there is no question photolithography and soft lithography are the two predominant microfluidic fabrication methods currently being employed, other techniques and methods are also available for consideration as potential microfabrication options.[69, 86, 87, 89-91, 328] Some of the other microfabrication methods available for technologists to consider include solid object printing,[329] embossing/imprinting,[212, 214, 215, 330-336] electrical discharge machining (EDM),[337-342] laser machining,[288, 343-354] microstereolithography,[355-362] lamination,[347, 363-368] powder blasting,[369, 370] computer numerically controlled (CNC) machining,[371, 372] and injection molding,[88, 373-384] along with an assortment of other promising, yet less utilized fabrication methodologies.[385-394] One of the most widely employed methods from this long list of fabrication methods, is that of injection molding. Injection molding is a commercial process of injecting a thermoplastic polymer into a cavity containing a template structure. This fabrication process is widely employed within industry, due to the high volume quantity of parts that can be produced within a short period of time, and additionally at a very low cost per plastic part.[395-397]

7) Packaging and Interconnect Technology

Microfluidic device packaging refers to fabrication processes such as bonding, surface modifications, physical isolation and encapsulation, providing mechanical support, controlling heat dissipation, and making connections to the outside world.[282, 398-403] The primary goals of packaging are device protection, as well as connection with the outside world. In the ideal case, the device would behave in a harsh environment,

identically as it would in a well defined and controlled laboratory environment. One of the most widely studied packaging fabrication processes is that of microfluidic interconnects, or also known as world-to-chip interface connections.[404, 405] These device connections to the macro world should ideally contain the following characteristics: 1) reversibility; 2) reliability; 3) low cost; 4) chemical compatibility; 5) ease of use and fabrication; 6) minimal dead volume; 7) ability to operate over a wide range of flow rates and pressure drops; 8) suitability for automation and high density integration; 9) provide minimal pressure drop; 10) allow for easy integration with other micro and macro instruments; and 11) not be susceptible to contamination. World-to-chip interfaces are anything but trivial, and oftentimes their importance placed secondary to other design aspects of the microdevice. This is especially true in academic research labs where the focus is not as heavily geared towards commercialization of the device, as it is in industrial laboratories. World-to-chip interfaces, and other packaging-related processes are of critical importance in taking devices from prototypes to products, where it has been stated that 50-90% of the total cost of a microdevice comes from packaging.[406, 407] While interconnects are only one aspect of packaging, their importance clearly cannot be overlooked in the business world. World-to-chip interfaces are one of the remaining technical challenges responsible for the slow integration of microfluidic devices as mainstream technology over some of their macro counterparts.[405, 408] Fused silica capillary tubing,[355, 384, 404, 409-413] as well as other types of tubing materials,[281, 414-418] have been successfully implemented as interconnects within microfluidic devices, where both interconnects have been shown to satisfy most of the ideal interconnect requirements.

Other successful interconnect technologies have made use of plug-in modular designs,[408, 419-427] as well as screw-connector unions.[428-430]

8) Microfluidic Device Transport Analysis

Once a microfluidic device has been successfully fabricated, it is oftentimes necessary or advantageous to characterize the microflow transport characteristics through the device.[5, 6, 431-445] Detailed flow visualizations can help characterize system performance, identify non-ideal flow characteristics, and validate simulation efforts.[446] Flow characterizations can be categorized into two categories, pointwise methods and full-field methods.[2] Pointwise methods yield information about a single point in a fluid flow, where full-field methods provide information about a two-dimensional flow field, with a minimum of two velocity vectors. Molecular tagging velocimetry (MTV) and particle image velocimetry (PIV), are two full-field methods commonly employed to characterize the transport characteristics through a microfluidic device.

MTV has shown great promise as a microfluidic device characterization technique.[447-450] MTV is able to characterize transport characteristics through a device, by making use of flow-tracing fluorescent molecules called tracers. An evenly dispersed solution containing tracers is pumped through the microfluidic device, where a light source excites these molecules. The source is pulsed with a line or grid, to excite the flowing fluid. At this point the excited line or grid is said to be "tagged." The tagged regions are then imaged at two successive time intervals within the lifetime of the tracers, where the image is sectioned into many smaller domains called interrogation regions. The displacement information provided by the moving line or grid can then be used to

obtain estimates of the velocity vector field. Computer algorithms have been written to aid in estimating the flow-fields Lagrangian displacement vectors.[451] One distinct advantage of this technique is the fact that molecular tracers will not become trapped in even the smallest of conduits within a microfluidic device. One disadvantage of MTV, is the fact that tracers have larger diffusion coefficients, in comparison to other techniques that use seed particles to trace out streamlines within a microfluidic device. This disadvantage has a tendency to lower spatial resolution and velocity resolution measurements.[2]

PIV is a technique that has been around for over 20 years,[452, 453] with the introduction of μPIV in 1998.[454, 455] While traditional macroscopic PIV is similar to μPIV, there are differences. μPIV differs for illumination and recording optics, flow-tracing particles, and image-processing algorithms.[456] μPIV has been referred to as analogous to MTV, since the two techniques are very similar in some regards.[447] μPIV resembles MTV in the sense that an optical pattern is written into the flowing fluid, where the evolution of the pattern is recorded by comparing two digital images captured in succession, with a short time delay placed between the two image acquisition events.[454, 457-459] Unlike MTV where a controlled and predetermined pattern is created in the flowing fluid, μPIV relies upon the random evolution of fluorescently labeled particles. These particles are used to trace out streamlines within a microfluidic device, and are referenced as, "seed" particles. With the aid of computer algorithms, the two digital images closely spaced in time, are used to estimate the velocity field profile.[460-463] Knowledge of the velocity field aids in identifying flow patterns and dead volume areas

within the conduits of a microfluidic device. The advantages of using μPIV over MTV is that μPIV provides better spatial and velocity resolution. MTV has a spatial resolution of around 20 μm, where typical μPIV values are reported as 7 μm, and even in some cases being reported as low as 1 μm.[2, 458] The biggest disadvantage of using μPIV is that the particles oftentimes become trapped within small passages, and therefore in turn can inhibit proper device function.[2, 464]

Microfluidic Platforms and Unit Operation Devices

9) Platforms and Unit Operations on a Microfluidic Chip

Microfluidic unit operations are a set of basic fluidic operations such as fluid transport, fluid metering, fluid valving, fluid mixing, analyte/compound separation, pre/concentration and/or amplification, detection and readout, reagent storage, and incubation.[465] Unit operations are performed with use of a reduced set of validated microfluidic elements such as microvalves, micropumps, micromixers, and flow meters, for example. When a set of microfluidic elements is combined onto a microfluidic chip, the chip can further be classified according to the particular platform. "A microfluidic platform provides a set of fluidic unit operations, which are designed for easy combination within a well-defined fabrication technology. A microfluidic platform paves a generic and consistent way for miniaturization, integration, automation and parallelization of (bio-)chemical processes." [70] The major microfluidic platforms can classified according to the main liquid propulsion principle, which include capillary, pressure-driven, centrifugal, electrokinetic, and acoustic modes of propulsion.[70]

A microfluidic platform can also be defined in other ways as well. The concept of "lab-on-a-*chip*" [70] has been derivatized to incorporate unit operations into different platforms defined as, "lab-on-a-*robot*," [466] "lab-on-a-*tube*," [467] "lab-on-a-*compact disc (CD)*," [468-470] "lab-on-a-*droplet*," [471, 472] and "lab-in-a-*cell*." [473]

In the sections that follow, a very brief and cursory introduction will be provided, to introduce microfluidic unit operation device technology. In some cases, thousands of designs have been reported for a single unit operation device, and therefore it is well beyond the scope of this dissertation to provide a thorough and detailed discussion of the many designs that have been reported within the literature. The focus instead will be placed on themes and concepts, with relevant discussion and salient examples provided for each of the respective unit operation device technologies.

10) Microvalves

Fluid control is one of the most fundamental and important operations on a microfluidic chip. Microvalves are unit operation actuator devices that are used to route and regulate fluid flows on a microchip, and in many instances, used as integral components within micropumps.[474-476] A microvalve can be characterized as a transduction element, where transducing elements convert one form of energy into another. Table I-2 illustrates many of the common transduction mechanisms exploited, for actuation of microvalves and other MEMS/microfluidic unit operation devices.[477, 478]

To / From	Electrical	Magnetic	Mechanical	Thermal	Chemical	Radiative
Electrical		Ampereís Law	Electrostatics, Electrophoresis	Resistive Heating	Electrolysis, Ionization	EM Transmission
Magnetic	Hall Effect, Mag. Resistance		Magnetostatics, Magnetostriction	Eddy Currents Hysteretic Loss	Magnetic Separation	Magneto-optics
Mechanical	Variable Cap. Piezoresistance Piezoelectricity	Magnetostriction		Friction	Phase Change	Tribo-luminescence
Thermal	Thermoelectric	Curie Point	Thermal Expansion		Reaction Rate Ignition	Thermal Radiation
Chemical	Electrochemical Potential	Chemomagnetic	Phase Change	Combustion		Chemo-luminescence
Radiative	Photoconductor, EM Receiving	Magneto-optics	Radiation Hardening	Photothermal	Photochemical	

Table I-2: Table of common transduction mechanisms used in microelectromechanical systems (MEMS). (Table I-2 from Judy, 2001)[477]

Microvalves are typically categorized as either active or passive, where actuation in both cases is accomplished using mechanical or nonmechanical mechanisms. Active valves are actuated irrespective of fluid flow direction, where passive valves typically respond to displaced fluids and only open in one direction, with flow control analogous to current flow through an electrical diode. Examples of common active mechanically-actuated microvalves would include pneumatic,[283, 479-492] piezoelectric,[326, 493-505] magnetic,[506-515] electrostatic,[516-520] thermopneumatic,[521-523] shape memory alloy,[524-528] and mechanical transduction,[529-535] with common examples of active nonmechanically-actuated microvalves using electrochemical,[536-540] hydrogel,[541-552] rheological,[553-556] and optical/electrical/thermal/phase change actuation[557-571] mechanisms. For passive microvalves, common mechanical designs incorporate ball or check valves,[572-584] with passive nonmechanical valves typically making use of capillary/surface mechanisms,[585-596] or geometrically-designed valving structures.[597-606]

Of the many microvalving mechanisms reported within the microfluidics literature, pneumatic microvalves are the most widely utilized valving structures incorporated into microchip platforms. Pneumatic microvalves are actuated using compressed gas canisters, with external mechanical switching mechanisms controlling the delivery and timing of pressure pulses. A common pneumatic microvalve design can be seen within Figure I-19.[283] This Figure illustrates three microvalves aligned in series, where the air in/out lines compress the microchannel below these gas conduits, in effect collapsing the microchannel below these gas lines, and therefore preventing fluid flow in either direction along the microchannel. This Figure is also representative of a peristaltic micropump, where three pneumatic gas conduits aligned in series over a fluidic microchannel, can be actuated over time to produce a peristaltic wave motion, and therefore produce a net fluid flow through the microchannel.

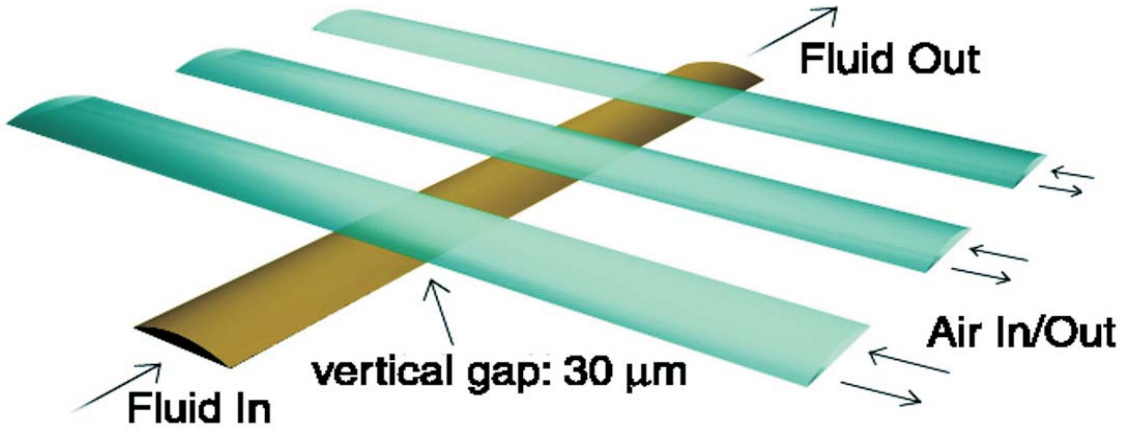

Figure I-19: A 3D scale diagram of an elastomeric peristaltic pump. The channels are 100 µm wide and 10 µm high. Peristalsis is typically actuated by the pattern 101, 100, 110, 010, 011, 001, where 0 and 1 indicate "valve open" and "valve closed," respectively. This pattern is named the "120°" pattern, referring to the phase angle of actuation between the three valves. Other patterns are possible, including 90° and 60° patterns. The differences in pumping rate at a given frequency of pattern cycling is minimal. (Figure I-19 from Unger et al., 2000)[283]

11) Micropumps

Micropumps perform fluidic propulsion unit operations on microchips. Fluidic transport can be performed either internally or externally across predetermined fluidic pathways. Micropumps are one of the very core elements integrated into any microfluidic chip format, and as such, many great reviews have been written to report the latest trends and advances in micropump technology.[607-620] Micropumps are actuated with many of the same microvalve actuation mechanisms, but are classified slightly different in comparison to microvalves. Micropumps have been classified as either: 1) mechanical or nonmechanical, or in other cases as; 2) displacement or dynamic. In both cases, a micropump is classified according to the physical pumping mechanism. Displacement pumps exert pressure forces on the working fluid through one or more moving boundaries, where dynamic pumps continuously add energy to the working fluid in a matter that increases either its momentum or its pressure directly.[609] Commonly reported displacement micropumps use pneumatic,[283, 621-635] piezoelectric,[326, 597, 636-654] magnetic,[655-668] thermopneumatic,[669-678] shape-memory alloy,[679, 680] electrostatic,[681-692] bio-powered,[693-697] electrochemical,[698-700] and mechanical[701-709] actuation mechanisms, with common dynamic micropumps using centrifugal,[468-470, 710, 711] optical,[712-718] electroosmotic,[719-738] electrohydrodynamic,[739-747] magnetohydrodynamic,[748-754] acoustic/ultrasonic,[755-760] bubble,[761-764] or surface tension[765-769] driving mechanisms. Considering all displacement micropumps, pneumatic and piezoelectric-actuated micropumps are the most widely employed within microfluidic device platforms. Piezoelectricity is a physical phenomena, where a piezoelectric material produces an electric charge on the surface of the material when stressed mechanically, or produces a

dimensional change when stressed electrically with a voltage.[770-780] Therefore, piezoelectric microvalves and micropumps are actuated when a voltage is applied to the piezoelectric structure.[781-791]

A pneumatic micropump design can be seen within Figure I-19, with a clever piezoelectric micropump design shown within Figure I-20.[654] The piezoelectric micropump in Figure I-20 employs Braille display pins as microvalves. When the Braille pins are actuated in series using a peristaltic wave, a net flow of fluid is propelled through the microchannel beneath the Braille pins.

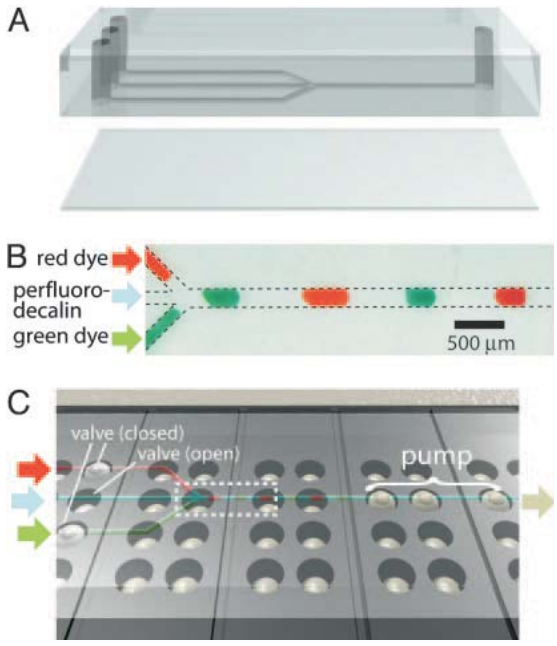

Figure I-20: Schematic representation of Braille display-based microfluidics. (A) A typical two-layer design for use with Braille displays. Both layers were composed of PDMS. Channels were face down and separated from the Braille display surface by a thin (140 µm) sheet of PDMS. Holes were punched with a 14-gauge blunt needle. (B) Segmented flow generated by integrating pumps and valves. The three inlets on the left, from top to bottom, contain red food dye, perfluorodecalin, and green food dye. The three components alternatively move toward the outlet on the right. (C) Overview of the typical experimental setup. The multilayer assembly is positioned on top of the Braille display so that channels are aligned above Braille pins, facing down. Three potential valves are on the left, and one pump is on the right. Retracted pins are situated directly below channels, and actuated pins are displayed upward against the PDMS sheet, closing channels directly above it. The dotted box refers to what is shown in B. (Figure I-20 from Gu et al., 2004)[654]

12) Micromixers

Fluid mixing is an important process on both micro and macro scale technology platforms. In microfluidics however, mixing is of great concern and continues to remain a serious challenge. Flows in microchannels are generally laminar, and therefore reagent mixing is primarily a result of molecular diffusion, which is an inherently slow process. As a result of the serious challenges that remain in mixing, many microfluidic mixing devices have been developed.[309, 792-804]

Micromixers are defined as either passive or active.[805, 806] Passive micromixers require no external energy, where the mixing process relies entirely upon diffusion or chaotic advection. Active micromixers in contrast use external fields to generate disturbances within a fluid. The performance of a micromixer can be characterized using the Reynolds number (Re), the Peclet number (Pe), or the Strouhal number (St). The Reynolds number is the ratio of inertial to viscous forces; the Peclet number representing the ratio between mass transport due to convection to diffusion; and the Strouhal number representing the ratio between the residence time of a species and the time period of its disturbance, where the Strouhal number is used to characterize active micromixer performance.

One design example of a microfluidic mixer is shown within Figure I-21.[807] This micromixer design employs the strategy of using mechanical grooves fabricated into the microchannel floor to rearrange and combine the component microfluidic streams. When a change in pneumatic pressure is applied to a pneumatic line, the microchannel groove depth changes on the microchannel floor. These depth-tunable channel floor grooves allow for stream mixing and tunable gradient concentration profile generation.

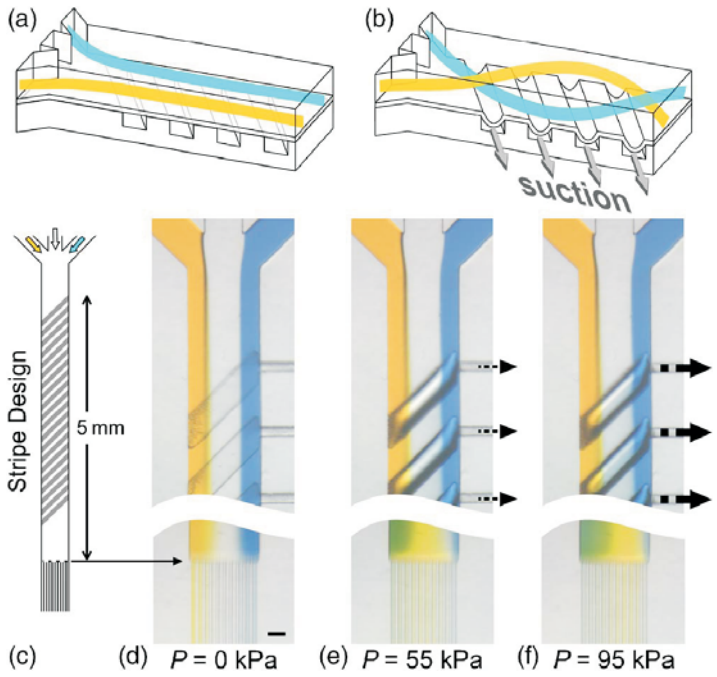

Figure I-21: Operation of a microfluidic "stirrer" (μFS). (a) Flow in the microchannel is not stirred when the PDMS membranes are not pressurized; flow is from left to right. (b) Flow is stirred when suction is applied to the pneumatic line, deflecting the membrane downwards (deflection depending on P), which forms grooves. (c) Schematic diagram of the μFS (with stripes at 45º angle, 100 μm wide, 50 μm deep and 100 μm separation). (d)–(f) Optical micrographs illustrating temporal sequences of concentration gradients of yellow dye, water, and blue dye generated by the μFS (the microchannel is 200 μm wide and 80 μm tall; the outlet channels are 10 μm wide and 20 μm tall) when P=0 kPa (d), 55 kPa (e), and 95 kPa (f) is applied to the pneumatic channel; flow is from top to bottom. Scale bar = 50 μm. (Figure I-21 from Hsu and Folch, 2006)[807]

13) Gradient Generators

Microfluidic gradient generators are unit operation devices that create spatiotemporal fluidic concentration gradients.[808-817] Gradient generators offer greater levels of precision, control, and quantification over traditional macroscopic methods, and are often used to enhance a scientist's ability to understand many biological phenomena.[818] One gradient generator design example can be seen within Figure I-22, where it is shown the gradient generator network repeatedly combines, mixes, and splits flow streams to yield distinct mixtures with distinct chemical compositions.[818]

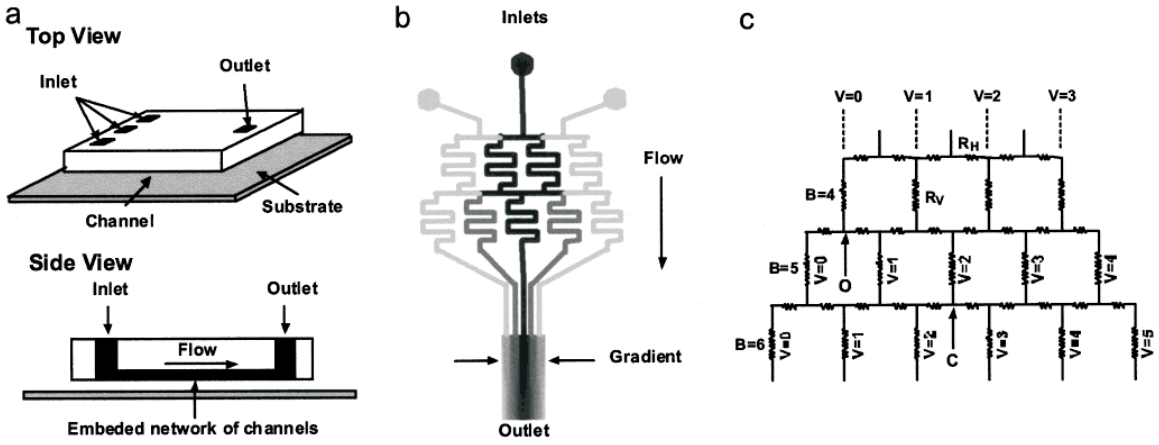

Figure I-22: (a) Scheme of a PDMS microfluidic gradient generator. (b) Schematic design of a representative gradient-generating microfluidic network. Solutions containing different chemicals are introduced from the top inlets and allowed to flow through the network. The gradient generator repeatedly combines, mixes, and splits the fluid streams to yield distinct mixtures with distinct compositions in each of the branch channels. When all the branches are combined, a concentration gradient is established across the outlet channel. The width of this channel and the total number of the branches determines the width of the gradient and the resolution of the steps making up the gradient, respectively. (c) Equivalent electronic circuit model of the pyramidal microfluidic network. (Figure I-22 from Jeon et al., 2000)[818]

14) Droplet / Emulsion Generators

Droplet generators, or also known as emulsion generators, generate a mixture of two or more immiscible (unblendable) microdroplets.[819-830] Microdroplets are typically defined as droplets that have micron-regime length scales, with volumes of less than 1 nL. [819, 828] Droplet generators have become widely utilized within microfluidic devices, and as a result have been widely studied for their ability to control and manipulate microdroplets. Emulsified droplets are commonly used as discrete chemical and biological microreactors, and in other contexts used for their ability to increase the rate of fluidic mixing. When droplet generators create emulsions for the purpose of limiting diffusion and dispersion, as shown within Figure I-23,[831] the individual droplets effectively form a train of digitally-saved chemical information packets. As a result of

this ability to "save" chemical information analogous to that of a solid state electronic device, the process of using microdroplets to retain chemical information is commonly referred to as, digital microfluidics.[832]

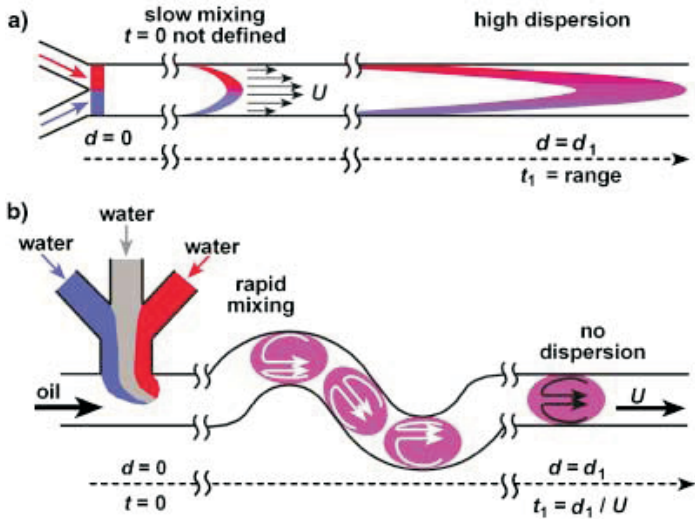

Figure I-23: Schematic comparison of a reaction A + B conducted in a standard pressure-driven microfluidic system device (a) and in an alternative microfluidic device format (b). a) Reaction time t≠d/U. b) Reaction time t=d/U. Two aqueous reagents (red, A and blue, B) can form laminar streams separated by a gray "divider" aqueous stream in a microchannel. When the three streams enter the channel with a flowing immiscible fluid, they form droplets (plugs). The reagents come into contact as the contents of the droplets are rapidly mixed. Internal recirculation within plugs flowing through channels of different geometries is shown schematically by arrows. (Figure I-23 from Song et al., 2003)[831]

15) Microfluidic Separators / Focusers

Microfluidic separators and focusers, are used to either separate or focus microdroplets or microparticles flowing through a microfluidic device.[833-840] Common microparticles introduced into a microfluidic device include cells, cell organelles, and micro and/or nanoparticles. Significant resources have been devoted to particle separator / focuser research, and as such, many unique microfluidic chip designs have been reported.[841-854] One such design can be seen in Figure I-24, where the separation and

aggregation characteristics of magnetic nanoparticles is controlled by manipulating experimental variables such as magnetic field strength, laminar flow conditions, and pH of the running buffers.[855]

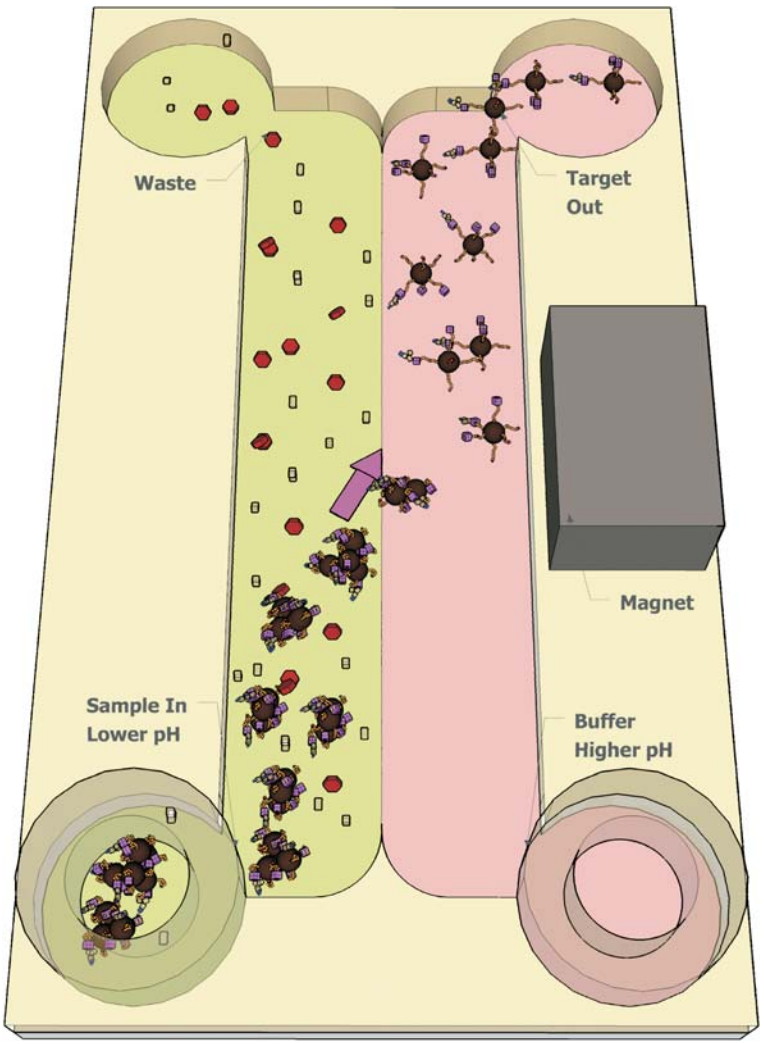

Figure I-24: Target analyte separation in a microfluidic channel facilitated by pH-responsive magnetic nanoparticles (mNPs) under isothermal conditions. The channel contains two flow streams. The left stream (green) is the sample that has been pre-incubated with mNPs. mNP aggregation is induced by using a lower pH buffer in this sample flowstream. The pH of the right stream (pink) is chosen to reverse mNP aggregation. A rare-earth magnet provides sufficient magnetic field to attract the aggregates laterally into the higher pH flowstream. The conjugate aggregates move out of the sample flowstream and in to the higher pH stream, where they return to a dispersed state, carrying the bound target analyte with them. Movement of other molecules across this interface is limited by diffusion due to low Reynolds number (laminar) fluid flow. (Figure I-24 from Lai et al., 2009)[855]

16) Microreactors

Microfluidic reactors are unit operation microfluidic devices that contain micro-structured features, with a sub-millimeter dimension, in which chemical reactions are performed in a continuous manner.[856] Microreactors are useful for prototyping, studying, and optimizing chemical reactions, and are devices of keen interest to the chemical, pharmaceutical, and biotechnology industries for commercial applications such as fine chemical synthesis, disease diagnosis, chemical crystallization, combinatorial synthesis, rapid chemical analyses, and high-throughput screening.[857] Microreactors have many advantages over batch reactor designs such as the enhancement of mass and heat transfer, reproducibility, high throughput, mass production process scale-up, potential for feedback control of temperature and feed streams, rapid screening of reaction conditions, low reagent consumption, the ability to cease reactions quickly after a product is formed, and the ability to perform reactions under more aggressive conditions with higher yields.[857-859] A safer operational environment is also provided with use of microreactors, where if a reaction were to fail, the safety and health issues could be minimized through easier containment of the miniaturized device and potentially toxic chemicals.[857-859] A wide array of microreactor designs have been reported within the literature,[856, 860-871] with one well designed microreactor shown within Figure I-25.[872] This microreactor design was used to coat colloidial silica core particles with titania layers of tunable thickness in a one-step, continuous flow process through controlled hydrolysis of titanium tetraethoxide (TEOT).[872] Titania-silica core shell particles in the sub-micron size range are of particular interest for applications such as catalysis, pigments (as whiteners), and imaging materials.[872]

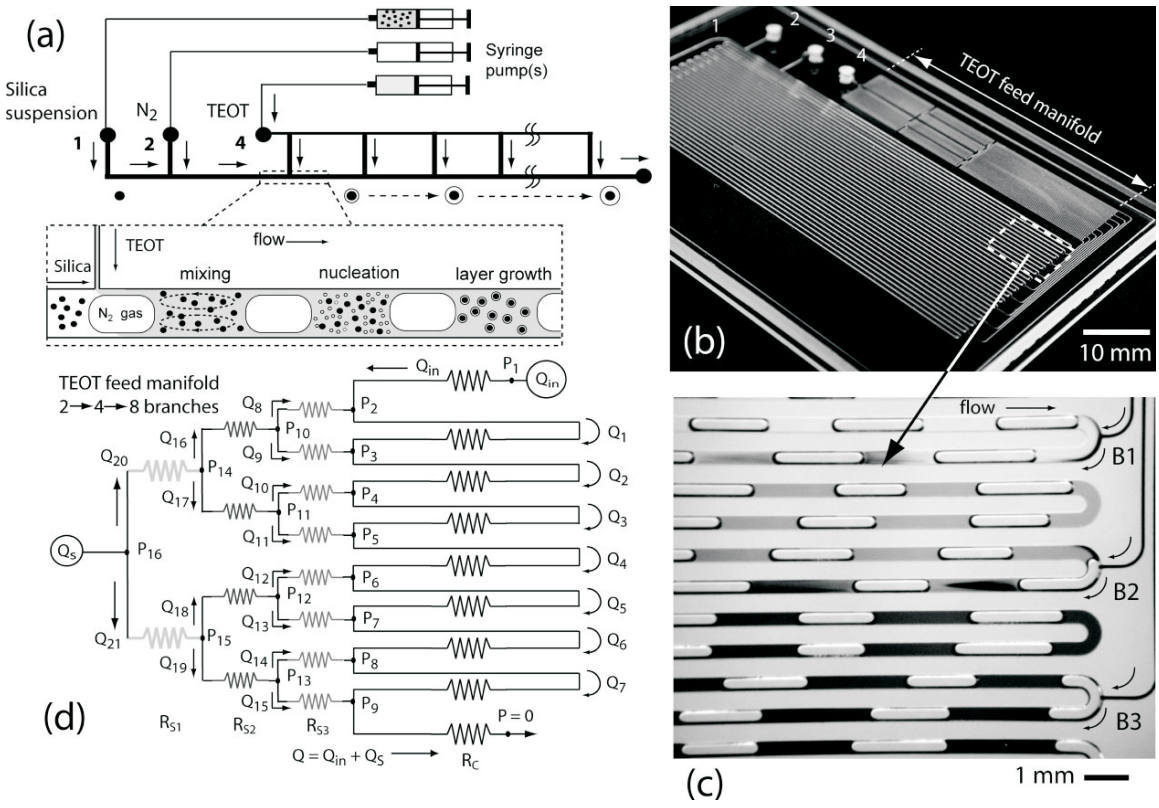

Figure I-25: a) Design concept for continuous-flow coating microreactor. b) Photograph of fabricated reactor. c) Stereomicroscope image of flow visualization experiment: ethanol dyed with black ink was introduced into a primary air—ethanol feed. The first three manifold branches (B1, B2, and B3) are seen feeding ethanol (dyed with black ink) into the gas-liquid flow (air-ethanol) in the main channel. d) Circuit model for microfluidic coating reactor showing hydraulic resistances R, flows Q and pressures P. R_{Si} (i=1-3) and R_C are the hydraulic resistances for the various manifold branches and the main reaction channel, respectively. Q_S represents the titanium tetraethoxide (TEOT) flow rate, with Q_{in} representing the flow rate for the silica particle suspension. (Figure I-25 from Khan and Jensen, 2007)[872]

17) Analytical Microfluidic Devices

Analytical microfluidic devices were among some of the very earliest reported microfluidic devices, since the beginning of modern microfluidic device technology.[23, 24, 873] Capillary electrophoresis (CE) microchips[874-881] are the most widely employed microfluidic separation devices, with common CE modes reported for isoelectric focusing,[882-886] capillary gel electrophoresis,[191, 887-889] isotachophoresis,[890-893] micellar

electrokinetic chromatography,[894-896] and immunoaffinity CE.[897-899] Other widely reported microchip separation devices would include micro free flow electrophoresis,[900-906] micro high performance liquid chromatography,[907-911] micro gas chromatography,[912-914] and micro solid phase extraction.[915-919] Two-dimensional microchip separation methods are also under active investigation.[920-923] A typical micro-CE chip design can be seen within Figure I-26, where this device was used to separate blood lactate and glucose.[924]

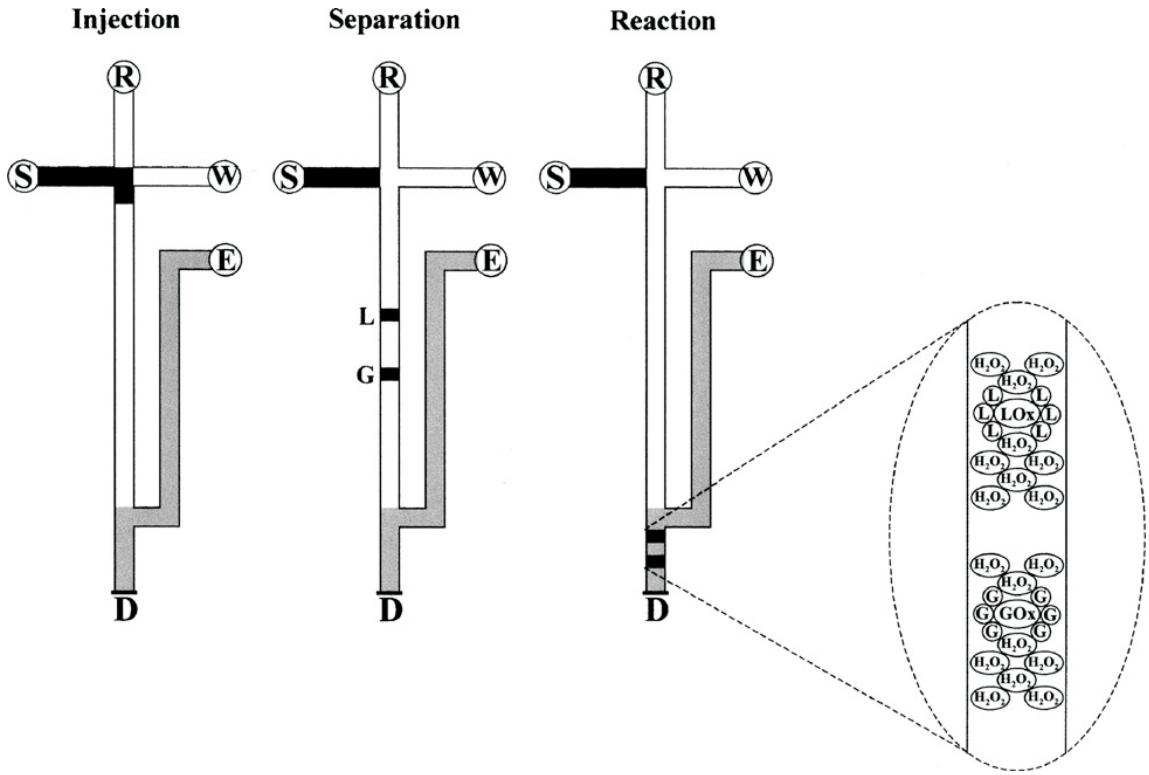

Figure I-26: Schematic of a capillary electrophoresis – electrochemical detector (CE-EC) microchip, with post-column enzymatic reaction, for the simultaneous measurement of glucose (G) and lactate (L). The individual analytical steps (injection, separation, reaction) are shown from left to right. Also shown (insert) is the post-column channel with the two hydrogen-peroxide zones. Reservoirs: (R) running buffer, (W) waste, (S) sample mixture, (E) "reagent" (enzyme) solution containing glucose oxidase (GOx) and lactate oxidase (LOx); (D) the amperometric detector. (Figure I-26 from Wang et al., 2007)[924]

Microchip separation devices remain the most widely reported microfluidic analytical devices, however other spectroscopic microfluidic devices are increasingly being reported. Such devices include micro spectrophotemeters[925-929] and micro nuclear magnetic resonance (NMR) chips.[930-933] One recent micro spectrophotometer design can be seen within Figure I-27, where an SU-8 microchannel module was integrated with a complementary metal-oxide-semiconductor (CMOS) microchip.[926] This integrated device was used to analyze human physiological fluids within a clinical setting.

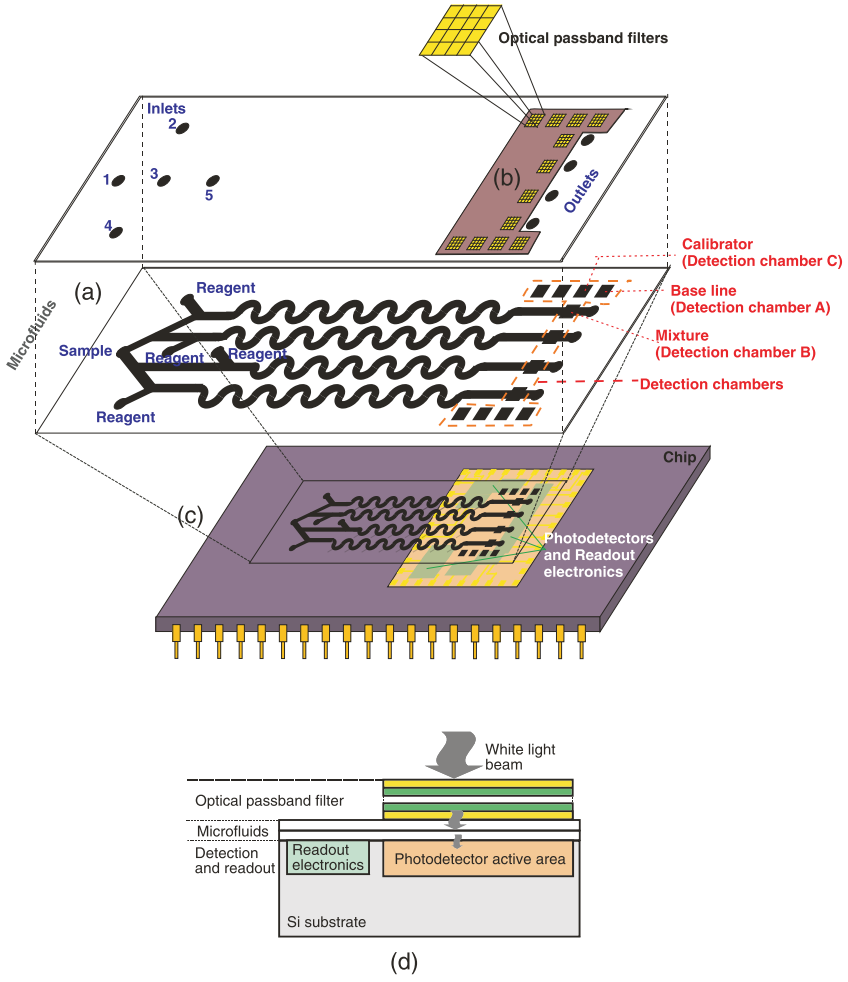

Figure I-27: Microlaboratory structure: (a) microfluidic system, the black squares are the detection chambers; (b) optical filtering system; (c) detection and readout system; (d) cross-section of the structure for a single optical-channel. (Figure I-27 from Minas et al., 2010)[926]

18) Miscellaneous Microfluidic Devices

A wide array of niche microfluidic devices have also been reported for their potential abilities to augment other microfluidic processes, or even in some cases enable completely new fluidic platforms for unique applications. Many electrically-equivalent microfluidic devices have been reported,[586, 603, 605, 934-950] along with other microfluidic device platforms that perform information processing operations, similar to that of computer microprocessors.[951-956] A recent report on microfluidic biological video games similar to PAC-man, Breakout, and Tic-Tac-Toe have also been reported.[957] One unique microfluidic device can be seen within Figure I-28,[958] where this schematic represents a micro electroporation device. This device was used to lyse cells being transported through a flow stream, with this device design having the capability to lyse cell membranes selectively, while leaving organelle membranes undamaged.[958]

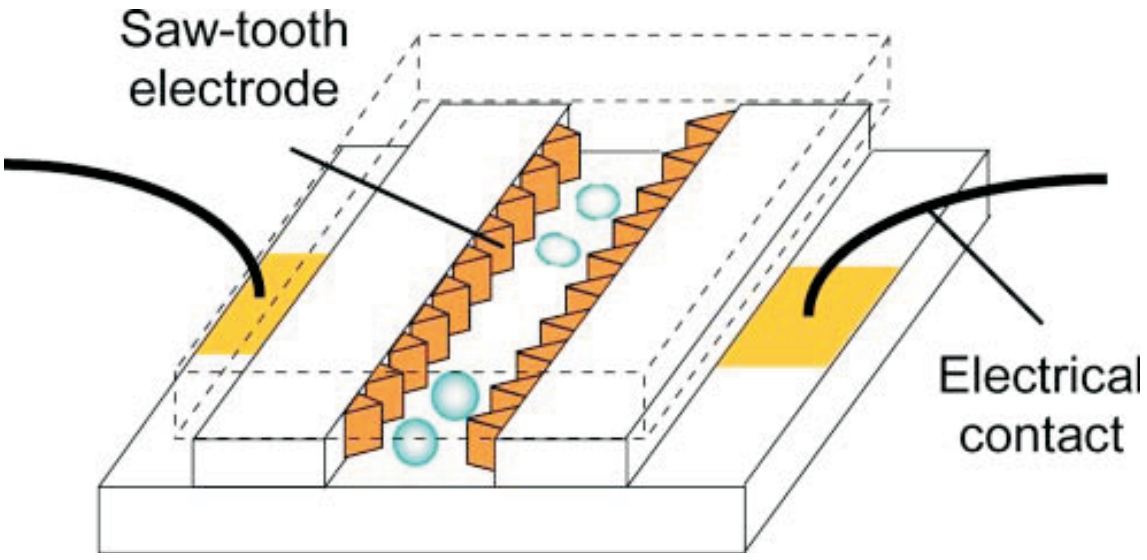

Figure I-28: Schematic of a micro electroporation device for cell lysis. Only one set of electrodes is shown for simplicity. (Figure I-28 from Lu et al., 2005)[958]

A second microfluidic device can be seen within Figure I-29, for the pair of electrically-equivalent fluidic devices.[959] These three-layer PDMS devices were formed using soft lithography replication techniques. The check valve device as illustrated for the top two rows, behaves in an analogous manner as an electrical diode, where fluid flow is allowed in only one direction. In the case of the switch-valve device shown for the bottom two rows, this device behaves analogous to a p-channel junction gate field-effect transistor (JFET), where a positive gate voltage would turn the JFET switch off.[959]

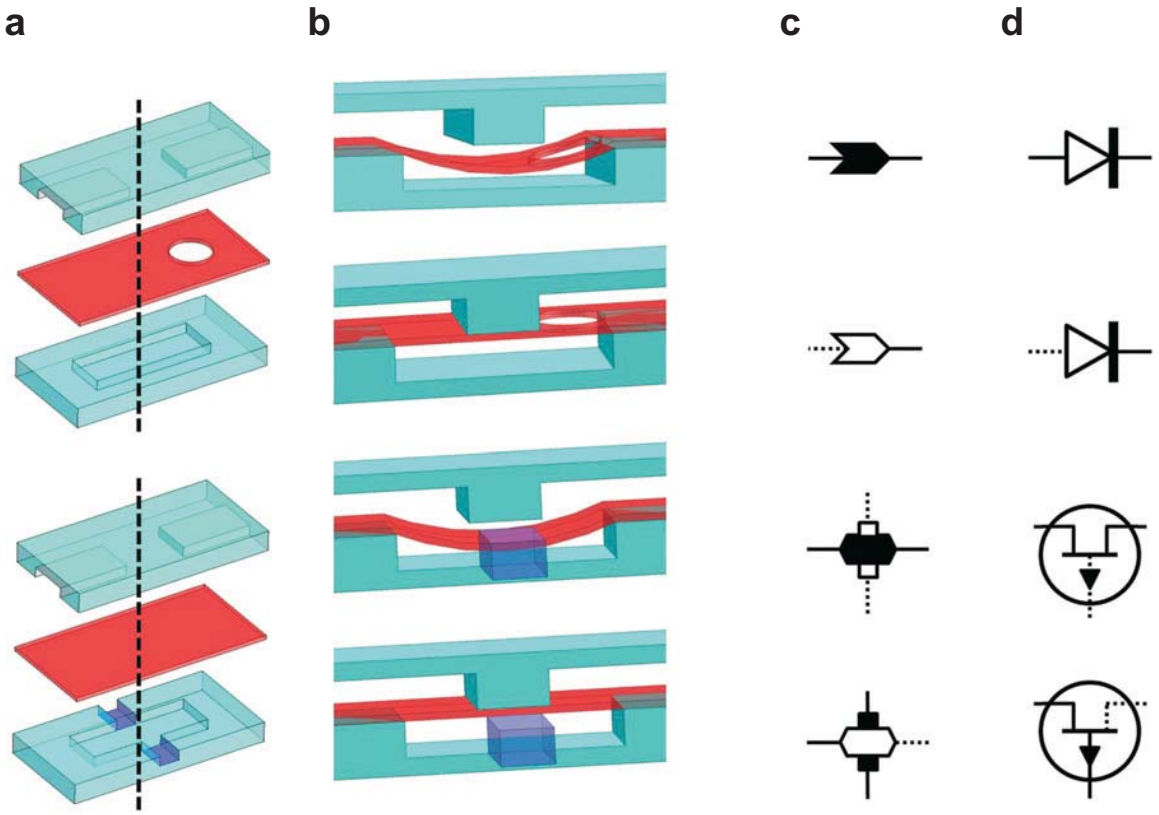

Figure I-29: Elastomeric components for autonomously controlled microfluidic devices. **a**, A three-layer composite of the check-valve and switch-valve. **b**, Cross-section schematic of the check-valve and switch-valve in both the open and closed state based on differential pressure. **c**, Corresponding component state symbol of the check-valve and switch-valve. Conducting current/flow is shown as solid lines and non-conducting current/flow is shown as dotted lines. **d**, The diode and p-channel JFET transistor shown as analogous electronic components to the check-valve and switch-valve, respectively. (Figure I-29 from Mosadegh et al., 2010)[959]

A third unique microfluidic device can be seen within Figure I-30.[960] This schematic image represents a microfluidic electronic wafer-probing tool, with similarities to a typical electrical wafer probe tool. The "microfluidic probe" was reported to allow for rapid and repeatable fluidic and electronic addressing of small die sites on a variety of substrate types, without the need for permanent modification or dicing of the device wafers.[960] The probe was also used to demonstrate locally patterned chemical modifications on a substrate surface, where it was shown the device could be used to acquire nanowire field-effect transistor (FET) sensor measurements.[960]

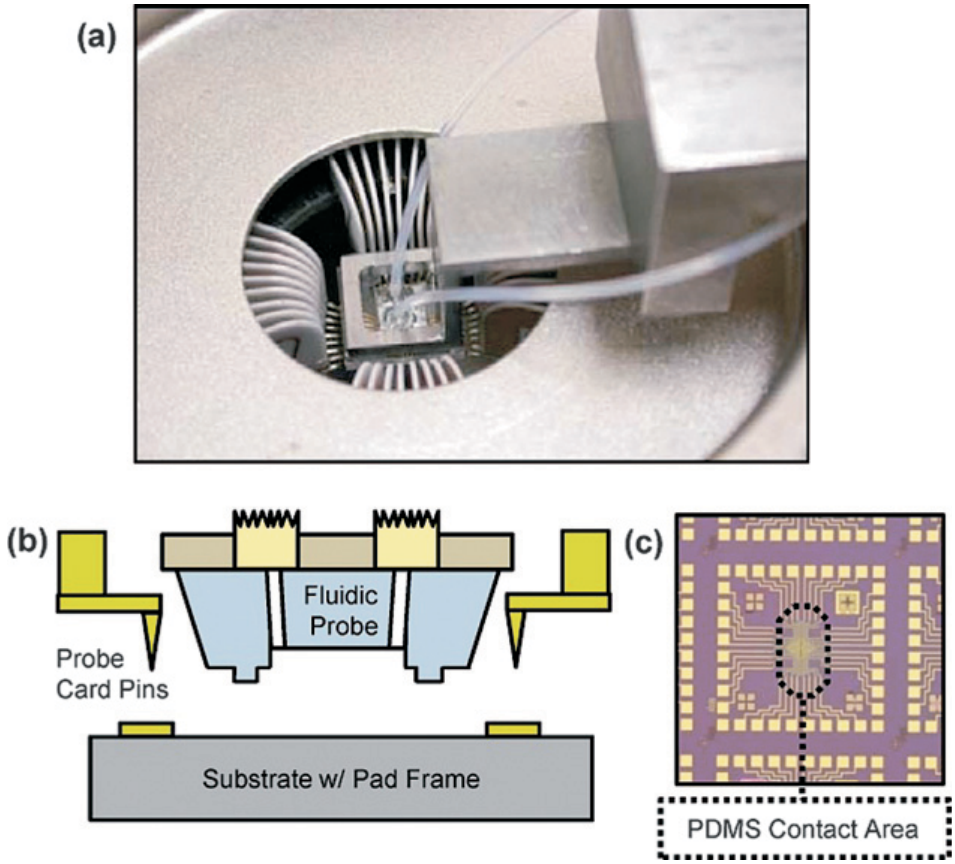

Figure I-30: (a) Microfluidic probe integrated with electronic probe card in automated wafer prober; (b) schematic cross-section and (c) die photo showing pad-frame and fluidic probe contact area. (Figure I-30 from Routenberg and Reed, 2010)[960]

19) Sample Injectors

Sample injection onto a microfluidic chip is a critical unit operation. When sample plugs are loaded onto a capillary electrophoresis separation column, the quantity and shape of the sample plug can negatively affect the efficiency and resolution of the separation, if the injection process is not optimized. Therefore, various sample injector designs have been studied for their ability to tightly control the length and reproducibility of an injected sample.[961-975] Sample injectors use either electrokinetic or hydrostatic actuation forces, with hydrostatic injections introduced using suction, pressure, or gravity.[976] One sample injection design can be seen in Figure I-31, where this design integrates both electrokinetic and pressure injection microfluidic options.[976]

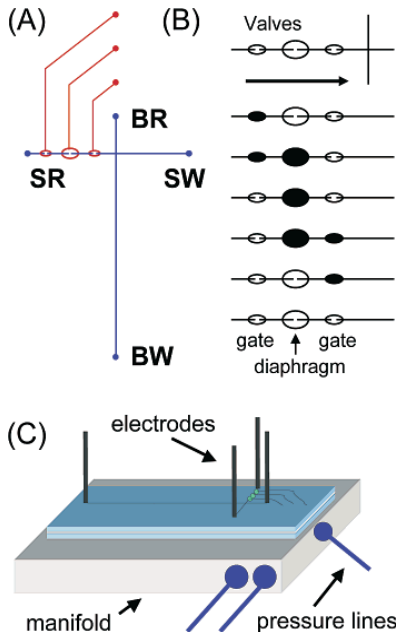

Figure I-31: Device schematics. (A) Channel design and dimensions. Distance from cross-T intersection to reservoirs: buffer reservoir (BR), 0.6 cm; buffer waste (BW), 7.9 cm; sample reservoir (SR) and sample waste (SW), 0.9 cm. Fluid channels (blue) etched 50 µm deep (50 µm original mask width). Valve channels (red) etched 60 µm deep. Volume of valve seats: gate, ~100 nL; diaphragm, ~200 nL. (B) Valve actuation sequence used to generate forward fluid pumping. Pressure injections presented as the number of cycles with the appropriate gate/diaphragm actuation times. (C) Assembled chip and pressure actuation manifold. (Figure I-31 from Karlinsey et al., 2005)[976]

20) Sensors and Detectors

Sensors and detectors are widely investigated for their use within microfluidic formats. A survey of the literature would turn up microfluidic sensor devices used to transduce physical variables such as temperature,[977-982] pressure,[983-988] fluid transport,[989-993] bio/chemical characteristics,[994-1003] mechanical forces,[1004-1007] and electrical properties.[1008-1014] Many of these microfluidic sensors can be integrated directly into a microchip, however this is oftentimes not the case with microfluidic detection systems. One remaining serious limitation for many microfluidic device formats, is the physical size of detection modules. One detection setup facing such challenges can be seen within Figure I-32, with this detection apparatus making use of multiple macro-sized electronic and optical components.[893]

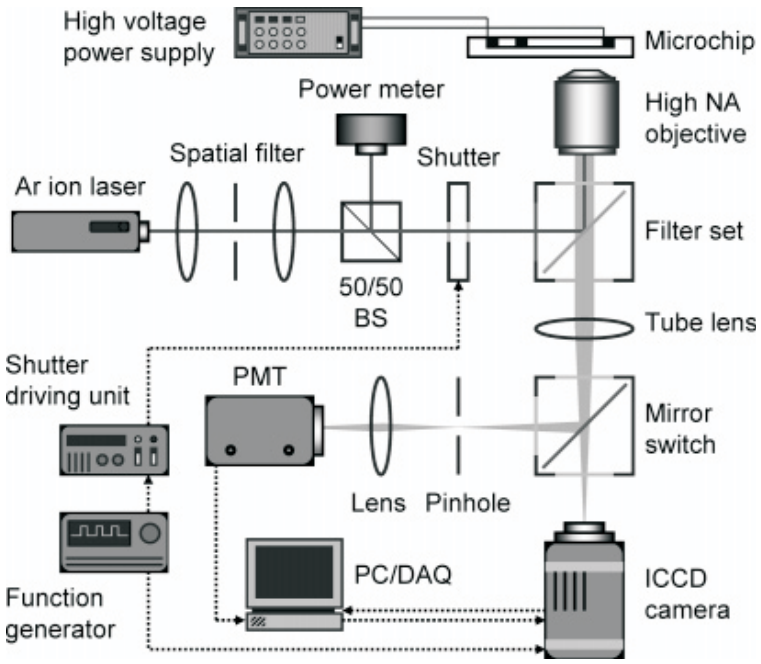

Figure I-32: Schematic of the high-sensitivity on-chip CE system showing argon ion laser illumination, light filter, shutter, color filters, detectors, and data acquisition PC. Actuation of a mirror switch provides switching from an intensified charge-coupled device (ICCD) camera to a custom-built confocal system with a photomultiplier tube (PMT). (Figure I-32 from Jung et al., 2007)[893]

The three primary detection systems employed within microfluidic systems include laser-induced fluorescence (LIF),[45, 1015-1025] electrochemical,[1026-1032] and mass spectrometric techniques,[881, 1033-1039] with other techniques such as infrared (IR), Raman, nuclear magnetic resonance (NMR), surface plasmon resonance (SPR), absorbance, thermal lens, chemiluminescence and electrochemiluminescence, refractive index (RI), and microplasma-optical emission detection (OED) schemes also being reported, albeit to a much lesser extent.[1040] In an attempt to decrease the size of microfluidic chip detection systems, various design strategies have been reported. In some cases new materials, detection schemes, and readouts are being investigated for their downsized lab-on-a-chip potential,[1041-1045] where in other instances cellular phones and common drugstore and/or household electrical devices are being explored for their possibilities as point-of-care detection systems.[1046-1055] These strategies are quite useful for field use and developing nation healthcare applications, but currently however, do not possess the same analyte detection capabilities as instrumentation employed within modern analytical laboratories. As a result, many scaled-down optical, electrochemical, and mass spectrometric detection systems have been reported for their applicability within microfluidic systems. One such scaled-down optical detection system is shown within Figure I-33.[1056] This microchip design employs four permanently bonded layers to form a sensor cartridge. The design does not eliminate the need for an external laser source, but does however integrate a miniaturized one-dimensional indium gallium arsenide (InGaAs) photodiode array for use as a collection device, and therefore eliminates the need for other commonly used macroscopic collection devices such as photomultiplier tubes (PMT).[1056]

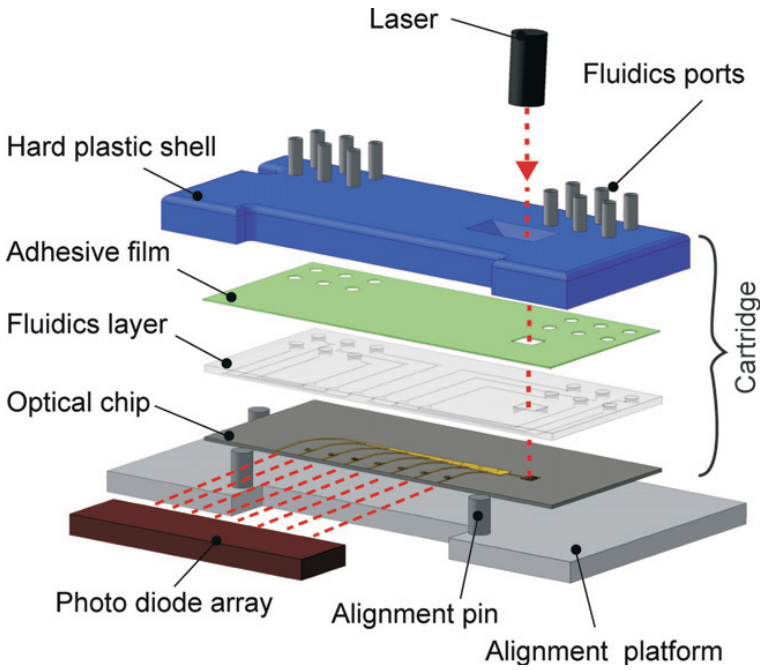

Figure I-33: A schematic exploded view of a sensor cartridge above an alignment platform, exposing 4 permanently bonded layers of the cartridge: the optical chip, the microfluidic layer, the adhesive film, and the hard plastic shell. Cutouts in the hard plastic shell free the edge of the precision cut silicon optical chip for accurate alignment against 3 pins protruding from the alignment platform of the read-out instrument. Light is coupled in from the top via a surface grating coupler, and collected at the long edge of the optical chip by imaging the output facets on a one-dimensional indium gallium arsenide (1D InGaAs) photodiode array. Fluidic ports for sample injection are formed by steel tubes glued into the hard plastic shell. (Figure I-33 from Carlborg et al., 2010)[1056]

Figure I-34 is an example of a scaled-down microfluidic electrochemical detection system.[1057] This design is an entirely polymeric microfluidic system, fabricated from the highly chemical resistant material cyclo olefin polymer (COP), where integrated gold micro electrodes were used for electrochemical detection in organic media.[1057] Another attempt to scale down parts of a microfluidic detection system can be observed within Figure I-35.[1058] This detection system illustrates a mass spectrometric setup, where a microreactor, a piezoelectric microdispenser, and nanovial target plates were employed to create the partial microtechnology-based detection platform.[1058]

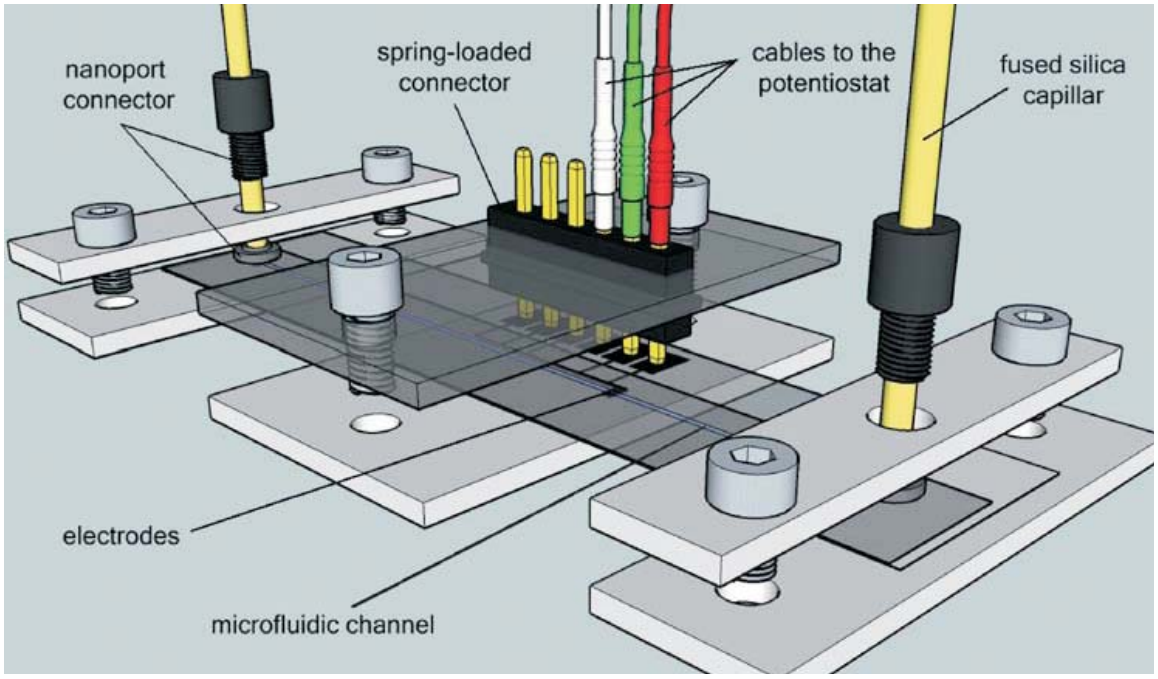

Figure I-34: Sketch of machined holders used to connect three electrochemical-sensing electrodes to a microfluidic chip. (Figure I-34 from Illa et al., 2010)[1057]

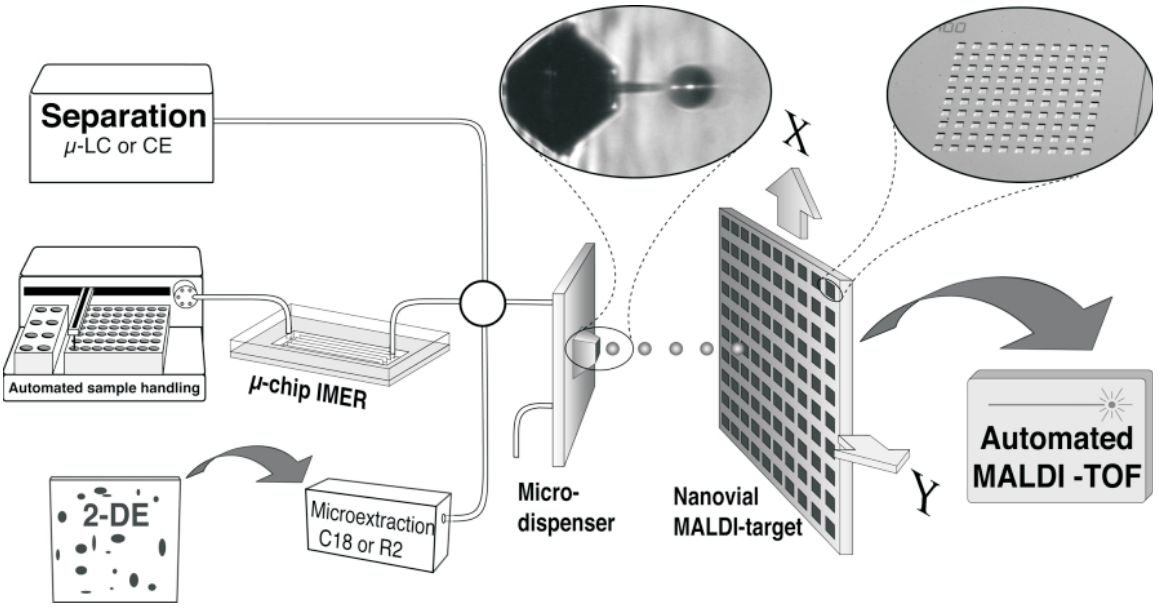

Figure I-35: Principal setup of a generic microtechnology matrix-assisted laser desorption time-of-flight mass spectrometry (MALDI TOF-MS) interface. (Figure I-35 from Laurell et al., 2001)[1058]

21) Micro-Total-Analysis-System (μTAS) Devices

When unit operation devices are combined onto a single microfluidic chip, the end-result is a micro-total-analysis-system (μTAS). An early μTAS design can be seen within Figure I-36.[1059] This device was fabricated entirely from silicon and glass, using conventional photolithographic micromachining techniques.[1059]

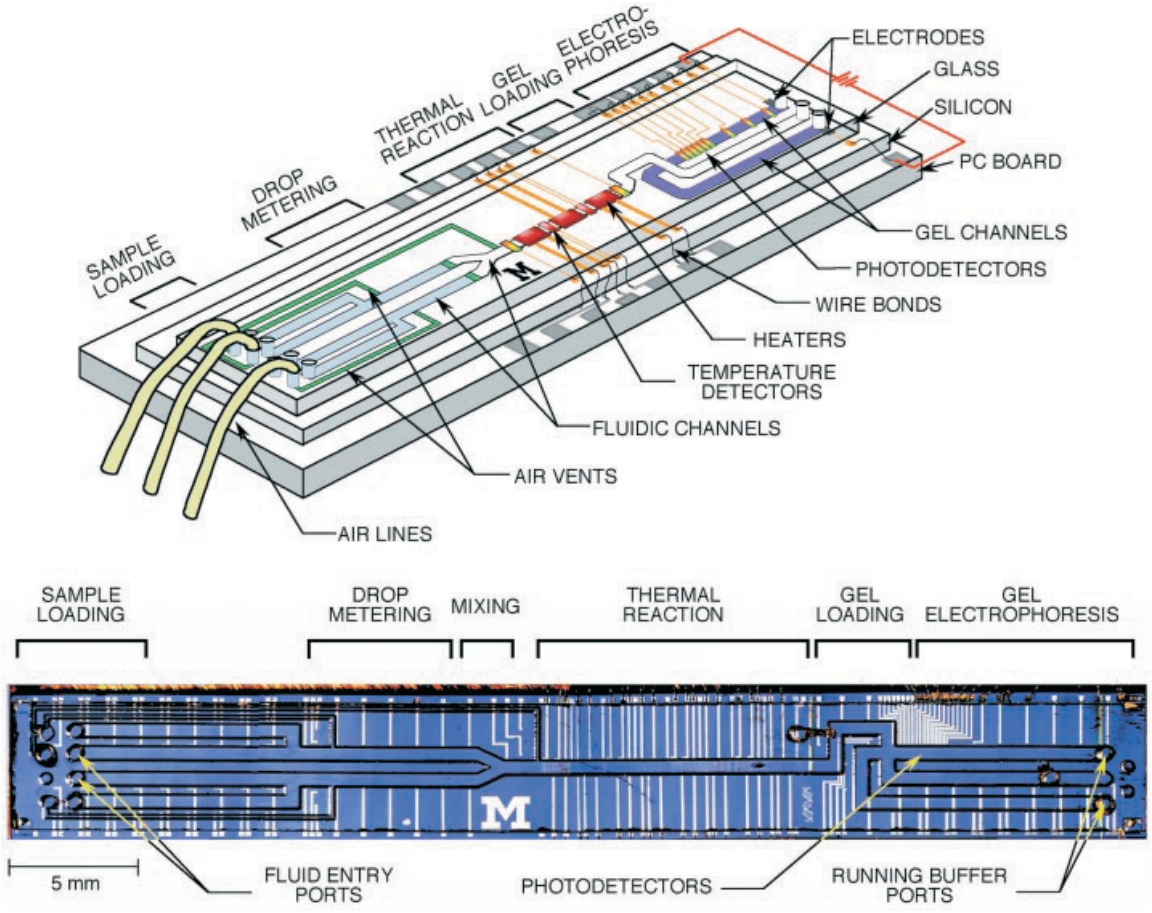

Figure I-36: (Top) Schematic of an integrated device with two liquid samples and an electrophoresis gel present. The only electronic component not fabricated on the silicon substrate, except for control and data processing electronics, is an excitation light source placed above the electrophoresis channel. Color code: blue, liquid sample (ready for metering); green, hydrophobic surfaces; purple, polyacrylamide gel. (Bottom) Optical micrograph of the device from above. Wire bonds to the printed circuit board can be seen along the top edge of the device. The blue tint is due to the interference filter reflecting the short-wavelength light. The pressure manifold and buffer wells that fit over the entry holes at each end of the device are not shown. (Figure I-36 from Burns et al., 1998)[1059]

A second more recent μTAS design can be seen within Figure I-37.[1060] This μTAS design was pneumatically actuated and fabricated from glass and PDMS.

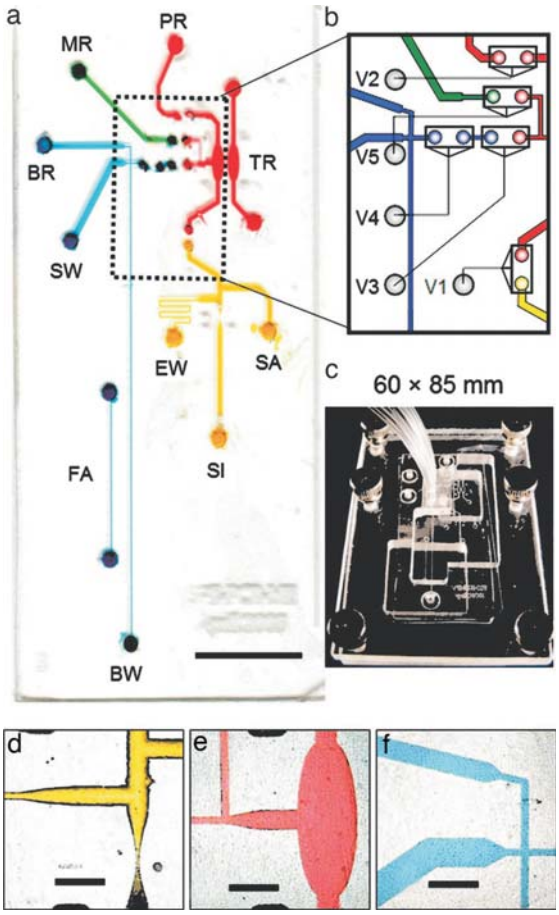

Figure I-37: Images of a microfluidic genetic analyzer (MGA) device. (a) Dyes are placed in the channels for visualization (Scale bar, 10 mm.). Domains for deoxyribonucleic acid (DNA) extraction (yellow), polymerase chain reaction (PCR) amplification (red), injection (green), and separation (blue) are connected through a network of channels and vias. Solid-phase extraction (SPE) reservoirs are labeled for sample inlet (SI), sidearm (SA), and extraction waste (EW). Injection reservoirs are labeled for PCR reservoir (PR), marker reservoir (MR), and sample waste (SW). Electrophoresis reservoirs are labeled for buffer reservoir (BR) and buffer waste (BW). Additional domains patterned onto the device include the temperature reference (TR) chamber and fluorescence alignment (FA) channel. The flow control region is outlined by a dashed box. Device dimensions are 30.0 x 63.5 mm, with a total solution volume <10 μL. (Scale bar, 10 mm.) (b) Schematic of flow control region. Valves are shown as open rectangles. V1 separates the SPE and PCR domains. V2 and V5 are inlet valves for the pumping injection, V3 is the diaphragm valve, and V4 is an outlet valve. (c) Device loaded into the manifold. (d) Intersection between SI and SA inlet channels, with the EW channel tapering to increase flow resistance. (Scale bar, 1 mm.) (e) Image of PCR chamber with exit channel tapering before intersecting with the MR inlet channel. (Scale bar, 1 mm.) (f) Image of cross-tee intersection. (Scale bar, 1 mm.) The relative sizes of the BR, SW, and BW channels create the difference in volume displacement during the pumping injection and affect how the resistance is dropped under an applied separation voltage. (Figure I-37 from Easley et al., 2006)[1060]

A third example of a modern μTAS design can be seen within Figure I-38.[1061] This particular design was fabricated from a plastic chip, a printed circuit board (PCB), and a Motorola eSensor microarray chip. This design in contrast to the μTAS design as shown within Figure I-37, employs thermopneumatic and electrochemical pumping mechanisms. The μTAS design as shown within Figure I-38 was also reportedly fully self-contained, where no external pressure sources, fluid storage, mechanical pumps, or valves were necessary for fluid manipulation, and thus eliminating possible sample contamination and simplifying device operation.

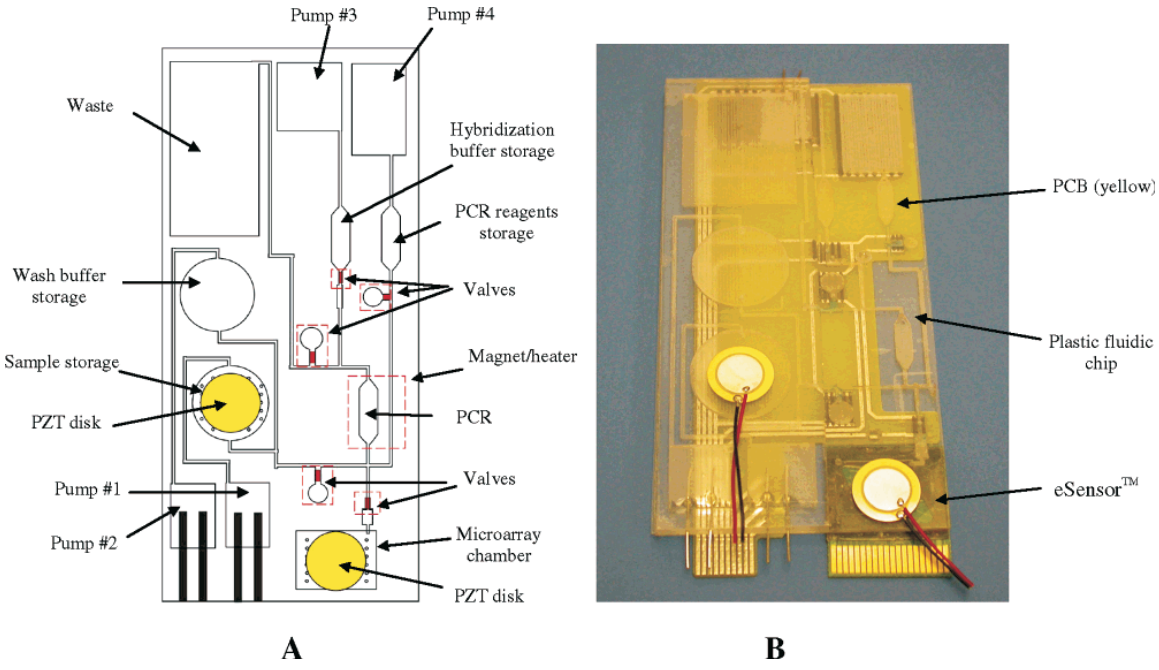

Figure I-38: (A) Schematic of a plastic fluidic chip. Pumps 1-3 are electrochemical pumps, and pump 4 is a thermopneumatic pump. (B) Photograph of the integrated device that consists of a plastic fluidic chip, a printed circuit board (PCB), and a Motorola eSensor microarray chip. (Figure I-38 from Liu et al., 2004)[1061]

A fourth and final μTAS example can be seen within Figure I-39.[470] This design leverages the capabilities of a compact disc microfluidic platform, employing laser irradiated ferrowax phase transition microvalve technology.[470] This particular design, like that of the previous three μTAS designs, was used to perform assay and genetic operations. The μTAS platform of Figure I-39 was designed to perform sample in-sample out analysis of whole blood samples, with both multiple biochemical analysis and sandwich type immunoassay analysis being performed simultaneously.

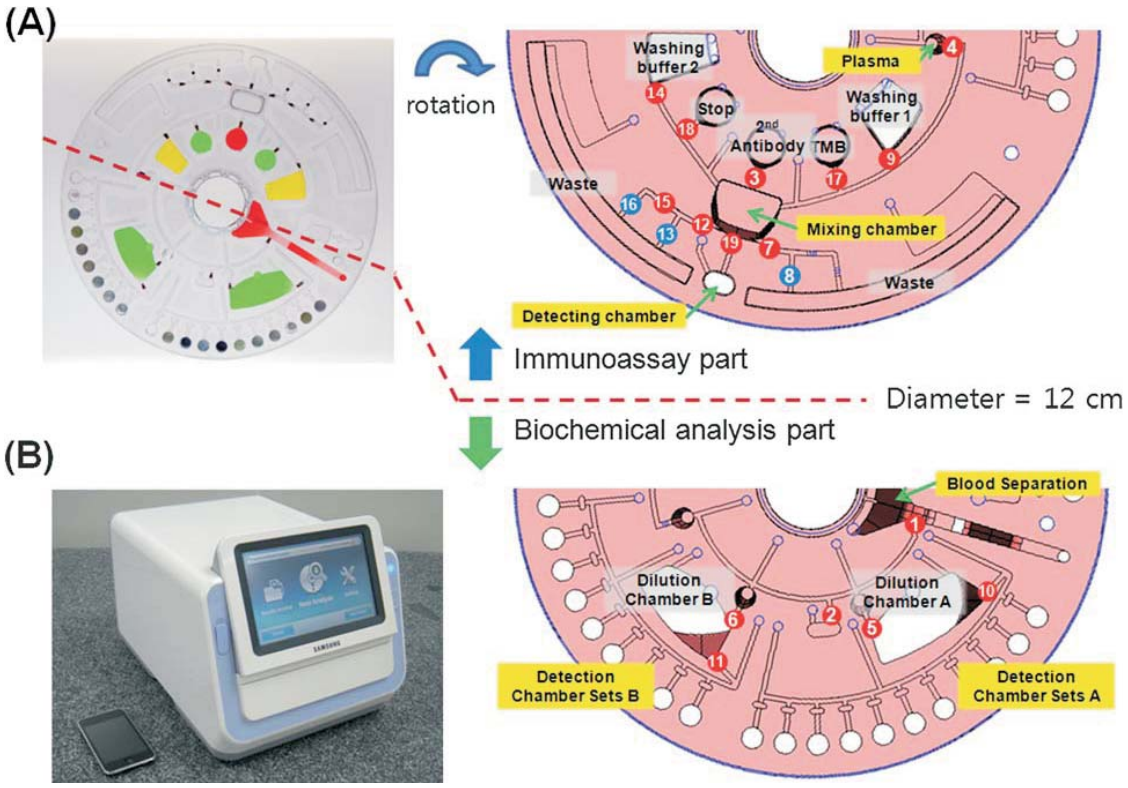

Figure I-39: (A) Photograph of a lab-on-a-disc. Detection wells on the clinical chemistry side are preloaded with lyophilized reagents. Other chambers for liquid type reagents are loaded with food dye solution for demonstration. In the right hand side, the disc design shows the detailed microfluidic layout. The number indicates the order of a laser irradiated ferrowax microvalve (LIFM) operation. The top half of the disc for the immunoassay part is rotated for easier demonstration. The blue circles with numbers are normally opened-LIFM (NO-LIFM). The other half of the disc for the clinical chemistry analysis part is shown in the bottom. (B) A photo image of the Samsung Blood Analyzer (25(W) x 35(D) x 25(H) cm). (Figure I-39 from Lee et al., 2011)[470]

The Study of Neuroscience using Microfluidic Device Technology

22) Neuroscience, a Cursory Introduction

The nervous system is one of the most intricately organized aggregate of matter on earth, where just 1 cm^3 of human brain tissue may contain several million nerve cells, each of which communicates with thousands of other neurons for data processing and communication purposes.[1062] The biological mechanisms at work within an individual neuron is shown within Figure I-40.[1063]

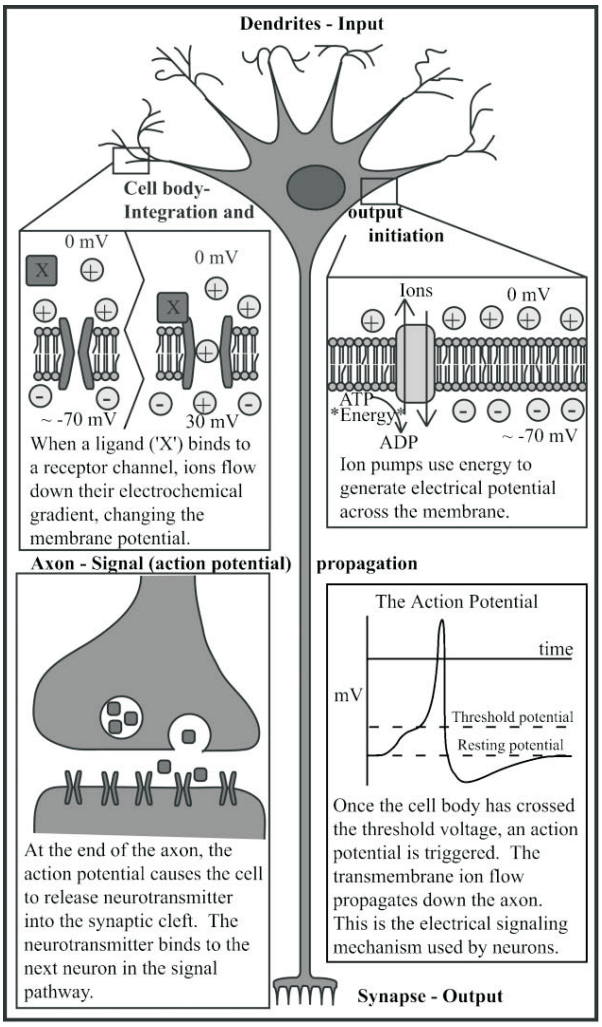

Figure I-40: The inner workings of a neuron. (Figure I-40 from Pearce and Williams, 2007)[1063]

The nervous system plays a critical role in complex functions such as perception, movement, learning, memory, and reasoning. When disease, accidents, or illness adversely affect the nervous system, it is often necessary to understand the neurochemical basis behind such problems. In today's research laboratories, neurochemists are primarily utilizing four techniques to elucidate neurochemical pathways. These techniques are microdialysis, push-pull perfusion, glutamate enzyme sensors, and fast scanning cyclic voltammetry (FSCV) / neural electrodes.

A) Microdialysis Probes

It is widely accepted, the most popular *in vivo* neuroscience probe monitoring technique is microdialysis.[1064-1077] This technique is commonly used in many branches of science and medicine including bioinorganic chemistry,[1078] renal analysis,[1079] cardiovascular experiments,[1080] and studies on neurological diseases such as schizophrenia.[1081] A typical microdialysis probe can be seen within Figure I-41. Microdialysis probes make use of the selective permeability of a membrane that allows small analytes to pass through, while excluding larger substances such as cells and proteins.[1082-1088] The permeability is based on pore size, where a molecular weight range is specified by the manufacturer. This technique has the advantages of having excellent chemical sensitivity, and being fairly selective in sampling for a specific analyte. These advantages are a result of the partially selective membrane and the fact that microdialysis sampling can be combined with powerful separation techniques like high performance liquid chromatography or capillary electrophoresis. With the selectivity and excellent

chemical sensitivity microdialysis possesses, this technique allows scientists to study signaling pathways from complex samples that oftentimes contain small quantities of the analyte under investigation.[1089]

Microdialysis is widely utilized for the attractive benefits associated with this technique, however this sampling technique does have shortcomings such as relatively poor temporal and spatial resolution. The sampling region of a microdialysis probe is usually 1-4 mm long, and 200 μm in diameter, with these dimensions being far too large to sample smaller brain regions of rats, and especially mice.[1090] The best temporal resolution to date has been reported as 3 to 10 seconds.[1082, 1091] Another shortcoming of microdialysis is that it cannot provide information on absolute analyte concentrations within the sampling region.[1092] This information cannot be obtained for two reasons. First, the detected analyte concentration represents a convolution of the total quantity of analyte crossing the microdialysis membrane. This is to say, analyte is continuously sampled across the microdialysis membrane for the entire flow path length of the microdialysis probe, and therefore the detected analyte concentration lacks specificity for any particular spatial brain region in contact with the microdialysis probe. The second reason microdialysis does not provide data on absolute analyte concentration, is because bulk fluid is not extracted from the sampling region. Microdialysis probes develop diffusive gradients in the vicinity of the probe sampling region, where this diffusive gradient does not allow for quantitation of absolute analyte concentration values, for surrounding brain areas in contact with the microdialysis probe membrane.

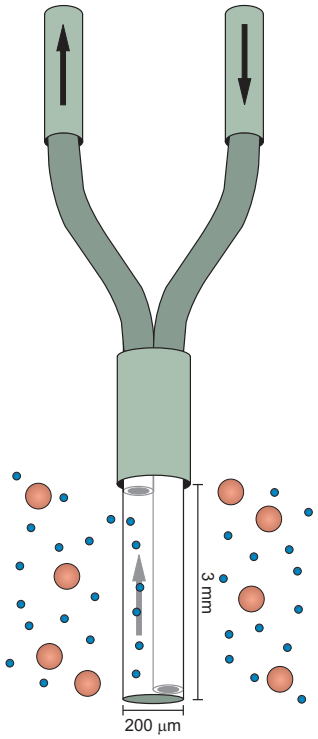

Figure I-41: Schematic of a typical microdialysis probe. Two fused silica capillary tubes are placed adjacent to one another, and further surrounded by a semipermeable molecular weight cutoff membrane. Typical dimensions for microdialysis probes measure 3-4 mm (L) x 1 mm (W). (Figure I-41 from M.T. Bowser, 2011)

B) Push-Pull Perfusion Probes

Push-pull perfusion is a second sampling technique used to study *in vivo* neurochemistry.[1093-1102] Push-pull perfusion probes straddle two pieces of capillary tubing side by side, or alternately placing one capillary tube within a second larger capillary tube. The later probe design can be observed within Figure I-42A.[1103] These probe designs sample *in vivo* analytes when buffer is perfused through one piece of capillary tubing, and pulled through the other capillary tube. Unlike microdialysis which utilizes a membrane to exclude larger analytes such as cells and proteins, push-pull perfusion is an open system where both adjacent capillary tube tips are exposed to the

in vivo microenvironment. Substances in the surrounding microenvironment are sampled when they diffuse into the perfusate making contact with the external microenvironment. The procedures name is self-explanatory in the sense that perfusate is "pushed" through one capillary tube into an open microenvironment, with the adjacent capillary tube "pulling" the solution near its tip back into the system for further chemical analysis. Figures I-42B and I-42C are schematics representing the overall push-pull perfusion sampling process, with flow injection sample analysis (FIA) represented in Figure I-42B, and high performance liquid chromatography (HPLC) sample analysis represented in Figure I-42C.[1103]

While this technique was abandoned for nearly 20 years due to the large amount of tissue damage created at the sampling site, it has seen a rebirth with the development of improved probes and sampling methodologies that allow for much lower flow rates. The spatial resolution for this techniques sampling region is equivalent to the surface area of two tips (e.g. 50/150 μm ID/OD) of capillary tubing placed adjacent to one other, or the surface area for one larger capillary tube tip (e.g. 100/250 μm ID/OD).[1093, 1099, 1103] Temporal resolution results have been reported to be 12-25 minutes to collect a 0.5-1 μL sample for offline capillary electrophoresis separation,[1093, 1095] and 111-317 seconds for online analysis.[1103]

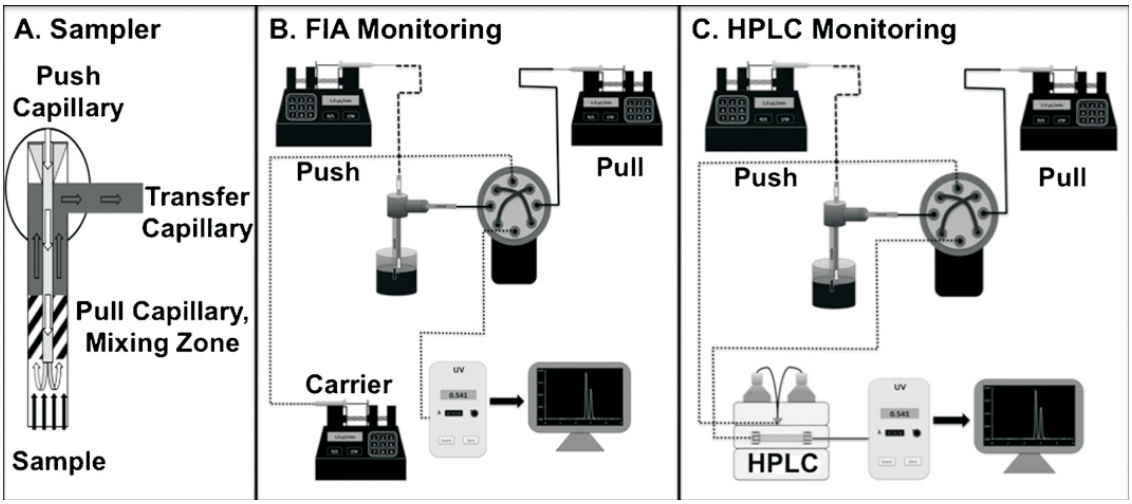

Figure I-42: Illustration of a sampling system showing (A) a detailed view of sample mixing with quenchant/diluent for a push-pull perfusion sampling probe, (B) an overview for flow injection analysis (FIA) monitoring, and (C) an overview for high performance liquid chromatography (HPLC) monitoring. (Figure I-42 from Chisolm et al., 2010)[1103]

C) Glutamate Enzyme Sensors

Glutamate enzyme sensors represent a third class of *in vivo* sampling probes.[1104-1115] These sensors have been specifically developed for *in vivo* glutamate detection. This technique immobilizes glutamate oxidase onto a substrate, where an enzymatic reaction with glutamate can be detected either optically or electrochemically. Glutamate oxidase has been linked to two types of substrates in past studies, including a fiber optic cable[1116] and a carbon-fiber electrode.[1116, 1117] One glutamate enzyme sensor design can be seen within Figure I-43, with this design representing an electrochemical sensing platform.[1118] The biggest drawback of glutamate enzyme sensors, is that only one neuroanalyte can be examined. The temporal and spatial resolutions reported for these electrodes however, position this sampling technique as a competitive *in vivo* brain science probe technology. Fiber optic probes are reported to have micrometer to submicrometer diameters, with

temporal resolutions reported as ~50 ms.[1116] Spatial resolutions of 2-10 μm have been reported using carbon-fiber microelectrodes, with temporal resolutions reported from 300 ms to 1 s.[1117, 1119]

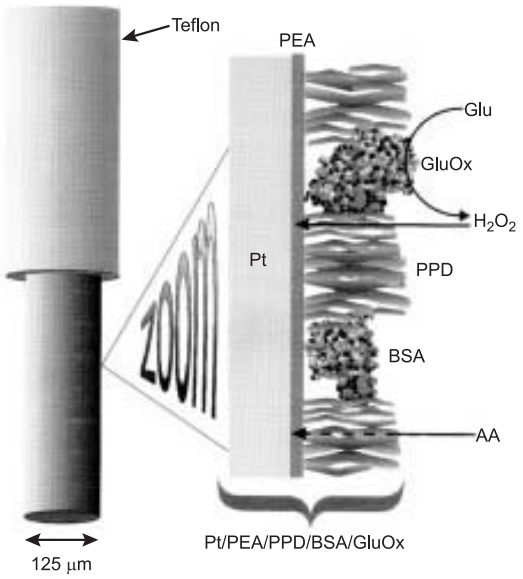

Figure I-43: Schematic illustration of a Pt/PEA/PPD/BSA/GluOx sensor fabricated by: dip coating the lipid phosphatidylethanolamine (PEA) from a chloroform solution onto bare platinum (Pt); adsorption and dip coating of l-glutamate oxidase (GluOx) from an aqueous buffer onto the PEA layer; and electrosynthesis of the non-conducting form of polyphenylenediamine (PPD) in a phosphate buffered saline (PBS) solution (pH 7.4) containing monomer and bovine serum albumin (BSA). The small H_2O_2 molecules can diffuse easily to the Pt surface to be electro-oxidized with a characteristic fast response time. Access to the metal by larger electroactive species, such as ascorbic acid (AA), is severely restricted by the PPD, PEA and proteins, with a correspondingly small and slow response. (Figure I-43 from Ryan et al., 1997)[1118]

D) Fast Scanning Cyclic Voltammetry (FSCV) Electrodes / Neural Electrodes

Fast scanning cyclic voltammetry (FSCV) is a fourth *in vivo* neurochemical sampling technique.[1120-1131] This technique is used to detect electroactive analytes in the brain, where these analytes are detected using a fine tip electrode. A FSCV probe can be seen within Figure I-44.[1065] Considering only *in vivo* electrochemical monitoring

methods, FSCV has emerged as the dominant technique.[1131] When it is desired that an *in vivo* electroactive analyte be characterized with very high spatial and temporal resolution, FSCV will likely be the neuroscientist's technique of choice. FSCV electrodes are typically made from carbon fibers with tip diameters in the range of 5-30 μm.[1064, 1132] Temporal resolution is usually around 100 ms.[1064, 1065, 1133] One downside of this technique is that only a few neurotransmitters can be monitored within the brain. Chemical selectivity can also be a problem, as there are many molecules within the brain that are easily oxidized and reduced, such as ascorbic acid and oxygen.[1065]

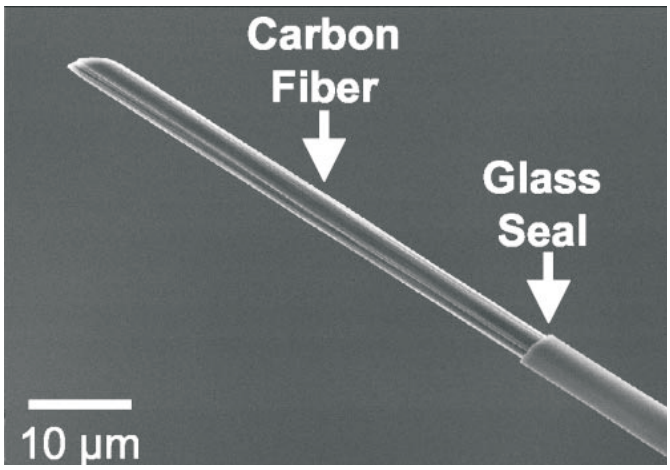

Figure I-44: Scanning electron microscope image of a cylindrical carbon-fiber microelectrode under x1200 magnification. The diameter of the fiber is ~5 μm. The length of the exposed carbon fiber extending from the glass seal is the electroactive area of the electrode. (Figure I-44 from Robinson et al., 2003)[1065]

An *in vivo* sampling technique closely related to FSCV, is that of neural electrodes.[1134-1146] Neural electrodes make use of modern micromachining techniques, and oftentimes incorporate on-board signal processing circuitry.[1147] These electrodes perform very similar to FSCV electrodes, however unlike FSCV electrodes, neural

electrodes are designed as multichannel probes. This multichannel capability allows for simultaneous stimulation and signal recording, from different spatial regions of the brain. One such neural electrode design providing such capabilities is shown within Figure I-45.[1147]

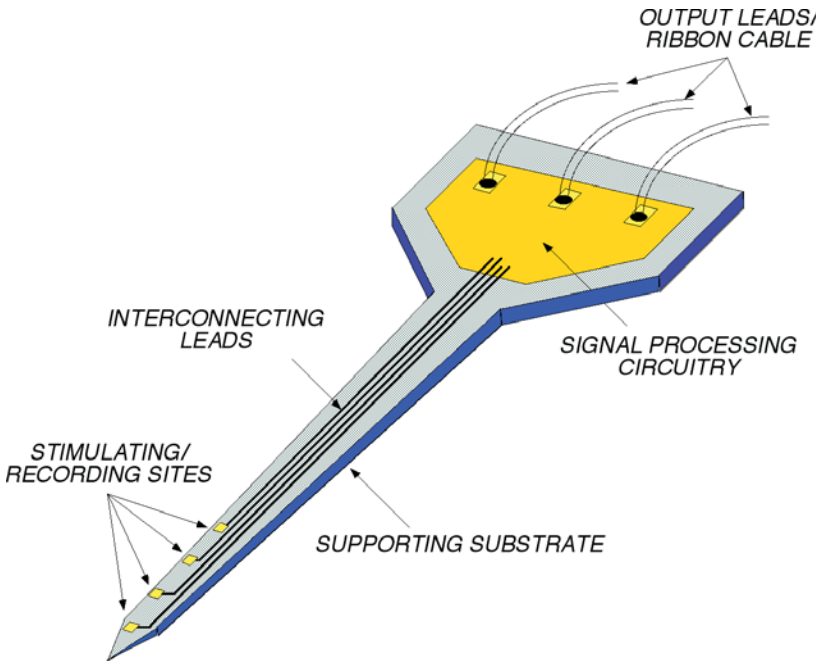

Figure I-45: Basic structure of a micromachined multielectrode probe for recording or stimulation in the central nervous system. (Figure I-45 from Wise et al., 2008)[1147]

Neural electrodes can be used to study *in vivo* brain chemistry, but have also been implemented as implantable prosthetic devices, to function as deep brain stimulators for treatment of diseases such as Parkinson's Disease.[1147] One experimental setup using neural electrodes can be seen within Figure I-46.[1147] This setup was used to study surgical implant trauma, by monitoring extracellular pH changes, as a function of surgical implant speed. It is also possible to implement a similar *in vivo* setup, by replacing the neural electrode with a microdialysis or push-pull perfusion probe, for example.

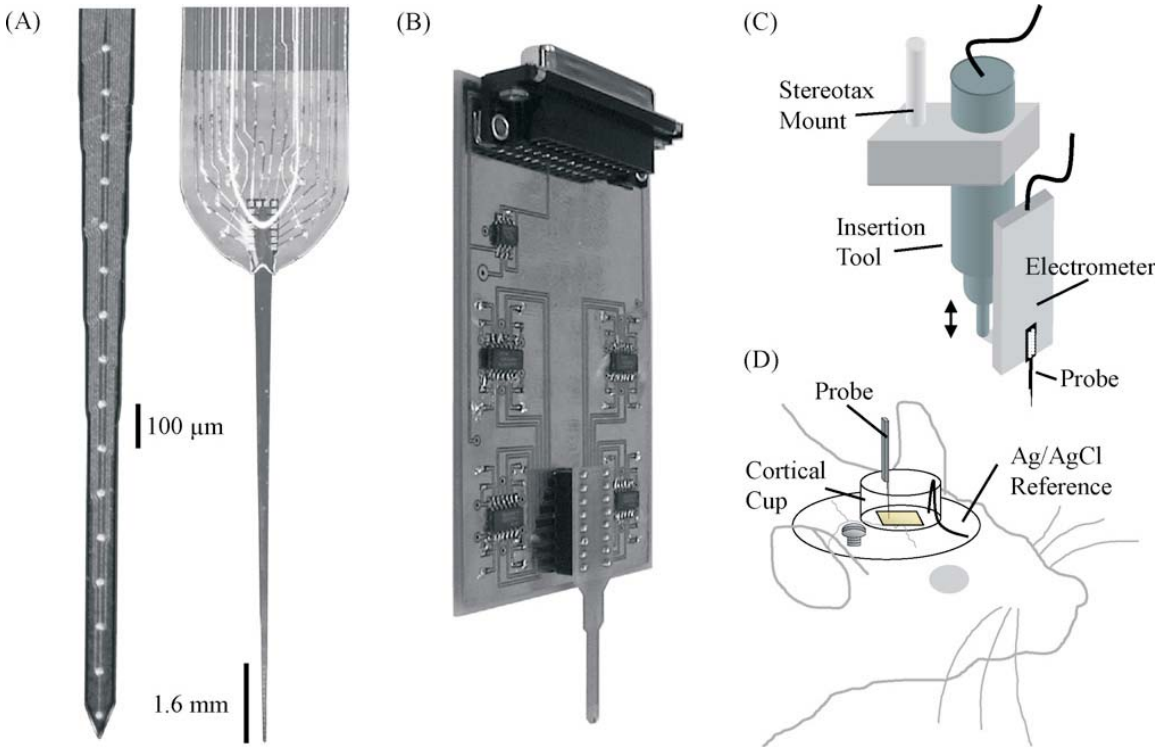

Figure I-46: Potentiometric extracellular pH (pH_e) responses are monitored with a potentiometric neural microelectrode array during insertion into the brain of an anesthetized rat. (A) Silicon-substrate probes with 16 hydrous iridium oxide (700 μm^2) contact sites spaced 100 µm apart transduce spatiotemporal pH_e dynamics through (B) a custom 16 channel electrometer circuit. (C) Microelectrode array insertion involves computer-controlled manipulations of a piezoelectric actuator, which adjusts the height of the electrometer and neural probe. A stereotaxic frame attachment secures the actuator base in place. (D) Probes are inserted through a cortical cup filled with 0.1M phosphate buffered saline (PBS) (pH 7.4) and into brain tissue. The cup solution provides single-point offset calibration prior to insertion and after explanting the microelectrode array. Measured potentials are referenced to an Ag/AgCl wire placed in the cortical cup. (Figure I-46 from Johnson et al., 2007)[1148]

E) Direct-Sampling Probes

Direct-sampling probes serve as a fifth *in vivo* sampling technique.[1090, 1149-1153] This technology is not as widely employed, in comparison to that of the above four techniques. Direct-sampling probes extract extracellular fluid from an *in vivo* brain using a single filament of capillary tubing. A direct-sampling probe would look similar to the FSCV electrode as shown within Figure I-44, however the central region would be

hollow, with the outer diameter of a direct-sampling probe measuring approximately 105 μm, in contrast to 5 μm as shown for the FSCV electrode. One report employed direct-sampling probe technology to study *in vivo* rodent brain chemistry, using a vacuum system with off-line capillary electrophoresis analysis.[1090] The Author's reported a spatial resolution of 18-40 μm ID and 90 μm OD, with a cited temporal resolution of better than 90 s.

F) Rodent Somatosensory Barrel Cortex

In the nervous system, various neurological functions such as motor control and sensation of the outside world, reside within specific regions of the brain and spinal cord. Of particular interest to many neuroscience experiments, are rodent bodily senses. The label for this division in the nervous system is the somatic (bodily) sensory system, or commonly also referenced as the somatosensory system. The somatosensory system receives sensory information from sight, sound, smell, taste, touch, pain, visceral, and body movement. These forms of stimuli can arise in the skin, joints, muscles, face, mouth, teeth, and jaw.[1154] When receptors in or on the body are stimulated in these regions, the stimulus is transduced into an electrical signal where the information contained in this signal is sent along neurons to specific regions of the brain and spinal cord, where the signal is processed. Somatosensory signals pass through bundles of cell bodies in the brain stem called nuclei. These nuclei are more specifically coined as, cranial nerve nuclei. There are a total of twelve cranial nerves, with cranial nerve V, the trigeminal nerve, of major importance for this dissertation. After the signal leaves the

brainstem, it passes through a central relay station in the brain called the thalamus. Once the signal has been routed by the thalamus, it is directed to the higher brain centers of the primary somatosensory cortex, often denoted as SI. This entire neurological pathway discussion can be referenced with respect to Figure I-47,[1155] with the stimulus originating on the face.

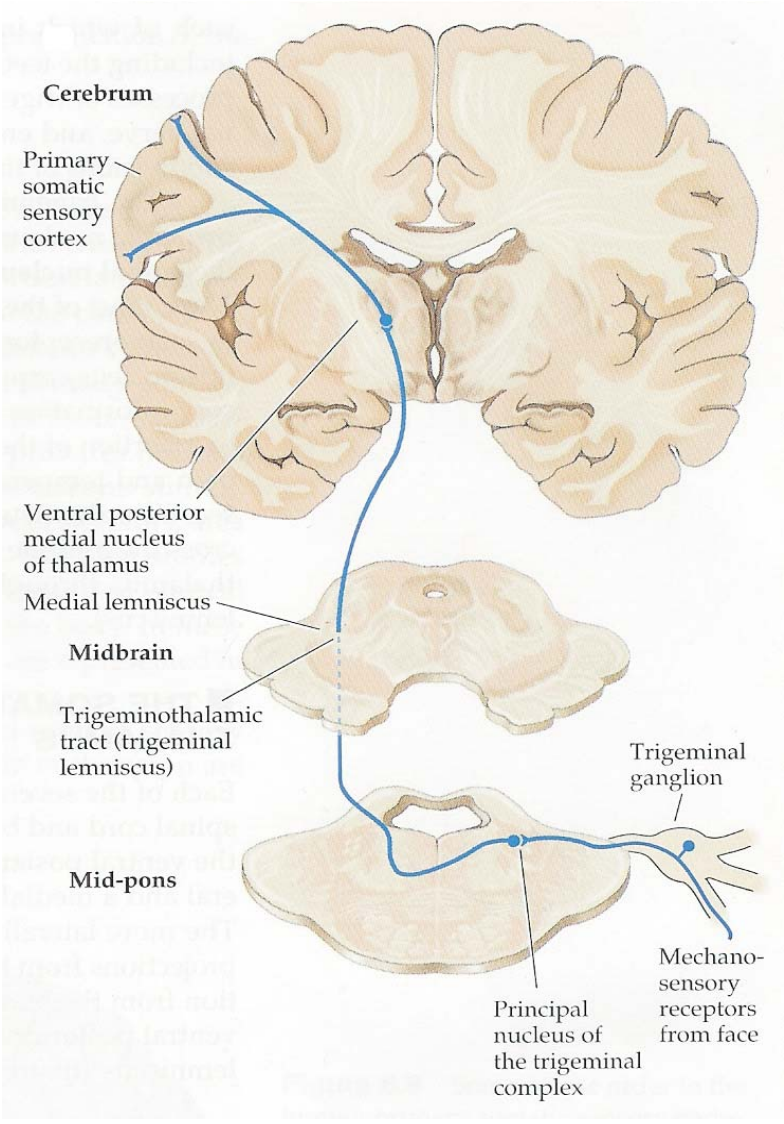

Figure I-47: The trigeminal nerve tract portion of the mechanosensory system. Action potential signal sent from receptors on face, to primary somatosensory cortex within the brain. (Figure I-47 from Purves et al., 1997)[1155]

The trigeminal pathway plays a key role in the survival of all mammals, but this is especially true for rodents. A region known as the barrel cortex,[1156-1164] occupies approximately 35% of a rodent's SI area.[1165] The name, "barrel cortex," was derived from the fact that reconstruction of three dimensional tangential slices through layer IV of the SI region in rodents, produces distinct elliptical-looking columns that resemble whisky barrels.[1164-1167] The most distinct and preserved anatomy from rodent to rodent within the barrel field, are the barrels located in the posteriomedial barrel subfield (PMBSF). These barrels range in size from 50-400 μm in diameter. The PMBSF region can be seen in images A and B of Figure I-48.[1154] This section of the barrel field has been shown to have a one-to-one correlation of individual barrels, to that of individual vibrissa on the contralateral vibrissa pad.[1168, 1169] That is, information from the opposite side of the whisker pad is processed in a specific barrel of the PMBSF region. The anatomical resemblance between patterns of the PMBSF and vibrissa pad, can be seen when comparing images A and B of Figure I-48, to image D of the same Figure.[1154] The term mystacial vibrissa is used as opposed to simply, whisker, to clearly separate bulk sinus hairs from the very large upper lip whiskers. Rodents mechanically deflect their upper lip whiskers to perform, "whisking." [1165, 1170, 1171] Whisking is the primary means by which rodents obtain tactile information from their surroundings, even over their paws.[1154] The frequency of whisking is also known to be in the 7-12 Hz range.[1165, 1170] The fact that a rodent's whiskers are so important to their survival presents many opportunities for neuroscientists to exploit this neurological/behavioral phenomena.[1167, 1172-1174] For example, whisking is known to be sensitive to mechanical properties such as

frequency, angular direction, velocity, amplitude, duration, and spatial and temporal patterns.[1175-1185] These characteristics elicit different neurological responses, and therefore produce different signals that can be studied in the PMBSF.[1186, 1187]

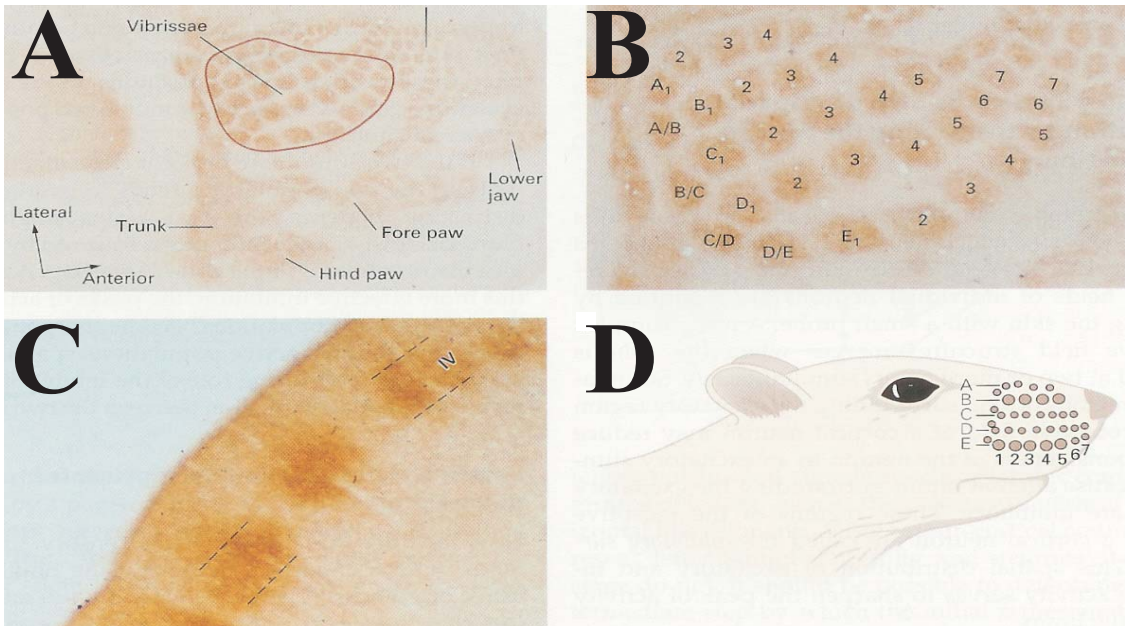

Figure I-48: Representation of whiskers in the somatosensory cortex of the rat. (A) Photomicrograph of a horizontal section through layer IV of the somatosensory cortex of a juvenile rat that has been stained with serotonin. The dark immunoreactive patches correspond to the cortical representations of specific parts of the body. The largest part of the cortical map is devoted to the face representation (whiskers, nose, and lower jaw). (B) Enlarged view of the whisker representation. Neurons that receive projections from the whisker fields are arranged in discrete circular units called *barrels*. Each barrel is most responsive to a single whisker. (C) Coronal section through the rat somatosensory cortex. The barrels form dense patches localized to layer IV of the cortex. (D) The topographic arrangement of the barrels in the cortex corresponds to the spatial arrangement of the whiskers in discrete rows and columns on the face. (Figure I-48 from Kandel et al., 2000)[1154]

23) Microfluidics Meets Neuroscience, and Beyond

The broad array of microfluidic unit operations in existence, provides many unique opportunities to study scientific phenomena in a microchip format. Microfluidic devices have been used to examine scientific phenomena in fields as far ranging as agriculture / food science,[1188-1192] to cancer research,[1193-1200] to infectious disease,[1201-1207] to point-of-care diagnostic devices for developing nations,[1208-1212] and even interplanetary space travel studies.[874, 916, 1213-1215] One area of particular interest for this body of research, is the study of neuroscience using microfluidic device technology.[1063, 1216-1218] Microfluidic devices have been used within the field of neuroscience to study scientific phenomena such as axon guidance,[1219-1223] ion transport in neuronal cells,[1224-1228] axon termination for spinal cord injuries,[1229-1233] neuron physiology using brain slices,[308, 1234-1237] and cell response to neurotoxins.[1238-1242] Figure I-49 illustrates one example of a microfluidic device applied within a neuroscience context.[1243] This microfluidic device was designed to incorporate a chip-based pixel sensor array, for high spatio-temporal resolution electrophysiological recordings from single, and large scale neuronal networks.[1243]

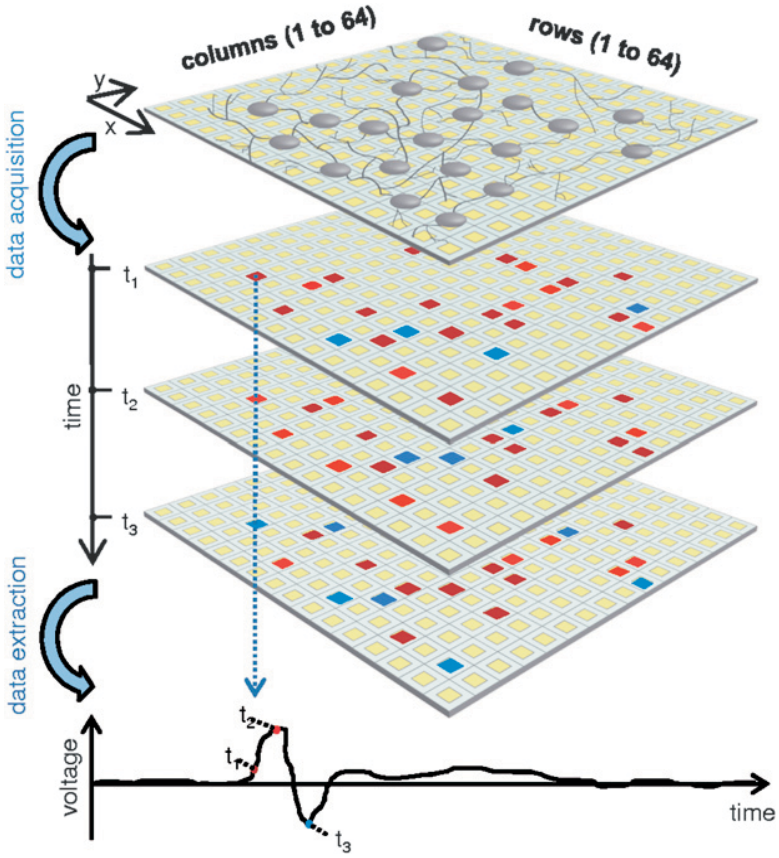

Figure I-49: Working principle of an *in vitro* neuronal active pixel sensor array platform, for high spatio-temporal resolution electrophysiological recordings. Neurons grow and develop chronically on the high-resolution microelectrode array. Fast acquisition of extracellular electrophysiological signals is performed as a sequence of frames by encoding extracellular voltage signals as pixels data. By using a false color map, this enables the video observation of the overall network activity as well as local activity on the basis of single pixel data. Single microelectrode raw data is reconstructed by combining single pixel data from sequential frames. (Figure I-49 from Berdondini et al., 2009)[1243]

Figure I-50 illustrates a second example of a microfluidic device, designed specifically for neuroscience applications.[1244] This device was used to sample *in vivo* rodent brain neurochemistry using a microdialysis probe. The design also incorporated a microfluidic droplet generator, a sample injector, and a capillary electrophoresis separation channel. The immiscible plugs generated by the droplet generator eliminated axial dispersion of analytes between plugs, where a temporal resolution of 2 s was reported for this particular microfluidic chip design.[1244]

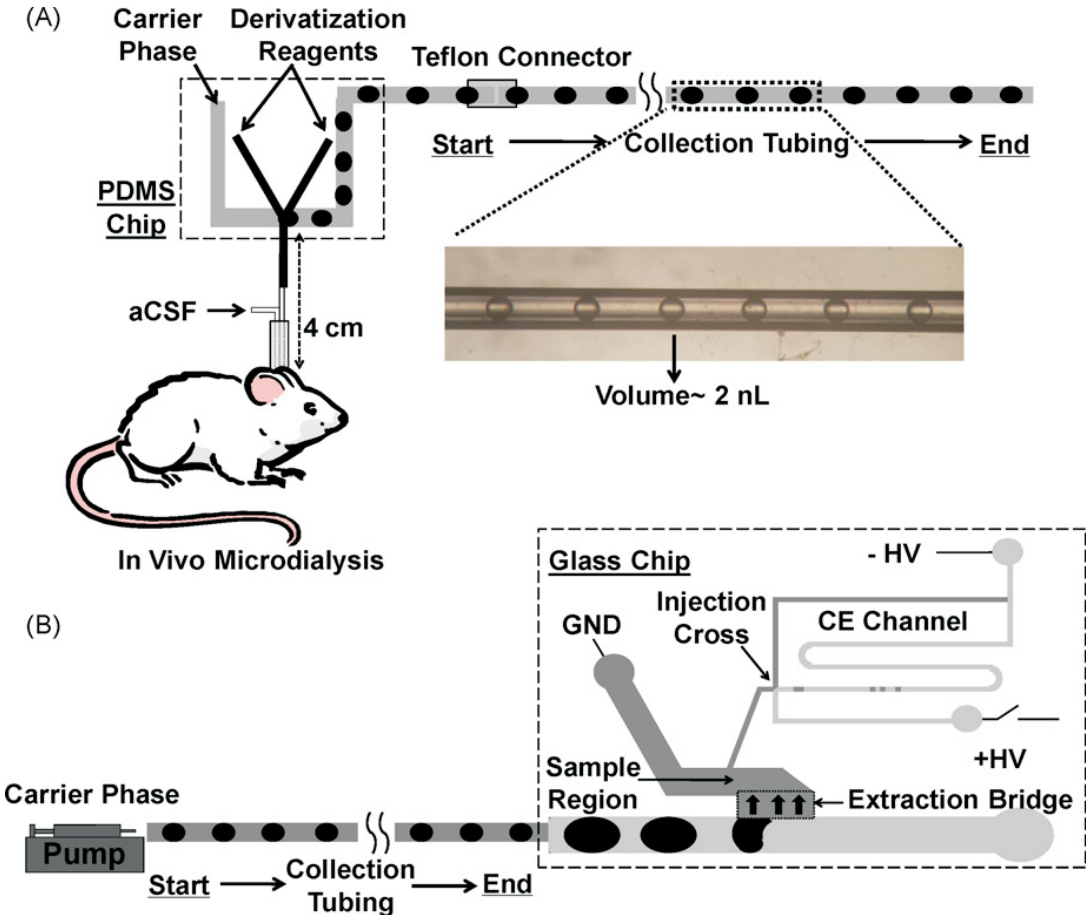

Figure I-50: Operational scheme of off-line capillary electrophoresis (CE)-based *in vivo* sensing using plugs as fraction collector. (A) *In vivo* dialysate is derivatized on-line and stored in collection tubing. (B) Plugs in the tubing are pumped to the microfluidic chip for electrophoretic analysis. The inset shows a brightfield picture of sample plugs stored in 150 µm inner diameter (ID) high-purity perfluoroalkoxy (HPFA) tubing. The volume of each plug is about 2 nL. (Figure I-50 from Wang et al., 2010)[1244]

Microfluidics has the potential to impact the future direction of both science and engineering. Very few disciplines in science and engineering can match the comprehensive interdisciplinary nature of microfluidics, where a technologist could be doing chemical engineering, electrical engineering, mechanical engineering, physics, chemistry, biology, and medicine, all at the same time, on a single palm-sized chip. Anywhere small quantities of fluids are of interest, microfluidic platforms should be considered seriously for their potential to solve or augment these scientific initiatives.

Scope of Dissertation

In a very broad and general sense, analytical chemistry could be characterized as the science of identification, and quantification, of small chemical quantities. Analytical chemists rely heavily upon instrumentation and device technology, in their endeavors to contribute to the advancement of fields as far ranging as materials science, archeology, forensics, food science, infectious disease, and neuroscience, just to name a few. The advancement of analytical chemistry typically takes one of two paths. One path is to advance the, "chemistry" side, of analytical chemistry, with the other path advancing the "instrumental" or "device" side, of analytical chemistry. This body of research was primarily devoted towards, the advancement of the latter.

This dissertation will present a body of research data for the design, fabrication, and characterization of a microfluidic device, for use in direct-sampling neuroscience experiments. To date, microdialysis remains the primary sampling technique, for research endeavors focused on advancing humanities basic science understanding of *in vivo* brain neurochemical dynamics. Other secondary techniques such as fast scanning cyclic voltammetry, are also widely reported within the neuroscience research literature. Very few research labs around the world utilize direct-sampling probe technology, to study *in vivo* brain science. Therefore, this technique is not well characterized. Very little precedence is available for researchers to rely upon, in considering this technique as an option, to study the chemical dynamics within a living, and fully functional brain.

One likely reason direct-sampling is not widely employed within neuroscience laboratories around the world, is due to the very specialized instrumentation required of

the technique, in addition to the very stringent performance demands placed upon the highly specialized instruments. Direct-sampling probes must extract cerebral spinal fluid (CSF) from a rodent's brain, where it is noted a rat's brain measures at most 1.5 cm in length, for any direction taken across the brain. The small volume rodent brain is primarily composed of tissue mass, in turn leaving very small quantities of CSF that are available for extraction, and subsequent chemical analysis. Therefore, the most obvious constraint of direct-sampling probe technology, is the requirement of a device to perform with very low flow rates, when extracting CSF from a rodent's brain. Direct-sampling device technology is expected to perform with flow rates on the order of sub-50 nL/min. To put this flow rate into perspective, it would take 69.4 days to create a 1 mL droplet of water, using a flow rate of 10 nL/min. The same 1 mL droplet of water could be created in a total of 13.8 days, using a flow rate corresponding to 50 nL/min.

A second major requirement expected of the direct-sampling fluidic extraction device, is the ability to work against very large backpressures. The tortuosity existing throughout a mammal's brain creates many small flow paths/channels (i.e. extracellular gaps between brain cells), where CSF is available for extraction.[1245-1254] A very high resistance is associated with transport of fluids throughout very small conduits, where as a baseline reference, the hydraulic resistance for laminar flow through a rigid straight pipe with circular cross-sectional geometry, scales as one over the fourth power of the pipes radius, and further, it is generally estimated the extracellular gap distance between brain cells, is approximately 20 nm.[1245] Therefore, the brains tortuosity leaves a very high inherent resistive threshold that must be surmounted, if the fluidic extraction device

is to be successful in transporting CSF from a rodent's brain, to a chemical analysis instrument. A physical representation of a brains inherent tortuosity can be referenced within Figure I-51.[1255] The top image illustrates the small flow channels that exist between brain cells of a healthy brain, and therefore represents normal tortuosity. The bottom image represents a proposed hypothesis, where an increase in tortuosity is proposed when the brain is affected by a pathological condition such as ischemia. An increase in tortuosity is produced when a decrease in gap distance between adjacent brain cells occurs, with this effect also producing an increase in flow resistance through these brain cell gap regions.

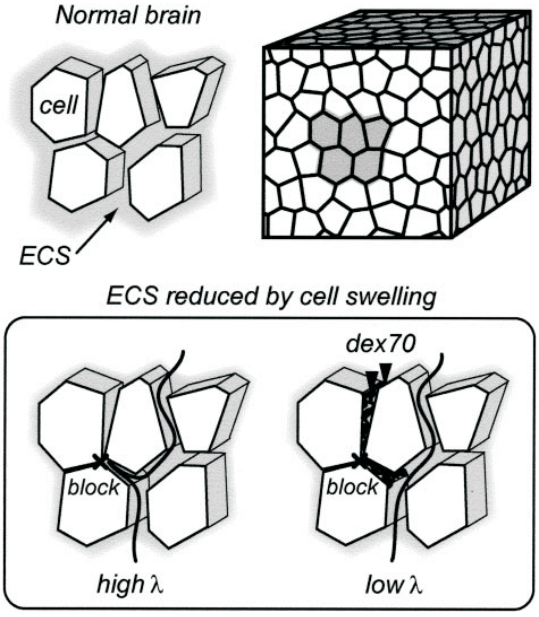

Figure I-51: Background macromolecules exclude dead-space diffusion: a hypothesis. Brain tissue is composed of cells surrounded by a thin layer of extracellular space (ECS). Because the interstitial spaces are interconnected, they form a system of channels where signaling molecules and substances diffuse (top image). During ischemia and other pathological conditions, cellular elements expand their volume as water moves from the extracellular to the cellular compartment, and blockages are formed in some interstitial planes. Diffusing molecules that enter these pocket-like regions are delayed and tortuosity increases (bottom left image). When background macromolecules, such as dex70, are added to this tissue, they become trapped in the dead spaces. By excluding the dead-space volume, dex70 prevents marker molecules from being delayed there, and tortuosity decreases (bottom right image). (Figure I-51 from Hrabetova et al., 2003)[1255]

Other critical requirements demanded of the fluidic extraction device are; very low dead volumes, biocompatibility, highly inert activity towards CSF, capability of being integrated in-line with modern analytical instrumentation, and a device with operational performance that is adjustable, highly stable, and reproducible. A device that meets all of the above requirements, would ideally allow a neuroscientist to obtain and analyze neurochemical information with both high spatial and temporal resolution. The device in every regard, *must*, perform as an analytical instrument, for the direct-sampling methodology to be considered a viable, and competitive brain sampling technique.

A microfluidic pump was chosen as the analytical device, to perform direct CSF sample extraction from the brain of an anesthetized rodent. The general design concept of the micropump can be seen within Figure I-52. This micropump was formed in-part by molding prepolymer polydimethylsiloxane (PDMS) against a template. This mold produced the micropump microchannel. Two capillary tube interconnects were placed partially within the microchannel, with subsequent bonding of a featureless layer of PDMS to seal the inlaid capillary tubes and microchannel, from exposure to the atmosphere. Piezoelectric cantilevers with precision machined external valves were employed as actuators. The cantilevers were driven with external electronic hardware, such that a peristaltic wave motion was created across the microchannel, in driving fluidic contents through the micropump, in the forward bias direction.

Micropump

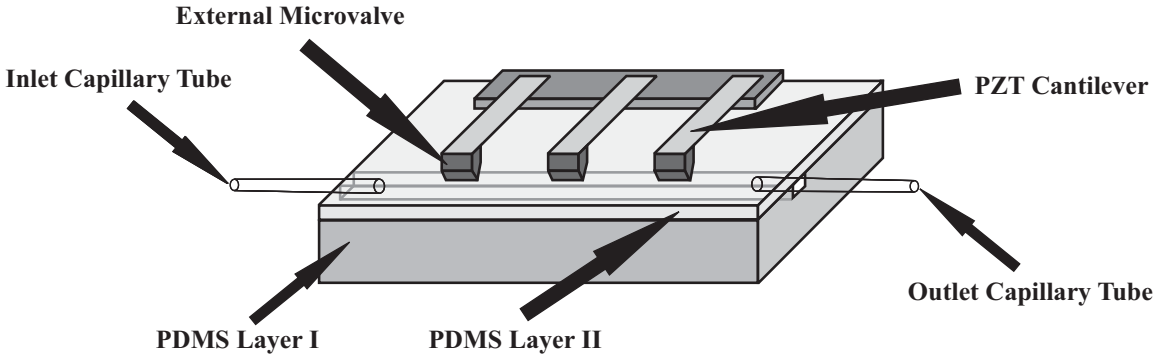

Figure I-52: Generalized micropump cartoon. The micropump cartoon illustrates the primary components of: two bonded PDMS layers, an inlet and outlet capillary tube, and piezoelectric cantilevers with precision machined external microvalves attached to each cantilever tip. (Figure I-52 adapted from M.T. Bowser, 2007).

The direct-sampling methodology is depicted within Figure I-53. The direct-sampling probe corresponds to the micropump inlet capillary tube interconnect. It is possible to chemically analyze neurotransmitter concentrations within CSF, when the micropump is connected in-line with a CE-LIF instrument. The electropherogram as shown, allows an analytical chemist/neuroscientist to correlate neurotransmitter release events within the rodent's brain, to various experimental stimuli induced over a specified period of time.

Direct-Sampling Methodology

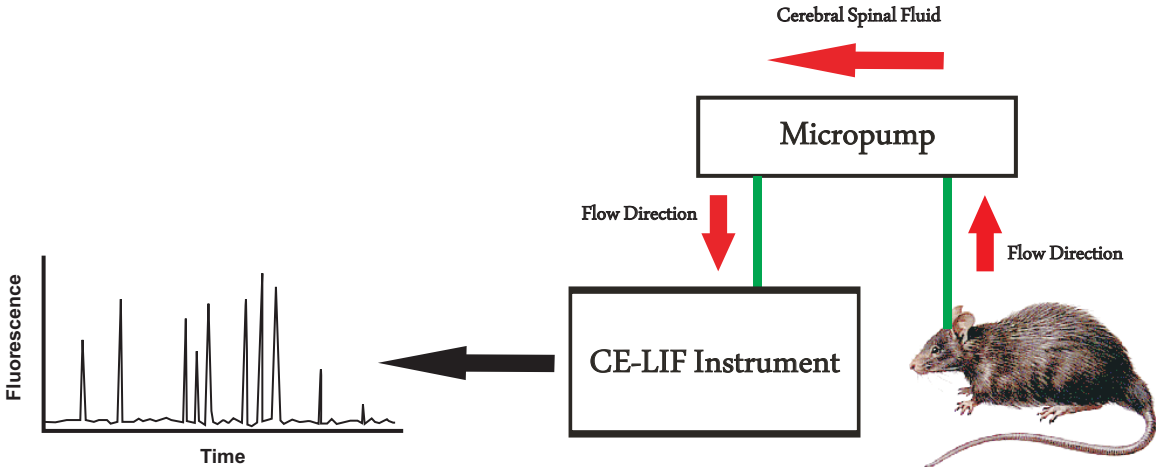

Figure I-53: Direct-sampling methodology. Schematic illustrates the process of directly extracting cerebral spinal fluid (CSF) from the brain of an anesthetized rodent, for subsequent CE-LIF neurochemical analysis.

The micropump as presented within the forthcoming Chapters, employed capillary tube interconnects with sizes of 105 / 40 µm (outer diameter / inner diameter). A reasonable estimate, of the average diameter for a single filament of human hair, is taken as 100 µm. Therefore the 40 µm inner diameter sampling area of the inlet capillary tube interconnect, is less than one half the average diameter of a single filament of human hair. In contrast, microdialysis probes have typical sampling area dimensions of, 4 mm x 1 mm (L x W). Contrasting the difference in sampling area of a direct-sampling probe, to that of a microdialysis probe, it is recognized the spatial resolution of a direct-sampling probe is improved over 5000-fold, compared to that of a microdialysis probe. The difference in sampling areas, when considered for a 2D diagram, can be seen within Figure I-54.[1256] The small dot would correspond to the 2D sampling area of a

direct-sampling probe with dimensions of 105 / 40 µm (outer diameter / inner diameter), with the large rectangular box corresponding to the 2D sampling area of a microdialysis probe with dimensions of 4 mm x 1 mm (L x W). The significant improvement in spatial resolution for a direct-sampling probe is clearly, indisputable.

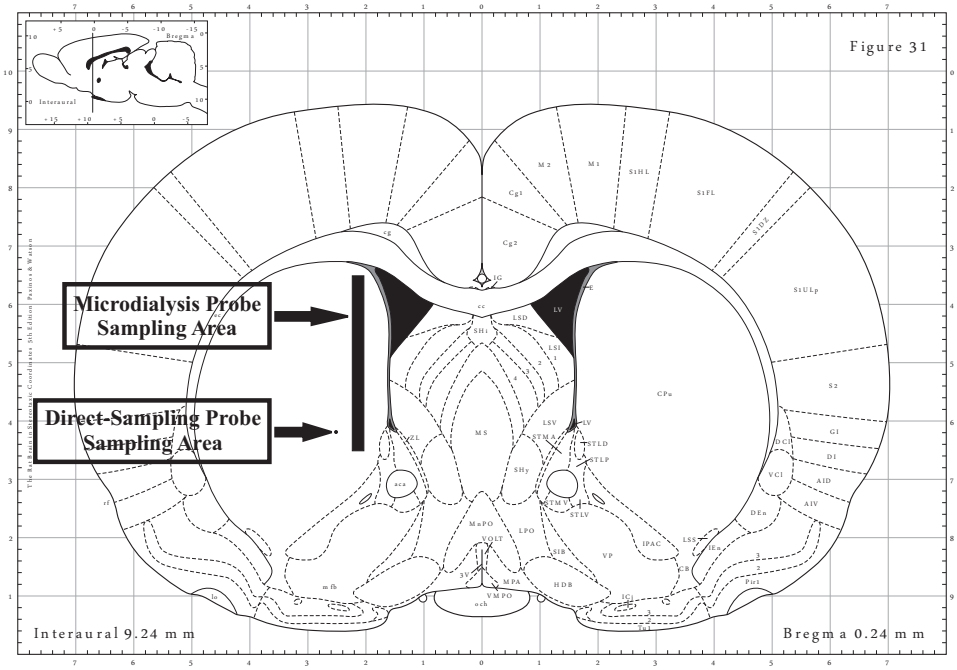

Figure I-54: Schematic to compare and contrast the difference in 2D spatial resolution of a microdialysis probe, to that of a direct-sampling probe. (Figure I-54 adapted from Paxinos and Watson, 2005)[1256]

The forthcoming Chapters, will present results as they pertain to the design, fabrication, and characterization of the micropump. The micropump in every regard performs as an analytical instrument, and therefore was characterized as such. The micropump metes and bounds were discovered through numerous detailed, and thorough characterization experiments. This detailed assessment was necessary to ensure future micropump success, when integrated as an analytical microfluidic add-on attachment

device, to an already existing CE-LIF instrument. The results that follow will allow an analytical chemist/neuroscientist to streamline and focus his/her efforts, towards the advancement of brain science studies. Future directions, along with preliminary pilot study direct-sampling data will be provided within Chapter IX.

Chapter II : *A Soft-Polymer Piezoelectric Bimorph Cantilever-Actuated Peristaltic Micropump*

Synopsis

A peristaltic micropump was fabricated and characterized. The micropump was fabricated using soft lithography, and actuated using piezoelectric bimorph cantilevers. The micropump channel was formed by bonding two layers of PDMS, mixed at 5 : 1 and 30 : 1 ratios. The channel was fabricated in the 5 : 1 layer using replica molding (REM), where a very simple and inexpensive template was made by straddling a 75 μm wire over a glass substrate, followed by covering and smoothing over the wire with a piece of aluminum foil. Not only was this template inexpensive and extremely simple to fabricate, it also created a rounded cross-sectional geometry which is favorable for complete valve shutoff. The cantilevers were driven at $V_p = \pm 90$ V with amplified square wave signals generated by a virtual function generator created in LabVIEW. Connections to the micropump were made by placing capillary tubes in the channel, and then sealed between the two layers of PDMS. Machined aluminum clamps were adhered to the tips of the cantilevers with general purpose adhesive. These clamps allowed for aluminum valves, with finely machined tips of dimensions 3 mm by 200 μm, to be held firmly in place. The variables characterized for this micropump were flow rate, maximum attainable backpressure, free cantilever deflection, valve shutoff, and valve leakage. Three actuation patterns with phase differences of 60º, 90º, and 120º were compared for flow rate and maximum backpressure. It was determined that the 120º signal outperformed the 60º and 90º signals for both maximum flow rate and maximum attainable backpressure. The maximum and minimum flow rates demonstrated by the micropump were 289 nL/min and 53 nL/min, respectively. The maximum backpressure

attained was 35,300 Pa. It was also demonstrated that the valves fully closed the channels upon actuation, with minimal observed leakage.

Introduction

An important aspect in the design of any microfluidic device is the method used to transport fluids through the devices internal conduits. Micropumps are commonly used for this purpose. Micropumps in the literature have generally been classified according to one of two schemes. The first is to classify a pump as either mechanical or non-mechanical (i.e. with or without moving parts).[2, 619] The more recently suggested method is to classify pumps as either displacement or dynamic.[609] Displacement pumps exert pressure forces on working fluids through one or more moving boundaries, where dynamic pumps continuously add energy to a working fluid in a manner that increases either its momentum or its pressure directly.[609] The majority of micropumps in the literature fall into the displacement category, where the moving boundary is a reciprocating diaphragm. Deflection of these pump diaphragms has been accomplished using many different types of actuators including pneumatic,[283, 628] thermopneumatic,[673, 1257] electrostatic,[684, 1258] electromagnetic,[659, 660] shape-memory alloy,[679] and piezoelectric.[1259, 1260] The choice of which actuation method to use in displacement and dynamic pumps depends on many variables including the working solution, size, power consumption, flow rate, frequency, and backpressure needs. The reader is referred to several excellent references that describe the pros and cons of each actuation principle for state-of-the-art micropump technology.[2, 608, 609, 616, 617, 619]

One relatively unexplored actuation method for soft polymer-based micropumps

is the use of piezoelectric materials. Piezoelectricity is a physical phenomena where a material will produce an electric charge when stressed mechanically, or produce a dimensional change when stressed electrically with a voltage.[1261] These materials are widely used for many sensing and actuator applications. The most common piezoelectric elements used for micropump applications are either rectangular bimorph (two-layers of piezoelectric material) cantilever beams or circular discs, both being made from a ceramic compound called PZT (lead zirconate titanate). Dimensions for these actuators vary depending on performance requirements, but can be as large as several centimeters for microdevice applications. One or more disks or cantilevers can be used to actuate a diaphragm. A single cantilever or disc is often used with check valve pumps, where the valves are passive and respond to pressure changes within the pump chamber. In other designs, piezoelectric elements can be combined in series to form peristaltic pumps. The series configuration of actuators in effect creates a pump with multiple chambers. By actuating the piezoelectric elements in series, a wavelike motion is created that propels solution with a net motion in one direction.

For the work presented within this Chapter, a peristaltic micropump was fabricated from PDMS and glass using soft lithography. A novel method was used to fabricate a simple, quick, and inexpensive template for prepolymer molding. This method also produces a cross sectional geometry that is favorable for increased device performance. Actuation of the micropump was performed using piezoelectric cantilevers. Aluminum clamps were adhered to the tips of the cantilevers, to hold precisely machined aluminum masses in place that served as valves for the micropump. Strict control of

registration for the valves over the channel was made possible with the aid of in-house manufactured micropositioners. The performance variables characterized for this micropump were flow rate, valve closure, valve leakage, and maximum backpressure.

Experimental Methods

1) Micropump Design

The peristaltic micropump, valves, and valve clamps are shown in Figure II-1A–C. The micropump is composed of a PDMS channel layer placed on a glass substrate, as shown in Figure II-1C. Three piezoelectric cantilevers are mounted on anodized aluminum micropositioners that allow for individual control of the horizontal and vertical position as well as the tilt of the valve tips. Adhered to the ends of the cantilevers are aluminum clamps that hold aluminum valve tips in place, with the valve tips used to control the open and closed states of the microchannel. A close up view of the clamps and valves can be seen in Figure II-1B, and a cross sectional schematic of the valve tips can be seen in Figure II-1A.

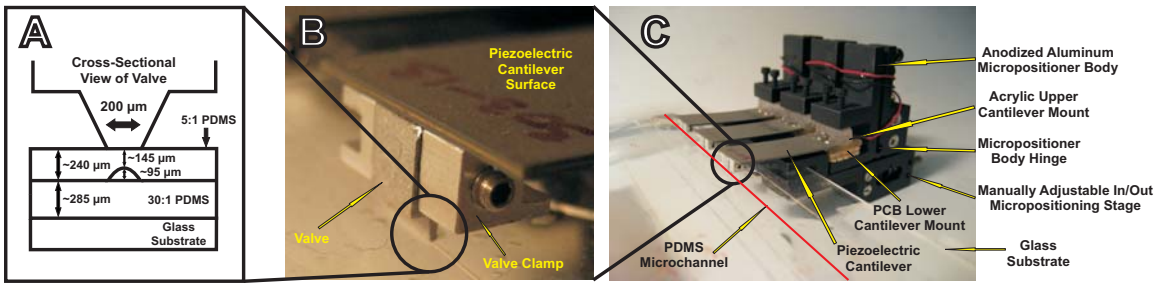

Figure II-1: Image of the micropump, micropositioners, and valves. (A) The cross-sectional geometry of the valve. The width of the microvalves was 200 µm, and the length was 3 mm. (B) A close-up image of the valve clamps used to secure the valves in place. (C) The full micropump design with the micropositioners, piezoelectric cantilevers, and PDMS channel structure on a glass substrate.

2) Micropump Fabrication

A) PDMS Channel and Base Layers

The micropump is composed of a single channel fabricated in PDMS. Fabrication begins with the creation of the master template. The template was formed by wrapping a 75 μm wire over a clean glass substrate, where the ends of the wire were adhered to the underside using Scotch tape. A thin layer of general purpose adhesive was then sprayed across the top of the glass surface. Aluminum foil was placed over the glass surface, in effect sandwiching the metal wire between the glass and aluminum foil. The aluminum was then gently smoothed over the wire using finger pressure to remove any air pockets. To complete the process, a square Teflon block with a carved out "C" was used to further smooth the aluminum foil. The narrow edge of the Teflon block was used to press the foil tightly against the covered metal wire.

After the template mask was fabricated, PDMS prepolymer (GE, RTV 615) was mixed in a 5 : 1 ratio and poured over the surface of the mask. Rectangular plastic spacers (~203 μm in height) were placed at the edges of the template to control the PDMS layer thickness. Next, a clean glass wafer was laid onto the mask surface with prepolymer and plastic spacers, to create a "sandwich" of PDMS. Gentle pressure was applied to both mask and glass wafer to extrude excess PDMS. Before heat curing, general laboratory tape was adhered to the top and bottom sandwich substrates to hold the two substrates in place. The PDMS sandwich was cured in a convection oven at 80º C for one or more hours. The 5 : 1 ratio yields a relatively firm PDMS layer that accurately reproduces the rounded shape of the template and is resistant to damage when

compressed by the metal tip of the actuator.

Fabrication of the second PDMS layer was similar. Prior to mixing the second layers prepolymer PDMS at a 30 : 1 ratio, two clean glass wafers were placed in a desiccator with tridecafluorooctyltrichlorosilane vapor (United Chemical Technologies, model T2492) for 1–2 h to reduce adhesion of the PDMS to the glass substrates. After removing the wafers from the desiccator, plastic spacers measuring ~203 μm were placed on one of the glass substrates to control the PDMS layers thickness. The 30 : 1 PDMS prepolymer was then poured over the glass surface, with subsequent addition of the second glass substrate to sandwich the 30 : 1 PDMS. Gentle pressure was applied to the glass substrates to extrude excess PDMS, and tape adhered to top and bottom glass substrates to hold them in place while curing. A partial cure of the 30 : 1 PDMS was performed in a convection oven for 45 min. The 30 : 1 ratio gives a more flexible, tackier PDMS layer that ensures a good seal with the channel layer.

Fused silica capillary tubing (Polymicro, 105 μm outer diameter/40 μm inner diameter) was used to make connections to the micropump. After separating the fully cured 5 : 1 wire molded PDMS sandwich, two ~30 cm long pieces of capillary tubing were placed approximately 1.5 cm into the PDMS channel. When the capillary tubes were properly aligned, a fresh 5 : 1 PDMS mixture was placed along the capillary tube in the channel to seal the void areas between the channel and tubing. At this point the partially cured 30 : 1 sandwich was separated and placed over the 5 : 1 layer with the capillary tubes in place. A heat cure was performed at 80º C for one or more hours to irreversibly bond the two layers. After removal of the sealed PDMS channel from the

convection oven, another fresh mixture of 5 : 1 PDMS was applied to the outer regions where the capillary tubes exited the PDMS, and cured again at 80º C for one or more hours. The 30 : 1 layer served as the base layer, where the 5 : 1 layer with the wire replica molded channel served as the membrane for the micropump. The membrane at its thinnest point measured ~140–145 μm.

B) Valves and Valve Clamps

Aluminum valve clamps were adhered to the tips of the piezoelectric cantilevers (see Figure II-1B). The valves for the piezoelectric cantilevers were fabricated from rectangular aluminum blocks using an electrical discharge machine (EDM). At one end of the blocks was a finely machined protruding structure (see Figure II-1A), with a cross sectional geometry resembling that of an obelisk. The protruding structures served as the valve tips that made contact with the PDMS membrane surface. The PDMS contact area of the valve tips were machined with a length and width of 3 mm and 200 μm, respectively.

C) Cantilevers, Stabilizer Blocks, and Micropositioners

Piezoelectric cantilevers were purchased from Piezo Systems (Q220-A4–303YB). This model cantilever comes with the PZT actuator bonded to a general quick mount system, with prewired electrical connections. In order to mount the cantilevers into the micropositioners and protect the cantilevers from being damaged, approximately 12 mm x 6 mm x 3.5 mm (L x W x H) acrylic blocks were hand machined and adhered to the top

of the quick mounts. Printed circuit board (PCB) material was hand machined and bonded to the bottom of the quick mount cantilevers. Both PCB and acrylic mounts were bonded to the quick mounts with a general purpose silicone adhesive (see Figure II-1C).

Micropositioners that allowed for adjustment of the valve position were fabricated in the Electrical Engineering Machine Shop at the University of Minnesota. Hand-turned adjustments were made possible with two manual micropositioning stages (Edmond Scientific, #56–416) and one metal hinge. The design of the micropositioners allowed for adjustments to be made horizontally (in/out), vertically (up/down), and tilt (up/down). The bulk material of the micropositioners was aluminum, where the aluminum was anodized to prevent any potential arcing from the cantilevers to the micropositioners. Metal screws were used to hold the cantilevers in place, where plastic screws were used to hold the micropositioners to the glass substrate where the PDMS channel resided. The micropositioners with the cantilevers and mounts can be seen in Figure II-1C.

D) Software and Hardware

A virtual function generator was created using National Instruments software and a data acquisition card (PCI-6259). The function generator had controls for signal type, frequency, amplitude, and phase adjustments. Three channels with individual phase adjustment were necessary to deliver signals to the cantilevers that would create a peristaltic motion. Actuation signals with phase differences of 60º, 90º, and 120º were compared with respect to flow rate and maximum attainable backpressure. Figure II-2 illustrates the three valve sequences for the 60º, 90º, and 120º signals. In-house

electronic hardware was fabricated to drive the piezoelectric cantilever actuators. High voltage amplifiers (Apex Microtechnology, PA15A) were used to amplify square waves generated by the virtual function generator to V_p = ±90 V, which was the maximum allowable driving potential for the cantilevers.

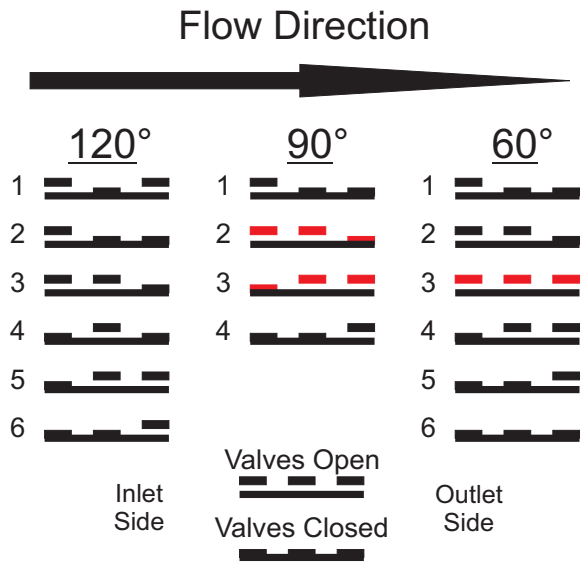

Figure II-2: Signal sequence for peristaltic micropump valves. Three unique square wave signal sequences are possible by varying the phase of the signal sent to each of the cantilever actuators. These three signal sequences can be referred to with respect to their phase variations of 120º, 90º, and 60º.

3) Characterization Experiments

E) Valve Alignment

With the cantilevers connected to the micropositioners, and the micropositioners connected to the glass substrate containing the PDMS channel, the valves were aligned over the channel using a microscope. The valves were aligned such that they were directly over the channel membrane, so that when actuated in the down position, the

channel was completely closed off from fluid flow in either direction. Valves not completely closing off flow (i.e. not 100%) were easily spotted using either fluorescence detection under the valves, or by observing cavitation, where bubbles would form in the channel under or adjacent to the valve.

F) Flow Rate

Flow rates were characterized by tracking the linear flow velocities of a small bubble introduced into the outlet line of the micropump, using distilled water as the working solution. Tracking the bubbles velocity over time allowed for a flow rate to be calculated using the formula $Q = Av$, where Q = flow rate, A = the cross sectional area of the flow, and v = linear flow velocity. The flow rate was characterized for signals with phase differences of 60º, 90º, and 120º. The standard errors were calculated and plotted as error bars for each set (n=4) of flow rate measurements taken at each frequency.

G) Maximum Backpressure

Backpressure measurements were taken by connecting the micropump outlet to an electronic pressure sensor (Honeywell, 40PC015G2A), that previously had its internal cavity completely filled with distilled water. The micropump was actuated to flow solution towards the pressure transducer. The pressure was monitored over time until a stable reading was obtained. The maximum attainable backpressure was characterized for actuation sequences with phase differences of 60º, 90º, and 120º.

H) Valve Deflection and Valve Shutoff Cycle

Valve deflection was measured by placing a micropositioner on its side and recording the no-load displacement of the valve at 30 V intervals from -90 V to 90 V. Displacement values were recorded using a microscope with an embedded optical reticle placed in the eyepiece of the microscope.

Valve shutoff data was collected independently from the valve deflection measurements. The collection of valve shutoff data began by placing the micropump in an inverted position, so that the PDMS channel under the valves was visible through an epifluorescence microscope. A working solution was flowed through the micropump using a syringe pump. After stopping the syringe pump, the solution was allowed to dissipate from the micropumps outlet for 30 s, where after this time, the outlet was capped off to prevent any further loss of solution. Intensity values were recorded for both distilled water and a 1 mM fluorescein solution, where these data were collected at 30 V intervals from -90 V to 90 V using a CCD camera. The background signal for the distilled water was subtracted from the fluorescein signal, where quantification of the signal intensities was performed using Metavue software.

I) Valve Leakage

Experiments to measure valve leakage began by filling the micropump with distilled water using a syringe pump. After the microchannel was filled, the inlet of the micropump was disconnected from the syringe pump and placed into a water-filled reservoir. The pump outlet was then connected to a pressure sensor that had been

previously filled with distilled water. The pump was operated at 40 Hz with a 120º signal, until the pressure stabilized at its maximum attainable value. After the backpressure stabilized, actuation of the cantilevers was stopped and the inlet of the micropump was removed from the reservoir, and laid on a flat surface. The cantilevers were then individually actuated with dc signals, so that two valves were in the open position, while one remained closed. Pressure measurements were recorded for 10 min with one valve closed, to examine pressure loss in the system. After the 10 min observation period, the pressure drop was recorded as the closed valve was opened.

Results and Discussion

4) Micropump Design

J) Peristaltic Design

Peristaltic pumps have several inherent advantages over other pump designs. Unlike micropumps that utilize check valve designs, peristaltic pumps usually involve a simpler design and fabrication process. For example, the micropump described for this work requires only one simple template, and no photolithography mask for fabrication of the PDMS channel, where other pumps made from PDMS require two or more templates and photolithographic masks.[105, 283] Devices that require two or more masks for fabrication can also have a difficult and/or complicated registration process for aligning multiple layers of PDMS.[105] Two other favorable design aspects for peristaltic pumps with designs similar to the one described within this Chapter are; (1) insensitivity to the working solution, and (2) little or no dead volume associated with the valving region.

K) Piezoelectric Actuation and Cantilever Valves

Piezoelectric actuation is a well-suited method for many micropump designs. This method of actuation has been widely utilized with glass and silicon-fabricated micropumps, but has remained a relatively unexplored actuation method for soft polymer-based micropumps. Compared to other external micropump actuators, piezoelectric actuators made from PZT can generate some of the largest actuation forces. PZT actuators also have some of the fastest response times, and are not limited to external on/off switching equipment like many pneumatic designs. Deflection displacement can be very large in comparison to other actuation methods, where less than 100 μm of free deflection is typical. Theoretical displacement values for the cantilevers used in this work is 630 μm.[1261] Lastly, external actuators like piezoelectric cantilevers allow for a partially disposable device design, where the actuators can be used repeatedly for disposable PDMS fabricated microchannel structures.

In spite of the many advantages piezoelectric actuators possess, this method of actuation, like that of all other methods, is not ideal in every way. The biggest disadvantage of using external piezoelectric actuators is their physical size. This property does not allow for an extremely high density of addressable valves like that of some pneumatic designs.[628, 945] The up-front design work in using piezoelectric actuators is also likely more complex and costly than most pneumatic designs, when in-house micropositioners are utilized for valve alignment. While it is possible to utilize primitive fixed-in-place clamping methods for valve alignment, it is highly advantageous to use micropositioning devices. Once fabricated, micropositioner devices have the advantages

of being reusable, and highly reproducible. Registration of valves over microchannels is also very quick and effortless. This may not always be the case with pneumatic designs, where alignment of a second PDMS valving layer over PDMS flow channel is required. Both the micropositioners and the precision-machined valves for this pump can provide the user with flexible options to modify the flow and valving characteristics of the pump. Only one valve-tip dimension was used for this micropump, however it is possible to fabricate other valves with different dimensions to tailor a micropumps flow and valving conditions to any specific device.

5) Fabrication

L) Replica Molding (REM) Template

The most common method for fabricating mask templates for the purpose of replica molding is to use soft lithography rapid prototyping methods.[274] This process creates a mylar mask using computer-aided drafting (CAD) software and high resolution printers. Typically, the mylar mask is used in a cleanroom, where photolithography is performed for creation of bas-relief structures. The use of cleanroom equipment can be expensive, and also requires the user to develop photolithography processing protocols. However, creation of master templates using photolithography has the advantage of allowing for complex and dense structures to be patterned.

In certain instances where simple structures such as long channels or flow crosses are needed for replica molding, it may not always be necessary to use clean-room equipment for template creation.[365, 887, 1262] This was the case for this work. Template

creation required very inexpensive and accessible supplies such as aluminum foil, glass, general purpose adhesive, small-gauge wire, and a soft plastic material such as Teflon. The simple nature of the template design eliminated the need for use of CAD software. While the method used for template creation in this work is limited to fabrication of simpler structures, it still has the advantages of being considerably faster, easier, and cheaper than using photolithography equipment in a cleanroom. It is conceivable this aluminum foil-wire template process could also be automated, as a result of the very simple template designs. Machines could use CAD file designs to lay wire down onto an adhesive surface, where the aluminum foil could be vacuum sealed over the wire. Another possibility would be to use the aluminum foil-wire template process in mix-and-match lithography. Complex design layers could be fabricated using templates created from traditional photolithography masks, where the simpler design layers could be created from templates fabricated using the aluminum foil-wire template process.

One last advantage of the template fabrication process described for this work has to do with the cross-sectional geometry of the channel. The rounded channel geometry produced for this work can be seen in Figure II-3. It has been shown that a rounded channel geometry is favorable for valving processes on microfluidic chips.[283] It is also common to find other applications that benefit from creation of microstructures with a rounded profile.[303, 1099, 1263]

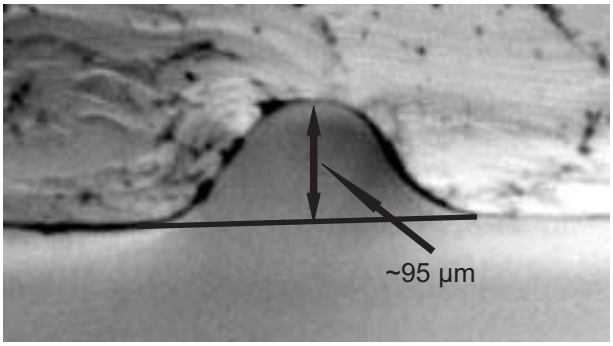

Figure II-3: Cross-sectional image illustrating the PDMS channel geometry. A smoothly rounded channel is produced using the aluminum foil/wire molding process.

6) Flow Rate

The effect of actuation frequency on flow rate is shown in Figure II-4. Actuation signals varying in phase by 60º, 90º, or 120º are also compared. All three curves demonstrate an initial sharp increase in flow rate, followed by a frequency range where flow rates increase linearly, and then either start to drop off (120º & 60º) or continue to increase slowly (90º). The overall trend in the magnitude of flow rates (120º > 90º > 60º) can be explained with a closer examination of Figure II-2. For the 120º signal, there is no point throughout the actuation cycle where at least one valve is not completely closed. For the 90º signal, as pressure builds at the outlet, backflow can occur between steps 2 and 3 when the outer valves change from open to closed, and closed to open, respectively. The situation is even more extreme in the 60º pattern, where in step 3 all three valves are open, allowing for complete backflow from outlet to inlet as pressure builds on the outlet side of the pump.

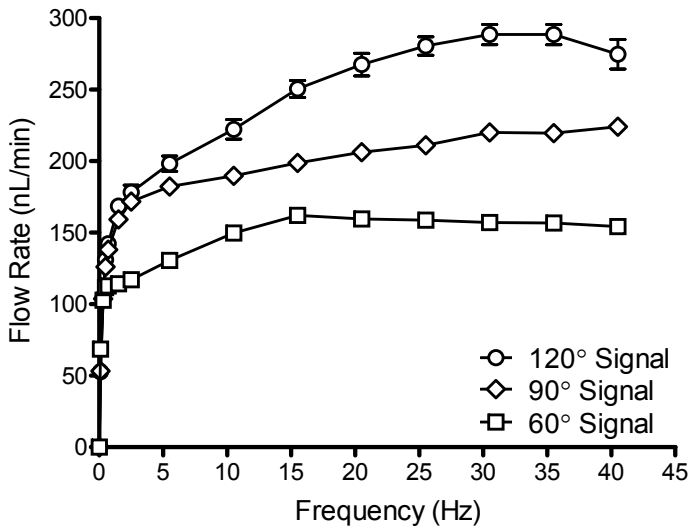

Figure II-4: Effect of actuation frequency on flow rate generated by the micropump. Actuation signals with 120º, 90º, and 60º phases were compared. Flow rate was measured by tracking the linear velocity of a small bubble introduced into the capillary attached to the micropump outlet. Error bars are the standard error of the mean (n = 4).

The largest range of flow rates was observed for the 120º signal, which varied from 53–289 nL/min (0.1–35 Hz). The ranges for the 90º and 60º signals were 53–224 nL/min (0.1–40 Hz) and 69–162 nL/min (0.1–15 Hz), respectively. Regions of each flow curve yielded very linear data. The 120º signal was linear from 2–20 Hz (178–268 nL/min), with an R^2 value of 0.9913. The 90º signal was linear from 5–30 Hz (182–220 nL/min) with R^2 = 0.9943. And lastly, the 60º signal was linear from 0.7–10 Hz (113–150 nL/min) with R^2 = 0.9962. The stability and reproducibility of these flow rate data makes this pump an ideal candidate for applications that require microdosing or microinjecting functions. The large range of frequency operation also allows users to more easily fine-tune desired flow rates, as opposed to other actuation methods such as thermopneumatic designs, where frequency of operation is limited to only a few Hertz. While no data were collected for flow in the opposite direction, the

micropump was tested, and easily reverses flow simply by inverting the signal sequence delivered to the cantilevers.

Flow rate data for each signal pattern were only collected up to 40 Hz. Above 40 Hz, the micropositioners had a tendency to vibrate out of place, moving the valves out of alignment over the channel. At frequencies higher than 40 Hz, flow rates decreased. Using a microscope, cross-sectional examination of the micropump cantilevers with a PDMS channel under the valves, reveals a sharp decrease in amplitude from 50–52 Hz. These data suggest that there is a physical response time limitation of the cantilevers themselves to fully respond to the input signals. However, this explanation cannot account for the flow rate data between 40 and 50 Hz, where flow rates start to decrease. A possible explanation would be that there is another response time limitation associated with the PDMS membrane, where above 40 Hz the membrane below the valve is not able to fully relax before the valve recloses the channel. The observation of cantilever deflection with PDMS channels below the valves also indicates that possible resonant frequencies exist at 33, 36, and 49 Hz.

7) Valve Deflection and Valve Shutoff Cycle

Valve performance in any pump is very important. Valves must reliably block backflow, as even the smallest amount of leakage could detrimentally affect device performance. The deflection of the cantilever with zero load was measured, to serve as a comparison to the situation where the cantilever movement was subjected to a load (i.e. closing off the PDMS channel). As shown in Figure II-5A, the cantilevers have an inherent hysteresis associated with their deflection. The data for experiments where a

PDMS channel is placed below the valves are shown in Figure II-5B. The fluorescent signal detected in the channel is nearly zero at voltages less than -30V, supporting the conclusion that the valve fully closes off the channel, impeding flow of channel contents in either direction.

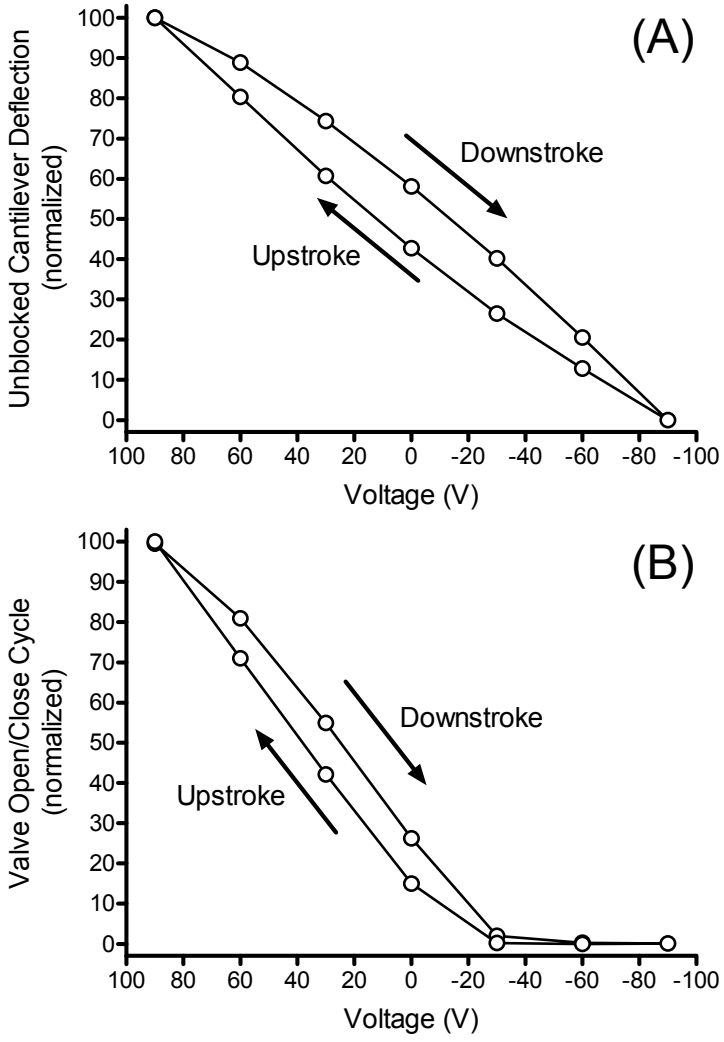

Figure II-5: (A) The deflection of an unblocked cantilever was measured with an optical reticle, by recording its displacement horizontally under a microscope. (B) The microvalve open/close cycle was recorded by filling the micropump with a fluorescein solution using a commercial syringe pump. After filling the micropump, a plug was placed over the outlet line of the micropump, trapping the fluorescein solution inside the micropump channel. Fluorescence intensity was then recorded using an epifluorescence microscope at various points throughout the actuation cycle. The data shown here are from a single representative experiment.

8) Valve Leakage

Another important performance metric for which pumps are evaluated is their valve leakage. The leakage of a valve can be improved by three to four orders of magnitude through the use of soft materials such as PDMS, when compared to devices fabricated in hard materials such as silicon, glass or silicon nitride.[2] The use of PDMS for the channel, combined with the high pressure resulting from the large force generated by the piezoelectric cantilevers, when applied to the small surface area of the valve tips, would be expected to minimize the potential for leakage through the valve when closed. Figure II-6 demonstrates the ability of a single closed valve to effectively seal the channel while under pressure. One valve in the closed position was able to hold a pressure of 36,700 Pa, where only a 2% pressure loss (827 Pa) was observed over ten minutes. It is believed that much of this pressure loss occurred at connections between the outlet of the micropump and the pressure sensor, since no backflow was observed through the valve. After ten minutes the piezoelectric actuator was opened and the rate of pressure loss increased 41-fold as fluid flowed through the open valve.

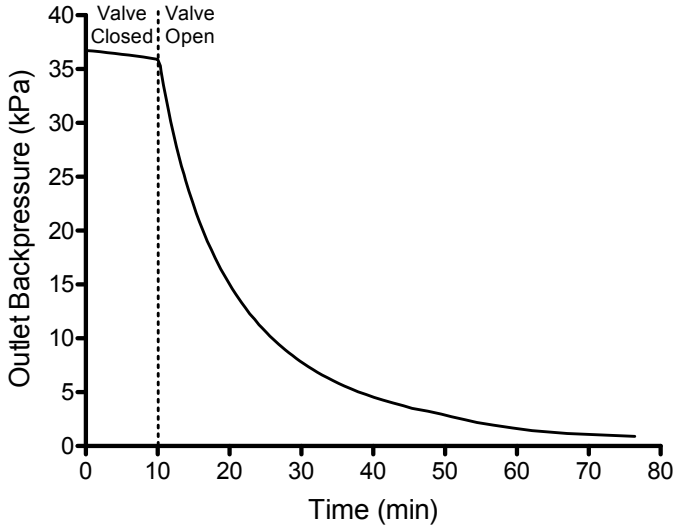

Figure II-6: Micropump valve shutoff/leakage curve. The micropump was allowed to fully pressurize the outlet line connected to a pressure sensor. Actuation was then stopped in a position with a single valve in the fully closed position. Pressure measurements were monitored for ten minutes to monitor leakage through the closed valve. After ten minutes the closed valve was opened and further pressure measurements were obtained for the depressurization of the outlet line. The rate of pressure loss increased 41-fold when the valve was opened. The data shown here are from a single representative experiment.

9) Maximum Attainable Backpressure

As shown within Figure II-7, both the effect of frequency, and the actuation signals phase, were examined for their effect on the micropumps maximum attainable backpressure. It can be observed the backpressure magnitudes followed the trend of; 120º > 90º > 60º for all frequencies. This trend can be explained by the potential for solution backflow when using the 60º and 90º signals, as discussed in the flow rate section above. The overall trend for the 120º and 90º signals was to increase to their maximum values of 35,300 Pa and 28,000 Pa respectively. For the 60º signal, maximum backpressure stabilized at 15 Hz, maintaining a pressure between 19,700 – 20,000 Pa up to 40 Hz. The backpressures this micropump can work against are higher than most previously reported peristaltic micropumps.[2, 609] The large actuation force generated

using external piezoelectric cantilevers, in conjunction with the small contact surface area of the valves with the PDMS membrane, make it possible for the valves to generate very large pressures that are able to fully close even when the valves are working against large backpressures. Subsequent Chapters that follow, will also discuss the effect of the peristaltic signals frequency, amplitude, shape, wavelength, and phase, and the effect these variables have on a micropumps maximum attainable backpressure. The high backpressures this pump can work against make it suitable for *in vivo* drug delivery applications, where it has been reported *in vivo* backpressures can be as high as 25,000 Pa.[609]

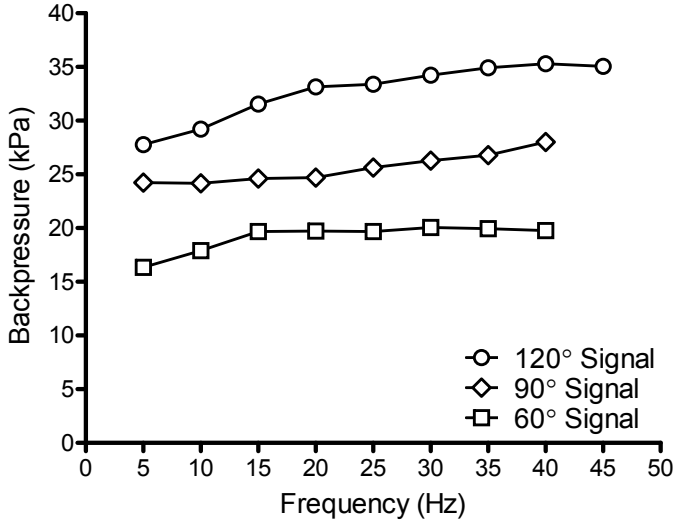

Figure II-7: Effect of actuation frequency on maximum attainable backpressure. Actuation patterns with phase differences of 120º, 90º, and 60º were compared. Backpressure was measured by connecting an electronic pressure sensor to the outlet line of the micropump. The data shown here are from a single representative experiment.

Conclusions

In conclusion, a piezoelectric bimorph cantilever-actuated peristaltic micropump was fabricated using soft lithography. The template fabrication method used for this work was extremely simple, cheap, and generated rounded cross-sectional geometries that are favorable for complete valve shutoff. The performance reported here suggests that this micropump is very robust and suitable for integration into many microfluidic device platforms. Flow rates are very reproducible, where measurements show little standard error at each frequency. Valve data indicate little if any backflow occurs across the valves, even when working against high back pressures. The alignment of the valves was also quick and effortless with the aid of machined micropositioners. The backpressures this micropump can work against show that it falls within the upper tier of what most micropumps are capable of generating. It was also demonstrated that the phase of the actuation signal was very important to overall performance of the micropumps flow rate and maximum attainable backpressure.

Chapter III : *Micropumps Fabricated from PDMS using: 1) SU-8 Replica Molding; 2) a Handheld Micro Injection Molding Apparatus, with Performance Analysis for Rectangular vs. Rounded/Gaussian-Shaped Microchannel Geometries*

Synopsis

The instant Chapter expands upon the previously presented fabrication methods of Chapter II, for realization of a peristaltic micropump with piezoelectric actuators. Two different fabrication methods were employed to fabricate micropumps with different cross-sectional channel geometries. The first was to fabricate rectangular cross-sectional microchannel geometries using the well known fabrication method of replica molding (REM).[271] The second, and far less utilized fabrication technique, was to create microchannel molds using an in-house fabricated handheld micro injection molding apparatus. The injection mold apparatus was designed for use with elastomeric room temperature vulcanization (RTV) polymers, as opposed to most other injection molding machines, which are designed for use with thermoplastic polymers. The injection molds bottom plate was used as a microchannel molding template. The molding template was created by threading a small-diameter wire (150 μm or less) through the injection molds bottom plate, with subsequent adhesion and smoothing of a thin piece of aluminum foil over the wire-raised injection mold template. When molded against, the template produced a rounded/Gaussian-shaped PDMS microchannel. The design of the injection mold will be presented, along with a direct comparison for micropump performance metrics such as flow rate, valving characteristics, and backpressures attainable for each of the respective micropump channel geometries.

Introduction

Microfabrication is at the very core of any microfluidic device, and therefore the pros and cons of any microfabrication technique must be considered carefully when choosing a fabrication methodology. Microfabrication is by no means trivial, and as such, a wide array of techniques and methodologies have been developed for the purpose of creating unique microfluidic device technologies.

Prior to the early 1990's, a time many regard as the beginning of modern microfluidic technology,[23, 873] a large portion of microfluidic devices were fabricated using traditional glass and silicon micromachining methods.[21, 262, 266, 267] Since the early 1990's however, microfluidic device technologies have been fabricated in large part using polymeric fabrication techniques. The most widely reported and characterized of these polymeric fabrication techniques is that of soft lithography.[271] Soft lithography has many attractive benefits such as rapid prototyping, use of well characterized materials such as SU-8 [230, 234, 235, 240, 245, 246, 1264] and PDMS,[108, 109, 1265] the ability to create nonplanar structures from elastomeric materials, and the ability to create micro and nano devices with minimal capital investment.[271, 274] While soft lithography is currently the predominant microfluidic fabrication method reported, other very useful and promising fabrication techniques also exist.[69, 86, 89-91, 277] A short list of other available microfabrication techniques includes embossing/imprinting,[212, 214, 215, 330, 333, 1266] laser machining,[288, 344, 348, 349] electrical discharge machining (EDM),[339, 341, 342] lamination techniques,[363, 365, 368] mechanical milling,[371, 372] 3D object printing,[329] microstereolithography,[359-361] injection molding,[88, 375-377, 379, 395, 397] and hybrid

approaches.[1267-1269]

Injection molding is a fabrication process widely utilized within industry, and often used for mass production purposes. Injection molding machines are capable of producing large quantities of plastic parts, at a minimal cost per molded part. Unlike soft lithography however, there are high initial start-up costs associated with injection molding fabrication methods. The two primary reasons for the high initial start-up costs are the machine/instruments cost, as well as the costly master template that must be fabricated for the injection molding machine.[233] Also in contrast to soft lithography, injection molding machines are primarily designed for use with thermoplastic materials, as opposed to other elastomeric compounds such as PDMS. Therefore, with the wide applicability of both soft lithography and injection molding, it would prove highly useful if technologists had the ability to combine the benefits of both fabrication techniques. Technologists would stand to benefit from an available cost-effective injection molding apparatus, with the capability of producing cost-effective molding templates, and further from the possibility of producing elastomeric PDMS injection molded parts.

A particular fabrication strategy in some cases depends upon variables such as working materials, cost, facilities, and availability of instrumentation. In other cases, the design of the device can be a determining factor in deciding upon which fabrication method to employ. With the high surface area to volume ratio of microfluidic technology, channel size and channel geometry are very important considerations.[435, 439, 440, 1270] Many channel geometries have been reported and characterized for microfluidic devices including rectangular,[440] rounded/bell/Gaussian-shaped,[283, 326, 1271, 1272

circular,[372, 1273, 1274] triangular,[1275, 1276] and arbitrary cross-sectional shaped channel geometries.[439, 1277]

For this Chapter, a cost-effective handheld injection molding apparatus will be presented. The design of the injection molding apparatus allows for a simple and cost-effective template fabrication scheme to be employed. In contrast to most commercial injection molding machines that employ thermoplastics, this injection molding apparatus makes use of PDMS as a working material. The handheld injection molding apparatus is further capable of producing rounded microchannel geometries, which are necessary for complete closure of a microchannel. The performance of these rounded microchannel geometries will also be compared to rectangular microchannel geometries, that were produced using SU-8 fabricated templates, in connection with replica molding procedures.

Experimental Methods

Readers are directed to Chapter II for additional details and information for sections I) through L).

1) Injection Mold Devices

A) Injection Mold Apparatus Fabrication, Parts, and Assembly

The injection mold apparatus as seen in Figure III-1 was fabricated primarily from aluminum (6061 T6) using a Haas (SMINIMILL) computer numerically controlled (CNC) milling machine, Bridgeport manual milling machine, and Hardinge manual lathe,

all within the University of Minnesota's Electrical Engineering Machine Shop. Parts as labeled represent: A) entire assembled injection mold apparatus; B) aluminum piston driver mount with stainless steel screw; C) stainless steel screws to secure top and bottom injection mold plates (parts labeled I and J); D) stainless steel cylinder spacers for placement between parts B) and E); E) aluminum cylinder body for containment of uncured PDMS, and subsequent injection into the injection mold cavity (bore diameter = 0.376" = 0.955 cm; machined for 0.0005" = ~1.3 μm cylindrical gap with piston (part F)); F) stainless steel piston (diameter = 0.375" = 0.953 cm; case hardened AISI 1566 steel, with outer surface of 60 Rockwell) with recessed divot for coupling with part G), with piston used for driving uncured PDMS into injection mold cavity; G) hardened stainless steel ball (alloy steel E52100, hardened to 60-70 Rockwell) for placement atop the piston, used to reduce torque piston experiences when driver screw from part B) drives piston into cylinder to inject uncured PDMS, thereby allowing the piston to move vertically throughout the aluminum cylinder block without twisting, and therefore preventing scoring of the cylinder walls by the pistons surface contact; H) stainless steel screws threaded through parts B), D), E), I), and J), to align and secure these parts together; I) bottom injection mold plate fabricated from aluminum, where molding feature (aluminum foil molded over small diameter wire (illustrated as dotted line)) resides, including a machined internal crevice (width = 0.063" = 1.6 mm), where the internal region of the crevice defines the injection mold cavity area (5.2" = 13 cm (L) x 0.81" = 2.1 cm (W)), and the region external to the cavity defines the gasket contact area; J) top injection mold plate fabricated from aluminum, which is smooth and featureless,

and contains a through via (diameter = 0.03" = 0.76 mm) for PDMS to be injected through, with compression of the PDMS contained within the cylinder block (part E)).

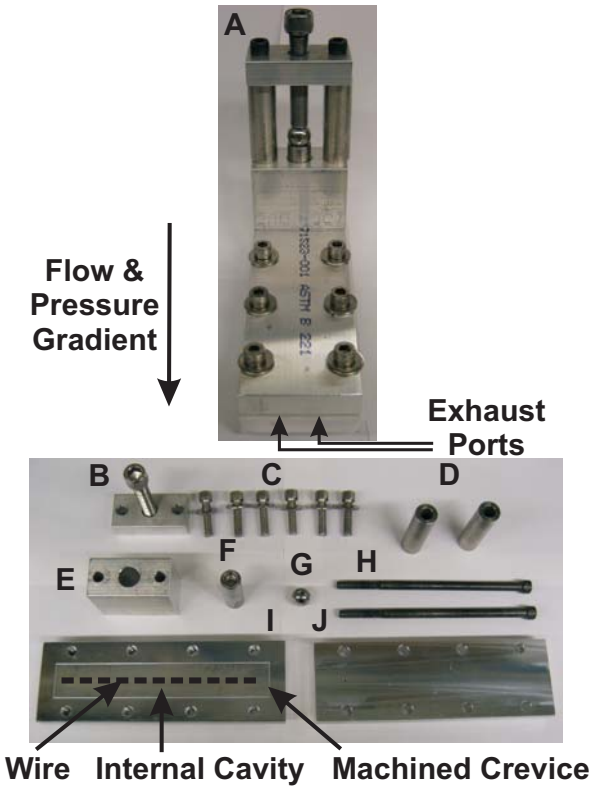

Figure III-1: Images of injection mold parts (bottom image) and entire assembled apparatus (top image). Exit region of two exhaust ports indicated with arrows, and machined into bottom injection mold plate (I). Gasket contained within apparatus and sealed between top and bottom injection mold plates not shown, where discussion for this component is provided within section A). Dotted line (wire) added as an image enhancement, for clarity and illustrative purposes only.

A polymeric gasket (not shown in Figure III-1) was utilized for placement between the top and bottom plates (parts I and J) when the injection mold was fully assembled. The thickness of the gasket regulated the overall thickness of the entire fully cured PDMS layer, and therefore the membrane thickness over the channel as well. Commercially available gasket material is somewhat limited with thicknesses available, where thicknesses were chosen that most closely matched the formula; (gasket thickness

= PDMS layer thickness desired = wire diameter + ~100 μm for membrane thickness + ~10 μm for aluminum foil thickness + ~20-30 μm compression factor for gasket material). Gaskets were fabricated using a CAD file in conjunction with laser machining (Epilog Helix 24). The CAD file was designed such that the gasket was cut from bulk polycarbonate material (McMaster-Carr P/N 9513K121) to be the same length and width as the top and bottom injection mold plates. The laser machine further cut holes in the gasket to allow for screws (parts C) and H)) to pass through the gasket material. Additionally, the gasket was cut to remove the central portion, corresponding to the internal cavity surface dimensions of the bottom plate, or put another way, the surface contained within the machined crevice of the bottom plate. Therefore the gasket material remaining only contacted the bottom plates surface external to the machined crevice (minus the holes removed for the screws to pass from top to bottom plate).

For the bottom injection mold plate, two recessed exhaust ports were machined (8.0 mm (L) x 1.6 mm (W) x 25 μm (D)) parallel to the lengthwise direction, that extended from the edge of the crevice to the outer edge of the injection mold plate (i.e. across the surface external to the machined crevice in the direction parallel to the lengthwise direction). Such exhaust ports were utilized to allow for the uncured PDMS being injected into the cavity from the cylinder block and piston, to exit the injection mold across the exhaust ports. The exhaust ports allowed for a pressure gradient to be developed throughout the injection mold cavity extending from the cylinder block and piston, to the exhaust ports. This pressure gradient provided flow directionality, as well as just enough resistance to extrude bubbles across the exhaust ports. The bubbles were

created and trapped within the injected uncured PDMS as a result of the mixing process for the base and curing agent. For other slightly modified injection mold designs, exhaust ports were laser machined into the gaskets themselves, instead of being machined into the actual bottom injection mold plate, where no difference in performance was noticed for the two designs.

B) Injection Mold Wire-Template Fabrication

The bottom plate of the injection mold (part I of Figure III-1) was utilized for the fabrication of the wire-template. Within the internal region enclosed by the crevice as shown in Figure III-1, were two machined holes (diameter = 762 μm) that spanned the entire depth of the block. A wire (illustrated as dotted line) of diameter ~152 μm (Small Parts, Inc., AWX-006-01-01) was threaded through the machined holes within the crevice region of the bottom plate, such that the wire spanned the entire length between the holes. The wire ends were then wrapped around metal posts built into the opposite side of the bottom plate, where the wrapped wire was then secured in place after a nut with a Teflon washer was tightened over the wrapped wire. If wound in the direction the screw was tightened, tightening of the screw would allow for the wire spanning the holes to be tightened even further, and therefore allowing the wire to remain taut.

With the wire secured in a taut state, general purpose adhesive was lightly and evenly sprayed across the wire and surface of the bottom plate. A piece of general purpose aluminum foil was then placed over the bottom plates surface, smoothed over gently with finger pressure, and further molded with a straight edge from a Teflon block.

The straight edge of the Teflon block was approximately 2 cm in length, where just prior to the smoothing process, the Teflon block was rubbed vigorously back and forth on a smooth slate lab bench. This ensured that a smooth and straight edge would be created and employed, so that tearing of the aluminum foil could be prevented. After the smoothing process, a razor blade was inserted and passed through the internal cavity created by the crevice, so that the aluminum foil external to the crevice (i.e. external plate surface as shown in Figure III-1) could be removed, thereby leaving aluminum foil remaining only within the internal cavity surface where the taut wire resided. Prior to assembling the injection mold, a general purpose citrus-based adhesive remover was used to remove excess adhesive that remained on the external surface area of the bottom plate. Acetone and IPA were then used as final cleaning steps, just prior to assembling the injection mold apparatus. Care was taken so as to avoid leaving the template with any contamination along the wire raised structure. Just prior to assembling the injection mold block, the template was observed carefully under a microscope to assure no contamination was left behind, and therefore preventing any contamination from being introduced into the fully cured PDMS injection mold.

C) Injection Mold CNC Machined Template Fabrication

A second approach was tested for the fabrication of a template structure to be molded to within the injection mold apparatus. This template structure was created from a bulk piece of aluminum, where a raised structure was machined across a flat bottom plate for the injection mold. The structure was machined using a Haas (SMINIMILL)

computer numerically controlled (CNC) milling machine, with a CAD file representing a square cross-sectional geometry with dimensions of ~10 cm (L), ~80 μm (W), and ~70 μm (H). The final machined cross-sectional geometry of the raised template structure retained burrs raised along the top surface (i.e. top width direction for the raised structure). When PDMS was molded to the raised template structure, the cross-sectional geometry revealed a silhouette akin to a shape similar to that of "Batman's head," with pointed burrs raised in the vertical direction above the top surface of the square/rectangular cross-sectional structure. To ameliorate these machining defects, a fine grit polishing compound (Happich Simichrome Polish P/N 390050) was rubbed over the structure to remove the defects. The polishing step produced a smooth cross-sectional geometry with a rounded profile.

D) Injection Mold Channel Layer Fabrication

The channel layer was fabricated from PDMS prepolymer (GE, RTV 615) with a 5 : 1 ratio of base to curing agent. The prepolymer was mixed for 5 minutes with a stir-rod, and then poured without a degassing step into the cylinder (part E) of the fully assembled injection mold apparatus. The laser cut gasket contained as a part of the fully assembled apparatus was cut from stock material with an overall thickness of ~318 μm (McMaster-Carr P/N 9513K121). The piston was then inserted slightly into the cylinder block, with the hardened stainless steel ball (part G) placed on top of the piston thereafter. The injecting screw (part B) was then secured against the stainless steel ball, and screwed downward to inject the PDMS prepolymer into the injection mold cavity.

Using a wrench, nearly maximum torsional force by hand was applied to the injection screw, so as to put the contents within the injection mold cavity under extreme pressure. In doing so, all bubbles that entered the injection mold cavity were forced out through the exhaust ports, leaving a bubble-free PDMS molded channel layer.

After injecting the PDMS prepolymer into the cavity, a quick cleanup of the extruded prepolymer was removed from the injection mold apparatus' outer body. The apparatus was then placed in an oven at 80º C for one or more hours. After removed from the oven, the injection mold apparatus was placed under running water to expedite the cooling-down of the apparatus. The injection mold was then disassembled, where the fully cured molded channel layer was carefully placed along a clean glass substrate. Cleanup of the injection mold parts was performed by first removing the aluminum foil over the wire, followed by a cleanup step using solvents (e.g. WD-40 or general purpose citrus-based cleaners) that would swell, and allow for easy removal of fully cured PDMS particulate matter.

E) Injection Mold Base Layer Fabrication

The base layer to be bonded to the wire template injection mold (as described in B) above) was fabricated from PDMS prepolymer (GE, RTV 615), using a 30 : 1 ratio of base to curing agent. A six inch glass wafer was initially placed inside a desiccator with vapor produced by tridecafluorooctyltrichlorosilane (United Chemical Technologies, model T2492). This antiadhesion vapor soak step was allowed to continue for 1-2 hours. After the vapor soak, the glass wafer was immediately placed in a photolithography

spinner (CEE Model 100), where the 30 : 1 prepolymer was poured over the glass wafer and spun using the program; 1) 400 RPM, 50 RPM/sec, 10 sec, 2) 1000 RPM, 200 RPM/sec, 45 seconds. After spinning the 30:1 PDMS, the glass wafer was baked in an oven at 80º C for 35 minutes to allow for a partially-cured 30 : 1 base layer to be formed. The base layer thickness was measured with a surface profilometer, and measured to be approximately 80 μm thick on average when measured across the diameter of the glass wafer.

Fabrication of the base layer to be bonded with the machined-block template injection mold (as described in C) above) was also fabricated using 30 : 1 PDMS prepolymer. The prepolymer however was not spun, where instead the prepolymer was cured between two glass wafers separated by spacers (~203 μm thick), with the two wafers being secured together using general purpose binder clips. Prior to pouring the 30 : 1 mixture, the two glass wafers were put through the same vapor soak step as that described above. The soak was performed with different time intervals for each wafer, where one wafer was allowed to soak for 15-30 minutes, and the other allowed to soak for 1 or more hours. The difference in soak times allowed for the ability to selectively control the separation of the wafers, where one wafer was rendered more prone to removal from the 30 : 1 layer over the other. A partial cure of the glass sandwich was performed for 35 minutes at 80º C in a convection oven.

F) Bonding of Injection Mold Channel and Base Layers

With the fully cured 5 : 1 channel layer already placed on a glass substrate with the molded channel exposed to the atmosphere, fused silica capillary tubes (Polymicro, 152 μm outer diameter / 40 μm inner diameter) each of length ~30-40 cm long were placed ~ 1.5 cm into the inlet and outlet regions of the channel, with the aid of a microscope (Nikon, SMZ1500). Uncured 5 : 1 prepolymer was then placed along the capillary tubes within the channel, so as to seal the void dead volume areas. A razor blade was dragged across the surface of the mold to remove excess 5 : 1 prepolymer. The partially cured 30 : 1 PDMS layer on the glass wafer was then placed on the surface of the 5 : 1 channel layer, containing the inlaid capillary tubes within the microchannel. Moderate pressure was applied to seal the layers and extrude trapped air bubbles between the layers. The 30 : 1 glass wafer was then carefully lifted, so as to remove the 5 : 1 layer from its original glass substrate. This step allowed for the 5 : 1 channel layer membrane to be exposed to the atmosphere, where a razor blade was further skimmed gently across the channel membrane surface to further seal the two layers as necessary. The bonded PMDS layers were then placed in an oven at 80º C for one or more hours to allow for an irreversible bond between the layers to occur. After bonding, the bulk PDMS region surrounding the enclosed microchannel was cut using a razor blade, and then transferred and aligned to a clean substrate. 5 : 1 PDMS prepolymer was then fully cured to the regions where the capillary tubes exited the bonded PDMS layers, so as to seal these regions further.

2) SU-8 REM Devices

G) SU-8 Photolithography Processing

A clean and six inch diameter glass wafer was dehydrated on a hotplate for 3 minutes at 120º C. After a brief cool-down, the glass wafer was placed in a photolithography spinner (CEE Model 100). SU-8 2025 (MicroChem Corp.) was next poured in the center of the glass wafer and spun using the program; 1) 200 RPM, 50 RPM/sec, 10 sec, 2) 2000 RPM, 300 RPM/sec, 45 sec., which produced an SU-8 thin film of thickness approximately equal to 37 μm near the center of the glass wafer, and approximately 40 μm near the edges of the glass wafer. The glass wafer was then softbaked using a two step process, where the first step was done for 2 minutes at 65º C, and then a second step of 5 minutes at 95º C. After soft baking, the wafer was placed under an Oriel flood exposure system (model 8095), which produces a collimated and uniform beam of UV radiation in the 350 – 450 nm wavelength range. A chrome photolithography mask was then placed in intimate contact with the SU-8 thin film. The chrome mask was fabricated with a 75 μm wide line extending the length of the mask in the diagonal direction from corner to corner. A 90 second exposure was next performed using the Oriel system, which provides a lamp intensity of approximately 5 mW/cm^2, and therefore providing a total dose of 450 mJ/cm^2 to the SU-8 thin film. This exposure time was used since it experimentally produced the desired vertical sidewalls, and therefore a perfectly square/rectangular cross-sectional SU-8 profile. The exposed SU-8 thin film was then put through a two step post exposure bake (PEB) process using two separate hot plates. The two step PEB used the following protocol; 1) 1 minute at 65º C, 2) 3 minutes

at 95º C. Due to the excess of SU-8 that remained unexposed (and therefore would be removed as a result of SU-8 being a negative tone resist), a final two step develop process was performed using PM Acetate, where the glass wafer was developed in a first container for 3 minutes, and 3 minutes in a second container.

H) REM Channel and Base Layer Fabrication, and Bonding

The exposed SU-8 feature was used as a template to perform replica molding (REM) against, using PDMS prepolymer (GE, RTV 615) mixed with a ratio of 5 : 1. The 5 : 1 PDMS was manually mixed for 5 minutes, and then spun in a centrifuge at 5000 RPM for 2-3 minutes to remove the bubbles introduced during the mixing step. The degassed PDMS was then poured over the SU-8 exposed structure, with spacers (~203 μm thick) placed on the outer regions of the glass wafer, serving as overall PDMS thickness regulators. After pouring the PDMS and placement of the spacers, a second bare glass plate was slowly placed over the top of the first glass wafer, effectively creating a sandwiched layer of PDMS regulated in thickness by the spacers. The excess prepolymer was extruded by applying pressure to the sandwich, where finally the sandwich was held together with binder clips and then placed in an oven to bake at 80º C for one or more hours. It is further noted an antiadhesion vapor soak was performed identically to that already described in E) above, with the shorter soak being performed on the second bare glass wafer of the sandwich, so as to allow selective removal of the fully cured mold from the SU-8 template.

The base layer was fabricated from PDMS prepolymer mixed in a ratio of 30 : 1.

The processing was identical to that already described for the wire template injection mold base layer fabrication process using a spinner, as described in E) above.

After the 5 : 1 sandwich was fully cured, the sandwich was removed from the oven, where the two glass substrates were separated. Removal of the excess fully cured PDMS was performed by cutting with a razor blade, the desired dimensions of bulk PDMS to remain surrounding the molded channel. The PDMS containing the molded microchannel was then transferred to a clean glass substrate, where bonding proceeded identically to that of the injection molding section F) as described above. In this case however, capillary tubing (Polymicro) with 105 μm outer diameter / 40 μm inner diameter was bonded into the SU-8 molded microchannel.

3) Micropump Actuation

I) Cantilevers, Microvalves, and Micropositioners

Actuation of the micropump was achieved with piezoelectric cantilevers (Piezo Systems, model Q220-A4-303YB). Precision machined aluminum valve clamps were adhered to the tips of the cantilevers with general purpose silicone, where precision machined aluminum microvalves were clamped within the adhered valve clamps. The contact area of each valve tip to the PDMS injection molded microchannel, measured 3 mm in the length direction, and 250 μm in the width direction. The SU-8 fabricated microchannel utilized valve tips of 3 mm in the length direction, and 150 μm in the width direction. These microvalve dimensions will explored more deeply within Chapter IV. The cantilevers as obtained from the manufacturer contain a general quick mount system,

where an acrylic block was adhered to the top surface of the quick mount, and an appropriately sized piece of printed circuit board material adhered to the bottom surface of the quick mount. The cantilever assembly was then secured in place within in-house fabricated micropositioners, that were fabricated in-part from preassembled stages (Edmond Scientific, #56-416), and provided for adjustments to be made in the horizontal (in/out), vertical (up/down), and tilt (angled up/down) directions. Such adjustments allowed for proper registration of the microvalves over the PDMS microchannel. Once the cantilever / microvalve / micropositioner assembly was in place, the assembly was then secured to the same glass substrate that the prior fabricated PDMS microchannel had been aligned and adhered to. For the current Chapter, the micropositioner clamping portion that attached to the glass substrate, had three Teflon screws threaded through the clamping portion of the micropositioners, in contrast to that as previously discussed within Chapter II. This additional threading allowed for a third Teflon screw to more fully secure the micropositioner assembly to the glass substrate, and therefore allowing for higher frequency measurements to be recorded without having the micropositioners vibrate out of place, in contrast to that as discussed within Chapter II. Final adjustments for alignment of the microvalves over the microchannel were made under a microscope (Nikon, SMZ1500), so as to allow for complete closure of the microchannel below each microvalve tip.

J) Software and Hardware

The cantilevers were actuated with square wave signals that were placed 120º out of phase, so as to create a peristaltic wave pattern. The signals were created with a virtual function generator (National Instruments) that allowed for control of signal shape, frequency, amplitude, and phase. The generated signals were amplified with in-house fabricated external electronic hardware, where high-voltage amplifiers (Apex Microtechnology, PA15A) were used to amplify the virtual function generator signals to $V_p = \pm 90$ V, which is the maximum driving potential for the cantilevers before depoling occurs, as reported by the manufacturer.

4) Characterization Experiments

K) Flow Rate

Flow rates for the micropump were obtained at specific frequencies by connecting the outlet capillary tube line of the micropump to an external piece of capillary tube ~1 m in length. The external piece of capillary tube was secured in place along a meter stick with mm ticks/gradations. The external capillary tube was filled with a blue food dye solution prior to mating with the outlet line of the micropump. The blue dye allowed for greater contrast and easier tracking of a 2-3 mm bubble that was intentionally introduced when the two capillary tubes were connected. Time of travel between selected intervals of the meter stick allowed for calculation of flow rate using the formula $Q = Av$, where "Q" being the flow rate, "A" the cross-sectional surface area of the flow channel, and "v" the linear flow velocity of the bubble. All flow rates were calculated while actuating the

micropump with a 120º square wave signal. The standard errors were calculated and plotted as error bars for each data set, where (n=4) for the SU-8 rectangular microchannel device, and (n=6) for the injection molded rounded/Gaussian shaped microchannel device.

L) Backpressure and Pressure Loss Measurements

Maximum attainable backpressure and valve leakage data were both obtained within a single experiment using the same setup. The micropump outlet capillary tube line was first connected to an electronic pressure sensor (Honeywell, 40PC015G2A) with the micropump being actuated to produce flow into the pressure sensor. The injection molded micropump was actuated at 25 Hz, with the SU-8 REM micropump actuated at 60 Hz, where in both cases for each set of experiments the micropump was allowed to attain the maximum attainable backpressure as indicated by the pressure sensor. After attaining this point, the micropump was stopped, where only one valve was left in the fully closed position. Pressure readings were recorded for 15 minutes to observe pressure loss within the system, where after this time the valve was fully opened. For each respective micropump, (n=3) experiments were performed.

M) Fluorescence Valve Closure Measurements

The micropump was placed in an inverted position under an epifluorescent microscope that was covered with a black cape, so as to block ambient light when taking measurements. All three microvalves were placed in the fully open position under the

microscope, where distilled water was forced through the channel of the micropump using a syringe pump. The syringe pump was then turned off, where after 30 s, the outlet line of the micropump was capped off. After allowing 30 min for the closed-off system to stabilize, fully open and fully closed valve intensities were recorded with the epifluorescent microscope (Nikon, SMZ1500 with filter cube 470/440/500 nm – excitation/emission/long pass). Without disturbing the micropump in the inverted position, the micropump channel was filled with a 10 mM fluorescein solution, where the same experiment was repeated as already described using distilled water. Background subtracted images were produced using Metavue, by subtracting the distilled water signal from the fluorescent recorded signal.

Results and Discussion

5) Cross-Sectional Microchannel Geometries

N) Injection Mold Wire-Template Channel

The cross-sectional geometry of the microchannel produced using the injection mold wire-template can be seen in Figure III-2. The overall height of the channel was measured to be ~198 μm, where the 5 : 1 PDMS membrane directly over the channel was observed to be ~155 μm thick. The maximum width at the base of the channel was measured at ~272 μm. Further the overall 5 : 1 thickness was recorded as ~330 μm, with the overall thickness of the 30 : 1 recorded as ~85 μm. As can be seen from Figure III-2, the wire molded channel geometry produced is very uniform/symmetric and resembles that of a Gaussian bell-shaped curve, where it has been shown how important this

characteristic is for microfluidic valving operations.[283, 1271, 1272] One further point to note is the measured channel height taken to be ~198 μm, where the wire molded to possessed a diameter of ~152 μm. The discrepancy in part could be attributed to an increase in molding wire height, created as a result of the general purpose spray adhesive and aluminum foil placed over the wire to create the template, however at most 10-20 μm of added thickness would be expected for these additions. It can be seen in the image that the top surface of the membrane is slightly bowed, where it is believed this effect is what accounts for the bulk of the additional and unexpected channel height. The slight bowing could be attributed to the bonding of the two PDMS layers, where it has been previously shown and described how various PDMS geometries can be distorted, especially with high-aspect-ratio PDMS structures.[275, 294] Other possible explanations to account for these observations, could be attributed in part to PDMS shrinkage[271, 293] during the curing process, and/or possibly stemming in part from the mismatch in molded PDMS channel height, to that of the inserted capillary tube diameter.

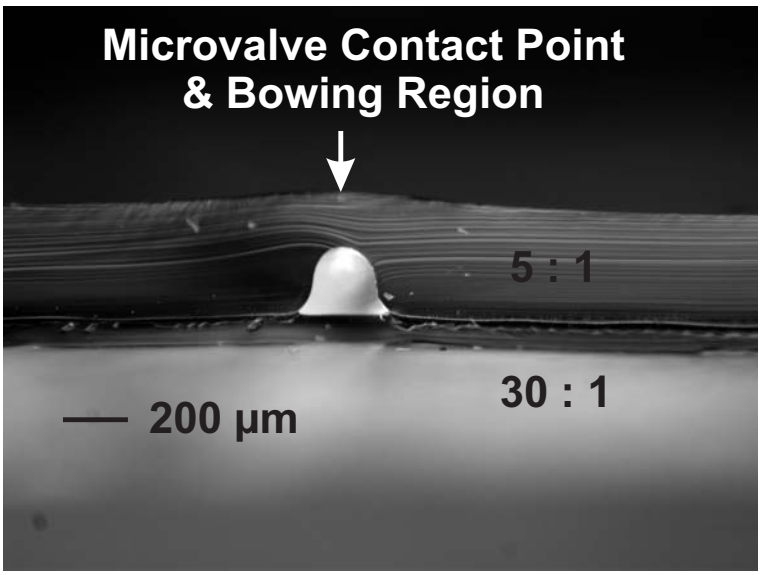

Figure III-2: Cross-sectional image of microchannel produced from injection mold wire-template. Template formed from aluminum foil and general purpose spray adhesive applied over a wire of diameter ~152 µm, and straddled across bottom plate of injection mold apparatus.

O) Injection Mold CNC Machined Template Channel

Figure III-3A shows a cross-sectional image of the 5 : 1 injection molded microchannel geometry before bonding of the 30 : 1 base layer, where III-3B shows the geometry after bonding of the 30 : 1 base layer. The images for this template show a rather dramatic distortion of the microchannel after bonding the base layer, where the channel height before bonding was measured to be ~77 µm, and ~114 µm after bonding, with the channel width at the base changing from ~65 µm to ~34 µm for before vs. after bonding, respectively. Therefore the aspect ratio as taken to be the ratio of the channel height, to channel width as measured at the base of the channel (i.e. opposite the membrane), changes from 1.2 to 3.4, representing a 2.8-fold overall change. This change in aspect ratio is believed to be due to the bowing effect as already described for the wire template injection mold.

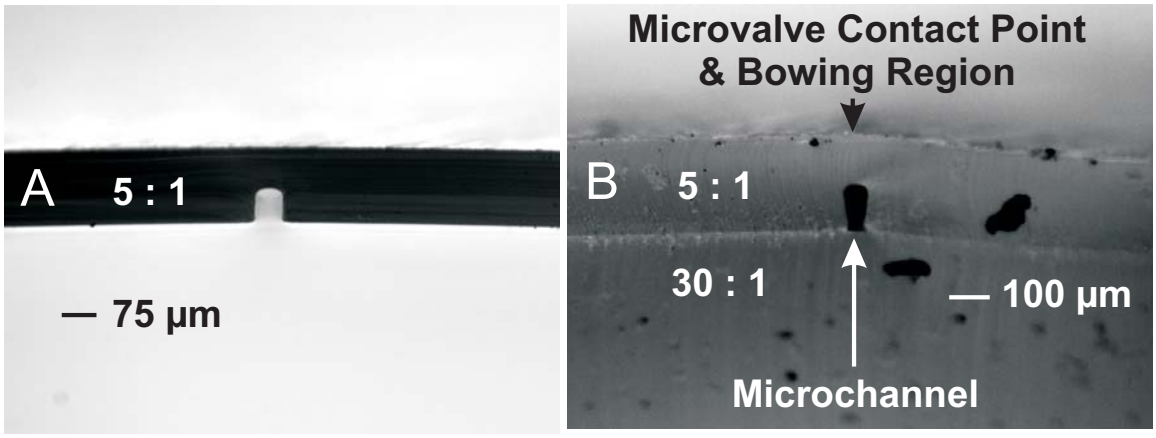

Figure III-3: Side-by-side images of before and after bonding of 30 : 1 base layer, to 5 : 1 mold produced from CNC machined template used within injection mold apparatus. Bonding of base layer shows distortion of final cross-sectional channel geometry.

P) SU-8 REM Channel

Figure III-4A shows a cross-sectional image of the 5 : 1 injection molded microchannel geometry before bonding of the 30 : 1 base layer, with III-4B showing the geometry after bonding of the 30 : 1 base layer.

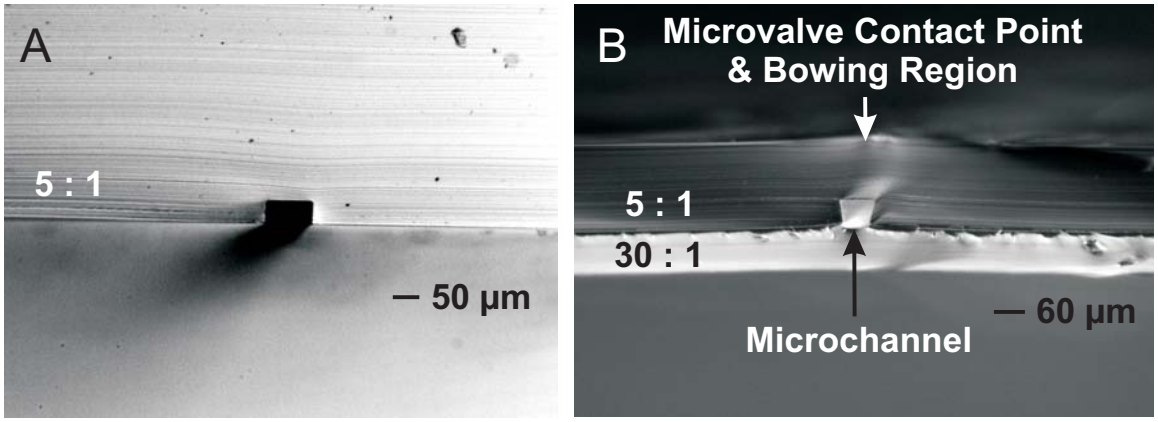

Figure III-4: Side-by-side images of before and after bonding of 30 : 1 base layer, to 5 : 1 mold produced from SU-8 fabricated template. Bonding of base layer shows distortion of final cross-sectional channel geometry.

The rather dramatic distortion in channel geometry can be seen to parallel that of the CNC machined template images as shown in Figure III-3. The aspect ratio taken as the dimensions of the channel height/width (taken at base of the channel, i.e. opposite the membrane) for III-4A was measured as 40/88 μm, and 57/57 μm for III-4B, or a 2.2-fold overall change with bonding of the 30 : 1 base layer. The bowing effect as described within the previous two sections of this Chapter is believed to be the reason for observation of these channel distortions.

It should be noted, not all cross-sectional channel geometries were observed with channel distortions. Figure III-5 shows a cross-sectional image of a microchannel fabricated using an SU-8 template, where the mask used was 50 μm in width. Before base layer bonding images were not captured, however the dimensions of the channel after base layer bonding were measured at 41/66 μm for the channel height/width as measured at the base of the channel (i.e. opposite the membrane), representing a final aspect ratio of 0.62. Presumably the microchannel aspect ratio was optimized before base layer bonding as shown within Figure III-5, in comparison to that as shown in Figure III-4. This hypothesis is consistent with previously discussed results for very high or very low aspect ratio PDMS structures.[275] It is further believed the likelihood of the channel experiencing serious distortions is significantly lessened when the channel layer is fabricated from; 1) a 5 : 1 PDMS ratio, and 2) an overall thicker piece of 5 : 1 PDMS, relatively speaking. This explanation could be attributed to the mechanical properties of the 5 : 1 ratio compared to that of the 30 : 1 ratio. The 6-fold increase in ratio of base/curing agent allows for a much higher density of cross-linking bonds to be formed

with base molecules, and therefore production of a much more rigid slab of PDMS, as compared to the same thickness sheet of fully cured 30 : 1 PDMS.

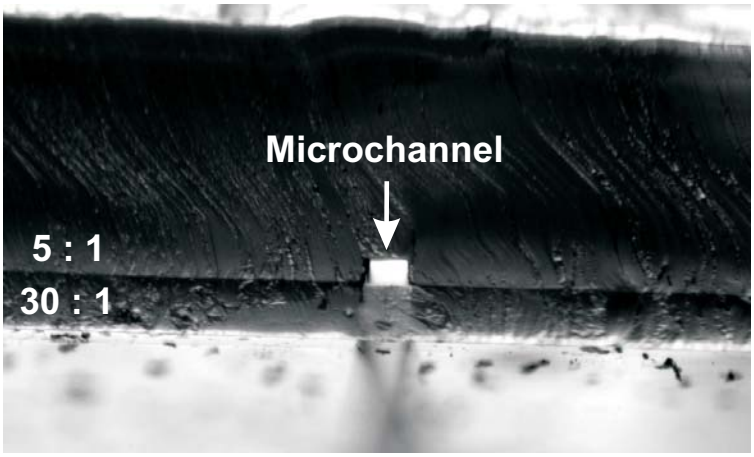

Figure III-5: Cross-sectional channel geometry for an SU-8 template fabricated microchannel. Channel formed using a photolithography mask of width 50 μm. Image shows vertical channel sidewalls, and therefore an undistorted cross-sectional channel geometry produced after bonding of 30 : 1 base layer.

6) Valve Closure Image Data

An image of a fully open vs. fully closed microvalve can be seen in Figure III-6. This Figure shows the micropump in an inverted position under an epifluorescent microscope, where observation of these states was recorded with fluorescein trapped within the channel. The image of the SU-8 channel in the fully closed position can be seen not fully closing the channel along the bottom right edge, as indicated between the arrows. The operation and stability of the SU-8 REM micropump proved to be a challenging task, where the non-ideal cross-sectional channel geometry is the expected culprit for these operational challenges.

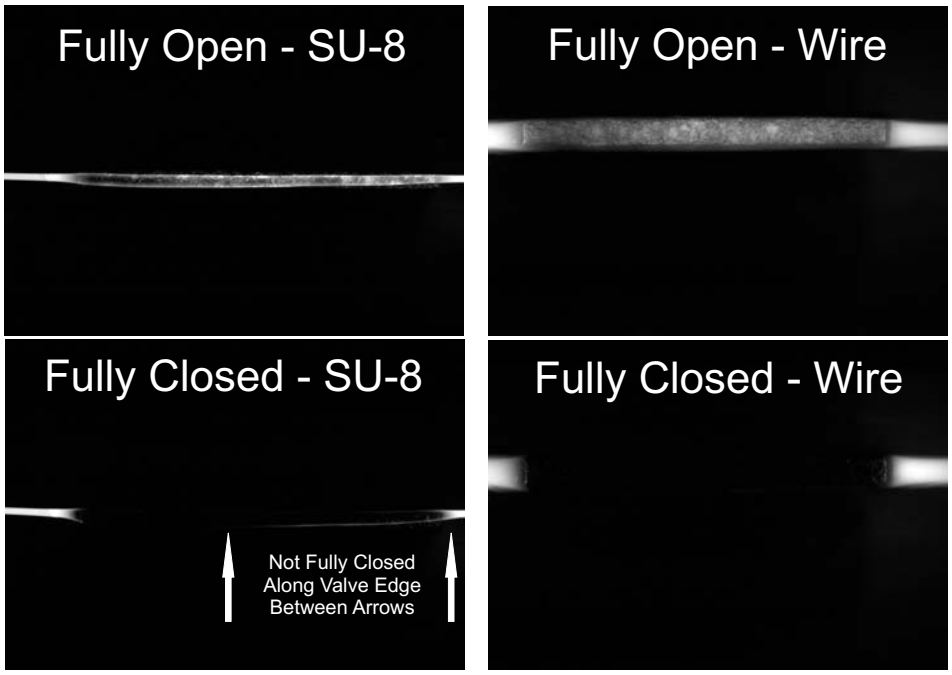

Figure III-6: Images of valve closure for SU-8 and wire-template molded microchannels. Images taken with micropump in an inverted position under an epifluorescent microscope, with fluorescein trapped within the microchannels. Image of fully closed SU-8 molded channel indicates channel not fully closed under microvalve contact/compression region, as indicated between the arrows at the bottom right edge of the channel. Image of wire-molded channel indicates valve successfully fully closed off channel, where no fluorescent signal was recorded.

The image of the wire-molded channel is shown on the right side of Figure III-6. As can be seen for the fully closed state, the channel was completely closed off, where no fluorescein was recorded under the closed valve region. The operation of this micropump was very stable, but, several adjustments to the microvalves were necessary. This process was qualitatively observed to be a result of the force output produced by the piezoelectric cantilevers, where the micropositioner adjustment was critical in allowing the cantilevers to fully collapse the microchannel. Wire molded micropumps were also fabricated using wire of diameter 55 μm, and 250 μm. The cantilevers were barely able to output enough force to fully close off the 250 μm channel, where operation was unstable. In contrast, the 55 μm wire molded channel allowed for the cantilevers to easily close the channel off

fully, however these pumps failed to produce a net flow. The hypothesized explanation is believed to be a result of the very high resistance that must be overcome, to produce a net flow through the small inner diameter capillary tubes (90/20 μm, OD/ID) used in the fabrication of the 55 μm wire molded micropump, where it is known the hydraulic resistance for laminar flow through a rigid straight pipe, with circular cross-sectional channel geometry, scales as $R_h \propto 1/r^4$, for "R_h" equal to the hydraulic resistance, and "r" equal to the radius of the circular pipe.[5, 6, 1278] Fabrication of micropumps with appropriately sized inlet and outlet capillary tube (90/20 μm, OD/ID) lengths, would likely produce a micropump capable of producing a net flow.

7) Backpressure and Pressure Loss Data

The backpressure data recorded for the two microchannel designs can be seen in Figure III-7. Three experiments were performed for each design, where the average maximum backpressure recorded for the SU-8 micropump was 51.5 kPa, and 25.8 kPa for the wire molded micropump. When factoring in the valve closure data as indicated in Figure III-6, it would be expected the SU-8 template molded micropump would have a higher average pressure loss due to valve leakage, but this was not the case. The average pressure loss for the first 15 minutes with only one valve in the fully closed position was recorded to be 5.9% for the SU-8 molded micropump, and 6.1% for the wire molded channel. It is believed from previous micropump experience that this pressure loss can be nearly, if not fully, attributed to pressure loss from the connections made to the inlet and outlet lines of the micropump, when fully pressurized.

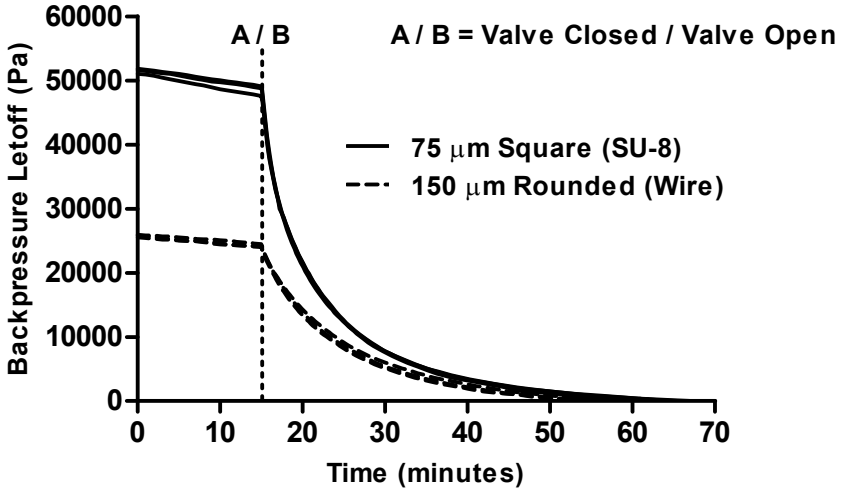

Figure III-7: Plot of backpressure and valve leakage characteristics for SU-8 and wire-template molded microchannels. Plot shows nearly same pressure loss recorded over the time-course of the first 15 minutes, where one valve was left in the fully closed position, with the respective micropump maintained in a fully maximal pressurized state. Pressure loss believed to be a result of losses in capillary tube connections, and not across the microvalve. An average maximum backpressure of 51.5 kPa and 25.8 kPa was recorded for the SU-8 and wire-molded micropumps, respectively. Three representative experiments were performed for each micropump design.

8) Flow Rate Data

The flow rate data collected for both micropump designs can be observed in Figure III-8. Up to approximately 20 Hz, the flow curves are very similar in nature. Past this frequency however, the flow curves diverge, where it can be seen with the error bars, how the flows became slightly erratic at higher frequencies for the SU-8 molded micropump. The flow rates for the wire template molded micropump however, remained quite stable throughout the entire range of characterized actuation frequencies. The instability of the SU-8 micropump curve is likely explained with the non-ideal rectangular cross-sectional channel geometry produced for this micropump.

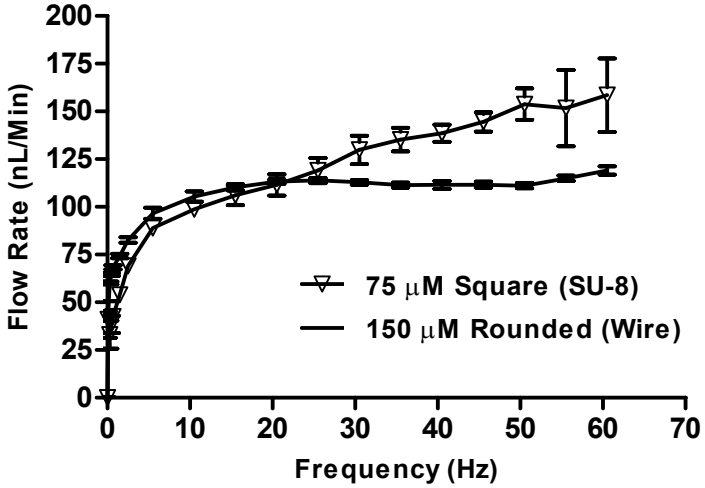

Figure III-8: Data shown for flow rate vs. frequency for SU-8 and wire-molded micropump designs. Data shows flow rate characteristics for the micropumps is very similar up to around 20 Hz, where after the data becomes slightly unstable for the SU-8 micropump, but continues to increase to an average maximum flow rate of 159 nL/min being recorded. An average maximum flow rate of 119 nL/min was recorded for the wire-molded micropump. Error bars plotted represent the standard error of the mean (n = 4 for SU-8 micropump, n = 6 for wire-molded micropump).

Figure III-9 is a plot of standard errors vs. frequency, for the SU-8 vs. wire molded microchannels, to further highlight the instability of the SU-8 micropump, compared to that of the wire molded micropump. The averaged range of flow rates recorded for the SU-8 micropump design was 33 – 159 nL/min (0.3 – 60 Hz), and 44 – 119 nL/min (0.1 – 60 Hz) for the wire molded micropump design.

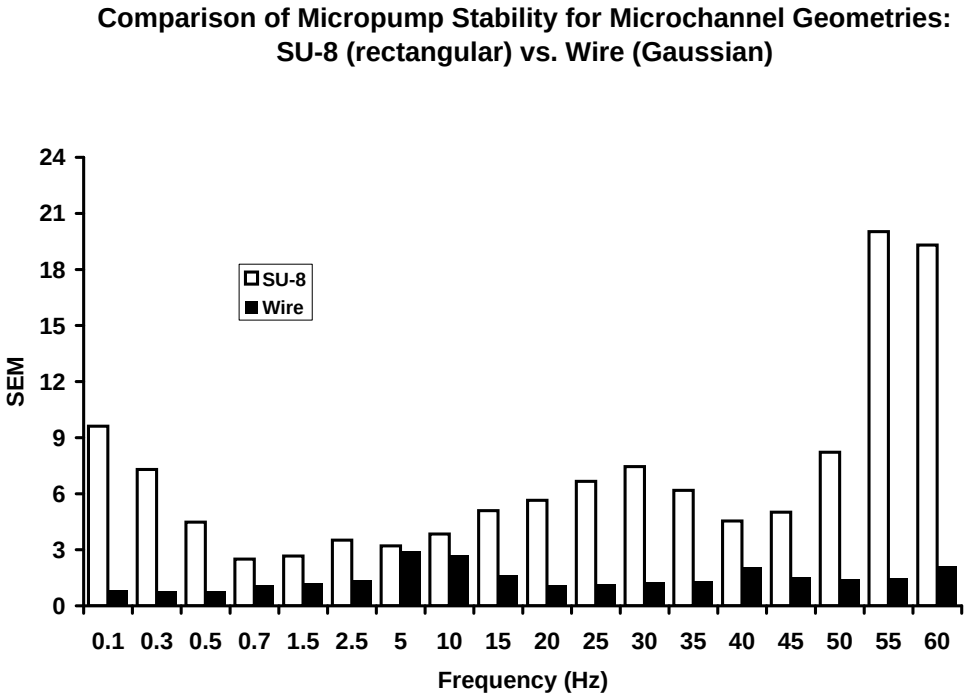

Figure III-9: Plot of standard errors for flow rate vs. frequency. Comparison is made for SU-8 vs. wire molded microchannels, for the data presented within Figure III-8. Plot shows the flow rate instability of the square (SU-8) vs. rounded/Gaussian (wire molded) shaped microchannel geometries.

Conclusions

The current work as presented within this Chapter, characterized the differences in two micropump fabrication methods, using; 1) SU-8 replica molding, and 2) micro injection molding. The two respective designs produced two very disparate cross-sectional channel geometries, with the SU-8 process producing a rectangular geometry, and the injection mold producing a Gaussian/rounded geometry. The results indicate both designs are capable of producing a net flow, with the SU-8 pump design proving to be slightly more delicate in its ability to operate in a consistently stable state. Distortion of the channel geometries after bonding of the 30 : 1 base layer was further

characterized in the current Chapter, where it has been shown in some instances, distortion can be rather extreme when comparing the final cross-sectional geometry of the channel to the initial geometry. The injection molding process proved to be a very simple, cheap, fast, and reproducible fabrication process, far superior to the glass substrate sandwich molding process used in fabricating SU-8 micropumps. The injection molding apparatus is also very unique compared to that of other micro injection molding machines, where the current disclosed apparatus is handheld and portable, and additionally designed for use with RTV polymers, as opposed to thermoplastic polymers used with most other injection molding machines.

Chapter IV : *Performance Characterization of a PDMS Soft Lithography-Fabricated Peristaltic Micropump, using Variable Cross-Sectional Surface Area Microvalves*

Synopsis

This Chapter presents a PZT cantilever-actuated peristaltic micropump with precision-machined microvalves. Fabrication of the micropump was performed using injection molding and PDMS soft lithography fabrication techniques, as previously presented within Chapters II and III. The current Chapter builds upon the functionality and versatile capabilities of this previously presented micropump (Chapters II and III), by exploiting the capacity of this pump to utilize interchangeable precision-machined external microvalves. The cross-sectional surface area of the interchangeable microvalve tips was varied in the lengthwise direction, and therefore allowing for relatively simple alteration of stroke volume for an individual microvalve. Alteration of stroke volume translates into the capability to further alter other metrics such as flow rate, backpressure, and valving characteristics. Such versatility, allows for flow rates and backpressures to span a much larger dynamic operating range as opposed to valves with a single set stroke volume. The range of flow rates spans from 14 - 138 nL/min, with maximum backpressures of approximately 15 - 24 kPa. Such a span of dynamic operating ranges allows for a single micropump design to be utilized across an array of fields where high and/or low flow rates and backpressures are required for a particular microanalytical / microfluidic application.

Introduction

The functionality of a microfluidic device is created from unit operations, with unit operations being defined as a set of basic fluidic operations such as fluid transport, fluid metering, fluid valving, fluid mixing, analyte/compound separation, pre/concentration and/or amplification, detection and readout, reagent storage, and incubation.[70, 465] One of the most widely studied set of unit operations is that of fluid transport and fluid routing on a microfluidic chip. These operations on a microfluidic chip are accomplished using micropumps and microvalves. Depending on the microfluidic platform, these operations can be accomplished using many different design and actuation strategies. Oftentimes microvalves are classified as either active or passive.[474] Active microvalves can include actuation means such as piezoelectric,[326, 493, 495, 497-499, 501] magnetic,[506, 508, 509, 511, 514, 515, 1279] pneumatic,[480, 483, 484, 486, 487, 490, 491] thermopneumatic,[522, 523] shape-memory alloy,[524, 527, 528] electrostatic,[516-518, 1280, 1281] and mechanical,[531, 532, 534, 1282] with passive valving schemes employing mechanisms such as capillary forces/surface chemistry,[586, 588, 594, 604, 1283] hydrogel responsive materials,[541, 545, 547, 548, 1284] geometric routing schemes,[597-599, 601, 603, 605] and check valves.[573, 575, 576, 579-581, 583] Likewise, micropumps can be classified as either active or passive, but are oftentimes categorized as either dynamic or displacement.[609] Displacement micropumps would include piezoelectric,[326, 641, 647, 654] pneumatic,[283, 621, 622, 626] magnetic,[665-668] mechanical,[702, 706, 708, 709] and thermal[672, 674, 680, 1285] formats, with dynamic designs making use of surface tension,[765, 767] bubble,[761, 762] acoustic,[757-760] or electrokinetic[732, 737, 738, 1286] actuation means, for example.

Active microvalves are oftentimes employed as fundamental elements within displacement micropumps. In the case of peristaltic micropumps three valves are aligned in series, to form a single functional micropump.[283, 326, 647, 654] In the case of microfluidic chips, the most widely reported microvalve and pumping technique is accomplished using pneumatic actuation. Pneumatic actuation offers the advantage of integrating high density valving operations onto a chip.[25, 635] Such designs however must employ an offline compressed gas source,[666, 1287] and also external pneumatic switching mechanisms. Therefore, depending on the particular design format and instrumental needs, other microvalve and micropump actuation means could prove advantageous. Piezoelectric microvalves and micropumps are favorable and/or additional options to consider, for applications where discrete electrical actuation is a priority, or where high density valving operations are not a requirement. Such applications could be found within macroscopic analytical instrumentation, where microfluidic devices are employed as an enabling form of technology.[32, 666, 963, 1244, 1288, 1289] The use of piezoelectric actuators also allows for offline adjustment of valve sizes, or even the placement of valves across a microfluidic chip, where additionally these adjustment operations could be performed without fabrication of a new chip. A change in valve size provides the option of tuning valve stroke volumes, and therefore micropump flow rates as well.[622, 667, 690, 1290, 1291] Such versatility would allow a stand-alone micropump to be used within both high and low flow rate microfluidic applications.

This Chapter will present a piezoelectric cantilever-actuated peristaltic micropump, employing external microvalve technology. The tip of each microvalve

makes contact with a PDMS membrane surface, with the microvalve tip dimensions determining microvalve stroke volume. The design as presented, allows for rapid offline tuning of valve sizes, and therefore valve stroke volume as well. Microvalves with tip dimensions of varying length were characterized for their effect on micropump flow rate and backpressure performance, and further for their valve leakage and valve cycling characteristics. The results will show a significant increase in both flow rate and backpressure performance, for the micropump actuated with microvalves of increasing tip length. The data will also establish this micropump and valving scheme as a potentially useful dosing or fluidic gating platform, where low flow rates and/or highly stable and reproducible flow rate and valving performance is a necessary requirement.

Experimental Methods

1) PDMS Micropump Fabrication

A) Channel Layer Fabrication using Injection Molding

The channel layer was fabricated from 5 : 1 PDMS (GE, RTV615) prepolymer using an in-house fabricated injection mold apparatus, as described within Chapter III. The injection mold was fabricated primarily from aluminum using computer numerically controlled (CNC) machinery. The apparatus contained an injection mold cavity, and was created by compressing a gasket between the top and bottom plates of the injection mold apparatus. The gasket was laser machined from a sheet of bulk polyester material (McMaster-Carr, 9513K118), with appropriate machining dimensions that allowed for formation of the cavity region when compressed between the two plates. The thickness

of the gasket determined the overall thickness of the PDMS mold formed. A microchannel was also created during the molding process, by utilizing the bottom plate of the injection mold as a template. The template was formed by threading a piece of 75 μm diameter (molybdenum) electrical discharge machine (EDM) wire through opposite ends of the bottom plate. The threaded wire was then wrapped around screw posts machined into the opposite side of the plate, where the wire was further stretched taut across the plate by tightening a nut and Teflon washer over the wrapped-wire. A thin film of general purpose spray adhesive was then applied over the bottom plate surface containing the taut wire, where shortly thereafter a piece of general purpose aluminum foil was molded against the wire using a straight edge of a Teflon block. Excess aluminum foil was then removed with a razor blade. Prior to assembling the injection mold, a cleanup of the template was performed using a citrus-based adhesive remover, with subsequent cleaning performed using common laboratory solvents such as acetone, methanol, and IPA. The final step before assembly of the apparatus was to inspect the template under a microscope, to ensure no contamination existed along the wire/aluminum foil template formed over the bottom plate of the injection mold.

The injection process was performed after formation of the template and complete assembly of the injection mold apparatus. Prepolymer 5 : 1 PDMS was first poured into the injection mold cylinder, and then compressed using a hardened stainless steel piston. Exhaust ports were machined into the bottom plate and positioned at the opposite end of the piston and cylinder, where excess PDMS was ejected across these ports. Such ports allowed for a pressure gradient to be formed throughout the injection mold cavity, where

the pressure differential allowed for the prepolymer PDMS to be injected without a degassing step. All bubbles were forced across the exhaust ports, leaving a bubble free micromolded slab of PDMS. Curing of the injected PDMS was hastened by placing the injection mold in a convection oven at 80º C, for one or more hours. After removing from the oven, the injection mold apparatus was placed under running water to expedite the cooling phase. The injection mold was then disassembled, where the PDMS mold was placed over a clean glass substrate. The injection molding process produced a 5 : 1 mold with overall thickness of ~176 μm for bulk regions of 5 : 1 (i.e. not near the molded microchannel region), a membrane of thickness of ~85 μm, and a channel height of ~119 μm.

B) Base Layer Fabrication with Photolithography Spinner

The base layer was formed by spinning 30 : 1 prepolymer over a six-inch glass wafer. Prior to spinning, the glass wafer was placed in a desiccator for 1-2 hours with vapor produced by tridecafluorooctyltricholorsilane (United Chemical Technologies, T2492). This vapor soak step was used to reduce the adhesion of the PDMS to the glass wafer. After spinning the 30 : 1 PDMS, the wafer was partially cured in a convection oven at 80º C for 35 minutes. This spinning process produced a base layer of thickness approximately equal to 83 μm, when measured directly below the microchannel.

C) Bonding Channel Layer with Base Layer

The previously fully cured 5 : 1 channel mold was first placed under a microscope with the channel region facing the atmosphere. Fused silica capillary tubing (Polymicro, 105/40 μm OD/ID) was then placed ~1.5 cm into the 5 : 1 molded channel. 5 : 1 prepolymer was then placed along the capillary tube regions that laid within the microchannel, so as to seal any and all void regions that could potentially exist after completion of the bonding step. Excess 5 : 1 was then gently removed by skimming a razor blade across the appropriate PDMS/capillary tube region. The partially cured 30 : 1 wafer was then placed over the 5 : 1 PDMS mold, so as to seal off the channel from atmospheric exposure. Moderate pressure was applied to optimize the bonding of the two layers, followed by application of prepolymer 5 : 1 PDMS to the capillary tubes, for the region where they exited the irreversibly bonded PDMS layers. The process was completed by baking the bonded layers for one or more hours in a convection oven heated to 80º C. The irreversibly sealed layers where then cut and positioned accordingly onto a clean glass substrate.

2) Microvalve Actuation, Registration, and Design

D) Microvalve Actuation and Registration

The micropump was actuated with piezoelectric cantilevers (Piezo Systems, Q220-A4-303YB), using a square wave signal, where the signal to each of the respective cantilevers was placed 120º out of phase, thereby creating a peristaltic wave motion. The signals were controlled using a virtual function generator created in LabVIEW (National

Instruments). These small signals were then amplified to ±90 V with high voltage external hardware that contained high-voltage op-amps (Apex Microtechnology, PA15A). Closure of the channel was achieved with precision-machined external microvalves clamped to the ends of the cantilevers. Three sets of valve tip dimensions were utilized for the current Chapter, where the length / width dimensions corresponded to 3 mm / 250 μm, 2 mm / 250 μm, and 1 mm / 250 μm. Registration of the valve tips over the microchannel was achieved using in-house machined micropositioners containing preassembled stage bodies (Edmond Scientific, #56-416), that allowed for adjustments to be made; in / out (horizontal), up / down (vertical), and angled up /down (vertical arc).

E) Microvalve Design

The schematic shown in Figure IV-1 shows a 3D schematic of a single external microvalve, with the length and width directions highlighted across the body of the microvalve. The external valve tip, is the active region that makes contact with the 5 : 1 PDMS membrane, which allows the microchannel to be placed in any state between fully open to fully closed. All microvalves were electrical discharge machined (Agie, AgieCut Classic) with the same length and width dimensions for the bulk portion of the microvalve body. The tip as shown was the portion of the microvalve that was varied for the current Chapter. All microvalves used for data presented within, had a 250 μm width, where the length direction was varied as 1, 2, and 3 mm. Experiments designated as "3 mm Valves" for example, indicates that all three valves for that particular experiment

had dimensions of 250 μm in width, and 3 mm in length (i.e. there was no mixing of valve sizes). Figure IV-1A shows a cross-sectional end image of a microvalve tip, where Figure IV-1B shows a valve tip spanning the entire width of the body (i.e. 3 mm), in contrast to that of the cartoon, where this image is representative of what a valve would look like with a 1 mm tip length, for example.

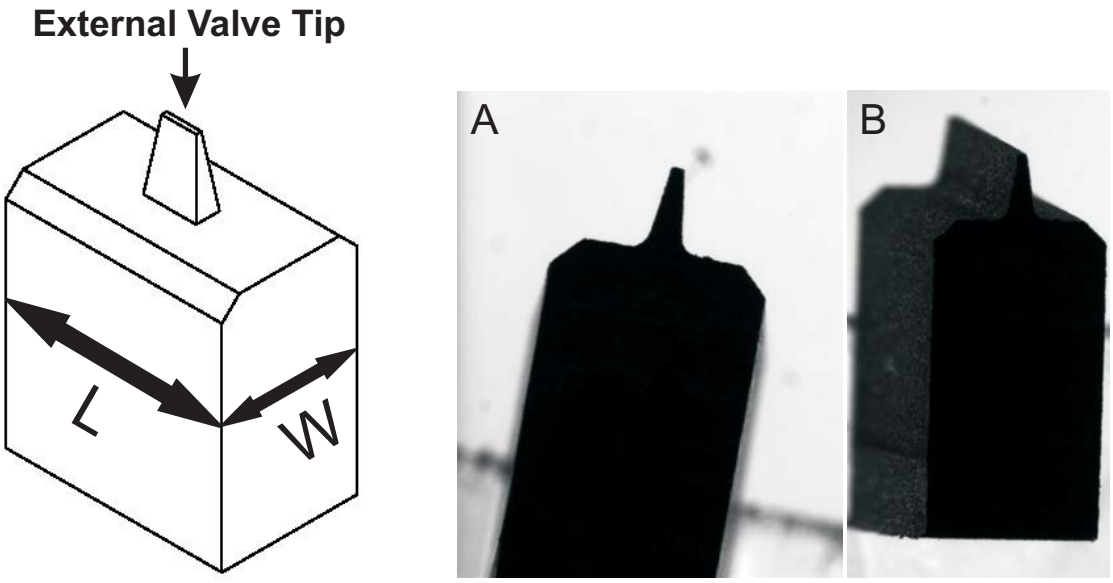

Figure IV-1: Cartoon and actual images of microvalves. Cartoon illustrates how valve tip dimensions were varied, where valve tip widths remained constant at 250 μm, with lengths being varied at 1 mm, 2 mm, and 3 mm. Image A shows a side cross-sectional view of a microvalve tip, with image B illustrating the full width of the valve tip, in contrast to that shown for the cartoon. All microvalves were precision machined from aluminum.

3) Micropump Characterization Experiments

F) Flow Rate Characterization

Flow rates were measured by connecting the outlet line of the micropump to a second piece of capillary tubing ~1 m in length, that had been previously filled with a blue food dye solution. The second piece of capillary tubing was placed in contact with a

meter stick. When connecting the outlet line of the micropump with the second piece of capillary tubing, a ~2 – 3 mm long bubble was intentionally introduced, allowing for tracking of the bubble against the ticks/gradations of the meter stick. The formula Q = Av was used to calculate flow rates, where Q = flow rate, A = cross sectional area of flow, and v = linear velocity recorded for the bubble. All measurements were taken with the cantilevers actuated with square waves, and placed out of phase by 120º. Error bars shown represent the standard error of the mean, with (n = 6) for each valve tip dimension tested (i.e. 1, 2, and 3 mm length valve tips).

G) Charging Profile Characterization

The micropump was first allowed to attain a steady state, with square wave signals actuating the cantilevers at 30 Hz and 120º out of phase. After this brief period, the outlet line of the capillary tube was connected to a pressure sensor (Honeywell, 40PC015G2A). Voltage readings from the pressure sensor were recorded over the course of two hours, and subsequently converted to pressure readings using the manufacturers sensitivity conversion of 266.6 mV/psi.

H) Backpressure Characterization

Maximum attainable backpressure data was collected similarly to that already described within the previous Charging Profile Characterization section. The outlet line of the micropump was connected to a pressure sensor and allowed to fully pressurize. All experiments performed utilized square waves actuated 120º out of phase. The frequency

chosen to pressurize the micropump, was 40 Hz for the 3 mm x 250 μm valves, 45 Hz for the 2 mm x 250 μm valves, and 25 Hz for the 1 mm x 250 μm valves. After achieving a stable maximum backpressure reading, the micropump was stopped, where one microvalve was left in the fully closed position. Pressure loss measurements were recorded over the course of a 15 minute interval, where at 15 minutes, the microvalve was actuated to the fully open position, and subsequent measurements were recorded until no pressure was recorded within the micropump system. For each of the respective valve sizes, (n = 3) experiments were performed.

I) Valve Leakage Characterization

Experiments were performed to test whether or not pressure losses within the system were likely due to blow-by past the microvalve, or losses due to other sources. The micropump was allowed to fully pressurize as already described within the Backpressure Characterization section above. After reaching a stable and steady maximal backpressure reading, the micropump was stopped, where in the first set of experiments, only one valve was left in the fully closed position. The second set of experiments kept all 3 valves in the fully closed position. Readings were recorded with the pressure sensor over the course of a 15 minute period, and then plotted as a summary for all experiments. For both sets of experiments using 1 vs. 3 microvalves, (n = 3) experiments were performed using valve tips with dimensions 2 mm x 250 μm.

J) Valve Shutoff Cycle Characterization

Data for these experiments were collected by placing the micropump in an inverted position under an epifluorescent microscope (Nikon SMZ1500 with filter cube 470/440/500 excitation/emission/long pass), where a black cape was placed around the micropump and objective lens so as to block the surrounding ambient light. A syringe pump was then used to flow solution through the micropump at 1 μL/min. After stopping the syringe pump, the solution was allowed to dissipate from the outlet line of the micropump for 30 s, where after this time-frame, the outlet line of the micropump was capped off. Intensity values were recorded at 30 V actuation intervals for the micropump, between -90 V and 90 V using a CCD camera. These measurements were first performed using distilled water as a working solution, and then using a 10 mM fluorescein solution. The water signal was subtracted from the fluorescein signal using Metavue software.

Results and Discussion

4) Flow Rate and Microvalve Design

Flow rate data collected for the current Chapter can be observed in Figure IV-2. This plot shows three flow curves for all three valves at the cantilever tips either 1, 2, or 3 mm in length, where in all cases the width remained constant at 250 μm. The overall flow rate range for the three curves is 14 – 138 nL/min. Figure IV-2 also indicates the 3 mm valves were able to produce the highest flow rates of the three lengths tested, with a maximum flow rate of 138 nL/min (25 Hz), where the 1 mm valves produced the

lowest flow rate, characterized as 14 nL/min (0.1 Hz). This finding was expected, and therefore not surprising. It was hypothesized, a microvalve tip with a larger contact surface area, would translate into a larger stroke volume produced, and therefore larger overall flow rates being observed for valve tips with larger overall footprint sizes. The trend of observing higher flow rates for larger contact surface area microvalves holds for the 1 mm and 2 mm valves past 30 Hz. Lower frequencies however show a reversal of the expected trend. For sub-30 Hz frequencies, the plot reveals that the 1 mm valves actually produced a higher flow rate than the 2 mm valves. It is hypothesized the reason this data shows this unexpected reversal is due to minor variations in tilt of the microvalve tips, with respect to the microchannel. More specifically, when the microvalves are placed in contact with the PDMS membrane, the plane that defines the tip surface is expected to be parallel to that of the plane that defines the PDMS membranes surface, where tilt in this case would refer to the valve tip being altered such that the tip surface plane would no longer be parallel to that of the PDMS membrane surface plane, where the net effect would translate to, the ends (along the length direction of the tip surface) of the valve tip retaining two distinct height values, when taken with respect to the PDMS membrane surface. This hypothesis could more generally be characterized as a "squeegee effect." A deeper discussion of the microvalve tilt/squeegee hypothesis is presented within Chapter VI.

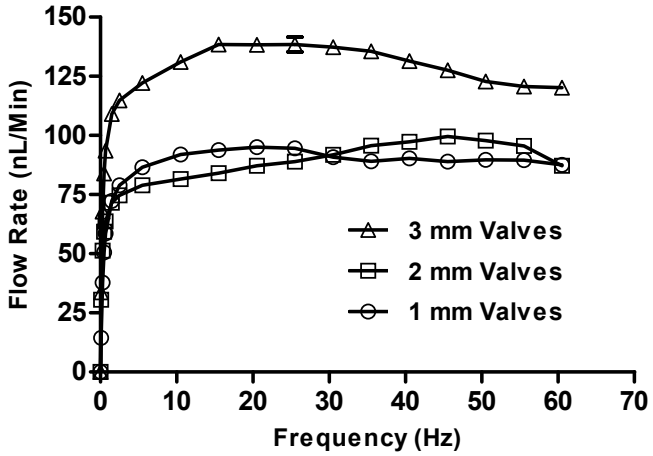

Figure IV-2: Plot of Flow Rate (nL/min) vs. Frequency (Hz) for microvalves with variable surface areas. Valves were machined as (1 mm x 250 µm), (2 mm x 250 µm), (3 mm x 250 µm). All experiments were performed by tracking a bubble 2 – 3 mm in length, while using a 120º square wave signal. Standard error bars plotted for (n = 6) experiments for each valve size.

5) Backpressure and Charging Profile for Microvalves

Figure IV-3 shows a plot of backpressure data collected for the three microvalve sizes tested. The data shows the trend; 3 mm valves > 2 mm valves > 1 mm valves for maximum backpressures achieved. It would be expected that a peristaltic pump with larger stroke volumes, would be able to work against higher backpressures, since the net flow produced by a 120º signal operates in part on the basis of the stroke volume produced by the microvalves. This plot also shows different discharge profiles, where the time observed for full dissipation of pressure within the system follows the trend; 3 mm valves > 2 mm valves > 1 mm valves. A possible explanation to explain this trend could be provided by noting that, when not in a fully open state, a larger surface area microvalve would be expected to provide more resistance to backflow over a smaller surface area microvalve. That is, in the instance the respective valve even slightly bowed

the membrane into the channel while in the fully open position, this bowing region produced below the valve would serve as a resistance point, and therefore impede flow past the valve as the system depressurized. A larger contact surface area microvalve would produce a larger bowing region into the channel, and therefore produce a larger resistance to backflow as well.

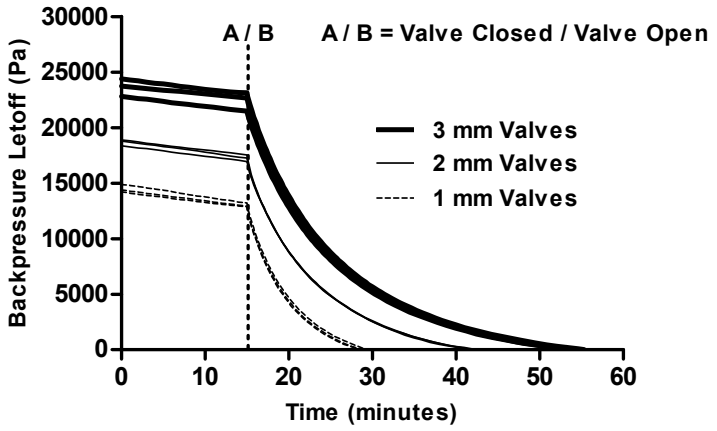

Figure IV-3: Plot of Backpressure (Pa) vs. Time (min). All experiments performed using a 120º square wave signal. The micropump was allowed to actuate and fully pressurize the outlet line connected to a pressure sensor. After reaching a fully pressurized state, the micropump was stopped, where only one valve was left in the fully closed state. After 15 minutes, the valve was opened, where subsequent measurements were taken until the pressure within the system had fully dissipated. For each of the valve dimensions, (n = 3) experiments were performed.

Figure IV-4 shows a plot of the time-course for fully charging the micropump system. It can be seen that the charging profile rapidly increases, and starts to plateau at approximately 30 minutes. The data indicates that ~90% of the maximum pressure, P_{max}, is achieved at ~26 minutes, ~95% of P_{max} achieved at ~33 minutes, and ~99% of P_{max} being achieved somewhere between ~54 - 60 minutes. Pressure readings fluctuate slightly when the pressure reaches ~99% of P_{max}, but does continue to rise overall until reaching an average maximal backpressure (i.e. P_{max} fluctuates slightly).

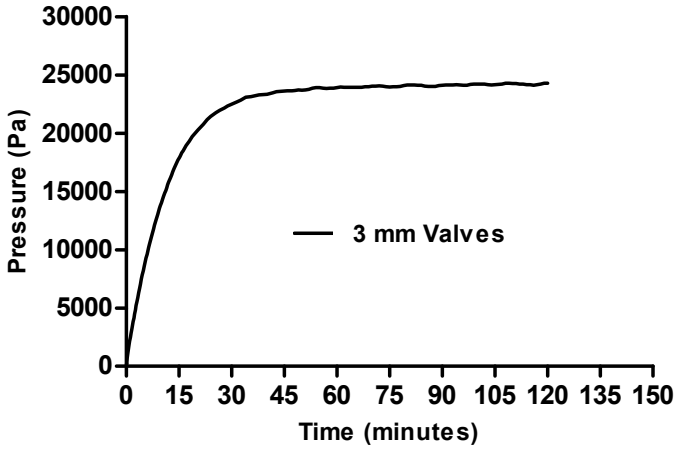

Figure IV-4: Plot of Pressure (Pa) vs. Time (min). Plot shows pressurization profile when the micropump outlet line is connected to a pressure sensor, and actuated at 30 Hz using a 120º square wave signal. Plot is for a single representative experiment.

6) Valve Leakage for 1 vs. 3 Microvalves

Figure IV-5 shows a plot of pressure loss recorded over a 15 minute time span for a fully pressurized micropump. The plot represents 6 total experiments, where (n = 3) experiments were performed for 3 valves in the fully closed position, as well as (n = 3) experiments for a single valve in the fully closed position. As the plot indicates, all 6 recordings show virtually the same rate of pressure loss, where the rates remain constant over the course of the 15 minute observation period. This same rate of pressure loss can also be observed in Figure IV-3, for readings taken over the course of the first 15 minutes. The pressure loss of Figure IV-5 indicates there is a consistent and inherent pressure loss that is observed when taking such readings. Had the pressure loss been a result of blow-by across the microvalve/s, the rate of pressure loss would be expected to be very different due to the significant difference in resistances for one vs. three fully closed microvalves. No experimental results have ever been consistent with a hypothesis

that this inherent pressure loss was a result of a partially closed microvalve, i.e. leakage/backflow across the microvalve. The current set of results solidifies the belief that the pressure loss is occurring in some other part of the pressurized system rather than loss due to valve leakage. It is believed the pressure loss is primarily due to the external connections made to the micropump outlet line, or possibly through the connection made to the pressure sensor input port.

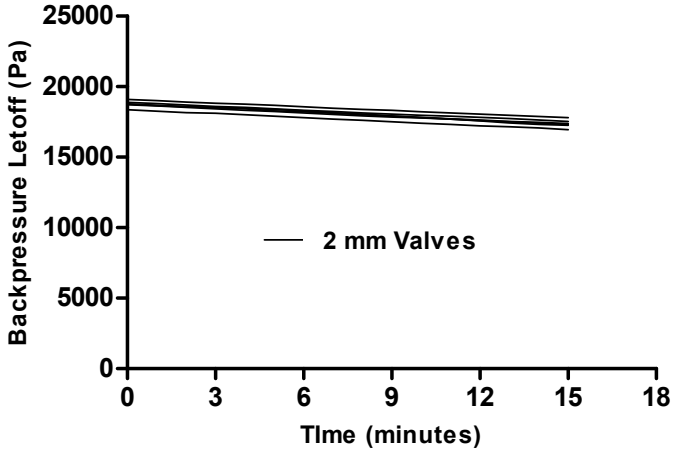

Figure IV-5: Plot of Backpressure Letoff (Pa) vs. Time (min). Plot to observe pressure loss within a fully pressurized micropump system. Two sets of three experiments were performed. The first was to test the effect of pressure loss for all three valves closed, and the second for only one valve closed.

7) Valve Shutoff Cycle for Microvalves

The valving cycle for the respective 1, 2, and 3 mm length microvalves can be observed in Figure IV-6. It can be seen that the three valve sizes produce data that shows the valves close the channel off with slightly different shutoff characteristics. It is noted for the 1, 2, and 3 mm length valves, that they show the channel being fully closed off at 0 V, -60 V, and -30 V respectively. It is believed this is due in part to the final

positioning of the microvalve over the microchannel, before actuation of the micropump is performed. Depending on the final adjustment state, it is possible the microvalves could travel along a slightly different actuation path with respect to the microchannel. One such instance of variability could be introduced if one cantilever (e.g. 1 mm valve) required a tilt adjustment of the micropositioner, to allow for proper registration of the microvalve over the microchannel, where the other cantilever (e.g. 3 mm valve) did not require such an adjustment for proper registration of the microvalve over the microchannel. Likewise, the final vertical positioning state of the microvalve over the microchannel could slightly alter the closing characteristics of the microchannel. In the instance however that the vertical positioning were maintained constant for all cantilevers and microvalves, the difference in pressure exerted by valves of different surface areas could also affect the measured valve cycle curves. The blocked force (maximal force output when recorded with zero deflection) for the cantilevers used for these experiments is reported as 0.24 N by the manufacturer. Therefore, the cantilevers with valve tip dimensions of (1 mm x 250 μm), (2 mm x 250 μm), and (3 mm x 250 μm), would be able to produce maximal pressures of 960 kPa, 480 kPa, and 320 kPa, respectively. The steep slope observed from 90 to 30 V for the 1 mm valve is likely due in part to the very large pressures that are generated when using these valves, as compared to that of using the 2 mm and 3 mm valves, where it would be expected a larger PDMS membrane deflection at each corresponding potential would result for the 1 mm valves (when compared to that of the 2 mm and 3 mm valves), due to the significantly higher pressures generated beneath these microvalves.

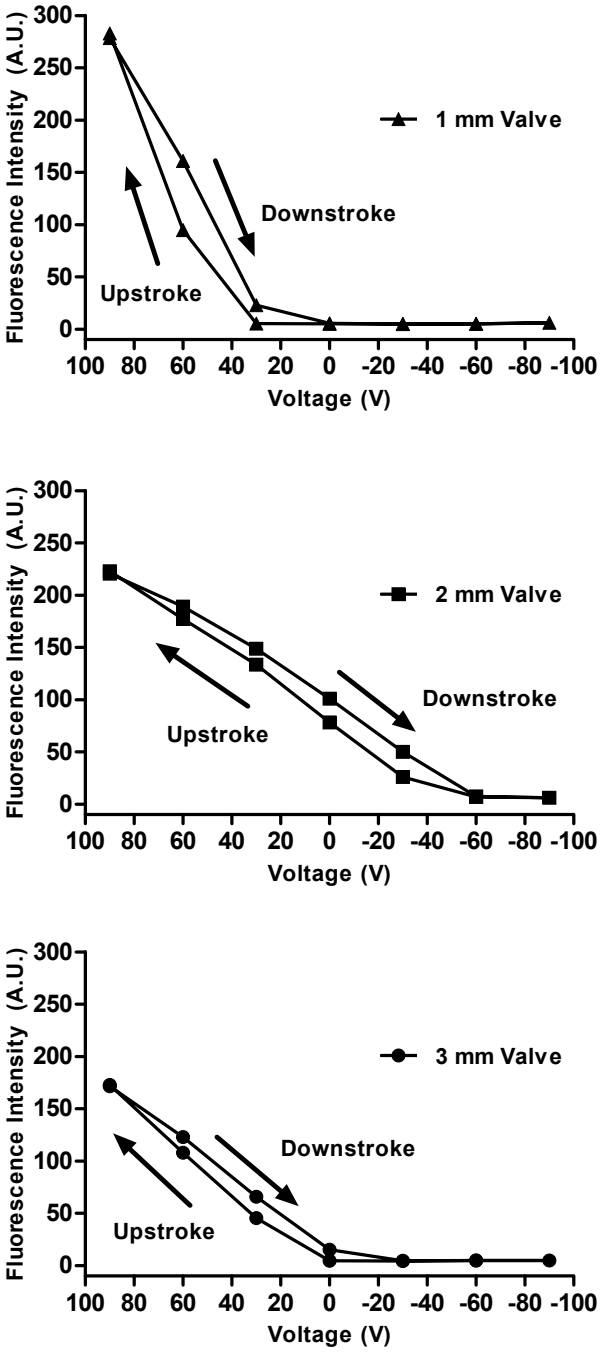

Figure IV-6: Plots of Fluorescent Intensity (A.U.) vs. Voltage (V). The micropump was placed in an inverted position and imaged using a CCD camera attached to an epifluorescent microscope. Data was collected by taking images of the microvalves, for 30 V cantilever actuation intervals. Distilled water was initially imaged within the channel, followed by imaging performed using 10 mM fluorescein. The water signal was background subtracted from the fluorescein signal using Metavue software.

Conclusions

The results presented within this Chapter focused on the characterization of external microvalves with variable cross-sectional surface areas, for a PZT piezoelectric cantilever-actuated PDMS peristaltic micropump. It was observed that the larger surface area microvalves tended to typically produce higher flow rates and backpressures. The flow rate results indicated a reversal of this general trend for frequencies up to ~25 Hz, for the 1 mm and 2 mm length microvalves. The overall flow rate range for the three valve sizes, was characterized as 14 – 138 nL/min. Pressure loss data was also collected, to further lend evidence to the belief that the current microvalving design is leak-free, and therefore indicating recorded pressure losses are likely due to other sources such as loss through capillary tube connections. Finally, valve cycling data provided evidence that the cantilever/microvalve assembly can fully close a microchannel easier when using smaller surface area microvalves, presumably due to the higher pressures generated over the microchannel when using smaller surface area microvalves. The microvalve characterization results provided within this Chapter allow for other microchip designs to be explored and utilized across a wide array of fields, where this micropump design may prove useful.

Chapter V : *A Comparison of Two Mechanical Micropositioner Designs, for Microvalve Registration within a PDMS Peristaltic Micropump*

Synopsis

A second generation (2G) micropositioner design was fabricated, and integrated within a peristaltic micropump. The 2G design was utilized for the purpose of positioning both piezoelectric cantilevers and microvalves over a PDMS fabricated microchannel. The 2G micropositioners allow for an increased degree of adjustment capability, in providing the option to laterally "tilt" the microvalves, such that each microvalve contact surface plane is brought from being parallel to the PDMS membrane surface plane, to a nonparallel state. The lateral tilt adjustment capability allows for the microvalve to be actuated as a "squeegee," in effect increasing the valve stroke volume in the peristaltic signal bias direction. Changes in microvalve lateral tilt, effectively translates into alteration of the peristaltic signal waveform shape. The 2G micropositioner design further allows for microvalve lateral tilt to be continuously altered on-the-fly in real-time. The first and second generation designs will be presented as a comparison, where additional data will be presented to highlight the improved vibration isolation of the second generation, over that of the first generation design.

Introduction

The fields of micro and nanotechnology provide many unique opportunities to study a wide array of scientific phenomena. In some cases, these opportunities are made possible when new or improved instrumentation becomes available, that allows for control of matter on such small length scales.[1292-1298] In the case of microfluidic device technology, self-alignment fabrication strategies have been proposed for fabrication of

multilayered device platforms.[289-291] In other cases where registration is a necessity, such as micropump or microvalve actuator alignment, these devices are oftentimes fabricated with one initial registration step that fixes the actuators in place for the entire life-cycle of the device. This is true for many monolithic pneumatic[629, 630] and piezoelectric[644, 645, 649, 1260, 1299] pump designs. Such designs are convenient for eliminating the need for any future registration steps, but do however limit the option of providing later actuator adjustments, should these adjustments be necessary or desired for any particular reason.

This Chapter will present a piezoelectric cantilever-actuated peristaltic micropump, designed for use with external microvalves. The external microvalves were placed in contact with a PDMS microchannel membrane, and positioned over the microchannel using in-house fabricated micropositioners. Two micropositioner designs will be reported, with the second generation micropositioner design allowing the option to provide tilt to the external microvalves. A tilted microvalve is capable of providing a microchannel squeegee action, in driving the microchannel contents preferentially in one direction over that of the opposite direction. The second generation micropositioner design provides significantly improved registration and positioning performance over the first generation design, in addition to providing greatly improved vibration isolation characteristics. The first and second generation micropositioner designs will be compared for their microvalve positioning capabilities, and additionally, experimental data will be provided to highlight the improved vibration isolation characteristics of the second generation design, over the first generation design.

Materials and Methods

1) PDMS Microchannel Fabrication

The PDMS microchannel with capillary tube interconnects, was fabricated by bonding two individual pieces of capillary tubing between two layers of PDMS. The PDMS molded microchannel layer was fabricated using a portable handheld injection mold apparatus that was manufactured in-house using CNC machinery. The injection mold was fabricated primarily from aluminum, where the specific design details are presented within Chapter III. Briefly however, the injection mold incorporated a cylinder and piston driving mechanism, that was used to inject 5 : 1 PDMS prepolymer (GE, RTV615) into a molding cavity. The molding cavity was created by compressing a laser machined gasket between the top and bottom plates of the injection mold. The machined gasket served a two-fold purpose, where the removed central-portion of the bulk gasket material (McMaster-Carr, 9513K118) created the injection mold cavity, and second, the thickness of the gasket material served to regulate the overall thickness of the PDMS layer, and therefore regulate the microchannel membrane thickness as well. A replica molding template was formed against the bottom plate of the injection mold, by threading a piece of 75 μm diameter wire (molybdenum) through opposite ends of the bottom plate. The threaded wire was then wrapped around posts machined into the backside of the bottom plate, where subsequently the wire was secured in a taut state by crimping a nut and Teflon washer over the threaded/wrapped wire. A thin film of general purpose spray adhesive was next applied across the surface of the bottom plate that contained the straddled wire. Soon after, a piece of general purpose aluminum foil was

molded against the taut wire, using a straight edge from a Teflon block. Just prior to assembling the injection mold apparatus, inspection of the molding template was performed under a microscope, where common laboratory solvents such as acetone and IPA were used to remove existing contaminants across the surface of the template.

Exhaust ports were machined into the bottom plate at the end opposite the pistons location, so as to allow for the injected 5 : 1 prepolymer to exit across these ports. These exhaust ports allowed for a pressure differential to be created across the entire length of the cavity, where the prepolymer was injected without performing a degassing step. The pressure differential was high enough, so as to allow for any and all bubbles trapped within the PDMS to be forced across the exhaust ports. A bubble-free mold was produced after placing the injection mold apparatus in an oven at 80º C, for one or more hours. Placing the injection mold into an oven expedited the curing process. Cooling of the apparatus was performed by placing the injection mold under a cold water faucet. The injection mold apparatus was then disassembled, with the mold being placed across a clean glass substrate. The channel height was measured as 102 μm for a first device, and 119 μm for a second device. The membrane thicknesses over the microchannel was 85 μm for both devices.

The two devices were bonded with a 30 : 1 PDMS base layer. The first device (i.e. 102 μm channel height device) base layer was fabricated using a sandwich PDMS molding process. This process began by placing two 6" glass wafers in separate desiccators, where the wafers were allowed to soak in a PDMS antiadhesion vapor (United Chemical Technologies, T2492) for different, yet overlapping time intervals.

This step allowed for selective removal of one wafer over the other. Prior to pouring the prepolymer PDMS, a degassing step was performed, by spinning the PDMS in a centrifuge at 5000 RPM for 2-3 minutes. The degassed PDMS was then poured over one wafer surface, with subsequent placement of the second wafer over the first wafer containing the poured PDMS. The sandwiched 30 : 1 PDMS layer thickness was regulated by placement of ~203 μm thick spacers between the first and second wafers. The two wafers were held in place using binder clips. The glass sandwich was then placed in an oven at 80º C for 35 minutes, to allow for partial curing of the 30 : 1 PDMS. The resulting 30 : 1 thickness was measured to be ~200 μm.

The second device (i.e. 119 μm channel height device) 30 : 1 base layer was fabricated using a photolithography spinner (CEE Model 100). Prior to spinning, an antiadhesion vapor soak was performed by placing a glass wafer in a desiccator for ~1 hour, as described above. The prepolymer PDMS was then spun using the program: 1) 400 RPM, 50 RPM/sec, 10 sec, 2) 1000 RPM, 200 RPM/sec, 45 sec.. The wafer was then placed in an oven at 80º C for 35 minutes, to allow for partial curing of the 30 : 1 PDMS. The resulting 30 : 1 thickness was measured to be ~83 μm.

Bonding of the 5 : 1 and 30 : 1 layers was performed under a microscope. The 5 : 1 channel layer was first placed under the microscope, where two separate pieces of capillary tubing (Polymicro, 105/40 μm – OD/ID) were placed ~1.5 cm into opposite ends of the molded microchannel. Prepolymer 5 : 1 PDMS was then lightly applied over the capillary tubes, to seal all void areas. Excess 5 : 1 was carefully removed using a razor blade. The respective partially cured 30 : 1 base layers were then placed in contact

with the 5 : 1 layer. Moderate pressure was applied to optimize the seal between the two layers of PDMS. The wafer adhered to the 5 : 1 channel layer was then removed, leaving the membrane surface of the 5 : 1 layer exposed to the atmosphere. Further smoothing of the PDMS was performed by grazing a razor blade gently across the membrane surface, to optimize the bonding of the two layers. The bonded layers were then placed in an oven at 80º C for one or more hours, to allow for an irreversible bond to occur between the two layers. The PDMS channel mold was then removed from the glass substrate, and aligned to a clean glass substrate. The final processing step was to apply 5 : 1 prepolymer to the ends of the microchannel, where the capillary tubes exited the bonded layers (i.e. the transition area in going from being bonded between the two PDMS layers, to being exposed to the atmosphere).

2) Micropositioner Fabrication

All aluminum parts used in the construction of the first generation (1G) and second generation (2G) micropositioners, were fabricated from 6061 T6 grade aluminum. The 1G micropositioners were fabricated as previously described within Chapter II. The bulk portion of the 1G micropositioners were CNC machined (Agie, AgieCut Classic) from aluminum, and thereafter anodized to prevent any possible arcing that might occur between the cantilevers and aluminum micropositioner bodies. The micropositioner bodies consisted of two machined aluminum sub-body parts being joined by two micropositioner stages (Edmond Scientific, #56-416). One of the sub-body parts was machined to integrate a flexible hinge, as a part of its physical design. The stages allowed for translational adjustments to be provided to the cantilevers and microvalves in

the Z-Y directions, with the hinge allowing for arc tilt adjustments (discussed more fully within the Results and Discussion section of this Chapter). Two metal screws were used to secure the cantilever mounts within the micropositioners. Three additional plastic screws were threaded through one of the aluminum bodies, and used to secure the micropositioners to the glass substrate containing the prior fabricated PDMS microchannel mold.

The 2G micropositioners were fabricated in-part using commercially available micropositioner bodies (Quater Research, XYZ 300MR). The micropositioner bodies allowed for X-Y-Z adjustments to be made (discussed more fully within the Results and Discussion section of this Chapter), and were attached to an aluminum base, where they could be guided along a "track" machined into the base. The track was formed by machining a lengthwise crevice through the base. The micropositioner bodies further had a "dummy" plate attached to their base, which contained a threaded hole. Allen screws were placed through the crevice from the backside of the plate, and tightened into the micropositioner "dummy" plate. Tightening of the Allen screws secured each individual 2G micropositioner body in place, and also served as a crude first positioning/adjustment step.

The 2G micropositioners had two further machined attachments connected to their bodies. The first attachment was an aluminum wishbone tilt arm mechanism, which allowed for lateral tilt adjustments to be performed. The second attachment was an aluminum part fabricated with both a clamping mechanism, and a hinge mechanism. The clamping mechanism served to secure the cantilevers in place, where the hinge

mechanism allowed for arc tilt adjustments to be provided to the cantilevers and microvalves. The second attachment was secured to the first attachment, with the first attachment secured to the micropositioner body. The adjustment capabilities for both micropositioner designs as a whole will be explored more deeply within the Results and Discussion section of this Chapter.

The final major design aspect of the 2G micropositioners was the use of a plastic screw clamping mechanism. This was a simple clamping system that was used to secure in place the glass substrate containing the PDMS microchannel mold. The glass substrate was secured flush to the aluminum base, to which the micropositioner bodies were also secured to.

3) Micropump Actuation

The micropump utilized external piezoelectric cantilevers (Piezo Systems, Q220-A4-303YB) as an actuation means. The cantilevers as supplied by the manufacturer come with a quick mount system, with pre-wired connections. An appropriately sized Delrin (or printed circuit board material) block was adhered to the bottom of the quick mount, with an in-house machined acrylic block adhered to the top of the quick mount. The mounts properly secured the cantilevers into the 1G and 2G micropositioners. Machined aluminum clamps were adhered to the tips of the cantilevers, with the clamps securing in place CNC machined (Agie, AgieCut Classic) microvalves. The microvalves were machined from aluminum, where each valve containing a finely machined valve tip. The contact surface area of each valve tip (see Chapter IV) to the PDMS membrane surface measured 3 mm by 250 μm (L x W).

Each of the cantilevers were actuated with a square wave signal, with each signal delivered 120º out of phase, in effect creating a peristaltic wave actuation motion across the membrane surface. The square wave signals were created using a virtual function generator (National Instruments), and further amplified using in-house fabricated electronic hardware that contained high voltage amplifiers (Apex Microtechnology, PA15A). Potentials of ±90 V were used to drive the cantilevers, where this was also the maximum allowable signal amplitude before depoling of the cantilevers starts to occur. Driving the cantilevers at this maximum allowable potential allowed for maximal tip deflection to be attained.

4) Flow Rate Characterization

All flow rate data for the current Chapter was collected by tracking a 2-3 mm bubble through an external piece of capillary tubing connected to the outlet capillary tube line of the micropump. Additionally, all flow rate data was collected using square wave signals actuated 120º out of phase. The external capillary tube was first filled with blue food dye, prior to mating with the outlet line of the micropump. The use of blue food dye allowed for better contrast and therefore increased tracking capabilities of the bubble. The bubble was tracked against the ticks/gradations of a meter stick, where the flow rate was calculated using the formula, $Q = Av$, with Q = flow rate, A = cross sectional surface area of the flow, and v = linear flow velocity of the bubble.

Flow rate data for the current Chapter were collected by utilizing micropumps fabricated with both 200 μm and 83 μm 30 : 1 base layers. In addition, flow rate data were also collected with both Generation I and II micropositioners. An additional

variable examined was to collect flow rate data for the Generation I micropositioners, with the glass substrate containing the PDMS microchannel mold being; 1) hoisted with use of substrate stabilizer blocks, or 2) not being hoisted at all. The stabilizer block experimental setup can be observed in Figure V-1. This Figure shows the micropositioner bodies hoisted, and therefore isolated from making contact with the base of the microscope stage. Without use of the stabilizer blocks, the micropositioner bodies rested fully upon the stage of the microscope base. All flow rate curves contain (n = 5) trials, with error bars representing the standard error of the mean.

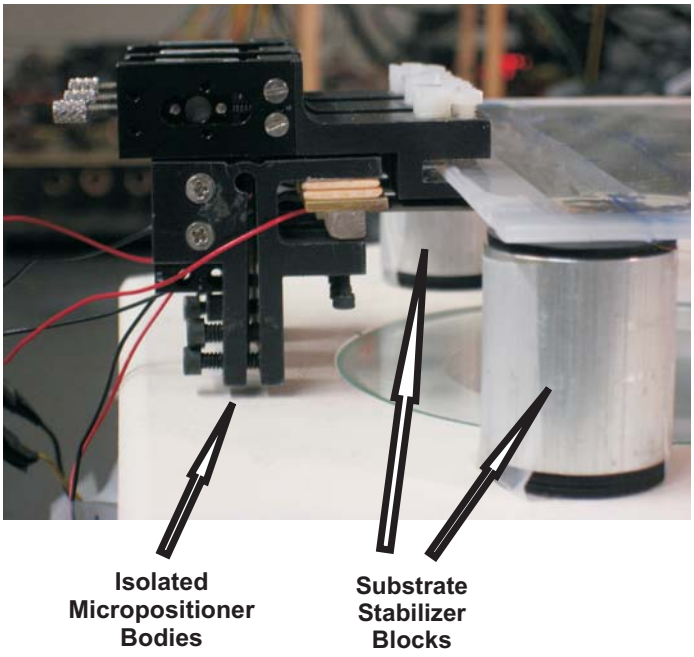

Figure V-1: Image of Generation I micropositioners, with use of substrate stabilizer blocks. The micropositioner bodies were isolated from the stage of the microscope base with placement of the stabilizer blocks beneath the glass substrate.

Results and Discussion

5) Micropositioner Design Features

The two micropositioner designs used within the current Chapter can be seen in Figure V-2. Image B of Figure V-2 is a side view of the Generation I (1G) micropositioners. This micropositioner design allowed for significantly less positioning capability of the cantilevers and microvalves, over that of the Generation II (2G) micropositioners, and additionally provided less vibration isolation in comparison to the 2G micropositioners. The 1G micropositioner design employed two integrated micropositioner stages, which provided adjustment capabilities in the Z and Y-directions. This design also incorporated a hinge mechanism similar to that utilized within the 2G design, with the hinge allowing for angled Y-axis (arc of Y-axis) adjustments to be provided to the cantilevers and microvalves. The summary of adjustments possible with the 1G design is shown for the 2D axis pasted within image B of Figure V-2. It should be noted, it was possible in a crude way, to alter the lateral tilt (shown for Figure V-3B) of the microvalves using the 1G micropositioners. This process was achieved by placing one or more small pieces of Scotch tape under the bottom mount of the cantilevers. This process did provide for some control over lateral tilt, but proved to be slightly unwieldy and erratic at times, especially as the number of small pieces of tape under the mounts increased. This crude lateral tilt capability however, provided pilot lateral tilt experimental data, which was useful for future 2G design considerations.

Image A of Figure 2 is a side view of the 2G micropositioner apparatus. Each micropositioner body for each individual cantilever, contains three knobs for adjusting

travel in the X-Y-Z directions, with these directions indicated by the 3D axis pasted within the image. The manufacturer reports a travel of 0.300" (7.62 mm) in each direction, where additionally it is reported the resolution per turn is 0.025" (635 μm). Integration of a hinge mechanism as shown by the arc tilt arm, allowed for angled Y-axis (arc of Y-axis) adjustments to be provided to the cantilevers and microvalves. This is to say, the Y-axis can be adjusted in a way such that the arrow at the tip of the Y-axis can be shifted in the Z-direction, while keeping the Y-axis origin fixed. This motion is depicted by the arcing arrow along the Y-axis.

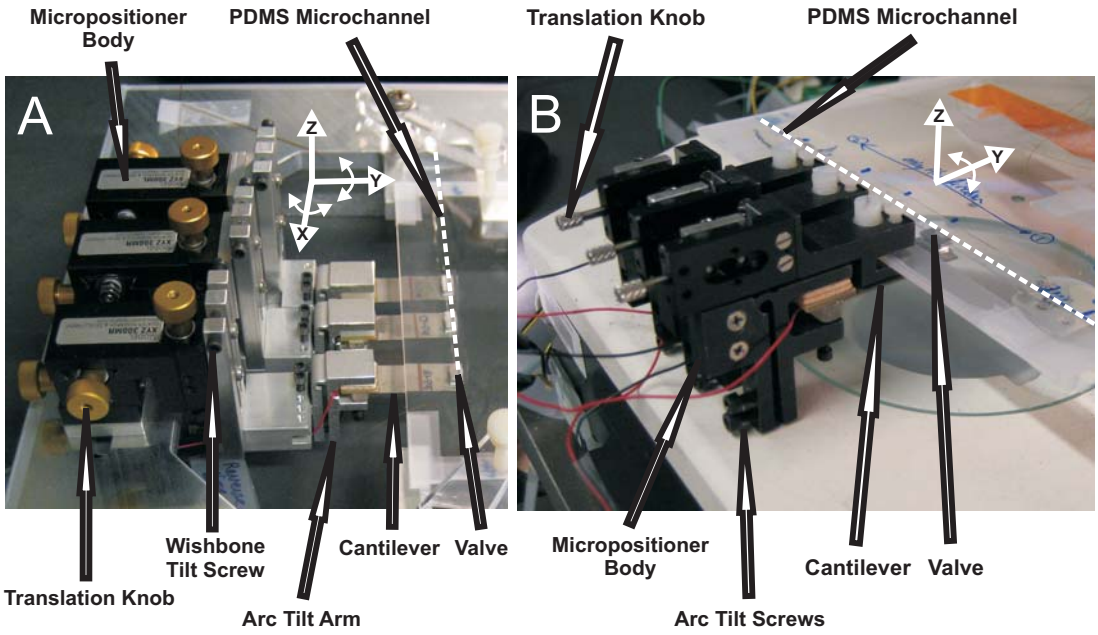

Figure V-2: Image of Generation I and II micropositioners. Images A and B show three micropositioner bodies placed adjacent to one another, for positioning the piezoelectric cantilevers and microvalves over the PDMS microchannel (depicted as dotted line). Image A is a representation of the Generation II micropositioner design, where the X-Y-Z adjustments are made with the translation knobs. The lateral tilt adjustment is made with the wishbone tilt screw, where the motion produced is indicated by the arced arrow on the X-axis. The arc tilt adjustment is made with a screw below the bodies, but is not visible as shown. The arced arrow on the Y-axis indicates the arc tilt motion. Image B is a representation of the Generation I micropositioner design. The Y-Z adjustments are made with translation knobs as shown, with the arc tilt adjustments being provided by the screws as indicated. The arced arrow along the Y-axis indicates the arc tilt motion.

The 2G micropositioners were also capable of providing a lateral tilt adjustment to the cantilevers and microvalves. This process was achieved by using a wishbone tilting mechanism, as shown more fully within Figure V-3. This mechanism employed three arms, with the center arm being fixed in place. Proper adjustment of the wishbone tilt screws allowed for both the cantilever and microvalve to be laterally tilted. That is, when the wishbone tilt screws are adjusted, the valve tip is spatially altered such that the valve tip surface would no longer be parallel to the membrane surface. An increase in lateral tilt is observed for the sequence of images proceeding to the right within image B) of Figure V-3. The overall effect is to not only spatially alter the X-axis' arrow tip (shown in Figure V-2), but also the location of the origin as a whole for all three major axis adjustments (when the origin is taken with respect to the center of the valve tip surface). This adjustment is depicted in a general sense for the arcing arrow on the X-axis as shown in image A of Figure V-2. It can also be noted, the lateral tilt adjustment capability allows for the microvalve to be actuated as a "squeegee," in effect increasing the microvalve stroke volume in the peristaltic signal bias direction, with a deeper discussion of the "squeegee" effect provided within Chapter VI. Changes in microvalve lateral tilt, effectively translates into alteration of the peristaltic signal waveform shape. Lastly, all adjustments for this particular micropositioner design are capable of providing real-time continuous on-the-fly microvalve adjustments.

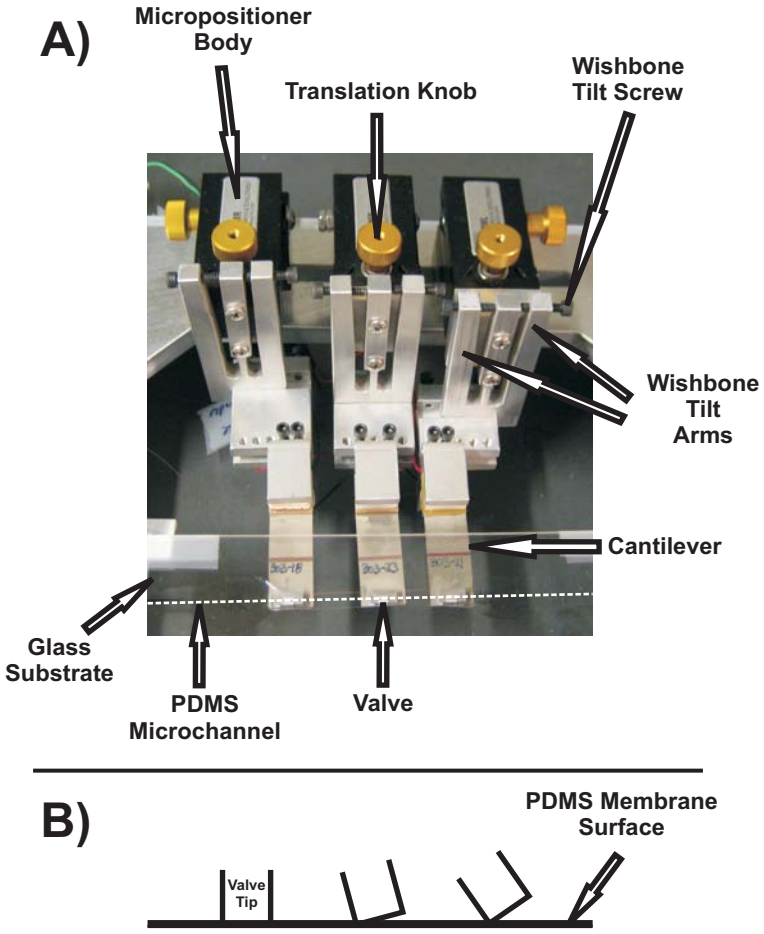

Figure V-3: Generation II micropositioners, with image A) providing a detailed head-on view of the wishbone tilt arms, and used to alter the lateral tilt of each microvalve. Image B) is a cartoon representation for a head-on view of microvalve tips, for a cross-sectional plane taken parallel to the longitudinal direction of the microchannel, and transverse to the PDMS membrane surface. The effect of increasing lateral tilt is shown with procession from left to right. This adjustment feature is provided by the wishbone tilt screws as shown in A).

6) Flow Rate and Vibrational Analysis

The 2G micropositioners were not only fabricated to increase the positional capabilities of each microvalve tip, but also to dampen and isolate vibrations arising from actuation of the cantilevers. Vibration of the entire micropump apparatus (image B of Figure V-2), often resulted when the cantilevers were actuated while being secured in place with the 1G micropositioners. The data of Figure V-4 shows flow rate data

collected using the 1G micropositioners, without placement of the stabilizer blocks under the glass substrate. The data was also compared for two different micropumps containing two different 30 : 1 base layer thicknesses. It can be observed the data is slightly unstable from about 25-35 Hz for the top curve, and from about 25-45 Hz for the bottom curve, where these frequency ranges correspond to a "resonant dip." The natural frequency for the top (curve A) vs. bottom (curve B) curve was observed to be 30 Hz vs. 35 Hz, respectively, where maximal vibrations at these frequencies was observed for the micropump apparatus as a whole. Video segments were also obtained, and show the significant increase in vibrations leading up to these frequencies. The micropump apparatus vibrations were a result of rotational motions produced within the internal sliding mechanism of the 1G micropositioner stages, which were in turn created as a result of cantilever actuation. The micropositioner stages as obtained from the manufacturer contain an internal sliding mechanism, with a sliding plastic part and two springs at opposite ends of the sliding part. Depending on how the stages are mounted, it is possible for the sliding plastic part to rotate slightly when enough force is applied to the stages. The integration of the stages with the 1G micropositioner sub-bodies allowed for such rotation to occur with actuation of the cantilevers. Essentially, actuation of the cantilevers induced a force to rotate one of the two sub-bodies with respect to the other, where this process was made possible by the rotational movement allowed for within the internal sliding mechanism of the stages.

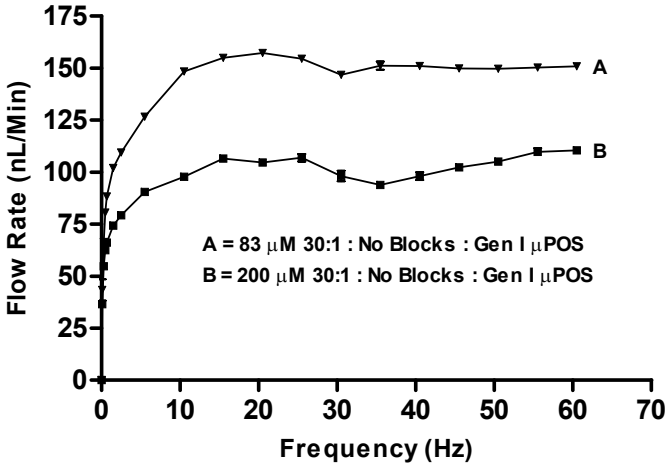

Figure V-4: Plot of flow rate vs. frequency. Plot shows two curves obtained with use of the Generation I micropositioners (represented as Gen I μPOS within plot), where in both cases, no stabilizer blocks were placed under the glass substrate. The curves also compare the effect of using two different thicknesses of 30 : 1 as a base layer, for two separate devices. Standard error bars plotted for (n = 5) experiments for each curve.

As shown in Figure V-4, the top curve (curve A) had less vibrational instability than the bottom curve (curve B). It is not believed the thickness of the 30 : 1 base layer had much of a direct effect on these results, but is believed to have played a significant indirect role. The 1G micropositioners required more torquing force to fully close the channel of the lower curve (thinner 30 : 1 base layer), and therefore in turn lessened the degree of rotation allowed for within the internal sliding mechanism of the stages. The overall effect was to dampen vibrations of the micropump apparatus as a whole.

Figure V-5 shows three flow data curves for both the 1G and 2G micropositioner designs. These curves more closely resemble the shape of an ideal set of flow rate curves, with smooth and predictable changes in flow rate being observed. The data shown for the 1G micropositioners, was taken with use of the stabilizer blocks (as discussed and shown within Figure V-1). The stabilizer blocks hoisted the 1G micropositioners off the

base of the microscope stage. It can be observed the 1G micropositioners with use of the stabilizer blocks, provided for stable flow data for both 30 : 1 base layer thicknesses. The vibrations of each individual micropositioner were still present, but not allowed to couple in a way such that they affected the vibration of the micropump apparatus as a whole. Therefore isolating the vibrations of each individual micropositioner to itself, allowed for stable flow data to be attained. It can also be observed within this Figure that the 2G micropositioners produced stable flow data. Use of the stabilizer blocks was not necessary, or even capable with this particular micropositioner design.

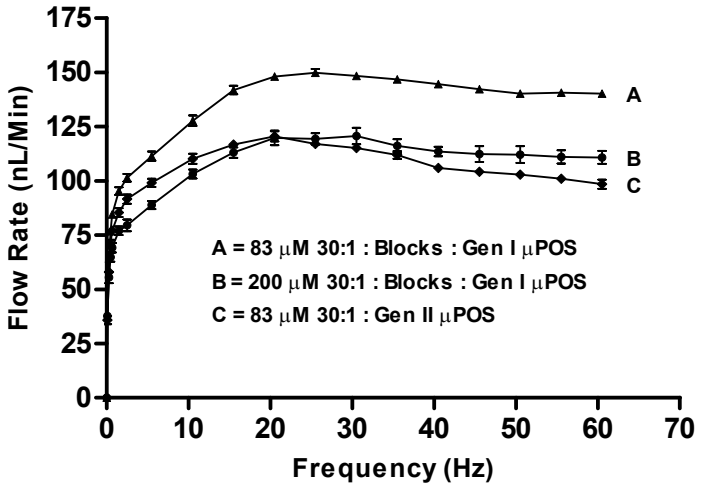

Figure V-5: Plot of flow rate vs. frequency. Plot shows three curves obtained using both Generation I and II micropositioners (represented as Gen I μPOS and Gen II μPOS within plot, respectively). The curves also examined the effect of altering the 30 : 1 base layer PDMS thickness, for two separate devices. Generation I micropositioners utilized substrate stabilizer blocks placed beneath the glass substrate, in effect hoisting the Generation I micropositioners off the base of the microscope stage. Standard error bars plotted for (n = 5) experiments for each curve.

Conclusions

The data presented within this Chapter introduced a new, and significantly improved second generation (2G) micropositioner apparatus, used for positioning piezoelectric cantilevers and microvalves over a PDMS microchannel. The 2G micropositioners allowed for considerably increased positioning capabilities with less effort, over that of the first generation design. The 2G design also provided for stable flow data, where vibrations arising from actuation of the cantilevers were eliminated, or dampened to the point of being undetectable, as determined from the flow rate curves. These micropositioners are not ideal from a size perspective, but do allow for an unprecedented level of control over microvalve registration, within this particular micropump design. The microvalve lateral tilt adjustment capability was introduced for the 2G micropositioners, which essentially allows for the microvalve to be actuated as a "squeegee," in effect increasing the valve stroke volume in the peristaltic signal bias direction, as discussed more fully within Chapter VI. Changes in microvalve lateral tilt, has a net effect of altering the peristaltic signal waveform shape. This micropositioner design is particularly suitable for benchtop and research-oriented applications, where real-time continuous on-the-fly microvalve adjustments are made possible. It is conceivable the 2G micropositioners could be integrated with an electronic feedback mechanism, to automatically adjust the lateral tilt of each microvalve. Such a feedback mechanism would allow the output characteristics of the micropump, to adapt as necessary, to the changing conditions of a particular microfluidic system.

Chapter VI : *Squeegee Microvalves: Alteration of Microvalve Tilt Angle for Enablement of a Micropump with On-The-Fly Tunable Performance Metrics*

Synopsis

The current Chapter reports on the performance characteristics of a PDMS fabricated peristaltic micropump, in response to changes in microvalve tilt angle. The micropump was actuated with PZT piezoelectric cantilevers, where the external microvalves were adhered to the tips of the cantilevers. The spatial orientation of the external microvalves was altered by tilting the microvalve tips, whereby the overall effect was to impart a gradient in height (z-direction) along the length of the microvalve tip, with the valve tip height being referenced with respect to the PDMS membrane surface plane. This gradient in height across the microvalve tip effectively created a "plowing" or "squeegee" bias effect, for driving fluid flow through the microchannel in the peristaltic signal bias direction. This change in microvalve tilt for creation of a "squeegee" effect, could more generally be characterized as changing the shape of the peristaltic waveform. A survey of the literature reveals that tilted "squeegee" microvalves remains an unexplored micropump design variable, to the best of the Author's knowledge. Integration of variable tilt microvalves within a single micropump allows for significantly higher maximum attainable backpressures and flow rates to be achieved, where the results presented within this Chapter, demonstrate the capacity to increase these metrics by as much as ~400%. Use of variable tilt microvalves further allowed for observation of an overall 10-fold increase in flow rate dynamic range. The increase in performance achieved through alteration of microvalve tilt, will further be analogized to the Affinity Laws, as applied to centrifugal pumps. Experiments were also undertaken to test the ability of the micropump to operate with the microvalves placed in

a nonideal tilt state, where the results demonstrate the robust ability of the pump to operate and function under such nonideal circumstances. Lastly, in some instances reversed flow was observed, contrary to that of the expected flow direction. These results indicate micropump valve tilt adjustments can in some instances have a dominant effect in controlling flow direction, even over the flow direction bias provided by the peristaltic signal. An analysis will be presented to account for these unexpected findings.

Introduction

Microfluidic device technology provides unique opportunities that can either augment traditional scientific platforms, or even create entirely new possibilities altogether. Microfluidic technologies have been employed within many domains of science and engineering, for purposes such as particle synthesis,[1193, 1300, 1301] cell studies,[1302-1305] separation science studies,[919, 1087, 1214, 1306] and point of care diagnostics for developing nations.[1051-1053]

Many microfluidic platforms exploit the phenomena of tunability. A survey of the microfluidics literature would turn up examples such as tunable microfluidic: flow resistances,[1307, 1308] electrical devices,[946, 947] pumps and valves,[1309, 1310] optofluidic devices,[1018, 1311-1315] gradient generators,[808, 809] droplet generators,[830, 1316] and separation devices.[877, 1298, 1317-1320] In some cases, tuning the performance of a microfluidic platform requires precise control over unit operation devices such as micropumps and microvalves.[628, 650, 653, 667, 690, 965, 967, 968, 1289] Options that exist to tune the performance of a microvalve and/or peristaltic micropump are to change the actuation signals frequency, shape, phase, amplitude, or wavelength.[283, 326, 1321] Additional options would include

altering the actuation force of a microvalve, or changing the footprint size of the microvalve.[667, 1290, 1291] With microvalves usually forming an integral part of micropump technology, it would be advantageous if other microvalve tuning options were available, as additional or alternative design options for fluidic control purposes on a microfluidic chip.

The current Chapter will present experimental data for a piezoelectric-actuated peristaltic micropump, with externally tilted microvalves. The tilted microvalves allow for a "squeegee" or "plowing" bias actuation, to preferentially drive the contents within the microchannel in one direction over that of the opposite direction. The Author is unaware of any existing report, characterizing the tilt of a microvalve. The results within the current Chapter will highlight the vastly improved flow rate and backpressure performance for tilted microvalves, over that of untilted microvalves. A sequence of tilted microvalves when actuated with a peristaltic waveform, is capable of providing a ~400% increase in flow rate, over that of the same valves when actuated without tilt. The predictable increase in flow rate performance for predictable increases in microvalve tilt, will also be presented as an analogy to the Affinity Laws, as commonly applied to centrifugal pump performance analysis.[1278] Lastly, data will also be presented for the characterized increases in working backpressures and power output, for the associated increase in degrees of microvalve tilt.

Experimental Methods

1) PDMS Micropump Fabrication

The micropump channel was fabricated by bonding two pieces of PDMS, with a derivatized sequence of previously described method steps, as described within Chapter II. The channel layer was fabricated using the portable handheld injection mold apparatus, presented within Chapter III. The apparatus was CNC machined in-house, using aluminum as the primary working material. The bottom plate of the apparatus was used for creation of the molding template. The process of creating the template involved; 1) straddling a 75 μm diameter wire across the bottom plate, 2) applying a thin film of general purpose spray adhesive over the wire/bottom plate surface, and 3) molding a piece of general purpose aluminum foil over the wire, using a Teflon block straight edge. Assembly of the injection mold included sandwiching a gasket between the top and bottom plates of the apparatus. The gasket was used to regulate the distance between the top and bottom plates, i.e. allowing for regulation of the overall thickness of the PDMS layer, in addition to the channel membrane thickness as well. The gasket was laser machined from bulk polyester material (McMaster-Carr, 9513K118), where the internal portion was cut-away. Removal of this material allowed for creation of a cavity when the laser machined gasket is compressed between the top and bottom plates. The Al foil wire-molded template also resided within this cavity region. After fully assembling the injection mold, 5 : 1 prepolymer PDMS (GE, RTV615) was injected into the cavity, and then placed in an oven at 80º C for one or more hours, to expedite curing of the PDMS. Once the bake step was completed, the injection mold was removed from the oven and

placed under running water to expedite cooling of the apparatus. The injection mold apparatus was then disassembled. The fully cured 5 : 1 mold was then removed and placed onto a clean glass substrate with the molded channel facing the atmosphere. The overall 5 : 1 membrane thickness over the channel region was measured to be approximately 80 μm, with the channel measuring ~100 μm in height.

A featureless 30 : 1 base layer was created using a glass wafer sandwich fabrication process, as previously discussed within Chapter II. An antiadhesion vapor soak of the wafers was first performed using tridecafluorooctyltrichlorosilane (United Chemical Technologies, model T2492). The wafers were placed in separate desiccators for two overlapping, yet different time intervals. This step allowed for preferential removal of one wafer over the other when the wafers were separated to access the sandwiched PDMS. After mixing the 30 : 1 PDMS, a degassing step was performed using a centrifuge (2-3 min at 5000 RPM). The prepolymer 30 : 1 PDMS was then cured between the two glass wafers, while being separated by ~203 μm thick spacers. The two wafers were secured in place using binder clips. The PDMS glass sandwich was then placed into a convection oven at 80º C for 35 minutes to allow for a partial cure. The overall thickness of the 30 : 1 layer was measured to be ~200 μm.

Bonding of the 5 : 1 and 30 : 1 layers was performed under a microscope, and began by placing two pieces of capillary tubing (Polymicro, 105 μm outer diameter / 40 μm inner diameter) ~1.5 cm within each end of the microchannel. Prepolymer 5 : 1 PDMS was then placed along the capillary tube/PDMS channel regions to seal all void areas. Excess PDMS was removed carefully with a razor blade. The 30 : 1 glass wafer

sandwich was next separated. The remaining wafer containing the partially cured 30 : 1 PDMS was then placed over, and bonded to the 5 : 1 layer. The two pieces of bonded PDMS were then placed in an oven at 80º C for one or more hours, to allow for an irreversible bond to be formed between the two layers. Final processing of the bonded PDMS layers consisted of removing excess cured PDMS, followed by alignment of the PDMS channel region across a new and clean glass substrate, with application of prepolymer 5 : 1 PDMS to the capillary tube regions, where they exited the bonded PDMS layers.

2) Micropump Actuation

The peristaltic micropump was actuated using external piezoelectric cantilevers (Piezo Systems, Q220-A4-303YB). Miniature aluminum clamps were adhered to the cantilever tips for the purpose of securing precision machined microvalves in place. The contact dimensions for the microvalves to the PDMS membrane surface was 3 mm by 250 μm (L x W), these dimensions being the same for all experiments presented within, and more fully understood with reference to Chapter IV. A peristaltic wave was created across the microchannel by actuating the cantilevers with square wave signals that were 120º out of phase. A small signal was created using a virtual function generator (National Instruments), where the small signals were amplified with external hardware containing high voltage amplifiers (Apex Microtechnologies, PA15A). The maximum driving potential of $V_p = \pm 90$ V was used to drive the cantilevers, so as to maximize deflection amplitude of the cantilevers.

3) Micropositioners

A second generation micropositioner apparatus was fabricated for the current set of experiments. A more detailed analysis and discussion is provided within Chapter V, for this newly fabricated micropositioner design. The micropositioners were fabricated to improve upon the earlier design, as presented within Chapter II. The improvements included allowing for greater stability of the micropositioners, dampening vibrations created by the piezoelectric cantilevers, and allowing for greater and more precise control over positioning of the microvalve tips over the microchannel region. The micropositioners contained three positioning bodies (Quater Research, XYZ 300MR) that were mounted to a bulk piece of machined aluminum (hereinafter, the bulk aluminum base). Further external machined parts were attached to the micropositioner bodies to allow for further adjustments to be made. The micropositioner bodies allowed for X-Y-Z induced movements, where the externally attached parts allowed for tilt induced adjustments (i.e. translations not perpendicular or parallel to X-Y-Z). These adjustments can be seen more clearly within Figure VI-1, of the 6) Valve Tilt Adjustments section. The summary of movements provided by the micropositioners (with respect to positioning of the microvalve tip over the PDMS microchannel, where the X-direction is defined as the direction parallel to both the microchannel and microvalve length-direction) included; 1) in/out (Y-direction), 2) lateral side-to-side (X-direction, and perpendicular to Z and Y-directions), 3) up/down (Z-direction), 4) angled tilt (arc in Z-direction), and 5) lateral tilt (tilt of microvalve surface plane in contact with the PDMS membrane surface plane, i.e. alteration of the microvalve contact surface direction/position, such that the end points of the microvalve length have different

z-vector components after being laterally tilted) The micropositioner design allows for real-time continuous on-the-fly change in microvalve position, with respect to any of 1) through 5). It should be noted, of particular interest for operation of the micropump, is the on-the-fly adjustment of 5) (lateral tilt) for the microvalves.

The PDMS channel adhered to the glass substrate (as described above) was easily secured in place over the bulk aluminum base using a simple clamping mechanism. Adjustment of each microvalve was made under a microscope, so as to impart a desired position of a microvalve tip over the microchannel region. Adjustments were provided using a dry microchannel, where release of the membrane from the base of the microchannel allowed for a clear indication of valving and tilt properties. Observation of membrane release enabled a quantitative eyeball assessment to be made, as to the degree of lateral tilt induced to the microvalves by the micropositioners. This quantitative assessment was recorded as X/Y%, with X and Y being a number value with the sum totaling 100%. The sum of 100% is the same for microvalves of any size, and is therefore a relative measure across the entire length of the microvalve (i.e. 25/75% indicates; 25% is 25% of the entire length across the microvalve when taken with respect to one microvalve end-point, with 75% representing 75% of the length across the microvalve when referenced with respect to the opposite microvalve end-point). The specific X and Y values were derived by observation of the membrane release characteristics from the bottom of the microchannel, as the valve was slowly actuated in increments from a fully closed to a fully open state. These adjustment characteristics will be explored more deeply with Figure VI-1, within the Results and Discussion section.

4) Flow Rate Characterization

Flow rates were characterized by tracking a 2-3 mm bubble through a piece of external capillary tubing. The external capillary tubing was filled with blue food dye and secured to a meter stick. The blue food dye allowed for better contrast of the bubble for tracking purposes. The micropump was allowed to actuate in a steady-state, where the outlet line was connected to the external blue-food dye filled capillary tube, such that the 2-3 mm bubble was intentionally introduced and tracked against the ticks/gradations of the meter stick. The formula Q = Av was used to calculate flow rates, with Q = flow rate, A = cross-sectional surface area of the flow, and v = linear flow velocity of the bubble. All flow rates were characterized using square waves out of phase by 120º. Standard errors were plotted as error bars for each flow rate plot, where (n = 4) for (50/50%), (35/65%), (25/75%), (10/90%), and (2@10/90%, 1@90/10%). The nomenclature (2@10/90%, 1@90/10%) represents two microvalves tilted in the forward bias peristaltic signal direction (i.e. 2@10/90%) and one microvalve tilted in the reverse peristaltic signal bias direction (i.e. 1@90/10%). Plots for (10/90 - RevSig), and (2@10/90%, 1@90/10% - RevSig), are representative of (n = 3) experiments.

5) Backpressure Characterization

Maximum attainable backpressure was characterized by connecting the outlet line of the micropump to an electronic pressure sensor (Honeywell, 40PC015G2A). The pump was allowed to actuate until a fully pressurized state was attained, as indicated by the pressure sensor reading. After achieving this stable and maximal pressure reading, the micropump was stopped, where one valve was left in the fully closed state. Pressure

readings were recorded over the course of a 15 minute time interval, where after this time-frame, the solely closed microvalve was opened, with further pressure readings obtained until no pressure remained within the system. The following ratio of (n/frequency) indicates the number of experiments performed, to the pressurization frequency: (3/30 Hz) for 10/90%; (3/20 Hz) for 25/75%; (3/20 Hz) for 35/65%; (3/20 Hz) for 50/50%; (1/200 Hz) for 10/90% - RevSig; (1/30 Hz) for 2@10/90%, 1@90/10%; (1/5 Hz) for 2@10/90%, 1@90/10% - RevSig. The nomenclature (2@10/90%, 1@90/10%) represents two microvalves tilted in the forward bias peristaltic signal direction (i.e. 2@10/90%) and one microvalve tilted in the reverse peristaltic signal bias direction (i.e. 1@90/10%).

Results and Discussion

6) Valve Tilt Adjustment

The lateral tilt adjustment process is front and center to the forthcoming experimental data that will be presented within. To the best of the Author's knowledge, microvalve lateral tilt remains an uncharacterized variable within the literature. Figure VI-1A) is an exaggerated cartoon representation of decreasing valve "tilt," when proceeding from V1 to V3. Unless otherwise noted, all discussions of "tilt" from this point forward, are directed towards lateral tilt adjustments, and therefore not that of angled tilt adjustments (see Micropositioners section of Experimental Methods). The designation of V1, V2, and V3, represents three valves aligned in succession along a PDMS microchannel. The general concept of valve tilt is shown in Figure VI-1A) to

decrease when moving from V1 to V3. That is to say, V1 would be expected to produce the largest "squeegee" effect of the three valves, when actuated downward along the depicted linear translation direction. The net effect of changing microvalve tilt, is to alter the shape of the peristaltic waveform, in morphing from a square wave, to a triangle-like waveform. The micropositioner design that was utilized to accomplish this tilt adjustment is presented within Chapter V.

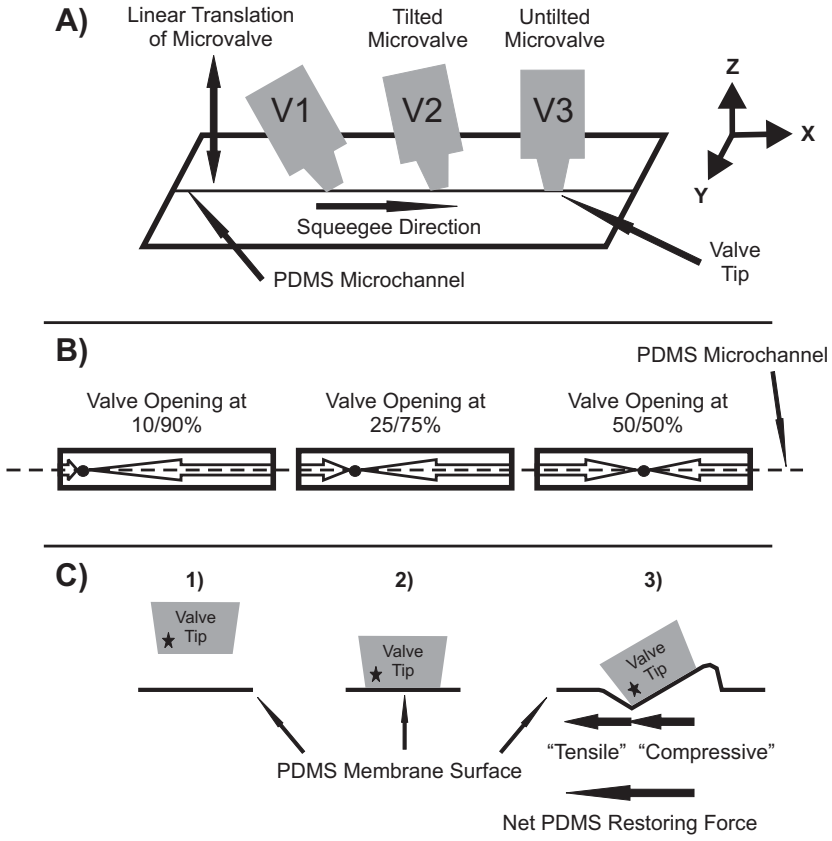

Figure VI-1: Image representations of microvalve lateral tilt dynamics. Image A) is an illustration representing the effect of decreasing lateral tilt to microvalves, when proceeding from V1 to V3, with V1, V2, and V3 being three valves aligned in sequence. Image B) is a schematic representation of membrane release dynamics from the bottom of the microchannel, when the microvalve is actuated from a fully closed state to a fully open state. The dot at the tip of the arrows for all three valves, represents the final point of release of the membrane from the base of the microchannel. This observation was taken under a microscope, with a dry microchannel. Image C) illustrates the sequence of steps used to impart lateral tilt to a microvalve tip. Part C)3) is the hypothesized surface deformations that result after the microvalve tilting process is complete. It is hypothesized the tilting process induces PDMS restoring forces, that explain the observations in Image B).

The degree of induced microvalve tilt was recorded with the micropump placed in an inverted position under a microscope. With the channel in a dry state, it was possible to observe the release of the membrane from the bottom of the channel, as the valve was actuated from a fully closed state to a fully open state. Figure VI-1B) is a cartoon representation that illustrates how the degree of tilt was characterized for each microvalve. The enclosed rectangular region represents the microvalve tip, for the region of the tip that makes contact with the PDMS membrane surface. The dot at the tip of the arrows is to designate the last point of release of the membrane from the bottom of the microchannel, as the valve actuates from being fully closed to fully open. Therefore, the rate of membrane release for the large arrow was much larger than the rate of membrane release for the small arrow, as shown within the 10/90% representation. At the other extreme, 50/50% indicates the rate of membrane release from the outer end-point of the microvalve towards the dot, was observed to be approximately equal when examined under a microscope. The percentage indication (e.g. 10/90%) therefore denotes a percentage of length across the valve tip, from the outer end-point of the microvalve tip, to the last point of membrane release represented by the dot at the tip of the arrow. This method of quantitation was recorded as an "eyeball" estimation, and believed to be accurate to within 5%. Another possibility for quantifying the degree of induced microvalve tilt would be to integrate micrometers into the micropositioners. This design feature was not utilized, but could easily be incorporated at a later point if necessary.

The %/% tilt phenomena is somewhat of an unexpected observation. It is believed the %/% tilt observations are a direct result of how the tilt adjustments were

performed. If the tilt adjustments had been made prior to placing the valve tips in contact with the membrane surface (i.e. at step 1) of Figure VI-1C), it would be expected based on qualitative reasoning that the first and last point of contact of the membrane to the bottom of the channel, when actuated from fully open to fully closed, would be the corner of the valve indicated by the star (if tilted such that the star corner was the first point of contact to the membrane surface). In other words, 0/100% would be the expected observation, regardless of the degree of induced tilt. For the current set of experiments however, the tilt adjustments were not made according to this scenario. The tilt adjustments were performed as indicated in steps 1) through 3) of Figure VI-1C). As shown, the valve tip was first placed in contact with the membrane surface using the micropositioner, and then tilted. It is hypothesized the final effect induced to the membrane surface would resemble the image shown in C3) of Figure VI-1. The contortion to the membrane surface is shown as an exaggeration for illustrative purposes, but nonetheless, still representative of the expected PDMS deformation that would result from an induced microvalve tilt. The elastomeric nature of PDMS would allow for such a distortion to take place, where it has been reported the shear modulus of PDMS can vary from 100 kPa to 3 MPa.[97] Relatively speaking, the degree of distortion would be expected to be on the smaller side, due to the membrane (channel layer) being fabricated from 5 : 1, as opposed to the mechanically softer 30 : 1 base layer. Further discussion can be found elsewhere, for the complexities surrounding induced mechanical deformations provided to polymeric surfaces.[294, 1322, 1323]

As a result of the proposed hypothesis for induced contortion to the PDMS

membrane surface, a restoring force would in turn be expected. This restoring force is shown broken into two parts, and indicated as "Compressive" and "Tensile" within C3) of Figure VI-1. It would be expected the star corner of the valve would essentially act as a divot when the valve is actuated. The "Tensile" side would be representative of one portion of the net restoring force, created as a result of the tensile stress provided to the PDMS. The "Compressive" portion of the net restoring force would be representative of the compressive volume stress experienced by the extruded PDMS, as indicated along the squeegee direction from the star to just past the opposite microvalve corner. The valve as shown in C3) corresponds to the neutral position, i.e. zero volts applied to the cantilever, where the "Compressive" and "Tensile" forces would be expected to increase and decrease in overall magnitude as the valve is actuated down vs. up, respectively. This trend would be expected as a result of the increased stress created by valve closure, where opening of the valve would result in relaxation of the PDMS. It should further be added that each valve remains in full contact with the membrane throughout the entire actuation cycle, and therefore the magnitude of change in these forces would be expected to cycle consistently throughout the entire valve cycling operation.

In summary, the restoring force discussion could be summarized by noting that a 10/90% observed tilt would be expected to create a larger net restoring force than a valve with no tilt (i.e. 50/50%), where this situation would be expected to produce a net restoring force of zero. Therefore, it is hypothesized that the magnitude and dynamics of the restoring forces, determines how the 5 : 1 membrane releases from the 30 : 1 PDMS at the base of the microchannel. Modeling studies are currently planned, to further

explore the basis of this hypothesis, in accounting for the proposed tilt and valving mechanisms, as described above. It is expected the valving results will be quite different than that described for other pneumatic valve designs.[283, 484]

7) Flow Rate Data

An array of experiments was undertaken to test the effects of valve tilt on flow rate. Figure VI-2 shows four curves for valve tilts corresponding to 50/50%, 35/65%, 25/75%, and 10/90%. For each individual curve, all three valves were adjusted such that each valve contained the same degree of tilt. The results show that the 10/90% valve tilt curve provided the highest overall flow rates, with the reduction in overall flow rates following a predictable trend for 25/75% > 35/65% > 50/50%. The average maximum flow rate recorded for the 10/90% curve was 120 nL/min, where the average maximum flow rate for the 50/50% curve was recorded as 32 nL/min. This represents a nearly 4-fold increase in observed maximum attainable flow rate, made possible by tilting the valves from a 50/50% configuration to a 10/90% configuration. The minimum averaged flow rate recorded for the four curves was 4.6 nL/min, for the 50/50% curve at 60 Hz, where further the minimum averaged flow rate for the 10/90% curve was 46 nL/min, recorded at 0.1 Hz.

For the current Chapter, a dynamic range is defined as the ratio of maximum to minimum flow rate values. It is noted a dynamic range value of 2.6 is observed when considering only the 10/90% curve, where this value changes to 26 when calculating the dynamic range for all curves considered. Therefore, tilted microvalves in this case is shown to increase the dynamic range by a factor of 10. This trend of increasing flow

rates for increasing tilt was not surprising once the data was placed into context. Using a 120º peristaltic signal, with progressively increasing degrees of valve tilt, one would expect to see an increase in micropump flow rates, resulting from the corresponding increase in microvalve "squeegee" action.

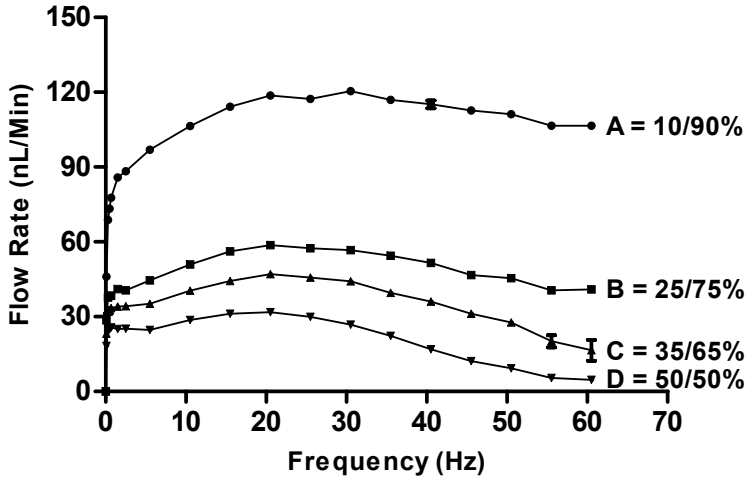

Figure VI-2: Flow rate curves for laterally tilted microvalves. All three valves for each individual curve, were adjusted such that each valve contained the same degree of induced tilt. Each curve is representative of (n = 4) experiments, with standard errors plotted with error bars.

The "squeegee" effect is best summarized as, providing a shape change to the peristaltic waveform. A microvalve tilt hypothesis is proposed to account for the expected increase in flow rates with increased microvalve tilt. First, it is expected a tilted microvalve would translate into a decrease in microvalve footprint length, for the vector component taken along the longitudinal direction (X-direction) of the microchannel. This is more easily understood with reference to Figure VI-1A), where it is easily visualized the x-component of the untilted microvalve shown as V3, is greater than the x-component of the tilted microvalve shown as V1. While it may be expected this decrease in length

taken along the x-direction, would translate into a decrease in displaced volume within the microchannel, it is hypothesized the edge of the microvalve denoted by the star within Figure VI-1C), acts as a "divot" in preventing backflow through the inlet of the micropump when V1 of Figure VI-1A) is progressively brought from a fully open to a fully closed state, and therefore a tilted microvalve actually provides a larger displaced stroke volume over that of an untilted microvalve. Increasing stroke volume by preventing backflow with a microvalve "divot" and "squeegee" action, would also allow for higher pressures to be trapped within the peristaltic chambers, and therefore in turn translate into higher working backpressures of the micropump. It has been shown and discussed previously within Chapter II, that a 120º peristaltic signal prevents backflow as a micropump pressurizes, unlike that of a 60º or 90º peristaltic signal, where if the proposed tilted microvalve hypothesis is correct, it might be said that "tilted" microvalves actuated with a 120º peristaltic signal, performs as, "an enhanced 120º peristaltic signal," in providing additional anti-backflow characteristics. A complex interplay between stroke volume, changes in linear momentum provided to the displaced volume, and PDMS compliance characteristics, could also be a factor that plays a role in fully explaining the "squeegee" effect observed with tilted microvalves.

Figure VI-2 indicates, there is nearly a uniform increase in flow rate values, when comparing the curves at each individual frequency value. This consistent and predictable increase in flow rate performance for increasing microvalve tilt, is analogous to the mathematical relationships expressed by the Affinity Laws for centrifugal pump performance.[1278] The Affinity Laws are a set of mathematical relationships, that express

changes in pump performance such as flow rate, when a change is made to another variable such as rotary pump speed or impeller diameter.[1278] That is, for a constant impeller diameter, $(Q_1 / Q_2) = (N_1 / N_2)$, where Q_1 represents the flow rate at a first value, Q_2 at a second flow rate valve, with N_1 representing the rotary pump speed at the Q_1 value, and N_2 the second rotary pump speed at Q_2. Likewise, for a constant rotary pump speed, the Affinity Laws for centrifugal pumps also state that, $(Q_1 / Q_2) = (D_1 / D_2)$, where a ratio of flow rate values is related to a ratio of impeller diameters, D_1 and D_2. Considering the micropump data of Figure VI-2 by analogy, the relationship $(Q_1 / Q_2) = (Tilt_1 / Tilt_2)$, could be used as a "micropump affinity relationship," similar in nature to that of the centrifugal pump Affinity Law relationships. Figure VI-3 is a plot of flow rate ratios, at each respective frequency value of Figure VI-2, with each curve referenced to the micropump with untilted microvalves (i.e. 50/50%). That is, the curves A, B, and C of Figure VI-3, are plotted representations of flow rate ratios vs. frequency for curves A / D, B / D, and C / D of Figure VI-2, respectively. It can be seen within Figure VI-3 that the "micropump affinity relationship" deviates from the relationship, $(Q_1 / Q_2) = (Tilt_1 / Tilt_2)$, for frequencies increasing past 25 Hz. The data as plotted within Figure VI-3 shows two regions, where the flow rate ratios follow the predictable trend for increasing degrees of microvalve tilt. These ranges correspond to: 0.1 – 2.5 Hz, and 5 – 25 Hz. For Figure VI-3, the standard deviation for the difference in flow rate ratios from 0.1 – 2.5 Hz, for curves (A – B), (B – C), and (A – C), is 0.35, 0.04, and 0.35, respectively. Similarly for Figure VI-3, the standard deviation for the difference in flow rate ratios from 5 – 25 Hz, for curves (A – B), (B – C), and (A – C) is 0.10, 0.01, and

0.11, respectively. Therefore, for the constant ratio of ($Tilt_1$ / $Tilt_2$), the data shows a fairly consistent and predictable change in ratio for (Q_1 / Q_2), especially for smaller relative alterations in microvalve tilt (i.e. for valve tilts closer to 50/50%, as opposed to that of the extreme case of 10/90%).

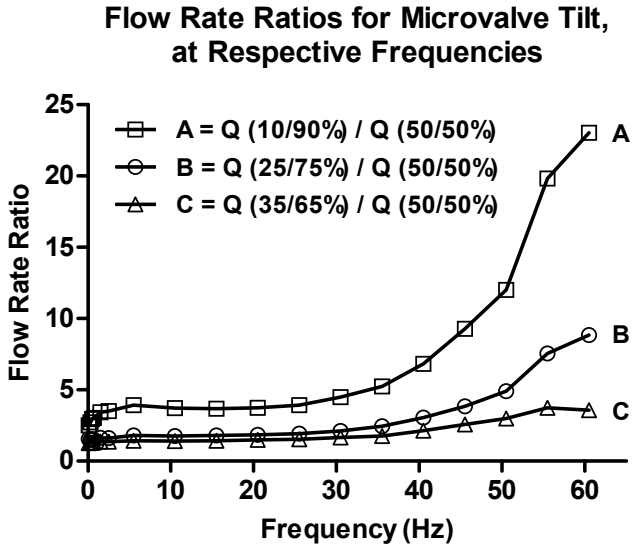

Figure VI-3: Flow rate ratio for microvalve tilts vs. frequency. Plot analogizes centrifugal pump Affinity Laws, to that of a peristaltic micropump, for the relationship taken as, (Q_1 / Q_2) = ($Tilt_1$ / $Tilt_2$). This relationship is predictable in relating flow rate (Q) changes to corresponding changes in microvalve tilt, for the frequency ranges of; 0.1 – 2.5 Hz, and 5 – 25 Hz.

Figure VI-4 shows two separate plots of flow rate data collected. Plot A) shows two curves for a micropump, configured with a mixed combination of microvalve tilts. The designation 2@10/90%, 1@90/10%, would correspond to Figure VI-1 as, V1 = 10/90%, V2 = 10/90%, V3 = 90/10%, with the 120º peristaltic signal biased in the forward flow direction, i.e. in the direction of V1 to V3. The designation of 2@10/90%, 1@90/10% - RevSig would correspond to the same valve tilt configuration, but indicates the 120º peristaltic signal was biased in the reverse flow direction. The data

for this Figure indicates flow patterns that are a little erratic, but nonetheless demonstrates the robust nature of the pump, where a net flow was produced in spite of the valve tilt combinations being altered such that the micropump was intentionally placed in an extreme and nonideal operating state. The data indicates the micropumps overall operation is very tolerant towards an array of valve tilt adjustments and/or combinations, and therefore in the instance there are uncontrolled or nonideal tilt adjustments, the micropump will be very "forgiving" towards this variable, as it relates to producing a net flow through the micropump. The data as shown in B) on the other hand, for valve tilts of 10/90% while using a 120º reversed square wave peristaltic signal, can be seen as very stable and capable of producing very high flow rates. The averaged maximum flow rate was recorded as 178 nL/min at 250 Hz.

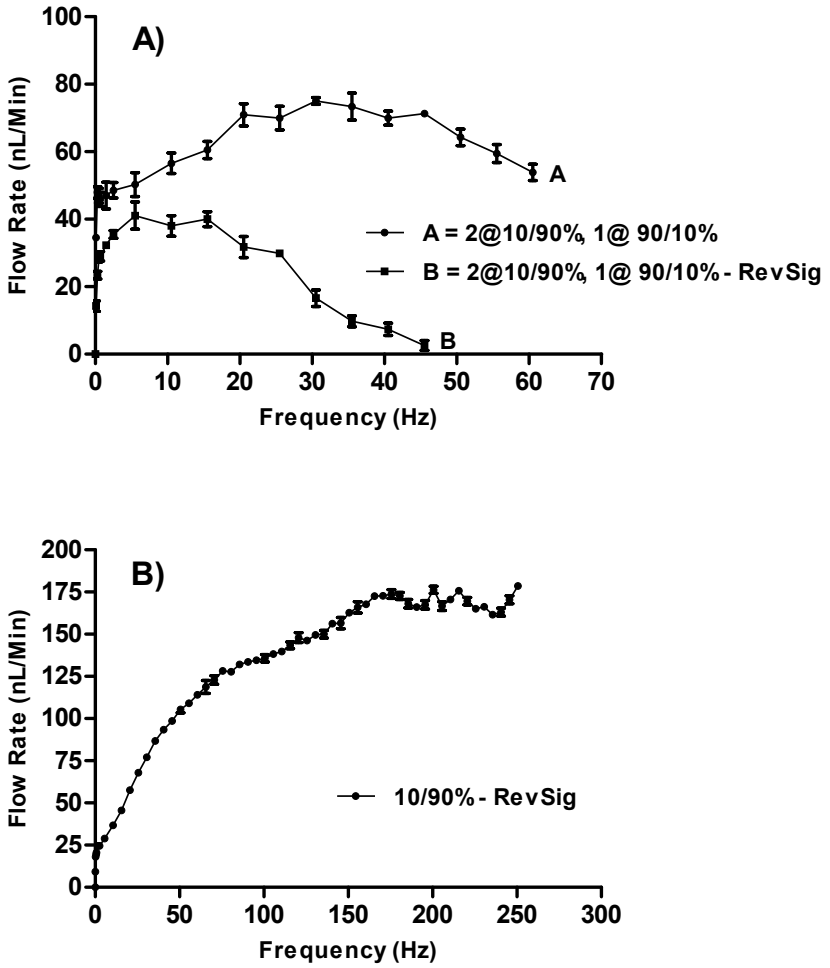

Figure VI-4: Flow rate curves for laterally tilted microvalves. The curves as shown in Plot A) are representative of a mixed combination of microvalve tilts. The bottom curve for A) was recorded with a reversed peristaltic signal bias, i.e. in the reverse flow direction. Plot B) illustrates valves with a uniform degree of induced lateral tilt, with the data being recorded for a reversed peristaltic signal bias. All curves indicate standard errors using error bars. The top curve for A) is representative of (n = 4) experiments, with the remaining curve for A), and the solo curve of B), being representative of (n = 3) experiments.

The flow rate data presented for Figure VI-4A) and Figure VI-4B) is certainly very disparate in many regards, however there is one unifying feature for both plots, relating to flow direction. It was observed the flow direction for both curves of plot A), was in the reversed signal direction. That is, the direction of flow through the micropump was the same for both plots, where the flow direction for curve A was against

the peristaltic signal bias direction (i.e. in the reverse flow direction), with the flow direction for curve B in the peristaltic signal bias direction (i.e. in the reverse flow direction). As for plot B) of Figure VI-4, the 120º peristaltic signal had a reverse flow bias, but the actual flow was observed and recorded in the forward direction. This observation was very unusual and unexpected, where in certain instances it appears the microvalves "squeegee" flow bias, overpowers/affects the peristaltic signal flow bias. A possible explanation to account for the high flow rates of the 10/90% reversed signal data of Figure VI-4B), as compared to the 10/90% flow rate data of Figure VI-2, would be provided if the 10/90% reversed signal had a counterflow microvortice driving force that was greater in magnitude, than that of the peristaltic signal driving force for the data presented within Figure VI-2.

8) Reverse Flow Discussion

An explanation to account for the reversed flow observations could be provided by considering the microvalve adjustment process, and the potential effects these adjustments could have on the valving operations of the micropump. Figure VI-5 is a schematic representation of the various microvalve adjustments that could alter the valving characteristics of the micropump. Figure VI-5A) is a top-down view of a cantilever and microvalve over a PDMS microchannel. This part of the Figure shows an exaggerated view of how, potentially the microvalve could be adjusted properly so as to completely close off the microchannel, and yet be placed in an adjusted state such that the microvalve tip was not completely parallel to the longitudinal direction of the microchannel. It should be noted this deviation was never observed, but could exist when

one considers micron-regime variations. These small variations in most cases would be expected to be undetectable, when observing valve alignment under a microscope.

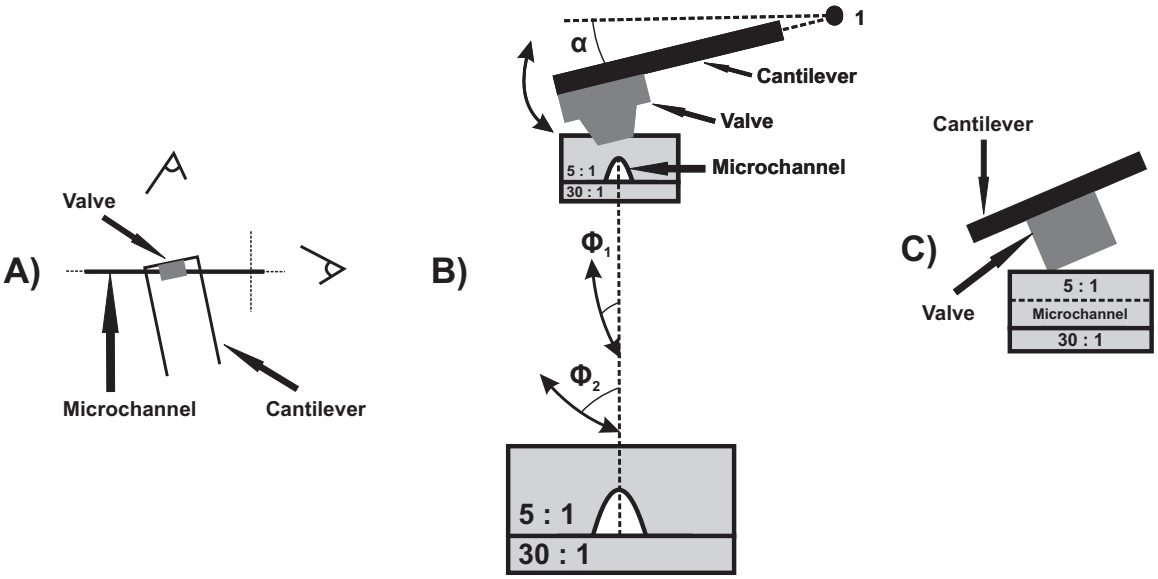

Figure VI-5: Sequence of illustrations to highlight potential valve adjustment variables, that could in turn affect channel collapse dynamics, and therefore valve performance as well. Image A) is a top-down illustration of how the microvalve could be aligned such that the channel fully closes, in spite of the cantilever not being aligned perfectly transverse to the longitudinal direction of the microchannel. Image B) is a cross-sectional image of the microchannel, and the image seen by the eye looking into the microchannel, as shown within Image A). Image B) depicts how alteration of the cantilever hinge-point angle α could impart a different "actuation arc" to the microvalve tip, with the actuation arc being characterized by angles Φ_1 and Φ_2. Alteration of α is accomplished by changing the angled tilt adjustment on the micropositioners. Image C) is an indication of lateral valve tilt. The image shown in C) would correspond to the image seen by the eye looking in the transverse direction to the longitudinal direction of the microchannel, as depicted within Image A).

Figure VI-5B) is a depiction of the microchannel when a cross-section is taken along the dotted line shown transverse to the longitudinal direction of the microchannel. The image observed for the eye looking into the channel, as shown in A), is the image shown in B). The top portion of B) is an illustration of the geometric variables influenced when angled tilt adjustments are provided by the micropositioners (not to be

confused with the lateral tilt adjustments as shown in C)). Angled tilt adjustments allow for the angle α to be varied, through rotation of the cantilever about hinge-point 1. Rotation about hinge-point 1 would in turn alter the degree of microvalve tip "actuation arcing" over the microchannel. It would be expected the channel would collapse nearly straight down if the angled tilt adjustment were made such that, the cantilever was oriented parallel to the dotted-line axis connected to hinge-point 1. This adjustment scenario would correspond to an actuation arc characterized by angle Φ_1, for example. If however, the cantilever were adjusted as illustrated, it would be expected the channel would collapse partially sideways as the cantilever was actuated in the downward direction. An example of this particular arcing motion is depicted in B), for the actuation arc characterized by angle Φ_2. Therefore, the extent to which the channel would collapse straight down vs. sideways, would likely depend in large part on Φ, and the overall magnitude of this angle. Smaller values would be expected to collapse the channel nearly straight down, with increasing collapse sideways being predicted for increasing values of Φ.

Figure VI-6 is an actual cross-sectional image, equivalent to the valve tip/microchannel region of Figure VI-5B). The sequence of images from A to C represents the progression of valve collapse as the valve tip actuates in the downward direction. The arrow shown in image C indicates a portion of the channel that did not fully collapse (as a result of the channel being square vs. rounded – see Chapter III). This portion of the microchannel would correspond to the top right corner of the microchannel shown within image A of Figure VI-6. The actuation arcing motion of the microvalve tip

is readily visible, when using this top right corner portion of the microchannel as a reference point. This sequence of images further illustrates the inextricable connection between actuation arcing, and microchannel collapse dynamics.

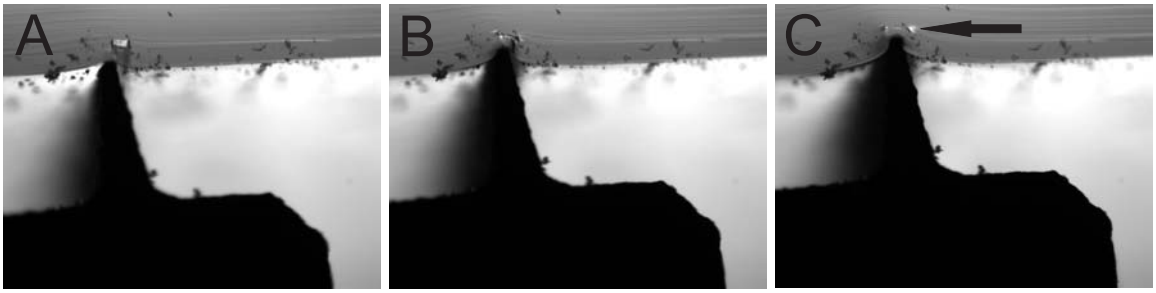

Figure VI-6: Cross-sectional PDMS channel geometry images, for observation of the microchannel being collapsed through actuation of a microvalve. Image A is for a fully open microchannel, with B showing an intermediate state, and C showing full closure of the microchannel. The arrow in C indicates a small portion of the channel that was not completely collapsed, as a result of the channel being square, versus rounded.

Figure VI-5C) is an illustration of a head-on view of the microvalve and microchannel. The image produced by the eye of A) looking in the direction transverse to the longitudinal direction of the microchannel, is the image illustrated within C). This image depicts the relative spatial orientation of the microvalves, after being laterally tilted by the micropositioners. This lateral tilt would further correspond to the tilted valve as shown in C3) of Figure VI-1.

Considering images A), B), and C) of Figure VI-5 in combination, it can be understood the valving mechanism for this micropump is complex. With all three images factored as a whole, it is possible the microchannel is not only being partially collapsed sideways, but additionally being "twisted" as the channel is collapsed sideways. The elastomeric nature of PDMS, combined with the complex adjustments and actuation

movements, make it possible that the channel is being "twisted" in a way, such that this complex 3D mechanical "twisting" motion creates or contributes to the process of producing reverse flows through the micropump. Therefore, it is believed the mechanical valving dynamics are not fully understood, solely based upon, the observed PDMS membrane release dynamics from the base of the microchannel, as studied/recorded through a microscope objective. The complex mechanical valving dynamics is a first proposed mechanism to account for the unexpected reversed flow results of Figure VI-4, where the data is indicative that valve tilt adjustments could have an overpowering effect on flow direction, trumping even the flow bias direction of the peristaltic signal.

A second possible explanation to account for the reversed flow observations, could be attributed to the creation of recirculatory flow patterns, induced as a result of microvalve tilt adjustments. It is possible components of the velocity flow field adjacent to the microvalves, could have deformed fluid elements such that counterflow microvortices or other complex flow patterns were created, whereby these counterflow patterns resulted in greater driving forces in the reverse flow direction, as opposed to the bias direction provided by the peristaltic signal. Microvortices, and reverse flow patterns for traveling wave micropumps have been discussed elsewhere.[1324-1328]

9) Backpressure Data

Figure VI-7 is a combined plot for all backpressure data produced for the current Chapter. Plot A) can be seen to produce a very predictable trend, where decreasing valve tilts corresponded to decreasing maximum attainable backpressures being recorded. For each set of curves corresponding to 1 through 4, the frequency the micropump was actuated at while pumping into the pressure sensor, was the frequency that corresponded to the averaged maximum flow rate of Figure VI-2. Therefore, the trend observed in plot A) is not unexpected, as higher backpressures would be expected for higher flow rates. The curves in plot B) are not comparable for valve tilts in the same way as those in plot A). The curves of plot B) however do follow the same trend as plot A), where a stepwise progression of decreasing maximum attainable backpressures for curves 1 through 3, corresponds to the same stepwise progression of decreasing averaged maximum flow rates for the respective valve tilts of Figure VI-4. The corresponding flow rate and backpressure values obey the physical relationship of $\Delta P = QR$ (ΔP = pressure drop, Q = flow rate, R = resistance), to produce linear data relating these two variables. This relationship is not unexpected since the micropump flow characteristics are dominated by laminar flow losses through straight pipe capillary tubing.

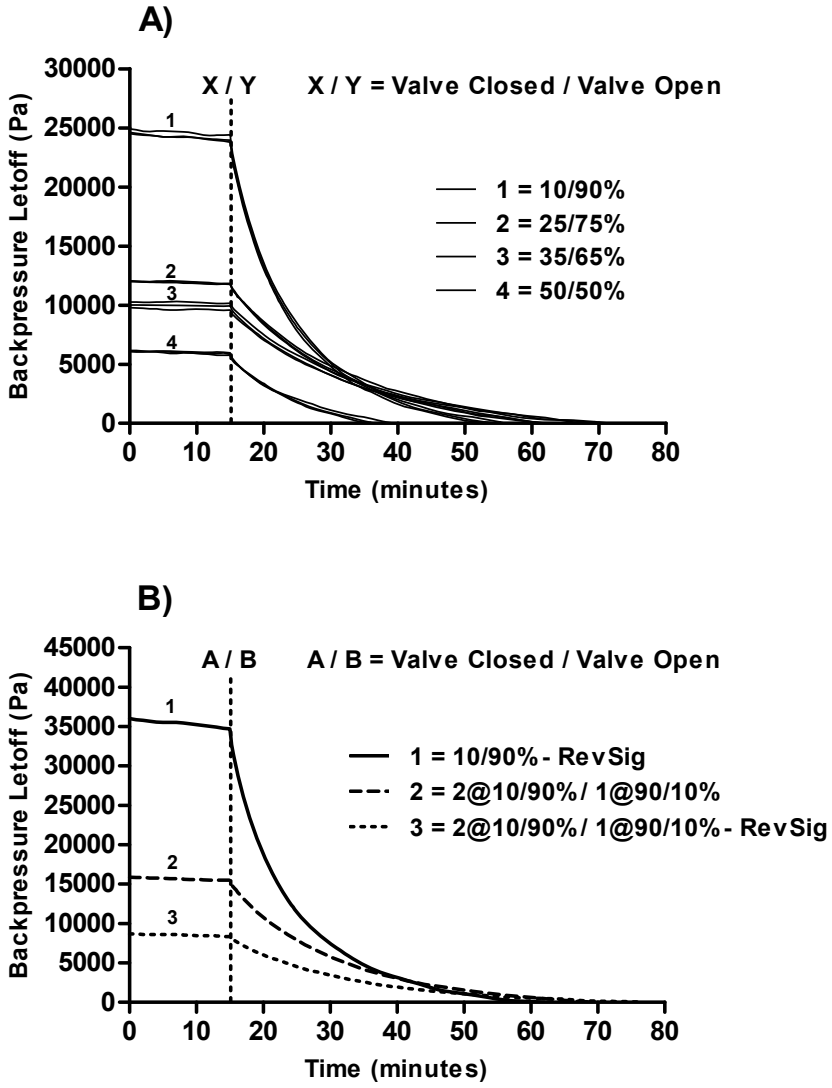

Figure VI-7: Cumulative summary of all backpressure data collected for the current Chapter. Plot A) shows data for four curve groupings (i.e. 1 to 4) corresponding to four separate lateral valve tilts. For each grouping, all three valves contained the same degree of tilt. Plot B) for curves 2-3 is a representation of backpressure data for mixed valve tilt combinations, with curve 3 further utilizing a reversed peristaltic signal bias (i.e. in the reverse flow direction). Curve 1 represents microvalves with uniform tilt, with the data being collected for a reversed peristaltic signal bias. Plot A) for groupings 1-4 are representative of (n = 3) curves, with Plot B) for groupings 1-3 being representative of (n = 1) curve.

Observation of stepwise increases in flow rates for Figure VI-2, with a likewise increase for observed backpressures as shown in Figure VI-7, further illustrates a corresponding increase in power output of the micropump for increases in microvalve tilt.

Figure VI-8 is an illustration of the increase in power output of the micropump (with all data points calculated for a frequency of 20 Hz) for corresponding increases in microvalve tilt, where it can be seen the curve follows the trend (25/75%) > (35/65%) > (50/50%). This trend would be expected for an increase in microvalve tilt, where the driving force of the peristaltic wave remains unaffected, for the proposed hypothesis of providing an increase in stroke volume for a corresponding increase in microvalve tilt. This change in power output for corresponding changes in microvalve tilt, when considered for a constant frequency peristaltic micropump, could be considered in some ways analogous to that of a constant speed centrifugal pump, when the vane angles of the impeller are altered.

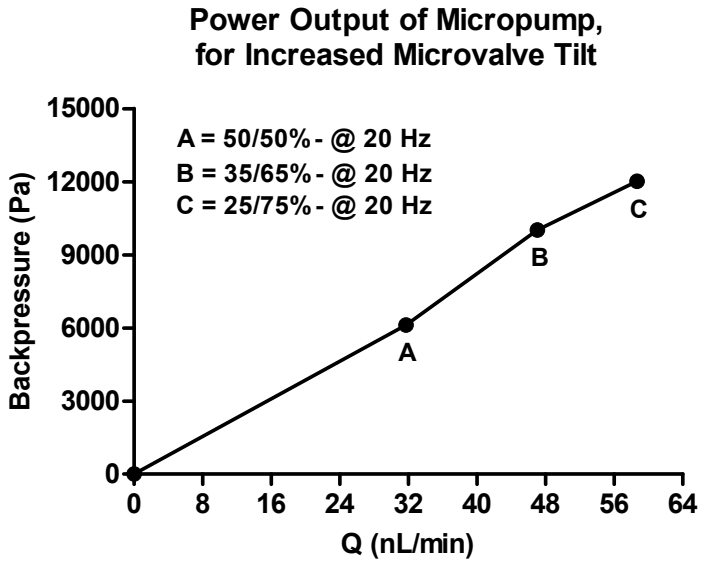

Figure VI-8: Plot of backpressure vs. flow rate, for illustration of micropump power output. All three data points are for backpressure and flow rates recorded at 20 Hz. Plot indicates an increase in power output of the micropump, for an increase in microvalve tilt, with the power output following the trend (25/75%) > (35/65%) > (50/50%). Flow rate values are for (n = 4) experiments, with backpressure values totaling (n = 3) experiments.

10) Microvalve Tilt Perspective

As is evidenced by the experimental data presented above, the lateral tilt of a microvalve can have a significant impact on micropump performance. This concept of microvalve tilt could bear relevance to other micropump designs as well. While in most cases it is not likely other micropump designs would be capable of integrating dynamically variable tilt microvalves, it is possible for other designs to incorporate design features that allow for a permanently "tilted" microvalve/s. This could be achieved using surface or bulk micromachining methods, where differences in material thicknesses and/or geometries could be varied such that an actuator could be mounted/integrated so as to create a "squeegee" effect when actuated. It is also possible to replica mold PDMS a membrane that contains a continuous gradient in membrane thickness, using gray-scale template fabrication methods.[1329-1331] Such membranes would function as squeegee microvalves when integrated into pneumatic micropump designs. Membranes fabricated with a spatially variable thickness would allow for the elasticity of the membrane to vary continuously across the length of the microvalve, and therefore when actuated, allow for a continuous difference in response times to exist across the membrane surface. It would be expected this variable response time for three valves taken in sequence, would allow for each microvalve to be actuated/closed with a "squeegee" effect, such that the net overall effect would be to alter the shape of the peristaltic waveform. Increasing the performance of a microvalve with tilt would allow pneumatic designs to integrate smaller microvalves, which are capable of performing identically as microvalves with larger footprint sizes. The effect of decreasing microvalve footprint size while maintaining equivalent performance as a larger

microvalve, would allow for less real estate to be used, and therefore provide an additional design variable that can be leveraged to continue the trend of increasing the number of valving operations on a microfluidic chip.[25, 635]

A measure of flow rate throughout a microfluidic chip is extremely important, when quantitative analysis is an objective. It is well known, changes in pressure drop or system resistance, create a change in flow rate throughout a microfluidic chip. As such, it is not surprising numerous approaches have been taken to study and characterize a microfluidic chips: 1) system resistance,[1307, 1308, 1332, 1333] 2) flow velocities for changes in backpressure[1334-1336] and pulsating flows,[1322, 1337, 1338] with flow velocities oftentimes being characterized using flow sensors[989, 990, 1339-1341] and techniques such as particle image velocimetry[454, 455, 459, 1342] (PIV), along with other optical,[446, 450, 1343] and thermal[1344] tagging techniques, and 3) pressure drops for various cross-sectional channel geometries,[1270, 1345-1348] channel distortions,[1322, 1323, 1349] channel surface textures,[1350, 1351] and fluidic contents.[1352-1354] Microfluidic chips oftentimes incorporate many valves for the purpose of directing and stopping flows throughout various sections of the microchip. These diversions in flow can create changes in pressure drop and system resistance throughout a microchip, and therefore, can create global and local changes in flow rate as well. Options that exist to change or control flow rate using a peristaltic micropump are to change the peristaltic signals shape, frequency, wavelength, amplitude, or phase.[283, 326, 1321] Another available option to change the flow rate of a peristaltic micropump is to change the valve footprint size/s.[1291]

The micropump reported within this Chapter, allows an experimentalist to alter

microvalve tilt, corresponding to a change in the peristaltic signals shape, and also a change in microvalve footprint size. Squeegee microvalves provide for an additional microchip design variable option beyond the ones mentioned above, in allowing for compensation or adjustment of flow rates throughout a microfluidic chip, as necessary. Squeegee microvalves could be placed in series or parallel with untilted microvalves, where the squeegee microvalves could be actuated as necessary to adjust flow rate and backpressures accordingly throughout a microfluidic chip. Likewise, forward or reverse squeegee microvalves could be employed either in series or parallel, as required by a particular microchip design. Such arrangements could be used to alter flow properties on a microfluidic chip, in addition to reversing flows either locally or globally. It is also conceivable that complex algorithms could be employed to calculate flow resistances throughout a microfluidic chip, as various combinations of microvalves are actuated, with the algorithm in turn actuating squeegee microvalves as necessary, to aid or assist in maintaining a constant or desired flow rate throughout a microfluidic chip (or chip sections). While this particular micropumps squeegee microvalves are designed with integrated piezoelectric cantilever actuators and external microvalves, it is possible as stated above, to integrate squeegee microvalves into pneumatic designs, using gray-scale template replica molding fabrication methods.[1329-1331]

The concept of valve tilt also extends beyond the notion of intentionally integrating such a feature into the valving mechanism of a micropump. While the data presented above indicates small variations in microvalve tilt would likely go unnoticed, it is still possible that irregularities or nonidealities could be introduced during the

micromachining process, whereby an undesired "squeegee" effect could be introduced as part of the micropump valve operating mechanism. Possible nonidealities or micromachining irregularities that could be introduced throughout the micromanufacturing process could include, but not limited to; external actuator mounting irregularities, local etch variations, variations in thin film and other material thicknesses, nonideal bonding of materials resulting in regional and local variations, dynamic variations in material dimensions due to a mismatch in coefficients of thermal expansion, contamination issues, defects in materials, variations in planarity of material surfaces, amongst many other possibilities as well. Therefore microvalve "tilt" is applicable beyond the current discussion. Taken as a general concept, "tilt," is relevant to many micro and nano device designs, where any form of mechanical actuation is incorporated into the fabrication process.

Conclusions

The current Chapter presented characterization results on the performance of a PDMS fabricated peristaltic micropump, when lateral tilt adjustments are provided to each respective microvalve tip. To the best of the Author's knowledge, no such micropump design variable has been previously reported within the literature. "Tilted" microvalves are best characterized as, "squeegee microvalves." The flow rate and backpressure data indicates very predictable and consistent trends for progressive increases and decreases of lateral tilt. Data was provided to illustrate these predictable and repeatable changes in micropump performance, and theory was developed analogous to the Affinity Laws commonly used to predict performance changes within a centrifugal

pump, as a result of induced operational changes provided to the centrifugal pump. Data was also provided to show that the power output of the micropump increases, for corresponding increases in microvalve tilts. Aside from redesigning and refabricating a new micropump, most fully functional peristaltic micropumps can alter actuation frequency or actuation force, to tailor the output performance of the micropump. This particular micropump design however, can not only alter actuation frequency and actuation force to change the output performance of a micropump, but further allows for alteration of microvalve tilt, which effectively equates to changing the shape of the peristaltic waveform. In situations with mixed lateral tilt combinations, it was observed the flow data was slightly erratic, but was still capable of producing a net flow in spite of these nonideal tilt combinations, thereby indicating this particular micropump design is "forgiving" towards nonideal tilt combinations, when considered with respect to its ability to produce a net flow.

It was observed the lateral tilt combination of the microvalves could in some instances overpower/affect the flow bias direction expected of the peristaltic signal. These reversed flows were observed in a few rare instances, where two hypotheses were put forth and discussed to account for these unexpected findings. The first hypothesis focused on the process of how lateral tilt adjustments were made, and the effect these adjustments could have on the valving dynamics of the micropump. It is hypothesized the microchannel in some instances is being collapsed sideways, in addition to being "twisted," such that this complex 3D mechanical "twisting" motion creates or contributes to the process of producing reverse flows through the micropump. A second hypothesis

put forth suggested that counterflow microvortices could possibly have been formed adjacent to the microvalves, and therefore provided a larger driving force in the flow direction opposite that of the peristaltic wave bias direction.

The current micropump valving mechanism was shown to be slightly complex, however this particular design allows for an increased array of options to continuously on-the-fly fine tune and adjust metrics such as flow rate and backpressure within a microfluidic system. These adjustment capabilities make this particular design a useful microfluidics research and/or benchtop tool for applications that may require additional real-time adjustment capabilities for micropump performance, beyond that of frequency or actuation driving force. It is conceivable an electronic feedback mechanism could be integrated and used to control microvalve lateral tilt in real-time, thereby allowing the micropump to adapt to a systems changing conditions, so that constant flow rates could be maintained. This tuning capability is fitting for use within the field of microfluidics where other applications have also demonstrated the process of tuning physical variables on a microchip.[808, 809, 830, 877, 946, 947, 1018, 1298, 1307-1320] Lastly, it was discussed how gray-scale fabrication methods could be employed, to integrate lateral tilt squeegee microvalves within pneumatic actuation microvalves and micropumps. Increasing the performance of a microvalve with tilt would allow pneumatic designs to integrate smaller microvalves, which are capable of performing identically as microvalves with larger footprint sizes. The overall effect would allow for less real estate consumption, and therefore provide an additional design variable that can be leveraged to continue the trend of increasing the number of valving operations on a microfluidic chip.[25, 635]

Chapter VII : *Chop and Sine Wave Signal Input to a Piezoelectric-Actuated Peristaltic Micropump*

Synopsis

A PDMS micropump, actuated with PZT piezoelectric cantilevers, was fabricated and characterized for the current data presented within this Chapter. Fabrication of the micropump was facilitated with use of an in-house portable handheld CNC machined injection molding apparatus. The micropump flow rate and backpressure performance was characterized for a sine wave actuation signal, as well as a "chop" actuation pattern. The chop actuation pattern corresponded to actuation of one cantilever actuated with a square wave signal, or two or three cantilevers actuated in unison with zero phase difference between the square wave signals. The flow rate and backpressure results for both signal patterns was further collected, with the microvalves "tilted," such that a "plowing" or "squeegee" action was created when each microvalve was actuated in the downward z-direction, for closure of the microchannel. A peristaltic micropump with "tilted" microvalves, is best described as providing an alteration to the shape of the peristaltic signal waveform, in morphing from a completely square wave (with zero microvalve tilt), to a triangular-like peristaltic signal (with microvalve tilt). An induced microvalve tilt was made possible, through fabrication and implementation of an in-house manufactured micropositioner setup. The results presented within this Chapter, characterize micropump variables not well characterized within the literature. Most peristaltic micropumps are actuated with square wave signals containing a phase difference, or with some other periodic actuation pattern, where the results presented within the current Chapter characterize a peristaltic micropump actuated with both a sine wave, and chop signal actuation pattern. In cases where micropumps are actuated with

"chop" signals, these micropumps typically employ a single cantilever with integrated check valves, where no such valves were incorporated into the current design. The performance of this micropump was further characterized for microvalves adjusted with "tilt," an unexplored experimental micropump design variable not found within the literature, to the best of the Author's knowledge.

Introduction

The field of microfluidics has experienced rapid growth over the past ten years, and shows no signs of slowing down any time soon.[62, 68, 71, 73-75] During this rapid growth phase, many unique device designs and microfluidic platforms have been reported, for their use and applications in studying and/or solving challenging scientific problems.

Microfluidic platforms are typically composed of multiple functional components commonly referred to as, unit operation devices.[70, 465] At the core of any fluidic platform are pumping and valving operations. Well characterized pumps and valves are critical, for microfluidic applications where quantitative analysis is dependent upon flow rate throughout a microchip. Many well designed and characterized micropumps have been reported for both displacement and dynamic pumps.[609] Pumps that fall within the displacement category commonly employ pneumatic,[628, 630, 633, 635] piezoelectric,[326, 646, 650, 654, 1326] magnetic,[659, 666, 668, 1355] mechanical,[702, 706, 708, 709] electrostatic,[684, 687, 691, 1356] electrochemical,[698, 700] and thermally-based[669, 678, 680, 1285] actuation means, with common dynamic pumps actuated with electrokinetic,[726, 728, 731, 734] acoustic,[757-760, 1327] and bubble[762-765] propulsion means.

In the case of displacement pumps, performance is typically characterized for

variables such as minimum and maximum flow rate, actuation signal characteristics such as frequency and phase, pressure pulsations, valving characteristics, and maximum working backpressures.[283, 326, 1322, 1323] Other variables such as valve footprint size and valve cycling characteristics have been characterized, for their effect on micropump performance.[326, 667, 1290, 1291] Each of these operational variables can have a large effect on device performance, and as such, characterization of these and other variables is critical for validation of microchip performance.

The current Chapter characterizes the performance of a piezoelectric cantilever-actuated peristaltic micropump, fabricated using injection molding and soft lithography fabrication techniques. The performance of the micropump is reported for two actuation signals, including a peristaltic sine wave and also a "chop" actuation signal. The chop signal is best referenced as a square wave actuation signal for actuation of one cantilever, or two or three cantilevers actuated in unison with zero phase difference placed between each of the cantilever signals. These actuation signals were further characterized for tilted microvalves, where these microvalves create a "plowing" or "squeegee" effect when actuated, and therefore preferentially drive the contents within the microchannel along the squeegee direction. The effect these variables have on micropump performance is significant, where these data can be used as a baseline reference, when considering how best to optimize the performance of a micropump.

Materials and Methods

1) Fabrication of PDMS Micropump

The closed channel of the micropump was fabricated from PDMS (GE, RTV615), with integrated capillary tube interconnects (Polymicro, 105/40 μm OD/ID). The microchannel was formed by irreversibly bonding a 5 : 1 micromolded PDMS microchannel, with a 30 : 1 featureless PDMS base layer. A portable handheld in-house CNC machined injection molding apparatus was used to fabricate the 5 : 1 channel layer. Details of this injection molding apparatus are provided within Chapter III. Briefly however, the injection molding apparatus was machined primarily from aluminum. The primary parts consisted of a top and bottom set of plates, a laser machined polymeric gasket (McMaster-Carr, 9513K118), a cylinder body, a piston, and a stainless steel ball with piston driving screw. The bottom plate was used to form the molding template, with the template formed using a derivatized sequence of previously described method steps, as discussed within Chapter II. The bottom plate was fabricated with through-hole vias, which allowed for a 75 μm electrical discharge machine (EDM) wire to be straddled across the surface of the bottom plate. The wire was threaded through the vias and wrapped around posts on the opposite side of the bottom plate, and thereafter secured in place using a nut and Teflon washer. General purpose spray adhesive was next applied across the bottom plate, for the side containing the straddled EDM wire. A piece of properly sized general purpose aluminum foil was then placed over the wire/spray adhesive atop the surface of the bottom plate, and smoothed over using finger pressure. A Teflon block was then used to further smooth over the aluminum foil, with excess foil

being trimmed using a razor blade. A citrus-based cleaner was used to remove excess spray adhesive from the surface of the template, followed by an IPA wipe. A final inspection was performed under a microscope, to remove any remaining contamination that was left behind.

After forming the molding template against the bottom plate of the injection mold, the injection molding apparatus was then fully assembled. The laser machined polymeric gasket was placed atop the bottom plate, with the top plate further placed over the polymeric gasket. The sandwiched gasket formed an internal molding cavity, which allowed for prepolymer PDMS to be injected and cured against the template formed across the surface of the bottom plate. The thickness of the gasket determined the thickness of the PDMS slab, and therefore the PDMS microchannel membrane thickness as well. The 5 : 1 PDMS was poured into the cylinder body, which was previously secured in place over the top plate of the injection mold. No degassing of the PDMS was necessary, prior to the injection step. The bubbles trapped within the 5 : 1 prepolymer PDMS as a result of the mixing process, were forced across exhaust ports, machined into either the polymeric gasket or the bottom plate. The exhaust ports and cylinder body were located at opposite ends of the injection molding apparatus, where such a spatial arrangement allowed for an extreme pressure differential to be formed across the injection mold cavity, when the PDMS contents of the cylinder were injected.

The PDMS-filled injection molding apparatus was briefly cleansed to remove any excess PDMS that exited across the exhaust ports, and then placed into a convection oven at 80º C for one or more hours. After the expedited curing process, the injection molding

apparatus was briefly placed under a cold water faucet, to bring the apparatus back down to room temperature. The injection molding apparatus was then disassembled to remove the molded 5 : 1 PDMS slab, with the slab being placed on a clean glass substrate, with the micromolded channel facing atmosphere. The membrane over the microchannel measured approximately 80 μm, with the microchannel height measuring approximately 100 μm.

The 30 : 1 PDMS base layer was formed concurrently with the injection molding process. The base layer was formed by sandwiching degassed 30 : 1 PDMS prepolymer between two glass substrates, with the substrates separated by ~203 μm spacers. This process began by placing two glass substrates into two separate desiccators containing a volatile antiadhesion vapor (United Chemical Technologies, model T2492). This antiadhesion vapor allowed for easier removal of PDMS from the glass substrates. The glass substrates were placed into their respective desiccators with two different yet overlapping time intervals. The overlapping time intervals allowed for one wafer to be preferentially removed over that of the other, when the glass substrates were separated. The 30 : 1 PDMS glass sandwich was secured together as a self-contained unit using binder clips, and thereafter placed into a convection oven at 80º C for 35 minutes, to allow for a partial cure of the 30 : 1 PDMS. The overall thickness of the 30 : 1 slab was measured using a surface profilometer, with the overall measured thickness recorded as ~200 μm.

With both the 5 : 1 microchannel layer and the 30 : 1 base layer formed, the process of bonding capillary tube interconnects between the two PDMS layers was next

performed. Two pieces of capillary tubing were placed ~1.5 cm into the microchannel under a microscope. A freshly mixed 5 : 1 prepolymer was lightly applied to the capillary tubes placed within the open microchannel. Excess prepolymer was removed using a razor blade. This step allowed for all excess void areas between the 5 : 1 microchannel and the capillary tubes, to be fully sealed. The 30 : 1 base layer was then applied atop the 5 : 1 microchannel layer, with the two bonded layers with capillary tube interconnects thereafter being placed into a convection oven at 80º C for one or more hours. After the convection oven cure step, the irreversibly bonded PDMS mold was then sectioned using a razor blade, and placed onto a clean glass substrate for further processing. The final step was to apply a freshly degassed 5 : 1 prepolymer PDMS solution to the exit regions of the capillary tube interconnects, where they exited the irreversibly bonded PDMS mold.

2) Micropump Cantilever Actuation

The micropump was actuated using PZT piezoelectric cantilevers (Piezo Systems, Q220-A4-303YB), with a miniature precision machined clamp adhered to each cantilever tip. The clamps allowed for a precision machined microvalve to be secured in place. Depending on the actuation signal, either one, two, or three cantilevers were actuated along the microchannel. The sine wave data presented within the current Chapter was collected with a 120º phase shift between each of the three cantilevers, with the "chop" actuation signal having a zero degree phase shift between two or three cantilevers. The "chop" signal is best described as actuating a single cantilever with a square wave signal, or actuating two or three cantilevers in unison with the same square wave signal, such

that their spatial and valving characteristics were identical over time. Small signals were created with a virtual function generator (National Instruments), with the small signals amplified using external high voltage electronic hardware containing high voltage amplifiers (Apex Microtechnologies, PA15A). The cantilevers were driven at their maximum driving potential of $V_p = \pm 90$ V, so as to maximize deflection amplitude.

3) Microvalves, Microvalve Micropositioners, and Microvalve "Tilt"

Precision machined microvalves were machined using an electrical discharge machine (Agie, AgieCut Classic), where each microvalve tip was machined with surface dimensions of 3 mm x 250 μm (L x W). Further microvalve design details are provided within Chapter IV. Each microvalve was positioned over the microchannel using an in-house fabricated micropositioning apparatus, which contained in-part, preassembled micropositioner bodies (Quater Research, XYZ 300MR), with the entire micropositioner apparatus described more fully within Chapter V. The micropositioner apparatus allowed each microvalve to be "tilted," such that the microvalves could be actuated to produce a "plowing" or "squeegee" action, in propelling the contents of the microchannel forward. The process of tilting a microvalve began by first placing the microvalve tip in contact with the PDMS membrane surface, such that the surface plane that defined the microvalve tip was placed parallel to the PDMS membrane surface plane. "Tilt," was then accomplished by adjusting the micropositioners, whereby the surface plane of the microvalve tip went from being parallel to the membrane surface plane, to nonparallel, with the overall change in position providing a "squeegee" actuation mechanism. This valve closure process can be seen more clearly as shown within Figure VII-1.

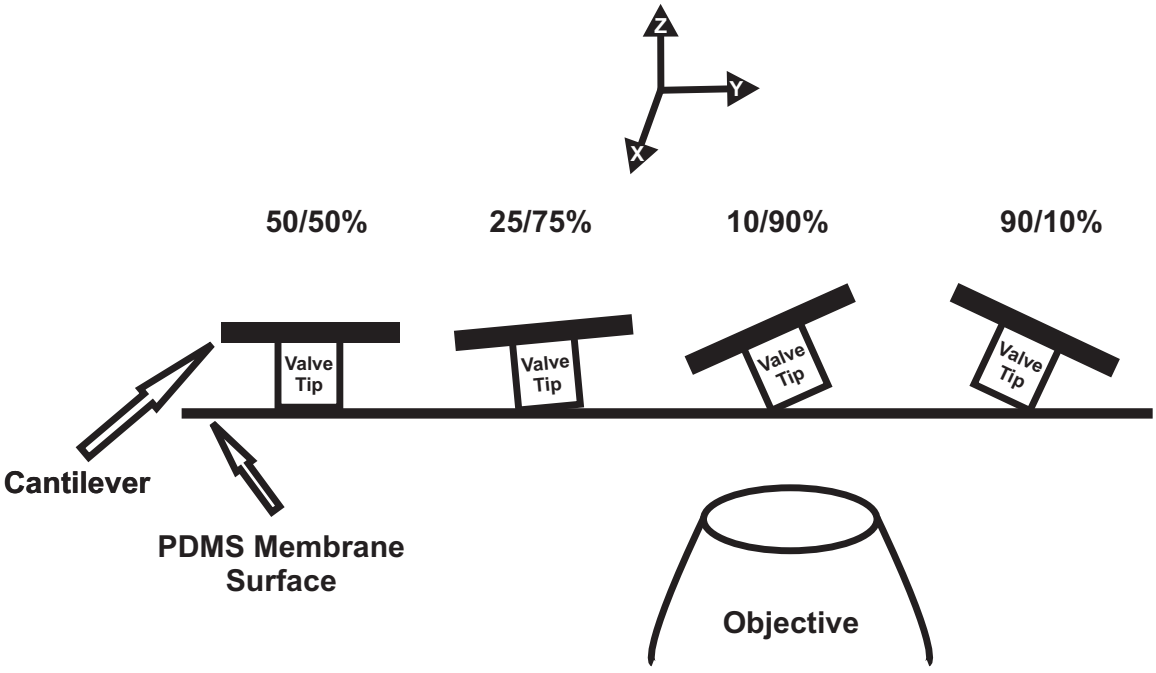

Figure VII-1: Microvalve "tilt" schematic. Illustration of various arbitrarily chosen microvalve tilts, where a tilt of 50/50% illustrates zero tilt, with any other %/% value indicating a quantitative measure, of a microvalve with a nonzero tilt. The degree of microvalve tilt increases as shown, with the trend going as; 10/90% > 25/75% > 50/50%, with 90/10% a mirror image of a microvalve with tilt, 10/90%. The degree of microvalve tilt was quantitated as an eyeball estimate using a microscope, and believed to be accurate to within 5%.

Various degrees of microvalve tilt were quantifiable with use of a microscope. Arbitrarily chosen degrees of induced microvalve tilt are shown within Figure VII-1, and indicated as a "%/%" quantity. A tilt corresponding to 50/50% is equivalent to a microvalve with zero induced tilt, with any other quantity corresponding to an induced tilt. The various degrees of tilt are seen increasing in order from 25/75% to 10/90%, with a mirror reflection of 10/90% shown as 90/10%, all within Figure VII-1. The microvalve tilt adjustment process effectively transforms the position of the microvalve, such that the opposite ends (considered with respect to the length direction) of the microvalve take on two separate height values (z-direction, referenced with respect to the PDMS membranes surface) after being, "tilted." The "squeegee" valving mechanism is easily observable

within Figure VII-1, for actuation of the microvalve along the Z-direction.

The process of quantifying the degree of microvalve tilt was accomplished using the microscope objective as shown within Figure VII-1. The microvalve was slowly actuated with a dry microchannel, where the PDMS membrane release dynamics from the base of the microchannel were recorded as the microvalve was actuated from a fully closed to a fully open state. The release dynamics were recorded as an eyeball estimate, and believed to be accurate to within 5% or less. The "%" quantities as recorded, effectively totaled a percentage of distance across the length of the microvalve. Therefore a tilt recorded as 50/50% indicated that the last point of membrane release from the base of the PDMS microchannel, was 50% of the total length across the microvalve, when considered from either opposing end (along Y-direction as shown within Figure VII-1) of the microvalve. A tilt of 10/90% however, would indicate that the last point of membrane release was 10% of the distance taken across the length of the microvalve (Y-direction) when referenced with respect to the left-most edge of the microvalve, and 90% of the distance taken across the length of the microvalve (Y-direction) when referenced with respect to the right-most edge of the microvalve. A more in-depth discussion of microvalve tilt is provided within Chapter VI, with "tilted" microvalves being coined within this Chapter as, "squeegee microvalves."

4) Flow Rate Characterization

Flow rate values for the micropump were recorded by tracking a small bubble (2-3 mm) along an external piece of capillary tubing (~1 m) connected to the micropump outlet capillary tube line. The external piece of capillary tubing was attached to a meter

stick, and also filled with blue food dye, so as to allow for better tracking contrast of the bubble. Flow rates were calculated using the formula, Q = Av, with "Q" equal to the flow rate, "A" equal to the cross-sectional surface area of the flow, and "v" equal to the linear flow velocity of the bubble. The sine signal data presented within this Chapter, was collected with the cantilevers placed 120º out of phase. No phase difference existed for the chop signal, as previously discussed. All error bars are shown for standard errors, with (n = 3) for the chop signal data, and (n = 4) for the sine signal data.

5) Backpressure Characterization

Maximum attainable backpressure data was obtained by connecting the outlet capillary tube line of the micropump to an electronic pressure sensor (Honeywell, 40PC015G2A), where a gage pressure reading was measured. The micropump was allowed to fully pressurize over time, with the pressure reading eventually attaining a steady-state value. Upon reaching this maximum backpressure, the micropump was stopped, where only one microvalve was left in the closed position. After recording pressure readings for a period of 15 minutes, the valve was opened, where additional pressure readings were recorded, until the micropump had fully depressurized. The pressurization frequency was 5 Hz for the sine signal, and also for the chop signals for one and two cantilevers, with the chop signal for three cantilevers actuated at 125 Hz. These frequencies corresponded to the frequencies that produced the highest flow rates, as determined from their respective flow rate curves. The sine backpressure plot is for (n = 3) experiments, with (n = 1) for the chop signal backpressure plots.

Results and Discussion

6) Flow Rate Data

Figure VII-2 represents the flow rate curve obtained for a 120º phase shifted sine wave peristaltic signal. Most characterized flow rate data for peristaltic micropumps is collected using periodic square wave signals, or with some other unique signal actuation pattern.[283, 326, 1321, 1335, 1357-1359] In spite of square wave actuation signals comprising the greatest number of publications for peristaltic micropumps, sine wave actuated micropumps have been characterized.[1324-1326] The flow rate curve shows a very smooth and predictable change in shape, when cycling throughout the various frequency intervals characterized. A microvalve tilt of 25/75% was characterized, where it would be expected a tilt greater than this value, would create a flow rate curve with higher flow rate values. Trends as such have been observed and reported within Chapter VI. The flow rate peaked at 5 Hz, with a flow rate corresponding to 79 nL/min. It is also noted, the 120º sine wave peristaltic actuation signal was qualitatively observed to be less pulsatile than that of a 120º square wave peristaltic actuation signal, when comparing both signals with the exact same microvalves containing identical tilt/positional settings. The study and use of pulsatile flow information within microfluidic devices has been presented elsewhere, and could therefore be employed as a means to quantitatively measure and further understand the pulsation dynamics of a sine wave peristaltic signal, in comparison to that of a square wave peristaltic signal.[1322, 1337, 1339]

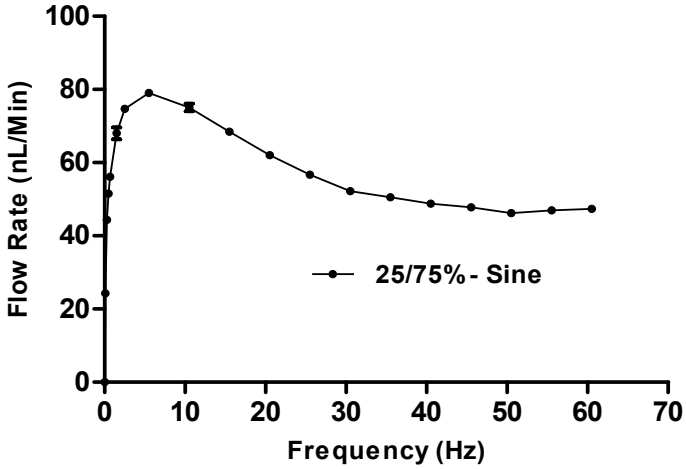

Figure VII-2: Plot of flow rate vs. frequency. Data was collected for the micropump actuated with a sine wave signal, with the cantilevers placed 120º out of phase. All three microvalves were quantitated with a tilt of 25/75%. Peak flow rate occurred at 5 Hz, with a flow rate corresponding to 79 nL/min. Error bars are representative of standard errors, and plotted for (n=4) experiments.

Figure VII-3 is a representation of the flow rate data obtained using the chop signals as described above. Most square wave "chop" actuation signals used with single actuator micropumps, contain integrated in-line valves,[597, 641, 645, 1336] where no such check valves were employed as a part of the current micropump design. All cantilevers used for obtaining the flow rate curves of Figure VII-3 were adjusted with a tilt corresponding to, 10/90%. A predictable trend was observed for maximum attainable flow rates, with increasing numbers of actuated cantilevers. The shape of the curves is similar and predictable for curves A and B, with an unusual shape for curve C. It is hypothesized curve C was able to attain much higher flow rates as a result of a possible complex multiple driving force mechanism, with the microvalve/s "squeegee" effect providing a first driving force, in addition to complex microvortice flow patterns adjacent the microvalves, creating a possible second added driving force. Such microvortice flow patterns have been studied elsewhere for both forward[1326] and reverse[1324, 1325, 1327, 1328

flows. It is additionally hypothesized the chop signal driving mechanism, is also a function of the mechanics associated with the nonuniform PDMS membrane surface deformation, as well as the microchannel collapse dynamics. The maximum flow rates peaked at 5 Hz for curves A and B, with flow rates corresponding to 28 nL/min and 39 nL/min, respectively. It is also noted that curves A and B were characterized for reverse flows, which were opposite that of the expected flow direction, when considered for the "squeegee" valving bias direction. As with the peristaltic sine wave actuation pattern, the chop signal flows were also qualitatively observed to be slightly less pulsatile than that of a peristaltic square wave actuation pattern, with three cantilevers placed 120º out of phase. The maximum flow rate for curve C peaked at 125 Hz, with a flow rate corresponding to 96 nL/min.

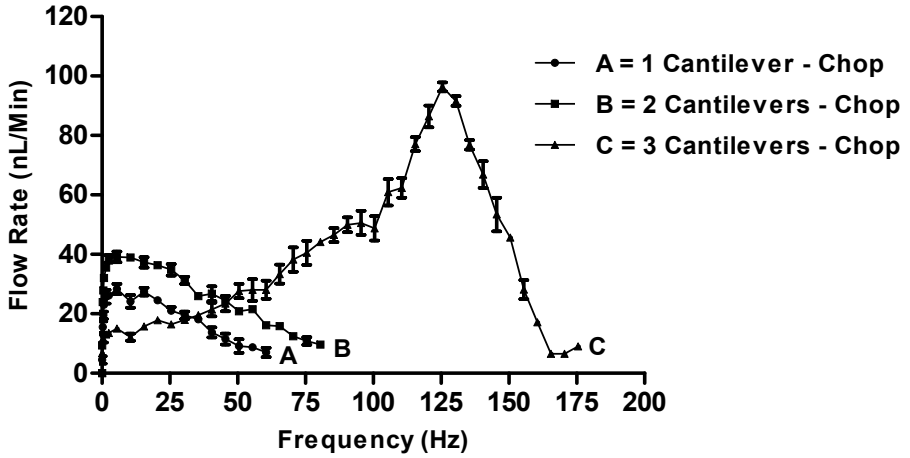

Figure VII-3: Plot of flow rate vs. frequency. Each of the three curves was characterized for a "chop" actuation signal, with a chop signal best characterized as actuating a single cantilever with a square wave signal, or two or three cantilevers actuated in unison with a square wave signal, such that zero phase difference existed between the two or three actuated cantilevers. All three curves characterized for microvalve/s with a tilt corresponding to 10/90%. The maximum flow rates go as, 96 nL/min > 39 nL/min > 28 nL/min, for curve C > B > A, respectively. Error bars are representative of standard errors, and plotted for (n=3) experiments, for each of the three curves.

7) Backpressure Data

Figure VII-4 is representative of the backpressure data collected for the 120º sine wave peristaltic actuation signal pattern. This plot was characterized for the micropump actuated at 5 Hz, corresponding to the maximum achievable flow rate for the micropump, as determined from Figure VII-2. The averaged maximum achievable backpressure of Figure VII-4 was computed as, 16,900 Pa.

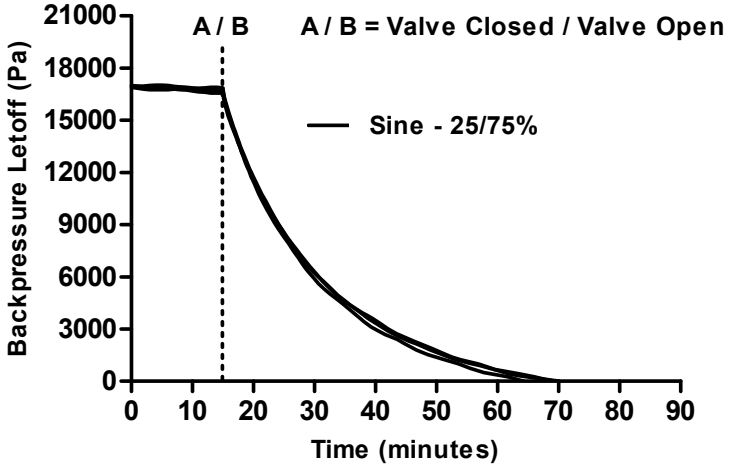

Figure VII-4: Plot of backpressure vs. time. The micropump was actuated with a peristaltic sine wave at 5 Hz, with the microvalves tilted as 25/75%. The outlet capillary tube line of the micropump was connected to an electronic pressure sensor, where upon reaching a stabilized backpressure (i.e. maximum backpressure value at time = zero), actuation of the micropump was stopped, with only one microvalve left in the closed position. After a period of 15 minutes, the single microvalve was opened, where backpressure readings were recorded until no pressure existed within the system. The averaged maximum backpressure was characterized as 16.9 kPa. The plot is shown for (n=3) experiments.

Figure VII-5 is a plot of the maximum achievable backpressures recorded for the chop signal actuation patterns. Curves A, B, and C of this plot follow a predictable trend of highest to lowest backpressure values going as, C > B > A. Curves A and B were characterized for actuation frequencies of 5 Hz, with curve C characterized for an actuation frequency corresponding to 125 Hz. These frequencies were chosen based

upon the flow rate data shown within Figure VII-3, where the maximum achievable flow rates of this Figure, corresponds to the pressurization frequencies chosen. The maximum achievable backpressures were recorded as, 20 kPa, 7.6 kPa, and 5.7 kPa, for curves C, B, and A, respectively. It is lastly noted, curves A and B of Figure VII-5, were characterized for a reverse flow direction, opposite that expected based upon the "squeegee" valving mechanism.

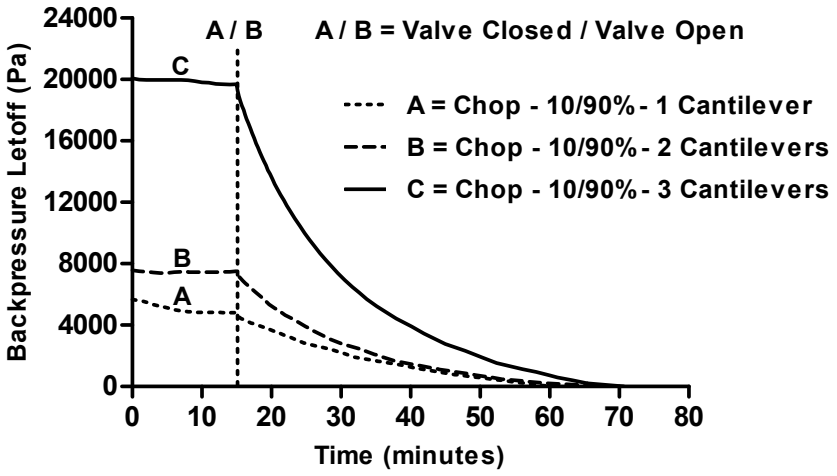

Figure VII-5: Plot of backpressure vs. time. The micropump was actuated with a chop signal, with the microvalves tilted as 10/90%. All three curves were characterized for a "chop" actuation signal, with a chop signal best characterized as actuating a single cantilever with a square wave signal, or two or three cantilevers actuated in unison with a square wave signal, such that zero phase difference existed between the two or three actuated cantilevers. The outlet capillary tube line of the micropump was connected to an electronic pressure sensor, where upon reaching a stabilized backpressure (i.e. maximum backpressure value at time = zero), actuation of the micropump was stopped, with only one microvalve left in the closed position. After a period of 15 minutes, the single microvalve was opened, where backpressure readings were recorded until no pressure existed within the system. The averaged maximum backpressure values are; 20 kPa > 7.6 kPa > 5.7 kPa, for curves C > B > A, respectively. The plot is shown for (n=1) experiments for each of the three curves.

Conclusions

The current Chapter reported the performance of a PDMS peristaltic micropump for both flow rate and backpressure, and additionally for both sine wave and chop signal actuation patterns. The results were characterized for each microvalve adjusted with a "tilt," such that a "squeegee" or "plowing" effect was created when each microvalve was actuated for closure of the microchannel. "Tilted" microvalves are best characterized as, "squeegee microvalves," as discussed within Chapter VI. Reversed flows were characterized for chop signals actuating either one or two cantilevers, where three cantilevers actuated in unison with a square wave chop actuation signal produced a flow in the expected microvalve squeegee direction. Predictable trends in magnitude were observed from highest to lowest, for both backpressure and flow rates, for the trend of three, two, and one cantilever/s actuated with a chop actuation signal. It was hypothesized the high flow rates recorded for three cantilevers actuated in unison with a square wave chop signal, was a result of a possible complex multiple driving force mechanism, with the microvalve/s "squeegee" effect accounting for one driving force, along with complex microvortice flow patterns adjacent the microvalves, creating a possible second added driving force. It was additionally hypothesized the chop signal driving mechanism, is also a function of the mechanics associated with the nonuniform PDMS membrane surface deformation, as well as the microchannel collapse dynamics. Qualitative observations were recorded for both sine wave and chop signal actuation patterns, where it was observed both actuation patterns produced less pulsatile flows, when compared to that of a square wave peristaltic signal actuation pattern, with three

cantilevers placed 120º out of phase. The results as presented within the current Chapter could be used as a baseline reference, when considering other actuation signals and valving mechanisms that could be utilized to a scientist or engineer's advantage, in controlling fluid flow throughout a microfluidic chip.

Chapter VIII : *A Method to Quantify in vivo Rodent Brain Direct-Sampling Suction Lift, using Micropump Performance Curve (H-Q Plot) Analysis*

Synopsis

The current Chapter will present a methodology for quantifying the suction lift required of a PDMS fabricated peristaltic micropump, to perform direct-sampling neuroscience experiments. The peristaltic micropump was fabricated in-part with the aid of a handheld PDMS injection molding apparatus. The injection molded microchannel was mounted to an in-house fabricated micropositioner apparatus, which provided microvalve lateral "tilt" adjustment capabilities. "Tilt" is accomplished when the micropositioners are adjusted, such that the plane that defines the microvalve tip, becomes non-parallel to the PDMS membrane surface plane, whereby a "plowing" or "squeegee" action is created when the microvalve is actuated, for closure of the microchannel. A more complete discussion of this "tilt" process will be provided below. Flow rate (Q) and backpressure (P) data was collected and plotted as a P-Q (or H-Q) plot, whereby this plot comprises fourteen data points, each with a unique combination of micropump variables (collectively defined within this Chapter as a micropump "state") for microvalve "tilt," microvalve size, number of cantilevers/microvalves actuated, and actuation signal/shape/frequency. The significance of this P-Q plot is four-fold. First, the plot provides useful data, as to how this particular micropump design can best be optimized to produce the highest possible flow rates and backpressures. Second, this plot provides a quantitative measure of the micropump power output. Third, the P-Q plot is equivalent to superimposing both a system curve, and pump performance curve upon one another. And fourth, the P-Q plot curves can be used to quantify the suction lift required of a micropump, when performing *in vivo* brain direct-sampling neuroscience

experiments, using anesthetized rodents. A quantitative measure of the suction lift resistance associated with the direct-sampling methodology is critical for four primary reasons, which include: 1) a quantitative measure of direct-sampling suction lift, will allow proper design of a micropump for intended use within rodent brain direct-sampling neuroscience experiments; 2) the micropump and direct-sampling probe will be connected in-line with a capillary electrophoresis instrument, whereby a quantitative direct-sampling suction lift assessment is required, if this instrumental arrangement is to yield high temporal resolution neurotransmitter release information; 3) the Author is unaware of any report, providing any such measure of the suction lift requirements associated with the direct-sampling methodology; and 4) the direct-sampling methodology remains far less utilized in proportion to many other neurotransmitter sampling techniques, such as that of microdialysis, whereby a quantitative measure of the direct-sampling suction lift requirements, will provide useful information in advancing the practicality, and usefulness of this particular brain sampling technique.

Introduction

A microfluidic system is composed of many generic components such as microchannels, interconnects, and unit operation devices such as valves and pumps.[70, 465] Central to any device platform or any particular intended use are microvalves and micropumps. One micropump classification scheme is to categorize micropumps as either displacement or dynamic pumps.[609] Commonly reported displacement micropumps include pneumatic,[283, 628, 629, 632] piezoelectric,[326, 638, 653, 654] magnetic,[659, 666-668] mechanical,[702, 706, 708, 709] and thermally-based[672, 678, 680, 1285] designs. Likewise,

commonly reported dynamic micropumps include surface tension,[765-768] bubble,[761-764] electrokinetic,[722, 730, 736, 1360] and acoustic[757-760, 1327] designs.

Once a micropump has been designed and successfully fabricated, characterization of the micropump is critical, especially in cases where quantitation is dependent upon flow rate throughout the microfluidic device. Typical characterization variables for micropumps include minimum and maximum flow rates, actuation signal characteristics such as frequency and phase, valve shutoff characteristics, maximum working backpressures, and pressure pulsations.[283, 326, 1322, 1323] Characterization of these variables is critical in many cases, as micropump and microvalving operations can drastically alter the performance of a microfluidic platform.

For microfluidic platforms containing a high number density of microvalves and micropumps, it is possible for flow rates and backpressures to change throughout portions of the microchip, as various fluidic routing operations are performed throughout the microchip.[1308, 1332, 1333] Therefore, it would be instructive and useful to have a methodology for understanding the performance of a micropump in relation to the entire fluidic system. In the case of centrifugal pump theory, pump performance curve analysis is used to understand a pump in relation to an industrial fluidic piping system.[1278]

This Chapter will present an analysis of a peristaltic micropump, where fourteen micropump operating "states" were characterized for both flow rate and backpressure. The plotted data for these fourteen micropump states can be used to understand how the performance of the micropump can be optimized for both flow rate and backpressure. The plot of backpressure vs. flow rate for the fourteen micropump states can also be used

to understand the performance of the micropump in relation to the simple microfluidic piping system. The forthcoming analysis and discussion will show this plot not only provides a means to understand how the micropump performance can best be optimized, but also provides the performance curve for the pump, as well as the microfluidic system curve. When the pump performance curve and system curve are superimposed, the relationship between micropump performance and flow throughout the entire microfluidic piping system, can be clearly understood. Therefore, the two superimposed curves can be used to optimize the performance of the micropump, with respect to fluidic transport throughout the piping system. An analysis for system changes is placed into a direct-sampling neuroscience context, however this analysis for system changes is applicable to nearly any microfluidic format where pumps and flow networks are in existence.

Experimental Methods

1) PDMS Micropump Fabrication

The PDMS micropump (GE, RTV615) channel layer was fabricated using a handheld injection molding apparatus, with the base layer fabricated by sandwiching PDMS between two glass plates, with spacers used to regulate the thickness of the base layer. The injection molding apparatus is described more fully within Chapter III. Briefly however, the injection mold was CNC machined in-house, primarily from aluminum. The bottom plate of the injection mold apparatus was used for creation of a PDMS molding template, with the template formed using a derivatized sequence of

previously described method steps, as presented within Chapter II. The template was created by first straddling a piece of 75 μm diameter electrical discharge machine (EDM) wire across the bottom plate, followed by application of a general purpose spray adhesive across the surface of the bottom plate. A piece of general purpose aluminum foil was next applied over the wire and adhesive, with the aluminum foil being smoothed over using a Teflon block. Removal of excess aluminum foil was performed by trimming the edges with a razor blade. The template was then placed through a citrus-based cleaning step, to remove excess spray adhesive. Final inspection of the template took place under a microscope, to ensure no contamination was left behind.

Assembly of the injection mold was performed in-part by sandwiching a laser-machined polymeric gasket (McMaster-Carr, 9513K118) between the top and bottom plates of the injection mold. The sandwiched laser-machined gasket created a microchannel molding cavity, where the thickness of the gasket further determined the thickness of the injection molded PDMS slab, and therefore the channel membrane thickness as well.

A fully assembled injection molding apparatus allowed for 5 : 1 PDMS to be poured directly into an injection cylinder, without performing a degassing step. A piston was compressed into the cylinder, to place the 5: 1 PDMS contents under extreme pressure in driving the prepolymer throughout the injection mold cavity. Exhaust ports were machined into the bottom plate of the injection molding apparatus, to further facilitate the creation of a pressure gradient throughout the molding cavity, whereby the excess injected prepolymer 5 : 1 PDMS was forced to exit across these exhaust ports.

The PDMS-filled injection molding apparatus was next placed into an oven at 80º C for one or more hours, to expedite curing of the PDMS within the injection mold cavity. Upon removal of the injection mold from the oven, the apparatus was briefly placed under a cold water faucet, to cool the apparatus back down to room temperature. The injection mold was then disassembled to remove the mold from the cavity. The mold was placed upon a clean glass substrate, with the channel facing atmosphere, to allow for further processing. The membrane over the microchannel measured approximately 80 μm, with the channel height measuring approximately 100 μm.

A partially cured 30 : 1 PDMS base layer was next fabricated. The process began by placing two glass substrates into two separate desiccators containing a volatile antiadhesion vapor (United Chemical Technologies, model T2492), where this step allowed for easy removal of the PDMS from the glass substrates. The glass substrates were placed into their respective desiccators with two overlapping, yet different time intervals, so as to allow for one of the glass substrates to be preferentially removed over that of the other. Degassed 30 : 1 PDMS was next sandwiched between the two vapor soaked glass substrates, with the glass substrates separated in height by ~203 μm spacers. Binder clips were used to secure the glass substrates into place, with the sandwiched PDMS thereafter being placed into an oven at 80º C for 35 minutes, to allow for a partial cure of the 30 : 1 PDMS. The overall 30 : 1 slab thickness measured ~200 μm.

Formation of the closed microchannel proceeded by first placing two pieces of capillary tubing (Polymicro, 105/40 μm OD/ID) ~1.5 cm into each end of the microchannel. A 5 : 1 prepolymer mixture was next placed over the capillary tubes to

seal all void areas adjacent the capillary tubes. Excess prepolymer 5 : 1 was removed with a razor blade, just prior to bonding the 5 : 1 microchannel mold with the 30 : 1 base layer. After bonding the capillary tubes between the microchannel and base layer, an irreversible bond was attained by placing the entire mold with capillary tube interconnects into an oven at 80º C, for one or more hours. After completion of the bonding step, the irreversibly bonded PDMS mold was placed onto a new and clean glass substrate. Lastly, the mold was sealed further from the atmosphere by applying prepolymer 5 : 1 PDMS to the exit regions of the mold, where the capillary tubes exited the bonded PDMS layers.

2) Micropump Cantilever Actuation

The micropump was actuated with either one, two, or three PZT piezoelectric cantilevers (Piezo Systems, Q220-A4-303YB) placed in series along the PDMS microchannel. A miniature precision machined aluminum clamp was adhered to each PZT cantilever tip, and used to fully secure a precision machined microvalve into place. The cantilevers were actuated with either: a peristaltic square wave with cantilever signals placed 120º out of phase; a peristaltic sine wave actuated with the cantilevers placed 120º out of phase; or actuated in unison with one, two, or three cantilevers, with zero phase difference between the two or three cantilevers (hereinafter referenced as a "chop" signal). In certain instances with use of a peristaltic wave, the wave bias was actuated to provide a reverse flow through the micropump. A full list of signal types, along with other experimental variables can be observed within Table VIII-1. A small signal for each cantilever was created using a virtual function generator (National

Instruments), with the small signals amplified with external high voltage electronic hardware containing high voltage amplifiers (Apex Microtechnologies, PA15A). The cantilevers were driven at their maximum driving potential of $V_p = \pm 90$ V, so as to maximize their deflection amplitudes.

3) Micropositioners, Microvalves, and Microvalve Tilt

Microvalves were precision machined using an electrical discharge machine (EDM), whereby the surface of the microvalve tip was fabricated with dimensions of either 3 mm x 250 μm (L x W), or 2 mm x 250 μm (L x W), with a more thorough discussion provided within Chapter IV. Positioning of each microvalve tip over the PDMS microchannel was made possible with use of an in-house fabricated micropositioner apparatus, fabricated in part with preassembled micropositioner bodies (Quater Research, XYZ 300MR), with the micropositioners discussed in greater detail within Chapter V. One variable characterized for the current Chapter, was to study the effect of microvalve "tilt." The process of tilting a microvalve begins by first placing the microvalve in contact with the PDMS membrane surface, whereby the surface plane that defines the microvalve tip, is placed parallel to the PDMS membrane surface plane. Tilt is next accomplished when the micropositioners are adjusted such that, the plane that defines the microvalve tip, becomes non-parallel to the PDMS membrane surface plane. A tilted microvalve creates a "plowing" or "squeegee" action throughout the microchannel region beneath the microvalve, when the microvalve is actuated for closure of the microchannel. The microvalve tilt process effectively transforms the position of the microvalve, such that the opposite ends (with respect to the length direction) of the

microvalve after being tilted, retain two separate heights (z-direction), when referenced with respect to the PDMS membrane surface. A schematic to depict this microvalve "tilt" process can be observed within Figure VIII-1. A tilt corresponding to 50/50% is equivalent to a microvalve with zero tilt. An increase in tilt is observed when proceeding from 25/75% to 10/90%, with a tilt of 90/10% corresponding to the mirror image of a microvalve with a tilt of 10/90%. When the microvalve is actuated into a closed state, flow beneath the microvalve would proceed along the Y-axis of Figure VIII-1, with the direction dependent upon the tilt direction of the microvalve. It is easy to visualize the "squeegee" action induced by a "tilted" microvalve, when the cantilevers are actuated along the Z-axis direction.

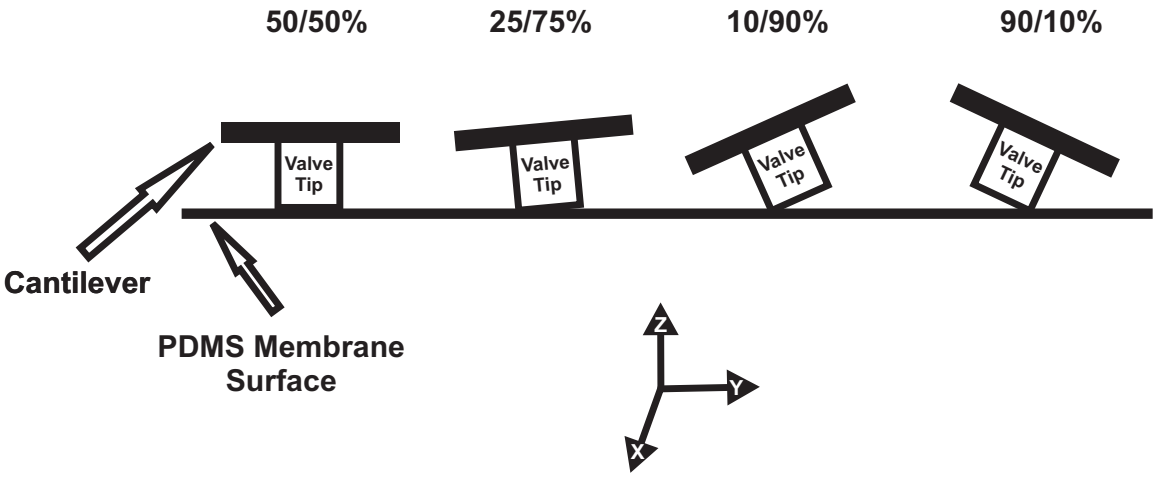

Figure VIII-1: Illustration of microvalve "tilt." A microvalves tilt is shown to sequentially increase in order, when proceeding as; 50/50% - 25/75% - 10/90%. Providing tilt to a microvalve was made possible with use of in-house fabricated micropositioners. A tilted microvalve created a "plowing" or "squeegee" effect, when actuated in the Z-direction, for closure of the microchannel below the microvalve.

The degree of induced microvalve tilt was quantitated with use of a microscope, and dry microchannel. The microvalve was observed, as it was slowly actuated from a fully closed to a fully open state. The release dynamics of the membrane from the base of the microchannel was quantifiable, with the quantity being recorded as an eyeball estimate, and further believed to be accurate to within 5%. A tilt assessment of 50/50% signified that the release of the PDMS membrane from the base of the microchannel was such that, the last point of release of the membrane was 50% of the length taken across the microvalve length direction (along Y-axis). A tilt of 25/75% however, would indicate the last point of membrane release from the base of the microchannel, was 25% of the distance taken across the microvalves length (Y-axis) when referenced with respect to the left-most edge of the microvalve, and 75% of the distance taken across the microvalve length (Y-axis) when referenced with respect to the right-most edge of the microvalve. Both uniform and mixed degrees of microvalve tilt were characterized for the current Chapter, where these variables along with others can be observed within Table VIII-1. Additionally, an in-depth discussion and analysis of the microvalve tilt process is provided within Chapter VI, with "tilted" microvalves being coined as, "squeegee microvalves."

4) Flow Rate Characterization

Flow rates were recorded by tracking a small bubble (2-3 mm) along an external piece of capillary tubing (Polymicro, 360/150 μm, OD/ID, ~1 m in length), secured in place along a meter stick. The external piece of capillary tubing was filled with blue food dye prior to mating with the outlet line of the micropump, so as to allow for easier

tracking of the bubble. The small bubble was tracked along the ticks/gradations of the meter stick, where the time interval between measurements was recorded. This data was then used with the formula Q = Av to calculate flow rates produced by the micropump, where Q = flow rate, A = cross-sectional surface area of the flow, and v = the linear flow velocity of the bubble. Fourteen flow rate curves (flow rate vs. frequency) were characterized for a unique combination of micropump variables, to yield maximal/minimal flow rate information. The combination of micropump variables for each flow rate curve, corresponded to a fixed and unique combination of: 1) microvalve/s tilt; 2) microvalve size; 3) number of cantilevers actuated; and 4) actuation signal/shape. Subsequent flow rate curves were thereafter obtained, with each curve characterized for a different unique combination of micropump variables. The fourteen individual flow rate curves are not presented within the current Chapter. A summary of the combination of micropump variables examined within the current Chapter is presented within Table VIII-1, with the significance of this table, and a deeper examination of the tables meaning, provided below.

5) Backpressure Characterization

The maximum attainable backpressure for the micropump was recorded with the aid of an electronic pressure sensor (Honeywell, 40PC015G2A). The micropump outlet capillary tube line was connected to the pressure sensor, where the pressure sensors electronic output was converted to a pressure reading using the manufacturers conversion factor of 266.6 mV/psi. The backpressure reading for the micropump increased over time, until finally reaching a steady value, whereby this steady pressure reading was

recorded as the micropumps maximum attainable backpressure. Fourteen maximum attainable backpressures were characterized for the micropump, with each value characterized for a fixed, yet unique combination of micropump variables (collectively defined within this Chapter as a micropump "state") corresponding to: 1) microvalve/s tilt; 2) microvalve size; 3) number of cantilevers actuated; and 4) actuation signal/shape/frequency. A summary of all characterized unique combinations of micropump variables is presented within Table VIII-1, with the significance of this table, and a deeper examination of the tables meaning, provided below. It should further be noted that the pressure values of the current Chapter correspond to gage pressure readings.

6) Formation of Micropump P-Q (H-Q) Plot

Prior to discussing the creation of the P-Q plot of Figure VIII-3, it is instructive to note, the designation "P" and "Q" goes as, P = backpressure (Pa – gage), and Q = flow rate (nL/min), where "H" can be substituted for "P" to represent a head of liquid, using the conversion, [Pressure (kPa) = (h x SG) / 0.102], where h = head of liquid (m), with SG representing the specific gravity of the liquid.

The plot as depicted within Figure VIII-3 was created by plotting fourteen data points, using the experimental methodology as presented within Figure VIII-2. To properly discuss the data/curve as shown within Figure VIII-3, a micropump "state" must first be defined. A micropump "state," corresponds to a fixed and unique combination of micropump variables for: 1) microvalve/s tilt; 2) microvalve size; 3) number of cantilevers actuated; and 4) actuation signal/shape/frequency. Each of the fourteen data

points shown within Figure VIII-3, was plotted for a fixed, and unique micropump "state." The experimental methodology shown within Figure VIII-2 depicts a micropump state as S1, S2,….up to the fourteenth micropump state, S14. The data collection process of Figure VIII-2 was employed, with the collected data plotted as shown within Figure VIII-3. The methodology of Figure VIII-2 is most clearly articulated by providing a sequential discussion for each data collection step.

The process of Figure VIII-2 began by adjusting/actuating the micropump such that it retained a unique combination of: 1) microvalve/s tilt; 2) microvalve size; 3) number of cantilevers actuated; and 4) actuation signal/shape. A flow rate curve for this unique combination of micropump variables was then collected for selected frequency intervals, as previously discussed within the Flow Rate Characterization section above. Based upon the flow rate curve, an actuation frequency was chosen, whereby this actuation frequency when combined with the unique combination of micropump variables (i.e. 1) microvalve/s tilt; 2) microvalve size; 3) number of cantilevers actuated; and 4) actuation signal/shape), defined a complete micropump "state." Fourteen micropump states were characterized within the current Chapter. Therefore, the methodology as depicted within Figure VIII-2 effectively follows the process of: 1) choosing a micropump state, 2) collecting a flow rate reading for this chosen micropump state, and 3) characterizing the maximum attainable backpressure (gage) for this micropump state. Steps 1) – 3) are shown for Figures VIII-2A) and VIII-2B). The two experimentally characterized variables of Figures VIII-2A) and VIII-2B), were then plotted as a first data point within Figure VIII-3, corresponding to

data for the micropump placed into state S1. The micropump was then placed into a different state, and further characterized for flow rate and backpressure. This process, and new state S2, is depicted within Figures VIII-2C) and VIII-2D). The experimental data for Figures VIII-2C) and VIII-2D) was then plotted as a second data point within Figure VIII-3. The process of collecting flow rate and backpressure data continued, until a total of fourteen unique micropump "states" had been fully characterized, for both flow rate and backpressure.

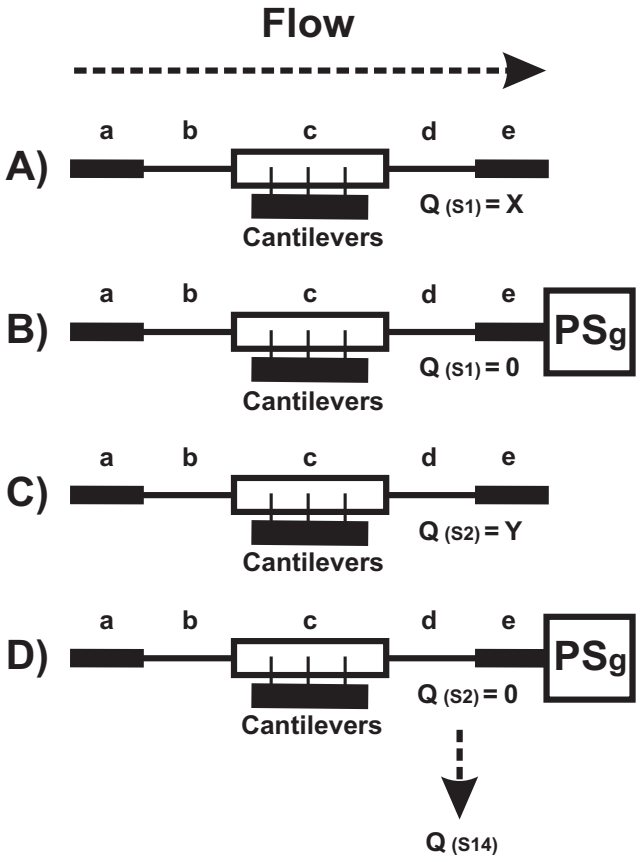

Figure VIII-2: Schematic for illustration of experimental methodology used to collect backpressure and flow rate data within the current Chapter. With the micropump placed into a "state" S1, a flow rate was recorded with the setup shown within A). The micropumps outlet line was then connected to a pressure sensor as shown within B), where a gage pressure reading was recorded. This experimental methodology was repeated, for a total of fourteen micropump "states." The data produced is illustrated within Figures VIII-3 and VIII-6, with a summary of the fourteen micropump states provided within Table VIII-1.

The linear curve shown within Figure VIII-3 shows the trend produced, for characterization of a total of fourteen unique micropump "states." The fourteen micropump states are summarized within Table VIII-1, and further correspond to the fourteen data points of column 2 within Table VIII-1. Actuation frequency is not shown within Table VIII-1, since flow rate curves are not presented within the current Chapter. The same micropump was used for collection of all fourteen data points, where the combined lengths for the flow system (section a to e) shown within Figure VIII-2 corresponds as: capillary tube extensions (a + e) = 15.6 cm, 360/150 μm OD/ID; inlet/outlet capillary tubes (b + d) = 80 cm, 105/40 μm OD/ID; PDMS microchannel (c) = 6.1 cm, rounded Gaussian/bell channel profile with channel height equal to ~100 μm.

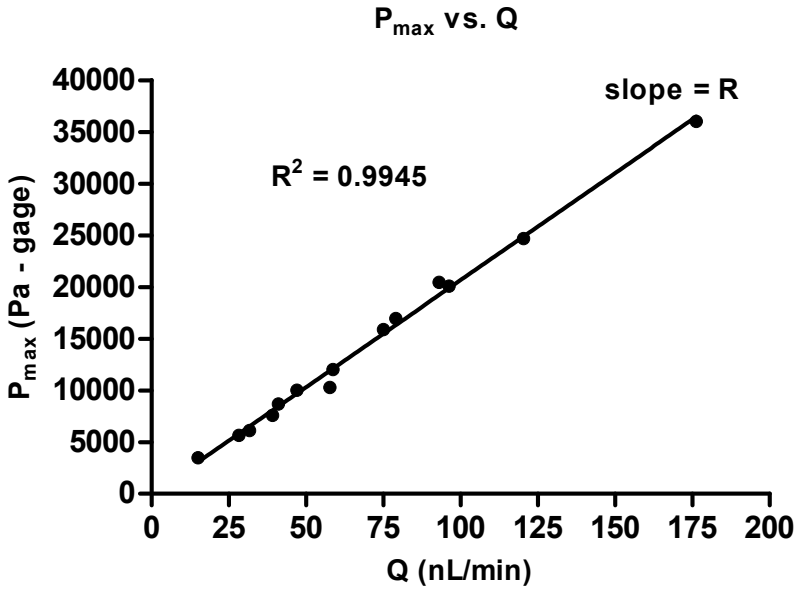

Figure VIII-3: Plot of backpressure vs. flow rate. This plot was created using the experimental methodology as shown within Figure VIII-2. The linear curve allows a scientist or engineer to determine which variables of the micropump can be tuned, to provide optimal backpressure and flow rate performance, for a particular microfluidic application. The identical plot is also shown within Figure VIII-6, where additional benefits of this linear plot can be realized.

To further distinguish between each operating state of the fourteen data points as presented within Table VIII-1, the variables were placed into five separate groups, with: groups A and B grouped for their valve tilt arrangements (i.e. column 3); group C for their unique actuation signals (i.e. column 4); group D for measuring a maximum backpressure value, that did not correspond to that particular operating states maximum achievable flow rate (i.e. column 7), as determined from the flow rate vs. frequency plot for that particular unique combination of micropump variables (i.e. 1) microvalve/s tilt; 2) microvalve size; 3) number of cantilevers actuated; and 4) actuation signal/shape), and; group E for this solo data point corresponding to the only data point with a different valve tip size (i.e. column 8). For additional clarity: column 1 is a representation of the various categorized groupings for the fourteen data points; column 2 a representation of each individual data point; column 3 an indication of the microvalve/s degree/combination of induced tilt, where group B indicates the first two microvalves proceeding in the direction of the signal bias, were tilted as 10/90%, with the most distant valve tilted as 90/10%, and for the remaining groups A, C-E of column 3, the reflected tilts indicate all three microvalves retained the same degree of tilt; column 4 the specific signal shape with corresponding signal phase; column 5 the number of cantilevers actuated in collecting backpressure and flow rate data for each individual data point; column 6 to indicate whether or not the peristaltic signal bias was opposite the squeegee bias direction, where the chop signals are not applicable since these signals actuated the cantilevers in unison as previously discussed (i.e. with zero signal phase); column 7 to indicate whether or not the maximum backpressure reading was recorded at the actuation

frequency that produced the maximum attainable flow rate value (as determined from the flow rate vs. frequency plot), where it is noted the only exception is that of group D for data points 12 and 13; column 8 to indicate the microvalve tip sizes (see Chapter IV) employed for actuation of the micropump; column 9 displaying the number of experiments performed in averaging the flow rate vs. frequency plots (not presented within the current Chapter); and, column 10 representing the number of maximum backpressure readings recorded and averaged for each data point of column 2.

1	2	3	4	5	6	7	8	9	10
Group	Data Point	Valve Tilt	Signal/Phase	# Cantilevers	Reversed Signal	Pmax Measured @ Qmax	Valve Sizes (L x W)	n for Q	n for P
A	1	50/50%	Square/120º	3	No	Yes	3 mm - 250 µm	4	3
	2	35/65%	Square/120º	3	No	Yes	3 mm - 250 µm	4	3
	3	25/75%	Square/120º	3	No	Yes	3 mm - 250 µm	4	3
	4	10/90%	Square/120º	3	No	Yes	3 mm - 250 µm	4	3
	5	10/90%	Square/120º	3	Yes	Yes	3 mm - 250 µm	3	1
B	6	2@ 10/90%, 1@90/10%	Square/120º	3	No	Yes	3 mm - 250 µm	4	1
	7	2@ 10/90%, 1@90/10%	Square/120º	3	Yes	Yes	3 mm - 250 µm	3	1
C	8	25/75%	Sine/120º	3	No	Yes	3 mm - 250 µm	4	3
	9	10/90%	Chop/0º	3	-	Yes	3 mm - 250 µm	3	1
	10	10/90%	Chop/0º	2	-	Yes	3 mm - 250 µm	3	1
	11	10/90%	Chop/0º	1	-	Yes	3 mm - 250 µm	3	1
D	12	10/90%	Chop/0º	3	-	No	3 mm - 250 µm	3	1
	13	10/90%	Square/120º	3	No	No	3 mm - 250 µm	4	1
E	14	25/75%	Square/120º	3	No	Yes	2 mm - 250 µm	3	1

Table VIII-1: Summary of micropump variables for each of the fourteen data points as plotted within Figures VIII-3 and VIII-6.

Results and Discussion

7) Micropump P-Q (H-Q) Plot

The linear curve as shown within Figure VIII-3, is the relationship produced when flow rate and backpressure data is collected, with the micropump placed into fourteen different operating states. A complete summary of the fourteen different micropump states is provided within Table VIII-1. A detailed and complete discussion, is also provided above within the Experimental Methods section, for both Table VIII-1, and for

the creation of Figure VIII-3.

The linear curve shown within Figure VIII-3 obeys the relationship, $\Delta P = QR$, with "ΔP" representing a pressure difference, "Q" representing a flow rate, and "R" equal to flow resistance. It is noted data points 5-6, 10-11 of Table VIII-1, were characterized for a reverse flow, opposite that of the expected direction (i.e. direction expected for net bias provided by summation of both the peristaltic signal bias and microvalve squeegee bias). Other than observation of a reversed flow, all other micropump operational characteristics were exactly as predicted and/or expected. It is likely reversed flows were observed due to either, the complex dynamics associated with valve closure as discussed within Chapter VI, or due to recirculatory flow patterns producing a stronger bias in the reverse flow direction, when referenced with respect to the signal wave bias direction. Microvortice flows for traveling wave micropumps,[1326] in addition to microfluidic reverse flows, opposite that of the traveling wave direction,[1324, 1325, 1327, 1328] have been discussed elsewhere. For the current Chapter however, a more detailed analysis and discussion is presented within Chapter VI, to account for these reversed flow observations.

The data points of Figure VIII-3 are expected to be slightly underestimated for the flow rate values recorded, due to recording these flow rate values with a capillary tube extension connected to the outlet line of the micropump (i.e. no capillary extension was used for backpressure characterization). It is possible to plot a correction curve, however, for a steady state flow analysis using the formula, $\Delta P = QR$, it is noted the added flow resistance contributed by the capillary tube extension, accounts for less than 1% of the

total resistance of the entire flow-through system of the current Chapter (i.e. combined length from a to e of Figure VIII-2). It is expected the time-averaged pulsatile flow rates as plotted within Figure VIII-3, would scale similarly, in making the assumption that the time-averaged pulsatile flow rates are well approximated for a steady-state, infinite-length tube Poiseuille flow rate relationship. Therefore, the plot of Figure VIII-3 is expected to be a strong/close approximation of the actual time-averaged pulsatile flow rate values expected, when characterized without a capillary tube extension.

The immediate significance of Figure VIII-3, is to illustrate how this particular micropump can best be optimized, in outputting the highest possible flow rates and backpressures. The micropump states as summarized within Table VIII-1, provide guidance in understanding how this micropump can best be optimized, for use within a particular microfluidic application. The data points within Figure VIII-3, proceed with the trend: 5 > 4 > 13 > 9 > 8 > 6 > 3 > 14 > 2 > 7 > 10 > 1 > 11 > 12, representing the data points in descending order of magnitude for both flow rate and backpressure.

The data of Figure VIII-3 can additionally be referenced, in providing a measure of the micropump power output, using the formula, [Power = (Q_{max} x P_{max}) / 2], with "Q_{max}" representing the maximum flow rate of the micropump, and "P_{max}" representing the maximum working backpressure of the micropump.[1361] Using this formula, the maximum power output recorded for this micropump equals 53 nW. The slope of the curve within Figure VIII-3, can also be used to calculate the power output of the micropump, with the slope corresponding to a resistance (R), analogous to the resistance extracted from an electrical I–V [current (I) – voltage (V)] plot, expressing the

relationship obeyed by Ohm's Law. The backpressure values plotted within Figure VIII-3 were characterized for zero flow rate through the micropump, where potentially it may not be clear as to how the micropump power output could be obtained using the backpressure values plotted within Figure VIII-3. A complete discussion however, is forthcoming within the Micropump Control Volume Analysis section that follows, that will clarify any such potential confusion.

There is further significance as to the meaning, and how Figure VIII-3 can be used to a technologist's advantage, beyond that immediately apparent, with quick observation of Figure VIII-3. A short diversion in providing a background discussion is necessary, to both realize and properly articulate, the additional lab on a chip science and engineering benefits, associated with the plot of Figure VIII-3.

8) H-Q Plot Theory and Analysis

A brief introduction to H-Q plot analysis, using centrifugal pumps within both laminar and turbulent flow regimes, is shown within Figure VIII-4, with supporting analysis provided within Figure VIII-5. The plots shown within Figure VIII-4, illustrate generalized behavior and expected changes to both system curves, and centrifugal pump curves, when changes are made to either the centrifugal pump or the system. Such plots are very commonplace, and widely utilized within industrial engineering applications, where turbopumps are employed.[1278, 1362] The "H" for "H-Q", represents a head of liquid, with "Q" representing a flow rate. Typical units for head are expressed in either feet or meters. A head of liquid is effectively an equivalent pressure taken at the base of a column of liquid, where the conversion between pressure and head using SI units is:

[Pressure (kPa) = (h x SG) / 0.102], with h = head of liquid (m), and SG representing the specific gravity of the liquid. Expressing pressure in terms of head is a matter of convention, and nearly always employed within centrifugal pump analysis. Pressures expressed in terms of head simplifies comparison between pumping systems, where a centrifugal pump will always develop the same head, in contrast to that of the pressure produced across a centrifugal pump, where the pressure will increase or decrease in direct proportion to a liquids specific gravity. That is, a head of liquid within a column can be expressed such that the head is the same for any number of different columns/solutions, where the pressure at the bottom of these columns (for the same head of liquid) can vary quite substantially, depending on the difference in specific gravities for the liquids contained within each column.

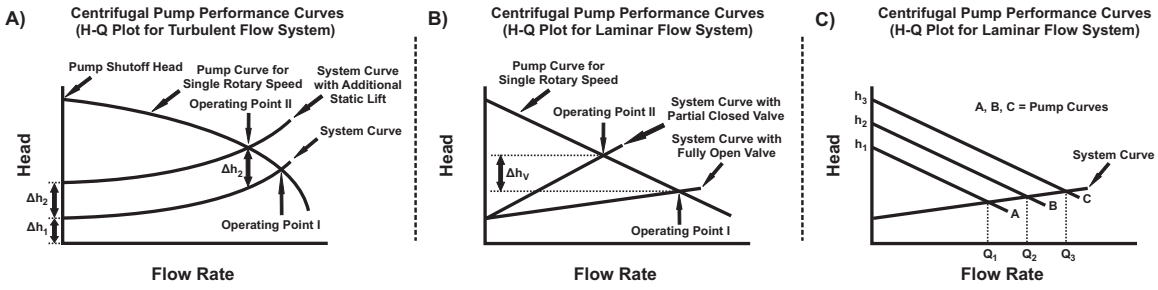

Figure VIII-4: Three generalized H-Q plots for a centrifugal pump. Illustration A) considers a turbulent flow regime, with change of the system curve reflecting an added static suction lift. Illustration B) considers a laminar flow regime, for a change in the system curve, reflecting a change in total dynamic losses throughout the piping system. Illustration C) considers a laminar flow regime, for changes brought to a centrifugal pumps performance, such as that of rotational velocity or impeller diameter. The shift in pump performance curves illustrates the effect of changing such pump variables. These generalized plots are useful as instructive guides, in understanding a pumps performance in relation to that of a system load, when placed across the pump.

Characterization of a system curve and centrifugal pump performance curve is performed separately, and therefore creation of a centrifugal pump performance curve is performed without the system demands placed across the pump. The general process used to characterize a centrifugal pump performance curve, is shown within Figure VIII-5A). The centrifugal pump inlet is placed into a reservoir, where the pump is set to operate with a fixed rotational velocity. The pressure/head differential across the centrifugal pump is characterized, for various control valve settings, with the control valve placed adjacent the outlet/discharge end of the pump. The point at which the pump continues to operate, while producing zero flow throughout the system (i.e. with the control valve fully closed), is regarded as the pump shutoff head. This point is seen as labeled within Figure VIII-4A). Operation of a centrifugal pump within a turbulent flow regime will produce a nonlinear pump curve like that shown within Figure VIII-4A), and a linear curve for laminar flows, as shown within Figures VIII-4B) and VIII-4C). Most centrifugal pumps operate within a turbulent flow regime, however linear centrifugal pump curves, do exist.[1363, 1364]

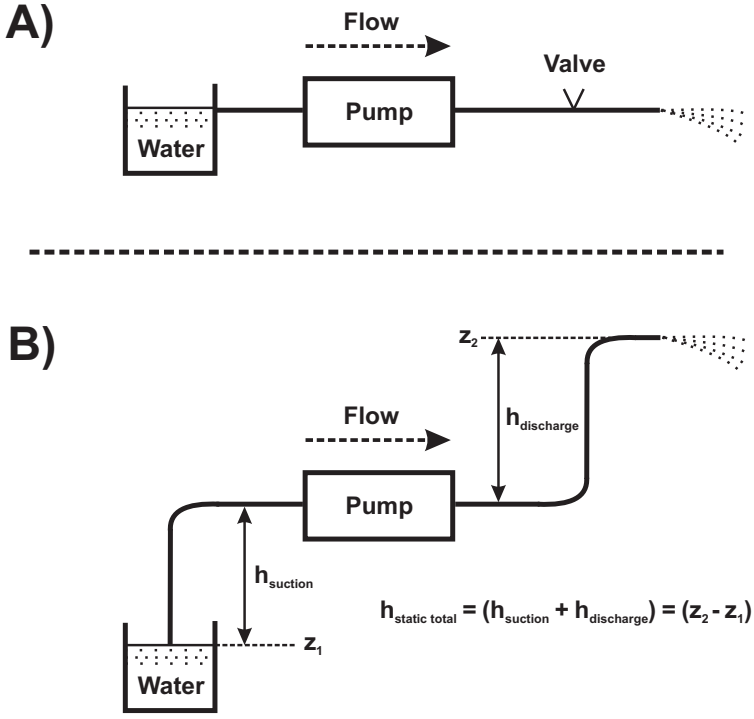

Figure VIII-5: Illustrations of static vs. dynamic losses, in support of Figure VIII-4. The control valve of illustration A), when closed, would increase the dynamic losses of a system, with the system curve shifting as shown within Figure VIII-4B). Illustration B) delineates between suction and discharge static heads, and how the two are related to total static head. A change in total static head is illustrated within Figure VIII-4A), for the added static lift scenario.

While experimentally characterized system curves have been reported,[1365] most system curves are numerically created, using both equations and tabulated data. A system curve is composed of two quantities, a static head, and a dynamic head. A static head is independent of flow, and is a representation of the difference in vertical height between the flow systems liquid surface at the source, to that of the liquids surface at the destination. The static head can further be broken down into a static discharge head and a static suction head (or static suction lift). With zero flow through the pump (i.e. no rotational velocity produced by the pump), a static suction head would be measured as the height from the liquid surface level of the source to that of the centerline

of the pump, with the static discharge head representing the vertical distance from the liquid surface level of the destination to the centerline of the pump. The sum of the static suction head and the static discharge head equals the total static head of the system. This discussion can be referenced with respect to Figure VIII-5B), where it can be seen the total static head of the system is equal to the difference in heights ($z_2 - z_1$).

Unlike that of static head, the dynamic head of a system is dependent upon flow through the system. Dynamic head losses are the numerically calculated friction losses associated with moving a liquid throughout the system. Dynamic losses are dependent upon: flow rate; the nature of the liquid; the size, condition, length, and type of pipe, and; the minor head losses that exist throughout the system, to include losses associated with any pipe fittings, tees, valves, pipe bends, and the like. For a turbulent flow regime, the frictional flow losses are proportional to the square of the flow rate, where for laminar flow regimes, the frictional losses are proportional to the first power of the flow rate. The difference in system curves for laminar vs. turbulent flow regimes can be observed when comparing Figure VIII-4A) to that of Figures VIII-4B) and VIII-4C).

The sum of all losses for a turbulent flow regime can be expressed as, [$h = (z_2 - z_1) + KQ^2$], with "h" representing the total head loss throughout the system, ($z_2 - z_1$) representing the total static head, "K" representing a constant that is dependent upon the physical characteristics of the piping system, and "Q" representing the flow rate.[1278] A laminar flow system would take the same form, however "Q^2 " would be replaced by "Q."

After obtaining an experimental pump performance curve and a numerically calculated system curve, the two curves can be superimposed onto one another, to obtain the operating point of the pump. The operating point will determine the flow rate produced throughout the system, and is further the point at which the system losses equals the increase in head across the centrifugal pump. This point is labeled as shown within Figures VIII-4A) and VIII-4B).

When the system curve or the pump performance curve is altered, a new operating point will be established. Figure VIII-4A) is indicative of a scenario, where the system takes on an additional static head, where it is shown the total static head increases from Δh_1 to, $(\Delta h_1 + \Delta h_2)$. The curves as shown represent no additional dynamic losses, and therefore are representative of the same system, with the added change being reflected as a new difference in height, $(z_2 - z_1)$, as shown within Figure VIII-5B).

Figure VIII-4B) represents a laminar system curve change, when the dynamic losses are increased. This change could manifest itself in many ways, but for the situation as shown, the increase in system losses reflects the effect produced when a system valve goes from being fully open, to partially closed, a process known as "throttling" a valve. Such a situation could result with partial closure of the valve as shown within Figure VIII-5A).

Finally, the operating point could be altered by changing an operating characteristic of the pump itself. Figure VIII-4C) represents a laminar flow regime, where it can be seen that both the operating point, as well as the pump shutoff head, are altered when the pump performance curve changes, in going from curve "A" to "B" to

"C." Changes to the impeller diameter, or an increase/decrease in the rotational velocity of the pump, are common centrifugal pump performance changes that would produce such shifts in the pump performance curve.

9) Superimposed System Curve and Micropump Performance Curve/s

The linear positive sloping solid curve of Figure VIII-6, is identical to that of Figure VIII-3. As it turns out, the solid curve of Figure VIII-6, is not only a curve that can be used to optimize micropump flow rates and backpressures, but is also an experimentally characterized system curve (i.e. for sections a to e of Figure VIII-2). The slope of the system curve represented as "R" within Figures VIII-3 and VIII-6, is a measure of the systems total resistance, at a particular flow rate through the system. As previously discussed, this resistance along with the micropump flow rate value, can be used to calculate the power output of the micropump. Additionally, the flat dotted lines of Figure VIII-6, connecting the pressure axis to the fourteen data points (details shown within Table VIII-1) of the system curve, are representations of the current peristaltic micropump performance curves. The differential pressure across the micropump was not measured experimentally, however it is known differential pressure is conserved for diaphragm pumps, and therefore does not change in response to system changes, unlike that of a centrifugal pump.[5, 6, 1362, 1366, 1367]

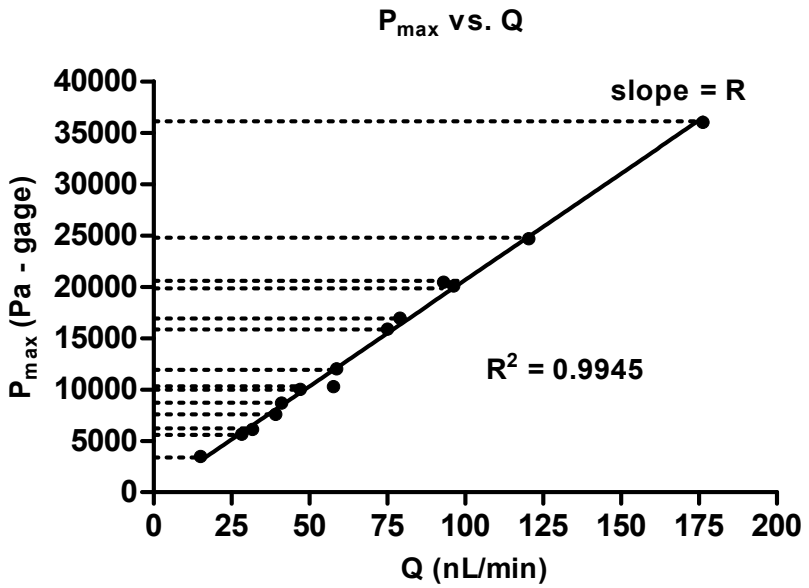

Figure VIII-6: Plot of micropump performance curves and system curve. The solid linear curve represents an experimentally measured system curve, with the horizontal dotted lines representing the micropumps experimentally characterized performance curves. The micropump performance curves are horizontal, since diaphragm pumps maintain a constant driving potential, when referenced with respect to the micropumps inlet and outlet. The point at which the pump curves cross the system curve, defines the micropumps operating point.

Experimental micropump P-Q (or H-Q) plots have been presented elsewhere to characterize a change in flow rate for a corresponding change in static head provided to the micropump inlet or outlet,[1260, 1299, 1334-1336, 1361, 1368-1370] where it is noted the micropump presented within this Chapter would respond in a similar manner. The P-Q plot of Figure VIII-6 however, not only provides a means to observe a change in micropump flow rate for a corresponding change in system losses, but also provides the additional benefit of being able to realize the analytical/numerical changes brought to the system curve, for a corresponding change in system losses. With a diaphragm micropump performing as a constant pressure source (i.e. considered for one pump performance curve), it is possible to take a ratio of the formula, $\Delta P = QR$, to predict a

systems increase in suction lift losses. The net result would produce, $(\Delta P_1 / \Delta P_2) = (Q_1 / Q_2)$, with "$Q_1$" and "$Q_2$" representing characterized micropump flow rates, with corresponding gage pressure magnitudes, "ΔP_1" and "ΔP_2." In contrast, a change in dynamic losses with consideration of a single micropump performance curve, would alter the slope of the system curve. The new slope could be determined with use of the formula, $\Delta P = QR$. Additional details pertaining to the system and experimental setup would be necessary, to determine whether the change in system losses was in the form of a static, or dynamic head change.

To provide a more rigorous discussion of the system curve and pump performance curves of Figure VIII-6, a control volume analysis using the linear momentum equation will be provided below.

10) Micropump Control Volume Analysis

For a control volume surface coincident with a system at any instant in time, the linear momentum equation states that, the time rate of change of the linear momentum of the system, is expressed as the sum of two components, to include; 1) the time rate of change of the linear momentum of the contents of the control volume, plus; 2) the net rate of flow of linear momentum through the control volume surface. For steady flows through fixed, nondeforming control volumes with uniform properties across the inlets and outlets, and additionally the velocity normal to the inlet and outlet areas, the linear momentum equation can be expressed as shown within Equation VIII-1,[1278]

$$\Sigma \mathbf{V}_{out} \rho_{out} A_{out} V_{out} - \Sigma \mathbf{V}_{in} \rho_{in} A_{in} V_{in} = \Sigma \mathbf{F}_{cv} \qquad \text{(Equation VIII-1)}$$

where $\mathbf{V}_{out}$ and $\mathbf{V}_{in}$ are the vector components of the inlet and outlet flow velocities; ρ_{out} and ρ_{in} the density of fluid at the inlet and outlet; A_{out} and A_{in} the cross-sectional areas for the flow into and out of the control volume; V_{out} and V_{in} the fluid flow speed across the inlet and outlet of the control volume; and $\mathbf{F}_{cv}$ representing the summation of forces acting on the contents of the coincident control volume. This form of the linear momentum equation, will be used for analysis of the current micropump, and associated capillary tube system (i.e. a to e of Figure VIII-2).

The current micropump control volume is depicted within Figure VIII-7, with the control volume taken as the liquid contents contained throughout the micropump from (a to e) of Figure VIII-2. This control volume does not include the surfaces containing the liquid contents of the micropump flow system, from (a to e) of Figure VIII-2. It is also noted the control volume of Figure VIII-7, does not reflect other minor losses such as those associated with entrance length effects, surface effects, and contractions/enlargements, where these effects are taken to be negligible for low Reynolds numbers.[1278, 1345, 1350] The largest Reynolds number for the current work corresponds to, Re = 0.02. As for the peristaltic wave placed across the control volume of Figure VIII-7, it is realized this is not fully consistent with the form of the linear momentum equation shown within Equation VIII-1. It is noted however that the current flow system is dominated by laminar flow through a rigid capillary tube system, as shown by [(a-b) + (d-e)] of Figure VIII-2, and further understood for the linear system curve shown within Figure VIII-6. For these reasons, the deforming PDMS membrane regions of the micropump are considered, but regarded as having a small effect upon the

control volume analysis that is forthcoming. As previously noted, the time-averaged pulsatile flow rates are approximated as a steady-state flow system, and considered within the context of an infinite-length tube Poiseuille flow rate relationship. Therefore in summary, the form of the linear momentum equation as expressed within Equation VIII-1 is considered for the above stated assumptions, and taken to be a very close approximation of the ideal form that would be representative of the micropump and capillary tube flow system, shown within Figure VIII-2 for sections (a to e).

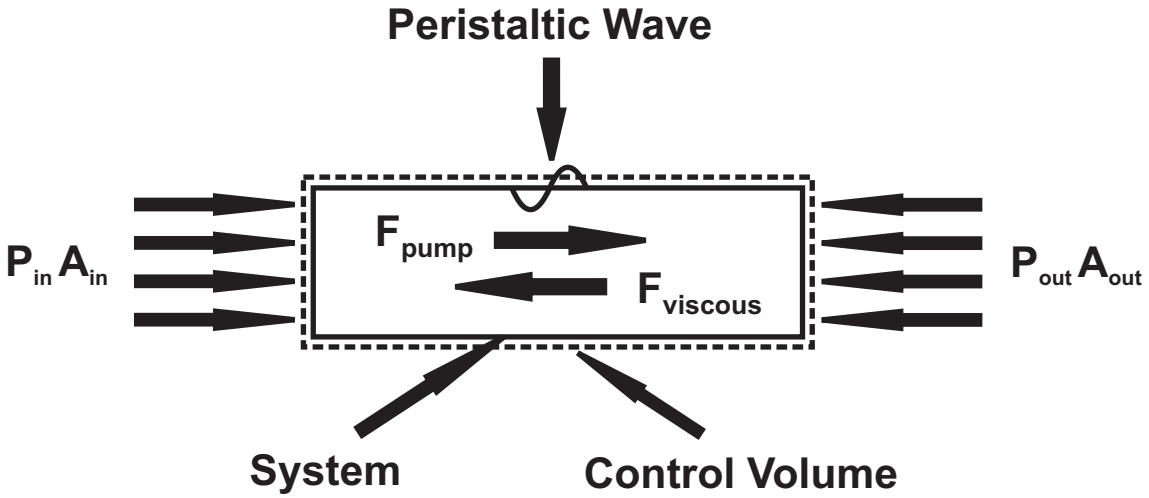

Figure VIII-7: Schematic of micropump control volume. The particular control volume as shown, is representative of the control volume taken for sections (a to e) of Figure VIII-2A). This control volume does not include the surfaces containing the liquid contents of the piping system. The same control volume was considered for all control volume analysis provided within the current Chapter, with the change in forces discussed within the context of supporting section discussions.

The control volume analysis for the linear system curve shown within Figures VIII-3 and VIII-6, begins by considering the fourteen data points experimentally characterized within these Figures. As previously noted, the fourteen data points were collected using the experimental methodology as shown within Figure VIII-2, and

characterized for the micropump variables as summarized within Table VIII-1. Considering Equation VIII-1, it is noted the control volume of Figure VIII-7 is taken for the entire system (i.e. from a to e) of Figure VIII-2A). With the velocity components of the flow equal at the inlet and outlet of the micropump, and further the inlet and outlet of the micropump equal to atmospheric pressure, Equation VIII-1 reduces to,

$$F_{MP} = F_{v1} \qquad \text{(Equation VIII-2)}$$

where "F_{v1}" represents the viscous drag force shown within Figure VIII-7, and "F_{MP}" representing the driving force of the micropump as shown within the same Figure. It is noted the driving force of the micropump is dependent upon the driving force of the peristaltic wave, which is a function of the peristaltic waves amplitude, shape, frequency, wavelength, and phase, and further, the viscous drag force is effectively a measure of all system losses, including those taken to be negligible, as previously discussed.

Figure VIII-2B), for the pressure sensor connected to the outlet line of the micropump, is considered for the same control volume of Figure VIII-7 (and Figure VIII-2A)). The control volume of Figure VIII-7, minus the viscous drag force, "F_{v1}," would represent the external forces acting upon the contents of the control volume considered for Figure VIII-2B). That is, Figure VIII-2B) is considered for a gage pressure reading, with zero flow velocity produced by the micropump. Thus, Equation VIII-1 reduces to,

$$F_{MP} = P_s A \qquad \text{(Equation VIII-3)}$$

where "P_s" represents the gage pressure reading of the pressure sensor, with "A" corresponding to the cross-sectional area of the pressure sensor transducer. It is noted the driving force of the micropump remains unchanged for both setups as shown within Figures VIII-2A) and VIII-2B), and further that the total driving force produced by the peristaltic wave of the micropump, is proportional to the gage pressure reading of the pressure sensor. Combining Equations VIII-2 and VIII-3, one attains,

$$F_{v1} = P_s A \qquad \text{(Equation VIII-4)}$$

where it is shown the gage pressure reading is proportional to the retarding viscous force produced by flow through the entire system, from (a to e) of Figure VIII-2.

The same flow rate and backpressure data collection process would be repeated for the remaining data points of Figure VIII-6, to produce the linear system curve as shown. Equation VIII-4 for each remaining data point would provide a measure of the systems total losses, as determined from the gage pressure reading of the pressure sensor. Superimposing the flat micropump performance curves onto the linear system curve as previously discussed, allows an experimentalist to evaluate a micropump and system together, as one combined entity, where optimal conditions and performance can be determined for a particular microfluidic platform. A new control volume analysis is next considered for an extended version of the methodology presented within Figure VIII-2. This analysis, along with Figure VIII-6, can be used to quantify the suction lift requirements associated with performing rodent brain direct-sampling neuroscience experiments. A very high fluidic extraction resistance likely exists for the

direct-sampling methodology, and is expected as a result of the small gap junctions between brain cells, in addition to the tortuosity that exists within an *in vivo* brain.[1245, 1246, 1255] Obtaining such a suction lift number would prove highly useful, as the Author is unaware of any such quantitative suction lift measurement associated with the direct-sampling methodology. While the following section is placed into a direct-sampling context, the analysis is applicable to any fluidic piping system where pumps exist, and therefore can be applied in a general sense to analytically understand a micropump in relation to a system, where dynamic changes are occurring over time.

11) Rodent Brain Suction Lift Quantitation using Peristaltic Micropump

After collecting the data of Figure VIII-6, an experimentalist could employ the methodology as depicted within Figures VIII-8A) to VIII-8C), to attain the suction lift requirements associated with the direct-sampling methodology. The micropump state, "S1," is reflected as remaining constant, in proceeding sequentially from the method step of Figure VIII-8A), to that of Figure VIII-8C). The flow system shown within Figure VIII-8A), is also identical to that of Figure VIII-2A), and therefore the pump performance curves and system curve of Figure VIII-6, would be the identical curves produced for the setup as illustrated within Figure VIII-8A).

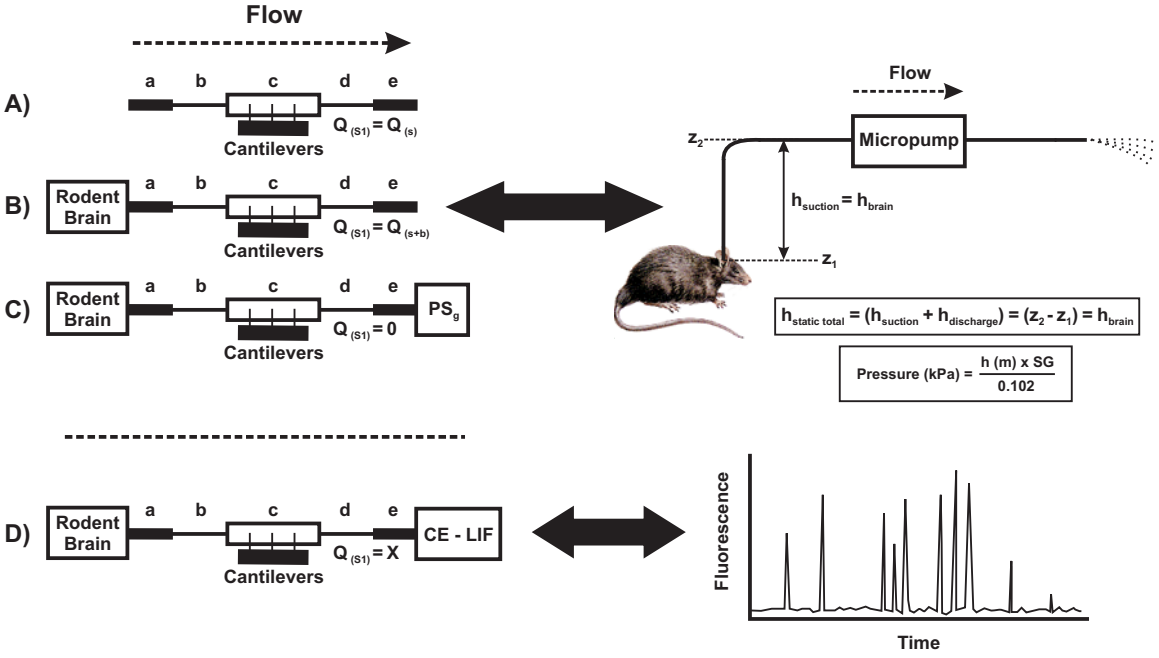

Figure VIII-8: Illustration of direct-sampling experimental methodology, with proposed capillary electrophoresis neurotransmitter analysis. Sections (a to e) are taken identical to that of the same sections depicted within Figure VIII-2. The sequential method steps from A) to C) would be employed to characterize the suction lift associated with direct-sampling neuroscience experiments. Step A) would first characterize a flow rate through the micropump, with the maximum backpressure for the micropumps operating state being obtained from Figure VIII-3 or VIII-6. Step B) illustrates the process of inserting the inlet capillary tube of the micropump into the brain of an anesthetized rodent, where a new flow rate would be measured. After measuring this new flow rate, the outlet capillary tube line of the micropump would be inserted into a pressure sensor, where a gage pressure reading would be recorded. The suction lift could then be computed directly by subtracting the gage pressure values of method steps A) and C). Conversely, it is possible to obtain the suction lift indirectly, using the methodology as shown within Figure VIII-9. Step D) represents the process of performing direct-sampling of a rodent's brain, with in-line capillary electrophoresis – laser-induced fluorescence neurotransmitter analysis.

Direct-sampling suction lift quantitation would first begin by operating the micropump with state "S1," to produce a system flow rate "$Q_{(s)}$," as shown within Figure VIII-8A). This flow rate is further illustrated within the generalized plot of Figure VIII-9, where an initial operating point, "$OP_{(s)}$," would be established. If the outlet capillary tube line of the micropump (as shown within Figure VIII-8A)) was connected to a pressure sensor, a gage pressure reading "$P_{(s)}$" would be recorded, with this value

indicated as shown within Figure VIII-9. As previously discussed, this gage pressure reading would correspond to the driving force of the peristaltic wave, as expressed within Equation VIII-3.

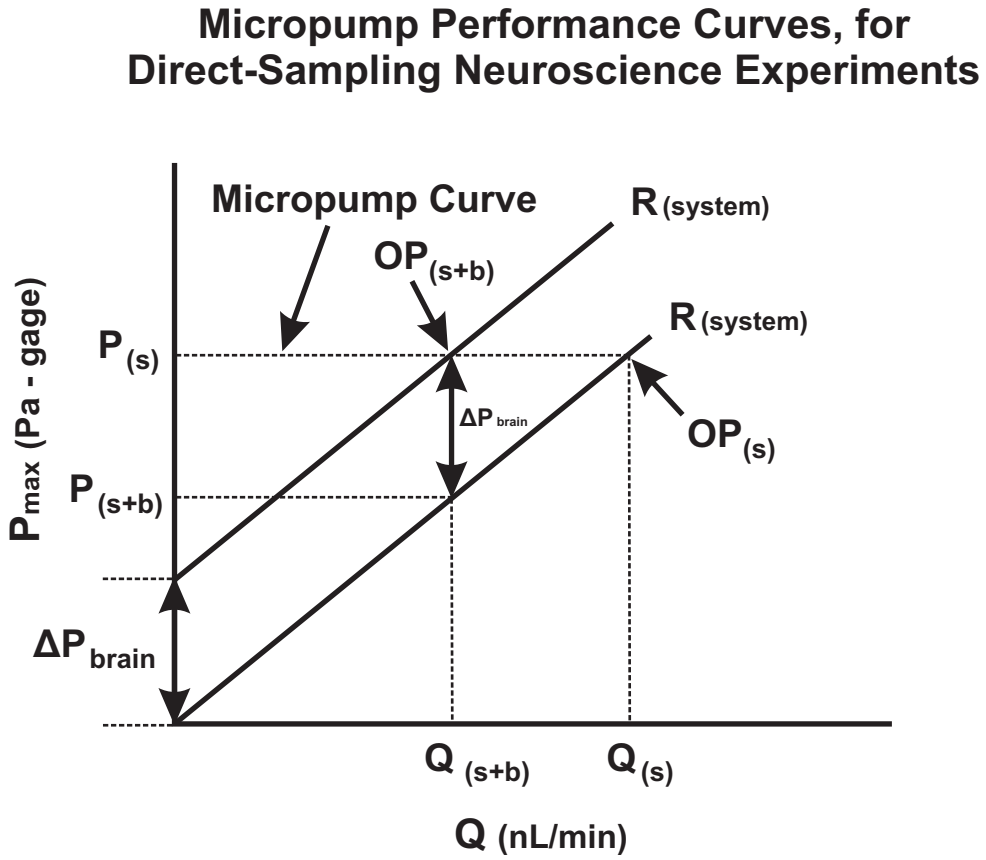

Figure VIII-9: Generalized P-Q plot utilized for micropump direct-sampling methodology. Quantification of rodent brain suction lift is determined by the magnitude of the system curve shift, with the suction lift indicated as ΔP_{brain}. Supporting analysis and discussion can be found within Figures VIII-8A) to VIII-8C).

With a rodent placed under anesthesia, the inlet capillary tube line of the micropump would next be placed into the rodent's brain, as shown within Figure VIII-8B). The added suction lift associated with direct-sampling of cerebral spinal fluid from the rodent's brain, would force the micropump to operate with a decreased flow rate

"$Q_{(s + b)}$," as shown within Figure VIII-8B). This decreased flow rate is also reflected within Figure VIII-9, where it is also shown a new operating point, "$OP_{(s + b)}$," is established. The subscript notation (s + b), is to reflect the meaning, (system + brain). This new operating point would be established in response to the additional static suction lift demands, associated with the direct-sampling methodology. Additionally shown within Figure VIII-9, the system curve slope would remain unchanged. An alternative graphical representation of the direct-sampling methodology can be seen with the connecting arrow of Figure VIII-8B). This graphic representation illustrates the suction head, "h_{brain}," is equivalent to the difference in static head represented as, $(z_2 - z_1)$, as shown within the Figure. For convenience, the formula for converting a head of liquid to a pressure is also provided within Figure VIII-8B).

To obtain a quantitative measure of the suction lift associated with direct-sampling, the methodology shown within Figure VIII-8C) would be employed, where it can be seen the outlet capillary tube line of the micropump would be connected to the pressure sensor, with the direct-sampling probe remaining untouched within the rodent's brain, as initially established within Figure VIII-8B). With the peristaltic pump performing as a diaphragm pump, the pressure differential across the pump would remain conserved for the process shown within Figure VIII-8C), and therefore remain as "$P_{(s)}$," when performing direct-sampling of the rodent's brain. The pressure sensor shown within Figure VIII-8C) however, would output a new gage pressure reading reflected as "$P_{(s + b)}$," within Figure VIII-9, with the subscript notation identical to that as previously discussed. The difference in gage pressures, "$P_{(s)}$," and "$P_{(s + b)}$," reflected as "ΔP_{brain},"

would be the change in pressure (or head) associated with the direct-sampling technique. Therefore, for a micropump performing with a constant state "S1," it is possible to obtain "ΔP_{brain}," by measuring a gage pressure reading as shown within Figure VIII-2B), and subtracting this value from the gage pressure reading obtained within Figure VIII-8C).

A control volume analysis, for the fluid contained within the system shown from (a to e) of Figure VIII-8B), would correspond to the control volume diagram of Figure VIII-7, with an added suction lift resistive force in the "$F_{viscous}$" direction. For the pressure within the rodent's brain taken as atmospheric pressure, with the inlet and outlet flow velocities equal, the momentum equation would reduce to,

$$F_{MP} = F_{v2} + F_{brain} \qquad \text{(Equation VIII-5)}$$

with "F_{MP}" representing the driving force of the micropump, "F_{v2}" representing the viscous drag force, and "F_{brain}" representing the resistive direct-sampling force, all considered for Figure VIII-7.

The control volume analysis corresponding to the system shown within Figure VIII-8C) for sections (a to e), is considered for the rodent's brain taken equal to atmospheric pressure, with zero inlet and outlet flow velocities. The momentum equation for this control volume would yield,

$$F_{MP} = P_{(s+b)}\, A + F_{brain} \qquad \text{(Equation VIII-6)}$$

with "F_{MP}" representing the driving force of the micropump, "$P_{(s+b)}$" representing the gage pressure reading of the pressure sensor, "A" corresponding to the cross-sectional

area of the pressure sensor transducer, and "F_{brain}" representing the resistive direct-sampling force, all considered for Figure VIII-7.

It is noted "F_{MP}" of Equations VIII-2-3, VIII-5-6 is identical, since the state of the micropump remains constant as, "S1," and therefore rearranging Equation VIII-6, with substitution of Equation VIII-3, yields,

$$F_{brain} = [P_{(s)} - P_{(s+b)}]\, A \qquad \text{(Equation VIII-7)}$$

Therefore the pressure values "$P_{(s)}$" and "$P_{(s\,+\,b)}$," of this control volume analysis, are shown to correspond one-for-one with the pressure values shown within Figure VIII-9. Obtaining experimental gage pressure readings, would allow an experimentalist to quantitate the suction lift resistance experienced by a peristaltic micropump, when working against the excess demands required of a direct-sampling load.

Another approach could be employed, to obtain a quantitative measure of the resistance associated with the direct-sampling methodology. This approach would associate a change in flow rates, to the expected change in gage pressure readings, before and after direct-sampling is performed. Starting from the equation, $\Delta P = QR$, one may subtract this equation from itself, with this equation considered for both, before, and after direct-sampling. The before and after data collection steps would correspond to flow rates obtained for Figures VIII-8A) and VIII-8B), respectively. The results would yield,

$$\Delta[P_{(s)} - P_{(s+b)}] = [Q_{(s)} - Q_{(s+b)}]\, R \qquad \text{(Equation VIII-8)}$$

where it is noted this case would correspond to measuring the difference in flow rates,

and therefore provide an indirect measure of the expected change in gage pressure readings.

An alternative approach of using the $\Delta P = QR$ equation, would be to divide this equation by itself, for the before and after recorded flow rates associated with the direct-sampling methodology. This approach would yield,

$$\Delta P_{(s+b)} = \Delta P_{(s)} [Q_{(s+b)} / Q_{(s)}] \qquad \text{(Equation VIII-9)}$$

After obtaining a quantitative measure of the suction lift requirements associated with the direct-sampling methodology, this information can further be used to obtain a quantitative measure of the neurotransmitter concentrations within the brain, when the micropump outlet capillary tube line is connected to a chemical analysis instrument, such as that of a capillary electrophoresis instrument, with laser-induced fluorescence (CE-LIF). This experimental setup is depicted within Figure VIII-8D), where it is easily observed how time-resolved neurochemical transmission events within the brain of a rodent, could be analyzed and quantitated over time, as shown with the generic electropherogram of Figure VIII-8D). Such CE-LIF experiments using microdialysis probes have proven effective in obtaining a better understanding of brain neurochemical dynamics within rodents.[1084, 1244]

Direct-sampling has great potential, to provide significant improvements upon many of the limitations associated with microdialysis. Direct-sampling probes can provide in excess of a 5000-fold improvement in spatial resolution, over that of microdialysis probes. This decrease in sampling/surface area of the probe, would in turn

be expected to yield less trauma to the rodent's brain, and therefore likely yield improved accuracy of neurochemical information.[1092] Lastly, it would be expected that direct-sampling would provide for a better understanding of absolute neurotransmitter concentrations within a rodent's brain, since bulk cerebral spinal fluid would be extracted from the brain for analysis, as opposed to a microdialysis probe, where sampling of the cerebral spinal fluid occurs across a diffusive region, adjacent the microdialysis membrane.[1072, 1073]

Conclusions

A peristaltic micropump was fabricated, characterized, and analyzed using control volume analysis, within the current Chapter. The micropump was fabricated in-part using injection molding technology, where a handheld PDMS injection molding apparatus was employed. The micropump was actuated using PZT cantilevers, with a precision machined microvalve attached to the tip of each cantilever. In-house fabricated micropositioners were employed to register the external microvalves over the PDMS microchannel. The micropositioners were assembled in-part with commercially available micropositioner bodies, which provided an array of microvalve adjustment capabilities. The concept of microvalve "tilt," was introduced, whereby this adjustment capability provided a means to position the microvalve/s over the PDMS microchannel, so that a "plowing" or "squeegee" effect could be employed as a part of the microvalve/s actuation mechanism. "Tilted" microvalves are coined within Chapter VI as, "squeegee microvalves."

A tilted microvalve (i.e. degree of squeegee bias), in addition to the microvalve

tip dimensions, the number of cantilevers actuated, and actuation signal/shape/frequency, was used to define a micropump, "state." Fourteen micropump states were characterized for both flow rate and backpressure. This information was plotted as a P-Q (or H-Q) plot, with "P" representing gage pressure, and "Q" representing flow rate. The use and advantages of the linear relationship produced within the P-Q plot were discussed. The P-Q plot was shown to be simple, yet potent, in serving as a 5-for-1, in terms of how the linear curve could be leveraged to a scientist or engineer's benefit. The single linear curve produced within the P-Q plot provided for: 1) a means to understand how the micropump "state" can best be optimized, to produce the most desirable flow rates and backpressures, for any particular microfluidic application, 2) an experimentally characterized system curve, 3) a set of experimentally characterized micropump performance curves, 4) a quantitative measure of the micropump power output, and 5) a means to acquire a quantitative measure of the suction lift requirements associated with direct-sampling neuroscience studies. A background discussion was provided for centrifugal pump performance curve and system curve analysis, to facilitate discussion of the current micropump performance curve and system curve analysis. The change brought to the simple piping system as presented within, was placed into a direct-sampling neuroscience context, however, this pump performance curve and system curve analysis is directly applicable to any fluidic piping system where pumps exist. Such analysis can be applied to other more complicated microfluidic formats, to better understand dynamic changes brought to a fluidic piping system.

An in-depth discussion was provided for the direct-sampling methodology, which encompassed a control volume analysis. This control volume analysis was used to articulate how the P-Q plot would be employed in practice, for obtaining a quantitative measure of the suction lift associated with micropump *in vivo* direct-sampling of a rodent's brain. The direct-sampling analysis as presented within this Chapter, is expected to yield critical information, in allowing for a better understanding of the use of direct-sampling probes within neuroscience studies. When compared to microdialysis, direct-sampling is expected to provide significant improvements in both spatial and temporal resolution, and therefore in turn, provide a better correlation of neurotransmitter release information, with *in vivo* experimental variables.

Chapter IX : *Research Significance and Future Directions*

Research Summary and Significance

A micropump was successfully designed, fabricated, and characterized for use as an analytical add-on attachment device to an already existing CE-LIF instrument. The micropump performs and passes all benchmark tests of: 1) biocompatibility, with inert activity towards CSF, 2) possessing low dead volumes, 3) implementation of interconnect technology that is fully compatible with macro-sized CE-LIF instrumentation, 4) successful implementation of a direct-sampling probe, with a spatial resolution corresponding to a 40 μm diameter circle, 5) integration of adjustment capabilities, that allows the micropump device to be adjusted in accordance with system load demands, 6) stable and reproducible output performance, and 7) nL/min flow rate performance, with high working backpressures.

The micropump was characterized for flow rates ranging from 2.6 - 289 nL/min, with working backpressures recorded as high as 51.5 kPa. The stability and reproducibility of these numbers, is understood with observation of the averaged flow rate curves, as presented within previous Chapters. It is noted, standard errors are represented as error bars for the flow rate curves, where it can be observed flow rate error is in the range of very small to not visible, at most actuation frequencies.

A control volume analysis was provided, to articulate a methodology that can be employed, to obtain a quantifiable measure of the suction lift demands associated with the direct-sampling technique. The Author is unaware of any such quantified suction lift number reported within the academic literature. Therefore, the significance of this methodology is considerable, in advancing the utility and practicality of the

direct-sampling method. An experimentally characterized suction lift value will allow proper design of in-line microfluidic pumps, when used to extract CSF directly from the brain of a living rodent, for subsequent neurochemical analysis. Successful design, characterization, and implementation of a direct-sampling microfluidic pump, will allow analytical chemists/neuroscientists to push the envelope of possibilities in asking bigger and better questions, in the continued quest to further unravel and understand the biological basis of both healthy and diseased states, within the human brain.

Future Research Experiments

The micropump as discussed within previous Chapters, was successfully designed, fabricated, and characterized. The micropump was characterized as a stand-alone analytical add-on attachment device, for future integration into an already existing and fully functional CE-LIF instrument. Currently, the micropump is immediately available, and ready for integration into the CE-LIF instrument.

1) Initial Integration of Micropump with CE-LIF Instrument

A first set of experiments is proposed, for integration of the micropump into the CE-LIF instrument. Acquisition of preliminary performance data for the fully integrated micropump-CE-LIF instrument would prove favorable, in gaining a broader understanding of the instrument as a whole. Figure IX-1 illustrates the general concept for these proposed experiments.

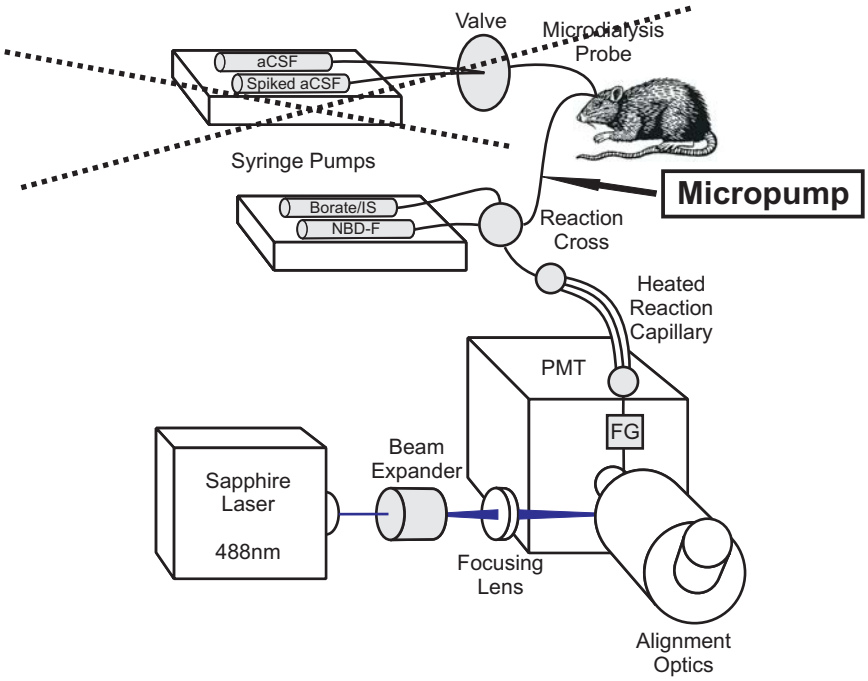

Figure IX-1: Schematic of fully integrated micropump-CE-LIF instrument. Schematic illustrates proposed first set of experiments, to fully characterize the integrated instrument as a single operational entity. Crossed-out dotted "X" would be the instrumental components removed, when the micropump is integrated into the current fully functional CE-LIF instrument. (Figure IX-1 adapted from Ciriacks Klinker and Bowser, 2007)[1371]

This Figure represents a generalized schematic, showing the functional components of the CE-LIF instrument. It is shown within this Figure, where the micropump would be inserted and integrated, for future use within direct-sampling studies. When integrated into the CE-LIF instrument, the micropump must be capable of pushing fluid from the micropump inlet capillary tube line into a reaction-cross. The reaction-cross is used to mix a fluorescent label with the CSF fluid, so that analytes of interest can be detected. It is expected the micropump will experience a backpressure, when pushing fluid into the reaction-cross. To test the ability of the micropump to overcome the expected increase in backpressure, a fluorescent solution would first be pulled from a beaker using the direct-sampling probe. For a set of calibrated micropump and CE-LIF parameters,

fluorescence and time delay from the start of pumping to the time of detection, would provide valuable flow rate information for both the micropump and CE-LIF instrument, when integrated as a single functional entity.

It is expected the micropump will need performance adjustment, so that optimal interaction with the current flow gate (the gap between the reaction and separation capillaries) design can be successfully achieved. Current flow velocities through the connecting 40 μm ID capillary tubing of the CE-LIF instrument while performing *in vivo* microdialysis, are typically 0.17-0.33 μm/min. Depending on the backpressure resistance experienced by the micropump, the flow velocity through the micropump may be smaller than desired, and therefore have the effect of increasing the time it would take for CSF to reach the separation capillary for plug injection. This increase in time could create negative consequences such as decreasing temporal resolution, and possibly causing dilution of the injected plug with flow gate buffer. To compensate for these potential negative offsets, the flow gate width (distance from reaction to separation capillary) could be decreased, with the expectation that this change in width would decrease the time needed to fill the flow gate region with CSF for plug injection. A decrease in flow gate width could also in turn allow CSF to enter the separation capillary when the flow gate is turned on. To offset this effect, the fluid velocity through the flow gate could be increased, so that contents within the reaction capillary are washed away to waste, as opposed to unnecessarily being pulled into the separation capillary.

2) Micropump Temporal Resolution Characterization

To characterize the micropump temporal resolution, the inlet capillary tube direct-sampling probe would first be inserted into a beaker of water, and therefore the rodent as shown within Figure IX-1, would be substituted for the beaker of water. With actuation of the micropump, a small amino acid liquid plug could be drawn into the micropump inlet capillary tube probe, by quickly transferring the inlet probe to a standardized amino acid solution, with rapid transfer back into the beaker of water. The plug flowing through the capillary tube interconnects would simulate an extracted plug of directly-sampled CSF. This amino acid plug would undergo derivatization within the reaction cross, and thereafter electrophoretic separation within the separation capillary column. The fluorescent signal would be detected with the photo multiplier tube (PMT), and thereafter converted into an electronic readout for quantitative peak analysis of the amino acid electropherogram. This set of experiments would allow an experimentalist to characterize the temporal resolution of the micropump direct-sampling technique.

3) In vivo Potassium Stimulation Experiments

After standardized amino acid liquid plug temporal resolution characterization of the micropump-CE-LIF instrument, a set of *in vivo* potassium stimulation experiments is proposed. These experiments would place the direct-sampling capillary tube probe directly into an *in vivo* rodent brain, in contrast to that as proposed above, with placement of the direct-sampling probe into a standardized amino acid solution contained within a beaker. These set of experiments are best understood with reference to Figure IX-1. A potassium stimulation is performed by applying a potassium solution to the surface or

interior of a rodent's brain. This external neurological stimuli is a well known excitatory neuroscience experiment, that is often used to characterize the release levels of glutamate and other neurotransmitters, in response to a potassium solution.[1088, 1372-1375] The basal concentration for glutamate has been reported to be in the range of 0.55-0.80 μM, when measured using a microdialysis probe.[1082, 1084]

Performing an *in vivo* potassium stimulation requires surgical removal of a skull section over the rat's cortex. The animal would be placed under anesthesia using Halothane, with the anesthesia delivered through a mask placed over the rodent's muzzle. A surgical platform with a built-in stereotaxic frame would be used to secure the rat's head firmly in place. To inject the high concentration potassium solution, a second micropump or external syringe pump could be used to push the potassium solution through a second capillary tube line that runs adjacent to the micropump direct-sampling probe. A flow rate of around 10 nL/min would be used to inject a bolus of 145 mM potassium chloride solution. This second capillary tube line would degrade the spatial resolution by a factor of two, however this offset is unavoidable if a high concentration potassium solution is to be injected at the sampling site. A second potassium delivery method reported within the literature uses a microdialysis probe while performing reverse dialysis.[1090] This approach however would create considerably more damage since the microdialysis probe has mm length dimensions, versus a second capillary tube line with micron-length dimensions.

Direct-sampling potassium stimulation data is expected to yield valuable information. This data can be used for comparison purposes, and compared with

microdialysis data that was collected using the same potassium stimulation experimental conditions. As opposed to a microdialysis probe that samples analyte across a diffusive gradient, a direct-sampling probe extracts bulk CSF from the rat's brain. As a result of this difference in physical sampling mechanisms, a contrast in neurotransmitter concentrations is expected.[1092] The exact magnitude of the expected difference in concentration levels would be extremely difficult to predict without undertaking a theoretical study of both direct-sampling and microdialysis probes. However, experiments injecting high potassium solutions have reported a change in glutamate release to be in the 600-700% range, when measured using a microdialysis probe.[1084] The percentage change for direct-sampling is expected to give similar to moderately different results of ±20%.

4) Histological Examinations, for Characterization of Direct-Sampling Probe Placement Accuracy and Neurological Tissue Damage

Histological examination of brain slices is proposed to characterize the extent of probe damage, and further to characterize direct-sampling probe placement accuracy. Many methods have been reported within the literature for sectioning and staining of brain slices.[1376-1378] The protocol proposed for these experiments begins by providing a lethal dose of Halothane to the rodent, and then perfusing the rodent transcardially with saline and 10% formalin solution. After fixing, the brain would be removed and sliced into 40 μm coronal sections and stained with potassium ferrocyanide. This first staining reaction would form a blue product.[1376] A second counterstaining would be performed using thionin, where this reaction would reveal the location of the lesion induced by

probe insertion into the brain. A light microscope would be used to characterize the extent of probe damage, and also the exact location of probe insertion into the brain. Brain slices would also be examined under an electron microscope, to characterize the fine microarchitectural damage induced by probe insertion. It is expected that cellular damage will be observed along the edges of the bore where the probe was inserted, but not at the tip of the probe where direct-sampling takes place.

5) Initial Barrel Cortex Direct-Sampling Experiments

After direct-sampling optimization of the micropump-CE-LIF instrument using an *in vivo* rodent brain, it is possible for an analytical chemist/neuroscientist to utilize the integrated instrument in such a way, so as to ask very specific and detailed neuroscience questions. A set of experiments designed to test the one barrel-one vibrissa hypothesis, would be an excellent choice of experiments to undertake, in utilizing the micropump-CE-LIF instrument as a means to address current and relevant *in vivo* brain science questions. As discussed within Chapter I, rodent somatosensory cortex barrels range in size from approximately 50 – 400 μm in diameter, with each barrel corresponding one-for-one to individual vibrissa on the contralateral vibrissa pad. The fact that a direct-sampling probe measures 105 / 40 μm (OD/ID), in comparison to barrels with diameters of 50 – 400 μm, would be of great significance in correlating the probes placement, to that of a barrels neurological response. The link between stimulation of a single predetermined vibrissa, and response of a discrete barrel, places the barrel cortex as an ideal candidate to study and advance humanities understanding of healthy, diseased, and injured somatosensory cortex states, using the micropump-CE-LIF instrument.

A first set of broadly-based barrel cortex experiments is proposed. For these experiments, the direct-sampling probe would be inserted into the posteriomedial barrel subfield (PMBSF) region of the barrel cortex, with the animal placed under anesthesia. Mechanical stimulations would be applied to the whiskers on the contralateral side of the whisker pad using an air-puff system.[1181, 1185] This stimulus would vigorously deflect many whiskers at once. Direct-sampling would be performed to establish a correlation between vibrissa deflection and PMBSF neurotransmitter release. It is hypothesized sub-10 second temporal resolution would be observed for the expected increase in glutamate concentration. Establishing a correlation between whisker stimulation and increased neurotransmitter release, would provide the necessary platform to undertake more challenging barrel cortex experiments, such as that of testing the one barrel-one vibrissa hypothesis.

6) One Barrel-One Vibrissa Hypothesis Direct-Sampling Experiments

Testing the one barrel-one vibrissa hypothesis using a direct-sampling probe would start by plucking all but one facial pad whisker from the rodent. After determining the surface location of the barrel that correlates to the solo remaining whisker, the probe would be inserted into layer IV for this chosen barrel. Detection of neurotransmitter release when mechanical deflections are provided to the individual whisker, would allow an experimentalist to validate proper placement of the direct-sampling probe. If a relationship was not established for whisker deflection and neurotransmitter release, the probe could be placed in nearby barrels to identify which barrel corresponds to the solo remaining whisker on the rodent's facial pad.

After establishing a one-to-one correlation between whisker deflection and neurotransmitter release within the rodent's barrel cortex, it is possible to study more complex barrel cortex variables. It is known the response of a barrel is different for a variety of stimulus parameters such as angular direction, velocity, amplitude, and frequency.[1175-1185] There have been reports of stimulating individual vibrissa using PZT cantilevers, to study these and other variables.[1175-1177] It is also possible to use an electric stepper motor to create controlled vibrissa deflections. Correlation of brain activity in the barrel cortex of rodents for experimental parameters such as vibrissa deflection frequency, amplitude, and velocity, would comprise a set of novel neuroscience data, as no such experiments have ever been undertaken using direct-sampling probe technology. Temporal resolution is expected to be sub-10 seconds for an increase in glutamate concentration.

7) Micropump and Micropump-CE-LIF Modeling / Computational Studies

Future proposed experiments beyond the set of experiments proposed above, would depend upon the results and data obtained. It is likely both the micropump and micropump-CE-LIF instrument would stand to benefit from modeling and/or computational studies. Numerical optimization of both the micropump and micropump-CE-LIF instrument as a whole, would provide for an additional means to further refine the direct-sampling methodology.

Preliminary Direct-Sampling Results

Preliminary direct-sampling data was obtained with use of a euthanized rodent. The micropump was used as a stand-alone microfluidic CSF extraction device, where the micropump inlet direct-sampling capillary tube probe was placed within the rodent's brain, and characterized for CSF extraction. The micropump was not connected with the already-existing CE-LIF instrument, in executing these preliminary pilot study direct-sampling experiments. It is also noted, these pilot study experiments were not performed using highly refined techniques, and therefore as a crude first approach, crude results were not unexpected.

Figure IX-2 is a partial summary of the direct-sampling proof-of-concept pilot experiments. After inserting the direct-sampling probe into the brain of a euthanized rodent, the micropump was actuated to output its maximum attainable flow rate, and therefore maximum operating backpressure as well. It is visualized the micropump was capable of generating enough suction lift, to core the rodent's brain. To a neuroscientist focused on elucidating the biochemical mechanisms at work within native brain tissue, Figure IX-2 would quite frankly be perceived as, frightening. To an analytical chemist/engineer focused on advancing microfluidic device instrumentation, for future application within *in vivo* brain science studies, Figure IX-2's pilot data was most certainly received with, pure joy. At the start of this research, it was not fully clear if the resistance created by the brains tortuosity, would be in excess of the micropumps performance capabilities. Had a quantitative measure of the direct-sampling suction lift requirements been reported or found within the academic literature, it would have been

possible to assess the output performance of the micropump in relation to the demands associated with the direct-sampling methodology. With the micropump capable of coring a rodent's brain, it is hypothesized the micropump will generate sufficient suction lift to extract CSF directly from the brain of an anesthetized rodent. It is expected however, that optimization of the direct-sampling methodology will be quite challenging. An extensive characterization process will likely be necessary, to understand how one can best obtain neurochemical information, with the highest possible temporal resolution.

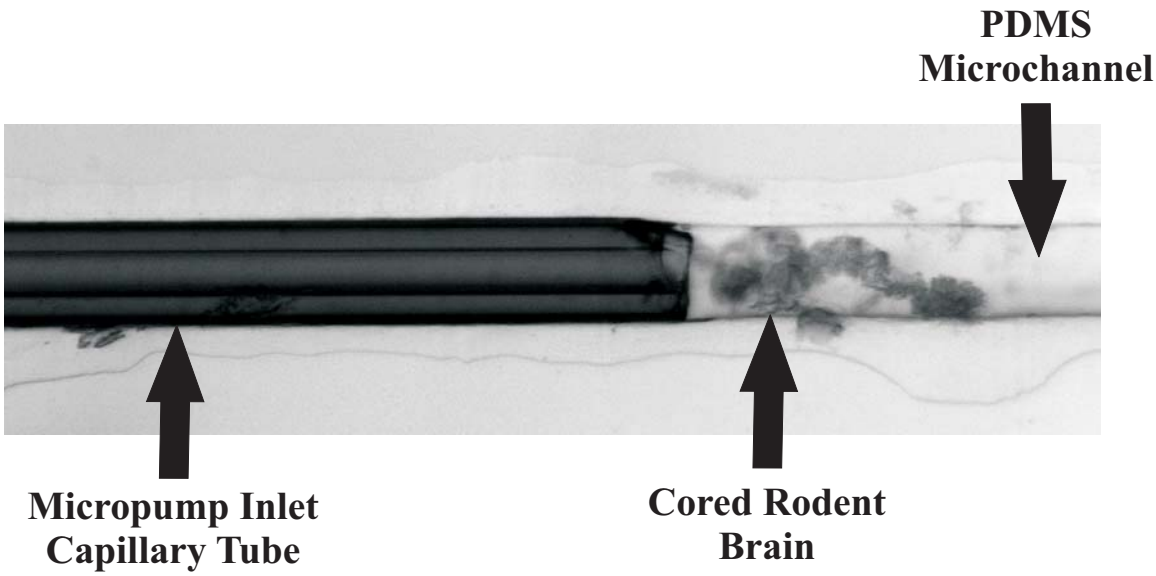

Figure IX-2: Pictorial image of cored rodent brain. Experiment was undertaken as a proof-of-concept pilot experiment, to prove viability of the direct-sampling methodology. The direct-sampling experiment was performed by placing the inlet of the micropump into the brain of a euthanized rodent. The micropump was actuated to produce its maximum possible flow rate, and therefore, maximum possible working backpressure as well.

Bibliography

1. Whitesides, G. M., The origins and the future of microfluidics. *Nature* **2006,** 442, (7101), 368-373.
2. Nguyen, N.-T.; Wereley, S. T., *Fundamentals and Applications of Microfluidics*. Artech House: 2002.
3. Saliterman, S. S., *Fundamentals of BioMEMS and Medical Microdevices*. SPIE - The International Society for Optical Engineering: 2006.
4. *Microfluidic Technologies for Miniaturized Analytical Systems*. Springer: 2007.
5. Kirby, B. J., *Micro- and Nanoscale Fluid Mechanics*. Cambridge University Press: 2010.
6. Bruus, H., *Theoretical Microfluidics*. Oxford University Press: 2008.
7. Engl, W.; Tachibana, M.; Panizza, P.; Backov, R., Millifluidic as a versatile reactor to tune size and aspect ratio of large polymerized objects. *International Journal of Multiphase Flow* **2007,** 33, (8), 897-903.
8. Tsukahara, T.; Mawatari, K.; Kitamori, T., Integrated extended-nano chemical systems on a chip. *Chemical Society Reviews* **2010,** 39, (3), 1000-1013.
9. Eijkel, J. C. T.; Berg, A. v. d., Nanofluidics: what is it and what can we expect from it? *Microfluidics and Nanofluidics* **2005,** 1, (3), 249-267.
10. Andrea, W. C., Lab-on-a-chip: Opportunities for chemical engineering. *AIChE Journal* **2002,** 48, (8), 1590-1595.
11. Erickson, D.; Li, D., Integrated microfluidic devices. *Analytica Chimica Acta* **2004,** 507, (1), 11-26.
12. Jindal, R., Hell's Bells Laboratory. *IEEE Transactions on Electron Devices* **2001,** 48, (11), 2453-2454.
13. *50 Years of Electron Devices*. The IEEE Electron Devices Society: 2002.
14. Warren, P., The future of computing: New architectures and new technologies Part 1: Biology versus silicon. *Engineering Science and Education Journal* **2002,** 11, (2), 44-48.
15. Moore's Law. http://www.intel.com/technology/mooreslaw/ (Accessed March 18, 2011).
16. Ramsey, J. M., The burgeoning power of the shrinking laboratory. *Nature Biotechnology* **1999,** 17, (11), 1061-1062.
17. Tay, F. E. H., *Microfluidics and BioMems Applications*. Kluwer Academic Publishers: 2002.
18. Thomas, L. J. Micro pump powered by piezoelectric disk benders. United States Patent US3963380, 1975.
19. Smits, J. G. Piezo-electrical micropump. European Patent EP0435653A1, 1984.
20. Voldman, J.; Gray, M. L.; Schmidt, M. A., Microfabrication in Biology and Medicine. *Annual Review of Biomedical Engineering* **1999,** 1, 401-425.
21. Madou, M. J., *Fundamentals of Microfabrication - The Science of Miniaturization*. Second ed.; CRC Press: 2002.

22. Sato, K.; Hibara, A.; Tokeshi, M.; Hisamoto, H.; Kitamori, T., Microchip-based chemical and biochemical analysis systems. *Advanced Drug Delivery Reviews* **2003,** 55, (3), 379-391.
23. Manz, A.; Graber, N.; Widmer, H. M., Miniaturized total chemical analysis systems: A novel concept for chemical sensing. *Sensors and Actuators B: Chemical* **1990,** 1, (1-6), 244-248.
24. Manz, A.; Harrison, D. J.; Verpoorte, E. M. J.; Fettinger, J. C.; Paulus, A.; Ludi, H.; Widmer, H. M., Planar chips technology for miniaturization and integration of separation techniques into monitoring systems : Capillary electrophoresis on a chip. *Journal of Chromatography A* **1992,** 593, (1-2), 253-258.
25. Hong, J. W.; Quake, S. R., Integrated nanoliter systems. *Nature Biotechnology* **2003,** 21, (10), 1179-1183.
26. Blow, N., Microfluidics: in search of a killer application. *Nature Methods* **2007,** 4, (8), 665-670.
27. Whitesides, G., Solving problems. *Lab on a Chip* **2010,** 10, (18), 2317-2318.
28. Whitesides, G. M., What Comes Next? *Lab on a Chip* **2011,** 11, (2), 191-193.
29. Clayton, J., Go with the microflow. *Nature Methods* **2005,** 2, (8), 621-627.
30. Blow, N., Microfluidics: the great divide. *Nature Methods* **2009,** 6, (9), 683-686.
31. Becker, H., Microfluidics: A Technology Coming of Age. *Medical Device Technology* **2008,** 19, 21-24.
32. Mukhopadhyay, R., Microfluidics: On the Slope of Enlightenment. *Analytical Chemistry* **2009,** 81, (11), 4169-4173.
33. Becker, H., Hype, hope and hubris: the quest for the killer application in microfluidics. *Lab on a Chip* **2009,** 9, (15), 2119-2122.
34. Janasek, D.; Franzke, J.; Manz, A., Scaling and the design of miniaturized chemical-analysis systems. *Nature* **2006,** 442, (7101), 374-380.
35. Manz, A.; Eijkel, J. C. T., Miniaturization and chip technology. What can we expect? *Pure and Applied Chemistry* **2001,** 10, (2001), 20011001.
36. Manz, A. In *Miniaturizing conventional analytical methods: electrophoresis, chemical reactors and detection*, Conference Proceedings. Second Joint EMBS-BMES Conference 2002 24th Annual International Conference of the Engineering in Medicine and Biology Society. Annual Fall Meeting of the Biomedical Engineering Society, 23-26 Oct. 2002, Houston, TX, USA, 2002; IEEE: Houston, TX, USA, 2002; pp 1638-9.
37. Nicoud, J.-D. In *Microengineering: when is small too small? Nanoengineering: when is large too large?*, MHS'95. Proceedings of the Sixth International Symposium on Micro Machine and Human Science, 4-6 Oct. 1995, Nagoya, Japan, 1995; IEEE: Nagoya, Japan, 1995; pp 1-6.
38. Madou, M. J.; Cubicciotti, R., Scaling issues in chemical and biological sensors. *Proceedings of the IEEE* **2003,** 91, (6), 830-8.
39. Wautelet, M., Scaling laws in the macro-, micro- and nanoworlds. *European Journal of Physics* **2001,** 22, (6), 601-11.
40. Dittrich, P. S.; Manz, A., Lab-on-a-chip: microfluidics in drug discovery. *Nature Reviews Drug Discovery* **2006,** 5, 210-218.

41. Jakeway, S. C.; de Mello, A. J.; Russell, E. L., Miniaturized total analysis systems for biological analysis. *Fresenius Journal of Analytical Chemistry* **2000,** 366, (6-7), 525-39.
42. Chovan, T.; Guttman, A., Microfabricated devices in biotechnology and biochemical processing. *Trends in Biotechnology* **2002,** 20, (3), 116-122.
43. Gardeniers, J. G. E.; van den Berg, A., Lab-on-a-chip systems for biomedical and environmental monitoring. *Analytical and Bioanalytical Chemistry* **2004,** 378, (7), 1700-1703.
44. Atencia, J.; Beebe, D. J., Controlled microfluidic interfaces. *Nature* **2005,** 437, (7059), 648-655.
45. Psaltis, D.; Quake, S. R.; Yang, C., Developing optofluidic technology through the fusion of microfluidics and optics. *Nature* **2006,** 442, (7101), 381-386.
46. deMello, A. J., Control and detection of chemical reactions in microfluidic systems. *Nature* **2006,** 442, (7101), 394-402.
47. El-Ali, J.; Sorger, P. K.; Jensen, K. F., Cells on chips. *Nature* **2006,** 442, (7101), 403-411.
48. Hansen, C.; Quake, S. R., Microfluidics in structural biology: smaller, faster... better. *Current Opinion in Structural Biology* **2003,** 13, (5), 538-544.
49. Sia, S. K.; Whitesides, G. M., Microfluidic devices fabricated in poly(dimethylsiloxane) for biological studies. *Electrophoresis* **2003,** 24, (21), 3563-76.
50. Weibel, D. B.; Whitesides, G. M., Applications of microfluidics in chemical biology. *Current Opinion in Chemical Biology* **2006,** 10, (6), 584-591.
51. Horsman, K. M.; Bienvenue, J. M.; Blasier, K. R.; Landers, J. P., Forensic DNA analysis on microfluidic devices: a review. *Journal of Forensic Sciences* **2007,** 52, (4), 784-799.
52. Lagally, E. T.; Mathies, R. A., Integrated genetic analysis microsystems. *Journal of Physics D: Applied Physics* **2004,** 37, (23), R245-R261.
53. Jacobson, S. C.; Hergenroeder, R.; Koutny, L. B.; Ramsey, J. M., High-speed separations on a microchip. *Analytical Chemistry* **1994,** 66, (7), 1114-1118.
54. Meldrum, D. R.; Holl, M. R., Microscale Bioanalytical Systems. *Science* **2002,** 297, (5584), 1197-1198.
55. Mitchell, P., Microfluidics - Downsizing large-scale biology. To what extent has microfluidics technology fulfilled life science researchers' expectations of creating a viable "lab-on-a-chip"? *Nature Biotechnology* **2001,** 19, (8), 717-721.
56. Daw, R.; Finkelstein, J., Lab on a chip. *Nature* **2006,** 442, (7101), 367-367.
57. Ramsey, J. M.; Jacobson, S. C.; Knapp, M. R., Microfabricated chemical measurement systems. *Nature Medicine* **1995,** 1, (10), 1093-1095.
58. Dittrich, P. S.; Manz, A., Single-molecule fluorescence detection in microfluidic channels—the Holy Grail in μTAS? *Analytical and Bioanalytical Chemistry* **2005,** 382, (8), 1771-1782.
59. Sjoelander, S.; Urbaniczky, C., Integrated fluid handling system for biomolecular interaction analysis. *Analytical Chemistry* **1991,** 63, (20), 2338-2345.

60. Paegel, B. M.; Blazej, R. G.; Mathies, R. A., Microfluidic devices for DNA sequencing: sample preparation and electrophoretic analysis. *Current Opinion in Biotechnology* **2003,** 14, (1), 42-50.
61. Hofmann, O.; Voirin, G.; Niedermann, P.; Manz, A., Three-Dimensional Microfluidic Confinement for Efficient Sample Delivery to Biosensor Surfaces. Application to Immunoassays on Planar Optical Waveguides. *Analytical Chemistry* **2002,** 74, (20), 5243-5250.
62. Arora, A.; Simone, G.; Salieb-Beugelaar, G. B.; Kim, J. T.; Manz, A., Latest Developments in Micro Total Analysis Systems. *Analytical Chemistry* **2010,** 82, (12), 4830-4847.
63. West, J.; Becker, M.; Tombrink, S.; Manz, A., Micro Total Analysis Systems: Latest Achievements. *Analytical Chemistry* **2008,** 80, (12), 4403-4419.
64. Dittrich, P. S.; Tachikawa, K.; Manz, A., Micro Total Analysis Systems. Latest Advancements and Trends. *Analytical Chemistry* **2006,** 78, (12), 3887-3908.
65. Vilkner, T.; Janazek, D.; Manz, A., Micro total analysis systems. Recent developments. *Analytical Chemistry* **2004,** 76, (12), 3373-3386.
66. Reyes, D. R.; Iossifidis, D.; Auroux, P.-A.; Manz, A., Micro total analysis systems. 1. Introduction, theory, and technology. *Analytical Chemistry* **2002,** 74, (12), 2623-2636.
67. Auroux, P.-A.; Iossifidis, D.; Reyes, D. R.; Manz, A., Micro total analysis systems. 2. Analytical standard operations and applications. *Analytical Chemistry* **2002,** 74, (12), 2637-2652.
68. Kamholz, A. E., Proliferation of microfluidics in literature and intellectual property. *Lab on a Chip* **2004,** 4, (2), 16N-20N.
69. Abgrall, P.; Gue, A.-M., Lab-on-chip technologies: making a microfluidic network and coupling it into a complete microsystem - a review. *Journal of Micromechanics and Microengineering* **2007,** 17, (5), R15 - R49.
70. Mark, D.; Haeberle, S.; Roth, G.; Stetten, F. v.; Zengerle, R., Microfluidic lab-on-a-chip platforms: requirements, characteristics and applications. *Chemical Society Reviews* **2010,** 39, (3), 1153-1182.
71. Van Den Berg, A.; Bergveld, P., Labs-on-a-Chip: origin, highlights and future perspectives - On the occasion of the 10th micro-TAS conference. *Lab on a Chip* **2006,** 6, (10), 1266-1273.
72. Zhao-Lun, F., Microfluidics in China. *Analytical & Bioanalytical Chemistry* **2005,** 381, (4), 807-808.
73. Minhas, H., Ten Years Strong. *Lab on a Chip* **2011,** 11, (1), 11-12.
74. Chang, H.-C., Editorial: A brief welcome to this new electronic journal on microfluidic applications to biology and medicine. *Biomicrofluidics* **2007,** 1, (1), 010901-1.
75. Li, D., The small flow becomes main stream. *Microfluidics and Nanofluidics* **2004,** 1, (1), 1-1.
76. Hubris. http://en.wikipedia.org/wiki/Hubris (Accessed March 22, 2011).
77. Zhang, Y.; Ozdemir, P., Microfluidic DNA amplification--A review. *Analytica Chimica Acta* **2009,** 638, (2), 115-125.

78. Microfluidics Technology. http://www.bccresearch.com/report/SMC036C.html (Accessed April 22, 2011).
79. Berg, A. v. d., Playing with space and time (on a chip). *Lab on a Chip* **2008,** 8, (11), 1779-1780.
80. Whitesides, G. M.; Deutch, J., Let's get practical. *Nature* **2011,** 469, (7328), 21-22.
81. Whitesides, G. M., Assumptions: Taking chemistry in new directions. *Angewandte Chemie, International Edition* **2004,** 43, (28), 3632-3641.
82. Quake, S. R.; Scherer, A., From micro- to nanofabrication with soft materials. *Science* **2000,** 290, (5496), 1536-40.
83. Schechter, B., Fantastic plastic. *New Scientist* **2003,** 177, (2379), 38-41.
84. Boone, T. D.; Hooper, H. H.; Ricco, A. J.; Tan, H.; Williams, S. J.; Hugh Fan, Z., Plastic advances microfluidic devices. *Analytical Chemistry* **2002,** 74, (3), A78-A86.
85. de Mello, A., Plastic fantastic? *Lab on a Chip* **2002,** 2, 31N-36N.
86. Becker, H.; Gartner, C., Polymer microfabrication technologies for microfluidic systems. *Analytical & Bioanalytical Chemistry* **2008,** 390, 89-111.
87. Sun, Y.; Kwok, Y. C., Polymeric microfluidic system for DNA analysis. *Analytica Chimica Acta* **2006,** 556, (1), 80-96.
88. Attia, U.; Marson, S.; Alcock, J., Micro-injection moulding of polymer microfluidic devices. *Microfluidics and Nanofluidics* **2009,** 7, (1), 1-28.
89. Heckele, M.; Schomburg, W. K., Review on micro molding of thermoplastic polymers. *Journal of Micromechanics and Microengineering* **2004,** 14, (3), R1 - R14.
90. Becker, H.; Locascio, L. E., Polymer microfluidic devices. *Talanta* **2002,** 56, (2), 267-287.
91. Becker, H.; Gartner, C., Polymer microfabrication methods for microfluidic analytical applications. *Electrophoresis* **2000,** 21, (1), 12-26.
92. Liu, C., Recent Developments in Polymer MEMS. *Advanced Materials* **2007,** 19, (22), 3783-3790.
93. Pouget, E.; Tonnar, J.; Lucas, P.; Lacroix-Desmazes, P.; Ganachaud, F.; Boutevin, B., Well-Architectured Poly(dimethylsiloxane)-Containing Copolymers Obtained by Radical Chemistry. *Chemical Reviews* **2009,** 110, (3), 1233-1277.
94. Xia, Y.; Whitesides, G. M., Soft lithography. *Annual Review of Materials Science* **1998**, 153-184.
95. Chaudhury, M. K.; Whitesides, G. M., Correlation Between Surface Free Energy and Surface Constitution. *Science* **1992,** 255, (5049), 1230-1232.
96. Chaudhury, M. K.; Whitesides, G. M., Direct measurement of interfacial interactions between semispherical lenses and flat sheets of poly(dimethylsiloxane) and their chemical derivatives. *Langmuir* **1991,** 7, (5), 1013-1025.
97. Lotters, J. C.; Olthuis, W.; Veltink, P. H.; Bergveld, P., Mechanical properties of the rubber elastic polymer polydimethylsiloxane for sensor applications. *Journal of Micromechanics and Microengineering* **1997,** 7, (3), 145-147.
98. Sun, J.; Vajandar, S.; Xu, D.; Kang, Y.; Hu, G.; Li, D.; Li, D., Experimental characterization of electrical current leakage in poly(dimethylsiloxane) microfluidic devices. *Microfluidics and Nanofluidics* **2009,** 6, (5), 589-598.

99. Schneider, F.; Draheim, J.; Kamberger, R.; Wallrabe, U., Process and material properties of polydimethylsiloxane (PDMS) for Optical MEMS. *Sensors and Actuators A: Physical* **2009,** 151, (2), 95-99.
100. Mata, A.; Fleischman, A.; Roy, S., Characterization of Polydimethylsiloxane (PDMS) Properties for Biomedical Micro/Nanosystems. *Biomedical Microdevices* **2005,** 7, (4), 281-293.
101. Vlachopoulou, M. E.; Tserepi, A.; Beltsios, K.; Boulousis, G.; Gogolides, E., Nanostructuring of PDMS surfaces: Dependence on casting solvents. *Microelectronic Engineering* **2007,** 84, (5-8), 1476-1479.
102. Garra, J.; Long, T.; Currie, J.; Schneider, T.; White, R.; Paranjape, M., Dry etching of polydimethylsiloxane for microfluidic systems. *Journal of Vacuum Science & Technology A* **2002,** 20, (3), 975-982.
103. Sung Jin, H.; et al., Dry etching of polydimethylsiloxane using microwave plasma. *Journal of Micromechanics and Microengineering* **2009,** 19, (9), 095010.
104. Whitesides, G. M.; Ostuni, E.; Takayama, S.; Jiang, X.; Ingber, D. E., Soft Lithography in Biology and Biochemistry. *Annual Review of Biomedical Engineering* **2001,** 3, 335-373.
105. Jeon, N. L.; Chiu, D. T.; Wargo, C. J.; Wu, H.; Choi, I. S.; Anderson, J. R.; Whitesides, G. M., Design and fabrication of integrated passive valves and pumps for flexible polymer 3-dimensional microfluidic systems. *Biomedical Microdevices* **2002,** 4, (2), 117-21.
106. Gates, B. D.; Xu, Q.; Love, J. C.; Wolfe, D. B.; Whitesides, G. M., Unconventional nanofabrication. *Annual Review of Materials Research* **2004,** 34, 339-372.
107. McDonald, J. C.; Duffy, D. C.; Anderson, J. R.; Chiu, D. T.; Wu, H.; Schueller, O. J.; Whitesides, G. M., Fabrication of microfluidic systems in poly(dimethylsiloxane). *Electrophoresis* **2000,** 21, (1), 27-40.
108. McDonald, J. C.; Whitesides, G. M., Poly(dimethylsiloxane) as a material for fabricating microfluidic devices. *Accounts of Chemical Research* **2002,** 35, (7), 491-9.
109. Mukhopadhyay, R., When PDMS isn't the best. *Analytical Chemistry* **2007,** 79, (9), 3248-3253.
110. Piruska, A.; Nikcevic, I.; Lee, S. H.; Ahn, C.; Heineman, W. R.; Limbach, P. A.; Seliskar, C. J., The autofluorescence of plastic materials and chips measured under laser irradiation. *Lab on a Chip* **2005,** 5, (12), 1348-1354.
111. Grainger, D. W.; Castner, D. G., Nanobiomaterials and Nanoanalysis: Opportunities for Improving the Science to Benefit Biomedical Technologies. *Advanced Materials* **2008,** 20, (5), 867-877.
112. Lange, J. J.; Culbertson, C. T.; Higgins, D. A., Single Molecule Studies of Solvent-Dependent Diffusion and Entrapment in Poly(dimethylsiloxane) Thin Films. *Analytical Chemistry* **2008,** 80, (24), 9726-9734.
113. Dangla, R.; Gallaire, F.; Baroud, C. N., Microchannel deformations due to solvent-induced PDMS swelling. *Lab on a Chip* **2010,** 10, (21), 2972-2978.

114. Lee, J. N.; Park, C.; Whitesides, G. M., Solvent Compatibility of Poly(dimethylsiloxane)-Based Microfluidic Devices. *Analytical Chemistry* **2003,** 75, (23), 6544-6554.
115. Regehr, K. J.; Domenech, M.; Koepsel, J. T.; Carver, K. C.; Ellison-Zelski, S. J.; Murphy, W. L.; Schuler, L. A.; Alarid, E. T.; Beebe, D. J., Biological implications of polydimethylsiloxane-based microfluidic cell culture. *Lab on a Chip* **2009,** 9, (15), 2132-2139.
116. Mukhopadhyay, R., Hard-soft microfluidic device bypasses drawbacks of PDMS. *Analytical Chemistry* **2009,** 81, (13), 5108-5108.
117. Stefanie, D.; Anne, H.; Astrid, E.; Ezequiel, F.-L.; Rainer, K.; Stephan, B.; Stephanus, B., Softlithographic partial integration of surface-active nanoparticles in a PDMS matrix for microfluidic biodevices. *physica status solidi (a)* **2010,** 207, (4), 898-903.
118. Bai, H.-J.; Gou, H.-L.; Xu, J.-J.; Chen, H.-Y., Molding a Silver Nanoparticle Template on Polydimethylsiloxane to Efficiently Capture Mammalian Cells. *Langmuir* **2009,** 26, (4), 2924-2929.
119. Llobera, A.; Demming, S.; Joensson, H. N.; Vila-Planas, J.; Andersson-Svahn, H.; Buttgenbach, S., Monolithic PDMS passband filters for fluorescence detection. *Lab on a Chip* **2010,** 10, (15), 1987-1992.
120. Glawdel, T.; Almutairi, Z.; Wang, S.; Ren, C., Photobleaching absorbed Rhodamine B to improve temperature measurements in PDMS microchannels. *Lab on a Chip* **2009,** 9, (1), 171-174.
121. Gong, X.; Wen, W., Polydimethylsiloxane-based conducting composites and their applications in microfluidic chip fabrication. *Biomicrofluidics* **2009,** 3, (1), 012007.
122. Niu, X. Z.; Peng, S. L.; Liu, L. Y.; Wen, W. J.; Sheng, P., Characterizing and Patterning of PDMS-Based Conducting Composites. *Advanced Materials* **2007,** 19, (18), 2682-2686.
123. Hailin, C.; Tingrui, P., Photopatternable Conductive PDMS Materials for Microfabrication. *Advanced Functional Materials* **2008,** 18, (13), 1912-1921.
124. Chao-Xuan Liu and Jin-Woo, C., Patterning conductive PDMS nanocomposite in an elastomer using microcontact printing. *Journal of Micromechanics and Microengineering* **2009,** 19, (8), 085019.
125. Choi, J.-W.; Rosset, S.; Niklaus, M.; Adleman, J. R.; Shea, H.; Psaltis, D. In *Tuning parameters of metal ion implantation within a microfluidic channel*, Microfluidics, BioMEMS, and Medical Microsystems VIII, San Francisco, California, USA, 2010; SPIE: San Francisco, California, USA, 2010; pp 75930D-7.
126. Khosla, A.; KorCok, J. L.; Gray, B. L.; Leznoff, D. B.; Herchenroeder, J. W.; Miller, D.; Chen, Z. In *Fabrication and testing of integrated permanent micromagnets for microfluidic systems*, Microfluidics, BioMEMS, and Medical Microsystems VIII, San Francisco, California, USA, 2010; SPIE: San Francisco, California, USA, 2010; pp 759316-8.
127. Choi Kyung, M., Photopatternable silicon elastomers with enhanced mechanical properties for high-fidelity nanoresolution soft lithography. *Journal of Physical Chemistry. B* **2005,** 109, (46), 21525-31.

128. Mills, K. L.; Zhu, X.; Takayama, S.; Thouless, M. D., The mechanical properties of a surface-modified layer on polydimethylsiloxane. *Journal of Materials Research* **2008,** 23, (1), 37-48.
129. Schmid, H.; Michel, B., Siloxane Polymers for High-Resolution, High-Accuracy Soft Lithography. *Macromolecules* **2000,** 33, (8), 3042-3049.
130. Elhadj, S.; Rioux, R. M.; Dickey, M. D.; DeYoreo, J. J.; Whitesides, G. M., Subnanometer Replica Molding of Molecular Steps on Ionic Crystals. *Nano Letters* **2010,** 10, (10), 4140-4145.
131. Preetha, J.; et al., Photodefinable PDMS thin films for microfabrication applications. *Journal of Micromechanics and Microengineering* **2009,** 19, (4), 045024.
132. Bhagat, A. A. S.; Jothimuthu, P.; Papautsky, I., Photodefinable polydimethylsiloxane (PDMS) for rapid lab-on-a-chip prototyping. *Lab on a Chip* **2007,** 7, (9), 1192-1197.
133. Choi, K. M.; Rogers, J. A., A Photocurable Poly(dimethylsiloxane) Chemistry Designed for Soft Lithographic Molding and Printing in the Nanometer Regime. *Journal of the American Chemical Society* **2003,** 125, (14), 4060-4061.
134. Jinwen, Z.; Amanda Vera, E.; Nicolas Hans, V., Recent developments in PDMS surface modification for microfluidic devices. *Electrophoresis* **2010,** 31, (1), 2-16.
135. Priest, C., Surface patterning of bonded microfluidic channels. *Biomicrofluidics* **2010,** 4, (3), 032206-13.
136. Belder, D.; Ludwig, M., Surface modification in microchip electrophoresis. *Electrophoresis* **2003,** 24, (21), 3595-606.
137. Makamba, H.; Kim, J. H.; Lim, K.; Park, N.; Hahn, J. H., Surface modification of poly(dimethylsiloxane) microchannels. *Electrophoresis* **2003,** 24, (21), 3607-19.
138. Doherty, E. A. S.; Meagher, R. J.; Albarghouthi, M. N.; Barron, A. E., Microchannel wall coatings for protein separations by capillary and chip electrophoresis. *Electrophoresis* **2003,** 24, (1), 34-54.
139. Muck, A.; Svatos, A., Chemical modification of polymeric microchip devices. *Talanta* **2007,** 74, (3), 333-341.
140. Jikun, L.; Milton, L. L., Permanent surface modification of polymeric capillary electrophoresis microchips for protein and peptide analysis. *Electrophoresis* **2006,** 27, (18), 3533-3546.
141. Kang, G. H.; No, K. Y.; Kim, G. M., Fabrication of Microchannel with Electrodes on Side Wall. *International Journal of Modern Physics B: Condensed Matter Physics; Statistical Physics; Applied Physics* **2006,** 20, 4493-4498.
142. Gao, Y.; Chen, L., Versatile control of multiphase laminar flow for in-channel microfabrication. *Lab on a Chip* **2008,** 8, (10), 1695-1699.
143. Graudejus, O.; Gorrn, P.; Wagner, S., Controlling the Morphology of Gold Films on Poly(dimethylsiloxane). *ACS Applied Materials & Interfaces* **2010,** 2, (7), 1927-1933.
144. Chen, Z.; Zhao, Y.; Wang, W.; Li, Z., Microfluidic patterning of nanoparticle monolayers. *Microfluidics and Nanofluidics* **2009,** 7, (4), 585-591.
145. Zhang, Q. L.; Xu, J. J.; Lian, H. Z.; Li, X. Y.; Chen, H. Y., Polycation coating poly(dimethylsiloxane) capillary electrophoresis microchip for rapid separation of ascorbic acid and uric acid. *Analytical & Bioanalytical Chemistry* **2007,** 387, 2699-2704.

146. Jian-Ding, Q.; Li, W.; Ru-Ping, L.; Jing-Wu, W., Microchip CE analysis of amino acids on a titanium dioxide nanoparticles-coated PDMS microfluidic device with in-channel indirect amperometric detection. *Electrophoresis* **2009,** 30, (19), 3472-3479.
147. Han, B.; Xu, Y.; Zhang, L.; Yang, X.; Wang, E., Surface modification of poly(dimethylsiloxane) microchips using a double-chained cationic surfactant for efficiently resolving fluorescent dye adsorption. *Talanta* **2009,** 79, (3), 959-962.
148. Wang, A.-J.; Xu, J.-J.; Zhang, Q.; Chen, H.-Y., The use of poly(dimethylsiloxane) surface modification with gold nanoparticles for the microchip electrophoresis. *Talanta* **2006,** 69, (1), 210-215.
149. Orhan, J. B.; Parashar, V. K.; Flueckiger, J.; Gijs, M. A. M., Internal Modification of Poly(dimethylsiloxane) Microchannels with a Borosilicate Glass Coating. *Langmuir* **2008,** 24, (16), 9154-9161.
150. Castellana, E. T.; Kataoka, S.; Albertorio, F.; Cremer, P. S., Direct Writing of Metal Nanoparticle Films Inside Sealed Microfluidic Channels. *Analytical Chemistry* **2005,** 78, (1), 107-112.
151. Luo, Y.; Huang, B.; Wu, H.; Zare, R. N., Controlling Electroosmotic Flow in Poly(dimethylsiloxane) Separation Channels by Means of Prepolymer Additives. *Analytical Chemistry* **2006,** 78, (13), 4588-4592.
152. Gomez-Sjoberg, R.; Leyrat, A. A.; Houseman, B. T.; Shokat, K.; Quake, S. R., Biocompatibility and Reduced Drug Absorption of Sol-Gel - Treated Poly(dimethyl siloxane) for Microfluidic Cell Culture Applications. *Analytical Chemistry* **2010,** 82, (21), 8954-8960.
153. Qing, Z.; Jing-Juan, X.; Hong-Yuan, C., Patterning microbeads inside poly(dimethylsiloxane) microfluidic channels and its application for immobilized microfluidic enzyme reactors. *Electrophoresis* **2006,** 27, (24), 4943-4951.
154. Roman, G. T.; Hlaus, T.; Bass, K. J.; Seelhammer, T. G.; Culbertson, C. T., Sol-Gel Modified Poly(dimethylsiloxane) Microfluidic Devices with High Electroosmotic Mobilities and Hydrophilic Channel Wall Characteristics. *Analytical Chemistry* **2005,** 77, (5), 1414-1422.
155. Zhang, Q.; Xu, J.-J.; Liu, Y.; Chen, H.-Y., In-situ synthesis of poly(dimethylsiloxane)-gold nanoparticles composite films and its application in microfluidic systems. *Lab on a Chip* **2008,** 8, (2), 352-357.
156. Khademhosseini, A.; Suh, K. Y.; Jon, S.; Eng, G.; Yeh, J.; Chen, G.-J.; Langer, R., A Soft Lithographic Approach To Fabricate Patterned Microfluidic Channels. *Analytical Chemistry* **2004,** 76, (13), 3675-3681.
157. Campbell, K.; Levy, U.; Fainman, Y.; Groisman, A., Pressure-driven devices with lithographically fabricated composite epoxy-elastomer membranes. *Applied Physics Letters* **2006,** 89, 154105.
158. Van Der Linden, H. J.; Jellema, L. C.; Holwerda, M.; Verpoorte, E., Stabilization of two-phase octanol/water flows inside poly(dimethylsiloxane) microchannels using polymer coatings. *Analytical & Bioanalytical Chemistry* **2006,** 385, 1376-1383.
159. Liang, R.; Hu, P.; Gan, G.; Qiu, J., Deoxyribonucleic acid modified poly(dimethylsiloxane) microfluidic channels for the enhancement of microchip electrophoresis. *Talanta* **2009,** 77, (5), 1647-1653.

160. Schneider, M. H.; Tran, Y.; Tabeling, P., Benzophenone Absorption and Diffusion in Poly(dimethylsiloxane) and Its Role in Graft Photo-polymerization for Surface Modification. *Langmuir* **2011,** 27, (3), 1232-1240.
161. Ebara, M.; Hoffman, J. M.; Hoffman, A. S.; Stayton, P. S., Switchable surface traps for injectable bead-based chromatography in PDMS microfluidic channels. *Lab on a Chip* **2006,** 6, (7), 843-848.
162. Cordeiro, A. L.; Zschoche, S.; Janke, A.; Nitschke, M.; Werner, C., Functionalization of Poly(dimethylsiloxane) Surfaces with Maleic Anhydride Copolymer Films. *Langmuir* **2009,** 25, (3), 1509-1517.
163. Lahann, J.; Balcells, M.; Lu, H.; Rodon, T.; Jensen, K. F.; Langer, R., Reactive polymer coatings: A first step toward surface engineering of microfluidic devices. *Analytical Chemistry* **2003,** 75, (9), 2117-2122.
164. Hu, S.; Ren, X.; Bachman, M.; Sims, C. E.; Allbritton, N.; Li, G. P., Surface modification of poly(dimethylsiloxane) microfluidic devices by ultraviolet polymer grafting. *Analytical Chemistry* **2002,** 74, (16), 4117-4123.
165. Wu, D.; Zhao, B.; Dai, Z.; Qin, J.; Lin, B., Grafting epoxy-modified hydrophilic polymers onto poly(dimethylsiloxane) microfluidic chip to resist nonspecific protein adsorption. *Lab on a Chip* **2006,** 6, (7), 942-947.
166. Wu, D.; Qin, J.; Lin, B., Self-assembled epoxy-modified polymer coating on a poly(dimethylsiloxane) microchip for EOF inhibition and biopolymers separation. *Lab on a Chip* **2007,** 7, (11), 1490-1496.
167. Sui, G.; Wang, J.; Lee, C.-C.; Lu, W.; Lee, S. P.; Leyton, J. V.; Wu, A. M.; Tseng, H.-R., Solution-Phase Surface Modification in Intact Poly(dimethylsiloxane) Microfluidic Channels. *Analytical Chemistry* **2006,** 78, (15), 5543-5551.
168. Wang, A.-J.; Feng, J.-J.; Fan, J., Covalent modified hydrophilic polymer brushes onto poly(dimethylsiloxane) microchannel surface for electrophoresis separation of amino acids. *Journal of Chromatography A* **2008,** 1192, (1), 173-179.
169. Guo, D.-J.; Han, H.-M.; Jing, W.; Xiao, S.-J.; Dai, Z.-D., Surface-hydrophilic and protein-resistant silicone elastomers prepared by hydrosilylation of vinyl poly(ethylene glycol) on hydrosilanes-poly(dimethylsiloxane) surfaces. *Colloids and Surfaces A: Physicochemical and Engineering Aspects* **2007,** 308, (1-3), 129-135.
170. Zhou, J.; Yan, H.; Ren, K.; Dai, W.; Wu, H., Convenient Method for Modifying Poly(dimethylsiloxane) with Poly(ethylene glycol) in Microfluidics. *Analytical Chemistry* **2009,** 81, (16), 6627-6632.
171. Cortese, G.; Martina, F.; Vasapollo, G.; Cingolani, R.; Gigli, G.; Ciccarella, G., Modification of micro-channel filling flow by poly(dimethylsiloxane) surface functionalization with fluorine--Substituted aminonaphthols. *Journal of Fluorine Chemistry* **2010,** 131, (3), 357-363.
172. Yu, L.; Li, C. M.; Liu, Y.; Gao, J.; Wang, W.; Gan, Y., Flow-through functionalized PDMS microfluidic channels with dextran derivative for ELISAs. *Lab on a Chip* **2009,** 9, (9), 1243-1247.
173. Ren, K.; Zhao, Y.; Su, J.; Ryan, D.; Wu, H., Convenient Method for Modifying Poly(dimethylsiloxane) To Be Airtight and Resistive against Absorption of Small Molecules. *Analytical Chemistry* **2010,** 82, (14), 5965-5971.

174. Poll, M. L. v.; Khodabakhsh, S.; Brewer, P. J.; Shard, A. G.; Ramstedt, M.; Huck, W. T. S., Surface modification of PDMS via self-organization of vinyl-terminated small molecules. *Soft Matter* **2009,** 5, (11), 2286-2293.
175. Klasner, S. A.; Metto, E. C.; Roman, G. T.; Culbertson, C. T., Synthesis and Characterization of a Poly(dimethylsiloxane)-Poly(ethylene oxide) Block Copolymer for Fabrication of Amphiphilic Surfaces on Microfluidic Devices. *Langmuir* **2009,** 25, (17), 10390-10396.
176. Romanowsky, M. B.; Heymann, M.; Abate, A. R.; Krummel, A. T.; Fraden, S.; Weitz, D. A., Functional patterning of PDMS microfluidic devices using integrated chemo-masks. *Lab on a Chip* **2010,** 10, (12), 1521-1524.
177. Nakajima, H.; Ishino, S.; Masuda, H.; Nakagama, T.; Shimosaka, T.; Uchiyama, K., Photochemical immobilization of protein on the inner wall of a microchannel and Its application in a glucose sensor. *Analytica Chimica Acta* **2006,** 562, (1), 103-109.
178. Thierry, B.; Kurkuri, M.; Shi, J. Y.; Lwin, L. E. M. P.; Palms, D., Herceptin functionalized microfluidic polydimethylsiloxane devices for the capture of human epidermal growth factor receptor 2 positive circulating breast cancer cells. *Biomicrofluidics* **2010,** 4, (3), 032205-10.
179. Fiddes, L. K.; Chan, H. K. C.; Lau, B.; Kumacheva, E.; Wheeler, A. R., Durable, region-specific protein patterning in microfluidic channels. *Biomaterials* **2010,** 31, (2), 315-320.
180. Linder, V.; Verpoorte, E.; Thormann, W.; De Rooij, N. F.; Sigrist, H., Surface biopassivation of replicated poly(dimethylsiloxane) microfluidic channels and application to heterogeneous immunoreaction with on-chip fluorescence detection. *Analytical Chemistry* **2001,** 73, (17), 4181-4189.
181. Frimat, J.-P.; Menne, H.; Michels, A.; Kittel, S.; Kettler, R.; Borgmann, S.; Franzke, J.; West, J., Plasma stencilling methods for cell patterning. *Analytical and Bioanalytical Chemistry* **2009,** 395, (3), 601-609.
182. Thorslund, S.; Larsson, R.; Nikolajeff, F.; Bergquist, J.; Sanchez, J., Bioactivated PDMS microchannel evaluated as sensor for human CD4+ cells--The concept of a point-of-care method for HIV monitoring. *Sensors and Actuators B: Chemical* **2007,** 123, (2), 847-855.
183. Thorslund, S.; Nikolajeff, F., Instant oxidation of closed microchannels. *Journal of Micromechanics and Microengineering* **2007,** 17, (4), N16.
184. Priest, C.; Gruner, P. J.; Szili, E. J.; Al-Bataineh, S. A.; Bradley, J. W.; Ralston, J.; Steele, D. A.; Short, R. D., Microplasma patterning of bonded microchannels using high-precision "injected" electrodes. *Lab on a Chip* **2011,** 11, (3), 541-544.
185. Berdichevsky, Y.; Khandurina, J.; Guttman, A.; Lo, Y. H., UV/ozone modification of poly(dimethylsiloxane) microfluidic channels. *Sensors and Actuators B: Chemical* **2004,** 97, (2-3), 402-408.
186. Vickers, J. A.; Caulum, M. M.; Henry, C. S., Generation of Hydrophilic Poly(dimethylsiloxane) for High-Performance Microchip Electrophoresis. *Analytical Chemistry* **2006,** 78, (21), 7446-7452.

187. Claus-Peter, K.; Alena, H.; Kristina, L.; Claudia, B.; Jochen, B.; Marko, E.; Margret von, H.; Antje, Z.; Michael, T., Surface Technology with Cold Microplasmas. *Plasma Processes and Polymers* **2007,** 4, (3), 208-218.
188. Barbier, V.; Tatoulian, M.; Li, H.; Arefi-Khonsari, F.; Ajdari, A.; Tabeling, P., Stable Modification of PDMS Surface Properties by Plasma Polymerization: Application to the Formation of Double Emulsions in Microfluidic Systems. *Langmuir* **2006,** 22, (12), 5230-5232.
189. Stroock, A. D.; Whitesides, G. M., Controlling Flows in Microchannels with Patterned Surface Charge and Topography. *Accounts of Chemical Research* **2003,** 36, (8), 597-604.
190. Juchniewicz, M.; Stadnik, D.; Biesiada, K.; Olszyna, A.; Chudy, M.; Brzózka, Z.; Dybko, A., Porous crosslinked PDMS-microchannels coatings. *Sensors and Actuators B: Chemical* **2007,** 126, (1), 68-72.
191. Arroyo, M. T.; et al., Novel all-polymer microfluidic devices monolithically integrated within metallic electrodes for SDS-CGE of proteins. *Journal of Micromechanics and Microengineering* **2007,** 17, (7), 1289.
192. Xu, G.; Wang, J.; Chen, Y.; Zhang, L.; Wang, D.; Chen, G., Fabrication of poly(methyl methacrylate) capillary electrophoresis microchips by in situ surface polymerization. *Lab on a Chip* **2006,** 6, (1), 145-148.
193. Haiducu, M.; et al., Deep-UV patterning of commercial grade PMMA for low-cost, large-scale microfluidics. *Journal of Micromechanics and Microengineering* **2008,** 18, (11), 115029.
194. Lee, S. J.; et al., Polymethylhydrosiloxane (PMHS) as a functional material for microfluidic chips. *Journal of Micromechanics and Microengineering* **2008,** 18, (2), 025026.
195. Fiorini, G. S.; Yim, M.; Jeffries, G. D. M.; Schiro, P. G.; Mutch, S. A.; Lorenz, R. M.; Chiu, D. T., Fabrication improvements for thermoset polyester (TPE) microfluidic devices. *Lab on a Chip* **2007,** 7, (7), 923-926.
196. Fiorini, G. S.; Lorenz, R. M.; Kuo, J. S.; Chiu, D. T., Rapid Prototyping of Thermoset Polyester Microfluidic Devices. *Analytical Chemistry* **2004,** 76, (16), 4697-4704.
197. Vickers, J. A.; Dressen, B. M.; Weston, M. C.; Boonsong, K.; Chailapakul, O.; Cropek, D. M.; Henry, C. S., Thermoset polyester as an alternative material for microchip electrophoresis/electrochemistry. *Electrophoresis* **2007,** 28, (7), 1123-1129.
198. Bartolo, D.; Degre, G.; Nghe, P.; Studer, V., Microfluidic stickers. *Lab on a Chip* **2008,** 8, (2), 274-279.
199. Hung, L.-H.; Lin, R.; Lee, A. P., Rapid microfabrication of solvent-resistant biocompatible microfluidic devices. *Lab on a Chip* **2008,** 8, (6), 983-987.
200. Sethu, P.; Mastrangelo, C. H., Cast epoxy-based microfluidic systems and their application in biotechnology. *Sensors and Actuators B: Chemical* **2004,** 98, (2-3), 337-346.

201. Piccin, E.; Coltro, W. K. T.; Fracassi da Silva, J. A.; Neto, S. C.; Mazo, L. H.; Carrilho, E., Polyurethane from biosource as a new material for fabrication of microfluidic devices by rapid prototyping. *Journal of Chromatography A* **2007,** 1173, (1-2), 151-158.
202. Kim, S. H.; Yang, Y.; Kim, M.; Nam, S. W.; Lee, K. M.; Lee, N. Y.; Kim, Y. S.; Park, S., Simple Route to Hydrophilic Microfluidic Chip Fabrication Using an Ultraviolet (UV)-Cured Polymer. *Advanced Functional Materials* **2007,** 17, (17), 3493-3498.
203. Sato, T.; Kawai, K.; Kanai, M.; Shoji, S., Development of an All-Fluoroplastic Microfluidic Device Applied as a Nanoliter Sample Injector. *Japanese Journal of Applied Physics* **2009,** 48, 06FJ03
204. Marco, C. D.; Girardo, S.; Mele, E.; Cingolani, R.; Pisignano, D., Ultraviolet-based bonding for perfluoropolyether low aspect-ratio microchannels and hybrid devices. *Lab on a Chip* **2008,** 8, (8), 1394-1397.
205. Schulte, V. A.; Hu, Y.; Diez, M.; Bünger, D.; Möller, M.; Lensen, M. C., A hydrophobic perfluoropolyether elastomer as a patternable biomaterial for cell culture and tissue engineering. *Biomaterials* **2010,** 31, (33), 8583-8595.
206. Begolo, S.; Colas, G.; Viovy, J.-L.; Malaquin, L., New family of fluorinated polymer chips for droplet and organic solvent microfluidics. *Lab on a Chip* **2011,** 11, (3), 508-512.
207. Rolland, J. P.; Van Dam, R. M.; Schorzman, D. A.; Quake, S. R.; DeSimone, J. M., Solvent-resistant photocurable "Liquid Teflon" for micro fluidic device fabrication. *Journal of the American Chemical Society* **2004,** 126, (8), 2322-2323.
208. Wang, X.; et al., Liquid crystal polymer (LCP) for MEMS: processes and applications. *Journal of Micromechanics and Microengineering* **2003,** 13, (5), 628.
209. Kuo, J. S.; Ng, L.; Yen, G. S.; Lorenz, R. M.; Schiro, P. G.; Edgar, J. S.; Zhao, Y.; Lim, D. S. W.; Allen, P. B.; Jeffries, G. D. M.; Chiu, D. T., A new USP Class VI-compliant substrate for manufacturing disposable microfluidic devices. *Lab on a Chip* **2009,** 9, (7), 870-876.
210. Liu, J.; Sun, X.; Lee, M. L., Adsorption-Resistant Acrylic Copolymer for Prototyping of Microfluidic Devices for Proteins and Peptides. *Analytical Chemistry* **2007,** 79, (5), 1926-1931.
211. Sudarsan, A. P.; Wang, J.; Ugaz, V. M., Thermoplastic Elastomer Gels: An Advanced Substrate for Microfluidic Chemical Analysis Systems. *Analytical Chemistry* **2005,** 77, (16), 5167-5173.
212. Mehta, G.; Lee, J.; Cha, W.; Tung, Y.-C.; Linderman, J. J.; Takayama, S., Hard Top Soft Bottom Microfluidic Devices for Cell Culture and Chemical Analysis. *Analytical Chemistry* **2009,** 81, (10), 3714-3722.
213. Bilenberg, B.; Hansen, M.; Johansen, D.; Ozkapici, V.; Jeppesen, C.; Szabo, P.; Obieta, I. M.; Arroyo, O.; Tegenfeldt, J. O.; Kristensen, A., Topas-based lab-on-a-chip microsystems fabricated by thermal nanoimprint lithography. *Journal of Vacuum Science & Technology A* **2005,** 23, (6), 2944-2949.
214. Gustafsson, O.; Mogensen, K. B.; Kutter, J. P., Underivatized cyclic olefin copolymer as substrate material and stationary phase for capillary and microchip electrochromatography. *Electrophoresis* **2008,** 29, 3145-3152.

215. Pemg, B.-Y.; Wu, C.-W.; Shen, Y.-K.; Lin, Y., Microfluidic chip fabrication using hot embossing and thermal bonding of COP. *Polymers for Advanced Technologies* **2010,** 21, 457-466.
216. Delille, R.; Urdaneta, M. G.; Moseley, S. J.; Smela, E., Benchtop Polymer MEMS. *Journal of Microelectromechanical Systems* **2006,** 15, (5), 1108-1120.
217. Carrilho, E.; Martinez, A. W.; Whitesides, G. M., Understanding Wax Printing: A Simple Micropatterning Process for Paper-Based Microfluidics. *Analytical Chemistry* **2009,** 81, (16), 7091-7095.
218. Bruzewicz, D. A.; Reches, M.; Whitesides, G. M., Low-Cost Printing of Poly(dimethylsiloxane) Barriers To Define Microchannels in Paper. *Analytical Chemistry* **2008,** 80, (9), 3387-3392.
219. Martinez, A. W.; Phillips, S. T.; Wiley, B. J.; Gupta, M.; Whitesides, G. M., FLASH: A rapid method for prototyping paper-based microfluidic devices. *Lab on a Chip* **2008,** 8, (12), 2146-2150.
220. Bracher, P. J.; Gupta, M.; Whitesides, G. M., Patterning precipitates of reactions in paper. *Journal of Materials Chemistry* **2010,** 20, (24), 5117-5122.
221. Coltro, W. K. T.; de Jesus, D. P.; da Silva, J. A. F.; do Lago, C. L.; Carrilho, E., Toner and paper-based fabrication techniques for microfluidic applications. *Electrophoresis* **2010,** 31, 2487-2498.
222. Ibáñez-García, N.; Alonso, J.; Martínez-Cisneros, C. S.; Valdés, F., Green-tape ceramics. New technological approach for integrating electronics and fluidics in microsystems. *TrAC Trends in Analytical Chemistry* **2008,** 27, (1), 24-33.
223. Ibanez-Garcia, N.; Mercader, M. B.; Mendes da Rocha, Z.; Seabra, C. A.; Gongora-Rubio, M. R.; Chamarro, J. A., Continuous Flow Analytical Microsystems Based on Low-Temperature Co-Fired Ceramic Technology. Integrated Potentiometric Detection Based on Solvent Polymeric Ion-Selective Electrodes. *Analytical Chemistry* **2006,** 78, (9), 2985-2992.
224. Golonka, L. J., Technology and applications of Low Temperature Cofired Ceramic (LTCC) based sensors and microsystems *Bulletin of the Polish Academy of Sciences: Technical sciences* **2006,** 54, (2), 221-231.
225. Sikanen, T.; Aura, S.; Heikkilal, L.; Kotiaho, T.; Franssila, S.; Kostiainen, R., Hybrid Ceramic Polymers: New, Nonbiofouling, and Optically Transparent Materials for Microfluidics. *Analytical Chemistry* **2010,** 82, (9), 3874-3882.
226. Aura, S.; Sikanen, T.; Kotiaho, T.; Franssila, S., Novel hybrid material for microfluidic devices. *Sensors and Actuators B: Chemical* **2008,** 132, (2), 397-403.
227. Lorenz, H.; et al., SU-8: a low-cost negative resist for MEMS. *Journal of Micromechanics and Microengineering* **1997,** 7, (3), 121.
228. Anhoj, T., A. ; et al., The effect of soft bake temperature on the polymerization of SU-8 photoresist. *Journal of Micromechanics and Microengineering* **2006,** 16, (9), 1819.
229. Liu, C.; Liu, Y.; Sokuler, M.; Fell, D.; Keller, S.; Boisen, A.; Butt, H.-J.; Auernhammer, G. K.; Bonaccurso, E., Diffusion of water into SU-8 microcantilevers. *Physical Chemistry Chemical Physics* **2010,** 12, (35), 10577-10583.

230. Abgrall, P.; Conedera, V.; Camon, H.; Gue, A.-M.; Nguyen, N.-T., SU-8 as a structural material for labs-on-chips and microelectromechanical systems. *Electrophoresis* **2007,** 28, (24), 4539-4551.
231. Ghantasala, M. K.; et al., Patterning, electroplating and removal of SU-8 moulds by excimer laser micromachining. *Journal of Micromechanics and Microengineering* **2001,** 11, (2), 133.
232. Wong, W. H.; Pun, E. Y. B., SU8C resist for electron beam lithography. *SPIE Proceedings Series* **2001,** 4345, 873-880.
233. Kim, S.-J.; Yang, H.; Kim, K.; Lim, Y. T.; Pyo, H.-B., Study of SU-8 to make a Ni master-mold: adhesion, sidewall profile, and removal. *Electrophoresis* **2006,** 27, (16), 3284-3296.
234. Zhang, J.; et al., Polymerization optimization of SU-8 photoresist and its applications in microfluidic systems and MEMS. *Journal of Micromechanics and Microengineering* **2001,** 11, (1), 20.
235. Campo, A. d.; Greiner, C., SU-8: a photoresist for high-aspect-ratio and 3D submicron lithography. *Journal of Micromechanics and Microengineering* **2007,** 17, (6), R81.
236. Bohl, B.; et al., Multi-layer SU-8 lift-off technology for microfluidic devices. *Journal of Micromechanics and Microengineering* **2005,** 15, (6), 1125.
237. Lin, C. H.; et al., A new fabrication process for ultra-thick microfluidic microstructures utilizing SU-8 photoresist. *Journal of Micromechanics and Microengineering* **2002,** 12, (5), 590.
238. Safavieh, R.; et al., Straight SU-8 pins. *Journal of Micromechanics and Microengineering* **2010,** 20, (5), 055001.
239. Dentinger, P. M.; Clift, W. M.; Goods, S. H., Removal of SU-8 photoresist for thick film applications. *Microelectronic Engineering* **2002,** 61-62, 993-1000.
240. Zhang, J.; Chan-Park, M. B.; Conner, S. R., Effect of exposure dose on the replication fidelity and profile of very high aspect ratio microchannels in SU-8. *Lab on a Chip* **2004,** 4, (6), 646-653.
241. Hagouel, P. I.; Karafyllidis, I.; Neureuther, A. R., Dependence of developed negative resist profiles on exposure energy dose: experiment, modeling, and simulation. *Microelectronic Engineering* **1998,** 41-42, 351-4.
242. Cheng, M.; Poppe, J.; Neureuther, A., Effects of treatment parameters in electric-field-enhanced postexposure bake. *Journal of Vacuum Science & Technology B: Microelectronics and Nanometer Structures* **2003,** 21, (4), 1428-32.
243. Cheng, M.; Yuan, L.; Croffie, E.; Neureuther, A., Improving resist resolution and sensitivity via electric-field enhanced postexposure baking. *Journal of Vacuum Science and Technology B: Microelectronics and Nanometer Structures* **2002,** 20, (2), 734-740.
244. Zheng, R.; et al., Characterizing and smoothing of striated sidewall morphology on UV-exposed thick SU-8 structures for micromachining millimeter wave circuits. *Journal of Micromechanics and Microengineering* **2010,** 20, (3), 035007.
245. Wouters, K.; Puers, R., Diffusing and swelling in SU-8: insight in material properties and processing. *Journal of Micromechanics and Microengineering* **2010,** 20, (9), 095013.

246. Sikanen, T.; Tuomikoski, S.; Ketola, R. A.; Kostiainen, R.; Franssila, S.; Kotiaho, T., Characterization of SU-8 for electrokinetic microfluidic applications. *Lab on a Chip* **2005,** 5, (8), 888-896.
247. Kuo, S.-M.; Lin, C.-H., The fabrication of non-spherical microlens arrays utilizing a novel SU-8 stamping method. *Journal of Micromechanics and Microengineering* **2008,** 18, (12), 125012.
248. Shields, E. A.; Williamson, F.; Leger, J. R., Electron-beam lithography for thick refractive optical elements in SU-8. *Journal of Vacuum Science & Technology B: Microelectronics and Nanometer Structures* **2003,** 21, (4), 1453-8.
249. Ruano-López, J. M.; Aguirregabiria, M.; Tijero, M.; Arroyo, M. T.; Elizalde, J.; Berganzo, J.; Aranburu, I.; Blanco, F. J.; Mayora, K., A new SU-8 process to integrate buried waveguides and sealed microchannels for a Lab-on-a-Chip. *Sensors and Actuators B: Chemical* **2006,** 114, (1), 542-551.
250. Kowpak, T.; Watts, B. R.; Zhang, Z.; Zhu, S.; Xu, C., Fabrication of Photonic/Microfluidic Integrated Devices Using an Epoxy Photoresist. *Macromolecular Materials and Engineering* **2010,** 295, 559-565.
251. Nakajima, A.; et al., Fabrication and high-speed characterization of SU-8 shrouded two-dimensional microimpellers. *Journal of Micromechanics and Microengineering* **2007,** 17, (9), S230.
252. Zhang, Y.; Lin, C.-T.; Yang, S., Fabrication of Hierarchical Pillar Arrays from Thermoplastic and Photosensitive SU-8. *Small* **2010,** 6, 768-775.
253. Choi, J.; et al., A microfluidic platform with a free-standing perforated polymer membrane. *Journal of Micromechanics and Microengineering* **2010,** 20, (8), 085011.
254. Nichols, K. P.; Eijkel, J. C. T.; Gardeniers, H. J. G. E., Nanochannels in SU-8 with floor and ceiling metal electrodes and integrated microchannels. *Lab on a Chip* **2008,** 8, (1), 173-175.
255. Chuang, Y.-J.; Tseng, F.-G.; Cheng, J.-H.; Lin, W.-K., A novel fabrication method of embedded micro-channels by using SU-8 thick-film photoresists. *Sensors and Actuators A: Physical* **2003,** 103, (1-2), 64-69.
256. Tay, F. E. H.; et al., A novel micro-machining method for the fabrication of thick-film SU-8 embedded micro-channels. *Journal of Micromechanics and Microengineering* **2001,** 11, (1), 27.
257. Frey, O.; Talaei, S.; van der Wal, P. D.; Koudelka-Hep, M.; de Rooij, N. F., Continuous-flow multi-analyte biosensor cartridge with controllable linear response range. *Lab on a Chip* **2010,** 10, (17), 2226-2234.
258. Nordman, N.; Sikanen, T.; Moilanen, M.-E.; Aura, S.; Kotiaho, T.; Franssila, S.; Kostiainen, R., Rapid and sensitive drug metabolism studies by SU-8 microchip capillary electrophoresis-electrospray ionization mass spectrometry. *Journal of Chromatography A* **2011,** 1218, (5), 739-745.
259. Jackman, R. J.; et al., Microfluidic systems with on-line UV detection fabricated in photodefinable epoxy. *Journal of Micromechanics and Microengineering* **2001,** 11, (3), 263.

260. Carlier, J.; et al., Integrated microfluidics based on multi-layered SU-8 for mass spectrometry analysis. *Journal of Micromechanics and Microengineering* **2004,** 14, (4), 619.
261. Campbell, S. A., *The Science and Engineering of Microelectronic Fabrication*. First ed.; Oxford University Press: 1996.
262. Campbell, S. A., *The Science and Engineering of Microelectronic Fabrication*. Second ed.; Oxford: 2001.
263. *Handbook of Microlithography, Micromachining, and Microfabrication*. SPIE Press and IEE: 1997; Vol. I: Microlithography.
264. *Handbook of Microlithography, Micromachining, and Microfabrication*. SPIE Press and IEE: 1997; Vol. II: Micromachining and Microfabrication.
265. Jaeger, R. C., *Introduction to Microelectronic Fabrication*. Second ed.; Prentice Hall: 2002; Vol. V.
266. Kovacs, G. T. A., *Micromachined Transducers Sourcebook*. McGraw Hill: New York, New York, 1998.
267. Senturia, S. D., *Microsystems Design*. Kluwer Academic Publishers: 2001.
268. Geissler, M.; Xia, Y., Patterning: Principles and some new developments. *Advanced Materials* **2004,** 16, (15), 1249-1269.
269. Mata, A.; et al., Fabrication of multi-layer SU-8 microstructures. *Journal of Micromechanics and Microengineering* **2006,** 16, (2), 276.
270. Xia, Y., Soft lithography and the art of patterning - A tribute to Professor George M. Whitesides. *Advanced Materials* **2004,** 16, (15), 1245-1246.
271. Xia, Y.; Whitesides, G. M., Soft Lithography. *Angewandte Chemie, International Edition* **1998,** 37, (5), 550-575.
272. Zhang, X.; Stuart, J. N.; Sweedler, J. V., Capillary electrophoresis with wavelength-resolved laser-induced fluorescence detection. *Analytical and Bioanalytical Chemistry* **2002,** 373, (6), 332-343.
273. Qin, D.; Xia, Y.; Rogers, J. A.; Jackman, R. J.; Zhao, X.-M.; Whitesides, G. M., Microfabrication, Microstructures, and Microsystems. *Topics in Current Chemistry* **1998,** 194, 1-20.
274. Duffy, D. C.; McDonald, J. C.; Schueller, O. J. A.; Whitesides, G. M., Rapid prototyping of microfluidic systems in poly(dimethylsiloxane). *Analytical Chemistry* **1998,** 70, (23), 4974-4984.
275. Qin, D.; Xia, Y.; Whitesides, G. M., Soft lithography for micro- and nanoscale patterning. *Nature Protocols* **2010,** 5, (3), 491-502.
276. Livingstone, P., George Whitesides - A Passion for Discovery. *R&D Magazine* **2007,** 49, (11), 12-14.
277. Quinn, D. J.; Spearing, S. M.; Ashby, M. F.; Fleck, N. A., A Systematic Approach to Process Selection in MEMS. *Journal of Microelectromechanical Systems* **2006,** 15, (5), 1039-1050.
278. Anderson, J. R.; Chiu, D. T.; Jackman, R. J.; Cherniavskaya, O.; McDonald, J. C.; Wu, H.; Whitesides, S. H.; Whitesides, G. M., Fabrication of topologically complex three-dimensional microfluidic systems in PDMS by rapid prototyping. *Analytical Chemistry* **2000,** 72, (14), 3158-3164.

279. Yang, X.; Grosjean, C.; Tai, Y.-C., Design, fabrication, and testing of micromachined silicone rubber membrane valves. *Journal of Microelectromechanical Systems* **1999,** 8, (4), 393-401.
280. Hosokawa, K.; Maeda, R., A pneumatically-actuated three-way microvalve fabricated with polydimethylsiloxane using the membrane transfer technique. *Journal of Micromechanics and Microengineering* **2000,** 10, (3), 415-20.
281. Chen, H.; Acharya, D.; Gajraj, A.; Meiners, J.-C., Robust interconnects and packaging for microfluidic elastomeric chips. *Analytical Chemistry* **2003,** 75, (19), 5287-5291.
282. Lai, S.; Cao, X.; Lee, L. J., A Packaging Technique for Polymer Microfluidic Platforms. *Analytical Chemistry* **2004,** 76, (4), 1175-1183.
283. Unger, M. A.; Chou, H.-P.; Thorsen, T.; Scherer, A.; Quake, S. R., Monolithic microfabricated valves and pumps by multilayer soft lithography. *Science* **2000,** 288, (5463), 113-16.
284. Lion, N.; Rohner, T. C.; Dayon, L.; Arnaud, I. L.; Damoc, E.; Youhnovski, N.; Wu, Z.-Y.; Roussel, C.; Josserand, J.; Jensen, H.; Rossier, J. S.; Przybylski, M.; Girault, H. H., Microfluidic systems in proteomics. *Electrophoresis* **2003,** 24, (21), 3533-62.
285. Huikko, K.; Kostiainen, R.; Kotiaho, T., Introduction to micro-analytical systems: Bioanalytical and pharmaceutical applications. *European Journal of Pharmaceutical Sciences* **2003,** 20, (2), 149-171.
286. Weigl, B. H.; Bardell, R. L.; Cabrera, C. R., Lab-on-a-chip for drug development. *Advanced Drug Delivery Reviews* **2003,** 55, (3), 349-377.
287. Verpoorte, E., Microfluidic chips for clinical and forensic analysis. *Electrophoresis* **2002,** 23, (5), 677-712.
288. Grzybowski, B. A.; Haag, R.; Bowden, N.; Whitesides, G. M., Generation of micrometer-sized patterns for microanalytical applications using a laser direct-write method and microcontact printing. *Analytical Chemistry* **1998,** 70, (22), 4645-4652.
289. Tien, J.; Nelson, C. M.; Chen, C. S., Fabrication of aligned microstructures with a single elastomeric stamp. *Proceedings of the National Academy of Sciences of the United States of America* **2002,** 99, (4), 1758-1762.
290. Choonee, K.; Syms, R. R. A., Multilevel Self-Aligned Microcontact Printing System. *Langmuir* **2010,** 26, (20), 16163-16170.
291. Kim, J. Y.; Baek, J. Y.; Lee, K. A.; Lee, S. H., Automatic aligning and bonding system of PDMS layer for the fabrication of 3D microfluidic channels. *Sensors and Actuators A: Physical* **2005,** 119, (2), 593-598.
292. Pagliara, S.; et al., Registration accuracy in multilevel soft lithography. *Nanotechnology* **2007,** 18, (17), 175302.
293. Moraes, C.; et al., Solving the shrinkage-induced PDMS alignment registration issue in multilayer soft lithography. *Journal of Micromechanics and Microengineering* **2009,** 19, (6), 065015.
294. Rogers, J. A.; Paul, K. E.; Whitesides, G. M., Quantifying distortions in soft lithography. *Journal of Vacuum Science & Technology, B: Microelectronics and Nanometer Structures* **1998,** 16, (1), 88-97.

295. Zhao, Y.; Zhang, X., Determination of the deformations in polymeric nanostructures using geometric moiré techniques for biological applications. *Sensors and Actuators B: Chemical* **2006,** 117, (2), 376-383.
296. Siegel, A. C.; Tang, S. K. Y.; Nijhuis, C. A.; Hashimoto, M.; Phillips, S. T.; Dickey, M. D.; Whitesides, G. M., Cofabrication: A Strategy for Building Multicomponent Microsystems. *Accounts of Chemical Research* **2010,** 43, (4), 518-528.
297. Kwak, M. K.; Jeong, H.-E.; Kim, T.-i.; Yoon, H.; Suh, K. Y., Bio-inspired slanted polymer nanohairs for anisotropic wetting and directional dry adhesion. *Soft Matter* **2010,** 6, (9), 1849-1857.
298. Boesel, L. F.; Greiner, C.; Arzt, E.; del Campo, A., Gecko-Inspired Surfaces: A Path to Strong and Reversible Dry Adhesives. *Advanced Materials* **2010,** 22, 2125-2137.
299. Goluch, E. D.; Shaikh, K. A.; Kee, R.; Chen, J.; Engel, J.; Chang, L., Microfluidic method for in-situ deposition and precision patterning of thin-film metals on curved surfaces. *Applied Physics Letters* **2004,** 85, 3629-3631.
300. Liu, X.; Wang, Q.; Qin, J.; Lin, B., A facile "liquid-molding" method to fabricate PDMS microdevices with 3-dimensional channel topography. *Lab on a Chip* **2009,** 9, (9), 1200-1205.
301. Xia, Y.; Whitesides, G. M., Extending Microcontact Printing as a Microlithographic Technique. *Langmuir* **1997,** 13, (7), 2059-2067.
302. Xia, Y.; Kim, E.; Whitesides, G. M., Micromolding of Polymers in Capillaries: Applications in Microfabrication. *Chemistry of Materials* **1996,** 8, (7), 1558-1567.
303. Xia, Y.; Kim, E.; Zhao, X.-M.; Rogers, J. A.; Prentiss, M.; Whitesides, G. M., Complex optical surfaces formed by replica molding against elastomeric masters. *Science* **1996,** 273, (5273), 347-349.
304. Wang, T.; Li, X.; Zhang, J.; Ren, Z.; Zhang, X.; Zhang, X.; Zhu, D.; Wang, Z.; Han, F.; Wang, X.; Yang, B., Morphology-controlled two-dimensional elliptical hemisphere arrays fabricated by a colloidal crystal based micromolding method. *Journal of Materials Chemistry* **2010,** 20, (1), 152-158.
305. Focke, M.; Stumpf, F.; Faltin, B.; Reith, P.; Bamarni, D.; Wadle, S.; Muller, C.; Reinecke, H.; Schrenzel, J.; Francois, P.; Mark, D.; Roth, G.; Zengerle, R.; von Stetten, F., Microstructuring of polymer films for sensitive genotyping by real-time PCR on a centrifugal microfluidic platform. *Lab on a Chip* **2010,** 10, (19), 2519-2526.
306. Dickey, M. D.; Russell, K. J.; Lipomi, D. J.; Narayanamurti, V.; Whitesides, G. M., Transistors Formed from a Single Lithography Step Using Information Encoded in Topography. *Small* **2010,** 6, 2050-2057.
307. Zhang, J.; Yang, B., Patterning Colloidal Crystals and Nanostructure Arrays by Soft Lithography. *Advanced Functional Materials* **2010,** 20, 3411-3424.
308. Rowe, L.; Almasri, M.; Lee, K.; Fogleman, N.; Brewer, G. J.; Nam, Y.; Wheeler, B. C.; Vukasinovic, J.; Glezer, A.; Frazier, A. B., Active 3-D microscaffold system with fluid perfusion for culturing in vitro neuronal networks. *Lab on a Chip* **2007,** 7, (4), 475-482.
309. Lim, T. W.; Son, Y.; Jeong, Y. J.; Yang, D.-Y.; Kong, H.-J.; Lee, K.-S.; Kim, D.-P., Three-dimensionally crossing manifold micro-mixer for fast mixing in a short channel length. *Lab on a Chip* **2011,** 11, (1), 100-103.

310. Randall, C. L.; Kalinin, Y. V.; Jamal, M.; Manohar, T.; Gracias, D. H., Three-dimensional microwell arrays for cell culture. *Lab on a Chip* **2011,** 11, (1), 127-131.
311. Nielson, R.; Kaehr, B.; Shear, J. B., Microreplication and Design of Biological Architectures Using Dynamic-Mask Multiphoton Lithography. *Small* **2009,** 5, (1), 120-125.
312. LaFratta Christopher, N.; Li, L.; Fourkas John, T., Soft-lithographic replication of 3D microstructures with closed loops. *Proceedings of the National Academy of Sciences of the United States of America* **2006,** 103, (23), 8589-94.
313. Luo, Y.; Zare, R. N., Perforated membrane method for fabricating three-dimensional polydimethylsiloxane microfluidic devices. *Lab on a Chip* **2008,** 8, (10), 1688-1694.
314. Yun, K.-S.; Yoon, E., Fabrication of complex multilevel microchannels in PDMS by using three-dimensional photoresist masters. *Lab on a Chip* **2008,** 8, (2), 245-250.
315. Carlborg, C. F.; Haraldsson, T.; Cornaglia, M.; Stemme, G.; van der Wijngaart, W., A High-Yield Process for 3-D Large-Scale Integrated Microfluidic Networks in PDMS. *Journal of Microelectromechanical Systems* **2010,** 19, (5), 1050-1057.
316. Martinez, A. W.; Phillips, S. T.; Whitesides, G. M., Three-dimensional microfluidic devices fabricated in layered paper and tape. *Proceedings of the National Academy of Sciences* **2008,** 105, (50), 19606-19611.
317. Yoon, Y.-K.; Park, J.-H.; Allen, M. G., Multidirectional UV Lithography for Complex 3-D MEMS Structures. *Journal of Microelectromechanical Systems* **2006,** 15, (5), 1121-1130.
318. Jackman, R. J.; Brittain, S. T.; Adams, A.; Wu, H.; Prentiss, M. G.; Whitesides, S.; Whitesides, G. M., Three-Dimensional Metallic Microstructures Fabricated by Soft Lithography and Microelectrodeposition. *Langmuir* **1999,** 15, (3), 826-836.
319. Brittain, S. T.; Schueller, O. J. A.; Wu, H.; Whitesides, S.; Whitesides, G. M., Microorigami: fabrication of small, three-dimensional, metallic structures. *Journal of Physical Chemistry B* **2001,** 105, (2), 347-350.
320. Wu, H.; Odom, T. W.; Chiu, D. T.; Whitesides, G. M., Fabrication of Complex Three-Dimensional Microchannel Systems in PDMS. *Journal of the American Chemical Society* **2003,** 125, (2), 554-559.
321. Jackman, R. J.; Brittain, S. T.; Whitesides, G. M., Fabrication of three-dimensional microstructures by electrochemically welding structures formed by microcontact printing on planar and curved substrates. *Journal of Microelectromechanical Systems* **1998,** 7, (2), 261-266.
322. Jackman, R. J.; Brittain, S. T.; Adams, A.; Prentiss, M. G.; Whitesides, G. M., Design and fabrication of topologically complex, three-dimensional microstructures. *Science* **1998,** 280, (5372), 2089-2091.
323. Lipomi, D. J.; Kats, M. A.; Kim, P.; Kang, S. H.; Aizenberg, J.; Capasso, F.; Whitesides, G. M., Fabrication and Replication of Arrays of Single- or Multicomponent Nanostructures by Replica Molding and Mechanical Sectioning. *ACS Nano* **2010,** 4, (7), 4017-4026.

324. Chang, C.-M.; Chiou, L.-F.; Lin, C.-C.; Shieh, D.-B.; Lee, G.-B., Three-dimensional microfluidic chip for the extraction of mitochondrial DNA. *Microfluidics and Nanofluidics* **2010,** 9, (2), 489-498.
325. Zhang, M.; Wu, J.; Wang, L.; Xiao, K.; Wen, W., A simple method for fabricating multi-layer PDMS structures for 3D microfluidic chips. *Lab on a Chip* **2010,** 10, (9), 1199-1203.
326. Graf, N. J.; Bowser, M. T., A soft-polymer piezoelectric bimorph cantilever-actuated peristaltic micropump. *Lab on a Chip* **2008,** 8, (10), 1664-1670.
327. Eddings, M., A. ; et al., Determining the optimal PDMS - PDMS bonding technique for microfluidic devices. *Journal of Micromechanics and Microengineering* **2008,** 18, (6), 067001.
328. Soper, S. A.; Ford, S. M.; Qi, S.; McCarley, R. L.; Kelly, K.; Murphy, M. C., Polymeric Microelectromechanical Systems. *Analytical Chemistry* **2000**, 643A-651A.
329. McDonald, J. C.; Chabinyc, M. L.; Metallo, S. J.; Anderson, J. R.; Stroock, A. D.; Whitesides, G. M., Prototyping of microfluidic devices in poly(dimethylsiloxane) using solid-object printing. *Analytical Chemistry* **2002,** 74, (7), 1537-1545.
330. Martynova, L.; Locascio, L. E.; Gaitan, M.; Kramer, G. W.; Christensen, R. G.; MacCrehan, W. A., Fabrication of Plastic Microfluid Channels by Imprinting Methods. *Analytical Chemistry* **1997,** 69, (23), 4783-4789.
331. Qi, S.; Liu, X.; Ford, S.; Barrows, J.; Thomas, G.; Kelly, K.; McCandless, A.; Lian, K.; Goettert, J.; Soper, S. A., Microfluidic devices fabricated in poly(methyl methacrylate) using hot-embossing with integrated sampling capillary and fiber optics for fluorescence detection. *Lab on a Chip* **2002,** 2, (2), 88-95.
332. Shiu, P. P.; et al., Rapid fabrication of tooling for microfluidic devices via laser micromachining and hot embossing. *Journal of Micromechanics and Microengineering* **2008,** 18, (2), 025012.
333. Li, J. M.; et al., Hot embossing/bonding of a poly(ethylene terephthalate) (PET) microfluidic chip. *Journal of Micromechanics and Microengineering* **2008,** 18, (1), 015008.
334. Park, J.; Li, J.; Han, A., Micro-macro hybrid soft-lithography master (MMHSM) fabrication for lab-on-a-chip applications. *Biomedical Microdevices* **2010,** 12, (2), 345-351.
335. Toh, A.; Ng, S.; Wang, Z., Fabrication and testing of embedded microvalves within PMMA microfluidic devices. *Microsystem Technologies* **2009,** 15, (9), 1335-1342.
336. Jeon, J.; Chung, S.; Kamm, R.; Charest, J., Hot embossing for fabrication of a microfluidic 3D cell culture platform. *Biomedical Microdevices* **2011,** 13, (2), 325-333.
337. Ekmekci, B.; et al., Geometry and surface damage in micro electrical discharge machining of micro-holes. *Journal of Micromechanics and Microengineering* **2009,** 19, (10), 105030.
338. Murali, M.; Yeo, S. H., Rapid Biocompatible Micro Device Fabrication by Micro Electro-Discharge Machining. *Biomedical Microdevices* **2004,** 6, (1), 41-45.
339. Chen, S.-T., Fabrication of high-density micro holes by upward batch micro EDM. *Journal of Micromechanics and Microengineering* **2008,** 18, (8), 085002.

340. Richardson , M., T. ; Gianchandani, Y. B., Achieving precision in high density batch mode micro-electro-discharge machining. *Journal of Micromechanics and Microengineering* **2008,** 18, (1), 015002.
341. Chen, S.-T.; et al., Study of an ultrafine w-EDM technique. *Journal of Micromechanics and Microengineering* **2009,** 19, (11), 115033.
342. Chaitanya, C. R. A.; Takahata, K., M^3 EDM: MEMS-enabled micro-electro-discharge machining. *Journal of Micromechanics and Microengineering* **2008,** 18, (10), 105009.
343. Huft, J.; Da Costa, D. J.; Walker, D.; Hansen, C. L., Three-dimensional large-scale microfluidic integration by laser ablation of interlayer connections. *Lab on a Chip* **2010,** 10, (18), 2358-2365.
344. Liu, H.-B.; Gong, H.-Q., Templateless prototyping of polydimethylsiloxane microfluidic structures using a pulsed CO2 laser. *Journal of Micromechanics and Microengineering* **2009,** 19, (3), 037002.
345. Wu, D.; Chen, Q.-D.; Niu, L.-G.; Wang, J.-N.; Wang, J.; Wang, R.; Xia, H.; Sun, H.-B., Femtosecond laser rapid prototyping of nanoshells and suspending components towards microfluidic devices. *Lab on a Chip* **2009,** 9, (16), 2391-2394.
346. Vishnubhatla, K. C.; Clark, J.; Lanzani, G.; Ramponi, R.; Osellame, R.; Virgili, T., Ultrafast optofluidic gain switch based on conjugated polymer in femtosecond laser fabricated microchannels. *Applied Physics Letters* **2009,** 94, (4), 041123-3.
347. Fercher, G.; Haller, A.; Smetana, W.; Vellekoop, M. J., Ceramic capillary electrophoresis chip for the measurement of inorganic ions in water samples. *Analyst* **2010,** 135, (5), 965-970.
348. Fogarty, B. A.; Heppert, K. E.; Cory, T. J.; Hulbutta, K. R.; Martin, R. S.; Lunte, S. M., Rapid fabrication of poly(dimethylsiloxane)-based microchip capillary electrophoresis devices using CO2 laser ablation. *The Analyst* **2005,** 130, (6), 924-930.
349. Klank, H.; Kutter, J. P.; Geschke, O., CO2-laser micromachining and back-end processing for rapid production of PMMA-based microfluidic systems. *Lab on a Chip* **2002,** 2, (4), 242-246.
350. Yu, H.; Balogun, O.; Li, B.; Murray, T. W.; Zhang, X., Fabrication of three-dimensional microstructures based on singled-layered SU-8 for lab-on-chip applications. *Sensors and Actuators A: Physical* **2006,** 127, (2), 228-234.
351. Chan, S. H.; et al., Development of a polymeric micro fuel cell containing laser-micromachined flow channels. *Journal of Micromechanics and Microengineering* **2005,** 15, (1), 231.
352. Sugioka, K.; Cheng, Y.; Midorikawa, K., Three-dimensional micromachining of glass using femtosecond laser for lab-on-a-chip device manufacture. *Applied Physics A: Materials Science & Processing* **2005,** 81, 1-10.
353. Malek, C. G. K., Laser processing for bio-microfluidics applications (part I). *Analytical & Bioanalytical Chemistry* **2006,** 385, 1351-1361.
354. Malek, C. G. K., Laser processing for bio-microfluidics applications (part II). *Analytical & Bioanalytical Chemistry* **2006,** 385, 1362-1369.

355. Han, K.-H.; McConnell, R. D.; Easley, C. J.; Bienvenue, J. M.; Ferrance, J. P.; Landers, J. P.; Frazier, A. B., An active microfluidic system packaging technology. *Sensors and Actuators B: Chemical* **2007,** B122, (1), 337-346.
356. Xia, C.; Fang, N., Fully three-dimensional microfabrication with a grayscale polymeric self-sacrificial structure. *Journal of Micromechanics and Microengineering* **2009,** 19, (11), 115029.
357. Haefliger, D.; Boisen, A., Three-dimensional microfabrication in negative resist using printed masks. *Journal of Micromechanics and Microengineering* **2006,** 16, (5), 951.
358. Teh, W. H.; Durig, U.; Drechsler, U.; Smith, C. G.; Guntherodt, H. J., Effect of low numerical-aperture femtosecond two-photon absorption on (SU-8) resist for ultrahigh-aspect-ratio microstereolithography. *Journal of Applied Physics* **2005,** 97, 054907.
359. Xia, C.; Fang, N., 3D microfabricated bioreactor with capillaries. *Biomedical Microdevices* **2009,** 11, (6), 1309-1315.
360. Conrad II, P. G.; Nishimura, P. T.; Aherne, D.; Schwartz, B. J.; Wu, D.; Fang, N.; Zhang, X.; Roberts, M. J.; Shea, K. J., Functional Molecularly Imprinted Polymer Microstructures Fabricated Using Microstereolithography. *Advanced Materials* **2003,** 15, (18), 1541-1544.
361. Snowden, M. E.; King, P. H.; Covington, J. A.; Macpherson, J. V.; Unwin, P. R., Fabrication of Versatile Channel Flow Cells for Quantitative Electroanalysis Using Prototyping. *Analytical Chemistry* **2010,** 82, (8), 3124-3131.
362. Kobayashi, K.; Ikuta, K., Three-dimensional magnetic microstructures fabricated by microstereolithography. *Applied Physics Letters* **2008,** 92, 262505.
363. Natali, M.; Begolo, S.; Carofiglio, T.; Mistura, G., Rapid prototyping of multilayer thiolene microfluidic chips by photopolymerization and transfer lamination. *Lab on a Chip* **2008,** 8, (3), 492-494.
364. Metz, S.; Trautmann, C.; Bertsch, A.; Renaud, P., Polyimide microfluidic devices with integrated nanoporous filtration areas manufactured by micromachining and ion track technology. *Journal of Micromechanics and Microengineering* **2004,** 14, (3), 324-331.
365. Paul, D.; Pallandre, A.; Miserere, S.; Weber, J.; Viovy, J.-L., Lamination-based rapid prototyping of microfluidic devices using flexible thermoplastic substrates. *Electrophoresis* **2007,** 28, (7), 1115-22.
366. Weigl, B. H.; Bardell, R.; Schulte, T.; Battrell, F.; Hayenga, J., Design and rapid prototyping of thin-film laminate-based microfluidic devices. *Biomedical Microdevices* **2001,** 3, (4), 267-74.
367. Guijt, R. M.; Candish, E.; Breadmore, M. C., Dry film microchips for miniaturised separations. *Electrophoresis* **2009,** 30, (24), 4219-4224.
368. Martin, P. M.; Matson, D. W.; Bennett, W. D.; Lin, Y.; Hammerstrom, D. J., Laminated plastic microfluidic components for biological and chemical systems. *Journal of Vacuum Science & Technology A* **1999,** 17, (4), 2264-2269.

369. Belloy, E.; Thurre, S.; Walckiers, E.; Sayah, A.; Gijs, M. A. M., Introduction of powder blasting for sensor and microsystem applications. *Sensors and Actuators A: Physical* **2000,** 84, (3), 330-337.
370. Lomas, T.; et al., A precision hot embossing mold fabricated by high-resolution powder blasting with polydimethylsiloxane and SU-8 masking technology. *Journal of Micromechanics and Microengineering* **2009,** 19, (3), 035002.
371. Mecomber, J. S.; Stalcup, A. M.; Hurd, D.; Halsall, H. B.; Heineman, W. R.; Seliskar, C. J.; Wehmeyer, K. R.; Limbach, P. A., Analytical Performance of Polymer-Based Microfluidic Devices Fabricated By Computer Numerical Controlled Machining. *Analytical Chemistry* **2005,** 78, (3), 936-941.
372. Wilson, M. E.; Kota, N.; Kim, Y.; Wang, Y.; Stolz, D. B.; LeDuc, P. R.; Ozdoganlar, O. B., Fabrication of circular microfluidic channels by combining mechanical micromilling and soft lithography. *Lab on a Chip* **2011,** 11, (8), 1550-1555.
373. Andresen, K. O.; et al., Injection molded chips with integrated conducting polymer electrodes for electroporation of cells. *Journal of Micromechanics and Microengineering* **2010,** 20, (5), 055010.
374. Schutte, J.; Freudigmann, C.; Benz, K.; Bottger, J.; Gebhardt, R.; Stelzle, M., A method for patterned in situ biofunctionalization in injection-molded microfluidic devices. *Lab on a Chip* **2010,** 10, (19), 2551-2558.
375. Utko, P.; Persson, F.; Kristensen, A.; Larsen, N. B., Injection molded nanofluidic chips: Fabrication method and functional tests using single-molecule DNA experiments. *Lab on a Chip* **2011,** 11, (2), 303-308.
376. Hansen, T. S.; et al., Fast prototyping of injection molded polymer microfluidic chips. *Journal of Micromechanics and Microengineering* **2010,** 20, (1), 015020.
377. Giboz, J.; et al., Microinjection molding of thermoplastic polymers: a review. *Journal of Micromechanics and Microengineering* **2007,** 17, (6), R96.
378. Matschuk, M.; Bruus, H.; Larsen, N. B., Nanostructures for all-polymer microfluidic systems. *Microelectronic Engineering* **2010,** 87, (5-8), 1379-1382.
379. Kim, D. S.; Lee, S. H.; Ahn, C. H.; Lee, J. Y.; Kwon, T. H., Disposable integrated microfluidic biochip for blood typing by plastic microinjection moulding. *Lab on a Chip* **2006,** 6, (6), 794-802.
380. Tai, L.-W.; Tseng, K.-Y.; Wang, S.-T.; Chiu, C.-C.; Kow, C. H.; Chang, P.; Chen, C.; Wang, J.-Y.; Webster, J. R., An automated microfluidic-based immunoassay cartridge for allergen screening and other multiplexed assays. *Analytical Biochemistry* **2009,** 391, (2), 98-105.
381. Huang, F.-C.; Chen, Y.-F.; Lee, G.-B., CE chips fabricated by injection molding and polyethylene/thermoplastic elastomer film packaging methods. *Electrophoresis* **2007,** 28, (7), 1130-1137.
382. Chang, P.-C.; Hwang, S.-J.; Lee, H.-H.; Huang, D.-Y., Development of an external-type microinjection molding module for thermoplastic polymer. *Journal of Materials Processing Technology* **2007,** 184, (1-3), 163-172.
383. McCormick, R. M.; Nelson, R. J.; Alonso-Amigo, M. G.; Benvegnu, D. J.; Hooper, H. H., Microchannel Electrophoretic Separations of DNA in Injection-Molded Plastic Substrates. *Analytical Chemistry* **1997,** 69, (14), 2626-2630.

384. Mair, D. A.; Geiger, E.; Pisano, A. P.; Frechet, J. M. J.; Svec, F., Injection molded microfluidic chips featuring integrated interconnects. *Lab on a Chip* **2006,** 6, (10), 1346-1354.
385. Sudarsan, A. P.; Ugaz, V. M., Printed circuit technology for fabrication of plastic-based microfluidic devices. *Analytical Chemistry* **2004,** 76, (11), 3229-35.
386. Abdelgawad, M.; Watson, M. W. L.; Young, E. W. K.; Mudrik, J. M.; Ungrin, M. D.; Wheeler, A. R., Soft lithography: masters on demand. *Lab on a Chip* **2008,** 8, (8), 1379-1385.
387. Mali, P.; Sarkar, A.; Lal, R., Facile fabrication of microfluidic systems using electron beam lithography. *Lab on a Chip* **2006,** 6, (2), 310-315.
388. Aracil, C.; et al., BETTS: bonding, exposing and transferring technique in SU-8 for microsystems fabrication. *Journal of Micromechanics and Microengineering* **2010,** 20, (3), 035008.
389. Chang, C.-H.; et al., Self-assembled ferrofluid lithography: patterning micro and nanostructures by controlling magnetic nanoparticles. *Nanotechnology* **2009,** 20, (49), 495301.
390. Watanabe, M., Refreshable microfluidic channels constructed using an inkjet printer. *Sensors and Actuators B: Chemical* **2007,** 122, (1), 141-147.
391. Merkel, T.; Graeber, M.; Pagel, L., A new technology for fluidic microsystems based on PCB technology. *Sensors and Actuators A: Physical* **1999,** 77, 98-105.
392. Shepherd, R., F. ; Panda, P.; Bao, Z.; Sandhage, K. H.; Hatton, T. A.; Lewis, J. A.; Doyle, P. S., Stop-Flow Lithography of Colloidal, Glass, and Silicon Microcomponents. *Advanced Materials* **2008,** 20, (24), 4734-4739.
393. Moorthy, J.; Mensing, G. A.; Kim, D.; Mohanty, S.; Eddington, D. T.; Tepp, W. H.; Johnson, E. A.; Beebe, D. J., Microfluidic tectonics platform: A colorimetric, disposable botulinum toxin enzyme-linked immunosorbent assay system. *Electrophoresis* **2004,** 25, (10-11), 1705-1713.
394. Beebe, D. J.; Moore, J. S.; Yu, Q.; Liu, R. H.; Kraft, M. L.; Jo, B.-H.; Devadoss, C., Microfluidic tectonics: A comprehensive construction platform for microfluidic systems. *Proceedings of the National Academy of Sciences of the United States of America* **2000,** 97, (25), 13488-13493.
395. Attia, U.; Alcock, J., Integration of functionality into polymer-based microfluidic devices produced by high-volume micro-moulding techniques. *The International Journal of Advanced Manufacturing Technology* **2010,** 48, (9), 973-991.
396. Bleul, R.; Ritzi-Lehnert, M.; Höth, J.; Scharpfenecker, N.; Frese, I.; Düchs, D.; Brunklaus, S.; Hansen-Hagge, T.; Meyer-Almes, F.-J.; Drese, K., Compact, cost-efficient microfluidics-based stopped-flow device. *Analytical and Bioanalytical Chemistry* **2011,** 399, (3), 1117-1125.
397. Fu, G.; et al., Fabrication of robust tooling for mass production of polymeric microfluidic devices. *Journal of Micromechanics and Microengineering* **2010,** 20, (8), 085019.
398. Jang, L.-S.; Wu, C.-C.; Liu, C.-F., Fabrication of microfluidic devices for packaging CMOS MEMS impedance sensors. *Microfluidics and Nanofluidics* **2009,** 7, (6), 869-875.

399. Wimberger-Friedl, R.; et al., Packaging of silicon sensors for microfluidic bio-analytical applications. *Journal of Micromechanics and Microengineering* **2009,** 19, (1), 015015.
400. Kelly, G.; Alderman, J.; Lyden, C.; Barrett, J., Microsystem packaging: lessons from conventional low cost IC packaging. *Journal of Micromechanics and Microengineering* **1996,** 7, (3), 99-103.
401. Esashi, M., Wafer level packaging of MEMS. *Journal of Micromechanics and Microengineering* **2008,** 18, (7), 073001.
402. Lu, C.; James Lee, L.; Juang, Y.-J., Packaging of microfluidic chips via interstitial bonding technique. *Electrophoresis* **2008,** 29, (7), 1407-1414.
403. Krulevitch, P.; Benett, W.; Hamilton, J.; Maghribi, M.; Rose, K., Polymer-based packaging platform for hybrid microfluidic systems. *Biomedical Microdevices* **2002,** 4, (4), 301-8.
404. Fredrickson, C. K.; Fan, Z. H., Macro-to-micro interfaces for microfluidic devices. *Lab on a Chip* **2004,** 4, (6), 526-533.
405. Liu, J.; Hansen, C.; Quake, S. R., Solving the "world-to-chip" interface problem with a microfluidic matrix. *Analytical Chemistry* **2003,** 75, (18), 4718-4723.
406. Lee, Y. C.; Amir Parviz, B.; Chiou, J. A.; Shaochen, C., Packaging for microelectromechanical and nanoelectromechanical systems. *IEEE Transactions on Advanced Packaging* **2003,** 26, (3), 217-26.
407. Ding, Y.; Hong, L.; Nie, B.; Lam, K. S.; Pan, T., Capillary-driven automatic packaging. *Lab on a Chip* **2011,** 11, (8), 1464-1469.
408. Chen, A.; Pan, T., Fit-to-Flow (F2F) interconnects: Universal reversible adhesive-free microfluidic adaptors for lab-on-a-chip systems. *Lab on a Chip* **2011,** 11, (4), 727-732.
409. Saarela, V.; Franssila, S.; Tuomikoski, S.; Marttila, S.; Östman, P.; Sikanen, T.; Kotiaho, T.; Kostiainen, R., Re-usable multi-inlet PDMS fluidic connector. *Sensors and Actuators B: Chemical* **2006,** 114, (1), 552-557.
410. Hashimoto, M.; Hupert, M. L.; Murphy, M. C.; Soper, S. A.; Cheng, Y.-W.; Barany, F., Ligase Detection Reaction/Hybridization Assays Using Three-Dimensional Microfluidic Networks for the Detection of Low-Abundant DNA Point Mutations. *Analytical Chemistry* **2005,** 77, (10), 3243-3255.
411. Sen, A.; Darabi, J.; Knapp, D., A fluidic interconnection system for polymer-based microfluidic devices. *Microsystem Technologies* **2010,** 16, (4), 617-623.
412. Hartmann, D. M.; Nevill, J. T.; Pettigrew, K. I.; Votaw, G.; Kung, P.-J.; Crenshaw, H. C., A low-cost, manufacturable method for fabricating capillary and optical fiber interconnects for microfluidic devices. *Lab on a Chip* **2008,** 8, (4), 609-616.
413. Nittis, V.; Fortt, R.; Legge, C. H.; de Mello, A. J., A high-pressure interconnect for chemical microsystem applications. *Lab on a Chip* **2001,** 1, (2), 148-52.
414. Pattekar, A. V.; Kothare, M. V., Novel microfluidic interconnectors for high temperature and pressure applications. *Journal of Micromechanics and Microengineering* **2003,** 13, (2), 337.

415. Sabourin, D.; et al., One-step fabrication of microfluidic chips with in-plane, adhesive-free interconnections. *Journal of Micromechanics and Microengineering* **2010,** 20, (3), 037001.
416. Murphy, E. R.; Inoue, T.; Sahoo, H. R.; Zaborenko, N.; Jensen, K. F., Solder-based chip-to-tube and chip-to-chip packaging for microfluidic devices. *Lab on a Chip* **2007,** 7, (10), 1309-1314.
417. Puntambekar, A.; Ahn, C. H., Self-aligning microfluidic interconnects for glass- and plastic-based microfluidic systems. *Journal of Micromechanics and Microengineering* **2002,** 12, (1), 35-40.
418. Chiou, C.-H.; Lee, G.-B., Minimal dead-volume connectors for microfluidics using PDMS casting techniques. *Journal of Micromechanics and Microengineering* **2004,** 14, (11), 1484.
419. Oh, K. W.; Park, C.; Namkoong, K.; Kim, J.; Ock, K.-S.; Kim, S.; Kim, Y.-A.; Cho, Y.-K.; Ko, C., World-to-chip microfluidic interface with built-in valves for multichamber chip-based PCR assays. *Lab on a Chip* **2005,** 5, (8), 845-850.
420. He, Q.-H.; Fang, Q.; Du, W.-B.; Fang, Z.-L., Fabrication of a monolithic sampling probe system for automated and continuous sample introduction in microchip-based CE. *Electrophoresis* **2007,** 28, (16), 2912-2919.
421. Jaffer, S.; Gray, B. L., Polymer mechanically interlocking structures as interconnects for microfluidic systems. *Journal of Micromechanics and Microengineering* **2008,** 18, (3), 035043.
422. Fujii, T.; Sando, Y.; Higashino, K.; Fujii, Y., A plug and play microfluidic device. *Lab on a Chip* **2003,** 3, (3), 193-197.
423. Johansson, A.; et al., SU-8 cantilever chip interconnection. *Journal of Micromechanics and Microengineering* **2006,** 16, (2), 314.
424. Perozziello, G.; Bundgaard, F.; Geschke, O., Fluidic interconnections for microfluidic systems: A new integrated fluidic interconnection allowing plug 'n' play functionality. *Sensors and Actuators B: Chemical* **2008,** 130, (2), 947-953.
425. Yuen, P. K.; Bliss, J. T.; Thompson, C. C.; Peterson, R. C., Multidimensional modular microfluidic system. *Lab on a Chip* **2009,** 9, (22), 3303-3305.
426. Yuen, P. K., SmartBuild-A truly plug-n-play modular microfluidic system. *Lab on a Chip* **2008,** 8, (8), 1374-1378.
427. Liou, D.-S.; Hsieh, Y.-F.; Kuo, L.-S.; Yang, C.-T.; Chen, P.-H., Modular component design for portable microfluidic devices. *Microfluidics and Nanofluidics* **2011,** 10, (2), 465-474.
428. Chen, C. F.; Liu, J.; Hromada, L. P.; Tsao, C. W.; Chang, C. C.; DeVoe, D. L., High-pressure needle interface for thermoplastic microfluidics. *Lab on a Chip* **2009,** 9, (1), 50-55.
429. Mogulkoc, B.; et al., Characterization of MEMS-on-tube assembly: reflow bonding of borosilicate glass (Duran®) tubes to silicon substrates. *Journal of Micromechanics and Microengineering* **2009,** 19, (8), 085027.
430. Unnikrishnan, S.; Jansen, H.; Berenschot, E.; Mogulkoc, B.; Elwenspoek, M., MEMS within a Swagelok®: a new platform for microfluidic devices. *Lab on a Chip* **2009,** 9, (13), 1966-1969.

431. Stone, H. A.; Kim, S., Microfluidics: Basic issues, applications, and challenges. *AIChE Journal* **2001,** 47, (6), 1250-1254.
432. Ho, C.-M.; Tai, Y.-C., Micro-Electro-Mechanical-Systems (MEMS) and Fluid Flows. *Annual Review of Fluid Mechanics* **1998,** 30, (1), 579-612.
433. Beebe, D. J.; Mensing, G. A.; Walker, G. M., Physics and applications of microfluidics in biology. *Annual Review of Biomedical Engineering* **2002,** 4, 261-86.
434. Stone, H. A.; Stroock, A. D.; Ajdari, A., Engineering Flows in Small Devices: Microfluidics Toward a Lab-on-a-Chip *Annual Review of Fluid Mechanics* **2004,** 36, (1), 381-411.
435. Squires, T. M.; Quake, S. R., Microfluidics: Fluid physics at the nanoliter scale. *Reviews of Modern Physics* **2005,** 77, (3), 977-1026.
436. Wu, Z.; Nguyen, N.-T.; Huang, X., Nonlinear diffusive mixing in microchannels: Theory and experiments. *Journal of Micromechanics and Microengineering* **2004,** 14, (4), 604-611.
437. Stay, M. S.; Barocas, V. H., Thin-domain modeling of mass transport in microchannels, with application to diffusive mixing. *Journal of Applied Physics* **2004,** 95, (11), 6435-6443.
438. Kamholz, A. E.; Yager, P., Theoretical analysis of molecular diffusion in pressure-driven laminar flow in microfluidic channels. *Biophysical Journal* **2001,** 80, (1), 155-60.
439. Ajdari, A.; Bontoux, N.; Stone, H. A., Hydrodynamic Dispersion in Shallow Microchannels: the Effect of Cross-Sectional Shape. *Analytical Chemistry* **2005,** 78, (2), 387-392.
440. Kreutzer, M. T.; Gunther, A.; Jensen, K. F., Sample Dispersion for Segmented Flow in Microchannels with Rectangular Cross Section. *Analytical Chemistry* **2008,** 80, (5), 1558-1567.
441. Gunther, A.; Jensen, K. F., Multiphase microfluidics: from flow characteristics to chemical and materials synthesis. *Lab on a Chip* **2006,** 6, (12), 1487-1503.
442. Balazs, A. C.; Verberg, R.; Pooley, C. M.; Kuksenok, O., Modeling the flow of complex fluids through heterogeneous channels. *Soft Matter* **2005,** 1, (1), 44-54.
443. Bocquet, L.; Barrat, J.-L., Flow boundary conditions from nano- to micro-scales. *Soft Matter* **2007,** 3, (6), 685-693.
444. Carlo, D. D., Inertial microfluidics. *Lab on a Chip* **2009,** 9, (21), 3038-3046.
445. Tabeling, P., A brief introduction to slippage, droplets and mixing in microfluidic systems. *Lab on a Chip* **2009,** 9, (17), 2428-2436.
446. Mosier, B. P.; Molho, J. I.; Santiago, J. G., Photobleached-fluorescence imaging of microflows. *Experiments in Fluids* **2002,** 33, (4), 545-54.
447. Bohl, D. G.; Koochesfahani, M. N.; Olson, B. J., Development of stereoscopic molecular tagging velocimetry. *Experiments in Fluids* **2001,** 30, (3), 302-8.
448. Sadr, R.; Klewicki, J. C., A spline-based technique for estimating flow velocities using two-camera multi-line MTV. *Experiments in Fluids* **2003,** 35, (3), 257-261.
449. Koochesfahani, M.; Cohn, R.; MacKinnon, C., Simultaneous whole-field measurements of velocity and concentration fields using a combination of MTV and LIF. *Measurement Science and Technology* **2000,** 11, (9), 1289-1300.

450. Maynes, D.; Webb, A. R., Velocity profile characterization in sub-millimeter diameter tubes using molecular tagging velocimetry. *Experiments in Fluids* **2002,** 32, (1), 3-15.
451. Zheng, Q.; Klewicki, J. C., Fast data reduction algorithm for molecular tagging velocimetry: The decoupled spatial correlation technique. *Measurement Science and Technology* **2000,** 11, (9), 1282-1288.
452. Adrian, R. J. In *Twenty Years of Particle Image Velocimetry*, 12th International Symposium on Applications of Laser Techniques to Fluid Mechanics, Lisbon, Portugal, July 12-15, 2004, 2004; Lisbon, Portugal, 2004.
453. Adrian, R. J. *Bibliography of Particle Velocimetry Using Imaging Methods*; TAM Report No. 817; University of Illinois at Urbana-Champaign: 1996, 1996; pp 1917-1995.
454. Santiago, J. G.; Wereley, S. T.; Meinhart, C. D.; Beebe, D. J.; Adrian, R. J., Particle image velocimetry system for microfluidics. *Experiments in Fluids* **1998,** 25, (4), 316-319.
455. Lindken, R.; Rossi, M.; Grobe, S.; Westerweel, J., Micro-Particle Image Velocimetry (micro-PIV): Recent developments, applications, and guidelines. *Lab on a Chip* **2009,** 9, (17), 2551-2567.
456. Meinhart, C. D.; Wereley, S. T., The theory of diffraction-limited resolution in microparticle image velocimetry. *Measurement Science & Technology* **2003,** 14, (7), 1047-53.
457. Devasenathipathy, S.; Santiago, J. G.; Takehara, K., Particle tracking techniques for electrokinetic microchannel flows. *Analytical Chemistry* **2002,** 74, (15), 3704-3713.
458. Meinhart, C. D.; Wereley, S. T.; Santiago, J. G., PIV measurements of a microchannel flow. *Experiments in Fluids* **1999,** 27, (5), 414-19.
459. Devasenathipathy, S.; Santiago, J. G.; Wereley, S. T.; Meinhart, C. D.; Takehara, K., Particle imaging techniques for microfabricated fluidic systems. *Experiments in Fluids* **2003,** 34, (4), 504-514.
460. Kobayashi, T.; Hu, H.; Saga, T. In *Optical Diagnostics for Velocity, Temperature, and Species Measurements of the Flow Field*, Proceeding of '99 Korea-Japan Joint Seminar on Particle Image Velocimetry, 1999; 1999; pp 15-31.
461. Hart, D. P. In *Sparse Array Image Correlation*, 8th International Symposium on Applications of Laser Techniques to Fluid Mechanics, Lisbon, Portugal, July 8-11, 2004, 1996; Lisbon, Portugal, 1996; pp 21.1.1-21.1.8.
462. Keane, R. D.; Adrian, R. J., Theory of Cross-Correlation Analysis of PIV Images. *University of Illinois, Applied Scientific Reseach* **1992,** 49, 1-27.
463. Wereley, S. T.; Gui, L.; Meinhart, C. D., Advanced algorithms for microscale particle image velocimetry. *AIAA Journal* **2002,** 40, (6), 1047-55.
464. Deshmukh, A. A.; Liepmann, D.; Pisano, A. P. In *Characterization of a micro-mixing, pumping, and valving system*, The 11th International Conference on Solid-State Sensors and Actuators, Munich, Germany, June 10-14, 2001, 2001; Obermeier, E., Ed. Transducers '01 Eurosensors XV: Munich, Germany, 2001; pp 950-953.
465. Haeberle, S.; Zengerle, R., Microfluidic platforms for lab-on-a-chip applications. *Lab on a Chip* **2007,** 7, (9), 1094-1110.

466. Berg, C.; Valdez, D. C.; Bergeron, P.; Mora, M. F.; Garcia, C. D.; Ayon, A., Lab-on-a-robot: Integrated microchip CE, power supply, electrochemical detector, wireless unit, and mobile platform. *Electrophoresis* **2008,** 29, (24), 4914-4921.
467. Li, C.; Wu, P.-M.; Jung, W.; Ahn, C. H.; Shutter, L. A.; Narayan, R. K., A novel lab-on-a-tube for multimodality neuromonitoring of patients with traumatic brain injury (TBI). *Lab on a Chip* **2009,** 9, (14), 1988-1990.
468. Cho, Y.-K.; Lee, J.-G.; Park, J.-M.; Lee, B.-S.; Lee, Y.; Ko, C., One-step pathogen specific DNA extraction from whole blood on a centrifugal microfluidic device. *Lab on a Chip* **2007,** 7, (5), 565-573.
469. Potyrailo, R. A.; Morris, W. G.; Leach, A. M.; Sivavec, T. M.; Wisnudel, M. B.; Boyette, S., Analog Signal Acquisition from Computer Optical Disk Drives for Quantitative Chemical Sensing. *Analytical Chemistry* **2006,** 78, (16), 5893-5899.
470. Lee, B. S.; Lee, Y. U.; Kim, H.-S.; Kim, T.-H.; Park, J.; Lee, J.-G.; Kim, J.; Kim, H.; Lee, W. G.; Cho, Y.-K., Fully integrated lab-on-a-disc for simultaneous analysis of biochemistry and immunoassay from whole blood. *Lab on a Chip* **2011,** 11, (1), 70-78.
471. Kelly, B. T.; Baret, J.-C.; Taly, V.; Griffiths, A. D., Miniaturizing chemistry and biology in microdroplets. *Chemical Communications* **2007**, (18), 1773-1788.
472. Dorvee, J. R.; Sailor, M. J.; Miskelly, G. M., Digital microfluidics and delivery of molecular payloads with magnetic porous silicon chaperones. *Dalton Transactions* **2008**, (6), 721-730.
473. Le Gac, S.; van den Berg, A., Single cells as experimentation units in lab-on-a-chip devices. *Trends in Biotechnology* **2010,** 28, (2), 55-62.
474. Oh, K., W. ; Ahn, C. H., A review of microvalves. *Journal of Micromechanics and Microengineering* **2006,** 16, (5), R13.
475. Gilbertson, R. G.; Busch, J. D., A Survey of Micro-Actuator Technologies for Future Spacecraft Missions. *The Journal of The British Interplanetary Society* **1996,** 49, 129-138.
476. De Volder, M.; Reynaerts, D., Pneumatic and hydraulic microactuators: a review. *Journal of Micromechanics and Microengineering* **2010,** 20, (4), 043001.
477. Judy, J. W., Microelectromechanical systems (MEMS): fabrication, design and applications. *Smart Materials and Structures* **2001,** 10, 1115-1134.
478. Wilson, S. A.; Jourdain, R. P. J.; Zhang, Q.; Dorey, R. A.; Bowen, C. R.; Willander, M.; Wahab, Q. U.; Willander, M.; Al-hilli, S. M.; Nur, O.; Quandt, E.; Johansson, C.; Pagounis, E.; Kohl, M.; Matovic, J.; Samel, B.; van der Wijngaart, W.; Jager, E. W. H.; Carlsson, D.; Djinovic, Z.; Wegener, M.; Moldovan, C.; Iosub, R.; Abad, E.; Wendlandt, M.; Rusu, C.; Persson, K., New materials for micro-scale sensors and actuators: An engineering review. *Materials Science and Engineering: R: Reports* **2007,** 56, (1-6), 1-129.
479. Studer, V.; Hang, G.; Pandolfi, A.; Ortiz, M.; Anderson, W. F.; Quake, S. R., Scaling properties of a low-actuation pressure microfluidic valve. *Journal of Applied Physics* **2004,** 95, (1), 393-398.
480. Nachef, K.; Bourouina, T.; Marty, F.; Danaie, K.; Bourlon, B.; Donzier, E., Microvalves for Natural-Gas Analysis With Poly Ether Ether Ketone Membranes. *Journal of Microelectromechanical Systems* **2010,** 19, (4), 973-981.

481. Ismagilov, R. F.; Rosmarin, D.; Kenis, P. J. A.; Chiu, D. T.; Zhang, W.; Stone, H. A.; Whitesides, G. M., Pressure-Driven Laminar Flow in Tangential Microchannels: an Elastomeric Microfluidic Switch. *Analytical Chemistry* **2001,** 73, (19), 4682-4687.
482. Maltezos, G.; Johnston, M.; Maltezos, D. G.; Scherer, A., Replication of three-dimensional valves from printed wax molds. *Sensors and Actuators A: Physical* **2007,** A135, (2), 620-624.
483. Willis, P. A.; Hunt, B. D.; White, V. E.; Lee, M. C.; Ikeda, M.; Bae, S.; Pelletier, M. J.; Grunthaner, F. J., Monolithic Teflon membrane valves and pumps for harsh chemical and low-temperature use. *Lab on a Chip* **2007,** 7, (11), 1469-1474.
484. Grover, W. H.; Ivester, R. H. C.; Jensen, E. C.; Mathies, R. A., Development and multiplexed control of latching pneumatic valves using microfluidic logical structures. *Lab on a Chip* **2006,** 6, (5), 623-631.
485. Hua, Z.; et al., A versatile microreactor platform featuring a chemical-resistant microvalve array for addressable multiplex syntheses and assays. *Journal of Micromechanics and Microengineering* **2006,** 16, (8), 1433.
486. Zeng, S.; Li, B.; Su, X. o.; Qin, J.; Lin, B., Microvalve-actuated precise control of individual droplets in microfluidic devices. *Lab on a Chip* **2009,** 9, (10), 1340-1343.
487. Abate, A. R.; Weitz, D. A., Single-layer membrane valves for elastomeric microfluidic devices. *Applied Physics Letters* **2008,** 92, 243509.
488. Frevert, C. W.; Boggy, G.; Keenan, T. M.; Folch, A., Measurement of cell migration in response to an evolving radial chemokine gradient triggered by a microvalve. *Lab on a Chip* **2006,** 6, (7), 849-856.
489. Li, N.; Hsu, C.-H.; Folch, A., Parallel mixing of photolithographically defined nanoliter volumes using elastomeric microvalve arrays. *Electrophoresis* **2005,** 26, (19), 3758-3764.
490. Xu, T.; Yue, W.; Li, C.-W.; Yao, X.; Cai, G.; Yang, M., Real-time monitoring of suspension cell-cell communication using an integrated microfluidics. *Lab on a Chip* **2010,** 10, (17), 2271-2278.
491. Fu, Z.; Shao, G.; Wang, J.; Lu, D.; Wang, W.; Lin, Y., Microfabricated Renewable Beads-Trapping/Releasing Flow Cell for Rapid Antigen - Antibody Reaction in Chemiluminescent Immunoassay. *Analytical Chemistry* **2011,** 83, (7), 2685-2690.
492. Zhang, Q.; Zeng, S.; Lin, B.; Qin, J., Controllable synthesis of anisotropic elongated particles using microvalve actuated microfluidic approach. *Journal of Materials Chemistry* **2011,** 21, (8), 2466-2469.
493. Motoo, K.; Toda, N.; Arai, F.; Fukuda, T.; Sekiyama, K.; Nakajima, M., Generation of concentration gradient from a wave-like pattern by high frequency vibration of liquid–liquid interface. *Biomedical Microdevices* **2008,** 10, (3), 329-335.
494. Park, J. M.; et al., A piezoelectric microvalve for cryogenic applications. *Journal of Micromechanics and Microengineering* **2008,** 18, (1), 015023.
495. Fazal, I.; Elwenspoek, M. C., Design and analysis of a high pressure piezoelectric actuated microvalve. *Journal of Micromechanics and Microengineering* **2007,** 17, (11), 2366.

496. Evans, A.; Park, J.; Chiravuri, S.; Gianchandani, Y., A low power, microvalve regulated architecture for drug delivery systems. *Biomedical Microdevices* **2010,** 12, (1), 159-168.
497. Wei, G.; Hao, C.; Yi-Chung, T.; Meiners, J.-C.; Takayama, S., Multiplexed hydraulic valve actuation using ionic liquid filled soft channels and Braille displays. *Applied Physics Letters* **2007,** 90, 033505.
498. Duggirala, R.; Lal, A., A hybrid PZT-silicon microvalve. *Journal of Microelectromechanical Systems* **2005,** 14, (3), 488-497.
499. Goettsche, T.; Kohnle, J.; Willmann, M.; Ernst, H.; Spieth, S.; Tischler, R.; Messner, S.; Zengerle, R.; Sandmaier, H., Novel approaches to particle tolerant valves for use in drug delivery systems. *Sensors and Actuators A: Physical* **2005,** 118, (1), 70-77.
500. Rogge, T.; Rummler, Z.; Schomburg, W. K., Polymer micro valve with a hydraulic piezo-drive fabricated by the AMANDA process. *Sensors and Actuators A: Physical* **2004,** 110, (1-3), 206-212.
501. Ninomiya, T.; Okayama, Y.; Matsumoto, Y.; Arouette, X.; Osawa, K.; Miki, N., MEMS-based hydraulic displacement amplification mechanism with completely encapsulated liquid. *Sensors and Actuators A: Physical* **2011,** 166, (2), 277-282.
502. Hensel, J. P.; Gemmen, R. S.; Thornton, J. D.; Vipperman, J. S.; Clark, W. W.; Bucci, B. A., Effects of cell-to-cell fuel mal-distribution on fuel cell performance and a means to reduce mal-distribution using MEMS micro-valves. *Journal of Power Sources* **2007,** 164, (1), 115-125.
503. Li, B.; Chen, Q., Solid micromechanical valves fabricated with in situ UV-LIGA assembled nickel. *Sensors and Actuators A: Physical* **2006,** 126, (1), 187-193.
504. Chakraborty, I.; Tang, W. C.; Bame, D. P.; Tang, T. K., MEMS micro-valve for space applications. *Sensors and Actuators A: Physical* **2000,** 83, 188-193.
505. Kim, H.; In, C.; Yoon, G.; Kim, J., A slim type microvalve driven by PZT films. *Sensors and Actuators A: Physical* **2005,** 121, (1), 162-171.
506. Gaspar, A.; Piyasena, M.; Daroczi, L.; Gomez, F., Magnetically controlled valve for flow manipulation in polymer microfluidic devices. *Microfluidics and Nanofluidics* **2008,** 4, (6), 525-531.
507. Casals-Terré, J.; Duch, M.; Plaza, J. A.; Esteve, J.; Pérez-Castillejos, R.; Vallés, E.; Gómez, E., Design, fabrication and characterization of an externally actuated ON/OFF microvalve. *Sensors and Actuators A: Physical* **2008,** 147, (2), 600-606.
508. Ducloux, O.; et al., A magnetically actuated, high momentum rate MEMS pulsed microjet for active flow control. *Journal of Micromechanics and Microengineering* **2009,** 19, (11), 115031.
509. Fazal, I.; et al., Design, fabrication and characterization of a novel gas microvalve using micro- and fine-machining. *Journal of Micromechanics and Microengineering* **2006,** 16, (7), 1207.
510. Bintoro, J. S.; Hesketh, P. J., An electromagnetic actuated on/off microvalve fabricated on top of a single wafer. *Journal of Micromechanics and Microengineering* **2005,** 15, (6), 1157.

511. Chen, C.-Y.; Chen, C.-H.; Tu, T.-Y.; Lin, C.-M.; Wo, A. M., Electrical isolation and characteristics of permanent magnet-actuated valves for PDMS microfluidics. *Lab on a Chip* **2011,** 11, (4), 733-737.
512. Luharuka, R.; Hesketh, P. J., A bistable electromagnetically actuated rotary gate microvalve. *Journal of Micromechanics and Microengineering* **2008,** 18, (3), 035015.
513. Sun, J.; Ng, J.; Fuh, Y.; Wong, Y.; Loh, H.; Xu, Q., Comparison of micro-dispensing performance between micro-valve and piezoelectric printhead. *Microsystem Technologies* **2009,** 15, (9), 1437-1448.
514. Churski, K.; Michalski, J.; Garstecki, P., Droplet on demand system utilizing a computer controlled microvalve integrated into a stiff polymeric microfluidic device. *Lab on a Chip* **2010,** 10, (4), 512-518.
515. Jackson, W. C.; Tran, H. D.; O'Brien, M. J.; Raninovich, E.; Lopez, G. P., Rapid prototyping of active microfluidic components based on magnetically modified elastomeric materials. *Journal of Vacuum Science and Technology* **2001,** B19, (2), 596-599.
516. Rosset, S.; Niklaus, M.; Dubois, P.; Shea, H. R., Large-Stroke Dielectric Elastomer Actuators With Ion-Implanted Electrodes. *Journal of Microelectromechanical Systems* **2009,** 18, (6), 1300-1308.
517. Chang, M.-P.; Maharbiz, M. M., Electrostatically-driven elastomer components for user-reconfigurable high density microfluidics. *Lab on a Chip* **2009,** 9, (9), 1274-1281.
518. Bansal, T.; Chang, M.-P.; Maharbiz, M. M., A class of low voltage, elastomer-metal 'wet' actuators for use in high-density microfluidics. *Lab on a Chip* **2007,** 7, (2), 164-166.
519. Yoshida, K.; Tanaka, S.; Hagihara, Y.; Tomonari, S.; Esashi, M., Normally closed electrostatic microvalve with pressure balance mechanism for portable fuel cell application. Part I: Design and simulation. *Sensors and Actuators A: Physical* **2010,** 157, (2), 299-306.
520. Yoshida, K.; Tanaka, S.; Hagihara, Y.; Tomonari, S.; Esashi, M., Normally closed electrostatic microvalve with pressure balance mechanism for portable fuel cell application. *Sensors and Actuators A: Physical* **2010,** 157, (2), 290-298.
521. Rich, C. A.; Wise, K. D. In *An 8-bit microflow controller using pneumatically-actuated microvalves*, 12th IEEE International Conference on Micro Electro Mechanical Systems, Piscataway, NJ, January 17-21, 1999, 1999; IEEE Robotics and Automation Society: Piscataway, NJ, 1999; pp 130-134.
522. Takao, H.; Miyamura, K.; Ebi, H.; Ashiki, M.; Sawada, K.; Ishida, M., A MEMS microvalve with PDMS diaphragm and two-chamber configuration of thermo-pneumatic actuator for integrated blood test system on silicon. *Sensors and Actuators A: Physical* **2005,** 119, (2), 468-475.
523. Yang, B.; et al., A thermopneumatically actuated bistable microvalve. *Journal of Micromechanics and Microengineering* **2010,** 20, (9), 095024.
524. Vyawahare, S.; Sitaula, S.; Martin, S.; Adalian, D.; Scherer, A., Electronic control of elastomeric microfluidic circuits with shape memory actuators. *Lab on a Chip* **2008,** 8, (9), 1530-1535.

525. Kohl, M.; Skrobanek, K. D.; Miyazaki, S., Development of stress-optimised shape memory microvalves. *Sensors and Actuators A: Physical* **1999,** 72, (3), 243-250.
526. Leester-Schädel, M.; Hoxhold, B.; Lesche, C.; Demming, S.; Büttgenbach, S., Micro actuators on the basis of thin SMA foils. *Microsystem Technologies* **2008,** 14, (4), 697-704.
527. Piccini, M. E.; Towe, B. C., A shape memory alloy microvalve with flow sensing. *Sensors and Actuators A: Physical* **2006,** 128, (2), 344-349.
528. Myunghoon, S.; et al., Development of a 'bi-layer lift-off' method for high flow rate and high frequency Nitinol MEMS valve fabrication. *Journal of Micromechanics and Microengineering* **2008,** 18, (7), 075034.
529. Hulme, S. E.; Shevkoplyas, S. S.; Whitesides, G. M., Incorporation of prefabricated screw, pneumatic, and solenoid valves into microfluidic devices. *Lab on a Chip* **2009,** 9, (1), 79-86.
530. Markov, D.; Manuel, S.; Shor, L.; Opalenik, S.; Wikswo, J.; Samson, P., Tape underlayment rotary-node (TURN) valves for simple on-chip microfluidic flow control. *Biomedical Microdevices* **2010,** 12, (1), 135-144.
531. Chen, C.-F.; Liu, J.; Chang, C.-C.; DeVoe, D. L., High-pressure on-chip mechanical valves for thermoplastic microfluidic devices. *Lab on a Chip* **2009,** 9, (24), 3511-3516.
532. Godino, N.; del Campo, F. J.; Munoz, F. X.; Hansen, M. F.; Kutter, J. P.; Snakenborg, D., Integration of a zero dead-volume PDMS rotary switch valve in a miniaturised (bio)electroanalytical system. *Lab on a Chip* **2010,** 10, (14), 1841-1847.
533. Yang, L.-J.; Wang, H.-H.; Wang, J.-M.; Liu, K.-C.; Ko, K.-C., Buckled-type valves integrated by parylene micro-tubes. *Sensors and Actuators A: Physical* **2006,** 130-131, 241-246.
534. Kim, J.; Chen, D.; Bau, H. H., An automated, pre-programmed, multiplexed, hydraulic microvalve. *Lab on a Chip* **2009,** 9, (24), 3594-3598.
535. Browne, A. W.; et al., A PDMS pinch-valve module embedded in rigid polymer lab chips for on-chip flow regulation. *Journal of Micromechanics and Microengineering* **2009,** 19, (11), 115012.
536. Pan, T.; Baldi, A.; Ziaie, B., Remotely adjustable check-valves with an electrochemical release mechanism for implantable biomedical microsystems. *Biomedical Microdevices* **2007,** 9, (3), 385-394.
537. Suhard, S.; Fau, P.; Chaudret, B.; Sabo-Etienne, S.; Mauzac, M.; Mingotaud, A.-F.; Ardila-Rodriguez, G.; Rossi, C.; Guimon, M.-F., When Energetic Materials, PDMS-Based Elastomers, and Microelectronic Processes Work Together: Fabrication of a Disposable Microactuator. *Chemistry of Materials* **2009,** 21, (6), 1069-1076.
538. Lee, D.; Soper, S.; Wang, W., Design and fabrication of an electrochemically actuated microvalve. *Microsystem Technologies* **2008,** 14, (9), 1751-1756.
539. Piyasena, M. E.; Newby, R.; Miller, T. J.; Shapiro, B.; Smela, E., Electroosmotically driven microfluidic actuators. *Sensors and Actuators B: Chemical* **2009,** 141, (1), 263-269.

540. Kirby, B. J.; Shepodd, T. J.; Hasselbrink Jr., E. F., Voltage-addressable on/off microvalves for high-pressure microchip separations. *Journal of Chromatography A* **2002,** 979, (1-2), 147-154.
541. Satarkar, N. S.; Zhang, W.; Eitel, R. E.; Hilt, J. Z., Magnetic hydrogel nanocomposites as remote controlled microfluidic valves. *Lab on a Chip* **2009,** 9, (12), 1773-1779.
542. Tehranirokh, M.; Majlis, B.; Bais, B., Design and simulation of a normally closed glucose sensitive hydrogel based microvalve. *Microsystem Technologies* **2009,** 15, (5), 753-762.
543. Ghosh, S.; et al., Oscillating magnetic field-actuated microvalves for micro- and nanofluidics. *Journal of Physics D: Applied Physics* **2009,** 42, (13), 135501.
544. Dong, L.; Jiang, H., Autonomous microfluidics with stimuli-responsive hydrogels. *Soft Matter* **2007,** 3, (10), 1223-1230.
545. Kim, D.; Beebe, D. J., A bi-polymer micro one-way valve. *Sensors and Actuators A: Physical* **2007,** 136, (1), 426-433.
546. Sugiura, S.; Szilagyi, A.; Sumaru, K.; Hattori, K.; Takagi, T.; Filipcsei, G.; Zrinyi, M.; Kanamori, T., On-demand microfluidic control by micropatterned light irradiation of a photoresponsive hydrogel sheet. *Lab on a Chip* **2009,** 9, (2), 196-198.
547. Yu, Q.; Bauer, J. M.; Moore, J. S., Responsive biomimetic hydrogel valve for microfluidics. *Applied Physics Letters* **2001,** 78, (17), 2589-2591.
548. Rahimi, S.; Sarraf, E.; Wong, G.; Takahata, K., Implantable drug delivery device using frequency-controlled wireless hydrogel microvalves. *Biomedical Microdevices* **2011,** 13, (2), 267-277.
549. Das, C.; Fredrickson, C. K.; Xia, Z.; Fan, Z. H., Device fabrication and integration with photodefinable microvalves for protein separation. *Sensors and Actuators A: Physical* **2007,** 134, (1), 271-277.
550. Seong, G. H.; Zhan, W.; Crooks, R. M., Fabrication of microchambers defined by photopolymerized hydrogels and weirs within microfluidic systems: Application to DNA hybridization. *Analytical Chemistry* **2002,** 74, (14), 3372-3377.
551. Wang, J.; Chen, Z.; Mauk, M.; Hong, K.-S.; Li, M.; Yang, S.; Bau, H., Self-Actuated, Thermo-Responsive Hydrogel Valves for Lab on a Chip. *Biomedical Microdevices* **2005,** 7, (4), 313-322.
552. Liu, C.; et al., Arrayed pH-responsive microvalves controlled by multiphase laminar flow. *Journal of Micromechanics and Microengineering* **2007,** 17, (10), 1985.
553. Yoshida, K.; Kikuchi, M.; Park, J.-H.; Yokota, S., Fabrication of micro electro-rheological valves (ER valves) by micromachining and experiments. *Sensors and Actuators A: Physical* **2002,** 95, 22-233.
554. Kim, J.-W.; Yoshida, K.; Kouda, K.; Yokota, S., A flexible electro-rheological microvalve (FERV) based on SU-8 cantilever structures and its application to microactuators. *Sensors and Actuators A: Physical* **2009,** 156, (2), 366-372.
555. Liu, L.; Niu, X.; Wen, W.; Sheng, P., Electrorheological fluid-actuated flexible platform. *Applied Physics Letters* **2006,** 88, 173505.
556. Niu, X.; Wen, W.; Lee, Y.-K., Electrorheological-fluid-based microvalves. *Applied Physics Letters* **2005,** 87, 243501.

557. Li, Z.; He, Q.; Ma, D.; Chen, H., On-chip integrated multi-thermo-actuated microvalves of poly(N-isopropylacrylamide) for microflow injection analysis. *Analytica Chimica Acta* **2010,** 665, (2), 107-112.
558. Luo, Q.; Mutlu, S.; Gianchandani, Y. B.; Svec, F.; Fréchet, J. M. J., Monolithic valves for microfluidic chips based on thermoresponsive polymer gels. *Electrophoresis* **2003,** 24, (21), 3694-3702.
559. Yu, C.; Mutlu, S.; Selvaganapathy, P.; Mastrangelo, C. H.; Svec, F.; Frechet, J. M. J., Flow Control Valves for Analytical Microfluidic Chips without Mechanical Parts Based on Thermally Responsive Monolithic Polymers. *Analytical Chemistry* **2003,** 75, (8), 1958-1961.
560. Pitchaimani, K.; Sapp, B. C.; Winter, A.; Gispanski, A.; Nishida, T.; Fan, Z. H., Manufacturable plastic microfluidic valves using thermal actuation. *Lab on a Chip* **2009,** 9, (21), 3082-3087.
561. Sershen, S. R.; Mensing, G. A.; Ng, M.; Halas, N. J.; Beebe, D. J.; West, J. L., Independent Optical Control of Microfluidic Valves Formed from Optomechanically Responsive Nanocomposite Hydrogels. *Advanced Materials* **2005,** 17, (11), 1366-1368.
562. Abi-Samra, K.; Hanson, R.; Madou, M.; Gorkin Iii, R. A., Infrared controlled waxes for liquid handling and storage on a CD-microfluidic platform. *Lab on a Chip* **2011,** 11, (4), 723-726.
563. Sugiura, S.; Sumaru, K.; Ohi, K.; Hiroki, K.; Takagi, T.; Kanamori, T., Photoresponsive polymer gel microvalves controlled by local light irradiation. *Sensors and Actuators A: Physical* **2007,** 140, (2), 176-184.
564. Chen, G.; Svec, F.; Knapp, D. R., Light-actuated high pressure-resisting microvalve for on-chip flow control based on thermo-responsive nanostructured polymer. *Lab on a Chip* **2008,** 8, (7), 1198-1204.
565. Feng, G.-H.; Chou, Y.-C., Fabrication and characterization of thermally driven fast turn-on microvalve with adjustable backpressure design. *Microelectronic Engineering* **2011,** 88, (2), 187-194.
566. Hua, Z.; Pal, R.; Srivannavit, O.; Burns, M. A.; Gulari, E., A light writable microfluidic "flash memory": Optically addressed actuator array with latched operation for microfluidic applications. *Lab on a Chip* **2008,** 8, (3), 488-491.
567. Song, W. H.; et al., Readily integrated, electrically controlled microvalves. *Journal of Micromechanics and Microengineering* **2008,** 18, (4), 045009.
568. Yang, B.; Lin, Q., A latchable microvalve using phase change of paraffin wax. *Sensors and Actuators A: Physical* **2007,** 134, (1), 194-200.
569. Park, J.-M.; Cho, Y.-K.; Lee, B.-S.; Lee, J.-G.; Ko, C., Multifunctional microvalves control by optical illumination on nanoheaters and its application in centrifugal microfluidic devices. *Lab on a Chip* **2007,** 7, (5), 557-564.
570. Kaigala, G. V.; Hoang, V. N.; Backhouse, C. J., Electrically controlled microvalves to integrate microchip polymerase chain reaction and capillary electrophoresis. *Lab on a Chip* **2008,** 8, (7), 1071-1078.
571. Debray, A.; et al., Thermal modification of the rigidity of micro-structures by the phase transition of a fusible alloy. *Journal of Micromechanics and Microengineering* **2009,** 19, (5), 055014.

572. Lee, D. G.; Shin, D. D.; Carman, G. P., Large flow rate/high frequency microvalve array for high performance actuators. *Sensors and Actuators A: Physical* **2007,** 134, (1), 257-263.
573. Chen, P.-J.; Rodger, D. C.; Humayun, M. S.; Tai, Y.-C., Floating-Disk Parylene Microvalves for Self-Pressure-Regulating Flow Controls. *Journal of Microelectromechanical Systems* **2008,** 17, (6), 1352-1361.
574. Nguyen, N.-T.; Truong, T.-Q.; Wong, K.-K.; Ho, S.-S.; Low, C. L.-N., Micro check valves for integration into polymeric microfluidic devices. *Journal of Micromechanics and Microengineering* **2004,** 14, (1), 69-75.
575. Li, B.; Chen, Q.; Lee, D.-G.; Woolman, J.; Carman, G. P., Development of large flow rate, robust, passive micro check valves for compact piezoelectrically actuated pumps. *Sensors and Actuators A: Physical* **2005,** A117, (2), 325-330.
576. Kim, J.; Baek, J.; Lee, K.; Park, Y.; Sun, K.; Lee, T.; Lee, S., Photopolymerized check valve and its integration into a pneumatic pumping system for biocompatible sample delivery. *Lab on a Chip* **2006,** 6, (8), 1091-1094.
577. Yang, B.; Lin, Q., Planar micro-check valves exploiting large polymer compliance. *Sensors and Actuators A: Physical* **2007,** 134, (1), 186-193.
578. Hirono-Hara, Y.; Noji, H.; Takeuchi, S., Single-biomolecule observation with micro one-way valves for rapid buffer exchange. *Journal of Applied Physics* **2009,** 105, (10), 102016-5.
579. Klammer, I.; et al., Numerical analysis and characterization of bionic valves for microfluidic PDMS-based systems. *Journal of Micromechanics and Microengineering* **2007,** 17, (7), S122.
580. Adams, M. L.; Johnston, M. L.; Scherer, A.; Quake, S. R., Polydimethylsiloxane based micro-fluidic diode. *Journal of Micromechanics and Microengineering* **2005,** 15, (8), 1517-1521.
581. Kirby, B. J.; Reichmuth, D. S.; Renzi, R. F.; Shepodd, T. J.; Wiedenman, B. J., Microfluidic routing of aqueous and organic flows at high pressures: fabrication and characterization of integrated polymer microvalve elements. *Lab on a Chip* **2005,** 5, (2), 184-190.
582. Seker, E.; Leslie, D. C.; Haj-Hariri, H.; Landers, J. P.; Utz, M.; Begley, M. R., Nonlinear pressure-flow relationships for passive microfluidic valves. *Lab on a Chip* **2009,** 9, (18), 2691-2697.
583. Hwang, H.; Kim, H.-H.; Cho, Y.-K., Elastomeric membrane valves in a disc. *Lab on a Chip* **2011,** 11, (8), 1434-1436.
584. Felton, M. J., The new generation of microvalves. *Analytical Chemistry* **2003,** 75, (19), A429-A432.
585. Hosokawa, K.; Omata, M.; Sato, K.; Maeda, M., Power-free sequential injection for microchip immunoassay toward point-of-care testing. *Lab on a Chip* **2006,** 6, (2), 236-241.
586. Melin, J.; Roxhed, N.; Gimenez, G.; Griss, P.; Van Der Wijngaart, W.; Stemme, G., A liquid-triggered liquid microvalve for on-chip flow control. *Sensors and Actuators B: Chemical* **2004,** 100, (3), 475-480.

587. Zhao, B.; Moore, J. S.; Beebe, D. J., Surface-Directed Liquid Flow Inside Microchannels. *Science* **2001,** 291, (5506), 1023-1026.
588. Takei, G.; Nonogi, M.; Hibara, A.; Kitamori, T.; Kim, H.-B., Tuning microchannel wettability and fabrication of multiple-step Laplace valves. *Lab on a Chip* **2007,** 7, (5), 596-602.
589. Feng, Y.; Zhou, Z.; Ye, X.; Xiong, J., Passive valves based on hydrophobic microfluidics. *Sensors and Actuators A: Physical* **2003,** 108, (1-3), 138-143.
590. Andersson, H.; van der Wijngaart, W.; Griss, P.; Niklaus, F.; Stemme, G., Hydrophobic valves of plasma deposited octafluorocyclobutane in DRIE channels. *Sensors and Actuators B: Chemical* **2001,** B75, (1-2), 136-41.
591. Glière, A.; Delattre, C., Modeling and fabrication of capillary stop valves for planar microfluidic systems. *Sensors and Actuators A: Physical* **2006,** 130-131, 601-608.
592. Cho, H.; Kim, H.-Y.; Kang, J. Y.; Kim, T. S., How the capillary burst microvalve works. *Journal of Colloid and Interface Science* **2007,** 306, (2), 379-385.
593. Zhao, B.; Moore, J. S.; Beebe, D. J., Pressure-Sensitive Microfluidic Gates Fabricated by Patterning Surface Free Energies Inside Microchannels. *Langmuir* **2002,** 19, (5), 1873-1879.
594. Nagai, H.; Irie, T.; Takahashi, J.; Wakida, S.-i., Flexible manipulation of microfluids using optically regulated adsorption/desorption of hydrophobic materials. *Biosensors and Bioelectronics* **2007,** 22, (9-10), 1968-1973.
595. Idota, N.; Kikuchi, A.; Kobayashi, J.; Sakai, K.; Okano, T., Microfluidic Valves Comprising Nanolayered Thermoresponsive Polymer-Grafted Capillaries. *Advanced Materials* **2005,** 17, (22), 2723-2727.
596. Londe, G.; Chunder, A.; Wesser, A.; Zhai, L.; Cho, H. J., Microfluidic valves based on superhydrophobic nanostructures and switchable thermosensitive surface for lab-on-a-chip (LOC) systems. *Sensors and Actuators B: Chemical* **2008,** 132, (2), 431-438.
597. Fadl, A.; Demming, S.; Zhang, Z.; Büttgenbach, S.; Krafczyk, M.; Meyer, D., A multifunction and bidirectional valve-less rectification micropump based on bifurcation geometry. *Microfluidics and Nanofluidics* **2010,** 9, (2), 267-280.
598. Lu, C.; Xie, Y.; Yang, Y.; Cheng, M. M. C.; Koh, C.-G.; Bai, Y.; Lee, L. J.; Juang, Y.-J., New Valve and Bonding Designs for Microfluidic Biochips Containing Proteins. *Analytical Chemistry* **2007,** 79, (3), 994-1001.
599. Izzo, I.; Accoto, D.; Menciassi, A.; Schmitt, L.; Dario, P., Modeling and experimental validation of a piezoelectric micropump with novel no-moving-part valves. *Sensors and Actuators A: Physical* **2007,** A133, (1), 128-140.
600. Singhal, V.; Garimella, S. V.; Murthy, J. Y., Low Reynolds number flow through nozzle-diffuser elements in valveless micropumps. *Sensors and Actuators A: Physical* **2004,** 113, (2), 226-235.
601. Nguyen, N.-T.; Lam, Y.-C.; Ho, S.-S.; Low, C. L.-N., Improvement of rectification effects in diffuser/nozzle structures with viscoelastic fluids. *Biomicrofluidics* **2008,** 2, (3), 034101-14.

602. Feldt, C.; Chew, L., Geometry-based macro-tool evaluation of non-moving-part valvular microchannels. *Journal of Micromechanics and Microengineering* **2002,** 12, 662-669.
603. Doh, I.; Cho, Y.-H., Passive flow-rate regulators using pressure-dependent autonomous deflection of parallel membrane valves. *Lab on a Chip* **2009,** 9, (14), 2070-2075.
604. Du, X.; Zhang, P.; Liu, Y.; Wu, Y., A passive through hole microvalve for capillary flow control in microfluidic systems. *Sensors and Actuators A: Physical* **2011,** 165, (2), 288-293.
605. Groisman, A.; Quake, S. R., A Microfluidic Rectifier: Anisotropic Flow Resistance at Low Reynolds Numbers. *Physical Review Letters* **2004,** 92, (9), 094501.
606. Frimat, J.-P.; Becker, M.; Chiang, Y.-Y.; Marggraf, U.; Janasek, D.; Hengstler, J. G.; Franzke, J.; West, J., A microfluidic array with cellular valving for single cell co-culture. *Lab on a Chip* **2011,** 11, (2), 231-237.
607. Zhang, C.; Xing, D.; Li, Y., Micropumps, microvalves, and micromixers within PCR microfluidic chips: Advances and trends. *Biotechnology Advances* **2007,** 25, (5), 483-514.
608. Nguyen, N.-T.; Huang, X.; Chuan, T. K., MEMS-Micropumps: A Review. *Journal of Fluids Engineering* **2002,** 124, (2), 384-392.
609. Laser, D. J.; Santiago, J. G., A review of micropumps. *Journal of Micromechanics and Microengineering* **2004,** 14, (6), 35-64.
610. Nisar, A.; Afzulpurkar, N.; Mahaisavariya, B.; Tuantranont, A., MEMS-based micropumps in drug delivery and biomedical applications. *Sensors and Actuators B: Chemical* **2008,** 130, (2), 917-942.
611. Amirouche, F.; Zhou, Y.; Johnson, T., Current micropump technologies and their biomedical applications. *Microsystem Technologies* **2009,** 15, (5), 647-666.
612. Iverson, B.; Garimella, S., Recent advances in microscale pumping technologies: a review and evaluation. *Microfluidics and Nanofluidics* **2008,** 5, (2), 145-174.
613. Luo, J. K.; et al., Moving-part-free microfluidic systems for lab-on-a-chip. *Journal of Micromechanics and Microengineering* **2009,** 19, (5), 054001.
614. Chen, L.; et al., Continuous dynamic flow micropumps for microfluid manipulation. *Journal of Micromechanics and Microengineering* **2008,** 18, (1), 013001.
615. Pamme, N., Magnetism and microfluidics. *Lab on a Chip* **2006,** 6, (1), 24-38.
616. Singhal, V.; Garimella, S. V.; Raman, A., Microscale pumping technologies for microchannel cooling systems. *Applied Mechanics Review* **2004,** 57, (3), 191-221.
617. Woias, P., Micropumps - past, progress and future prospects. *Sensors and Actuators B: Chemical* **2005,** B105, (1), 28-38.
618. Elwenspoek, M.; Lammerink, T. S. J.; Miyake, R.; Fluitman, J. H. J., Towards integrated microliquid handling systems. *Journal of Micromechanics and Microengineering* **1994,** 4, 227-245.
619. Shoji, S.; Esashi, M., Microflow devices and systems. *Journal of Micromechanics and Microengineering* **1994,** 4, 157-71.
620. Gravesen, P.; Branebjerg, J.; Jensen, O. S., Microfluidics - a review. *Journal of Micromechanics and Microengineering* **1993,** 3, (4), 168-182.

621. Grover, W. H.; Muhlen, M. G. v.; Manalis, S. R., Teflon films for chemically-inert microfluidic valves and pumps. *Lab on a Chip* **2008,** 8, (6), 913-918.
622. Zhang, W.; Lin, S.; Wang, C.; Hu, J.; Li, C.; Zhuang, Z.; Zhou, Y.; Mathies, R. A.; Yang, C. J., PMMA/PDMS valves and pumps for disposable microfluidics. *Lab on a Chip* **2009,** 9, (21), 3088-3094.
623. Jeong, O. C.; Konishi, S., The self-generated peristaltic motion of cascaded pneumatic actuators for micro pumps. *Journal of Micromechanics and Microengineering* **2008,** 18, (8), 085017.
624. Jeong, O. C.; Konishi, S., Fabrication of Peristaltic Micropump Driven by a Single-Phase Pneumatic Force. *Japanese Journal of Applied Physics* **2010,** 49, 056506.
625. Yang, Y.-N.; Hsiung, S.-K.; Lee, G.-B., A pneumatic micropump incorporated with a normally closed valve capable of generating a high pumping rate and a high back pressure. *Microfluidics and Nanofluidics* **2009,** 6, (6), 823-833.
626. Liu, C.-Y.; Rick, J.; Chou, T.-C.; Lee, H.-H.; Lee, G.-B., Integrated microfluidic system for electrochemical sensing of urinary proteins. *Biomedical Microdevices* **2009,** 11, (1), 201-211.
627. Wang, C.-H.; Lee, G.-B., Automatic bio-sampling chips integrated with micro-pumps and micro-valves for disease detection. *Biosensors and Bioelectronics* **2005,** 21, (3), 419-425.
628. Grover, W. H.; Skelley, A. M.; Liu, C. N.; Lagally, E. T.; Mathies, R. A., Monolithic membrane valves and diaphragm pumps for practical large-scale integration into glass microfluidic devices. *Sensors and Actuators B: Chemical* **2003,** 89, (3), 315-323.
629. Sundararajan, N.; Kim, D.; Berlin, A. A., Microfluidic operations using deformable polymer membranes fabricated by single layer soft lithography. *Lab on a Chip* **2005,** 5, (3), 350-354.
630. Ni, J.; et al., A planar PDMS micropump using in-contact minimized-leakage check valves. *Journal of Micromechanics and Microengineering* **2010,** 20, (9), 095033.
631. Goulpeau, J.; Trouchet, D.; Ajdari, A.; Tabeling, P., Experimental study and modeling of polydimethylsiloxane peristaltic micropumps. *Journal of Applied Physics* **2005,** 98, (4), 044914/1-044914/9.
632. Huang, S.; Li, C.; Lin, B.; Qin, J., Microvalve and micropump controlled shuttle flow microfluidic device for rapid DNA hybridization. *Lab on a Chip* **2010,** 10, (21), 2925-2931.
633. Tseng, H.-Y.; Wang, C.-H.; Lin, W.-Y.; Lee, G.-B., Membrane-activated microfluidic rotary devices for pumping and mixing. *Biomedical Microdevices* **2007,** 9, (4), 545-54.
634. Huang, C.-W.; et al., Pneumatic micropumps with serially connected actuation chambers. *Journal of Micromechanics and Microengineering* **2006,** 16, (11), 2265.
635. Cole, M. C.; Desai, A. V.; Kenis, P. J. A., Two-layer multiplexed peristaltic pumps for high-density integrated microfluidics. *Sensors and Actuators B: Chemical* **2011,** 151, (2), 384-393.

636. Geipel, A.; Goldschmidtböing, F.; Doll, A.; Jantscheff, P.; Esser, N.; Massing, U.; Woias, P., An implantable active microport based on a self-priming high-performance two-stage micropump. *Sensors and Actuators A: Physical* **2008,** 145-146, 414-422.
637. Doll, A. F.; Wischke, M.; Geipel, A.; Goldschmidtboeing, F.; Ruthmann, O.; Hopt, U. T.; Schrag, H.-J.; Woias, P., A novel artificial sphincter prosthesis driven by a four-membrane silicon micropump. *Sensors and Actuators A: Physical* **2007,** 139, (1-2), 203-209.
638. Geipel, A.; Goldschmidtboeing, F.; Jantscheff, P.; Esser, N.; Massing, U.; Woias, P., Design of an implantable active microport system for patient specific drug release. *Biomedical Microdevices* **2008,** 10, (4), 469-478.
639. Wang, S.; Huang, X.; Yang, C., Valveless micropump with acoustically featured pumping chamber. *Microfluidics and Nanofluidics* **2010,** 8, (4), 549-555.
640. Olsson, A.; Enoksson, P.; Stemme, G.; Stemme, E., Micromachined Flat-Walled Valveless Diffuser Pumps. *Journal of Microelectromechanical Systems* **1997,** 6, (2), 161-166.
641. Hwang, I.-H.; et al., A novel micropump with fixed-geometry valves and low leakage flow. *Journal of Micromechanics and Microengineering* **2007,** 17, (8), 1632.
642. Hayamizu, S.; Higashino, K.; Fujii, Y.; Sando, Y.; Yamamoto, K., Development of a bi-directional valve-less silicon micro pump controlled by driving waveform. *Sensors and Actuators A: Physical* **2003,** A103, (1-2), 83-7.
643. Husband, B.; Bu, M.; Evans, A. G. R.; Melvin, T., Investigation for the operation of an integrated peristaltic micropump. *Journal of Micromechanics and Microengineering* **2004,** 14, (9), S64-S69.
644. Truong, T.-Q.; Nguyen, N.-T., A polymeric piezoelectric micropump based on lamination technology. *Journal of Micromechanics and Microengineering* **2004,** 14, (4), 632-638.
645. Feng, G.-H.; Kim, E. S., Micropump based on PZT unimorph and one-way parylene valves. *Journal of Micromechanics and Microengineering* **2004,** 14, (4), 429-435.
646. Kan, J.; Tang, K.; Liu, G.; Zhu, G.; Shao, C., Development of serial-connection piezoelectric pumps. *Sensors and Actuators A: Physical* **2008,** 144, (2), 321-327.
647. Hsu, Y. C.; Le, N. B., Equivalent electrical network for performance characterization of piezoelectric peristaltic micropump. *Microfluidics and Nanofluidics* **2009,** 7, (2), 237-248.
648. Jang, L.-S.; Yu, Y.-C., Peristaltic micropump system with piezoelectric actuators. *Microsystem Technologies* **2008,** 14, (2), 241-248.
649. Dinh, T. X.; Dau, V. T.; Sugiyama, S.; Pham, P. H., Fluidic device with pumping and sensing functions for precise flow control. *Sensors and Actuators B: Chemical* **2010,** 150, (2), 819-824.
650. Liu, G.; Shen, C.; Yang, Z.; Cai, X.; Zhang, H., A disposable piezoelectric micropump with high performance for closed-loop insulin therapy system. *Sensors and Actuators A: Physical* **2010,** 163, (1), 291-296.
651. Su, G.; Pidaparti, R., Transport of drug particles in micropumps through novel actuation. *Microsystem Technologies* **2010,** 16, (4), 595-606.

652. Trenkle, F.; Haeberle, S.; Zengerle, R., Normally-closed peristaltic micropump with re-usable actuator and disposable fluidic chip. *Procedia Chemistry* **2009,** 1, (1), 1515-1518.
653. Yokokawa, R.; Saika, T.; Nakayama, T.; Fujita, H.; Konishi, S., On-chip syringe pumps for picoliter-scale liquid manipulation. *Lab on a Chip* **2006,** 6, (8), 1062-1066.
654. Gu, W.; Zhu, X.; Futai, N.; Cho, B. S.; Takayama, S., Computerized microfluidic cell culture using elastomeric channels and Braille displays. *Proceedings of the National Academy of Sciences of the United States of America* **2004,** 101, (45), 15861-15866.
655. Lee, C.-Y.; et al., A MEMS-based valveless impedance pump utilizing electromagnetic actuation. *Journal of Micromechanics and Microengineering* **2008,** 18, (3), 035044.
656. Shen, M.; et al., A high-performance compact electromagnetic actuator for a PMMA ball-valve micropump. *Journal of Micromechanics and Microengineering* **2008,** 18, (2), 025031.
657. Hatch, A.; Kamholz, A. E.; Holman, G.; Yager, P.; Bohringer, K. F., A ferrofluidic magnetic micropump. *Journal of Microelectromechanical Systems* **2001,** 10, (2), 215-221.
658. Khoo, M.; Liu, C., Micro magnetic silicone elastomer membrane actuator. *Sensors and Actuators A: Physical* **2001,** 89, (3), 259-266.
659. Pan, T.; McDonald, S. J.; Kai, E. M.; Ziaie, B., A magnetically driven PDMS micropump with ball check-valves. *Journal of Micromechanics and Microengineering* **2005,** 15, (5), 1021-1026.
660. Santra, S.; Holloway, P.; Batich, C. D., Fabrication and testing of a magnetically actuated micropump. *Sensors and Actuators B: Chemical* **2002,** B87, (2), 358-64.
661. Yin, H.-L.; Huang, Y.-C.; Fang, W.; Hsieh, J., A novel electromagnetic elastomer membrane actuator with a semi-embedded coil. *Sensors and Actuators A: Physical* **2007,** 139, (1-2), 194-202.
662. Kim, E.-G.; Oh, J.-g.; Choi, B., A study on the development of a continuous peristaltic micropump using magnetic fluids. *Sensors and Actuators A: Physical* **2006,** A128, (1), 43-51.
663. Lee, C.-Y.; Chen, Z.-H., Valveless impedance micropump with integrated magnetic diaphragm. *Biomedical Microdevices* **2010,** 12, (2), 197-205.
664. Kavcic, B.; Babic, D.; Osterman, N.; Podobnik, B.; Poberaj, I., Magnetically actuated microrotors with individual pumping speed and direction control. *Applied Physics Letters* **2009,** 95, (2), 023504-3.
665. Zordan, E.; Amirouche, F.; Zhou, Y., Principle design and actuation of a dual chamber electromagnetic micropump with coaxial cantilever valves. *Biomedical Microdevices* **2010,** 12, (1), 55-62.
666. Addae-Mensah, K. A.; Cheung, Y. K.; Fekete, V.; Rendely, M. S.; Sia, S. K., Actuation of elastomeric microvalves in point-of-care settings using handheld, battery-powered instrumentation. *Lab on a Chip* **2010,** 10, (12), 1618-1622.
667. Malouin Jr, B. A.; Vogel, M. J.; Olles, J. D.; Cheng, L.; Hirsa, A. H., Electromagnetic liquid pistons for capillarity-based pumping. *Lab on a Chip* **2011,** 11, (3), 393-397.

668. Pilarski, P. M.; Adamia, S.; Backhouse, C. J., An adaptable microvalving system for on-chip polymerase chain reactions. *Journal of Immunological Methods* **2005,** 305, (1), 48-58.
669. Yoo, J.-C.; Choi, Y. J.; Kang, C. J.; Kim, Y.-S., A novel polydimethylsiloxane microfluidic system including thermopneumatic-actuated micropump and Paraffin-actuated microvalve. *Sensors and Actuators A: Physical* **2007,** 139, (1-2), 216-220.
670. Yoo, J.-C.; Moon, M.-C.; Kang, C. J.; Jeon, D.; Kim, Y.-S., Dynamic Characteristics of the Micro-Fluidic Systems Actuated by Thermopneumatic-Method. *Japanese Journal of Applied Physics* **2006,** 45 519.
671. Kim, J.-H.; Na, K.-H.; Kang, C. J.; Kim, Y.-S., A disposable thermopneumatic-actuated micropump stacked with PDMS layers and ITO-coated glass. *Sensors and Actuators A: Physical* **2005,** A120, (2), 365-369.
672. Samel, B.; Sandstrom, N.; Griss, P.; Stemme, G., Liquid Aspiration and Dispensing Based on an Expanding PDMS Composite. *Journal of Microelectromechanical Systems* **2008,** 17, (5), 1254-1262.
673. Jeong, O. C.; Park, S. W.; Yang, S. S.; Pak, J. J., Fabrication of a peristaltic PDMS micropump. *Sensors and Actuators A: Physical* **2005,** A123-A124, 453-458.
674. Yang, Y.-J.; Liao, H.-H., Development and characterization of thermopneumatic peristaltic micropumps. *Journal of Micromechanics and Microengineering* **2009,** 19, (2), 025003.
675. Cooney, C. G.; Towe, B. C., A thermopneumatic dispensing micropump. *Sensors and Actuators A: Physical* **2004,** A116, (3), 519-524.
676. Jun, D. H.; Sim, W. Y.; Yang, S. S., A novel constant delivery thermopneumatic micropump using surface tensions. *Sensors and Actuators A: Physical* **2007,** 139, (1-2), 210-215.
677. Ha, S.-M.; Cho, W.; Ahn, Y., Disposable thermo-pneumatic micropump for bio lab-on-a-chip application. *Microelectronic Engineering* **2009,** 86, (4-6), 1337-1339.
678. Chia, B. T.; Liao, H.-H.; Yang, Y.-J., A novel thermo-pneumatic peristaltic micropump with low temperature elevation on working fluid. *Sensors and Actuators A: Physical* **2011,** 165, (1), 86-93.
679. Benard, W. L.; Kahn, H.; Heuer, A. H.; Huff, M. A., Thin-film shape-memory alloy actuated micropumps. *Journal of Microelectromechanical Systems* **1998,** 7, (2), 245-251.
680. Shkolnikov, V.; Ramunas, J.; Santiago, J. G., A self-priming, roller-free, miniature, peristaltic pump operable with a single, reciprocating actuator. *Sensors and Actuators A: Physical* **2010,** 160, (1-2), 141-146.
681. Bertarelli, E.; Corigliano, A.; Greiner, A.; Korvink, J. G., Design of high stroke electrostatic micropumps: a charge control approach with ring electrodes. *Microsystem Technologies* **2011,** 17, 165-173.
682. Astle, A. A.; Kim, H. S.; Bernal, L. P.; Najafi, K.; Washabaugh, P. D., Theoretical and experimental performance of a high frequency gas micropump. *Sensors and Actuators A: Physical* **2007,** 134, (1), 245-256.

683. Teymoori, M. M.; Abbaspour-Sani, E., Design and simulation of a novel electrostatic peristaltic micromachined pump for drug delivery applications. *Sensors and Actuators A: Physical* **2005,** A117, (2), 222-229.
684. Xie, J.; Shih, J.; Lin, Q.; Yang, B.; Tai, Y.-C., Surface micromachined electrostatically actuated micro peristaltic pump. *Lab on a Chip* **2004,** 4, (5), 495-501.
685. Machauf, A.; et al., A membrane micropump electrostatically actuated across the working fluid. *Journal of Micromechanics and Microengineering* **2005,** 15, (12), 2309.
686. Tsai, N.-C.; Sue, C.-Y., Fabrication and analysis of ionic conductive polymer films for micro drug delivery systems. *Sensors and Actuators A: Physical* **2008,** 141, (2), 670-676.
687. Loverich, J. J.; Kanno, I.; Kotera, H., Concepts for a new class of all-polymer micropumps. *Lab on a Chip* **2006,** 6, (9), 1147-1154.
688. Santos, J.; Lopes, B.; Branco, P. J. C., Ionic polymer-metal composite material as a diaphragm for micropump devices. *Sensors and Actuators A: Physical* **2010,** 161, (1-2), 225-233.
689. Nguyen, T. T.; Goo, N. S.; Nguyen, V. K.; Yoo, Y.; Park, S., Design, fabrication, and experimental characterization of a flap valve IPMC micropump with a flexibly supported diaphragm. *Sensors and Actuators A: Physical* **2008,** 141, (2), 640-648.
690. Price, A. K.; Anderson, K. M.; Culbertson, C. T., Demonstration of an integrated electroactive polymer actuator on a microfluidic electrophoresis device. *Lab on a Chip* **2009,** 9, (14), 2076-2084.
691. Fang, Y.; Tan, X., A novel diaphragm micropump actuated by conjugated polymer petals: Fabrication, modeling, and experimental results. *Sensors and Actuators A: Physical* **2010,** 158, (1), 121-131.
692. Naka, Y.; Fuchiwaki, M.; Tanaka, K., A micropump driven by a polypyrrole-based conducting polymer soft actuator. *Polymer International* **2010,** 59, (3), 352-356.
693. Park, J.; Kim, I. C.; Baek, J.; Cha, M.; Kim, J.; Park, S.; Lee, J.; Kim, B., Micro pumping with cardiomyocyte-polymer hybrid. *Lab on a Chip* **2007,** 7, (10), 1367-1370.
694. Tanaka, Y.; Sato, K.; Shimizu, T.; Yamato, M.; Okano, T.; Kitamori, T., A micro-spherical heart pump powered by cultured cardiomyocytes. *Lab on a Chip* **2007,** 7, (2), 207-212.
695. Kim, Min J.; Breuer, K. S., Microfluidic Pump Powered by Self-Organizing Bacteria. *Small* **2008,** 4, (1), 111-118.
696. Spetzler, D.; York, J.; Dobbin, C.; Martin, J.; Ishmukhametov, R.; Day, L.; Yu, J.; Kang, H.; Porter, K.; Hornung, T.; Frasch, W. D., Recent developments of bio-molecular motors as on-chip devices using single molecule techniques. *Lab on a Chip* **2007,** 7, (12), 1633-1643.
697. Tanaka, Y.; Morishima, K.; Shimizu, T.; Kikuchi, A.; Yamato, M.; Okano, T.; Kitamori, T., An actuated pump on-chip powered by cultured cardiomyocytes. *Lab on a Chip* **2006,** 6, (3), 362-368.
698. Lui, C.; Stelick, S.; Cady, N.; Batt, C., Low-power microfluidic electro-hydraulic pump (EHP). *Lab on a Chip* **2010,** 10, (1), 74-79.
699. Yang, K.; Wu, J., Investigation of microflow reversal by ac electrokinetics in orthogonal electrodes for micropump design. *Biomicrofluidics* **2008,** 2, (2), 024101-8.

700. Takashima, A.; Kojima, K.; Suzuki, H., Autonomous Microfluidic Control by Chemically Actuated Micropumps and Its Application to Chemical Analyses. *Analytical Chemistry* **2010,** 82, (16), 6870-6876.
701. da Silva, A. K.; Kobayashi, M. H.; Coimbra, C. F. M., Optimal design of non-Newtonian, micro-scale viscous pumps for biomedical devices. *Biotechnology and Bioengineering* **2007,** 96, (1), 37-47.
702. Yobas, L.; Tang, K.-C.; Yong, S.-E.; Ong, E. K.-Z., A disposable planar peristaltic pump for lab-on-a-chip. *Lab on a Chip* **2008,** 8, (5), 660-662.
703. El-Sadi, H.; Esmail, N., Simulation of three-dimensional transient performance in micro-pump. *Sensors and Actuators B: Chemical* **2006,** 115, (1), 510-518.
704. Lei, K. F.; Law, W. C.; Suen, Y.-K.; Li, W. J.; Yam, Y.; Ho, H. P.; Kong, S.-K., A vortex pump-based optically-transparent microfluidic platform for biotech and medical applications. *Proceedings of the Institution of Mechanical Engineers -- Part H -- Journal of Engineering in Medicine* **2007,** 221, 129-141.
705. Matteucci, M.; Casella, M.; Bedoni, M.; Donetti, E.; Fanetti, M.; De Angelis, F.; Gramatica, F.; Di Fabrizio, E., A compact and disposable transdermal drug delivery system. *Microelectronic Engineering* **2008,** 85, (5-6), 1066-1073.
706. Lim, K.; Kim, S.; Hahn, J. H., Roller-type squeezing pump with picoliter handling capability. *Sensors and Actuators B: Chemical* **2003,** B92, (1-2), 208-14.
707. Waldschik, A.; Büttgenbach, S., Micro gear pump with internal electromagnetic drive. *Microsystem Technologies* **2010,** 16, (8), 1581-1587.
708. Skafte-Pedersen, P.; Sabourin, D.; Dufva, M.; Snakenborg, D., Multi-channel peristaltic pump for microfluidic applications featuring monolithic PDMS inlay. *Lab on a Chip* **2009,** 9, (20), 3003-3006.
709. Koch, C.; Remcho, V.; Ingle, J., PDMS and tubing-based peristaltic micropumps with direct actuation. *Sensors and Actuators B: Chemical* **2009,** 135, (2), 664-670.
710. Ducree, J.; et al., The centrifugal microfluidic Bio-Disk platform. *Journal of Micromechanics and Microengineering* **2007,** 17, (7), S103.
711. Zoval, J. V.; Madou, M. J., Centrifuge-based fluidic platforms. *Proceedings of the IEEE* **2004,** 92, (1), 140-53.
712. Chen, M.; Xing, X.; Liu, Z.; Zhu, Y.; Liu, H.; Yu, Y.; Cheng, F., Photodeformable polymer material: towards light-driven micropump applications. *Applied Physics A: Materials Science and Processing* **2010,** 100, (1), 39-43.
713. Adamiak, K.; Mizuno, A.; Nakano, M., Electrohydrodynamic Flow in Optoelectrostatic Micropump: Experiment Versus Numerical Simulation. *IEEE Transactions on Industry Applications* **2009,** 45, (2), 615-622.
714. Terray, A.; Oakey, J.; Marr, D. W. M., Microfluidic control using colloidal devices. *Science* **2002,** 296, (5574), 1841-4.
715. Maruo, S.; Inoue, H., Optically driven micropump produced by three-dimensional two-photon microfabrication. *Applied Physics Letters* **2006,** 89, (14), 144101/1-144101/3.
716. Dijkink, R.; Ohl, C.-D., Laser-induced cavitation based micropump. *Lab on a Chip* **2008,** 8, (10), 1676-1681.

717. Liu, G. L.; Kim, J.; Lu, Y.; Lee, L. P., Optofluidic control using photothermal nanoparticles. *Nature Materials* **2006,** 5, (1), 27-32.
718. Leoni, M.; Kotar, J.; Bassetti, B.; Cicuta, P.; Lagomarsino, M. C., A basic swimmer at low Reynolds number. *Soft Matter* **2009,** 5, (2), 472-476.
719. Squires, T. M., Induced-charge electrokinetics: fundamental challenges and opportunities. *Lab on a Chip* **2009,** 9, (17), 2477-2483.
720. Wang, X.; Wang, S.; Gendhar, B.; Cheng, C.; Byun, C. K.; Li, G.; Zhao, M.; Liu, S.; Byun, C. K.; Zhao, M., Electroosmotic pumps for microflow analysis. *TrAC Trends in Analytical Chemistry* **2009,** 28, (1), 64-74.
721. Wang, X.; Cheng, C.; Wang, S.; Liu, S., Electroosmotic pumps and their applications in microfluidic systems. *Microfluidics and Nanofluidics* **2009,** 6, (2), 145-162.
722. Huang, C.-C.; Bazant, M. Z.; Thorsen, T., Ultrafast high-pressure AC electro-osmotic pumps for portable biomedical microfluidics. *Lab on a Chip* **2010,** 10, (1), 80-85.
723. Kivanc, F. C.; Litster, S., Pumping with electroosmosis of the second kind in mesoporous skeletons. *Sensors and Actuators B: Chemical* **2011,** 151, (2), 394-401.
724. Wang, P.; Chen, Z.; Chang, H.-C., A new electro-osmotic pump based on silica monoliths. *Sensors and Actuators B: Chemical* **2006,** 113, (1), 500-509.
725. Gitlin, I.; Stroock, A. D.; Whitesides, G. M.; Ajdari, A., Pumping based on transverse electrokinetic effects. *Applied Physics Letters* **2003,** 83, 1486.
726. Yairi, M.; Richter, C., Massively parallel microfluidic pump. *Sensors and Actuators A: Physical* **2007,** A137, (2), 350-356.
727. Hilber, W.; Weiss, B.; Saeed, A.; Holly, R.; Jakoby, B., Density-dependent particle separation in microchannels using 3D AC-driven electro-osmotic pumps. *Sensors and Actuators A: Physical* **2009,** 156, (1), 115-120.
728. Mruetusatorn, P.; Mahfouz, M. R.; Wu, J., Low-voltage dynamic control for DC electroosmotic devices. *Sensors and Actuators A: Physical* **2009,** 153, (2), 237-243.
729. McKnight, T. E.; Culbertson, C. T.; Jacobson, S. C.; Ramsey, J. M., Electroosmotically Induced Hydraulic Pumping with Integrated Electrodes on Microfluidic Devices. *Analytical Chemistry* **2001,** 73, (16), 4045-4049.
730. Brask, A.; Snakenborg, D.; Kutter, J. P.; Bruus, H., AC electroosmotic pump with bubble-free palladium electrodes and rectifying polymer membrane valves. *Lab on a Chip* **2006,** 6, (2), 280-288.
731. Lu, Q.; Collins, G. E., A fritless, EOF microchip pump for high pressure pumping of aqueous and organic solvents. *Lab on a Chip* **2009,** 9, (7), 954-960.
732. Lazar, I. M.; Karger, B. L., Multiple Open-Channel Electroosmotic Pumping System for Microfluidic Sample Handling. *Analytical Chemistry* **2002,** 74, (24), 6259-6268.
733. Seibel, K.; et al., A programmable planar electroosmotic micropump for lab-on-a-chip applications. *Journal of Micromechanics and Microengineering* **2008,** 18, (2), 025008.

734. Joo, S.; Chung, T. D.; Kim, H. C., A rapid field-free electroosmotic micropump incorporating charged microchannel surfaces. *Sensors and Actuators B: Chemical* **2007,** 123, (2), 1161-1168.
735. Nie, F.-Q.; Macka, M.; Barron, L.; Connolly, D.; Kent, N.; Paull, B., Robust monolithic silica-based on-chip electro-osmotic micro-pump. *The Analyst* **2007,** 132, (5), 417-424.
736. Chang, S. T.; Paunov, V. N.; Petsev, D. N.; Velev, O. D., Remotely powered self-propelling particles and micropumps based on miniature diodes. *Nature Materials* **2007,** 6, (3), 235-240.
737. He, C.; Lu, J. J.; Jia, Z.; Wang, W.; Wang, X.; Dasgupta, P. K.; Liu, S., Flow Batteries for Microfluidic Networks: Configuring An Electroosmotic Pump for Nonterminal Positions. *Analytical Chemistry* **2011,** 83, (7), 2430-2433.
738. Shin, W.; Lee, J. M.; Nagarale, R. K.; Shin, S. J.; Heller, A., A Miniature, Nongassing Electroosmotic Pump Operating at 0.5 V. *Journal of the American Chemical Society* **2011,** 133, (8), 2374-2377.
739. Holtappels, M.; Stubbe, M.; Gimsa, J., ac-field-induced fluid pumping in microsystems with asymmetric temperature gradients. *Physical Review E* **2009,** 79, (2), 026309.
740. Felten, M.; Staroske, W.; Jaeger, M. S.; Schwille, P.; Duschl, C., Accumulation and filtering of nanoparticles in microchannels using electrohydrodynamically induced vortical flows. *Electrophoresis* **2008,** 29, (14), 2987-2996.
741. Felten, M.; Geggier, P.; Jager, M.; Duschl, C., Controlling electrohydrodynamic pumping in microchannels through defined temperature fields. *Physics of Fluids* **2006,** 18, 051707.
742. Yang, L.-J.; Wang, J.-M.; Ko, K.-C.; Shih, W.-P.; Dai, C.-L., A circular microchannel integrated with embedded sprial electrodes used for fluid transportation. *Sensors and Actuators A: Physical* **2007,** 139, (1-2), 172-177.
743. Singhal, V.; Garimella, S. V., Induction electrohydrodynamics micropump for high heat flux cooling. *Sensors and Actuators A: Physical* **2007,** 134, (2), 650-659.
744. Stubbe, M.; et al., A new working principle for ac electro-hydrodynamic on-chip micro-pumps. *Journal of Physics D: Applied Physics* **2007,** 40, (21), 6850.
745. Foroughi, P.; Shooshtari, A.; Dessiatoun, S.; Ohadi, M. M., Experimental Characterization of an Electrohydrodynamic Micropump for Cryogenic Spot Cooling Applications. *Heat Transfer Engineering* **2010,** 31, (2), 119 - 126.
746. Iverson, B.; Cremaschi, L.; Garimella, S., Effects of discrete-electrode configuration on traveling-wave electrohydrodynamic pumping. *Microfluidics and Nanofluidics* **2009,** 6, (2), 221-230.
747. Zeng, J.; Korsmeyer, T., Principles of droplet electrohydrodynamics for lab-on-a-chip. *Lab on a Chip* **2004,** 4, (4), 265-277.
748. Eijkel, J. C. T.; Dalton, C.; Hayden, C. J.; Burt, J. P. H.; Manz, A., A circular ac magnetohydrodynamic micropump for chromatographic applications. *Sensors and Actuators B: Chemical* **2003,** B92, (1-2), 215-21.

749. Homsy, A.; Koster, S.; Eijkel, J. C. T.; van den Berg, A.; Lucklum, F.; Verpoorte, E.; de Rooij, N. F., A high current density DC magnetohydrodynamic (MHD) micropump. *Lab on a Chip* **2005,** 5, (4), 466-471.
750. Kang, H.-J.; Choi, B., Development of the MHD micropump with mixing function. *Sensors and Actuators A: Physical* **2011,** 165, (2), 439-445.
751. Lemoff, A. V.; Lee, A. P., AC magnetohydrodynamic micropump. *Sensors and Actuators B: Chemical* **2000,** 63, (3), 178-185.
752. Jang, J.; Lee, S. S., Theoretical and experimental study of MHD (magnetohydrodynamic) micropump. *Sensors and Actuators A: Physical* **2000,** 80, (1), 84-89.
753. Patel, V.; Kassegne, S. K., Electroosmosis and thermal effects in magnetohydrodynamic (MHD) micropumps using 3D MHD equations. *Sensors and Actuators B: Chemical* **2007,** 122, (1), 42-52.
754. Homsy, A.; Linder, V.; Lucklum, F.; de Rooij, N. F., Magnetohydrodynamic pumping in nuclear magnetic resonance environments. *Sensors and Actuators B: Chemical* **2007,** 123, (1), 636-646.
755. Nabavi, M.; Mongeau, L., Numerical analysis of high frequency pulsating flows through a diffuser-nozzle element in valveless acoustic micropumps. *Microfluidics and Nanofluidics* **2009,** 7, (5), 669-681.
756. Dissanayake, D. W.; et al., Finite element modelling of surface acoustic wave device based corrugated microdiaphragms. *Smart Materials and Structures* **2009,** 18, (9), 095030.
757. Guttenberg, Z.; Muller, H.; Habermuller, H.; Geisbauer, A.; Pipper, J.; Felbel, J.; Kielpinski, M.; Scriba, J.; Wixforth, A., Planar chip device for PCR and hybridization with surface acoustic wave pump. *Lab on a Chip* **2005,** 5, (3), 308-317.
758. Yeo, L. Y.; Friend, J. R., Ultrafast microfluidics using surface acoustic waves. *Biomicrofluidics* **2009,** 3, (1), 012002-23.
759. Nguyen, N.-T.; Meng, A. H.; Black, J.; White, R. M., Integrated flow sensor for in situ measurement and control of acoustic streaming in flexural plate wave micropumps. *Sensors and Actuators A: Physical* **2000,** 79, (2), 115-121.
760. Girardo, S.; Cecchini, M.; Beltram, F.; Cingolani, R.; Pisignano, D., Polydimethylsiloxane-LiNbO3 surface acoustic wave micropump devices for fluid control into microchannels. *Lab on a Chip* **2008,** 8, (9), 1557-1563.
761. Chiu, S.-H.; Liu, C.-H., An air-bubble-actuated micropump for on-chip blood transportation. *Lab on a Chip* **2009,** 9, (11), 1524-1533.
762. Cheng, C.-M.; Liu, C.-H., An Electrolysis-Bubble-Actuated Micropump Based on the Roughness Gradient Design of Hydrophobic Surface. *Journal of Microelectromechanical Systems* **2007,** 16, (5), 1095-1105.
763. Chan, S.-C.; Chen, C.-R.; Liu, C.-H., A bubble-activated micropump with high-frequency flow reversal. *Sensors and Actuators A: Physical* **2010,** 163, (2), 501-509.
764. Meng, D. D.; Kim, C.-J. C. J., Micropumping of liquid by directional growth and selective venting of gas bubbles. *Lab on a Chip* **2008,** 8, (6), 958-968.
765. Peng, X. Y., A micro surface tension pump (MISPU) in a glass microchip. *Lab on a Chip* **2011,** 11, (1), 132-138.

766. Resto, P. J.; Mogen, B. J.; Berthier, E.; Williams, J. C., An automated microdroplet passive pumping platform for high-speed and packeted microfluidic flow applications. *Lab on a Chip* **2010,** 10, (1), 23-26.
767. Berthier, E.; Beebe, D. J., Flow rate analysis of a surface tension driven passive micropump. *Lab on a Chip* **2007,** 7, (11), 1475-1478.
768. Xu, Z.-R.; Zhong, C.-H.; Guan, Y.-X.; Chen, X.-W.; Wang, J.-H.; Fang, Z.-L., A microfluidic flow injection system for DNA assay with fluids driven by an on-chip integrated pump based on capillary and evaporation effects. *Lab on a Chip* **2008,** 8, (10), 1658-1663.
769. Chen, I. J.; Eckstein, E. C.; Lindner, E., Computation of transient flow rates in passive pumping micro-fluidic systems. *Lab on a Chip* **2009,** 9, (1), 107-114.
770. Tadigadapa, S.; Mateti, K., Piezoelectric MEMS sensors: state-of-the-art and perspectives. *Measurement Science and Technology* **2009,** 20, (9), 092001.
771. Xu, X.-H.; Chu, J.-R., Preparation of a high-quality PZT thick film with performance comparable to those of bulk materials for applications in MEMS. *Journal of Micromechanics and Microengineering* **2008,** 18, (6), 065001.
772. Hindrichsen, C. G.; Lou-Møller, R.; Hansen, K.; Thomsen, E. V., Advantages of PZT thick film for MEMS sensors. *Sensors and Actuators A: Physical* **2010,** 163, (1), 9-14.
773. Muralt, P., Recent Progress in Materials Issues for Piezoelectric MEMS. *Journal of the American Ceramic Society* **2008,** 91, 1385-1396.
774. Safari, A.; Akdogan, E. K., Rapid Prototyping of Novel Piezoelectric Composites. *Ferroelectrics* **2006,** 331, 153-179.
775. Kryszewski, M., Fifty Years of Study of the Piezoelectric Properties of Macromolecular Structured Biological Materials. *Acta Physica Polonica, A* **2004,** 105, (4), 389-408.
776. Panda, P., Review: environmental friendly lead-free piezoelectric materials. *Journal of Materials Science* **2009,** 44, (19), 5049-5062.
777. Jürgen, R.; Wook, J.; Klaus, T. P. S.; Eva-Maria, A.; Torsten, G.; Dragan, D., Perspective on the Development of Lead-free Piezoceramics. *Journal of the American Ceramic Society* **2009,** 92, (6), 1153-1177.
778. *An American National Standard IEEE Standard on Piezoelectricity*; ANSI/IEEE Std 176-1987; IEEE Ultrasonics, Ferroelectrics, and Frequency Control Society: 1988, 1988; pp 1-66.
779. Polla, D. L.; Francis, L. F., Processing and characterization of piezoelectric materials and integration into microelectromechanical systems. *Annual Review of Materials Science* **1998,** 28, 563-597.
780. Buck, R. P.; Lindner, E.; Kutner, W.; Inzelt, G., Piezoelectric chemical sensors (IUPAC Technical Report). *Pure and Applied Chemistry* **2004,** 76, (6), 1139-1160.
781. Paganelli, R. P.; Romani, A.; Golfarelli, A.; Magi, M.; Sangiorgi, E.; Tartagni, M., Modeling and characterization of piezoelectric transducers by means of scattering parameters. Part I: Theory. *Sensors and Actuators A: Physical* **2010,** 160, (1-2), 9-18.

782. Paganelli, R. P.; Romani, A.; Golfarelli, A.; Magi, M.; Sangiorgi, E.; Tartagni, M., Modeling and characterization of piezoelectric transducers by means of scattering parameters. Part II: Application on colloidal suspension monitoring. *Sensors and Actuators A: Physical* **2010,** 160, (1-2), 1-8.
783. Watson, B.; Friend, J.; Yeo, L., Piezoelectric ultrasonic micro/milli-scale actuators. *Sensors and Actuators A: Physical* **2009,** 152, (2), 219-233.
784. Ni, S. S.; Li, T.; Ma, J., Polymeric piezoelectric cantilever and tubular actuators. *Polymers for Advanced Technologies* **2010,** 21, 591-597.
785. Ajitsaria, J.; et al., Modeling and analysis of a bimorph piezoelectric cantilever beam for voltage generation. *Smart Materials and Structures* **2007,** 16, (2), 447.
786. Liu, M.; et al., Deposition and characterization of Pb(Zr,Ti)O3 sol-gel thin films for piezoelectric cantilever beams. *Smart Materials and Structures* **2007,** 16, (1), 93.
787. DeVoe, D. L.; Pisano, A. P., Modeling and optimal design of piezoelectric cantilever microactuators. *Journal of Microelectromechanical Systems* **1997,** 6, (3), 266-270.
788. Fu, Y. Q.; Luo, J. K.; Du, X. Y.; Flewitt, A. J.; Li, Y.; Markx, G. H.; Walton, A. J.; Milne, W. I., Recent developments on ZnO films for acoustic wave based bio-sensing and microfluidic applications: a review. *Sensors and Actuators B: Chemical* **2010,** 143, (2), 606-619.
789. Zheng, S.; Choi, J. H.; Lee, S. M.; Hwang, K. S.; Kim, S. K.; Kim, T. S., Analysis of DNA hybridization regarding the conformation of molecular layer with piezoelectric microcantilevers. *Lab on a Chip* **2011,** 11, (1), 63-69.
790. Tandiono; Ohl, S.-W.; Ow, D. S.-W.; Klaseboer, E.; Wong, V. V. T.; Camattari, A.; Ohl, C.-D., Creation of cavitation activity in a microfluidic device through acoustically driven capillary waves. *Lab on a Chip* **2010,** 10, (14), 1848-1855.
791. Lang, S. B.; Muensit, S., Review of some lesser-known applications of piezoelectric and pyroelectric polymers. *Applied Physics A: Materials Science & Processing* **2006,** 85, 125-134.
792. Stroock, A. D.; Dertinger, S. K.; Whitesides, G. M.; Ajdari, A., Patterning Flows Using Grooved Surfaces. *Analytical Chemistry* **2002,** 74, (20), 5306-5312.
793. Lee, N. Y.; Yamada, M.; Seki, M., Development of a passive micromixer based on repeated fluid twisting and flattening, and its application to DNA purification. *Analytical & Bioanalytical Chemistry* **2005,** 383, 776-782.
794. Gambin, Y.; Simonnet, C.; VanDelinder, V.; Deniz, A.; Groisman, A., Ultrafast microfluidic mixer with three-dimensional flow focusing for studies of biochemical kinetics. *Lab on a Chip* **2010,** 10, (5), 598-609.
795. Liu, M. C.; Ho, D.; Tai, Y.-C., Monolithic fabrication of three-dimensional microfluidic networks for constructing cell culture array with an integrated combinatorial mixer. *Sensors and Actuators B: Chemical* **2008,** 129, (2), 826-833.
796. Neils, C.; Tyree, Z.; Finlayson, B.; Folch, A., Combinatorial mixing of microfluidic streams. *Lab on a Chip* **2004,** 4, (4), 342-350.
797. Garstecki, P.; Fuerstman, M. J.; Fischbach, M. A.; Sia, S. K.; Whitesides, G. M., Mixing with bubbles: a practical technology for use with portable microfluidic devices. *Lab on a Chip* **2006,** 6, (2), 207-212.

798. Chang, C.-C.; Yang, R.-J., Electrokinetic mixing in microfluidic systems. *Microfluidics and Nanofluidics* **2007,** 3, (5), 501-525.
799. Sudarsan, A. P.; Ugaz, V. M., Fluid mixing in planar spiral microchannels. *Lab on a chip* **2006,** 6, (1), 74-82.
800. Fu, B. R.; Pan, C., Simple Channel Geometry for Enhancement of Chemical Reactions in Microchannels. *Industrial & Engineering Chemistry Research* **2010,** 49, (19), 9413-9422.
801. Bertsch, A.; Heimgartner, S.; Cousseau, P.; Renaud, P., Static micromixers based on large-scale industrial mixer geometry. *Lab on a Chip* **2001,** 1, 56-60.
802. Luong, T.-D.; Phan, V.-N.; Nguyen, N.-T., High-throughput micromixers based on acoustic streaming induced by surface acoustic wave. *Microfluidics and Nanofluidics* **2011,** 10, (3), 619-625.
803. Yang, S.-Y.; Cheng, F.-Y.; Yeh, C.-S.; Lee, G.-B., Size-controlled synthesis of gold nanoparticles using a micro-mixing system. *Microfluidics and Nanofluidics* **2010,** 8, (3), 303-311.
804. Liu, J.; Williams, B. A.; Gwirtz, R. M.; Wold, B. J.; Quake, S., Enhanced Signals and Fast Nucleic Acid Hybridization By Microfluidic Chaotic Mixing. *Angewandte Chemie International Edition* **2006,** 45, (22), 3618-3623.
805. Jeong, G. S.; Chung, S.; Kim, C.-B.; Lee, S.-H., Applications of micromixing technology. *The Analyst* **2010,** 135, (3), 460-473.
806. Nguyen, N.-T.; Wu, Z., Micromixers - a review. *Journal of Micromechanics and Microengineering* **2005,** 15, (2), R1.
807. Hsu, C.-H.; Folch, A., Spatio-temporally-complex concentration profiles using a tunable chaotic micromixer. *Applied Physics Letters* **2006,** 89, (14), 144102-3.
808. Kim, D.; Lokuta, M. A.; Huttenlocher, A.; Beebe, D. J., Selective and tunable gradient device for cell culture and chemotaxis study. *Lab on a Chip* **2009,** 9, (12), 1797-1800.
809. Sun, K.; Wang, Z.; Jiang, X., Modular microfluidics for gradient generation. *Lab on a Chip* **2008,** 8, (9), 1536-1543.
810. Irimia, D.; Liu, S.-Y.; Tharp, W. G.; Samadani, A.; Toner, M.; Poznansky, M. C., Microfluidic system for measuring neutrophil migratory responses to fast switches of chemical gradients. *Lab on a Chip* **2006,** 6, (2), 191-198.
811. Hattori, K.; Sugiura, S.; Kanamori, T., Generation of arbitrary monotonic concentration profiles by a serial dilution microfluidic network composed of microchannels with a high fluidic-resistance ratio. *Lab on a Chip* **2009,** 9, (12), 1763-1772.
812. Chen, L.; Azizi, F.; Mastrangelo, C. H., Generation of dynamic chemical signals with microfluidic C-DACs. *Lab on a Chip* **2007,** 7, (7), 850-855.
813. Azizi, F.; Mastrangelo, C. H., Generation of dynamic chemical signals with pulse code modulators. *Lab on a Chip* **2008,** 8, (6), 907-912.
814. Lin, F.; Saadi, W.; Rhee, S. W.; Wang, S.-J.; Mittal, S.; Jeon, N. L., Generation of dynamic temporal and spatial concentration gradients using microfluidic devices. *Lab on a Chip* **2004,** 4, (3), 164-167.

815. Chung, B. G.; Lin, F.; Jeon, N. L., A microfluidic multi-injector for gradient generation. *Lab on a Chip* **2006,** 6, (6), 764-768.
816. Keenan, T. M.; Folch, A., Biomolecular gradients in cell culture systems. *Lab on a Chip* **2008,** 8, (1), 34-57.
817. Chung, B. G.; Choo, J., Microfluidic gradient platforms for controlling cellular behavior. *Electrophoresis* **2010,** 31, 3014-3027.
818. Jeon, N. L.; Dertinger, S. K. W.; Chiu, D. T.; Choi, I. S.; Stroock, A. D.; Whitesides, G. M., Generation of Solution and Surface Gradients Using Microfluidic Systems. *Langmuir* **2000,** 16, (22), 8311-8316.
819. Huebner, A.; Sharma, S.; Srisa-Art, M.; Hollfelder, F.; Edel, J. B.; deMello, A. J., Microdroplets: A sea of applications? *Lab on a Chip* **2008,** 8, (8), 1244-1254.
820. Shah, R. K.; Kim, J.-W.; Agresti, J. J.; Weitz, D. A.; Chu, L.-Y., Fabrication of monodisperse thermosensitive microgels and gel capsules in microfluidic devices. *Soft Matter* **2008,** 4, (12), 2303-2309.
821. Nie, J.; Kennedy, R. T., Sampling from Nanoliter Plugs via Asymmetrical Splitting of Segmented Flow. *Analytical Chemistry* **2010,** 82, (18), 7852-7856.
822. Surenjav, E.; Priest, C.; Herminghaus, S.; Seemann, R., Manipulation of gel emulsions by variable microchannel geometry. *Lab on a Chip* **2009,** 9, (2), 325-330.
823. Zeng, Y.; Novak, R.; Shuga, J.; Smith, M. T.; Mathies, R. A., High-Performance Single Cell Genetic Analysis Using Microfluidic Emulsion Generator Arrays. *Analytical Chemistry* **2010,** 82, (8), 3183-3190.
824. Nisisako, T.; Torii, T., Microfluidic large-scale integration on a chip for mass production of monodisperse droplets and particles. *Lab on a Chip* **2008,** 8, (2), 287-293.
825. Damean, N.; Olguin, L. F.; Hollfelder, F.; Abell, C.; Huck, W. T. S., Simultaneous measurement of reactions in microdroplets filled by concentration gradients. *Lab on a Chip* **2009,** 9, (12), 1707-1713.
826. Adamson, D. N.; Mustafi, D.; Zhang, J. X. J.; Zheng, B.; Ismagilov, R. F., Production of arrays of chemically distinct nanolitre plugs via repeated splitting in microfluidic devices. *Lab on a Chip* **2006,** 6, (9), 1178-1186.
827. Stride, E.; Edirisinghe, M., Novel microbubble preparation technologies. *Soft Matter* **2008,** 4, (12), 2350-2359.
828. Christopher, G. F.; Anna, S. L., Microfluidic methods for generating continuous droplet streams. *Journal of Physics D: Applied Physics* **2007,** 40, (19), R319.
829. Song, H.; Chen, D. L.; Ismagilov, R. F., Reactions in Droplets in Microfluidic Channels. *Angewandte Chemie International Edition* **2006,** 45, (44), 7336-7356.
830. Miller, E.; Rotea, M.; Rothstein, J. P., Microfluidic device incorporating closed loop feedback control for uniform and tunable production of micro-droplets. *Lab on a Chip* **2010,** 10, (10), 1293-1301.
831. Song, H.; Tice, J. D.; Ismagilov, R. F., A Microfluidic System for Controlling Reaction Networks in Time. *Angewandte Chemie International Edition* **2003,** 42, (7), 768-772.
832. Miller, E.; Wheeler, A., Digital bioanalysis. *Analytical and Bioanalytical Chemistry* **2009,** 393, (2), 419-426.

833. Wang, Z.; Zhe, J., Recent advances in particle and droplet manipulation for lab-on-a-chip devices based on surface acoustic waves. *Lab on a Chip* **2011,** 11, (7), 1280-1285.
834. Jonáscaron, A.; Zemánek, P., Light at work: The use of optical forces for particle manipulation, sorting, and analysis. *Electrophoresis* **2008,** 29, (24), 4813-4851.
835. Hwang, H.; Park, J.-K., Optoelectrofluidic platforms for chemistry and biology. *Lab on a Chip* **2011,** 11, (1), 33-47.
836. Lenshof, A.; Laurell, T., Continuous separation of cells and particles in microfluidic systems. *Chemical Society Reviews* **2010,** 39, (3), 1203-1217.
837. Pamme, N., Continuous flow separations in microfluidic devices. *Lab on a Chip* **2007,** 7, (12), 1644-1659.
838. Kersaudy-Kerhoas, M.; Dhariwal, R.; Desmulliez, M. P. Y., Recent advances in microparticle continuous separation. *IET Nanobiotechnology* **2008,** 2, 1-13.
839. Nilsson, J.; Evander, M.; Hammarström, B.; Laurell, T., Review of cell and particle trapping in microfluidic systems. *Analytica Chimica Acta* **2009,** 649, (2), 141-157.
840. Kang, Y.; Li, D., Electrokinetic motion of particles and cells in microchannels. *Microfluidics and Nanofluidics* **2009,** 6, (4), 431-460.
841. Shi, J.; Mao, X.; Ahmed, D.; Colletti, A.; Huang, T. J., Focusing microparticles in a microfluidic channel with standing surface acoustic waves (SSAW). *Lab on a Chip* **2008,** 8, (2), 221-223.
842. Petersson, F.; Aberg, L.; Sward-Nilsson, A.-M.; Laurell, T., Free Flow Acoustophoresis: Microfluidic-Based Mode of Particle and Cell Separation. *Analytical Chemistry* **2007,** 79, (14), 5117-5123.
843. Choi, S.; Park, J.-K., Continuous hydrophoretic separation and sizing of microparticles using slanted obstacles in a microchannel. *Lab on a Chip* **2007,** 7, (7), 890-897.
844. Kim, H. C.; Park, J.; Cho, Y.; Park, H.; Han, A.; Cheng, X., Lateral-flow particle filtration and separation with multilayer microfluidic channels. *Journal of Vacuum Science & Technology B: Microelectronics and Nanometer Structures* **2009,** 27, (6), 3115-3119.
845. Yeo, L. Y.; Friend, J. R.; Arifin, D. R., Electric tempest in a teacup: The tea leaf analogy to microfluidic blood plasma separation. *Applied Physics Letters* **2006,** 89, 103516.
846. Kuntaegowdanahalli, S. S.; Bhagat, A. A. S.; Kumar, G.; Papautsky, I., Inertial microfluidics for continuous particle separation in spiral microchannels. *Lab on a Chip* **2009,** 9, (20), 2973-2980.
847. Huh, D.; Bahng, J. H.; Ling, Y.; Wei, H.-H.; Kripfgans, O. D.; Fowlkes, J. B.; Grotberg, J. B.; Takayama, S., Gravity-Driven Microfluidic Particle Sorting Device with Hydrodynamic Separation Amplification. *Analytical Chemistry* **2007,** 79, (4), 1369-1376.
848. Stan, C. A.; Tang, S. K. Y.; Whitesides, G. M., Independent Control of Drop Size and Velocity in Microfluidic Flow-Focusing Generators Using Variable Temperature and Flow Rate. *Analytical Chemistry* **2009,** 81, (6), 2399-2402.

849. Lai, C.-W.; Hsiung, S.-K.; Yeh, C.-L.; Chiou, A.; Lee, G.-B., A cell delivery and pre-positioning system utilizing microfluidic devices for dual-beam optical trap-and-stretch. *Sensors and Actuators B: Chemical* **2008,** 135, (1), 388-397.
850. Hulme, S. E.; DiLuzio, W. R.; Shevkoplyas, S. S.; Turner, L.; Mayer, M.; Berg, H. C.; Whitesides, G. M., Using ratchets and sorters to fractionate motile cells of Escherichia coli by length. *Lab on a Chip* **2008,** 8, (11), 1888-1895.
851. Mao, X.; Lin, S.-C. S.; Dong, C.; Huang, T. J., Single-layer planar on-chip flow cytometer using microfluidic drifting based three-dimensional (3D) hydrodynamic focusing. *Lab on a Chip* **2009,** 9, (11), 1583-1589.
852. Tai, C.-H.; Hsiung, S.-K.; Chen, C.-Y.; Tsai, M.-L.; Lee, G.-B., Automatic microfluidic platform for cell separation and nucleus collection. *Biomedical Microdevices* **2007,** 9, (4), 533-543.
853. Christofer, E. W.; Rajat, A. D.; Ciarán, F. D.; Edgar, A. A., Determining under- and oversampling of individual particle distributions in microfluidic electrophoresis with orthogonal laser-induced fluorescence detection. *Electrophoresis* **2008,** 29, (7), 1431-1440.
854. Nam, K.-H.; Yong, W.; Harvat, T.; Adewola, A.; Wang, S.; Oberholzer, J.; Eddington, D., Size-based separation and collection of mouse pancreatic islets for functional analysis. *Biomedical Microdevices* **2010,** 12, (5), 865-874.
855. Lai, J. J.; Nelson, K. E.; Nash, M. A.; Hoffman, A. S.; Yager, P.; Stayton, P. S., Dynamic bioprocessing and microfluidic transport control with smart magnetic nanoparticles in laminar-flow devices. *Lab on a Chip* **2009,** 9, (14), 1997-2002.
856. Watts, P.; Wiles, C., Recent advances in synthetic micro reaction technology. *Chemical Communications* **2007**, (5), 443-467.
857. Yujun, S.; Hormes, J.; Kumar, C. S. S. R., Microfluidic Synthesis of Nanomaterials. *Small* **2008,** 4, (6), 698-711.
858. Marre, S.; Jensen, K. F., Synthesis of micro and nanostructures in microfluidic systems. *Chemical Society Reviews* **2010,** 39, (3), 1183-1202.
859. Jensen, K. F., Microreaction engineering-is small better? *Chemical Engineering Science* **2001,** 56, (2), 293-303.
860. Schäpper, D.; Alam, M.; Szita, N.; Eliasson Lantz, A.; Gernaey, K., Application of microbioreactors in fermentation process development: a review. *Analytical and Bioanalytical Chemistry* **2009,** 395, (3), 679-695.
861. Geyer, K.; Gustafsson, T.; Seeberger, P. H., Developing Continuous-Flow Microreactors as Tools for Synthetic Chemists. *Synlett* **2009,** 2009, (15), 2382-2391.
862. Brivio, M.; Verboom, W.; Reinhoudt, D. N., Miniaturized continuous flow reaction vessels: influence on chemical reactions. *Lab on a Chip* **2006,** 6, (3), 329-344.
863. Churski, K.; Korczyk, P.; Garstecki, P., High-throughput automated droplet microfluidic system for screening of reaction conditions. *Lab on a Chip* **2010,** 10, (7), 816-818.
864. Hoang, P. H.; Nguyen, C. T.; Perumal, J.; Kim, D.-P., Droplet synthesis of well-defined block copolymers using solvent-resistant microfluidic device. *Lab on a Chip* **2011,** 11, (2), 329-335.

865. Nightingale, A. M.; de Mello, J. C., Controlled Synthesis of III-V Quantum Dots in Microfluidic Reactors. *ChemPhysChem* **2009,** 10, (15), 2612-2614.
866. Kikkeri, R.; Laurino, P.; Odedra, A.; Seeberger, Peter H., Synthesis of Carbohydrate-Functionalized Quantum Dots in Microreactors. *Angewandte Chemie International Edition* **2010,** 49, (11), 2054-2057.
867. Lee, H. L. T.; Boccazzi, P.; Ram, R. J.; Sinskey, A. J., Microbioreactor arrays with integrated mixers and fluid injectors for high-throughput experimentation with pH and dissolved oxygen control. *Lab on a Chip* **2006,** 6, (9), 1229-1235.
868. Yoon, T.-H.; Park, S.-H.; Min, K.-I.; Zhang, X.; Haswell, S. J.; Kim, D.-P., Novel inorganic polymer derived microreactors for organic microchemistry applications. *Lab on a Chip* **2008,** 8, (9), 1454-1459.
869. Zourob, M.; Mohr, S.; Mayes, A. G.; Macaskill, A.; Perez-Moral, N.; Fielden, P. R.; Goddard, N. J., A micro-reactor for preparing uniform molecularly imprinted polymer beads. *Lab on a Chip* **2006,** 6, (2), 296-301.
870. Yu, X.; David, L. In *Parallel Microfluidic Synthesis of Conductive Biopolymers*, Mechatronic and Embedded Systems and Applications, Proceedings of the 2nd IEEE/ASME International Conference on, Aug. 2006, 2006; 2006; pp 1-5.
871. Geyer, K.; Codée, J. D. C.; Seeberger, P. H., Microreactors as Tools for Synthetic Chemists - The Chemists' Round-Bottomed Flask of the 21st Century? *Chemistry - A European Journal* **2006,** 12, (33), 8434-8442.
872. Khan, S. A.; Jensen, K. F., Microfluidic Synthesis of Titania Shells on Colloidal Silica. *Advanced Materials* **2007,** 19, (18), 2556-2560.
873. Harrison, D. J.; Fluri, K.; Seiler, K.; Fan, Z.; Effenhauser, C. S.; Manz, A., Micromachining a Miniaturized Capillary Electrophoresis-Based Chemical Analysis System on a Chip. *Science* **1993,** 261, (5123), 895-897.
874. Stockton, A. M.; Tjin, C. C.; Huang, G. L.; Benhabib, M.; Chiesl, T. N.; Mathies, R. A., Analysis of carbonaceous biomarkers with the Mars Organic Analyzer microchip capillary electrophoresis system: Aldehydes and ketones. *Electrophoresis* **2010,** 31, 3642-3649.
875. Long, Z.; Shen, Z.; Wu, D.; Qin, J.; Lin, B., Integrated multilayer microfluidic device with a nanoporous membrane interconnect for online coupling of solid-phase extraction to microchip electrophoresis. *Lab on a Chip* **2007,** 7, (12), 1819-1824.
876. Kuroda, D.; Zhang, Y.; Wang, J.; Kaji, N.; Tokeshi, M.; Baba, Y., A viscosity-tunable polymer for DNA separation by microchip electrophoresis. *Analytical and Bioanalytical Chemistry* **2008,** 391, (7), 2543-2549.
877. Plecis, A.; Tazid, J.; Pallandre, A.; Martinhon, P.; Deslouis, C.; Chen, Y.; Haghiri-Gosnet, A. M., Flow field effect transistors with polarisable interface for EOF tunable microfluidic separation devices. *Lab on a Chip* **2010,** 10, (10), 1245-1253.
878. Reid, K. R.; Kennedy, R. T., Continuous Operation of Microfabricated Electrophoresis Devices for 24 Hours and Application to Chemical Monitoring of Living Cells. *Analytical Chemistry* **2009,** 81, (16), 6837-6842.
879. Coltro, W. K. T.; Lunte, S. M.; Carrilho, E., Comparison of the analytical performance of electrophoresis microchannels fabricated in PDMS, glass, and polyester-toner. *Electrophoresis* **2008,** 29, (24), 4928-4937.

880. Emrich, C. A.; Tian, H.; Medintz, I. L.; Mathies, R. A., Microfabricated 384-lane capillary array electrophoresis bioanalyzer for ultrahigh-throughput genetic analysis. *Analytical Chemistry* **2002,** 74, (19), 5076-5083.
881. Fritzsche, S.; Hoffmann, P.; Belder, D., Chip electrophoresis with mass spectrometric detection in record speed. *Lab on a Chip* **2010,** 10, (10), 1227-1230.
882. Guillo, C.; Karlinsey, J. M.; Landers, J. P., On-chip pumping for pressure mobilization of the focused zones following microchip isoelectric focusing. *Lab on a Chip* **2007,** 7, (1), 112-118.
883. Cui, H.; Horiuchi, K.; Dutta, P.; Ivory, C. F., Multistage Isoelectric Focusing in a Polymeric Microfluidic Chip. *Analytical Chemistry* **2005,** 77, (24), 7878-7886.
884. Ou, J.; Glawdel, T.; Samy, R.; Wang, S.; Liu, Z.; Ren, C. L.; Pawliszyn, J., Integration of Dialysis Membranes into a Poly(dimethylsiloxane) Microfluidic Chip for Isoelectric Focusing of Proteins Using Whole-Channel Imaging Detection. *Analytical Chemistry* **2008,** 80, (19), 7401-7407.
885. Ou, J.; Glawdel, T.; Ren, C. L.; Pawliszyn, J., Fabrication of a hybrid PDMS/SU-8/quartz microfluidic chip for enhancing UV absorption whole-channel imaging detection sensitivity and application for isoelectric focusing of proteins. *Lab on a Chip* **2009,** 9, (13), 1926-1932.
886. Sommer, G. J.; Hatch, A. V., IEF in microfluidic devices. *Electrophoresis* **2009,** 30, (5), 742-757.
887. Zhao, D. S.; Roy, B.; McCormick, M. T.; Kuhr, W. G.; Brazill, S. A., Rapid fabrication of a poly(dimethysiloxane) microfluidic capillary gel electrophoresis system utilizing high precision machining. *Lab on a Chip* **2003,** 3, (2), 93-9.
888. Agirregabiria, M.; Blanco, F. J.; Berganzo, J.; Fullaondo, A.; Zubiaga, A. M.; Mayora, K.; Ruano-López, J. M., SDS-CGE of proteins in microchannels made of SU-8 films. *Electrophoresis* **2006,** 27, (18), 3627-3634.
889. Zeng, H.-L.; Li, H.-F.; Wang, X.; Lin, J.-M., Development of a gel monolithic column polydimethylsiloxane microfluidic device for rapid electrophoresis separation. *Talanta* **2006,** 69, (1), 226-231.
890. Grass, B.; Neyer, A.; Joehnck, M.; Siepe, D.; Eisenbeiss, F.; Weber, G.; Hergenroeder, R., New PMMA-microchip device for isotachophoresis with integrated conductivity detector. *Sensors and Actuators B: Chemical* **2001,** 72, (3), 249-258.
891. Baldock, S. J.; Fielden, P. R.; Goddard, N. J.; Kretschmer, H. R.; Prest, J. E.; Treves Brown, B. J., Novel variable volume injector for performing sample introduction in a miniaturised isotachophoresis device. *Journal of Chromatography A* **2004,** 1042, (1-2), 181-188.
892. Jung, B.; Bharadwaj, R.; Santiago, J. G., On-Chip Millionfold Sample Stacking Using Transient Isotachophoresis. *Analytical Chemistry* **2006,** 78, (7), 2319-2327.
893. Jung, B.; Zhu, Y.; Santiago, J. G., Detection of 100 aM Fluorophores Using a High-Sensitivity On-Chip CE System and Transient Isotachophoresis. *Analytical Chemistry* **2006,** 79, (1), 345-349.
894. Shou, M.; Ferrario, C. R.; Schultz, K. N.; Robinson, T. E.; Kennedy, R. T., Monitoring Dopamine in Vivo by Microdialysis Sampling and On-Line CE-Laser-Induced Fluorescence. *Analytical Chemistry* **2006,** 78, (19), 6717-6725.

895. Wang, J.; Zhou, S.; Huang, W.; Liu, Y.; Cheng, C.; Lu, X.; Cheng, J., CE-based analysis of hemoglobin and its applications in clinical analysis. *Electrophoresis* **2006,** 27, (15), 3108-3124.
896. Abdelgawad, M.; Watson, M. W. L.; Wheeler, A. R., Hybrid microfluidics: A digital-to-channel interface for in-line sample processing and chemical separations. *Lab on a Chip* **2009,** 9, (8), 1046-1051.
897. Amundsen, L. K.; Sirén, H., Immunoaffinity CE in clinical analysis of body fluids and tissues. *Electrophoresis* **2007,** 28, (1-2), 99-113.
898. Peoples, M. C.; Phillips, T. M.; Karnes, H. T., A capillary-based microfluidic instrument suitable for immunoaffinity chromatography. *Journal of Chromatography B* **2007,** 848, (2), 200-207.
899. Peoples, M. C.; Karnes, H. T., Microfluidic immunoaffinity separations for bioanalysis. *Journal of Chromatography B* **2008,** 866, (1-2), 14-25.
900. Turgeon, R. T.; Fonslow, B. R.; Jing, M.; Bowser, M. T., Measuring Aptamer Equilibria Using Gradient Micro Free Flow Electrophoresis. *Analytical Chemistry* **2010,** 82, (9), 3636-3641.
901. Fonslow, B. R.; Bowser, M. T., Free-Flow Electrophoresis on an Anodic Bonded Glass Microchip. *Analytical Chemistry* **2005,** 77, (17), 5706-5710.
902. Fonslow, B. R.; Barocas, V. H.; Bowser, M. T., Using Channel Depth To Isolate and Control Flow in a Micro Free-Flow Electrophoresis Device. *Analytical Chemistry* **2006,** 78, (15), 5369-5374.
903. Zhang, C.-X.; Manz, A., High-Speed Free-Flow Electrophoresis on Chip. *Analytical Chemistry* **2003,** 75, (21), 5759-5766.
904. Kohler, S.; Weilbeer, C.; Howitz, S.; Becker, H.; Beushausen, V.; Belder, D., PDMS free-flow electrophoresis chips with integrated partitioning bars for bubble segregation. *Lab on a Chip* **2011,** 11, (2), 309-314.
905. Turgeon, R.; Bowser, M., Micro free-flow electrophoresis: theory and applications. *Analytical and Bioanalytical Chemistry* **2009,** 394, (1), 187-198.
906. Kohlheyer, D.; Eijkel, J. C. T.; van den Berg, A.; Schasfoort, R. B. M., Miniaturizing free-flow electrophoresis - a critical review. *Electrophoresis* **2008,** 29, (5), 977-993.
907. Morf, W. E.; van der Wal, P. D.; de Rooij, N. F., Computer simulation and theory of the diffusion- and flow-induced concentration dispersion in microfluidic devices and HPLC systems based on rectangular microchannels. *Analytica Chimica Acta* **2008,** 622, (1-2), 175-181.
908. Shintani, Y.; Hirako, K.; Motokawa, M.; Iwano, T.; Zhou, X.; Takano, Y.; Furuno, M.; Minakuchi, H.; Ueda, M., Development of miniaturized multi-channel high-performance liquid chromatography for high-throughput analysis. *Journal of Chromatography A* **2005,** 1073, (1-2), 17-23.
909. Hasselbrink, E. F.; Shepodd, T. J.; Rehm, J. E., High-Pressure Microfluidic Control in Lab-on-a-Chip Devices Using Mobile Polymer Monoliths. *Analytical Chemistry* **2002,** 74, (19), 4913-4918.

910. Fuentes, H. V.; Woolley, A. T., Electrically actuated, pressure-driven liquid chromatography separations in microfabricated devices. *Lab on a Chip* **2007,** 7, (11), 1524-1531.
911. Yin, H.; Killeen, K., The fundamental aspects and applications of Agilent HPLC-Chip. *Journal of Separation Science* **2007,** 30, (10), 1427-1434.
912. Zeng, H.-L.; Seino, N.; Nakagama, T.; Kikuchi, Y.; Nagano, H.; Uchiyama, K., Accurate nano-injection system for capillary gas chromatography. *Journal of Chromatography A* **2009,** 1216, (15), 3337-3342.
913. Ohira, S.-I.; Toda, K., Micro gas analyzers for environmental and medical applications. *Analytica Chimica Acta* **2008,** 619, (2), 143-156.
914. Agah, M.; Lambertus, G. R.; Sacks, R.; Wise, K., High-Speed MEMS-Based Gas Chromatography. *Journal of Microelectromechanical Systems* **2006,** 15, (5), 1371-1378.
915. Han, S.-I.; Han, K.-H.; Frazier, A.; Ferrance, J.; Landers, J., An automated micro-solid phase extraction device involving integrated high-pressure microvalves for genetic sample preparation. *Biomedical Microdevices* **2009,** 11, (4), 935-942.
916. Marchiarullo, D. J.; Lim, J. Y.; Vaksman, Z.; Ferrance, J. P.; Putcha, L.; Landers, J. P., Towards an integrated microfluidic device for spaceflight clinical diagnostics: Microchip-based solid-phase extraction of hydroxyl radical markers. *Journal of Chromatography A* **2008,** 1200, (2), 198-203.
917. Duarte, G. R. M.; Price, C. W.; Littlewood, J. L.; Haverstick, D. M.; Ferrance, J. P.; Carrilho, E.; Landers, J. P., Characterization of dynamic solid phase DNA extraction from blood with magnetically controlled silica beads. *The Analyst* **2010,** 135, (3), 531-537.
918. Arce, L.; Nozal, L.; Simonet, B. M.; Valcárcel, M.; Ríos, A., Liquid-phase microextraction techniques for simplifying sample treatment in capillary electrophoresis. *TrAC Trends in Analytical Chemistry* **2009,** 28, (7), 842-853.
919. Hagan, K. A.; Bienvenue, J. M.; Moskaluk, C. A.; Landers, J. P., Microchip-Based Solid-Phase Purification of RNA from Biological Samples. *Analytical Chemistry* **2008,** 80, (22), 8453-8460.
920. Liu, J.; Chen, C.-F.; Yang, S.; Chang, C.-C.; DeVoe, D. L., Mixed-mode electrokinetic and chromatographic peptide separations in a microvalve-integrated polymer chip. *Lab on a Chip* **2010,** 10, (16), 2122-2129.
921. Wang, Y.-C.; Choi, M. H.; Han, J., Two-Dimensional Protein Separation with Advanced Sample and Buffer Isolation Using Microfluidic Valves. *Analytical Chemistry* **2004,** 76, (15), 4426-4431.
922. Tia, S.; Herr, A. E., On-chip technologies for multidimensional separations. *Lab on a Chip* **2009,** 9, (17), 2524-2536.
923. Chen, H.; Fan, Z. H., Two-dimensional protein separation in microfluidic devices. *Electrophoresis* **2009,** 30, (5), 758-765.
924. Wang, J.; Chatrathi, M. P.; Collins, G. E., Simultaneous microchip enzymatic measurements of blood lactate and glucose. *Analytica Chimica Acta* **2007,** 585, (1), 11-16.
925. Schuler, L. P.; et al., MEMS-based microspectrometer technologies for NIR and MIR wavelengths. *Journal of Physics D: Applied Physics* **2009,** 42, (13), 133001.

926. Minas, G.; Wolffenbuttel, R.; Correia, J., MCM-based microlaboratory for simultaneous measurement of several biochemical parameters by spectrophotometry. *Biomedical Microdevices* **2010,** 12, (4), 727-736.
927. Adams, M. L.; Enzelberger, M.; Quake, S.; Scherer, A., Microfluidic integration on detector arrays for absorption and fluorescence micro-spectrometers. *Sensors and Actuators A: Physical* **2003,** A104, (1), 25-31.
928. Minas, G.; Wolffenbuttel, R. F.; Correia, J. H., A lab-on-a-chip for spectrophotometric analysis of biological fluids. *Lab on a Chip* **2005,** 5, (11), 1303-1309.
929. Syms, R., Advances in microfabricated mass spectrometers. *Analytical and Bioanalytical Chemistry* **2009,** 393, (2), 427-429.
930. Lam, M. H. C.; et al., Sub-nanoliter nuclear magnetic resonance coils fabricated with multilayer soft lithography. *Journal of Micromechanics and Microengineering* **2009,** 19, (9), 095001.
931. Wensink, H.; Benito-Lopez, F.; Hermes, D. C.; Verboom, W.; Gardeniers, H. J. G. E.; Reinhoudt, D. N.; van den Berg, A., Measuring reaction kinetics in a lab-on-a-chip by microcoil NMR. *Lab on a Chip* **2005,** 5, (3), 280-284.
932. Lee, H.; Yoon, T.-J.; Weissleder, R., Ultrasensitive Detection of Bacteria Using Core-Shell Nanoparticles and an NMR-Filter System. *Angewandte Chemie International Edition* **2009,** 48, (31), 5657-5660.
933. Lee, H.; Sun, E.; Ham, D.; Weissleder, R., Chip-NMR biosensor for detection and molecular analysis of cells. *Nature Medicine* **2008,** 14, (8), 869-874.
934. Horiuchi, K.; Dutta, P., Electrokinetic flow control in microfluidic chips using a field-effect transistor. *Lab on a chip* **2006,** 6, (6), 714-23.
935. Cheng, L.-J.; Guo, L. J., Nanofluidic diodes. *Chemical Society Reviews* **2010,** 39, (3), 923-938.
936. Liu, Y.-J.; Guo, S.-S.; Zhang, Z.-L.; Huang, W.-H.; Baigl, D.; Chen, Y.; Pang, D.-W., Integration of minisolenoids in microfluidic device for magnetic bead-based immunoassays. *Journal of Applied Physics* **2007,** 102, 084911.
937. Razunguzwa, T. T.; Lenke, J.; Timperman, A. T., An electrokinetic/hydrodynamic flow microfluidic CE-ESI-MS interface utilizing a hydrodynamic flow restrictor for delivery of samples under low EOF conditions. *Lab on a Chip* **2005,** 5, (8), 851-855.
938. Hsu, C.-J.; Sheen, H.-J., A microfluidic flow-converter based on a double-chamber planar micropump. *Microfluidics and Nanofluidics* **2009,** 6, (5), 669-678.
939. Schasfoort, R. B.; Schlautmann, S.; Hendrikse, J.; van den Berg, A., Field-Effect Flow Control for Microfabricated Fluidic Networks. *Science* **1999,** 286, (5441), 942-945.
940. Groisman, A.; Enzelberger, M.; Quake, S. R., Microfluidic Memory and Control Devices. *Science* **2003,** 300, 955.
941. Liu, J.; Chen, Y.; Taylor, C. R.; Scherer, A.; Kartalov, E. P., Elastomeric microfluidic diode and rectifier work with Newtonian fluids. *Journal of Applied Physics* **2009,** 106, (11), 114311-5.

942. Kartalov, E. P.; Walker, C.; Taylor, C. R.; Anderson, W. F.; Scherer, A., Microfluidic vias enable nested bioarrays and autoregulatory devices in Newtonian fluids. *Proceedings of the National Academy of Sciences of the United States of America* **2006,** 103, (33), 12280-12284.
943. Leslie, D. C.; Easley, C. J.; Seker, E.; Karlinsey, J. M.; Utz, M.; Begley, M. R.; Landers, J. P., Frequency-specific flow control in microfluidic circuits with passive elastomeric features. *Nature Physics* **2009,** 5, (3), 231-235.
944. Kou, S.; Lee, Han N.; van Noort, D.; Swamy, K. M. K.; Kim, So H.; Soh, Jung H.; Lee, K.-M.; Nam, S.-W.; Yoon, J.; Park, S., Fluorescent Molecular Logic Gates Using Microfluidic Devices. *Angewandte Chemie International Edition* **2008,** 47, (5), 872-876.
945. Thorsen, T.; Maerki, S. J.; Quake, S. R., Microfluidic large-scale integration. *Science* **2002,** 298, 580-584.
946. Maltezos, G.; Nortrup, R.; Jeon, S.; Zaumseil, J.; Rogers, J. A., Tunable organic transistors that use microfluidic source and drain electrodes. *Applied Physics Letters* **2003,** 83, (10), 2067-2069.
947. So, J.-H.; Thelen, J.; Qusba, A.; Hayes, G. J.; Lazzi, G.; Dickey, M. D., Reversibly Deformable and Mechanically Tunable Fluidic Antennas. *Advanced Functional Materials* **2009,** 19, 3632-3637.
948. Kubo, M.; Li, X.; Kim, C.; Hashimoto, M.; Wiley, B. J.; Ham, D.; Whitesides, G. M., Stretchable Microfluidic Radiofrequency Antennas. *Advanced Materials* **2010,** 22, (25), 2749-2752.
949. Weaver, J. A.; Melin, J.; Stark, D.; Quake, S. R.; Horowitz, M. A., Static control logic for microfluidic devices using pressure-gain valves. *Nature Physics* **2010,** 6, (3), 218-223.
950. Chen, D.; Du, W.; Liu, Y.; Liu, W.; Kuznetsov, A.; Mendez, F. E.; Philipson, L. H.; Ismagilov, R. F., The chemistrode: A droplet-based microfluidic device for stimulation and recording with high temporal, spatial, and chemical resolution. *Proceedings of the National Academy of Sciences* **2008,** 105, (44), 16843-16848.
951. Fuerstman, M. J.; Deschatelets, P.; Kane, R.; Schwartz, A.; Kenis, P. J. A.; Deutch, J. M.; Whitesides, G. M., Solving mazes using microfluidic networks. *Langmuir* **2003,** 19, (11), 4714-4722.
952. Hashimoto, M.; Feng, J.; York, R. L.; Ellerbee, A. K.; Morrison, G.; Thomas Iii, S. W.; Mahadevan, L.; Whitesides, G. M., Infochemistry: Encoding Information as Optical Pulses Using Droplets in a Microfluidic Device. *Journal of the American Chemical Society* **2009,** 131, (34), 12420-12429.
953. Grover, W. H.; Mathies, R. A., An integrated microfluidic processor for single nucleotide polymorphism-based DNA computing. *Lab on a Chip* **2005,** 5, (10), 1033-1040.
954. Riesco-Chueca, P.; Gañán-Calvo, Alfonso M., Microfluidic Codecs. *Small* **2007,** 3, (7), 1140-1142.
955. Prakash, M.; Gershenfeld, N., Microfluidic Bubble Logic. *Science* **2007,** 315, (5813), 832-835.

956. Fuerstman, M. J.; Garstecki, P.; Whitesides, G. M., Coding/Decoding and Reversibility of Droplet Trains in Microfluidic Networks. *Science* **2007,** 315, (5813), 828-832.
957. Riedel-Kruse, I. H.; Chung, A. M.; Dura, B.; Hamilton, A. L.; Lee, B. C., Design, engineering and utility of biotic games. *Lab on a Chip* **2011,** 11, (1), 14-22.
958. Lu, H.; Schmidt, M. A.; Jensen, K. F., A microfluidic electroporation device for cell lysis. *Lab on a Chip* **2005,** 5, (1), 23-29.
959. Mosadegh, B.; Kuo, C.-H.; Tung, Y.-C.; Torisawa, Y.-s.; Bersano-Begey, T.; Tavana, H.; Takayama, S., Integrated elastomeric components for autonomous regulation of sequential and oscillatory flow switching in microfluidic devices. *Nature Physics* **2010,** 6, (6), 433-437.
960. Routenberg, D. A.; Reed, M. A., Microfluidic probe: a new tool for integrating microfluidic environments and electronic wafer-probing. *Lab on a Chip* **2010,** 10, (1), 123-127.
961. Blazej, R. G.; Kumaresan, P.; Cronier, S. A.; Mathies, R. A., Inline Injection Microdevice for Attomole-Scale Sanger DNA Sequencing. *Analytical Chemistry* **2007,** 79, (12), 4499-4506.
962. Gorbounov, V.; Kuban, P.; Dasgupta, P. K.; Temkin, H., A nanoinjector for microanalysis. *Analytical Chemistry* **2003,** 75, (15), 3919-3923.
963. Xu, J.; Attinger, D., Drop on demand in a microfluidic chip. *Journal of Micromechanics and Microengineering* **2008,** 18, (6), 065020.
964. Qi, L.-Y.; Yin, X.-F.; Zhang, L.; Wang, M., Rapid and variable-volume sample loading in sieving electrophoresis microchips using negative pressure combined with electrokinetic force. *Lab on a Chip* **2008,** 8, (7), 1137-1144.
965. Easley, C. J.; Karlinsey, J. M.; Landers, J. P., On-chip pressure injection for integration of infrared-mediated DNA amplification with electrophoretic separation. *Lab on a Chip* **2006,** 6, (5), 601-610.
966. Hansen, C. L.; Skordalakes, E.; Berger, J. M.; Quake, S. R., A robust and scalable microfluidic metering method that allows protein crystal growth by free interface diffusion. *Proceedings of the National Academy of Sciences of the United States of America* **2002,** 99, (26), 16531-16536.
967. Leach, A. M.; Wheeler, A. R.; Zare, R. N., Flow injection analysis in a microfluidic format. *Analytical Chemistry* **2003,** 75, (4), 967-972.
968. Li, M. W.; Huynh, B. H.; Hulvey, M. K.; Lunte, S. M.; Martin, R. S., Design and Characterization of Poly(dimethylsiloxane)-Based Valves for Interfacing Continuous-Flow Sampling to Microchip Electrophoresis. *Analytical Chemistry* **2006,** 78, (4), 1042-1051.
969. Luo, Y.; Wu, D.; Zeng, S.; Gai, H.; Long, Z.; Shen, Z.; Dai, Z.; Qin, J.; Lin, B., Double-Cross Hydrostatic Pressure Sample Injection for Chip CE: Variable Sample Plug Volume and Minimum Number of Electrodes. *Analytical Chemistry* **2006,** 78, (17), 6074-6080.
970. Li, Q.; Zhang, H.; Wang, Y.; Tang, B.; Liu, X.; Gong, X., Versatile programmable eight-path-electrode power supply for automatic manipulating microfluids of a microfluidic chip. *Sensors and Actuators B: Chemical* **2009,** 136, (1), 265-274.

971. Pei, J.; Nie, J.; Kennedy, R. T., Parallel Electrophoretic Analysis of Segmented Samples On Chip for High-Throughput Determination of Enzyme Activities. *Analytical Chemistry* **2010,** 82, (22), 9261-9267.
972. Cannon, D. M., Jr.; Kuo, T.-C.; Bohn, P. W.; Sweedler, J. V., Nanocapillary Array Interconnects for Gated Analyte Injections and Electrophoretic Separations in Multilayer Microfluidic Architectures. *Analytical Chemistry* **2003,** 75, (10), 2224-2230.
973. Blas, M.; Delaunay, N.; Rocca, J.-L., Electrokinetic-based injection modes for separative microsystems. *Electrophoresis* **2008,** 29, (1), 20-32.
974. Roddy, E. S.; Xu, H.; Ewing, A. G., Sample introduction techniques for microfabricated separation devices. *Electrophoresis* **2004,** 25, (2), 229-242.
975. Kubán, P.; Karlberg, B., Flow/sequential injection sample treatment coupled to capillary electrophoresis. A review. *Analytica Chimica Acta* **2009,** 648, (2), 129-145.
976. Karlinsey, J. M.; Monahan, J.; Marchiarullo, D. J.; Ferrance, J. P.; Landers, J. P., Pressure Injection on a Valved Microdevice for Electrophoretic Analysis of Submicroliter Samples. *Analytical Chemistry* **2005,** 77, (11), 3637-3643.
977. Reinhardt, H.; Dittrich, P. S.; Manz, A.; Franzke, J., micro-Hotplate enhanced optical heating by infrared light for single cell treatment. *Lab on a Chip* **2007,** 7, (11), 1509-1514.
978. Zhong, R.; Xiaoyan, P.; Jiang, L.; Dai, Z.; Qin, J.; Lin, B., Simply and reliably integrating micro heaters/sensors in a monolithic PCR-CE microfluidic genetic analysis system. *Electrophoresis* **2009,** 30, (8), 1297-1305.
979. Lee, W.; Fon, W.; Axelrod, B. W.; Roukes, M. L., High-sensitivity microfluidic calorimeters for biological and chemical applications. *Proceedings of the National Academy of Sciences* **2009,** 106, (36), 15225-15230.
980. Samy, R.; Glawdel, T.; Ren, C. L., Method for Microfluidic Whole-Chip Temperature Measurement Using Thin-Film Poly(dimethylsiloxane)/Rhodamine B. *Analytical Chemistry* **2007,** 80, (2), 369-375.
981. Choi, S. R.; Kim, D., Real-time thermal characterization of 12 nl fluid samples in a microchannel. *Review of Scientific Instruments*, **2008,** 79, 064901.
982. Velve Casquillas, G.; Fu, C.; Le Berre, M.; Cramer, J.; Meance, S.; Plecis, A.; Baigl, D.; Greffet, J.-J.; Chen, Y.; Piel, M.; Tran, P. T., Fast microfluidic temperature control for high resolution live cell imaging. *Lab on a Chip* **2011,** 11, (3), 484-489.
983. Li, H.; Luo, C. X.; Ji, H.; Ouyang, Q.; Chen, Y., Micro-pressure sensor made of conductive PDMS for microfluidic applications. *Microelectronic Engineering* **2010,** 87, (5-8), 1266-1269.
984. Chihyung, H.; Gregory, J. W.; Sullivan, J. P., Microchannel Pressure Measurements Using Molecular Sensors. *Journal of Microelectromechanical Systems* **2007,** 16, (4), 777-785.
985. Ko, H. S.; et al., Flow characteristics in a microchannel system integrated with arrays of micro-pressure sensors using a polymer material. *Journal of Micromechanics and Microengineering* **2008,** 18, (7), 075016.
986. Abeysinghe, D. C.; et al., Novel MEMS pressure and temperature sensors fabricated on optical fibers. *Journal of Micromechanics and Microengineering* **2002,** 12, (3), 229.

987. Kartalov, E. P.; Maltezos, G.; French Anderson, W.; Taylor, C. R.; Scherer, A., Electrical microfluidic pressure gauge for elastomer microelectromechanical systems. *Journal of Applied Physics*, **2007,** 102, 084909.
988. Wang, L.; Zhang, M.; Yang, M.; Zhu, W.; Wu, J.; Gong, X.; Wen, W., Polydimethylsiloxane-integratable micropressure sensor for microfluidic chips. *Biomicrofluidics* **2009,** 3, 034105.
989. Vilares, R.; Hunter, C.; Ugarte, I.; Aranburu, I.; Berganzo, J.; Elizalde, J.; Fernandez, L. J., Fabrication and testing of a SU-8 thermal flow sensor. *Sensors and Actuators B: Chemical* **2010,** 147, (2), 411-417.
990. Sengupta, S.; Ziaie, B.; Barocas, V. H., Lag-after-pulsed-separation microfluidic flowmeter for biomacromolecular solutions. *Sensors and Actuators B: Chemical* **2004,** 99, (1), 25-29.
991. van Honschoten, J. W.; Svetovoy, V. B.; Lammerink, T. S. J.; Krijnen, G. J. M.; Elwenspoek, M. C., Determination of the sensitivity behavior of an acoustic, thermal flow sensor by electronic characterization. *Sensors and Actuators A: Physical* **2004,** 112, (1), 1-9.
992. Berthet, H.; Jundt, J.; Durivault, J.; Mercier, B.; Angelescu, D., Time-of-flight thermal flowrate sensor for lab-on-chip applications. *Lab on a Chip* **2011,** 11, (2), 215-223.
993. Wu, S.; Lin, Q.; Yuen, Y.; Tai, Y.-C., MEMS flow sensors for nano-fluidic applications. *Sensors and Actuators A: Physical* **2001,** A89, (1-2), 152-8.
994. Huang, S.-C.; et al., A microfluidic system with integrated molecular imprinting polymer films for surface plasmon resonance detection. *Journal of Micromechanics and Microengineering* **2006,** 16, (7), 1251.
995. Weng, C.-H.; Yeh, W.-M.; Ho, K.-C.; Lee, G.-B., A microfluidic system utilizing molecularly imprinted polymer films for amperometric detection of morphine. *Sensors and Actuators B: Chemical* **2007,** 121, (2), 576-582.
996. Birnbaumer, G. M.; Lieberzeit, P. A.; Richter, L.; Schirhagl, R.; Milnera, M.; Dickert, F. L.; Bailey, A.; Ertl, P., Detection of viruses with molecularly imprinted polymers integrated on a microfluidic biochip using contact-less dielectric microsensors. *Lab on a Chip* **2009,** 9, (24), 3549-3556.
997. Guillon, S.; Lemaire, R.; Linares, A. V.; Haupt, K.; Ayela, C., Single step patterning of molecularly imprinted polymers for large scale fabrication of microbiochips. *Lab on a Chip* **2009,** 9, (20), 2987-2991.
998. Abe, K.; Suzuki, K.; Citterio, D., Inkjet-Printed Microfluidic Multianalyte Chemical Sensing Paper. *Analytical Chemistry* **2008,** 80, (18), 6928-6934.
999. Piorek, B. D.; Lee, S. J.; Santiago, J. G.; Moskovits, M.; Banerjee, S.; Meinhart, C. D., Free-surface microfluidic control of surface-enhanced Raman spectroscopy for the optimized detection of airborne molecules. *Proceedings of the National Academy of Sciences* **2007,** 104, (48), 18898-18901.
1000. Scarano, S.; Mascini, M.; Turner, A. P. F.; Minunni, M., Surface plasmon resonance imaging for affinity-based biosensors. *Biosensors and Bioelectronics* **2010,** 25, (5), 957-966.

1001. Varshney, M.; Li, Y.; Srinivasan, B.; Tung, S., A label-free, microfluidics and interdigitated array microelectrode-based impedance biosensor in combination with nanoparticles immunoseparation for detection of Escherichia coli O157:H7 in food samples. *Sensors and Actuators B: Chemical* **2007,** 128, (1), 99-107.
1002. Zhang, S.; Xie, C.; Zeng, D.; Zhang, Q.; Li, H.; Bi, Z., A feature extraction method and a sampling system for fast recognition of flammable liquids with a portable E-nose. *Sensors and Actuators B: Chemical* **2007,** 124, (2), 437-443.
1003. Berdat, D.; Rodriguez, A. C. M.; Herrera, F.; Gijs, M. A. M., Label-free detection of DNA with interdigitated micro-electrodes in a fluidic cell. *Lab on a Chip* **2008,** 8, (2), 302-308.
1004. Uludag, Y.; Piletsky, S. A.; Turner, A. P. F.; Cooper, M. A., Piezoelectric sensors based on molecular imprinted polymers for detection of low molecular mass analytes. *FEBS Journal*, **2007,** 274, 5471-5480.
1005. Waggoner, P. S.; Craighead, H. G., Micro- and nanomechanical sensors for environmental, chemical, and biological detection. *Lab on a Chip* **2007,** 7, (10), 1238-1255.
1006. Janshoff, A.; Galla, H.-J.; Steinem, C., Piezoelectric Mass-Sensing Devices as Biosensors - An Alternative to Optical Biosensors? *Angewandte Chemie* **2000,** 39, (22), 4004-4032.
1007. Craighead, H. G., Nanoelectromechanical Systems. *Science* **2000,** 290, (5496), 1532-1535.
1008. Truman, P.; Uhlmann, P.; Stamm, M., Monitoring liquid transport and chemical composition in lab on a chip systems using ion sensitive FET devices. *Lab on a Chip* **2006,** 6, (9), 1220-1228.
1009. Oh, Y.-J.; Gamble, T. C.; Leonhardt, D.; Chung, C.-H.; Brueck, S. R. J.; Ivory, C. F.; Lopez, G. P.; Petsev, D. N.; Han, S. M., Monitoring FET flow control and wall adsorption of charged fluorescent dye molecules in nanochannels integrated into a multiple internal reflection infrared waveguide. *Lab on a Chip* **2008,** 8, (2), 251-258.
1010. Chang, S. R.; et al., Die-level, post-CMOS processes for fabricating open-gate, field-effect biosensor arrays with on-chip circuitry. *Journal of Micromechanics and Microengineering* **2008,** 18, (11), 115032.
1011. Wijaya, I. P. M.; Nie, T. J.; Rodriguez, I.; Mhaisalkar, S. G., Investigation of sensing mechanism and signal amplification in carbon nanotube based microfluidic liquid-gated transistors via pulsating gate bias. *Lab on a Chip* **2010,** 10, (11), 1454-1458.
1012. Shen, N. Y.; Liu, Z.; Jacquot, B. C.; Minch, B. A.; Kan, E. C., Integration of chemical sensing and electrowetting actuation on chemoreceptive neuron MOS (CvMOS) transistors. *Sensors and Actuators B: Chemical* **2004,** 102, (1), 35-43.
1013. Jacquot, B.; Chungho, L.; Shen, Y. N.; Kan, E. C., Time-Resolved Charge Transport Sensing by Chemoreceptive Neuron MOS Transistors (CvMOS) With Microfluidic Channels. *IEEE Sensors Journal* **2007,** 7, (10), 1429-1434.
1014. Kim, D.-S.; Park, J.-E.; Shin, J.-K.; Kim, P. K.; Lim, G.; Shoji, S., An extended gate FET-based biosensor integrated with a Si microfluidic channel for detection of protein complexes. *Sensors and Actuators B: Chemical* **2006,** 117, (2), 488-494.

1015. Karlinsey, J. M.; Landers, J. P., AOTF-based multicolor fluorescence detection for short tandem repeat (STR) analysis in an electrophoretic microdevice. *Lab on a Chip* **2008,** 8, (8), 1285-1291.
1016. Karlinsey, J. M.; Landers, J. P., Multicolor Fluorescence Detection on an Electrophoretic Microdevice Using an Acoustooptic Tunable Filter. *Analytical Chemistry* **2006,** 78, (15), 5590-5596.
1017. Tang, S. K. Y.; Li, Z.; Abate, A. R.; Agresti, J. J.; Weitz, D. A.; Psaltis, D.; Whitesides, G. M., A multi-color fast-switching microfluidic droplet dye laser. *Lab on a Chip* **2009,** 9, (19), 2767-2771.
1018. Zhenyu, L.; Psaltis, D., Optofluidic Distributed Feedback Dye Lasers. *IEEE Journal of Selected Topics in Quantum Electronics* **2007,** 13, (2), 185-193.
1019. Vezenov, D. V.; Mayers, B. T.; Conroy, R. S.; Whitesides, G. M.; Snee, P. T.; Chan, Y.; Nocera, D. G.; Bawendi, M. G., A Low-Threshold, High-Efficiency Microfluidic Waveguide Laser. *Journal of the American Chemical Society* **2005,** 127, (25), 8952-8953.
1020. Song, W.; Psaltis, D., Pneumatically tunable optofluidic dye laser. *Applied Physics Letters* **2010,** 96, (8), 081101-3.
1021. Monat, C.; Domachuk, P.; Eggleton, B. J., Integrated optofluidics: A new river of light. *Nature Photonics* **2007,** 1, (2), 106-114.
1022. Li, Z.; Psaltis, D., Optofluidic dye lasers. *Microfluidics and Nanofluidics* **2008,** 4, (1), 145-158.
1023. Mogensen, K. B.; Kutter, J. P., Optical detection in microfluidic systems. *Electrophoresis* **2009,** 30, (S1), S92-S100.
1024. Kuswandi, B.; Nuriman; Huskens, J.; Verboom, W., Optical sensing systems for microfluidic devices: A review. *Analytica Chimica Acta* **2007,** 601, (2), 141-155.
1025. Brennan, D.; Justice, J.; Corbett, B.; McCarthy, T.; Galvin, P., Emerging optofluidic technologies for point-of-care genetic analysis systems: a review. *Analytical and Bioanalytical Chemistry* **2009,** 395, (3), 621-636.
1026. Lacher, N. A.; Lunte, S. M.; Martin, R. S., Development of a Microfabricated Palladium Decoupler/Electrochemical Detector for Microchip Capillary Electrophoresis Using a Hybrid Glass/Poly(dimethylsiloxane) Device. *Analytical Chemistry* **2004,** 76, (9), 2482-2491.
1027. Goral, V. N.; Zaytseva, N. V.; Baeumner, A. J., Electrochemical microfluidic biosensor for the detection of nucleic acid sequences. *Lab on a Chip* **2006,** 6, (3), 414-421.
1028. Wang, Y.; He, Q.; Dong, Y.; Chen, H., In-channel modification of biosensor electrodes integrated on a polycarbonate microfluidic chip for micro flow-injection amperometric determination of glucose. *Sensors and Actuators B: Chemical* **2010,** 145, (1), 553-560.
1029. Pumera, M.; Escarpa, A., Nanomaterials as electrochemical detectors in microfluidics and CE: Fundamentals, designs, and applications. *Electrophoresis* **2009,** 30, (19), 3315-3323.

1030. Cai, D.; Ren, L.; Zhao, H.; Xu, C.; Zhang, L.; Yu, Y.; Wang, H.; Lan, Y.; Roberts, M. F.; Chuang, J. H.; Naughton, M. J.; Ren, Z.; Chiles, T. C., A molecular-imprint nanosensor for ultrasensitive detection of proteins. *Nature Nanotechnology* **2010,** 5, (8), 597-601.
1031. Dungchai, W.; Chailapakul, O.; Henry, C. S., Electrochemical Detection for Paper-Based Microfluidics. *Analytical Chemistry* **2009,** 81, (14), 5821-5826.
1032. Mannoor, M. S.; Zhang, S.; Link, A. J.; McAlpine, M. C., Electrical detection of pathogenic bacteria via immobilized antimicrobial peptides. *Proceedings of the National Academy of Sciences* **2010,** 107, (45), 19207-19212.
1033. Lee, J.; Soper, S. A.; Murray, K. K., Microfluidic chips for mass spectrometry-based proteomics. *Journal of Mass Spectrometry* **2009,** 44, (5), 579-593.
1034. Dahlin, A. P.; Wetterhall, M.; Liljegren, G.; Bergstrom, S. K.; Andren, P.; Nyholm, L.; Markides, K. E.; Bergquist, J., Capillary electrophoresis coupled to mass spectrometry from a polymer modified poly(dimethylsiloxane) microchip with an integrated graphite electrospray tip. *The Analyst* **2005,** 130, (2), 193-199.
1035. Sikanen, T.; Tuomikoski, S.; Ketola, R. A.; Kostiainen, R.; Franssila, S.; Kotiaho, T., Fully Microfabricated and Integrated SU-8-Based Capillary Electrophoresis-Electrospray Ionization Microchips for Mass Spectrometry. *Analytical Chemistry* **2007,** 79, (23), 9135-9144.
1036. Park, S.-m.; Lee, K.; Craighead, H., On-chip coupling of electrochemical pumps and an SU-8 tip for electrospray ionization mass spectrometry. *Biomedical Microdevices* **2008,** 10, (6), 891-897.
1037. Wang, P.; Chen, Z.; Chang, H.-C., An integrated micropump and electrospray emitter system based on porous silica monoliths. *Electrophoresis* **2006,** 27, (20), 3964-3970.
1038. Lazar, I. M.; Grym, J.; Foret, F., Microfabricated devices: A new sample introduction approach to mass spectrometry. *Mass Spectrometry Reviews* **2006,** 25, (4), 573-594.
1039. Koster, S.; Verpoorte, E., A decade of microfluidic analysis coupled with electrospray mass spectrometry: An overview. *Lab on a Chip* **2007,** 7, (11), 1394-1412.
1040. Viskari, P. J.; Landers, J. P., Unconventional detection methods for microfluidic devices. *Electrophoresis* **2006,** 27, (9), 1797-1810.
1041. Liu, Y.; Sun, Y.; Sun, K.; Song, L.; Jiang, X., Recent developments employing new materials for readout in lab-on-a-chip. *Journal of Materials Chemistry* **2010,** 20, (35), 7305-7311.
1042. Nie, Z.; Nijhuis, C. A.; Gong, J.; Chen, X.; Kumachev, A.; Martinez, A. W.; Narovlyansky, M.; Whitesides, G. M., Electrochemical sensing in paper-based microfluidic devices. *Lab on a Chip* **2010,** 10, (4), 477-483.
1043. Siegel, A. C.; Phillips, S. T.; Wiley, B. J.; Whitesides, G. M., Thin, lightweight, foldable thermochromic displays on paper. *Lab on a Chip* **2009,** 9, (19), 2775-2781.
1044. Dungchai, W.; Chailapakul, O.; Henry, C. S., Use of multiple colorimetric indicators for paper-based microfluidic devices. *Analytica Chimica Acta* **2010,** 674, (2), 227-233.

1045. Pumera, M.; Merkoçi, A.; Alegret, S., New materials for electrochemical sensing VII. Microfluidic chip platforms. *TrAC Trends in Analytical Chemistry* **2006,** 25, (3), 219-235.
1046. Weigl, B.; Domingo, G.; LaBarre, P.; Gerlach, J., Towards non- and minimally instrumented, microfluidics-based diagnostic devices. *Lab on a Chip* **2008,** 8, (12), 1999-2014.
1047. Ellerbee, A. K.; Phillips, S. T.; Siegel, A. C.; Mirica, K. A.; Martinez, A. W.; Striehl, P.; Jain, N.; Prentiss, M.; Whitesides, G. M., Quantifying Colorimetric Assays in Paper-Based Microfluidic Devices by Measuring the Transmission of Light through Paper. *Analytical Chemistry* **2009,** 81, (20), 8447-8452.
1048. Lu, Y.; Shi, W.; Qin, J.; Lin, B., Low cost, portable detection of gold nanoparticle-labeled microfluidic immunoassay with camera cell phone. *Electrophoresis* **2009,** 30, (4), 579-582.
1049. Ruano-Lopez, J. M.; Agirregabiria, M.; Olabarria, G.; Verdoy, D.; Bang, D. D.; Bu, M.; Wolff, A.; Voigt, A.; Dziuban, J. A.; Walczak, R.; Berganzo, J., The SmartBioPhone[trade mark sign], a point of care vision under development through two European projects: OPTOLABCARD and LABONFOIL. *Lab on a Chip* **2009,** 9, (11), 1495-1499.
1050. Ahn, C. H.; Jin-Woo, C.; Beaucage, G.; Nevin, J. H.; Jeong-Bong, L.; Puntambekar, A.; Lee, J. Y., Disposable smart lab on a chip for point-of-care clinical diagnostics. *Proceedings of the IEEE* **2004,** 92, (1), 154-173.
1051. Gaster, R. S.; Hall, D. A.; Wang, S. X., nanoLAB: An ultraportable, handheld diagnostic laboratory for global health. *Lab on a Chip* **2011,** 11, (5), 950-956.
1052. Nie, Z.; Deiss, F.; Liu, X.; Akbulut, O.; Whitesides, G. M., Integration of paper-based microfluidic devices with commercial electrochemical readers. *Lab on a Chip* **2010,** 10, (22), 3163-3169.
1053. Lee, D.-S.; Jeon, B. G.; Ihm, C.; Park, J.-K.; Jung, M. Y., A simple and smart telemedicine device for developing regions: a pocket-sized colorimetric reader. *Lab on a Chip* **2011,** 11, (1), 120-126.
1054. Martinez, A. W.; Phillips, S. T.; Carrilho, E.; Thomas, S. W.; Sindi, H.; Whitesides, G. M., Simple Telemedicine for Developing Regions: Camera Phones and Paper-Based Microfluidic Devices for Real-Time, Off-Site Diagnosis. *Analytical Chemistry* **2008,** 80, (10), 3699-3707.
1055. Myers, F. B.; Lee, L. P., Innovations in optical microfluidic technologies for point-of-care diagnostics. *Lab on a Chip* **2008,** 8, (12), 2015-2031.
1056. Carlborg, C. F.; Gylfason, K. B.; Kazmierczak, A.; Dortu, F.; Banuls Polo, M. J.; Maquieira Catala, A.; Kresbach, G. M.; Sohlstrom, H.; Moh, T.; Vivien, L.; Popplewell, J.; Ronan, G.; Barrios, C. A.; Stemme, G.; van der Wijngaart, W., A packaged optical slot-waveguide ring resonator sensor array for multiplex label-free assays in labs-on-chips. *Lab on a Chip* **2010,** 10, (3), 281-290.
1057. Illa, X.; Ordeig, O.; Snakenborg, D.; Romano-Rodriguez, A.; Compton, R. G.; Kutter, J. P., A cyclo olefin polymer microfluidic chip with integrated gold microelectrodes for aqueous and non-aqueous electrochemistry. *Lab on a Chip* **2010,** 10, (10), 1254-1261.

1058. Laurell, T.; Marko-Varga, G.; Ekström, S.; Bengtsson, M.; Nilsson, J., Microfluidic components for protein characterization. *Reviews in Molecular Biotechnology* **2001,** 82, (2), 161-175.
1059. Burns, M. A.; Johnson, B. N.; Brahmasandra, S. N.; Handique, K.; Webster, J. R.; Krishnan, M.; Sammarco, T. S.; Man, P. M.; Jones, D.; Heldsinger, D.; Mastrangelo, C. H.; Burke, D. T., An Integrated Nanoliter DNA Analysis Device. *Science* **1998,** 282, (5388), 484-487.
1060. Easley, C. J.; Karlinsey, J. M.; Bienvenue, J. M.; Legendre, L. A.; Roper, M. G.; Feldman, S. H.; Hughes, M. A.; Hewlett, E. L.; Merkel, T. J.; Ferrance, J. P.; Landers, J. P., A fully integrated microfluidic genetic analysis system with sample-in-answer-out capability. *Proceedings of the National Academy of Sciences of the United States of America* **2006,** 103, (51), 19272-19277.
1061. Liu, R. H.; Yang, J.; Lenigk, R.; Bonanno, J.; Grodzinski, P., Self-Contained, Fully Integrated Biochip for Sample Preparation, Polymerase Chain Reaction Amplification, and DNA Microarray Detection. *Analytical Chemistry* **2004,** 76, (7), 1824-1831.
1062. Campbell, N. A., *Biology*. Third ed.; The Benjamin/Cummings Publishing Company, Inc.: 1993.
1063. Pearce, T. M.; Williams, J. C., Microtechnology: Meet neurobiology. *Lab on a Chip* **2007,** 7, (1), 30-40.
1064. Wightman, R. M.; Robinson, D. L., Transient changes in mesolimbic dopamine and their association with "reward". *Journal of Neurochemistry* **2002,** 82, (4), 721-735.
1065. Robinson, D. L.; Venton, B. J.; Heien, M. L. A. V.; Wightman, R. M., Detecting subsecond dopamine release with fast-scan cyclic voltammetry in vivo. *Clinical Chemistry* **2003,** 49, (10), 1763-1773.
1066. Singewald, N.; Philippu, A., Release of neurotransmitters in the locus coeruleus. *Progress in Neurobiology* **1998,** 56, (2), 237-267.
1067. Wang, M.; Roman, G. T.; Schultz, K.; Jennings, C.; Kennedy, R. T., Improved Temporal Resolution for in Vivo Microdialysis by Using Segmented Flow. *Analytical Chemistry* **2008,** 80, (14), 5607-5615.
1068. Cooper, J. D.; Heppert, K. E.; Davies, M. I.; Lunte, S. M., Evaluation of an osmotic pump for microdialysis sampling in an awake and untethered rat. *Journal of Neuroscience Methods* **2007,** 160, (2), 269-275.
1069. Nandi, P.; Lunte, S. M., Recent trends in microdialysis sampling integrated with conventional and microanalytical systems for monitoring biological events: A review. *Analytica Chimica Acta* **2009,** 651, (1), 1-14.
1070. Watson, C. J.; Venton, B. J.; Kennedy, R. T., In Vivo Measurements of Neurotransmitters by Microdialysis Sampling. *Analytical Chemistry* **2006,** 78, (5), 1391-1399.
1071. Guihen, E.; O'Connor, W., T. , Capillary and microchip electrophoresis in microdialysis: Recent applications. *Electrophoresis* **2010,** 31, (1), 55-64.
1072. Benveniste, H.; Hüttemeier, P. C., Microdialysis--Theory and application. *Progress in Neurobiology* **1990,** 35, (3), 195-215.

1073. Korf, J.; Huinink, K. D.; Posthuma-Trumpie, G. A., Ultraslow microdialysis and microfiltration for in-line, on-line and off-line monitoring. *Trends in Biotechnology* **2010,** 28, (3), 150-158.
1074. Lee, G. J.; Park, J. H.; Park, H. K., Microdialysis applications in neuroscience. *Neurological Research* **2008,** 30, 661-668.
1075. Fillenz, M., In vivo neurochemical monitoring and the study of behaviour. *Neuroscience & Biobehavioral Reviews* **2005,** 29, (6), 949-962.
1076. Yang, H.; Peters, J. L.; Allen, C.; Chern, S.-S.; Coalson, R. D.; Michael, A. C., A Theoretical Description of Microdialysis with Mass Transport Coupled to Chemical Events. *Analytical Chemistry* **2000,** 72, (9), 2042-2049.
1077. van der Zeyden, M.; Oldenziel, W. H.; Rea, K.; Cremers, T. I.; Westerink, B. H., Microdialysis of GABA and glutamate: Analysis, interpretation and comparison with microsensors. *Pharmacology Biochemistry and Behavior* **2008,** 90, (2), 135-147.
1078. Canales, J. J.; Corbalan, R.; Montoliu, C.; Llansola, M.; Monfort, P.; Erceg, S.; Hernandez-Viadel, M.; Felipo, V., Aluminium impairs the glutamate-nitric oxide-cGMP pathway in cultured neurons and in rat brain in vivo: molecular mechanisms and implications for neuropathology. *Journal of Inorganic Biochemistry* **2001,** 87, (1-2), 63-69.
1079. Nishiyama, A.; Abe, Y., Potential roles of interstitial fluid adenosine in the regulation of renal hemodynamics. *Biogenic Amines* **2003,** 17, (4-6), 459-474.
1080. Chan, S. H. H.; Chan, J. Y. H., Application of reverse microdialysis in the evaluation of neural regulation of cardiovascular functions. *Analytica Chimica Acta* **1999,** 379, (3), 275-279.
1081. O'Connor, W. T., Functional neuroanatomy of the ventral striopallidal GABA pathway. New sites of intervention in the treatment of schizophrenia. *Journal of Neuroscience Methods* **2001,** 109, (1), 31-39.
1082. Bowser, M. T.; Kennedy, R. T., In vivo monitoring of amine neurotransmitters using microdialysis with on-line capillary electrophoresis. *Electrophoresis* **2001,** 22, (17), 3668-76.
1083. O'Brien, K. B.; Esguerra, M.; Klug, C. T.; Miller, R. F.; Bowser, M. T., A high-throughput on-line microdialysis-capillary assay for D-serine. *Electrophoresis* **2003,** 24, (7-8), 1227-1235.
1084. Ciriacks, C. M.; Bowser, M. T., Monitoring d-Serine Dynamics in the Rat Brain Using Online Microdialysis-Capillary Electrophoresis. *Analytical Chemistry* **2004,** 76, (22), 6582-6587.
1085. Nandi, P.; Desai, D. P.; Lunte, S. M., Development of a PDMS-based microchip electrophoresis device for continuous online in vivo monitoring of microdialysis samples. *Electrophoresis* **2010,** 31, (8), 1414-1422.
1086. Sandlin, Z. D.; Shou, M.; Shackman, J. G.; Kennedy, R. T., Microfluidic Electrophoresis Chip Coupled to Microdialysis for in Vivo Monitoring of Amino Acid Neurotransmitters. *Analytical Chemistry* **2005,** 77, (23), 7702-7708.
1087. Wang, M.; Roman, G. T.; Perry, M. L.; Kennedy, R. T., Microfluidic Chip for High Efficiency Electrophoretic Analysis of Segmented Flow from a Microdialysis Probe and in Vivo Chemical Monitoring. *Analytical Chemistry* **2009,** 81, (21), 9072-9078.

1088. Mecker, L. C.; Martin, R. S., Integration of Microdialysis Sampling and Microchip Electrophoresis with Electrochemical Detection. *Analytical Chemistry* **2008,** 80, (23), 9257-9264.
1089. Presti, M. F.; Watson, C. J.; Kennedy, R. T.; Yang, M.; Lewis, M. H., Behavior-related alterations of striatal neurochemistry in a mouse model of stereotyped movement disorder. *Pharmacology, Biochemistry and Behavior* **2004,** 77, (3), 501-507.
1090. Kennedy, R. T.; Thompson, J. E.; Vickroy, T. W., In vivo monitoring of amino acids by direct sampling of brain extracellular fluid at ultralow flow rates and capillary electrophoresis. *Journal of Neuroscience Methods* **2002,** 114, (1), 39-49.
1091. Lada, M. W.; Vickroy, T. W.; Kennedy, R. T., High Temporal Resolution Monitoring of Glutamate and Aspartate in Vivo Using Microdialysis Online with Capillary Electrophoresis with Laser-Induced Fluorescence Detection. *Analytical Chemistry* **1997,** 69, (22), 4560-4565.
1092. Robinson, D. L.; Hermans, A.; Seipel, A. T.; Wightman, R. M., Monitoring Rapid Chemical Communication in the Brain. *Chemical Reviews* **2008,** 108, (7), 2554-2584.
1093. Kottegoda, S.; Shaik, I.; Shippy Scott, A., Demonstration of low flow push-pull perfusion. *Journal of Neuroscience Methods* **2002,** 121, (1), 93-101.
1094. Thongkhao-on, K.; Wirtshafter, D.; Shippy, S. A., Feeding specific glutamate surge in the rat lateral hypothalamus revealed by low-flow push-pull perfusion. *Pharmacology Biochemistry and Behavior* **2008,** 89, (4), 591-597.
1095. Gao, L.; Barber-Singh, J.; Kottegoda, S.; Wirtshafter, D.; Shippy, S. A., Determination of nitrate and nitrite in rat brain perfusates by capillary electrophoresis. *Electrophoresis* **2004,** 25, (9), 1264-1269.
1096. Gao, L.; Patterson II, E. E.; Shippy, S. A., Multiplexed detection of nitrate and nitrite for capillary electrophoresis with an automated device for high injection efficiency. *The Analyst* **2006,** 131, (2), 222-228.
1097. Patterson II, E. E.; Pritchett, J. S.; Shippy, S. A., High temporal resolution coupling of low-flow push-pull perfusion to capillary electrophoresis for ascorbate analysis at the rat vitreoretinal interface. *The Analyst* **2009,** 134, (2), 401-406.
1098. Pritchett, J. S.; Pulido, J. S.; Shippy, S. A., Measurement of Region-Specific Nitrate Levels of the Posterior Chamber of the Rat Eye Using Low-Flow Push-Pull Perfusion. *Analytical Chemistry* **2008,** 80, (14), 5342-5349.
1099. Cellar, N. A.; Burns, S. T.; Meiners, J.-C.; Chen, H.; Kennedy, R. T., Microfluidic chip for low-flow push-pull perfusion sampling in vivo with on-line analysis of amino acids. *Analytical chemistry* **2005,** 77, (21), 7067-73.
1100. Cellar, N. A.; Kennedy, R. T., A capillary-PDMS hybrid chip for separations-based sensing of neurotransmitters in vivo. *Lab on a Chip* **2006,** 6, (9), 1205-1212.
1101. Privette, T. H.; Myers, R. D., Peristaltic versus syringe pumps for push-pull perfusion: tissue pathology and dopamine recovery in rat neostriatum. *Journal of Neuroscience Methods* **1989,** 26, (3), 195-202.
1102. Myers, R. D.; Adell, A.; Lankford, M. F., Simultaneous comparison of cerebral dialysis and push-pull perfusion in the brain of rats: a critical review. *Neuroscience & Biobehavioral Reviews* **1998,** 22, (3), 371-387.

1103. Chisolm, C. N.; Evans, C. R.; Jennings, C.; Black, W. A.; Antosz, F. J.; Qiang, Y.; Diaz, A. R.; Kennedy, R. T., Development and characterization of "push-pull" sampling device with fast reaction quenching coupled to high-performance liquid chromatography for pharmaceutical process analytical technologies. *Journal of Chromatography A* **2010,** 1217, (48), 7471-7477.
1104. Tian, F.; Gourine, A. V.; Huckstepp, R. T. R.; Dale, N., A microelectrode biosensor for real time monitoring of l-glutamate release. *Analytica Chimica Acta* **2009,** 645, (1-2), 86-91.
1105. Oldenziel, W. H.; Dijkstra, G.; Cremers, T. I. F. H.; Westerink, B. H. C., In vivo monitoring of extracellular glutamate in the brain with a microsensor. *Brain Research* **2006,** 1118, (1), 34-42.
1106. Doong, R.-a.; Shih, H.-m., Glutamate optical biosensor based on the immobilization of glutamate dehydrogenase in titanium dioxide sol-gel matrix. *Biosensors and Bioelectronics* **2006,** 22, (2), 185-191.
1107. Oldenziel, W. H.; Dijkstra, G.; Cremers, T. I. F. H.; Westerink, B. H. C., Evaluation of Hydrogel-Coated Glutamate Microsensors. *Analytical Chemistry* **2006,** 78, (10), 3366-3378.
1108. Rutherford, E. C.; Pomerleau, F.; Huettl, P.; Stromberg, I.; Gerhardt, G. A., Chronic second-by-second measures ofl-glutamate in the central nervous system of freely moving rats. *Journal of Neurochemistry* **2007,** 102, 712-722.
1109. O'Neill, R. D.; Chang, S.-C.; Lowry, J. P.; McNeil, C. J., Comparisons of platinum, gold, palladium and glassy carbon as electrode materials in the design of biosensors for glutamate. *Biosensors and Bioelectronics* **2004,** 19, (11), 1521-1528.
1110. Pantano, P.; Kuhr, W. G., Enzyme-modified microelectrodes for in vivo neurochemical measurements. *Electroanalysis* **1995,** 7, (5), 405-416.
1111. Green, R. A.; et al., Conducting polymer-hydrogels for medical electrode applications. *Science and Technology of Advanced Materials* **2010,** 11, (1), 014107.
1112. O'Neill, R. D.; Rocchitta, G.; McMahon, C. P.; Serra, P. A.; Lowry, J. P., Designing sensitive and selective polymer/enzyme composite biosensors for brain monitoring in vivo. *TrAC Trends in Analytical Chemistry* **2008,** 27, (1), 78-88.
1113. Wilson, G. S.; Johnson, M. A., In-Vivo Electrochemistry: What Can We Learn about Living Systems? *Chemical Reviews* **2008,** 108, (7), 2462-2481.
1114. Alaejos, M. S.; Montelongo, F. J. G., Application of amperometric biosensors to the determination of vitamins and alpha-amino acids. *Chemical Reviews* **2004,** 104, (7), 3239-3265.
1115. Qin, S.; van der Zeyden, M.; Oldenziel, W.; Cremers, T.; Westerink, B., Microsensors for in vivo Measurement of Glutamate in Brain Tissue. *Sensors* **2008,** 8, (11), 6860-6884.
1116. Cordek, J.; Wang, X.; Tan, W., Direct immobilization of glutamate dehydrogenase on optical fiber probes for ultrasensitive glutamate detection. *Analytical Chemistry* **1999,** 71, (8), 1529-1533.
1117. Burmeister, J. J.; Pomerleau, F.; Palmer, M.; Day, B. K.; Huettl, P.; Gerhardt, G. A., Improved ceramic-based multisite microelectrode for rapid measurements of L-glutamate in the CNS. *Journal of Neuroscience Methods* **2002,** 119, (2), 163-71.

1118. Ryan, M. R.; Lowry, J. P.; ONeill, R. D., Biosensor for Neurotransmitter L-Glutamic Acid Designed for Efficient Use of L-Glutamate Oxidase and Effective Rejection of Interference. *Analyst* **1997,** 122, (1419-1424).
1119. Pantano, P.; Kuhr, W. G., Dehydrogenase-Modified Carbon-Fiber Microelectrodes for the Measurement of Neurotransmitter Dynamics. 2. Covalent Modification Utilizing Avidin-Biotin Technology. *Analytical Chemistry* **1993,** 65, 623-630.
1120. Pennington, J. M.; Millar, J.; Jones, C. P. L.; Owesson, C. Å.; McLaughlin, D. P.; Stamford, J. A., Simultaneous real-time amperometric measurement of catecholamines and serotonin at carbon fibre 'dident' microelectrodes. *Journal of Neuroscience Methods* **2004,** 140, (1-2), 5-13.
1121. Dressman, S. F.; Peters, J. L.; Michael, A. C., Carbon fiber microelectrodes with multiple sensing elements for in vivo voltammetry. *Journal of Neuroscience Methods* **2002,** 119, (1), 75-81.
1122. Garris, P. A.; Ensman, R.; Poehlman, J.; Alexander, A.; Langley, P. E.; Sandberg, S. G.; Greco, P. G.; Wightman, R. M.; Rebec, G. V., Wireless transmission of fast-scan cyclic voltammetry at a carbon-fiber microelectrode: proof of principle. *Journal of Neuroscience Methods* **2004,** 140, (1-2), 103-115.
1123. Bledsoe, J. M.; Kimble, C. J.; Covey, D. P.; Blaha, C. D.; Agnesi, F.; Mohseni, P.; Whitlock, S.; Johnson, D. M.; Horne, A.; Bennet, K. E.; Lee, K. H.; Garris, P. A., Development of the Wireless Instantaneous Neurotransmitter Concentration System for intraoperative neurochemical monitoring using fast-scan cyclic voltammetry. *Journal of neurosurgery* **2009,** 111, (4), 712-23.
1124. Heien, M. L. A. V.; Khan, A. S.; Ariansen, J. L.; Cheer, J. F.; Phillips, P. E. M.; Wassum, K. M.; Wightman, R. M., Real-time measurement of dopamine fluctuations after cocaine in the brain of behaving rats. *Proceedings of the National Academy of Sciences of the United States of America* **2005,** 102, (29), 10023-10028.
1125. Heien, M. L. A. V.; Johnson, M. A.; Wightman, R. M., Resolving Neurotransmitters Detected by Fast-Scan Cyclic Voltammetry. *Analytical Chemistry* **2004,** 76, (19), 5697-5704.
1126. Singh, Y. S.; Sawarynski, L. E.; Michael, H. M.; Ferrell, R. E.; Murphey-Corb, M. A.; Swain, G. M.; Patel, B. A.; Andrews, A. M., Boron-Doped Diamond Microelectrodes Reveal Reduced Serotonin Uptake Rates in Lymphocytes from Adult Rhesus Monkeys Carrying the Short Allele of the 5-HTTLPR. *ACS Chemical Neuroscience* **2009,** 1, (1), 49-64.
1127. Makos, M. A.; Han, K.-A.; Heien, M. L.; Ewing, A. G., Using in Vivo Electrochemistry To Study the Physiological Effects of Cocaine and Other Stimulants on the Drosophila melanogaster Dopamine Transporter. *ACS Chemical Neuroscience* **2009,** 1, (1), 74-83.
1128. Maina, F. K.; Mathews, T. A., Functional Fast Scan Cyclic Voltammetry Assay to Characterize Dopamine D2 and D3 Autoreceptors in the Mouse Striatum. *ACS Chemical Neuroscience* **2010,** 1, (6), 450-462.

1129. Zachek, M. K.; Takmakov, P.; Park, J.; Wightman, R. M.; McCarty, G. S., Simultaneous monitoring of dopamine concentration at spatially different brain locations in vivo. *Biosensors and Bioelectronics* **2010,** 25, (5), 1179-1185.
1130. Phillips, P. E. M.; Wightman, R. M., Critical guidelines for validation of the selectivity of in-vivo chemical microsensors. *TrAC Trends in Analytical Chemistry* **2003,** 22, (8), 509-514.
1131. Venton, B. J.; Wightman, R. M., Psychoanalytical electrochemistry: dopamine and behavior. *Analytical Chemistry* **2003,** 75, (19), 414A-421A.
1132. Ewing, A. G.; Strein, T. G.; Lau, Y. Y., Analytical chemistry in microenvironments: single nerve cells. *Accounts of Chemical Research* **1992,** 25, (10), 440-7.
1133. Bunin, M. A.; Prioleau, C.; Mailman, R. B.; Wightman, R. M., Release and uptake rates of 5-hydroxytryptamine in the dorsal raphe and substantia nigra reticulata of the rat brain. *Journal of Neurochemistry* **1998,** 70, (3), 1077-1087.
1134. Yoon, H.; et al., Aligned nanowire growth using lithography-assisted bonding of a polycarbonate template for neural probe electrodes. *Nanotechnology* **2008,** 19, (2), 025304.
1135. HajjHassan, M.; Chodavarapu, V.; Musallam, S., NeuroMEMS: Neural Probe Microtechnologies. *Sensors* **2008,** 8, (10), 6704-6726.
1136. Takeuchi, S.; Ziegler, D.; Yoshida, Y.; Mabuchi, K.; Suzuki, T., Parylene flexible neural probes integrated with microfluidic channels. *Lab on a Chip* **2005,** 5, (5), 519-523.
1137. Kozai, T. D. Y.; Kipke, D. R., Insertion shuttle with carboxyl terminated self-assembled monolayer coatings for implanting flexible polymer neural probes in the brain. *Journal of Neuroscience Methods* **2009,** 184, (2), 199-205.
1138. Mercanzini, A.; Cheung, K.; Buhl, D. L.; Boers, M.; Maillard, A.; Colin, P.; Bensadoun, J.-C.; Bertsch, A.; Renaud, P., Demonstration of cortical recording using novel flexible polymer neural probes. *Sensors and Actuators A: Physical* **2008,** 143, (1), 90-96.
1139. Tagawa, A.; Minami, H.; Mitani, M.; Noda, T.; Sasagawa, K.; Tokuda, T.; Tamura, H.; Hatanaka, Y.; Ishikawa, Y.; Shiosaka, S.; Ohta, J., Multimodal Complementary Metal–Oxide–Semiconductor Sensor Device for Imaging of Fluorescence and Electrical Potential in Deep Brain of Mouse. *Japanese Journal of Applied Physics* **2010,** 49, 01AG02.
1140. Kanno, S.; Kobayashi, R.; Sanghoon, L.; Jicheol, B.; Fukushima, T.; Sakamoto, K.; Katayama, N.; Mushiake, H.; Tanaka, T.; Koyanagi, M., Development of Si Neural Probe with Microfluidic Channel Fabricated Using Wafer Direct Bonding. *Japanese Journal of Applied Physics* **2009,** 48, 04C189.
1141. Ziegler, D.; Suzuki, T.; Takeuchi, S., Fabrication of Flexible Neural Probes With Built-In Microfluidic Channels by Thermal Bonding of Parylene. *Journal of Microelectromechanical Systems* **2006,** 15, (6), 1477-1482.
1142. Cheung, K. C.; Djupsund, K.; Dan, Y.; Lee, L. P., Implantable multichannel electrode array based on SOI technology. *Journal of Microelectromechanical Systems* **2003,** 12, (2), 179-184.

1143. Herwik, S.; et al., Fabrication technology for silicon-based microprobe arrays used in acute and sub-chronic neural recording. *Journal of Micromechanics and Microengineering* **2009,** 19, (7), 074008.
1144. Schneider, A.; Frasson, L.; Parittotokkaporn, T.; Rodriguez y Baena, F. M.; Davies, B. L.; Huq, S. E., Biomimetic microtexturing for neurosurgical probe surfaces to influence tribological characteristics during tissue penetration. *Microelectronic Engineering* **2009,** 86, (4-6), 1515-1517.
1145. Buzsaki, G., Large-scale recording of neuronal ensembles. *Nature Neuroscience* **2004,** 7, 446-451.
1146. Metz, S.; Bertsch, A.; Bertrand, D.; Renaud, P., Flexible polyimide probes with microelectrodes and embedded microfluidic channels for simultaneous drug delivery and multi-channel monitoring of bioelectric activity. *Biosensors and Bioelectronics* **2004,** 19, (10), 1309-1318.
1147. Wise, K. D.; Sodagar, A. M.; Ying, Y.; Gulari, M. N.; Perlin, G. E.; Najafi, K., Microelectrodes, Microelectronics, and Implantable Neural Microsystems. *Proceedings of the IEEE* **2008,** 96, (7), 1184-1202.
1148. Johnson, M. D.; Kao, O. E.; Kipke, D. R., Spatiotemporal pH dynamics following insertion of neural microelectrode arrays. *Journal of Neuroscience Methods* **2007,** 160, (2), 276-287.
1149. Musteata, F. M.; de Lannoy, I.; Gien, B.; Pawliszyn, J., Blood sampling without blood draws for in vivo pharmacokinetic studies in rats. *Journal of Pharmaceutical and Biomedical Analysis* **2008,** 47, (4-5), 907-912.
1150. Cobbe, S.; Connolly, S.; Ryan, D.; Nagle, L.; Eritja, R.; Fitzmaurice, D., DNA-Controlled Assembly of Protein-Modified Gold Nanoparticles. *Journal of Physical Chemistry B* **2003,** 107, 470-477.
1151. Perry, M.; Li, Q.; Kennedy, R. T., Review of recent advances in analytical techniques for the determination of neurotransmitters. *Analytica Chimica Acta* **2009,** 653, (1), 1-22.
1152. Lapainis, T.; Sweedler, J. V., Contributions of capillary electrophoresis to neuroscience. *Journal of Chromatography A* **2008,** 1184, (1-2), 144-158.
1153. Oguri, S.; Nomura, M.; Fujita, Y., Site-specific sampling of taurine from rat brain followed by on-line sample pre-concentration, throughout in-capillary derivatization and capillary electrophoresis. *Journal of Chromatography B* **2006,** 843, (2), 194-201.
1154. Kandel, E. R.; Schwartz, J. H.; Jessell, T. M., *Principles of Neural Science*. McGraw-Hill: 2000.
1155. Purves, D.; Augustine, G. J.; Fitzpatrick, D.; Katz, L. C.; LaMantia, A.-S.; McNamara, J. O., *Neuroscience*. Sinauer: 1997.
1156. Dykes, R. W.; Dudar, J. D.; Tanji, D. G.; Publicover, N. G., Somatotopic Projections of Mystacial Vibrissae on Cerebral Cortex of Cats. *Journal of Neurophysiology* **1977,** 40, (5), 997-1014.
1157. Welker, C.; Woolsey, T. A., Structure of Layer IV in the Somatosensory Neocortex of the Rat: Description and Comparison with the Mouse. *Journal of Comparative Neurology* **1974,** 158, 437-454.

1158. Simons, D. J.; Woolsey, T. A., Functional organization in mouse barrel cortex. *Brain Research* **1979,** 165, 327-332.
1159. Kim, U.; Ebner, F. F., Barrels and Septa: Separate Circuits in Rat Barrel Field Cortex. *The Journal of Comparative Neurology* **1999,** 408, 489-505.
1160. Lee, S.; Carvell, G. E.; Simons, D. J., Motor modulation of afferent somatosensory circuits. *Nature Neuroscience* **2008,** 11, (12), 1430-1438.
1161. Sato, T. R.; Svoboda, K., The Functional Properties of Barrel Cortex Neurons Projecting to the Primary Motor Cortex. *Journal of Neuroscience* **2010,** 30, (12), 4256-4260.
1162. Inan, M.; Crair, M. C., Development of Cortical Maps: Perspectives From the Barrel Cortex. *Neuroscientist* **2007,** 13, 49-61.
1163. Petersen, C. C. H., The Functional Organization of the Barrel Cortex. *Neuron* **2007,** 56, (2), 339-355.
1164. Giaume, C.; Maravall, M.; Welker, E.; Bonvento, G., The Barrel Cortex as a Model to Study Dynamic Neuroglial Interaction. *Neuroscientist* **2009,** 15, 351-366.
1165. Woolsey, T. A.; Van Der Loos, H., The Structural Organization of Layer IV in the Somatosensory Region (SI) of Mouse Cerebral Cortex. *Brain Research* **1970,** 17, (2), 205-242.
1166. Brecht, M., Barrel cortex and whisker-mediated behaviors. *Current Opinion in Neurobiology* **2007,** 17, (4), 408-416.
1167. Woolsey, T. A., Barrels: 25 Years Later. *Somatosensory and Motor Research* **1996,** 13, (3-4), 181-186.
1168. Hutson, K. A.; Masterton, R. B., The Sensory Contribution of a Single Vibrissa's Cortical Barrel. *Journal of Neurophysiology* **1996,** 56, (4), 1196-1223.
1169. Simons, D. J., Response Properties of Vibrissa Units in Rat SI Somatosensory Neocortex. *Journal of Neurophysiology* **1978,** 41, (3), 798-820.
1170. Bermejo, R.; Harvey, M.; Gao, P.; Zeigler, P., Conditioned Whisking in the Rat. *Somatosensory and Motor Research* **1996,** 13, (3-4), 225-233.
1171. Stanley, G. B., It's not you, it's me. Really. *Nature Neuroscience* **2009,** 12, (4), 374-375.
1172. Masino, S. A.; Kwon, M. C.; Dory, Y.; Frostig, R. D., Characterization of functional organization within rat barrel cortex using intrinsic signal optical imaging through a thinned skull. *Proceedings of the National Academy of Sciences USA* **1993,** 90, 9998-10002.
1173. Shimegi, S.; Akasaki, T.; Ichikawa, T.; Sato, H., Physiological and Anatomical Organization of Multiwhisker Response Interactions in the Barrel Cortex of Rats. *The Journal of Neuroscience* **2000,** 20, (16), 6241-6248.
1174. Kyriazi, H. T.; Carvell, G. E.; Simons, D. J., Off Response Transformations in the Whisker/Barrel System. *Journal of Neurophysiology* **1994,** 72, (1), 392-401.
1175. Simmons, D. J., Multi-whisker stimulation and its effects on vibrissa units in rat Sml barrel cortex. *Brain Research* **1983,** 276, 178-182.
1176. Corey, D. P.; Hudspeth, A. J., Mechanical stimulation and micromanipulation with piezoelectric bimorph elements. *Journal of Neuroscience Methods* **1980,** 3, 183-202.

1177. Peterson, B. E.; Goldreich, D., A new approach to optical imaging applied to rat barrel cortex. *Journal of Neuroscience Methods* **1994,** 54, 39-47.
1178. Peterson, B. E.; Goldreich, D.; Merzenich, M. M., Optical Imaging and Electrophysiology of Rat Barrel Cortex. I. Responses to Small Single-vibrissa Deflections. *Cerebral Cortex* **1998,** 8, 173-183.
1179. Goldreich, D.; Peterson, B. E.; Merzenich, M. M., Optical Imaging and Electrophysiology of Rat Barrel Cortex. II. Responses to Paired-vibrissa Deflections. *Cerebral Cortex* **1998,** 8, 184-192.
1180. Shimegi, S.; Ichikawa, T.; Akasaki, T.; Sato, H., Temporal Characteristics of Response Integration Evoked by Multiple Whisker Stimulations in the Barrel Cortex of Rats. *The Journal of Neuroscience* **1999,** 19, (22), 10164-10175.
1181. Sachdev, R. N. S.; Sellien, H.; Ebner, F. F., Direct Inhibition Evoked by Whisker Stimulation in Somatic Sensory (SI) Barrel Field Cortex of the Awake Rat. *The American Physiological Society* **2000,** 84, (3), 1497-1504.
1182. Temereanca, S.; Brown, E. N.; Simons, D. J., Rapid Changes in Thalamic Firing Synchrony during Repetitive Whisker Stimulation. *Journal of Neuroscience* **2008,** 28, (44), 11153-11164.
1183. Lak, A.; Arabzadeh, E.; Harris, J. A.; Diamond, M. E., Correlated physiological and perceptual effects of noise in a tactile stimulus. *Proceedings of the National Academy of Sciences* **2010,** 107, (17), 7981-7986.
1184. O'Connor, D. H.; Peron, S. P.; Huber, D.; Svoboda, K., Neural Activity in Barrel Cortex Underlying Vibrissa-Based Object Localization in Mice. *Neuron* **2010,** 67, (6), 1048-1061.
1185. Takuwa, H.; Autio, J.; Nakayama, H.; Matsuura, T.; Obata, T.; Okada, E.; Masamoto, K.; Kanno, I., Reproducibility and variance of a stimulation-induced hemodynamic response in barrel cortex of awake behaving mice. *Brain Research* **2011,** 1369, 103-111.
1186. Armstrong-James, M.; Fox, K.; Ashis, D.-G., Flow of Excitation Within Rat Barrel Cortex on Striking a Single Vibrissa. *Journal of Neurophysiology* **1992,** 68, (4), 1345-1358.
1187. Zhu, J. J.; Connors, B. W., Intrinsic Firing Patterns and Whisker-Evoked Synaptic Responses of Neurons in the Rat Barrel Cortex. *The American Physiological Society* **1999,** 81, (3), 1171-1183.
1188. Asensio-Ramos, M.; Hernández-Borges, J.; Rocco, A.; Fanali, S., Food analysis: A continuous challenge for miniaturized separation techniques. *Journal of Separation Science* **2009,** 32, (21), 3764-3800.
1189. Herrero, M.; García-Cañas, V.; Simo, C.; Cifuentes, A., Recent advances in the application of capillary electromigration methods for food analysis and Foodomics. *Electrophoresis* **2010,** 31, (1), 205-228.
1190. Ávila, M.; González, M. C.; Zougagh, M.; Escarpa, A.; Ríos, Á., Rapid sample screening method for authenticity controlling vanilla flavors using a CE microchip approach with electrochemical detection. *Electrophoresis* **2007,** 28, (22), 4233-4239.

1191. Xuan, Y.; Scheuermann, E. B.; Meda, A. R.; Jacob, P.; von Wirén, N.; Weber, G., CE of phytosiderophores and related metal species in plants. *Electrophoresis* **2007,** 28, (19), 3507-3519.
1192. Fouad, M.; Jabasini, M.; Kaji, N.; Terasaka, K.; Tokeshi, M.; Mizukami, H.; Baba, Y., Microchip analysis of plant glucosinolates. *Electrophoresis* **2008,** 29, (11), 2280-2287.
1193. Yang, C. H.; Huang, K. S.; Lin, Y. S.; Lu, K.; Tzeng, C. C.; Wang, E. C.; Lin, C. H.; Hsu, W. Y.; Chang, J. Y., Microfluidic assisted synthesis of multi-functional polycaprolactone microcapsules: incorporation of CdTe quantum dots, Fe3O4 superparamagnetic nanoparticles and tamoxifen anticancer drugs. *Lab on a Chip* **2009,** 9, (7), 961-965.
1194. Samsuri, F.; Alkaisi, M. M.; Mitchell, J. S.; Evans, J. J., Replication of cancer cells using soft lithography bioimprint technique. *Microelectronic Engineering* **2010,** 87, (5-8), 699-703.
1195. den Toonder, J., Circulating tumor cells: the Grand Challenge. *Lab on a Chip* **2011,** 11, (3), 375-377.
1196. Kaji, H.; Yokoi, T.; Kawashima, T.; Nishizawa, M., Controlled cocultures of HeLa cells and human umbilical vein endothelial cells on detachable substrates. *Lab on a Chip* **2009,** 9, (3), 427-432.
1197. Vincent, M. E.; Liu, W.; Haney, E. B.; Ismagilov, R. F., Microfluidic stochastic confinement enhances analysis of rare cells by isolating cells and creating high density environments for control of diffusible signals. *Chemical Society Reviews* **2010,** 39, (3), 974-984.
1198. Day, P. J. R., Miniaturized PCR systems for cancer diagnosis. *Biochemical Society Transactions* **2009,** 037, (2), 424-426.
1199. Liu, W.; Sun, P.; Yang, L.; Wang, J.; Li, L.; Wang, J., Assay of glioma cell responses to an anticancer drug in a cell-based microfluidic device. *Microfluidics and Nanofluidics* **2010,** 9, (4), 717-725.
1200. Sun, J.; Masterman-Smith, M. D.; Graham, N. A.; Jiao, J.; Mottahedeh, J.; Laks, D. R.; Ohashi, M.; DeJesus, J.; Kamei, K.-i.; Lee, K.-B.; Wang, H.; Yu, Z. T. F.; Lu, Y.-T.; Hou, S.; Li, K.; Liu, M.; Zhang, N.; Wang, S.; Angenieux, B.; Panosyan, E.; Samuels, E. R.; Park, J.; Williams, D.; Konkankit, V.; Nathanson, D.; van Dam, R. M.; Phelps, M. E.; Wu, H.; Liau, L. M.; Mischel, P. S.; Lazareff, J. A.; Kornblum, H. I.; Yong, W. H.; Graeber, T. G.; Tseng, H.-R., A Microfluidic Platform for Systems Pathology: Multiparameter Single-Cell Signaling Measurements of Clinical Brain Tumor Specimens. *Cancer Research* **2010,** 70, (15), 6128-6138.
1201. Klostranec, J. M.; Xiang, Q.; Farcas, G. A.; Lee, J. A.; Rhee, A.; Lafferty, E. I.; Perrault, S. D.; Kain, K. C.; Chan, W. C. W., Convergence of Quantum Dot Barcodes with Microfluidics and Signal Processing for Multiplexed High-Throughput Infectious Disease Diagnostics. *Nano Letters* **2007,** 7, (9), 2812-2818.
1202. Lagally, E. T.; Scherer, J. R.; Blazej, R. G.; Toriello, N. M.; Diep, B. A.; Ramchandani, M.; Sensabaugh, G. F.; Riley, L. W.; Mathies, R. A., Integrated Portable Genetic Analysis Microsystem for Pathogen/Infectious Disease Detection. *Analytical Chemistry* **2004,** 76, (11), 3162-3170.

1203. Liu, R. H.; Lodes, M. J.; Nguyen, T.; Siuda, T.; Slota, M.; Fuji, H. S.; McShea, A., Validation of A Fully Integrated Microfluidic Array Device for Influenza A Subtype Identification and Sequencing. *Analytical Chemistry* **2006,** 78, (12), 4184-4193.
1204. Chun, A. L., Nanoparticles offer hope for TB detection. *Nature Nanotechnology* **2009,** 4, (11), 698-699.
1205. Antia, M.; Herricks, T.; Rathod, P. K., Microfluidic approaches to malaria pathogenesis. *Cellular Microbiology*, **2008, (**10), 1968-1974.
1206. Lee, Y.-F.; Lien, K.-Y.; Lei, H.-Y.; Lee, G.-B., An integrated microfluidic system for rapid diagnosis of dengue virus infection. *Biosensors and Bioelectronics* **2009,** 25, (4), 745-752.
1207. Pal, R.; Yang, M.; Lin, R.; Johnson, B. N.; Srivastava, N.; Razzacki, S. Z.; Chomistek, K. J.; Heldsinger, D. C.; Haque, R. M.; Ugaz, V. M.; Thwar, P. K.; Chen, Z.; Alfano, K.; Yim, M. B.; Krishnan, M.; Fuller, A. O.; Larson, R. G.; Burke, D. T.; Burns, M. A., An integrated microfluidic device for influenza and other genetic analyses. *Lab on a Chip* **2005,** 5, (10), 1024-1032.
1208. Desai, D.; Wu, G.; Zaman, M. H., Tackling HIV through robust diagnostics in the developing world: current status and future opportunities. *Lab on a Chip* **2011,** 11, (2), 194-211.
1209. Lee, W. G.; Kim, Y.-G.; Chung, B. G.; Demirci, U.; Khademhosseini, A., Nano/Microfluidics for diagnosis of infectious diseases in developing countries. *Advanced Drug Delivery Reviews* **2010,** 62, (4-5), 449-457.
1210. Wong, A. P.; Gupta, M.; Shevkoplyas, S. S.; Whitesides, G. M., Egg beater as centrifuge: isolating human blood plasma from whole blood in resource-poor settings. *Lab on a Chip* **2008,** 8, (12), 2032-2037.
1211. Yager, P.; Edwards, T.; Fu, E.; Helton, K.; Nelson, K.; Tam, M. R.; Weigl, B. H., Microfluidic diagnostic technologies for global public health. *Nature* **2006,** 442, (7101), 412-418.
1212. Martinez, A. W.; Phillips, S. T.; Whitesides, G. M.; Carrilho, E., Diagnostics for the Developing World: Microfluidic Paper-Based Analytical Devices. *Analytical Chemistry* **2009,** 82, (1), 3-10.
1213. Skelley, A. M.; Scherer, J. R.; Aubrey, A. D.; Grover, W. H.; Ivester, R. H. C.; Ehrenfreund, P.; Grunthaner, F. J.; Bada, J. L.; Mathies, R. A., Development and evaluation of a microdevice for amino acid biomarker detection and analysis on Mars. *Proceedings of the National Academy of Sciences of the United States of America* **2005,** 102, (4), 1041-1046.
1214. Benhabib, M.; Chiesl, T. N.; Stockton, A. M.; Scherer, J. R.; Mathies, R. A., Multichannel Capillary Electrophoresis Microdevice and Instrumentation for in Situ Planetary Analysis of Organic Molecules and Biomarkers. *Analytical Chemistry* **2010,** 82, (6), 2372-2379.
1215. Stockton, A. M.; Chiesl, T. N.; Scherer, J. R.; Mathies, R. A., Polycyclic Aromatic Hydrocarbon Analysis with the Mars Organic Analyzer Microchip Capillary Electrophoresis System. *Analytical Chemistry* **2008,** 81, (2), 790-796.
1216. Wang, J.; Ren, L.; Li, L.; Liu, W.; Zhou, J.; Yu, W.; Tong, D.; Chen, S., Microfluidics: A new cosset for neurobiology. *Lab on a Chip* **2009,** 9, (5), 644-652.

1217. Weibel, D. B.; Garstecki, P.; Whitesides, G. M., Combining microscience and neurobiology. *Current Opinion in Neurobiology* **2005,** 15, (5), 560-567.
1218. Taylor, A. M.; Jeon, N. L., Micro-scale and microfluidic devices for neurobiology. *Current Opinion in Neurobiology* **2010,** 20, (5), 640-647.
1219. Shige, X.; Wenwen, L.; Zhuo, H.; Long, C.; Kang, S.; Dong, H.; Wei, Z.; Xingyu, J., Development of neurons on micropatterns reveals that growth cone responds to a sharp change of concentration of laminin. *Electrophoresis* **2010,** 31, 3144-3151.
1220. Millet, L. J.; Stewart, M. E.; Nuzzo, R. G.; Gillette, M. U., Guiding neuron development with planar surface gradients of substrate cues deposited using microfluidic devices. *Lab on a Chip* **2010,** 10, (12), 1525-1535.
1221. Kothapalli, C. R.; van Veen, E.; de Valence, S.; Chung, S.; Zervantonakis, I. K.; Gertler, F. B.; Kamm, R. D., A high-throughput microfluidic assay to study neurite response to growth factor gradients. *Lab on a Chip* **2011,** 11, (3), 497-507.
1222. Zhang, K.; Osakada, Y.; Vrljic, M.; Chen, L.; Mudrakola, H. V.; Cui, B., Single-molecule imaging of NGF axonal transport in microfluidic devices. *Lab on a Chip* **2010,** 10, (19), 2566-2573.
1223. Wang, C. J.; Li, X.; Lin, B.; Shim, S.; Ming, G.-l.; Levchenko, A., A microfluidics-based turning assay reveals complex growth cone responses to integrated gradients of substrate-bound ECM molecules and diffusible guidance cues. *Lab on a Chip* **2008,** 8, (2), 227-237.
1224. Lau, A. Y.; Hung, P. J.; Wu, A. R.; Lee, L. P., Open-access microfluidic patch-clamp array with raised lateral cell trapping sites. *Lab on a Chip* **2006,** 6, (12), 1510-1515.
1225. Chen, C.; Folch, A., A high-performance elastomeric patch clamp chip. *Lab on a Chip* **2006,** 6, (10), 1338-1345.
1226. Xu, B.; Liu, Z.; Lee, Y.-K.; Mak, A.; Yang, M., A PDMS microfluidic system with poly(ethylene glycol)/SU-8 based apertures for planar whole cell-patch-clamp recordings. *Sensors and Actuators A: Physical* **2011,** 166, (2), 219-225.
1227. Koester, P. J.; Buehler, S. M.; Stubbe, M.; Tautorat, C.; Niendorf, M.; Baumann, W.; Gimsa, J., Modular glass chip system measuring the electric activity and adhesion of neuronal cells-application and drug testing with sodium valproic acid. *Lab on a Chip* **2010,** 10, (12), 1579-1586.
1228. Dahan, E.; Bize, V.; Lehnert, T.; Horisberger, J. D.; Gijs, M. A. M., Rapid fluidic exchange microsystem for recording of fast ion channel kinetics in Xenopus oocytes. *Lab on a Chip* **2008,** 8, (11), 1809-1818.
1229. Ben-Yakar, A.; Bourgeois, F., Ultrafast laser nanosurgery in microfluidics for genome-wide screenings. *Current Opinion in Biotechnology* **2009,** 20, (1), 100-105.
1230. Taylor, A. M.; Blurton-Jones, M.; Rhee, S. W.; Cribbs, D. H.; Cotman, C. W.; Jeon, N. L., A microfluidic culture platform for CNS axonal injury, regeneration and transport. *Nature Methods* **2005,** 2, (8), 599-605.
1231. Guo, S. X.; Bourgeois, F.; Chokshi, T.; Durr, N. J.; Hilliard, M. A.; Chronis, N.; Ben-Yakar, A., Femtosecond laser nanoaxotomy lab-on-a-chip for in vivo nerve regeneration studies. *Nature Methods* **2008,** 5, (6), 531-533.

1232. Kim, Y.-t.; Karthikeyan, K.; Chirvi, S.; Dave, D. P., Neuro-optical microfluidic platform to study injury and regeneration of single axons. *Lab on a Chip* **2009,** 9, (17), 2576-2581.
1233. Vahidi, B.; Park, J. W.; Kim, H. J.; Jeon, N. L., Microfluidic-based strip assay for testing the effects of various surface-bound inhibitors in spinal cord injury. *Journal of Neuroscience Methods* **2008,** 170, (2), 188-196.
1234. Blake, A. J.; Rodgers, F. C.; Bassuener, A.; Hippensteel, J. A.; Pearce, T. M.; Pearce, T. R.; Zarnowska, E. D.; Pearce, R. A.; Williams, J. C., A microfluidic brain slice perfusion chamber for multisite recording using penetrating electrodes. *Journal of Neuroscience Methods* **2010,** 189, (1), 5-13.
1235. Choi, Y.; McClain, M.; LaPlaca, M.; Frazier, A.; Allen, M., Three dimensional MEMS microfluidic perfusion system for thick brain slice cultures. *Biomedical Microdevices* **2007,** 9, (1), 7-13.
1236. Blake, A. J.; Pearce, T. M.; Rao, N. S.; Johnson, S. M.; Williams, J. C., Multilayer PDMS microfluidic chamber for controlling brain slice microenvironment. *Lab on a Chip* **2007,** 7, (7), 842-849.
1237. Queval, A.; Ghattamaneni, N. R.; Perrault, C. M.; Gill, R.; Mirzaei, M.; McKinney, R. A.; Juncker, D., Chamber and microfluidic probe for microperfusion of organotypic brain slices. *Lab on a Chip* **2010,** 10, (3), 326-334.
1238. Shi, W.; Qin, J.; Ye, N.; Lin, B., Droplet-based microfluidic system for individual Caenorhabditis elegans assay. *Lab on a Chip* **2008,** 8, (9), 1432-1435.
1239. Wang, Y.; Wang, J.; Du, W.; Feng, X.; Liu, B.-F., Identification of the neuronal effects of ethanol on C. elegans by in vivo fluorescence imaging on a microfluidic chip. *Analytical and Bioanalytical Chemistry* **2011,** 399, (10), 3475-3481.
1240. Ma, H.; Jiang, L.; Shi, W.; Qin, J.; Lin, B., A programmable microvalve-based microfluidic array for characterization of neurotoxin-induced responses of individual C. elegans. *Biomicrofluidics* **2009,** 3, (4), 044114-8.
1241. Shi, W.; Wen, H.; Lu, Y.; Shi, Y.; Lin, B.; Qin, J., Droplet microfluidics for characterizing the neurotoxin-induced responses in individual Caenorhabditis elegans. *Lab on a Chip* **2010,** 10, (21), 2855-2863.
1242. Tan, H. Y.; Loke, W. K.; Tan, Y. T.; Nguyen, N.-T., A lab-on-a-chip for detection of nerve agent sarin in blood. *Lab on a Chip* **2008,** 8, (6), 885-891.
1243. Berdondini, L.; Imfeld, K.; Maccione, A.; Tedesco, M.; Neukom, S.; Koudelka-Hep, M.; Martinoia, S., Active pixel sensor array for high spatio-temporal resolution electrophysiological recordings from single cell to large scale neuronal networks. *Lab on a Chip* **2009,** 9, (18), 2644-2651.
1244. Wang, M.; Slaney, T.; Mabrouk, O.; Kennedy, R. T., Collection of nanoliter microdialysate fractions in plugs for off-line in vivo chemical monitoring with up to 2 s temporal resolution. *Journal of Neuroscience Methods* **2010,** 190, (1), 39-48.
1245. Nandigam, R. K.; Kroll, D. M., Three-Dimensional Modeling of the Brain's ECS by Minimum Configurational Energy Packing of Fluid Vesicles. *Biophysical Journal* **2007,** 92, (10), 3368-3378.

1246. Thorne, R. G.; Hrabetova, S.; Nicholson, C., Diffusion of Epidermal Growth Factor in Rat Brain Extracellular Space Measured by Integrative Optical Imaging. *Journal of Neurophysiology* **2004,** 92, (6), 3471-3481.
1247. Rusakov, D. A.; Kullmann, D. M., Geometric and viscous components of the tortuosity of the extracellular space in the brain. *Proceedings of the National Academy of Sciences of the United States of America* **1998,** 95, (15), 8975-8980.
1248. Chen, K. C.; Nicholson, C., Changes in brain cell shape create residual extracellular space volume and explain tortuosity behavior during osmotic challenge. *Proceedings of the National Academy of Sciences of the United States of America* **2000,** 97, (15), 8306-8311.
1249. Guy, Y.; Muha, R. J.; Sandberg, M.; Weber, S. G., Determination of zeta-Potential and Tortuosity in Rat Organotypic Hippocampal Cultures from Electroosmotic Velocity Measurements under Feedback Control. *Analytical Chemistry* **2009,** 81, (8), 3001-3007.
1250. Perez-Pinzon, M. A.; Tao, L.; Nicholson, C., Extracellular potassium, volume fraction, and tortuosity in rat hippocampal CA1, CA3, and cortical slices during ischemia. *Journal of Neurophysiology* **1995,** 74, (2), 565-573.
1251. Vorisek, I.; Sykova, E., Measuring diffusion parameters in the brain: comparing the real-time iontophoretic method and diffusion-weighted magnetic resonance. *Acta Physiologica* **2009,** 195, (1), 101-110.
1252. Sykova, E.; Nicholson, C., Diffusion in Brain Extracellular Space. *Physiological Reviews* **2008,** 88, (4), 1277-1340.
1253. Hrabetová, S.; Nicholson, C., Contribution of dead-space microdomains to tortuosity of brain extracellular space. *Neurochemistry International* **2004,** 45, (4), 467-477.
1254. Hrabe, J.; Hrabetová, S.; Segeth, K., A Model of Effective Diffusion and Tortuosity in the Extracellular Space of the Brain. *Biophysical Journal* **2004,** 87, (3), 1606-1617.
1255. Hrabetova, S.; Hrabe, J.; Nicholson, C., Dead-Space Microdomains Hinder Extracellular Diffusion in Rat Neocortex during Ischemia. *The Journal of Neuroscience* **2003,** 23, (23), 8351-8359.
1256. Paxinos, G.; Watson, C., *The Rat Brain in Stereotaxic Coordinates*. Fifth ed.; Elsevier Academic Press: 2005.
1257. Handique, K.; Burke, D. T.; Mastrangelo, C. H.; Burns, M. A., On-Chip Thermopneumatic Pressure for Discrete Drop Pumping. *Analytical Chemistry* **2001,** 73, (8), 1831-1838.
1258. Machauf (Prochaska), A.; Nemirovsky, Y.; Dinnar, U., A membrane micropump electrostatically actuated across the working fluid. *Journal of Micromechanics and Microengineering* **2005,** 15, 2309-2316.
1259. Koch, M.; Harris, N.; Evans, A. G. R.; White, N. M.; Brunnschweiler, A., A novel micromachined pump based on thick-film piezoelectric actuation. *Sensors and Actuators A: Physical* **1998,** A70, (1-2), 98-103.

1260. Jang, L.-S.; Li, Y.-J.; Lin, S.-J.; Hsu, Y.-C.; Yao, W.-S.; Tsai, M.-C.; Hou, C.-C., A stand-alone peristaltic micropump based on piezoelectric actuation. *Biomedical Microdevices* **2007,** 9, (2), 185-94.
1261. Piezo Systems, Inc. - Catalog #7B. www.piezo.com/catalog7B.pdf
1262. Sudarsan Arjun, P.; Ugaz Victor, M., Printed circuit technology for fabrication of plastic-based microfluidic devices. *Analytical Chemistry* **2004,** 76, (11), 3229-35.
1263. He, M.; Yuan, X.; Bu, J.; Cheong Wai, C., Hybrid sample-inverted reflow and soft-lithography technique for fabrication of conicoid microlens arrays. *Applied optics* **2005,** 44, (19), 4130-5.
1264. Keller, S.; et al., Processing of thin SU-8 films. *Journal of Micromechanics and Microengineering* **2008,** 18, (12), 125020.
1265. Choi, K. M., Photopatternable silicon elastomers with enhanced mechanical properties for high-fidelity nanoresolution soft lithography. *Journal of Physical Chemistry B* **2005,** 109, (46), 21525-31.
1266. Koesdjojo, M. T.; Tennico, Y. H.; Remcho, V. T., Fabrication of a Microfluidic System for Capillary Electrophoresis Using a Two-Stage Embossing Technique and Solvent Welding on Poly(methyl methacrylate) with Water as a Sacrificial Layer. *Analytical Chemistry* **2008,** 80, (7), 2311-2318.
1267. Han, A.; Wang, O.; Graff, M.; Mohanty, S. K.; Edwards, T. L.; Han, K.-H.; Frazier, A. B., Multi-layer plastic/glass microfluidic systems containing electrical and mechanical functionality. *Lab on a Chip* **2003,** 3, (3), 150-157.
1268. Steigert, J.; et al., Rapid prototyping of microfluidic chips in COC. *Journal of Micromechanics and Microengineering* **2007,** 17, (2), 333.
1269. Kim, S.; et al., Hybrid micromachining using a nanosecond pulsed laser and micro EDM. *Journal of Micromechanics and Microengineering* **2010,** 20, (1), 015037.
1270. Damean, N.; Regtien, P. P. L., Poiseuille number for the fully developed laminar flow through hexagonal ducts etched in <1 0 0> silicon. *Sensors and Actuators A: Physical* **2001,** 90, (1-2), 96-101.
1271. Futai, N.; Gu, W.; Takayama, S., Rapid Prototyping of Microstructures with Bell-Shaped Cross-Sections and Its Application to Deformation-Based Microfluidic Valves. *Advanced Materials* **2004,** 16, (15), 1320-1323.
1272. Park, W.; Han, S.; Kwon, S., Fabrication of membrane-type microvalves in rectangular microfluidic channels via seal photopolymerization. *Lab on a Chip* **2010,** 10, (20), 2814-2817.
1273. Abdelgawad, M.; Wu, C.; Chien, W.-Y.; Geddie, W. R.; Jewett, M. A. S.; Sun, Y., A fast and simple method to fabricate circular microchannels in polydimethylsiloxane (PDMS). *Lab on a Chip* **2011,** 11, (3), 545-551.
1274. Wang, G.-J.; Ho, K.-H.; Hsu, S.-H.; Wang, K.-P., Microvessel scaffold with circular microchannels by photoresist melting. *Biomedical Microdevices* **2007,** 9, (5), 657-63.
1275. Park, J.; Kim, D.-H.; Kim, G.; Kim, Y.; Choi, E.; Levchenko, A., Simple haptotactic gradient generation within a triangular microfluidic channel. *Lab on a Chip* **2010,** 10, (16), 2130-2138.

1276. Wen, J.; Albrecht, J. W.; Jensen, K. F., Microfluidic preparative free-flow isoelectric focusing in a triangular channel: System development and characterization. *Electrophoresis* **2010,** 31, 1606-1614.
1277. Kumi, G.; Yanez, C. O.; Belfield, K. D.; Fourkas, J. T., High-speed multiphoton absorption polymerization: fabrication of microfluidic channels with arbitrary cross-sections and high aspect ratios. *Lab on a Chip* **2010,** 10, (8), 1057-1060.
1278. Young, D. F.; Munson, B. R.; Okiishi, T. H., *A Brief Introduction to Fluid Mechanics*. Third ed.; John Wiley & Sons, Inc.: 2004.
1279. Sutanto, J.; et al., Design, microfabrication and testing of a CMOS compatible bistable electromagnetic microvalve with latching/unlatching mechanism on a single wafer. *Journal of Micromechanics and Microengineering* **2006,** 16, (2), 266.
1280. Fuchiwaki, M.; Tanaka, K.; Kaneto, K., Planate conducting polymer actuator based on polypyrrole and its application. *Sensors and Actuators A: Physical* **2009,** 150, (2), 272-276.
1281. van der Wijngaart, W.; Ask, H.; Enoksson, P.; Stemme, G., A high-stroke, high pressure electrostatic actuator for valve applications. *Sensors and Actuators A: Physical* **2002,** 100, 264-271.
1282. Weibel, D. B.; Kruithof, M.; Potenta, S.; Sia, S. K.; Lee, A.; Whitesides, G. M., Torque-Actuated Valves for Microfluidics. *Analytical Chemistry* **2005,** 77, (15), 4726-4733.
1283. Zhao, B.; Moore, J. S.; Beebe, D. J., Principles of Surface-Directed Liquid Flow in Microfluidic Channels. *Analytical Chemistry* **2002,** 74, (16), 4259-4268.
1284. Baldi, A.; Lei, M.; Gu, Y.; Siegel, R. A.; Ziaie, B., A microstructured silicon membrane with entrapped hydrogels for environmentally sensitive fluid gating. *Sensors and Actuators B: Chemical* **2006,** 114, (1), 9-18.
1285. Richter, A.; Klatt, S.; Paschew, G.; Klenke, C., Micropumps operated by swelling and shrinking of temperature-sensitive hydrogels. *Lab on a Chip* **2009,** 9, (4), 613-618.
1286. Takamura, Y.; Onoda, H.; Inokuchi, H.; Adachi, S.; Oki, A.; Horiike, Y., Low-voltage electroosmosis pump for stand-alone microfluidics devices. *Electrophoresis* **2003,** 24, (1-2), 185-192.
1287. Bong, K. W.; Chapin, S. C.; Pregibon, D. C.; Baah, D.; Floyd-Smith, T. M.; Doyle, P. S., Compressed-air flow control system. *Lab on a Chip* **2011,** 11, (4), 743-747.
1288. Cabal, A.; Ross, D. S.; Lebens, J. A.; Trauernicht, D. P., Thermal actuator with optimized heater for liquid drop ejectors. *Sensors and Actuators A: Physical* **2005,** 123-124, 531-539.
1289. Shemesh, J.; Bransky, A.; Khoury, M.; Levenberg, S., Advanced microfluidic droplet manipulation based on piezoelectric actuation. *Biomedical Microdevices* **2010,** 12, (5), 907-914.
1290. Tan, H. Y.; Loke, W. K.; Nguyen, N.-T., A reliable method for bonding polydimethylsiloxane (PDMS) to polymethylmethacrylate (PMMA) and its application in micropumps. *Sensors and Actuators B: Chemical* **2010,** 151, (1), 133-139.
1291. Lai, H.; Folch, A., Design and dynamic characterization of "single-stroke" peristaltic PDMS micropumps. *Lab on a Chip* **2011,** 11, (2), 336-342.

1292. Shim, W.; Braunschweig, A. B.; Liao, X.; Chai, J.; Lim, J. K.; Zheng, G.; Mirkin, C. A., Hard-tip, soft-spring lithography. *Nature* **2011,** 469, (7331), 516-520.
1293. Feldmann, M.; Buttgenbach, S., Novel Microrobots and Micromotors Using Lorentz Force Driven Linear Microactuators Based on Polymer Magnets. *IEEE Transactions on Magnetics* **2007,** 43, (10), 3891-3895.
1294. Vozzi, G.; Flaim, C.; Ahluwalia, A.; Bhatia, S., Fabrication of PLGA scaffolds using soft lithography and microsyringe deposition. *Biomaterials* **2003,** 24, (14), 2533-2540.
1295. Beyaz, M. I.; McCarthy, M.; Ghalichechian, N.; Ghodssi, R., Closed-loop control of a long-range micropositioner using integrated photodiode sensors. *Sensors and Actuators A: Physical* **2009,** 151, (2), 187-194.
1296. Millet, O.; Bernardoni, P.; Régnier, S.; Bidaud, P.; Tsitsiris, E.; Collard, D.; Buchaillot, L., Electrostatic actuated micro gripper using an amplification mechanism. *Sensors and Actuators A: Physical* **2004,** 114, (2-3), 371-378.
1297. Park, J.; et al., Fabrication of complex 3D polymer structures for cell-polymer hybrid systems. *Journal of Micromechanics and Microengineering* **2006,** 16, (8), 1614.
1298. Choi, S.; Park, J.-K., Tuneable hydrophoretic separation using elastic deformation of poly(dimethylsiloxane). *Lab on a Chip* **2009,** 9, (13), 1962-1965.
1299. Schabmueller, C. G. J.; Koch, M.; Mokhtari, M. E.; Evans, A. G. R.; Brunnschweiler, A.; Sehr, H., Self-aligning gas/liquid micropump. *Journal of Micromechanics and Microengineering* **2002,** 12, 420-424.
1300. Xu, Q.; Hashimoto, M.; Dang, T. T.; Hoare, T.; Kohane, D. S.; Whitesides, G. M.; Langer, R.; Anderson, D. G., Preparation of Monodisperse Biodegradable Polymer Microparticles Using a Microfluidic Flow-Focusing Device for Controlled Drug Delivery. *Small* **2009,** 5, (13), 1575-1581.
1301. Dendukuri, D.; Gu, S. S.; Pregibon, D. C.; Hatton, T. A.; Doyle, P. S., Stop-flow lithography in a microfluidic device. *Lab on a Chip* **2007,** 7, (7), 818-828.
1302. Lii, J.; Hsu, W.-J.; Parsa, H.; Das, A.; Rouse, R.; Sia, S. K., Real-Time Microfluidic System for Studying Mammalian Cells in 3D Microenvironments. *Analytical Chemistry* **2008,** 80, (10), 3640-3647.
1303. Tkachenko, E.; Gutierrez, E.; Ginsberg, M. H.; Groisman, A., An easy to assemble microfluidic perfusion device with a magnetic clamp. *Lab on a Chip* **2009,** 9, (8), 1085-1095.
1304. Hufnagel, H.; Huebner, A.; Gulch, C.; Guse, K.; Abell, C.; Hollfelder, F., An integrated cell culture lab on a chip: modular microdevices for cultivation of mammalian cells and delivery into microfluidic microdroplets. *Lab on a Chip* **2009,** 9, (11), 1576-1582.
1305. Wang, Z.; Kim, M.-C.; Marquez, M.; Thorsen, T., High-density microfluidic arrays for cell cytotoxicity analysis. *Lab on a Chip* **2007,** 7, (6), 740-745.
1306. Fonslow, B. R.; Bowser, M. T., Optimizing Band Width and Resolution in Micro-Free Flow Electrophoresis. *Analytical Chemistry* **2006,** 78, (24), 8236-8244.
1307. Lam, E. W.; Cooksey, G. A.; Finlayson, B. A.; Folch, A., Microfluidic circuits with tunable flow resistances. *Applied Physics Letters* **2006,** 89, 164105.

1308. Huang, S.-B.; et al., A membrane-based serpentine-shape pneumatic micropump with pumping performance modulated by fluidic resistance. *Journal of Micromechanics and Microengineering* **2008,** 18, (4), 045008.
1309. Langelier, S. M.; Chang, D. S.; Zeitoun, R. I.; Burns, M. A., Acoustically driven programmable liquid motion using resonance cavities. *Proceedings of the National Academy of Sciences* **2009,** 106, (31), 12617-12622.
1310. Benito-Lopez, F.; Byrne, R.; Raduta, A. M.; Vrana, N. E.; McGuinness, G.; Diamond, D., Ionogel-based light-actuated valves for controlling liquid flow in micro-fluidic manifolds. *Lab on a Chip* **2010,** 10, (2), 195-201.
1311. Kayani, A. A.; Zhang, C.; Khoshmanesh, K.; Campbell, J. L.; Mitchell, A.; Kalantar-zadeh, K., Novel tuneable optical elements based on nanoparticle suspensions in microfluidics. *Electrophoresis* **2010,** 31, (6), 1071-1079.
1312. Chin, L. K.; Liu, A. Q.; Soh, Y. C.; Lim, C. S.; Lin, C. L., A reconfigurable optofluidic Michelson interferometer using tunable droplet grating. *Lab on a Chip* **2010,** 10, (8), 1072-1078.
1313. Hashimoto, M.; Mayers, B.; Garstecki, P.; Whitesides, G. M., Flowing Lattices of Bubbles as Tunable, Self-Assembled Diffraction Gratings. *Small* **2006,** 2, (11), 1292-1298.
1314. Mao, X.; Lin, S.-C. S.; Lapsley, M. I.; Shi, J.; Juluri, B. K.; Huang, T. J., Tunable Liquid Gradient Refractive Index (L-GRIN) lens with two degrees of freedom. *Lab on a Chip* **2009,** 9, (14), 2050-2058.
1315. Cadarso, V. J.; Llobera, A.; Villanueva, G.; Plaza, J. A.; Brugger, J.; Dominguez, C., Mechanically tuneable microoptical structure based on PDMS. *Sensors and Actuators A: Physical* **2010,** 162, (2), 260-266.
1316. Lee, C.-H.; et al., A tunable microflow focusing device utilizing controllable moving walls and its applications for formation of micro-droplets in liquids. *Journal of Micromechanics and Microengineering* **2007,** 17, (6), 1121.
1317. Anand, R. K.; Sheridan, E.; Hlushkou, D.; Tallarek, U.; Crooks, R. M., Bipolar electrode focusing: tuning the electric field gradient. *Lab on a Chip* **2011,** 11, (3), 518-527.
1318. Qu, P.; Lei, J.; Zhang, L.; Ouyang, R.; Ju, H., Molecularly imprinted magnetic nanoparticles as tunable stationary phase located in microfluidic channel for enantioseparation. *Journal of Chromatography A* **2010,** 1217, (39), 6115-6121.
1319. Huh, D.; Mills, K. L.; Zhu, X.; Burns, M. A.; Thouless, M. D.; Takayama, S., Tuneable elastomeric nanochannels for nanofluidic manipulation. *Nature Materials* **2007,** 6, (6), 424-428.
1320. Jellema, L.-J. C.; Markesteijn, A. P.; Westerweel, J.; Verpoorte, E., Tunable Hydrodynamic Chromatography of Microparticles Localized in Short Microchannels. *Analytical Chemistry* **2010,** 82, (10), 4027-4035.
1321. Jang, L.-S.; Shu, K.; Yu, Y.-C.; Li, Y.-J.; Chen, C.-H., Effect of actuation sequence on flow rates of peristaltic micropumps with PZT actuators. *Biomedical Microdevices* **2009,** 11, (1), 173-181.

1322. Wunderlich, B. K.; Klebinger, U. A.; Bausch, A. R., Diffusive spreading of time-dependent pressures in elastic microfluidic devices. *Lab on a Chip* **2010,** 10, (8), 1025-1029.
1323. Hardy, B. S.; Uechi, K.; Zhen, J.; Kavehpour, H. P., The deformation of flexible PDMS microchannels under a pressure driven flow. *Lab on a Chip* **2009,** 9, (7), 935-938.
1324. Tabak, A.; Yesilyurt, S., Simulation-based analysis of flow due to traveling-plane-wave deformations on elastic thin-film actuators in micropumps. *Microfluidics and Nanofluidics* **2008,** 4, (6), 489-500.
1325. Tabak, A. F.; Yesilyurt, S. In *Numerical simulations and analysis of a micropump actuated by traveling plane waves*, Microfluidics, BioMEMS, and Medical Microsystems V, San Jose, CA, USA, 2007; SPIE: San Jose, CA, USA, 2007; pp 64650Z-11.
1326. Ogawa, J.; Kanno, I.; Kotera, H.; Wasa, K.; Suzuki, T., Development of liquid pumping devices using vibrating microchannel walls. *Sensors and Actuators A: Physical* **2009,** 152, (2), 211-218.
1327. Masini, L.; Cecchini, M.; Girardo, S.; Cingolani, R.; Pisignano, D.; Beltram, F., Surface-acoustic-wave counterflow micropumps for on-chip liquid motion control in two-dimensional microchannel arrays. *Lab on a Chip* **2010,** 10, (15), 1997-2000.
1328. Cecchini, M.; Girardo, S.; Pisignano, D.; Cingolani, R.; Beltram, F., Acoustic-counterflow microfluidics by surface acoustic waves. *Applied Physics Letters* **2008,** 92, 104103.
1329. Taff, J.; Kashte, Y.; Spinella-Mamo, V.; Paranjape, M., Fabricating multilevel SU-8 structures in a single photolithographic step using colored masking patterns. *Journal of Vacuum Science & Technology A* **2006,** 24, (3), 742-746.
1330. Chen, C.; Hirdes, D.; Folch, A., Gray-scale photolithography using microfluidic photomasks. *Proceedings of the National Academy of Sciences of the United States of America* **2003,** 100, (4), 1499-1504.
1331. Waits, C., M. ; Modafe, A.; Ghodssi, R., Investigation of gray-scale technology for large area 3D silicon MEMS structures. *Journal of Micromechanics and Microengineering* **2003,** 13, (2), 170.
1332. Leslie, D. C.; Melnikoff, B. A.; Marchiarullo, D. J.; Cash, D. R.; Ferrance, J. P.; Landers, J. P., A simple method for the evaluation of microfluidic architecture using flow quantitation via a multiplexed fluidic resistance measurement. *Lab on a Chip* **2010,** 10, (15), 1960-1966.
1333. Kim, D.; Chesler, N. C.; Beebe, D. J., A method for dynamic system characterization using hydraulic series resistance. *Lab on a Chip* **2006,** 6, (5), 639-644.
1334. Wang, C.-H.; Lee, G.-B., Pneumatically driven peristaltic micropumps utilizing serpentine-shape channels. *Journal of Micromechanics and Microengineering* **2006,** 16, (2), 341-348.
1335. Nguyen, N.-T.; Huang, X., Miniature valveless pumps based on printed circuit board technique. *Sensors and Actuators A: Physical* **2001,** 88, (2), 104-111.
1336. Bohm, S.; Olthuis, W.; Bergveld, P., A plastic micropump constructed with conventional techniques and materials. *Sensors and Actuators A: Physical* **1999,** A77, (3), 223-8.

1337. Vedel, S.; Olesen, L. H.; Bruus, H., Pulsatile microfluidics as an analytical tool for determining the dynamic characteristics of microfluidic systems. *Journal of Micromechanics and Microengineering* **2010,** 20, (3), 035026.
1338. Majid Nabavi and Kamran, S., A critical review on advanced velocity measurement techniques in pulsating flows. *Measurement Science and Technology* **2010,** 21, (4), 042002.
1339. Ahrens, R.; Festa, M., Polymer-based micro flow sensor for dynamical flow measurements in hydraulic systems. *Journal of Micromechanics and Microengineering* **2010,** 20, (6), 064004.
1340. Okulan, N.; Henderson, H. T.; Ahn, C. H., A pulsed mode micromachined flow sensor with temperature drift compensation. *IEEE Transactions on Electron Devices* **2000,** 47, (2), 340-7.
1341. Mogensen, K. B.; Kwok, Y. C.; Eijkel, J. C. T.; Petersen, N. J.; Manz, A.; Kutter, J. r. P., A Microfluidic Device with an Integrated Waveguide Beam Splitter for Velocity Measurements of Flowing Particles by Fourier Transformation. *Analytical Chemistry* **2003,** 75, (18), 4931-4936.
1342. Hsieh, S.-S.; Lin, C.-Y.; Huang, C.-F.; Tsai, H.-H., Liquid flow in a micro-channel. *Journal of Micromechanics and Microengineering* **2004,** 14, (4), 436-45.
1343. Arbour, T. J.; Enderlein, J., Application of dual-focus fluorescence correlation spectroscopy to microfluidic flow-velocity measurement. *Lab on a Chip* **2010,** 10, (10), 1286-1292.
1344. Chung, J.; Grigoropoulos, C. P.; Greif, R., Infrared thermal velocimetry for nonintrusive flow measurement in silicon microfluidic devices. *Review of Scientific Instruments* **2003,** 74, (5), 2911-17.
1345. Akbari, M.; Sinton, D.; Bahrami, M., Pressure Drop in Rectangular Microchannels as Compared With Theory Based on Arbitrary Cross Section. *Journal of Fluids Engineering* **2009,** 131, (4), 041202-8.
1346. Urbanek, W.; Zemel, J. N.; Bau, H. H., An investigation of the temperature dependence of Poiseuille numbers in microchannel flow. *Journal of Micromechanics and Microengineering* **1993,** 3, (4), 206-9.
1347. Dutkowski, K., Experimental investigations of Poiseuille number laminar flow of water and air in minichannels. *International Journal of Heat and Mass Transfer* **2008,** 51, (25-26), 5983-5990.
1348. Fischer, L.; Martin, H., Friction factors for fully developed laminar flow in ducts confined by corrugated parallel walls. *International Journal of Heat and Mass Transfer* **1997,** 40, (3), 635-639.
1349. Gervais, T.; El-Ali, J.; Gunther, A.; Jensen, K. F., Flow-induced deformation of shallow microfluidic channels. *Lab on a Chip* **2006,** 6, (4), 500-507.
1350. Wang, H.; Wang, Y., Flow in microchannels with rough walls: flow pattern and pressure drop. *Journal of Micromechanics and Microengineering* **2007,** 17, (3), 586.
1351. Chakraborty, S.; Das, T.; Chattoraj, S., A generalized model for probing frictional characteristics of pressure-driven liquid microflows. *Journal of Applied Physics* **2007,** 102, 104907.

1352. Perry, S. L.; Higdon, J. J. L.; Kenis, P. J. A., Design rules for pumping and metering of highly viscous fluids in microfluidics. *Lab on a Chip* **2010,** 10, (22), 3112-3124.
1353. Fuerstman, M. J.; Lai, A.; Thurlow, M. E.; Shevkoplyas, S. S.; Stone, H. A.; Whitesides, G. M., The pressure drop along rectangular microchannels containing bubbles. *Lab on a Chip* **2007,** 7, (11), 1479-1489.
1354. Adzima, B., J. ; Velankar, S. S., Pressure drops for droplet flows in microfluidic channels. *Journal of Micromechanics and Microengineering* **2006,** 16, (8), 1504.
1355. Yamahata, C.; Lacharme, F.; Burri, Y.; Gijs, M. A. M., A ball valve micropump in glass fabricated by powder blasting. *Sensors and Actuators B: Chemical* **2005,** 110, (1), 1-7.
1356. Kim, J. H.; Lau, K. T.; Shepherd, R.; Wu, Y.; Wallace, G.; Diamond, D., Performance characteristics of a polypyrrole modified polydimethylsiloxane (PDMS) membrane based microfluidic pump. *Sensors and Actuators A: Physical* **2008,** 148, (1), 239-244.
1357. Husband, B.; Bu, M.; Apostolopoulos, V.; Melvin, T.; Evans, A. G. R. In *Novel actuation of an integrated peristaltic micropump*, Micro and Nano Engineering 2003, Sep 22-25 2003, Cambridge, United Kingdom, 2004; Elsevier: Cambridge, United Kingdom, 2004; pp 858-863.
1358. Zhu, M.; Kirby, P.; Wacklerle, M.; Herz, M.; Richter, M., Optimization design of multi-material micropump using finite element method. *Sensors and Actuators A: Physical* **2009,** 149, (1), 130-135.
1359. Berg, J. M.; Anderson, R.; Anaya, M.; Lahlouh, B.; Holtz, M.; Dallas, T., A two-stage discrete peristaltic micropump. *Sensors and Actuators A: Physical* **2003,** 104, (1), 6-10.
1360. Nie, F.-Q.; Macka, M.; Paull, B., Micro-flow injection analysis system: on-chip sample preconcentration, injection and delivery using coupled monolithic electroosmotic pumps. *Lab on a Chip* **2007,** 7, (11), 1597-1599.
1361. Nguyen, N.-T.; Truong, T.-Q., A fully polymeric micropump with piezoelectric actuator. *Sensors and Actuators B: Chemical* **2004,** 97, (1), 137-143.
1362. Karassik, I. J.; Messina, J. P.; Cooper, P.; Heald, C. C., *Pump Handbook*. Fourth ed.; McGraw-Hill: 2008.
1363. Rossetti, A.; et al., Experimental and numerical analyses of micro rotary shaft pumps. *Journal of Micromechanics and Microengineering* **2009,** 19, (12), 125013.
1364. Tagusari, O.; Yamazaki, K.; Litwak, P.; Antaki, J. F.; Watach, M.; Gordon, L. M.; Kono, K.; Mori, T.; Koyanagi, H.; Griffith, B. P.; Kormos, R. L., Effect of Pressure-Flow Relationship of Centrifugal Pump on In Vivo Hemodynamics: A. *Artificial Organs* **1998,** 22, 399-404.
1365. Ma, H.; Hou, B.; Wu, H.; Lin, C.; Gao, J.; Kou, M., Development and application of a diaphragm micro-pump with piezoelectric device. *Microsystem Technologies* **2008,** 14, (7), 1001-1007.
1366. Dickenson, C., *Pumping Manual*. Eighth ed.; The Trade & Technical Press Limited: 1988.

1367. Mohitpour, M.; Botros, K. K.; Van Hardeveld, T., *Pipeline Pumping and Compression Systems*. ASME Press: 2008.
1368. Lee, D.-S.; Ko, J. S.; Kim, Y. T., Bidirectional pumping properties of a peristaltic piezoelectric micropump with simple design and chemical resistance. *Thin Solid Films* **2004,** 468, (1-2), 285-290.
1369. Linnemann, R.; Woias, P.; Senfft, C.-D.; Ditterich, J. A. In *A self-priming and bubble-tolerant piezoelectric silicon micropump for liquids and gases*, Proceedings IEEE Eleventh Annual International Workshop on Micro Electro Mechanical Systems An Investigation of Micro Structures, Sensors, Actuators, Machines and Systems, 25-29 Jan. 1998, Heidelberg, Germany, 1998; IEEE: Heidelberg, Germany, 1998; pp 532-7.
1370. Wego, A.; Pagel, L., A self-filling micropump based on PCB technology. *Sensors and Actuators A: Physical* **2001,** 88, (3), 220-226.
1371. Ciriacks Klinker, C.; Bowser, M. T., 4-Fluoro-7-nitro-2,1,3-benzoxadiazole as a Fluorogenic Labeling Reagent for the in Vivo Analysis of Amino Acid Neurotransmitters Using Online Microdialysis-Capillary Electrophoresis. *Analytical Chemistry* **2007,** 79, (22), 8747-8754.
1372. Young, A. M.; Rees, K. R., Dopamine release in the amygdaloid complex of the rat, studied by brain microdialysis. *Neuroscience Letters* **1998,** 249, (1), 49-52.
1373. Meredith, R. M.; McCabe, B. J.; Kendrick, K. M.; Horn, G., Amino acid neurotransmitter release and learning: a study of visual imprinting. *Neuroscience* **2004,** 126, (2), 249-56.
1374. Varea, E.; Ponsoda, X.; Molowny, A.; Danscher, G.; Lopez-Garcia, C., Imaging synaptic zinc release in living nervous tissue. *Journal of Neuroscience Methods* **2001,** 110, (1-2), 57-63.
1375. Morgenthaler, F. D.; Knott, G. W.; Floyd Sarria, J. C.; Wang, X.; Staple, J. K.; Catsicas, S.; Hirling, H., Morphological and molecular heterogeneity in release sites of single neurons. *European Journal of Neuroscience* **2003,** 17, (7), 1365-74.
1376. Roitman, M. F.; Stuber, G. D.; Phillips, P. E. M.; Wightman, R. M.; Carelli, R. M., Dopamine operates as a subsecond modulator of food seeking. *Journal of Neuroscience* **2004,** 24, (6), 1265-1271.
1377. Robinson, D. L.; Heien, M. L. A. V.; Wightman, R. M., Frequency of dopamine concentration transients increases in dorsal and ventral striatum of male rats during introduction of conspecifics. *Journal of Neuroscience* **2002,** 22, (23), 10477-10486.
1378. Rentero, N.; Bruandet, N.; Quintin, L., Rostral ventrolateral medulla catechol involvement upon sino-aortic deafferentation: an in vivo voltammetric study. *Life Sciences* **2000,** 68, (2), 177-189.

Appendix

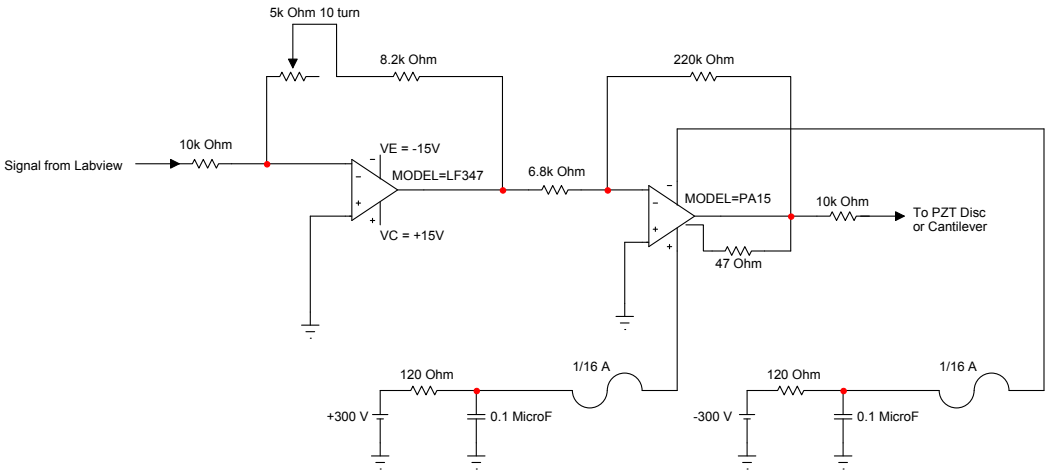

Figure A-1: High voltage circuit schematic. Circuit design fabricated to power and drive piezoelectric actuator elements. (Figure A-1 adapted from D. J. Simons, 2005)

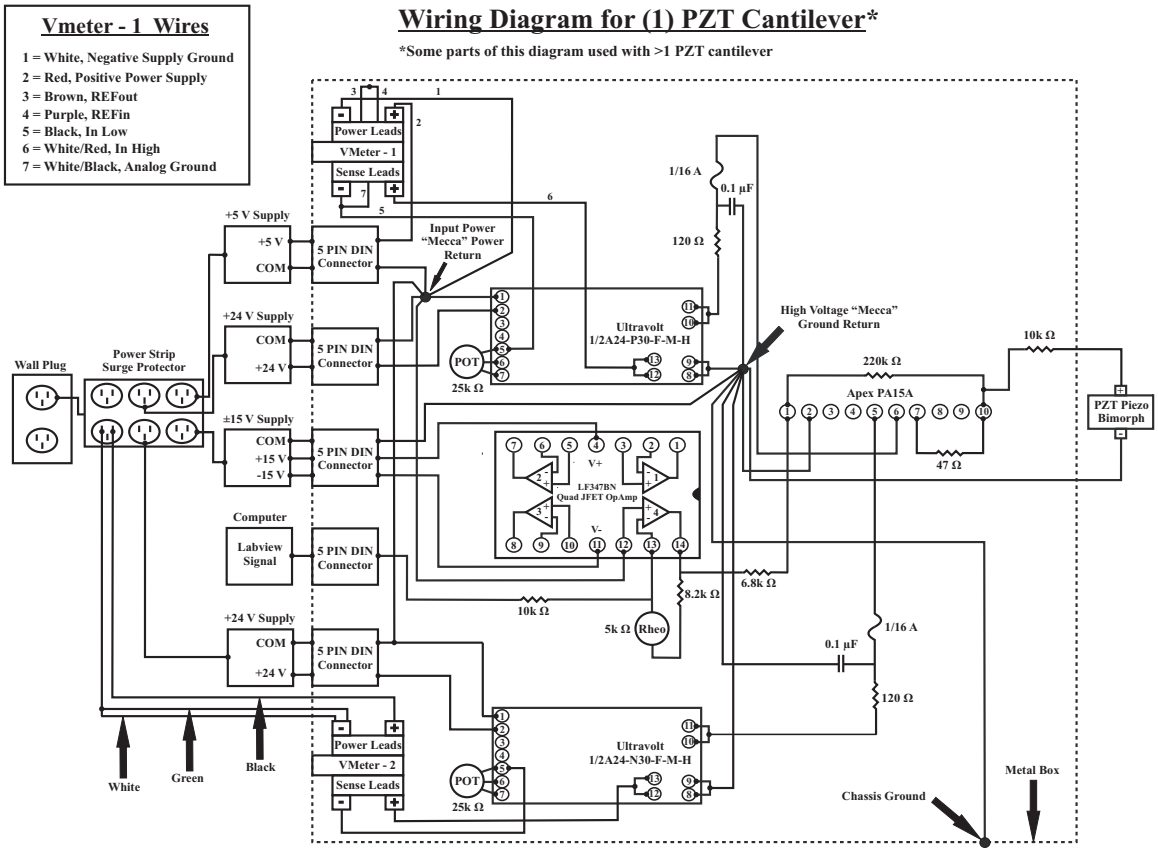

Figure A-2: Wiring diagram for electronic apparatus used to power and drive micropump piezoelectric cantilever actuators.